THE MODERN AND LATE HOLOCENE MARINE ENVIRONMENTS OF LOCH SUNART, N.W. SCOTLAND

Alix Gayle Cage

A Thesis Submitted for the Degree of PhD
at the
University of St Andrews

2006

Please use this identifier to cite or link to this item:
http://hdl.handle.net/10023/15910

THE MODERN AND LATE HOLOCENE MARINE ENVIRONMENTS OF LOCH SUNART, N.W. SCOTLAND.

Alix Gayle Cage

A thesis submitted to the University of St Andrews for the degree of
Doctor of Philosophy

School of Geography & Geosciences
University of St Andrews

May 2005

DECLARATION

i I, Alix Gayle Cage, hereby certify that this thesis, which is approximately 84,000 words in length, has been written by me, that it is the record of work carried out by me and that it has not been submitted in any previous application for a higher degree.

Date....27/5/2005 Signature of candidat

ii I was admitted as a research student in October, 2000 and as a candidate for the degree of Ph.D. in October, 2001; the higher study for which this is a record was carried out in the University of St Andrews between 2000 and 2005.

Date..27/5/2005 Signature of candidate

iii I hereby certify that the candidate has fulfilled the conditions of the Resolution and Regulations appropriate for the degree of Ph.D. in the University of St Andrews and that the candidate is qualified to submit this thesis in application for that degree.

Date..27/5/2005 Signature of supervisor

Unrestricted

In submitting this thesis to the University of St Andrews, I understand that I am giving permission for it to be made available for use in accordance with the regulations of the University Library for the time being in force subject to any copyright vested in the work not being affected thereby. I also understand that the title and abstract will be published, and that a copy of the work may be made and supplied to any bona fide library or research worker.

Date...27/5/2005 Signature of candidate

ABSTRACT

The first study to exploit the sedimentary archives of Loch Sunart, a relatively well-flushed fjord on the NW coast of Scotland, for palaeoenvironmental reconstruction is presented. In order to understand environmental influences on past environments, the modern physical, chemical and biological conditions of the loch and surrounding catchment were studied. Both observational and computer modelled annual inner basin salinity show a clear response to climatic forcing, modulated by NAO behaviour. Main basin salinity appears to remain very stable and a well-defined salinity:$\delta^{18}O$ relationship suggests excellent potential for palaeotemperature reconstructions based on foraminiferal $\delta^{18}O$.

Multi-variate statistical analyses identified 4 benthic foraminiferal assemblage groups in the surface sediments of the loch: A) restricted basin (*E. scaber)*; B) very high current activity (*C. lobatulus-A. mammilla –A. beccarii*); C) calm environment under a stratified water column (*B. marginata-N. turgida-S. fusiformis*) and D) coastal water influence and mild/episodic current activity (*A. beccarii-C. lobatulus-S. wrightii-E. excavatum*). Using assemblage data, an existing benthic foraminiferal transfer function was modified in order to reconstruct Loch Sunart bottom water temperature (BWS); these reconstructions agree well with Scottish coastal temperature series (Millport).

C. lobatulus appears to calcify close to theoretical equilibrium $\delta^{18}O$ calcite ($\Delta\delta^{18}O = -0.11 \pm 0.17$ ‰), probably during the warm bottom water temperatures (BWT) of late autumn, and predominantly reflects changes in BWT rather than BWS in the main basin of Loch Sunart.

The first late Holocene high resolution palaeoenvironmental reconstruction from the deep (121 m) main basin of Loch Sunart is presented; gravity core (GC023) is 3 m long and spans the last 2,000 years. Despite difficulties with geochronology, palaeoenvironmental reconstructions from Loch Sunart suggest that these high resolution sedimentary archives have the potential to resolve inter-annual marine climate variability of the order of 1-2°C and capture an integrated record of changes in the catchment and marine environment.

ACKNOWLEDGMENTS

Firstly I would like to thank my supervisor, Dr. Bill Austin, for providing me with the opportunity to pursue this Ph.D. and for his help, support, funding, expertise and guidance throughout.

Many thanks to Dr. P. Gillibrand (formerly of FRS, Aberdeen, now based at SAMS, Oban), whose collaboration allowed the fjordic circulation of Loch Sunart to be observed and modelled; contributing to my first publication! Also, many thanks to Dr. P. Barnett (University Marine Biological Station, Millport), Mr. I. Harris (UEA), Dr. M. Inall (SAMS) and Dr. B. Turrell (FRS) for sharing their data with me and for providing useful advice, and to Sankurie Pye (National Museum of Scotland) for allowing me to use their historical mollusc collection for destructive analyses. Many thanks to Prof. J. Scourse whose inspirational lectures led me down this path.

A large proportion of work included in this thesis was carried out at other institutes. Prof. Jan Heinemeier kindly invited me to visit the University of Aarhus to carry out AMS radiocarbon dating and thanks goes to his research group, particularly Ann-Berit Jensen, who was a great help and a friendly face. The trip was funded through grants awarded by The Scottish International Education Trust and the University of St Andrews Russell Trust. Thanks to Prof. Karen Luise Knudsen and Dr. P. Kristensen for their useful discussion on benthic foraminiferal taxonomy. Stable isotopic analyses were carried out with the guidance and help of Dr. Ulysses Ninneman and Rune Sørås during my 4 month pre-doctoral fellowship at the University of Bergen, Norway. I appreciate the help given by Dr. J. Birks and Dr. R. Telford on transfer function techniques. Many thanks to Dr. Dorthe Klitgaard-Kristensen, for her help, advice and friendship (particularly as an avid dancing diva!) during my stay in Bergen - it was very much appreciated!

I'm hugely indebted to the University of St Andrews for providing funding and laboratory assistance. Particular thanks goes to Colin Cameron, who has saved me more than once! Dr. Richard Bates provided data for use in GIS and Mr. G. Sandeman taught

me the joys of Illustrator! Thanks to Dr. Niels Norgaard-Pedersen, who assisted on field work and provided the bulk sediment data , grain size data and isotopic analyses for cores GC023 and SC023 (chapter 8). Dr. Tracy Shimmield provided the geochemical data for cores GC023 and SC023 and Prof. G. Shimmield made useful suggestions. Thanks to Mr and Mrs Campbell of Ariundle and Dr. Jack Jarvis who helped out with Ariundle weather station, and also thanks to Matt, Andrew and Emilie who provided me with laughs, good music (sometimes!) and an extra pair of hands on my frequent tramps over to Strontian.

My friends and family, both near and far, have been a great source of entertainment and support over the years, and much love and thanks goes out to Jamie, Jojo, Caroline, Ele, Lindsey, Andrew, Pig, Maerkey, Mog, Beccy, Nick, Chrispy, Tom, Zoe, Goose, Marci and Dave.

But the best friends I have, and who I couldn't have done this without, are my parents and Matt. Their love, affection, support and constant encouragement throughout (and Matt's amazing thesis compilation skills!), have kept me going and I cannot even begin to thank them enough. I hope I can make them proud.

TABLE OF CONTENTS

CHAPTER 7 – A BENTHIC FORAMINIFERAL TRANSFER FUNCTION APPROACH TO RECONSTRUCT SCOTTISH WEST COAST FJORDIC PALAEOENVIRONMENTS 260

CHAPTER 8 – LATE HOLOCENE PALAEOENVIRONMENTAL HISTORY OF LOCH SUNART 291

APPENDICES

FIGURES

TABLES

CHAPTER 1 – INTRODUCTION

1.1. Project rationale

Oceans play an important role in the regulation of global climate (Clark *et al.*, 2002), particularly the sub-polar/polar North Atlantic Ocean, where the formation of deep water is the primary driver of the thermohaline circulation (Broecker *et al.*, 1990). Palaeoclimatic studies utilising marine, terrestrial and ice core archives have therefore been carried out in the North Atlantic because this region provides a globally significant perspective of the magnitude and rate of climate change (e.g. Cortijo *et al.*, 2000).

Within a palaeoceanographic context, the majority of studies have employed deep sea sediment cores to provide an insight into ocean circulation dynamics and global climate change over recent geological time, particularly across the glacial-interglacial transitions of the current Quaternary period (e.g. Bond *et al.*, 1992; Seidenkrantz *et al.*, 1995; Austin & Evans, 2000). Seminal work within the last 2 decades noted the presence of millennial-scale climate cycles pervading late Quaternary marine archives and high resolution ice core records in a penecontemporaneous fashion (Bond *et al.*, 1999). This millennial-scale variability is often attributed to changes in the global thermohaline circulation (THC), however the recent identification of centennial and decadal-scale variability in palaeoclimatic records (e.g. Hall *et al.*, 2004; Andresen *et al.*, 2005) suggests factors other than the rate and location of deep ocean ventilation, such as solar variability or an Atlantic multi-decadal oscillation (Kerr, 2000), are playing an important role in driving long-term climate change. In addition, deep ocean environments typically have low sediment accumulation rates (<0.01 cm yr^{-1}) which are often affected by bioturbation, thus creating the need for high resolution marine sedimentary archives in order to investigate the Atlantic's multi-decadal climate oscillations.

High sediment accumulation rates (~ 0.5 cm yr^{-1}) in sea loch (or fjord) environments provide the potential for high resolution palaeoenvironmental studies and present a unique opportunity to study land-ocean interactions. Palaeoenvironmental studies from W Norwegian fjords, for example, have demonstrated that sediments and benthic foraminifera from these environments capture and record centennial and decadal variability in the coastal environment and climate of western Norway (e.g. Mikalsen *et al.*, 2001; Kristensen *et al.*, 2004). Climatically driven circulation changes linking Scottish coastal regions to the North Atlantic have been illustrated by Holliday (2003). At a regional scale, recent work by Gillibrand *et al.,* (2005) and Austin & Inall (2002) exemplify the potential for regional changes in fjordic hydrography to be captured in the carbonate shells of marine organisms. Since the west coast of Scotland lies in a climatically sensitive region of the North Atlantic it is also likely that Scottish sea loch sediments capture North Atlantic climatic variability, possibly with sub-decadal resolution.

Despite this potential, few palaeoenvironmental studies have been carried out in Scottish sea lochs. Those that exist have focused upon the last glacial – interglacial transition (LGIT; Dix & Duck, 2000; Howe *et al.*, 2002) or cover only the past few centuries (Murray *et al.*, 2003). Thus, the sea lochs (fjords) of NW Scotland have been generally overlooked in terms of palaeoenvironmental work and neglected in the context of late-Holocene climatic variability.

1.2 The role of oceans in modulating global climate

Whilst the orbital forcing of the Earth's climate primarily drives the large glacial-interglacial cycles (Lowe & Walker, 1997), the oceans play an important role in the modulation of climate variability. This is due to the strong ocean-atmospheric coupling and subsequent transfer of both sensible and latent heat (Cayan, 1992; Bigg, 1996) and latitudinal heat transfer from the tropics poleward (Ganachaud & Wunsch, 2000). The majority of the ocean's energy comes from solar radiation heating of the surface layer (Bigg, 1996) and the high specific heat capacity of the ocean influences atmospheric climate on daily, seasonal and inter-annual time scales (Clark *et al.*, 2002). Additionally, the ocean can retain a 'memory' of atmospheric climate (see section 1.3.1).

1.2.1 Thermohaline circulation

Global thermohaline circulation (THC) and it's role as a conveyor of heat around the globe is well documented (see Rahmstorf, 2002 and references within). Warm saline water flows from the tropical Atlantic region towards the high latitudes, in particular the North Atlantic, due to differential solar heating of the surface ocean at high and low latitudes (Bond *et al.*, 1999; Clark *et al.*, 2002). At around 60 °N, surface water is cooled, subsequently causing an increase in surface water density. The formation of sea ice can also result in brine formation, providing an additional mechanism that creates dense water. This dense water, collectively known as North Atlantic Deep Water (NADW), sinks and flows southward, eventually upwelling in the Pacific Ocean where it is heated and returns to the North Atlantic as surface water. Antartic Bottom Water (AABW) and Lower Circumpolar Deep Water (LCDW), which are also important sources of deep water in the global ocean, are formed around Antarctica.

NADW formation is thought to be the main 'driver' of the THC (Broecker *et al.*, 1990) and plays a particularly important role in millennial-scale climate variability (e.g. Weaver & Hughes, 1994; Marchitto *et al.*, 1998; Bianchi & McCave, 1999; Curry *et al.*, 1999; Rodwell *et al.*, 1999; Broecker, 2000; Keigwin & Boyle, 2000; Marotzke, 2000; Arz *et al.*, 2001; Clark *et al.*, 2002; Marchitto & deMenocal, 2003; Oppo *et al.*, 2003; Giraudeau *et al.*, 2004; Hall *et al.*, 2004). The formation of NADW is often referred to as ocean 'ventilation' and ventilation rates can change over time, depending on the 'mode' of the THC in operation (Bond *et al.*, 1999; Curry *et al.*, 1999). The THC system is sensitively balanced and though the THC is primarily forced by thermically driven density differences, freshwater inputs significantly impact upon the system (figure 1.1 and Rahmstorf, 1995, 1996, 2000). Such freshwater injections have been attributed as the cause of the temporary slowdown (or shutdown) of the THC during the Younger Dryas phase and the Holocene 8,200 year event (Broecker, 2003), though both Piotrowski *et al.,* (2004) and Rohling & Pälike (2005) suggest the causal factor of the 8.2 kyr BP cool event (and also the Younger Dryas phase) is yet to be determined.

Recent instrumental studies have shown large inter-annual and decadal variability in North Atlantic Ocean conditions (Cayan, 1992; Chen & Ghil, 1995; Dickson *et al.*, 1996; Macdonald & Wunsch, 1996; Reverdin *et al.*, 1997; Sutton & Allen, 1997;

White *et al.*, 1997; Ezer, 1999; Ganachaud & Wunsch, 2000; Ezer, 2001b, a; Furevik, 2001; Marshall *et al.*, 2001; Greene & Pershing, 2003; Keim *et al.*, 2004; Wu & Liu, 2005). This variability is often linked to the North Atlantic Oscillation (NAO; section 1.3) due to the strong atmosphere-ocean coupling (Marshall *et al.*, 2001; Visbeck *et al.*, 2003 and references within); for example, the decadal frequency of the 'Great Salinity Anomalies' (GSA) appear to coincide with NAO phases (e.g. Dickson *et al.*, 1988; Belkin *et al.*, 1998; Greene & Pershing, 2003; Belkin, 2004). Holliday (2003) demonstrated that water masses in the Rockall Trough (which contribute to NW Scottish coastal waters) were strongly coupled with the state of the NAO (section 2.17) and Kershaw *et al.*, (2004) used geochemical tracers to show that North Atlantic current strengths were significantly influenced by the NAO.

The seminal study by Hansen *et al.*, (2001) showed that the overflow of dense, cold water (one of the main sources of NADW) south across the Greenland-Scotland ridge has reduced within the past 4 decades and recent studies have also shown that subpolar North Atlantic water is gradually becoming fresher (Dickson *et al.*, 2002; Curry *et al.*, 2003; Dickson & Curry, 2003). Blindheim *et al.*, (2000) links the freshening surface layer of the Norwegian Sea to the prolonged positive NAO state. Hansen *et al.*, (2001) suggest a reduced overflow may signify a reduction in NADW formation and ventilation, with the possibility of reduced latitudinal heat transport. However, Dickson & Curry (2003) report no evidence of a change in the THC during the same period. Despite these uncertainties, the sensitivity of the THC to freshwater input at high and mid latitudes in clear (figure 1.1).

1.2.2 The ocean's role in the global carbon cycle

The oceans (particularly the surface oceans) are one of the largest of the fast exchanging reservoirs in the global carbon cycle (Stocker, 2000), capable of significantly influencing atmospheric carbon dioxide (CO_2) concentration and subsequently global temperatures (e.g. Petit *et al.*, 1999). Oceanic processes can modulate atmospheric CO_2 concentration via: (i) changes in ventilation rates, with higher natural CO_2 (i.e. non-anthropogenic) during reduced NADW formation (Broecker, 1997); (ii) increased upwelling, releasing stored deep ocean CO_2 into the atmosphere; (iii) marine primary productivity (Bigg, 1996); (iv) ocean temperature, with CO_2 typically more soluble in cooler waters (Chester, 1990) and (v) CO_2 storage in marine calcium carbonate ($CaCO_3$) which regulates the CO_2 saturation point of ocean water (Maslin *et al.*, 2003). Recent anthropogenic forcing of climate, including increased CO_2 emissions and ocean warming, has raised concerns regarding the future role of oceanic uptake of CO_2, particularly since the impact of anthropogenic CO_2 is already evident in the ocean (e.g. Broecker, 1997; Stocker & Schmittner, 1997; Keir *et al.*, 1998; Gruber *et al.*, 1999; Joos *et al.*, 1999; Sonnerup *et al.*, 1999; Gruber & Keeling, 2001; Clark *et al.*, 2002; Körtzinger *et al.*, 2003; Quay *et al.*, 2003; Feely *et al.*, 2004; Sabine *et al.*, 2004).

1.3 The North Atlantic Oscillation

The surface layer of the North Atlantic Ocean is strongly coupled with the overlying atmosphere (Czaja *et al.*, 2003) and strong ocean-atmosphere interactions play an important role in the climate of the North Atlantic region (e.g. Holliday, 2003).

The North Atlantic Oscillation (NAO) is the large-scale alternation of atmospheric mass between the Icelandic Low and the Azores High and is determined by sea-level pressure (SLP) differences between these two regions (figure 1.2). For instance, a positive NAO phase occurs when a strong high pressure system lies over the Azores region and a strong low pressure system lies over Iceland, resulting in a strong pressure gradient between the two regions. During a negative NAO phase, the pressure systems are much weaker, leading to a weaker pressure gradient. Wanner *et al.,* (2001) and Hurrell *et al.,* (2003) provide excellent overviews of the NAO.

The NAO is the dominant mode of atmospheric behaviour in the Northern Hemisphere throughout the year, becoming more prevalent during the winter months where it accounts for more than one-third of the total variance in sea-level pressure (Cayan, 1992) and is typically determined by the averaged monthly NAO indices from December-January-February-March (Jones *et al.*, 1997). Hurrell (1995) used data obtained from stations at Lisbon, Portugal and Stykkisholmur, Iceland, and Jones *et al.,* (1997) used instrumental records from Gibraltar and Reykjavik. Although such records differ in detail, the inter-annual trends seen within the two different indices are generally consistent, showing for example, a positive phase between 1900 - 1930 AD,

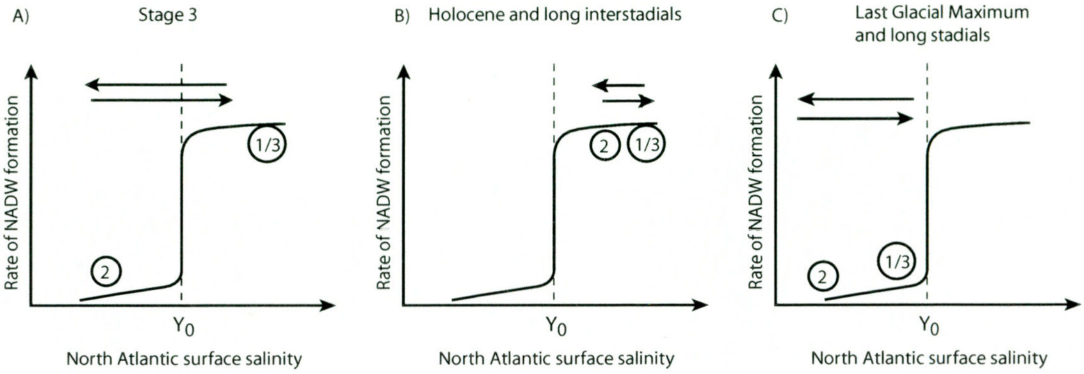

Figure 1.1 Threshold diagrams depicting one way in which 1-2 kyr climate cycle might have been amplified into Dansgaard/Oeschger cycles of the glaciation. Y_0 is the threshold value at which a mode switch in ocean circulation occurs. Parallel arrows give a hyopthetical range of changes in surface salinities as might result from increases and decreases in freshwater input regulated by the climate cycle. 1. is the intial state, 3 is a final state and 2 is a new equilibrium state of the system. A) Increases in freshwater fluxes exceed the threshold value, forcing recurring non-linear response. Here, freshwater injection is a transient process and the system returns to its initial state after each mode switch. B) Recurring shifts in fresh water fluxes during warmer intervals are small and do not exceed the threshold value. That mode might have characterised the Holocene and the long interstadials of the early glaciation. C) A low overall surface salinity prevents the system from returning to the inital state. That mode may have dominated during the long stadials of the glaciation. Redrawn from Bond *et al.*, (1999).

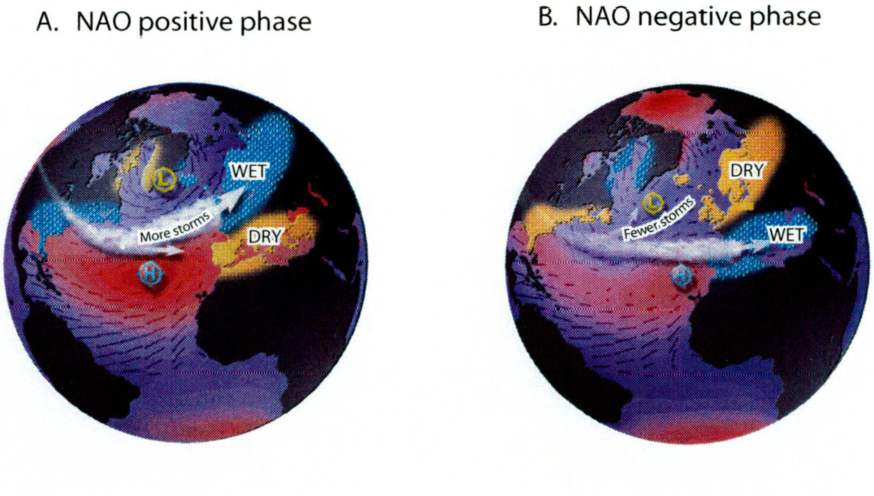

Figure 1.2 Atmospheric circulation and associated storm track positions during A) positive or high index North Atlantic Oscillation (NAO) phases and B) negative or low index NAO phases. During positive NAO years, NW Europe typically experiences warmer and wetter winters and vica versa for negative years. Graphics from http://www.ldeo.columbia.edu/NAO/

an extended negative phase between 1930-1970 AD and a prolonged positive phase in the indices since the 1980's (Jones *et al.*, 1997).

Atmospheric circulation changes associated with the NAO typically occur when the index is either 1.0 deviation above or below the zero axis (Hurrell, 1995). Positive (or high index) phases of the NAO index are characterised by stronger than normal mid-latitude westerly winds (>8 ms^{-1} above normal; Hurrell, 1995) and this storm track is deflected northwards by the high pressure system over the Azores, resulting in warmer and wetter winters over NW Europe as the air masses travel over the warm Atlantic ocean. Conversely, a negative (low index) year sees a change in atmospheric circulation with the storm tracks deflected towards Southern Europe, resulting in cold, dry winter conditions over NW Europe (e.g. Slonosky & Yiou, 2001; Ruprecht *et al.*, 2002; Trigo *et al.*, 2002). Hurrell (1995) showed that correlation coefficients between winter (December-March) precipitation and the winter NAO index are stronger for European coastal stations (e.g. Bergen: 0.77 and Stornoway: 0.75) than for inland stations (Oslo: 0.21 and Frankfurt: 0.19). Chandler and Wheater (2002) have also demonstrated the seasonally varying impact of the NAO upon rainfall variability from the west of Ireland.

1.3.1 Forcing mechanisms and cyclicity of the NAO

The NAO is responsible for generating systematic large-amplitude changes of wind speed, latent and sensible heat fluxes, and hence sea surface temperatures over much of the mid-latitude North Atlantic (Cayan, 1992; Reverdin *et al.*, 1997; Visbeck *et al.*, 2003). In turn, the inter-annual and longer-term changes in the NAO index may determine or modulate deep temperature and salinity (Reverdin *et al.*, 1997) and hence deep convection in the Atlantic (Dickson *et al.*, 1996). Inter-annual sea surface temperature (SST) anomalies generated by atmospheric variability in the NAO may be 'stored' underneath the seasonally stratified surface ocean layer and released during winter water column mixing, thus providing the ocean with a 'memory' of atmospheric climate (e.g. McCartney, 1997; Sutton & Allen, 1997; White *et al.*, 1997). Czaja *et al.*, (2003) suggests that whilst the Atlantic Ocean responds strongly to NAO changes, the Atlantic Ocean modulates NAO variability rather than exhibiting coupled ocean-atmosphere dynamics as does the Pacific Ocean with the El Niño-Southern Oscillation.

Long-term variability in the NAO index, reflecting the dominant mode of atmospheric behaviour in the North Atlantic region, has been observed at periodicities of around ~2, 7-10, 20-23, 70 and 80-90 years (Appenzeller *et al.*, 1998 and references in O'Sullivan *et al.*, 2002) and the NAO has been identified as the likely mechanism responsible for periodic behaviour in the $\delta^{18}O$ record of the GISP2 ice-core record from central Greenland (White *et al.*, 1996) during the late Holocene. However, many of the observed cycles reported are statistically insignificant and hard to distinguish from 'red noise' (Appenzeller *et al.*, 1998; Hurrell *et al.*, 2003).

1.4 Millennial Scale Climate variability in the Late Quaternary

The current geological period, the Quaternary, began around 2.1 million years before present (Ma BP) and consists of two geological epochs; the Pleistocene and the Holocene. The Pleistocene lasted from ~2.1 Ma BP to ~ 10 kyr BP (kyr BP = thousand years before present) and is characterised by high amplitude and frequent oscillations between cold glacial periods and warm interglacial periods with at least 50 cold-temperature cycles occurring throughout this geological period (Lowe & Walker, 1997). The Holocene (meaning 'wholly recent') is the most recent epoch of the Quaternary period (though some regard it as the current interglacial of the Pleistocene; Lowe & Walker, 1997) commencing around 11.5 ka cal yr BP; Roberts, 1998).

The seminal work of Emiliani (1955) and Shackleton (1967, 1974, 1977, 1987) on stable oxygen isotope stratigraphy led to the subsequent identification of glacial-interglacial cycles and their pacing in marine sediment cores. Glacial-interglacial cycles are primarily driven by the 'Milankovitch' orbital cycles with periodicities of ~100ka (eccentricity), ~41ka (obliquity) and ~23ka and ~19ka (precessional cycles) and are clearly evident in both ocean and ice cores (Lowe & Walker, 1997). However, the recent advent of high-resolution proxy records from ice core, terrestrial and marine sediment archives have demonstrated that climatic cycles on sub-Milankovitch (or millennial) time-scales also exist (e.g. table 1.1); exemplifying the potential for abrupt and rapid climate change to occur throughout recent Earth history (e.g. Alley, 2000).

Stable oxygen isotope records ($\delta^{18}O$; proxies of temperature at the time of precipitation and deposition) from high resolution, often annually layered, Greenland ice cores, clearly exemplify the pervasive millennial-scale climatic variability of the late Quaternary (figure 1.3 and Johnsen *et al.*, 1992; Dansgaard *et al.*, 1993; Larsen *et al.*, 1995; White *et al.*, 1996; Dahl-Jensen *et al.*, 1998; Stauffer, 1999; Walker *et al.*, 1999; Chambers & Brain, 2002; Andersen *et al.*, 2004). Such millennial-scale climate cycles are particularly evident in glacial periods, where short ~1,500 year Dansgaard-Oeschger (DO) cycles result in alternating warm interstadials and cold stadials (Dansgaard *et al.*, 1993), and are characteristically grouped into longer Bond cycles (Alley, 1998) in North Atlantic marine sediment cores. Bond *et al.,* (1993) demonstrated that the millennial scale glacial DO events evident in the Greenland ice cores were strongly coupled with ocean proxies suggesting cool temperatures and 'Heinrich events' (ice rafted detritus or IRD, in marine sediment) deposited during the discharge of icebergs into the North Atlantic (Bond *et al.*, 1992; Bond & Lotti, 1995; Andrews, 1998). The penecontemporeanous occurrence of DO cycles in the ice core and millennial-scale cycles in marine cores point to a closely coupled ocean-atmosphere climate system at least throughout the last glacial maximum (LGM).

1.5 Holocene Climate

1.5.1 Millennial-scale variability in the Holocene

There is no doubt that Holocene climate is more stable than that of the last glacial period (figure 1.3). However, Denton & Karlen (1973) studied glacier advances across Europe and were the first to suggest that Holocene climate demonstrated millennial-scale climate variability. Despite this early find, Holocene climate was still perceived as being relatively stable well into the 1990s (e.g. Dansgaard *et al.*, 1993). It wasn't until O' Brien *et al.,* (1995) illustrated the complexity of salts and terrestrial dust in a Greenland ice core that the concept of an unstable Holocene climate began to be more widely accepted (Bond *et al.*, 1997). Records of atmospheric climate change had already been correlated with marine climate records for the last glacial period (Bond *et al.*, 1993), and seminal work carried out by Bond *et al.,* (1997) demonstrated

Table 1.1

Selected Holocene (quasi)-periods from palaeoclimate proxy records from the North Atlantic region (NA) and the Greenland GISP2 ice core. Taken from Schulz *et al.*, 2004

Proxy record	Periodicity (years)	Reference
NA, drift ice	400-500, 900 - 1100	Bond *et al.*, 2001
NA, benthic foraminiferal abundance	~ 400 - 1300	Sarnthein *et al.*, 2003
NA, sediment colour	550, 1000, ~ 1600?	Chapman & Shackleton, 2000
NA, planktonic foraminifera $\delta^{18}O$	550 and 1150	Risebrobakken *et al.*, 2003
NA, mean size of sortable silt	400 and ~ 1000	Hall *et al.*, 2004
GISP2, $\delta^{18}O$,	900	Schulz & Paul, 2002
GISP2, potassium	2600	O'Brien *et al.*, 1995

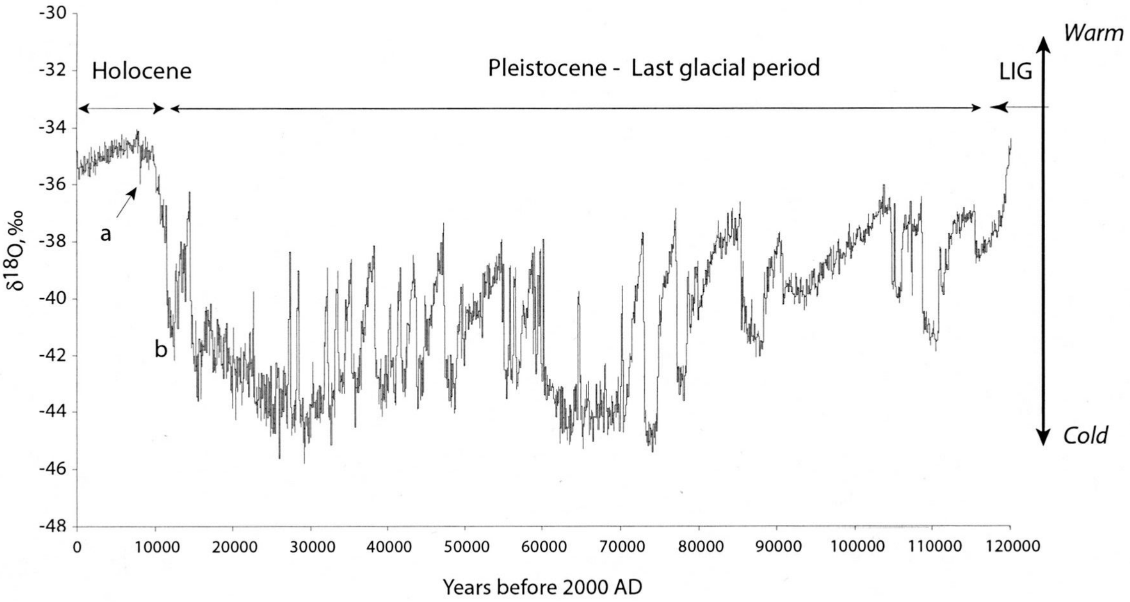

Figure 1.3 Stable oxygen isotopic compositions from the Greenland ice core NorthGRIP for the past 120,000 years. The Holocene, the last glacial period and the end of theLast Interglacial (LIG) are marked out, as are a) the Holocene 8.2 kyr BP event (Andersen *et al.*, 2004) and b) the Younger Dryas. Data obtained from ftp://ftp.ncdc.noaa.gov/pub/data/paleo/icecore/greenland/summit/ngrip/isotopes/ngrip-d18o-50yr.txt

that ice rafting events similar to the glacial Heinrich and DO events occurred in the North Atlantic throughout the Holocene with a similar millennial-scale cyclicity.

Since then, more studies have turned to investigating Holocene climate change and an excellent synopsis of this work is provided by Mayewski *et al.,* (2004; figure 1.4), who use a compilation of studies (references contained within figure caption) to produce a synthesis of global rapid climate change (RCC) events occurring throughout the Holocene. Climate records show 6 RCC events occurring at cycles of 2800-2000 years and 1500 years in the North Atlantic region. The most severe of these climatic deteriorations occurred between 9 – 8 kyr BP, termed the Glacial aftermath RCC (GA-RCC) by Mayewski *et al.,* (2004), where most of the northern hemisphere experienced high latitude cooling and low latitude aridity (Mayewski *et al.*, 2004). Initially this cooling event, easily visible in Greenland ice core records (temperature decrease of ~ 4 - 8 °C) and North Atlantic records (~ 1.5 – 3 °C decrease) was attributed to a slow-down/stagnation of the THC arising from a freshwater pulse into the North Atlantic from the Laurentide ice sheet, occurring around 8.2 kyr BP (Alley *et al.*, 1997; Barber *et al.*, 1999a). However, Rohling & Pälike (2005) point out that climatic deterioration preceded the 8.2 kyr BP meltwater spike (figure 1.4), suggesting a cause other than THC variability is responsible for the GA-RCC cooling. This view is supported by Piotrowski *et al.,* (2004) who report a strong link between North Atlantic climate and deep ocean circulation but no evidence of meltwater pulses significantly influencing NADW formation. Additionally, Mayewski *et al.,* (2004) suggest that a decrease in summer insolation and volcanically forced climate may have lead to the climatic deterioration in the GA-RCC.

1.5.2 Possible causes of climatic variability in the Holocene

Though the GA-RCC provides an insight of how possible THC stagnation can abruptly affect global climate, the event occurred during a time when ice sheets were still retreating, thus such large changes invoked by meltwater pulses are unlikely to occur in modern times. However, after the GA-RCC, climatic deteriorations can be seen to pervade the Holocene on millennial time scales. For example, Mayewski *et al.,* (2004 and references within) show fairly severe and extensive Holocene climatic deteriorations occurring between 6-5 kyr BP and 3.5-2.5 kyr BP, with a global climate

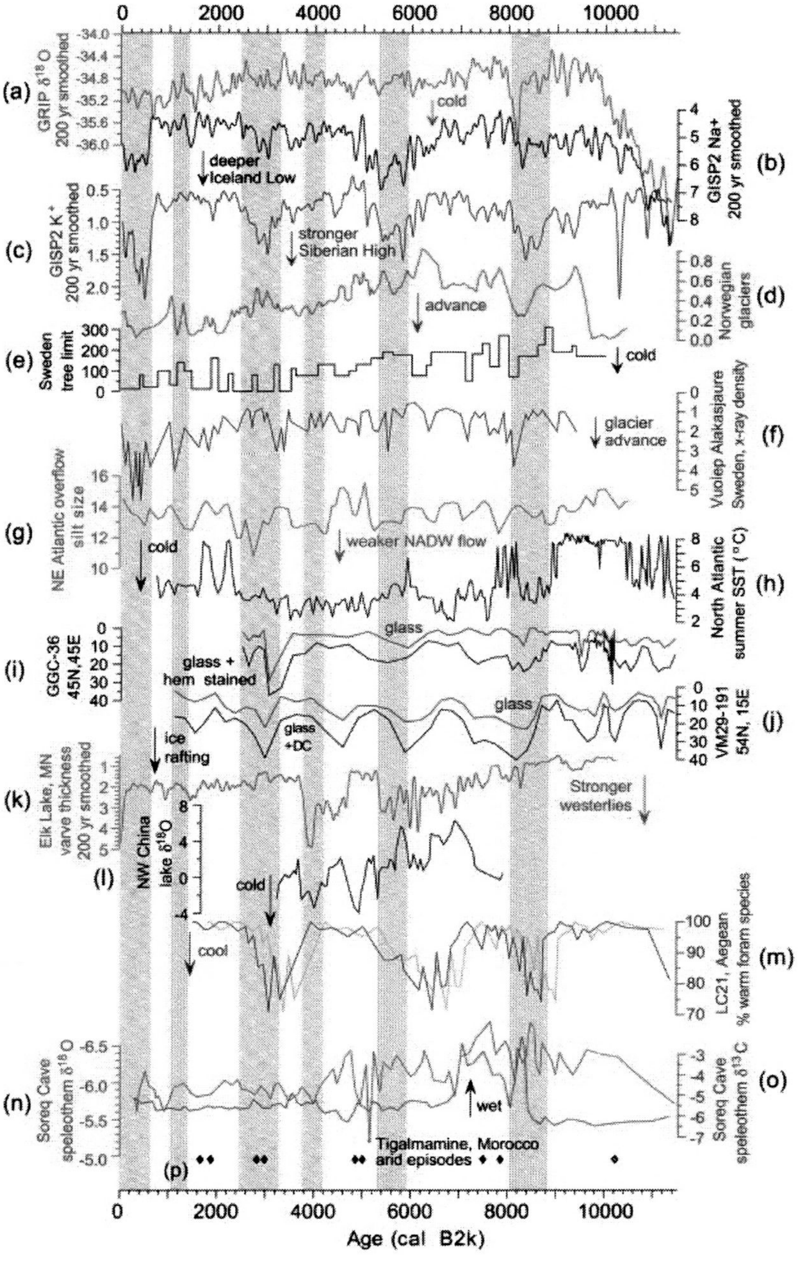

Fig. 1.4 Northern Hemisphere paleoclimate series, arranged generally by latitude (north, top), with state of climate proxy noted. Green bands represent timing of RCC, tuned to high-resolution GISP2 record. (a) Gaussian smoothed (200 yr) GRIP $\delta^{18}O$ (‰) proxy for temperature (Johnsen *et al.*, 1992). (b) Gaussian smoothed (200 yr) GISP2 sodium (Na+; parts per billion, ppb) ion proxy for the Icelandic Low (Mayewski *et al.*, 1997 and Meeker and Mayewski, 2002). (c) Gaussian smoothed (200 yr) GISP2 potassium (K+; ppb) ion proxy for the Siberian High (Mayewski *et al.*, 1997 and Meeker and Mayewski, 2002). (d) Norwegian glacier advance record (units) (Nesje *et al.*, 2001). (e) Treeline limit shifts in Sweden (units relative to the present) (Karlén and Kuylenstierna, 1996). (f) X-ray density measurements [relative scale of increasing density (i.e., increased silt influx, downward)] for sediments in Lake Vuolep Alakasjaure, northern Sweden (Karlén and Larsson, in review). (g) Northeast Atlantic overflow recorded in silt-sized particles (10–64 m) for NEAP-15K with Gaussian interpolation using a 300-yr window (Bianchi and McCave, 1999). (h) Summer sea surface temperatures (°C) for the North Atlantic (Irminger Sea) from a planktonic foraminiferal modern analogue function (this study). (i) Abundances of volcanic glass particles and hematite-stained grains in sediment core GGC-36 from 45°N, 45°W (Bond *et al.*, 1997 and Bond *et al.*, 1999). (j) Abundances of volcanic glass particles and hematite stained grains in sediment core VM29-191 from 54°N, 15°W (Bond *et al.*, 1997). (k) Gaussian smoothed (200 yr) varve thickness (mm) record from Elk Lake (Minnesota, USA) (Bradbury *et al.*, 1993). (l) Isotopic temperature (°C) reconstruction based on $\delta^{18}O$ (‰) of lacustrine carbonates, lake section from Hongshui River, northwest China (Zang *et al.*, 2000). (m) Relative abundance (%) of Aegean core LC21 planktonic foraminiferal species with warm-water affinities (Rohling *et al.*, 2002). Light line represents original calibrated AMS 14C chronology, and heavy line indicates maximum (three to four centuries) correction required to match the Minoan eruption of Santorini to its actual age. (n) $\delta^{18}O$ (‰) for speleothem in Soreq Cave, Israel (Bar-Matthews *et al.*, 1999). (o) $\delta^{13}C$ record (‰) for speleothem in Soreq Cave, Israel (Bar-Matthews *et al.*, 1999). (p) Arid episodes identified in Moroccan Lake Tigalmammine (van Campo and Gasse, 1993). Taken from Mayewski *et al.*, 2004.

pattern of ‘cool poles, dry tropics’ synonymous with Pleistocene climate trends. These RCCs display IRD events, strengthened westerlies and glacier advances and Mayewski *et al.,* (2004) suggest ice core ^{10}Be and Δ^{14}C point to solar forcing as a driving mechanism (figure 1.5). Two other RCC events occurring between 4.2-3.8 kyr BP and 1.2-1 kyr BP are less extensive and their causal factors are harder to pinpoint. The last event, lasting from 0.6 kyr BP differs from the others in that it displays ‘cool poles, wet tropics’ and again this has been linked to changes in solar forcing (e.g. Beer *et al.*, 2000; Bond *et al.*, 2001; Mayewski *et al.*, 2004).
Many late Holocene records show periodicities on millennial, centennial and decadal scales (e.g. O'Sullivan *et al.*, 2002). The pacing of the Holocene RCC events at 1450 ± 500 years appears to be statistically similar to the glacial DO events (Bond *et al.*, 1997) and Bond *et al.,* (1999) suggest that the North Atlantic possess a 1-2 kyr climate rhythm, with glacial DO events representing amplifications of the Holocene RCC millennial cycles brought about by THC sensitivity to freshwater injections into the North Atlantic. However, the actual driving mechanisms of these millennial scale changes are yet to be established.

Internal forcing

The volume, high specific heat capacity, inertia and response time on the scale of hundreds to thousands of years, make the oceans a prime candidate for driving and sustaining internal Holocene climate change on millennial time scales (Maslin *et al.*, 2003). The seminal work of Bianchi & McCave (1999) investigating sediment grain sizes in North Atlantic marine sediment cores illustrated the importance of the ocean in driving millennial-scale climate change. They suggest that decreases in the mean size of the sortable silt fraction point to a reduction in the intensity of NADW formation and link these periods of sluggish current activity to proxies of climatic deteriorations in the GISP2 ice core.

However, external forcing must often be invoked to account for ocean variability (e.g. Elliot *et al.*, 2002) and suggestions include ice sheet instability with internal oscillations resulting in episodic freshwater injections into the region of NADW

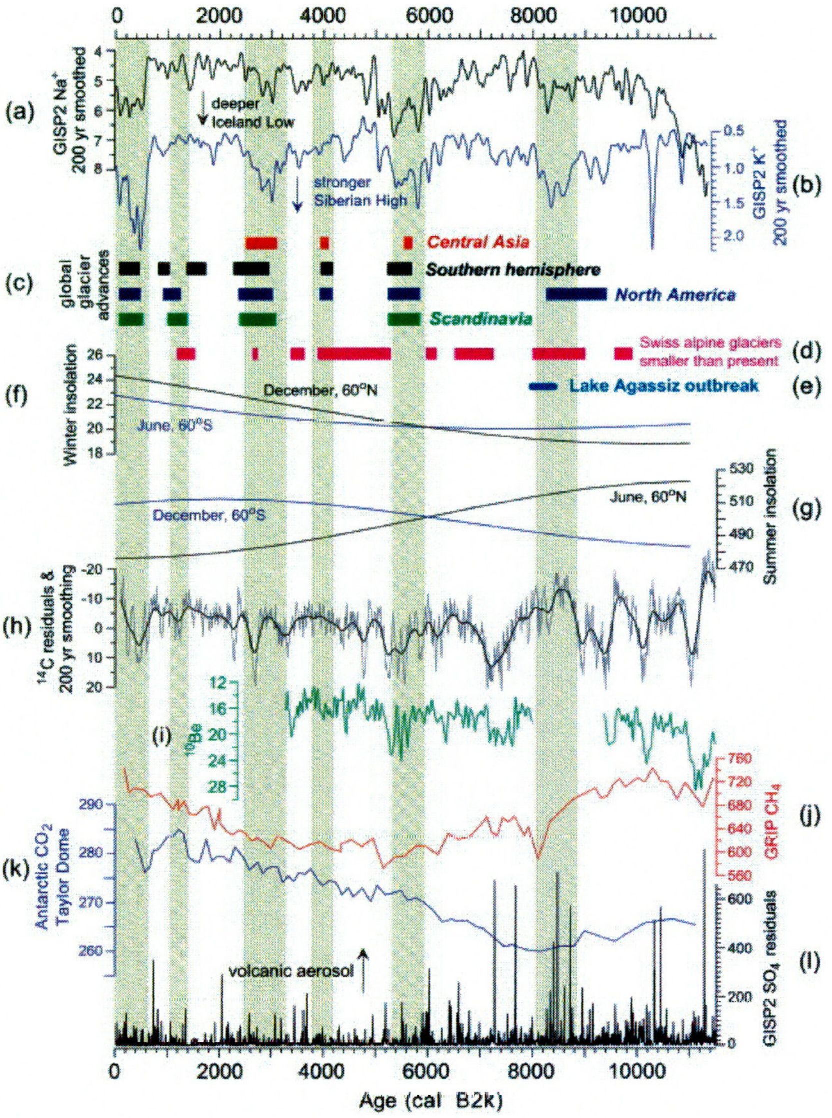

Figure 1.5 Climate forcing series and globally distributed discontinuous glacier advance records plus GISP2 proxy for atmospheric circulation, included as a continuous record example. Green bands represent timing of RCC tuned to high-resolution GISP2 record. (a) Gaussian smoothed (200 yr) GISP2 Na+ (ppb) ion proxy for the Icelandic Low (Mayewski *et al.*, 1997 and Meeker & Mayewski, 2002). (b) Gaussian smoothed (200 yr) GISP2 K+ (ppb) ion proxy for the Siberian High (Mayewski *et al.*, 1997 and Meeker & Mayewski, 2002). (c) Episodes of distinct glacier advances: European, North American, and Southern Hemisphere (Denton & Karlén, 1973), and central Asia (Haug *et al.*, 2001). (d) Episodes during which Swiss alpine glaciers were smaller than today, derived from dating of emerging tree-stumps (Hormes *et al.*, 2001). (e) Timing of the Holocene outburst of the North American meltwater from Lake Agassiz (Barber *et al.*, 1999). (f) Winter insolation values (W m−2) at 60°N (black curve) and 60°S latitude (blue curve) (Berger & Loutre, 1991). (g) Summer insolation values (W m−2) at 60°N (black curve) and 60°S latitude (blue curve) (Berger & Loutre, 1991). (h) $\Delta^{14}C$ residuals (Stuiver *et al.*, 1998): raw data (light line) and with 200-yr Gaussian smoothing (bold line). (i) ^{10}Be concentrations in the GISP2 ice core (103 atoms g−1) (Finkel & Nishizumi, 1997). (j) Atmospheric CH_4 (ppbv) concentrations in the GRIP ice core, Greenland (Chappellaz *et al.*, 1993). (k) Atmospheric CO_2 (ppmv) concentrations in the Taylor Dome, Antarctica, ice core (Indermühle *et al.*, 1999). (l) SO_4^{2-} residuals (ppb) from the GISP2 ice core, Greenland (Zielinski *et al.*, 1996). Taken from Mayewski *et al., (*2004).

formation (e.g. van Kreveld *et al.*, 2000), and the 'bipolar seesaw' ocean oscillator and subsequent inter-hemispheric heat piracy (e.g. Seidov & Maslin, 2001).

External forcing

Another possible external forcing mechanism is solar variability (e.g. Chambers *et al.*, 1999). Bond *et al.,* (2001) showed that proxies of North Atlantic drift ice (IRD events) are strongly coupled with proxies of solar variability (^{10}Be and ^{14}C) in Greenland ice cores, and suggested that changes in solar output during the Holocene influenced the surface hydrography of the North Atlantic and thus NADW formation (see also van Geel *et al.*, 2003). However, Maslin *et al.,* (2003) question how robust the Bond *et al.,* (2001) hypothesis can be, given that both ^{10}Be and ^{14}C can be influenced by climate change, such as ocean ventilation (Campin *et al.*, 1999; Beck *et al.*, 2001) and precipitation. Irrespective of this, van Geel *et al.,* (2003) point out that given the similarity between the DO-like events during both glacial and interglacial periods (Bond *et al.*, 1997; Bond *et al.*, 1999) and the identification of climatic variability close to this periodicity across the globe (e.g. Campbell *et al.*, 1998;Voelker, 2002), it is likely that these RCC events are driven by an external forcing, most likely solar output. Rial (2004) suggests that DO oscillations may be linked to a frequency modulate harmonic of precessional (orbital) forcing, with climate operating between chaos and order, again linking millennial scale variability to solar forcing mechanisms. Rahmstorf (2003) also suggests that the precise pacing of the 1,470 cycles points to an external forcing mechanism, whilst Clemens (2005) implies that the 1,470 cycle is an artifact of the ice core age model and that millennial-scale abrupt climate changes are linked to centennial (probably solar) variability. Schulz *et al.,* (2004) also suggests no dominant periodicity exists in the Holocene and questions the link between solar forcing and the 1,470 cycle.

1.5.3 Centennial and decadal-scale climatic variability in the Holocene

The recent increase in the number of high resolution palaeoclimatic studies has brought centennial and decadal variability to the fore-front of research and some studies suggest that millennial-scale variability seen in palaeoclimatic archives are likely to be a reflection of centennial-scale climate cycles (e.g. Wunsch, 2000; Clemens, 2005).

Centennial-scale climate variability (coherent with ice core climate cycles) has been observed in North Atlantic marine sediment cores (e.g. table 1.1), in ice core records (e.g. Meeker & Mayewski, 2002), in peat bog records (e.g. Chambers & Blackford, 2001), in speleothem records (McDermott *et al.*, 2001) and in instrumental records (O'Sullivan *et al.*, 2002). Though solar forcing is most likely responsible for centennial climate change, Hall *et al.,* (2004) present data which suggest a direct linkage between surface processes and circulation changes in the deep Iceland-Scotland overflow component of meridional overturning circulation.

Improved understanding of the North Atlantic Oscillation (e.g. Marshall *et al.*, 2001; Wu & Liu, 2005) and it's strong coupling with the ocean (section 1.3) has sparked interest in the influence of this ocean-atmosphere interaction upon climate (e.g. Drinkwater *et al.*, 2003; Mysterud *et al.*, 2003). For example, in the NE Atlantic region, NAO variability has been observed in the Greenland ice cores (e.g. Appenzeller *et al.*, 1998; Barlow, 2001; Meeker & Mayewski, 2002; Dawson *et al.*, 2003). Radiocarbon tracers ($\Delta^{14}C$) from the annual growth bands of tropical corals suggest the North Atlantic Ocean has experienced several 'pulses' in ventilation during the last century (Druffel, 1997), whilst $\Delta^{14}C$ records from the long-lived mollusc *Arctica islandica* records mixing at the Georges Bank/Labrador Sea region of the North Atlantic and points to periods of reduced NADW between 1960-1970 (Weidman & Jones, 1993). Additionally, Abrantes *et al.*, (in press) relate the Tagus River (Portugal) discharge to NAO forced climate; Schone *et al.,* (2003) have observed NAO driven changes in molluscan shell chemistry; Proctor *et al.,* (2002) link changes in speleothem geochemistry to the NAO, and hydrographic changes in Scandinavian fjords have been attributed to the NAO (section 1.8.5).

O'Sullivan *et al.,* (2002) suggest that many palaeorecords detecting NAO periodicities are in fact artefacts of the smoothing of the data, however it is likely that the North Atlantic may be modulating climatic variability at a multidecadal time scale (Chen & Ghil, 1995; Chapman & Shackleton, 2000; Cooper *et al.*, 2000; Delworth & Mann, 2000; Kerr, 2000; McDermott *et al.*, 2001; Meeker & Mayewski, 2002; O'Sullivan *et al.*, 2002; Rohling *et al.*, 2002; Risebrobakken *et al.*, 2003; Schonfeld *et al.*, 2003; Hall *et al.*, 2004; Andresen *et al.*, 2005), and Kerr (2000) suggests this multidecadal pacemaker could go by the name of the 'Atlantic Multidecadal Oscillation'.

1.6 Late Holocene climate in the North Atlantic region

Within the past few decades attention has turned to late Holocene (past 2 kyr) climate variability (e.g. Barber *et al.*, 1999b; Chambers & Brain, 2002) and research generated in this thesis comntributed to the European Union funded Framework V project HOLSMEER (Late Holocene Shallow Marine Environments of Europe).

In the North Atlantic region, the last 2 millennia are marked by 4 climatic phases: the Roman Warm Period (RWP), the Dark Ages Cold Period (DACP), the Medieval Warm Period (MWP) and the Little Ice Age (LIA). The latter climatic event, the LIA, is particularly important since it: (i) coincides with the Maunder Minimum of solar activity (Reid, 1997; Beer *et al.*, 2000; Luterbacher *et al.*, 2001; Shindell *et al.*, 2001); (ii) occurs during a phase of sluggish current activity in the NE Atlantic (Bianchi & McCave, 1999); and (iii) is thought to be linked to the 1-2 kyr climate cycles which pervade palaeorecords from the late Quaternary (Bond *et al.*, 1999). Volcanic eruptions can impact upon global climate (Zielinski, 2000) and volcanic aerosols may have also contributed to LIA cooling, particularly at the time of its onset (e.g. Shindell *et al.*, 2003; Mayewski *et al.*, 2004). The LIA also provides a good test of palaeo-data, since it has a small but defined signal relative to the deglaciation signal (Jennings *et al.*, 2001) and coincides with the commencement of instrumental data collection.

1.6.1 Anthropogenic influence on Late Holocene climate

Chambers & Brain (2002) report a paradigm shift in the study of Late Holocene climate, primarily due to interest in anthropogenic activity upon natural climate variability. Excellent reviews of climate during the past two millennia can be found in Mann & Park (1994), Mann *et al.*, (1998), Crowley (2000), Mann (2001), Shindell *et al.*, (2001), Mann & Jones (2003) and Moberg *et al.*, (2005).

Prior to 1800 AD (i.e. before the Industrial Revolution) decadal climate variability was significantly influenced by natural factors with solar irradiance and volcanic forcing accounting for 41-64 % of climate variability (Crowley, 2000). Mann & Jones (2003) report that the northern hemisphere is currently experiencing the highest temperatures of the past 2 millennia, i.e. significantly warmer than the regional 'Medieval Warm Period', and it is now widely accepted that 20th and 21st century climate has and continues to be forced by anthropogenic activity (Mann *et al.*, 1998; Crowley, 2000), to the point that Crutzen (2002) suggests the last ~ 150 years should be renamed the 'Anthropocene'. However, recent work by Moberg *et al.,* (2005) using combined high and low resolution proxies from marine and terrestrial archives, suggests climatic variations are likely to have been much more variable than those proposed by previous studies (figure 1.6). This corroborates the earlier suggestions of Marchitto & deMenocal (2003), whose reconstruction of NADW bottom water temperature suggests greater temporal variability (~2 °C) than reported in previous studies. Moberg *et al.,* (2005) also propose that natural climate variability is still a significant factor in global climate change, despite anthropogenic forcing and suggest natural climate variability could amplify or attenuate anthropogenic climate change.

Despite global attempts, such as the Kyoto Protocol, to curb anthropogenic greenhouse gas exports into the atmosphere (e.g. Reilly *et al.*, 1999; O'Neill & Oppenheimer, 2002), the Earth's energy balance and large thermal inertia is such that global temperatures are predicted to continue to rise. The climatic implications of rising global temperatures are likely to be severe (Hansen *et al.*, 2004) and the feedback mechanisms from the underlying natural variability of the climate system are unknown. The need to improve the understanding of natural climatic variability and the role of the oceans in future climate is both clear and urgent (cf. NERC RAPID thematic programme: http://www.soc.soton.ac.uk/rapid/rapid.php).

1.7 Previous high-resolution palaeoceanographic studies in the North East Atlantic Ocean region

The importance of the North East Atlantic region to global climate variability has resulted in many seminal palaeoceanographic studies being undertaken in the region. Recent high-resolution palaeoceanographic studies in the North Atlantic, particularly

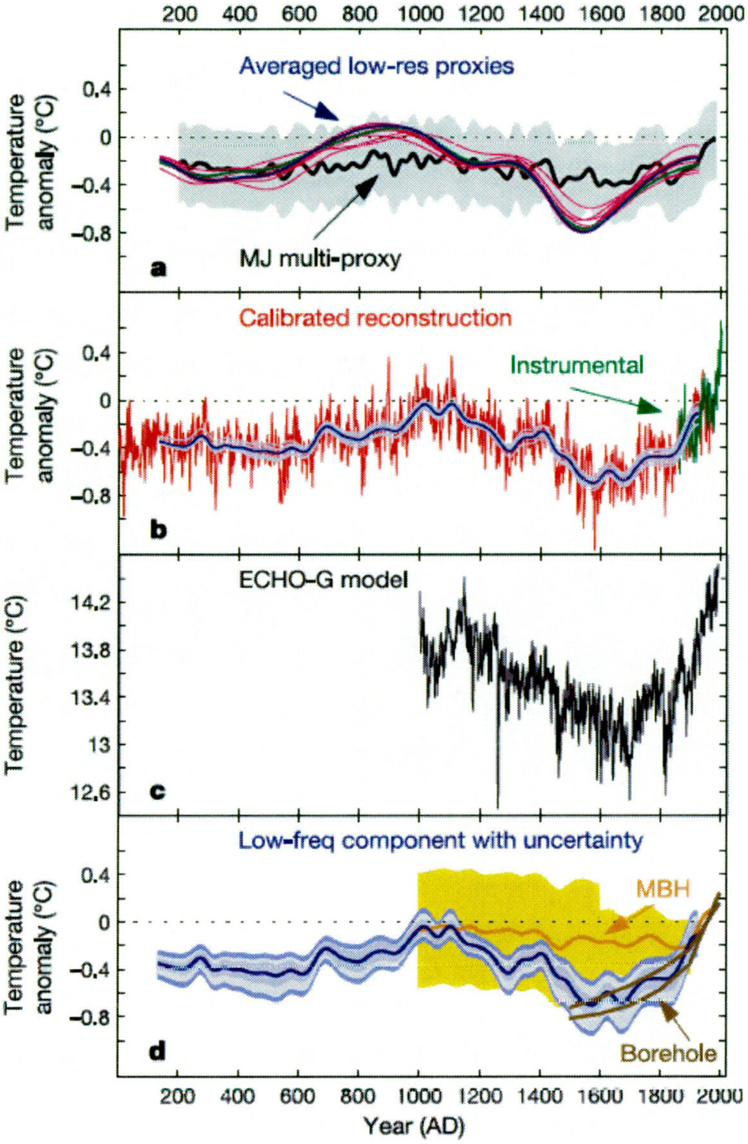

Figure 1.6 Estimations of Northern Hemisphere mean temperature variations. a, Previous multi-proxy reconstruction (MJ: from Mann & Jones, 2003, black line) with ~2 s.d. uncertainty (grey shading), and various averages (blue, green, magenta) of smoothed low-resolution temperature indicators (see see Moberg *et al.*, 2005). b, Moberg *et al.*, 2005 multi-proxy reconstruction AD 1–1979 (red) with its 80-yr component AD 133–1925 (blue) and its jack-knifed estimates (light blue), and the instrumental record green; Jones & Moberg, 2003). c, Forced ECHO-G model1 (see Moberg *et al.*,, 2005 for references. d, Low-f requency component of multi-proxy reconstruction in b (blue curve) with confidence intervals for three separate uncertainties. The innermost medium-blue band shows the uncertainty due to variance among the low-resolution proxy series. The two outer bands show the uncertainty in the variance scaling factor (light blue) and the constant adjustment (outermost blue band) separately. Each uncertainty is illustrated with an approximate 95% confidence interval (see Supplementary Information). Also shown are ground surface temperatures estimated from boreholes with their uncertainty interval (brown; see Moberg *et al.*, 2005, and the 80-yr component of a previous multi-proxy reconstruction (MBH: from Mann et al. 1998; 1999 orange) with ~2 s.d. uncertainty (yellow). Taken from Moberg *et al.*,, 2005.

focusing on Holocene climate or millennial-scale variability include Chapman & Shackleton (2000), Eiríksson *et al.,* (2000), Kroon *et al.,* (2000), Rohling *et al.,* (2002), Scourse *et al.,* (2002), Berstad *et al.,* (2003), Marchitto & deMenocal (2003), Risebrobakken *et al.,* (2003), Giraudeau *et al.,* (2004), Hall *et al.,* (2004), Kristensen *et al.,* (2004), Andresen *et al.,* (2005) and Jiang & Eiríksson (2005).

However, whilst deep sea cores provide an excellent record of ocean-modulated long-term climate changes and climatic reorganisations, they can often have low sediment accumulation rates resulting in low resolution reconstructions which can be sensitive to reworking and bioturbation (e.g.Conradsen & Heier-Nielsen, 1995). Additionally, the deep sea record may not be responsive enough to account for the rapid millennial-scale changes documented in terrestrial archives.

1.7.1 Shelf seas as sites of palaeoenvironmental interest

Shallow shelf seas and slope regions are usually areas of high sediment accumulation rates, proffering the potential for high resolution palaeoclimatic studies. Shelf seas typically experience seasonal stratification (e.g. Pingree & Griffiths, 1978) and subsequently are zones of enhanced primary production (Berger *et al.*, 1989). They contribute at least 20 % of global marine primary productivity (net production ~ 6 x 10^9 tons yr^{-1}; Walsh *et al.*, 1981) whilst accounting for only ~ 10 % of the ocean floor area. Shelf sea areas are sensitive to climatic processes (e.g. Backhaus, 1989, 1990, 1996) and provide a link between the terrestrial and deep-sea environments. Scourse & Austin (2002 and references within) note their importance in studies of palaeoclimate, glacio-eustatic sea-level change and potential to capture land-ocean interactions.

1.7.2 Fjords as recorders of palaeoenvironmental and palaeoclimate change

Fjords (sea lochs) are unique shelf sea marine environments in the sense that they bridge the land-ocean interface, maintaining contact with the global oceans but also penetrating deep into the coastline. The geomorphology of the fjordic catchment and associated weathering processes, together with enhanced flocculation processes due to the mixing of freshwater and saline water within the fjord (Open University, 1997), combine to produce a marine environment with very high sediment accumulation rates (e.g. Gilbert, 2000). The underlying geology of the fjords with their deep basins separated by shallow sills, often provide areas of sediment focussing thereby increasing the potential for high-resolution studies (e.g. Howe *et al.*, 2002).

1.8 Background to Fjords: hydrographic processes and previous studies

1.8.1 Definition

Scottish sea lochs (or fjords) are essentially glacially carved valleys which have been inundated by the sea, thus they are similar to the fjords, sounds and inlets found in other high-latitude locations (such as Norway, Sweden, Iceland, Greenland, Canada, New Zealand and Chile).

Classification of fjordic hydrography is difficult due to different schemes and variability in circulation due to climatic forcing (Farmer & Freeland, 1983). However, fjords are usually much longer than they are wide and are characterised by their steep sided walls, usually contain a number of shallow submarine sills which separate deep basins and have a relatively large fluvial input at the loch head (Farmer & Freeland, 1983).

1.8.2 Fjordic hydrography

Coastal water conditions can influence the circulation in a sea loch or fjord system, e.g. wind conditions and resulting geostrophic currents (Klinck *et al.*, 1981) and differences in offshore density conditions (Aure *et al.*, 1996). However, the interaction between coastal waters and fjordic circulation is complex (Farmer & Freeland, 1983) and will not be discussed here.

1.8.2.1 Stratified water columns

Sea lochs typically display fjordic hydrography which differs from other estuarine circulation types (Farmer & Freeland, 1983; OpenUniversity, 1997). Physical oceanographical processes (such as mixing via wind stress, diffusivity, and internal and barotropic tides) occurring within most fjords are complex (figure 1.7) and are covered in great detail by Farmer & Freeland (1983).

A fjordic water column usually consists of three water masses. A brackish surface water layer, where high freshwater inputs from rivers and surface runoff mixes with basin waters, is characterised by salinities as low as 10. This layer is usually fairly thin (~ 5-10 m in Loch Sunart; figure 1.8) but can be modified with varying freshwater inputs. A well defined halocline separates the brackish surface water layer from the intermediate layer (figure 1.8). At the sill region, mixing of the surface water with coastal waters (Elliott *et al.*, 1992) and the subsequent entrainment of this low salinity water into the basin results in the formation of an intermediate layer of higher salinity than the surface water but lower salinity than coastal water (figure 1.8). Saline deep water enters the basin via exchange or flushing of the fjord by coastal waters during an important process in fjordic hydrography: deep water renewal events (section 1.8.2.3).

1.8.2.2 Seasonal stratification

As Farmer & Freeland (1983) point out, fjordic hydrography is not constant throughout the year. Periods of high runoff typically result in a strongly stratified water column with the brackish surface layer extending far along the axis of the fjord, whereas during periods of low freshwater inputs stratification is much weaker (figure 1.9).

Hydrography also changes due to seasonal stratification. Increased warming of the surface water layer due to increased mid- to high-latitude summer insolation strengthens the thermocline and results in a stratified water column. The break-down of the seasonal thermocline during the winter months along with strong mixing processes and convective overturning (figure 1.7) leads to a fairly homogenous water column. Whilst sea lochs with a very high freshwater input may experience year-long stratification (as with the Clyde Sea; Bock *et al.*, 1999), seasonal observational data from Loch Sunart suggests a mixed water column during the winter months (figure 1.10, data from Dr. P. Gillibrand).

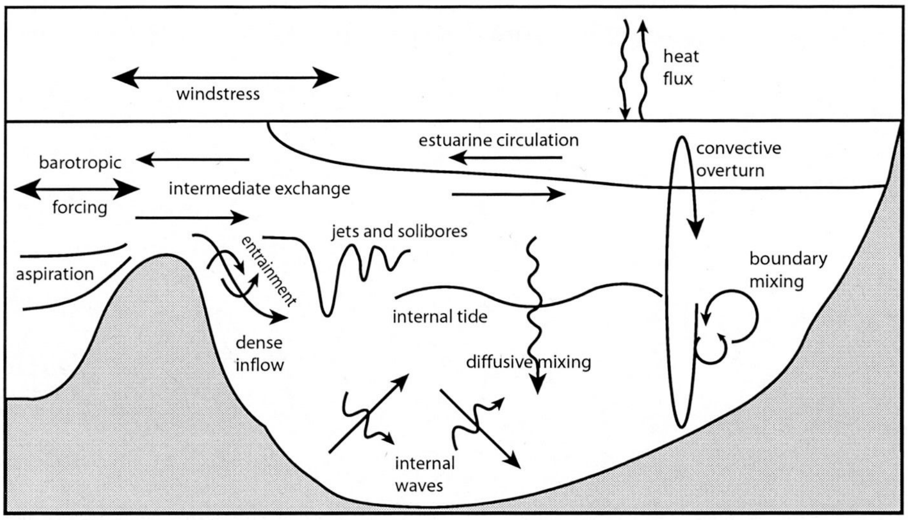

Figure 1.7. The complexity of physical processes occurring in a fjord. Full descriptions of these processes are covered in Farmer & Freeland (1983). Figure modified from http://www.sams.ac.uk/research/marine%20physics/fjords.htm.

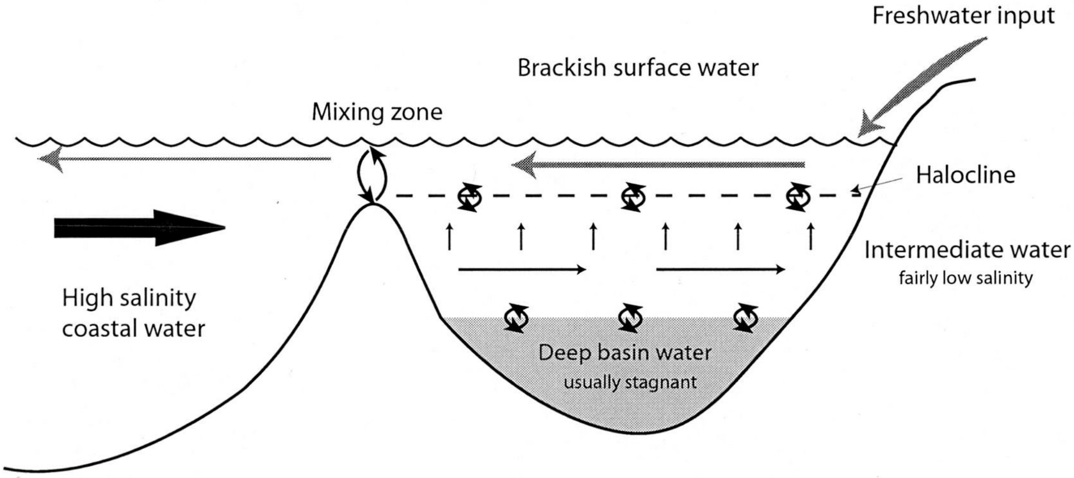

Figure 1.8. Typical structure of the water column in a fjord. Arrows represent mixing processes or direction of water transport.

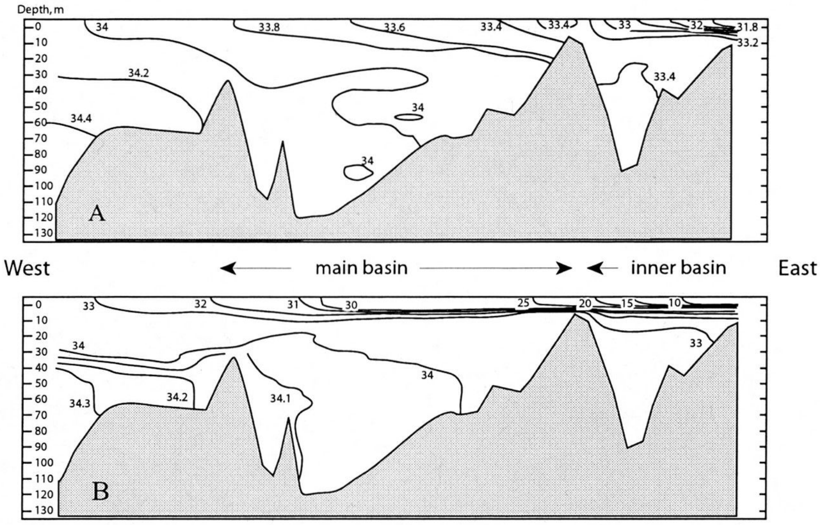

Figure 1.9 Salinity distributions along the axis of Loch Sunart on A) 12 July, 1989 during a period of low freshwater input and B) 14-15 August, 1989 following high freshwater input. Hydrographic conditions in A are more typical. Re-drawn from Gillibrand *et al., (*1995).

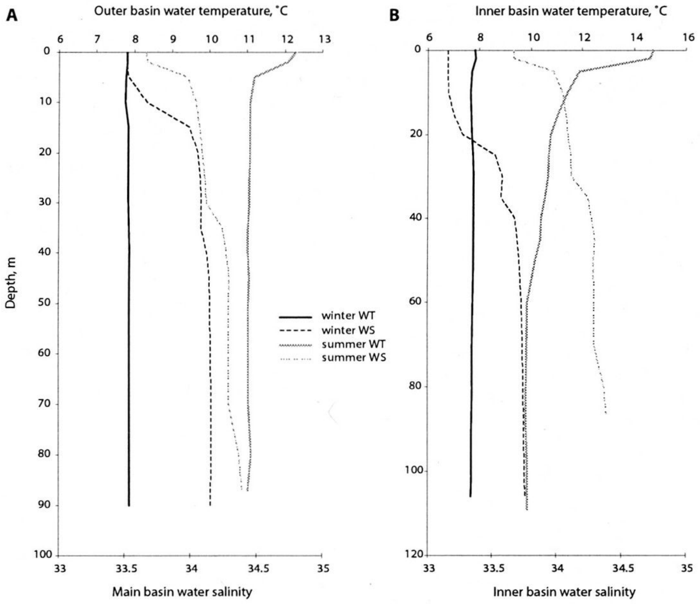

Figure 1.10 Seasonal differences (i.e. winter vs summer) in Loch Sunart basin water properties for A) the outer basin and B) the inner basin. Winter water column properties (measured 1/5/1991) are represented by black lines; solid for water temperature (WT) and dashed for water salinity (WS). Summer water column properties (measured 2/7/1991) are represented by grey lines. Data courtesy of Dr. P. A. Gillibrand and The Fisheries Research Services, Aberdeen.

1.8.2.3 Deep water renewal events

An excellent overview of deep water renewal events (DWREs) is provided by Gade & Edwards (1980). Deep basin water is usually stagnant and isolated from saline coastal waters (via sills and a stratified water column) and experiences gradual freshening via diffusive mixing with the overlying lower salinity intermediate water (Inall & Rippeth, 2002 and figure 1.8). When the density of the sill water exceeds the density of the deep basin water, saline dense coastal water flows into the basin to replace the less dense and fresher deep basin water (e.g. Gillibrand *et al.*, 1995; Allen & Simpson, 1998). During this process, 'old' deep basin water is 'lifted' up and transported out of the loch. DWREs often occur during periods of low runoff into the fjord, since a shallow halocline allows coastal water to 'slip' over the sill and 'renew' the salinity of the deep basin water. Though deep water renewal events in sea lochs are driven largely by the easily identifiable density changes associated with salinity fluctuations (e.g. Gade & Edwards, 1980; Farmer & Freeland, 1983), temperature changes (positive or negative) may accompany the inflow of coastal waters depending on the surface water temperature at the time of the DWRE (e.g. Gillibrand *et al.*, 1995; Allen & Simpson, 1998; Austin & Inall, 2002).

1.8.3 Response of fjordic hydrography to climatic change

The sensitivity of fjordic circulation to wind forcing and freshwater inputs (e.g. Gade & Edwards, 1980; Farmer & Freeland, 1983) means that the variability in both coastal and catchment conditions is likely to impact upon these environments. This can be tested through the comparison of climatic data series (such as the NAO index) with instrumental records of fjordic hydrography. For instance, Kristensen *et al.,* (2004) demonstrated that basin water temperatures in Sognesjøen (at 300 m water depth) reflected marine temperatures recorded at the coastal station OWS Mike and air temperatures recorded in Bergen, and showed good agreement with the Hurrell (1995) NAO index. Recently, Gillibrand *et al.,* (2005) utilised exisiting circulation models from Loch Sunart (Elliott *et al.*, 1992; Gillibrand *et al.*, 1995) to explore the response of main basin and inner basin circulation to climatic forcing during two recent extreme NAO years, namely 1988/89 (+2.86) and 1995/96 (-2.32; Jones *et al.*, 1997). Full details of the latter study are presented in chapter 3. In summary, the main basin showed a negligible salinity change to recent NAO forcing, whilst the inner basin showed a clear response, with frequent DWREs occurring during negative NAO years and less frequent DWREs during the positive NAO state. However, Arneborg (2004) finds no link between the NAO and instrumental data recording basin exchange in the Gullmar fjord between 1956 – 1984. This may be a function of the fairly deep sill (~ 42 m) in the Gullmar Fjord, somewhat analogous to the deep sill (~31 m) at the entrance of the main basin of Loch Sunart.

Since marine ecosystems typically show a strong response to NAO-forced oceanic conditions (e.g. Drinkwater *et al.*, 2003 and references within), climatic data series such as the NAO index can be compared with instrumental records of fjordic hydrography or with recent palaeoenvironmental records (usually spanning less than 100 years). The majority of such studies have focused on the shallow silled, restricted fjords of Sweden (e.g. Gustafsson & Nordberg, 2000; Nordberg *et al.*, 2000; Gustafsson & Nordberg, 2001; Nordberg *et al.*, 2001; Gustafsson & Nordberg, 2002; Filipsson & Nordberg, 2004a, b) with periods of infrequent basin exchange and associated low oxygen concentration occuring during phases of positive NAO index. Kristensen *et al.,* (2004) also demonstrate good agreement between palaeoclimate, as recorded by benthic foraminiferal proxies from a deep silled Norwegian fjord and North Atlantic temperature changes over the past 100 years.

1.8.4 Fjords as recorders of palaeoenvironmental and palaeoclimate change

On a centennial/millennial time-scale, palaeoclimatic and palaeoenvironmental studies have been carried out in many Scandinavian and Icelandic fjordic environments, particularly during the past decade (e.g. Alve, 1995; Kristensen *et al.*, 1995; Aarseth, 1997; Grosfjeld *et al.*, 1999; Kelly *et al.*, 1999; Nordberg *et al.*, 2000; Mikalsen *et al.*, 2001; Nordberg *et al.*, 2001; Sejrup *et al.*, 2001; Gustafsson & Nordberg, 2002; Howe *et al.*, 2002; Plassen & Vorren, 2002; Hald *et al.*, 2003; Filipsson & Nordberg, 2004b; Husum & Hald, 2004; Kristensen *et al.*, 2004; Lysa *et al.*, 2004; Smittenberg *et al.*, 2005). Where the fjord is deep silled, palaeoenvironmental proxies suggest fjordic bottom water reliably records NE Atlantic circulation (e.g. Mikalsen *et al.*, 2001; Kristensen *et al.*, 2004), whilst shallow-silled, restricted fjords provide good records of NAO influence (e.g. Nordberg *et al.*, 2000; Nordberg *et al.*, 2001; Filipsson & Nordberg, 2004b).

Despite the clear potential for obtaining high-resolution palaeoenvironmental records from fjords, few studies have addressed palaeoenvironmental change in temperate Scottish sea lochs. Palaeoenvironmental work in the sea lochs of NW Scotland have focused upon depositional regimes across the Late Glacial – Holocene transition (Dix & Duck, 2000; Howe *et al.*, 2002) or recent (last 200 years) environmental change in the near-anoxic Loch Etive (Murray *et al.*, 2003) which is not comparable to the well ventilated Loch Sunart (Edwards & Sharples, 1986). Modern studies in Loch Sunart and other sea lochs have primarily been concerned with circulation processes (Elliott *et al.*, 1992; Gillibrand *et al.*, 1995; Gillibrand *et al.*, 2005) or fishery studies (Treasurer, 2001; McKenzie *et al.*, 2004). Thus, the work presented in this thesis is the first attempt to provide a synthesis of modern surface samples (sedimentological, faunal and geochemical) related to modern environmental gradients, framed by an evaluation of processes and aimed at generating high resolution palaeoclimatic records.

1.9 Thesis aims and objectives

The main aim of this thesis is to investigate the potential of obtaining high resolution palaeoenvironmental records from Loch Sunart, a fjord on the NW coast of Scotland. For this purpose, a ~3 m sediment core was obtained from the main basin of Loch Sunart during April 2001 (chapter 2) with a resolution of approximately 0.1 cm yr^{-1} back to 2090 ± 120 years BP.

Little palaeoenvironmental work has been undertaken in Scottish sea lochs and there is a need to understand how modern processes influence the study site before reliable reconstructions of these palaeoenvironments can be achieved. To this end, the objectives of this thesis can be broadly divided into two parts; an improved understanding of modern processes and the generation of palaeoenvironmental records. Given the broad spectrum of work presented here, each chapter of this thesis is intended to provide a short introduction and a full discussion of the data relating to the major theme studied. It is hoped that each chapter will eventually yield a peer-reviewed publication.

Following an introduction to the topic (chapter 1) and a materials and methods section (chapter 2), the thesis is structured so that modern processes are dealt with first (chapters 3, 4, 5 and 6) and then palaeoenvironmental reconstructions follow in chapters 7 and 8. A final chapter (chapter 9) provides an overview of the main findings and a conclusion to the thesis.

The aims of the thesis are as follows:

1.9.1 Modern processes:

Chapter 3 -Instrumental records from NW Scotland: Climate and Hydrography

a) To determine whether regional indices of long-term climate (Jones & Lister, 2004) can explain the weather experienced by the Loch Sunart catchment area, and to investigate the link between regional marine temperatures and air temperatures in context with indices of inter-annual climatic variability such as the North Atlantic Oscillation (NAO).

b) To test whether the fjordic circulation of Loch Sunart is influenced by extreme states of the NAO. This work was carried out in collaboration with Dr. P. A. Gillibrand (from hereon PAG; formerly at Fisheries Research Services, Aberdeen, now based at Scottish Association of Marine Science, Oban) and Dr. W. E. N. Austin (from hereon WENA), and published as 'Gillibrand, P.A., Cage, A.G. and Austin, W.E.N., 2005. A preliminary investigation of basin water response to climate forcing in a Scottish fjord: evaluating the influence of the NAO. *Continental Shelf Research,* **25** (5-6): 571-587'.

Chapter 4 – Marine reservoir ages in Scottish coastal waters and Loch Sunart core chronology

c) To investigate whether the restricted exchange of fjord water with coastal waters affects the marine radiocarbon reservoir age in Scottish sea lochs and quantify the regional marine radiocarbon reservoir age in order to improve radiocarbon age models from these environments.

Chapter 5 – Distribution of modern benthic foraminifera in Loch Sunart surface sediments

d) To document the modern distribution of benthic foraminifera (planktonic foraminifera are typically rare in coastal regions) in Loch Sunart and identify assemblage groups and their spatial distribution.

Chapter 6 – Stable isotopic compositions in modern benthic foraminifera

e) To study modern stable carbon and oxygen isotopes in benthic foraminifera and investigate possible ecological controls on test isotopic composition.

f) To investigate whether the benthic foraminifera *Cibicides lobatulus* calcifies in isotopic equilibrium with seawater.

1.9.2 Palaeoenvironmental reconstructions

Chapter 7 – A benthic foraminiferal transfer function approach to reconstruct bottom water temperature in NW Scottish fjordic environments.

g) To establish whether the benthic foraminiferal transfer function model of Sejrup *et al.*, (2004) can be used to obtain an independent proxy of palaeotemperature from a Loch Sunart sediment core, via calibration with instrumental records.

Chapter 8 – Late Holocene palaeoenvironmental history of Loch Sunart, a fjord on the NW coast of Scotland

h) To construct a geochronology for Loch Sunart sediment cores GC023 and SC023 using radiocarbon and geochemical methods.

i) To obtain high resolution sedimentological, geochemical, stable carbon and oxygen isotope data for core GC023.

j) To apply transfer function techniques to low resolution benthic foraminiferal assemblages spanning the last 2000 years in core GC023.

k) To place the palaeoenvironmental history of Loch Sunart in context with other North Atlantic palaeoclimate and palaeoceanographical records.

CHAPTER 2 – STUDY AREA, MATERIALS AND METHODS

2.1 Site Context

2.1.1 Location of Loch Sunart

Loch Sunart is a sea loch located on the NW coast of Scotland, approximately 35 km north of Oban (see figure 2.1). The loch is approximately 31 km long and averages at 1.5 km wide, with a total of 6 sills (Edwards & Sharples, 1986 and table 2.1). However, two sills (1 and 6; table 2.1) essentially section the loch into three basins. The inner basin has a maximum depth of 96 m and a sill depth of ~10 m; the main basin is 124 m deep with a sill depth of ~35 m, and the outer basin has an average depth of around 60 m with no sill restricting connection with the Sound of Mull. The bathymetry of Loch Sunart is summarised figure 2.2.

The catchment area (299 km^2) of Loch Sunart is predominantly high relief land (> 600 m; figure 2.1) with relatively thin and poorly developed soils, rapidly translating rainfall into surface runoff (Black & Cranston, 1995). Bare surfaces are common, particularly on the steep high slopes, though vegetation exists around streams and woodland occurs around the shores of the loch, particularly on the northern side (figure 1.13). As with most places in the Highlands, the area around Loch Sunart has experienced deforestation, particularly during the Highland Clearances (www.sunartoaklands.co.uk), however there has been a recent move towards reforestation of the Sunart oaklands during the past decade (*pers. comm.,* Ms. E. Madden, Lochaber Countryside Ranger, Highland Council, 2002).

2.1.2 Formation of Loch Sunart and local geology

Sea lochs are glacially carved valleys which have been inundated by the sea, thus they are similar to the fjords found in Norway, and are remnants of the glacial history of Scotland and the controls imposed by the underlying bedrock geology. Glacier tongues spreading west from the centre of ice accumulation around Rannoch Moor eroded the local geology creating overdeepend valleys. During the Last Glacial Maximum (LGM), the British ice sheet extended beyond the present day shoreline and onto the continental shelf, and geomorphological observations in the area around Loch Sunart suggests the Loch Lomond (Younger Dryas) Re-advance reached the inner

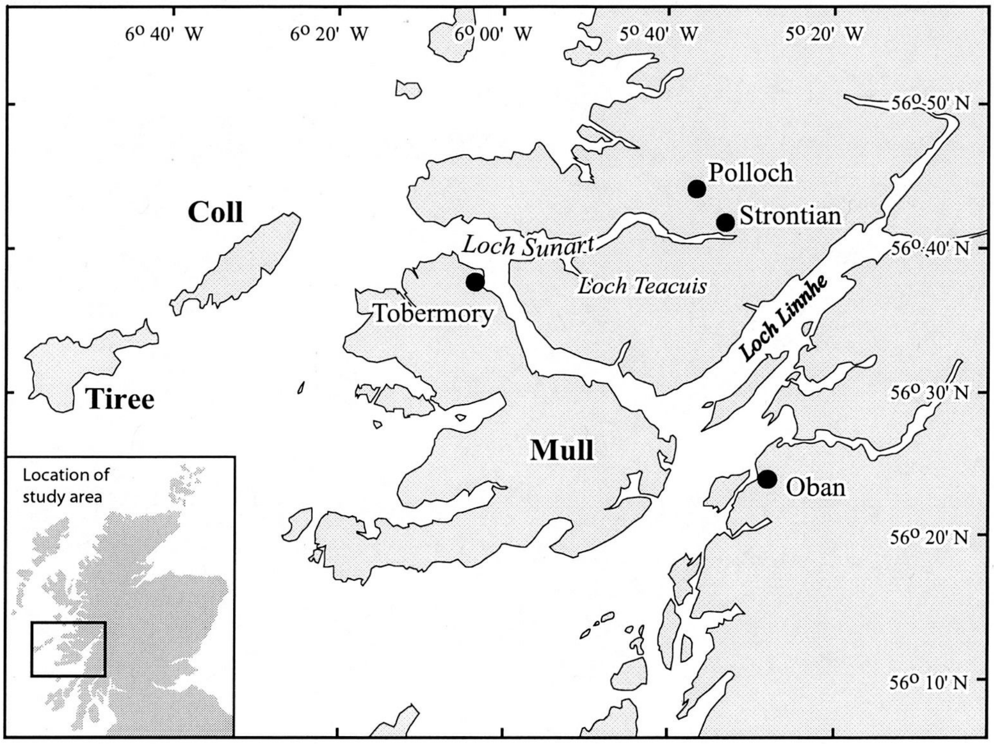

Figure 2.1 Location of Loch Sunart on the NW coast of Scotland. For geographical context, Oban is shown, as are sites of importance in chapter 3.

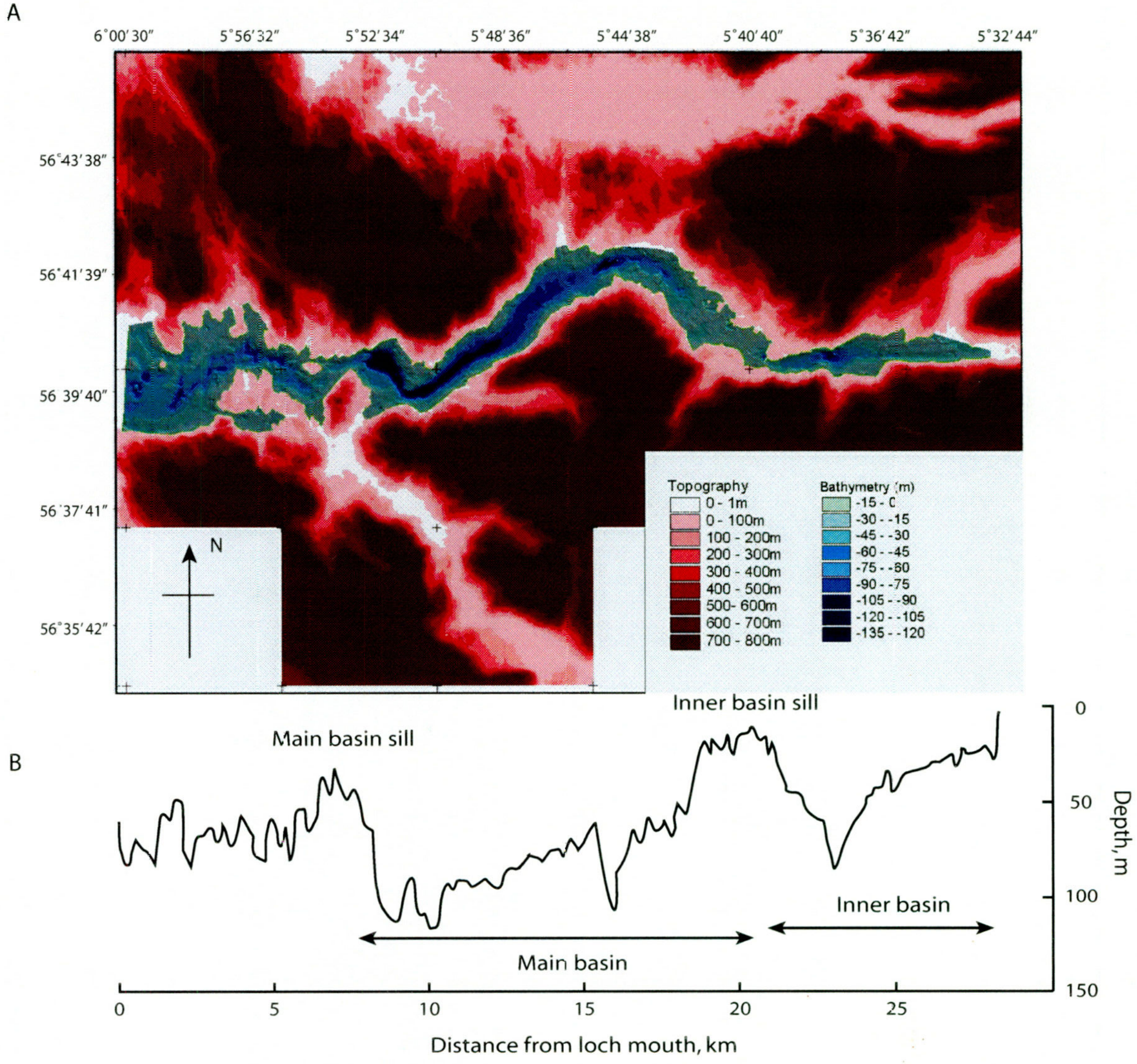

Figure 2.2 A) Geographical Information System (GIS) bathymetry of Loch Sunart with greatest depths represented by the darkest blue. Catchment relief (via a digital elevation model) is also shown with deep red representing highest relief. GIS map created by AGC using ArcGIS and data obtained from Dr. R. Bates, School of Geography & Geosciences, University of St Andrews.

Table 2.1 A) Summary Information regarding Loch Sunart basin, catchment area, annual freshwater input, and hydrographic properties. B) Information regarding the separate basins of Loch Sunart. Data obtained from Edwards & Sharples (1986).

A

OS Reference	NM570580
Chart number	2394
Chart Scale	25000
Loch length (km)	30.7
Tidal range (m)	4
Maximum depth (m)	124
High water area (km^2)	54.1
Low water area (km^2)	47.3
2 m area (km^2)	43.9
5 m area (km^2)	39.8
10 m area	36.2
Low water volume (million m^3)	1839.7
Catchment area (km^2)	299
Annual rainfall (mm)	2000
Catchment freshwater runoff (million m^3 year^{-1})	523.3
Kinetic energy supply (Kw)	208.5
Mean depth at low water (m)	38.9
Fresh/tidal ratio (salinity reduction)	5.3 (0.2)
Runoff/width ratio (m^{2}day^{-1})	868
Mixing depth (m)	2
Mixing depth to maximum depth (m)	15
Flushing time (days)	7

B

Sill number[§]	1	2	3	4	5	6
Length (m)	450	520	4270	1250	420	600
High water width (m)	820	1470	1220	1170	1220	690
Low water width (m)	800	1450	1200	1150	1200	670
Depth (m)	31	70	69	45	15	6
Mean depth (m)	20	37	43	23	9	3
X-area (m^2)	16000	53000	52000	27000	11000	2200
Hwup area[†] (km^2)	29.4	25.3	15.1	11.5	9.7	7.1
Lwup area[‡] (km^2)	24.7	21.1	12.2	9.1	7.5	5.5
Current over sill (cms^{-1})	25	7	4	6	10	23
Basin depth (m)	113	124	113	76	40	91

§. Sill number from the fjord mouth progressing inwards.

†. Upstream area at high water = surface area of the loch and any side arms upstream of the sill was measured planimetrically in km^2.

‡. Upstream area at low water = surface area of the loch and any side arms upstream of the sill was measured planimetrically in km^2 where intertidal areas are more than 20 % of the surface area of the loch.

basin of Loch Sunart (Benn, 1997; figure 2.4). Additionally, glacial features can be seen in seismic surveys of the loch, e.g. de Greer type glacial moraines, possible kettle holes and pro-glacial delta stratigraphies (Baltzer *et al, in press*).

The bedrock geology of the Ardnamurchan peninsula and area surrounding Loch Sunart comprises primarily of igneous and metamorphic rocks which are relatively resistant to glacial erosion. Inner basin bedrock geology is primarily intrusive granite, whilst the main and outer basin bedrock geology consists of metamorphic rocks from the Moine formation (British Geological Survey, 1979). Sill locations coincide with belts of extremely resistant schists and both the inner basin and the main basin show classical glacial over-deepening towards the western end of basins, attributed to glacial pinching controlled by the resistant bedrock at sill locations (*pers. comm.,* Dr. Richard Bates, from hereon CRB, University of St Andrews, 2004). The Quaternary geology of the area shows areas of peat (particularly in the upper basin catchment), boulder clay and morainic drift (British Geological Survey, 1977).

2.1.3 Sedimentary characteristics of Loch Sunart

Biotype mapping via geophysical techniques were carried out during a recent Scottish Natural Heritage survey (figures 2.5; Bates *et al.*, 2002). Sediments in the basins of Loch Sunart are typically fine grained (< 63 μm) with high organic matter content, particularly in the inner basin, where inputs of terrigeneous matter become trapped (chapter 8), whilst sill areas are characterised by either thin packages of coarse grained sediment overlying sill rock or by bare rock. Sediment focussing does not necessarily occur in deep areas due to the influences of current activity (e.g. tidal currents can propagate to the sea floor; Gillibrand *et al.*, 1996). Sediment accumulation is not even throughout the loch (exemplified by figure 2.6) and thin sediment packages can occur in deep basins whilst thicker packages may be found on shallow shelf areas (*pers. comm.*, CRB, 2004).

Figure 2.3 Satellite image of Loch Sunart (A) and the surrounding catchment area. Areas of dense woodland (B) are shown by deep green shading and moorland, peatland or sparse vegetation (C) are represented by light green. The pink areas are likely to be bare upland terrain (D) and the blue area is in the location of Kentra Moss (E). Dark green areas show inland freshwater bodies.

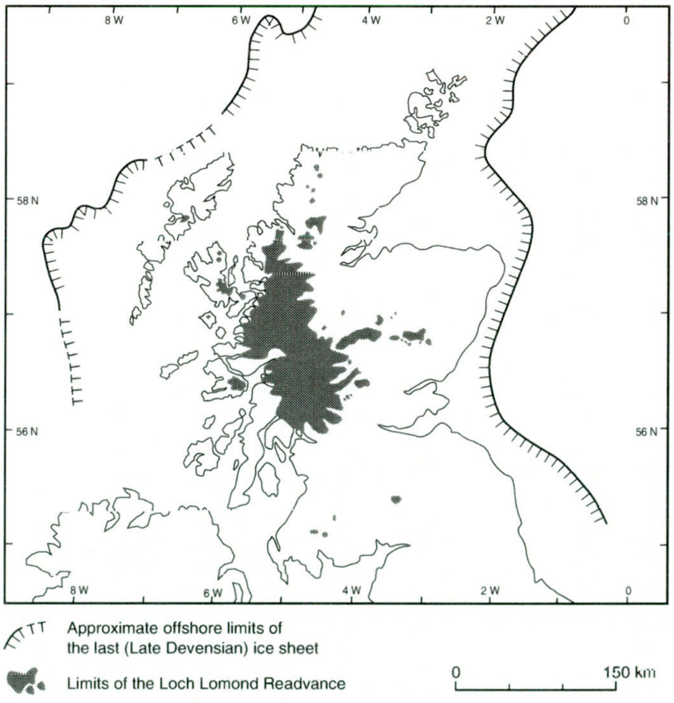

Figure 2.4 Extent of the British Ice Sheet over Scotland during the Last Glacial Maximum (late Devensian; black line) and the Loch Lomond (or Younger Dryas Readvance; grey solid fill). Modified after Ballantyne (1997).

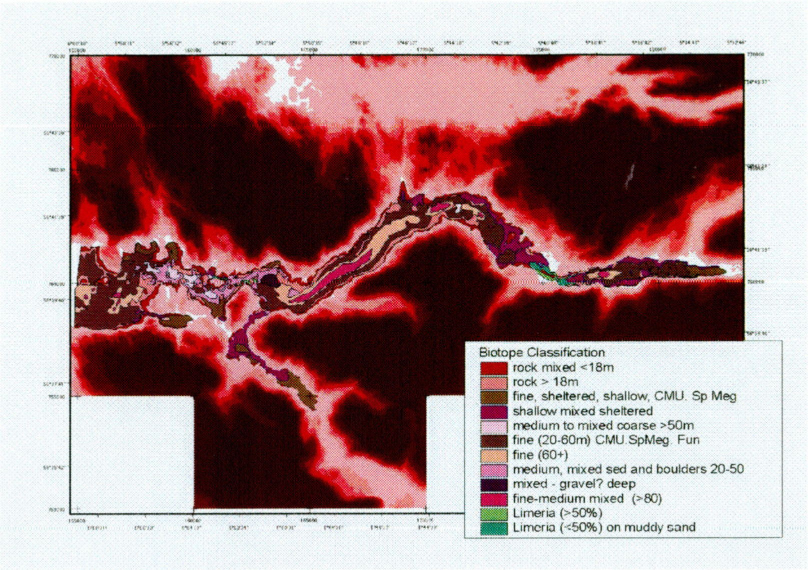

Figure 2.5 Biotype mapping of Loch Sunart using geophysical techniques and ground truth mapping. Figure courtesy of Dr. R. Bates, from Bates *et al.*, (2002).

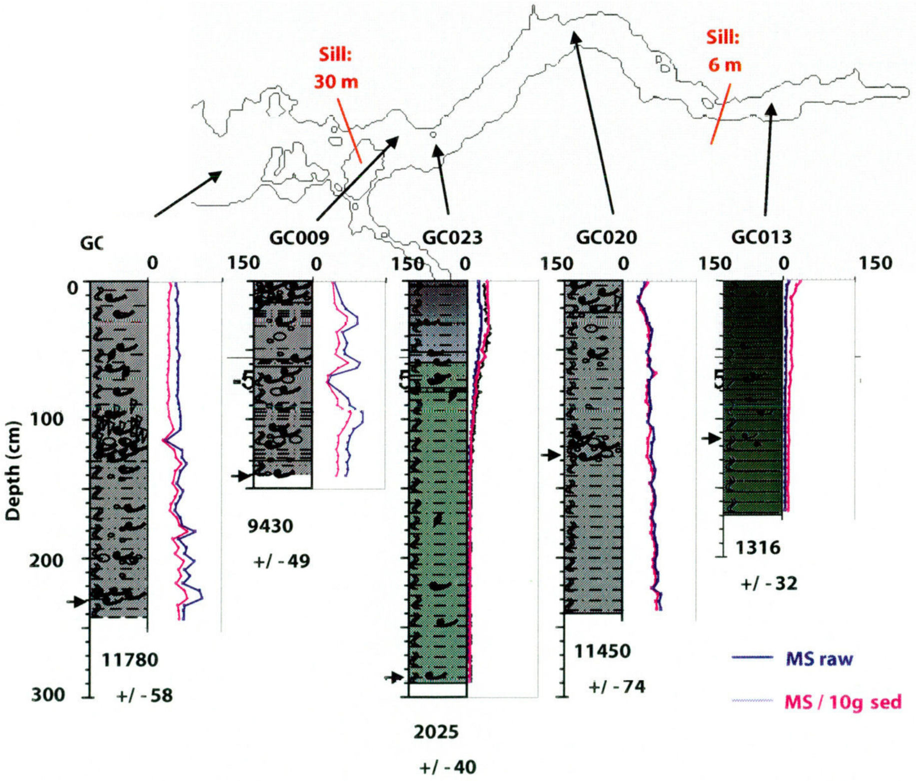

Figure 2.6 Stratigraphic summary of cores obtained from Loch Sunart during the R.V *Calanus* 2001 cruise. The core lithology is represented (green colour indicating high organic matter content), as is the degree of bioturbation in the cores (high) and the presence of molluscs (shell symbols). The magnetic susceptibility (MS; SI units) is indicated at the right side of each core and the position of the calibrated basal radiocarbon age is indicated by an arrow-head and reported as years BP (± 1σ).

2.1.4 *Hydrography of Loch Sunart*

The physical oceanography of Loch Sunart has been studied in detail by Elliott (1992), Gillibrand (1993) and Gillibrand *et al.,* (1995; 2005). Loch Sunart exhibits typical fjordic hydrography (see section 1.8.2), with a brackish surface layer and generally higher salinity waters with increasing depth (figures 1.9 and 1.10). The water column is highly stratified in the summer months and well mixed in the winter months (figure 1.10).

Approximately 50% of the freshwater input to the loch enters the upper basin, primarily via the sub-catchment areas of the major rivers Strontian and Carnoch, which account for ~70 km^2 of the total sea loch catchment area. Loch Sunart experiences semi-diurnal tides with ranges of 4 m for spring tides and 1 m for neaps. The small freshwater discharge: tidal ratio of Loch Sunart with respect to other Scottish sea lochs (e.g. Loch Etive; Edwards & Sharples, 1986) likely contributes to the frequent flushing of this sea loch (Gillibrand *et al.*, 1995).

The deep waters of the main basin are typically more saline (~ 34) than the inner basin deep waters (~33; figures 1.9 and 1.10), due to the proximity to the saline coastal water source and the main basin's deep sill which results in fairly unrestricted connection to Atlantic coastal waters. DWREs occur at least monthly in the inner basin (Gillibrand *et al.*, 1995) when south-westerly winds enhance estuarine circulation thus increasing the density of water at sill depth by removing low salinity water from the sill region. In combinations with a low runoff, this results in a weakly stratified water column and increased likelihood of a DWRE.

2.1.5 *Loch Sunart basin water response to climatic forcing*

The coastal catchments of NW Scotland are often the first areas of the UK mainland to receive weather systems from the North Atlantic, hence along with the high relief of the land promoting orographic rainfall, these catchments fall into high annual precipitation bands (table 2.1; Gillibrand *et al.*, 2005). Inter-annual variability in the location of the North Atlantic storm track due to the NAO strongly influences the wind patterns and precipitation received by NW European coastal locations (section 1.3). Since DWREs appear to respond to coupled wind direction, wind strength and runoff forcing (Gillibrand *et al.*, 1995), Loch Sunart circulation was expected to show a response to the regional climatic forcing of the NAO. Gillibrand *et al.,* (2005) modelled the response of main basin and inner basin circulation to extreme NAO forcing (section 1.8.3. and chapter 3) and showed that Loch Sunart main basin salinity showed a negligible change whilst the inner basin showed a clear response, with frequent basin exchange (thus higher salinity basin water) occurring during negative NAO years and less frequent DWREs during the positive NAO state. The implications of this hydrographic response are of great importance to the Scottish fisheries industry, since many fish farms are located in NW Scottish sea lochs and an extended period of the positive NAO phase and response to anthropogenic forcing (section 1.3) may result in basin water stagnation, oxygen depletion and other factors associated with infrequent flushing such as nutrient enrichment (e.g. Gillibrand *et al.*, 1996; Gillibrand & Turrell, 1997).

2.1.6 Coastal hydrography

The hydrography of the Scottish shelf and slope region is complex and has been documented by Craig (1953), Ellett (1979), Ellett & Edwards (1983), Simpson & Rippeth (1993), Hill *et al.,* (1997), Thomason *et al.,* (1997), Xing & Davies (2001), Holliday (2003), Inall & Griffiths (2003) and Kershaw *et al.,* (2004). The North Atlantic Current (NAC) typically follows the bathymetry of the Hebridean slope (figure 2.7) and incursions of saline North Atlantic water flow onto the shelf north of Ireland as the N. Atlantic Slope Current (NASC), mixing with the Scottish Coastal Current (SCC; Ellett, 1979), and are thought to be an important component of water within, for example, the Tiree Passage (McKay *et al.*, 1986; Inall & Griffiths, 2003). Additionally, a small branch of highly saline water (> 35) of Atlantic origin is present in the deep (>100 m) waters west of Tiree (Hill *et al.*, 1997) and the well defined 'Islay front' (an area of typically high productivity, where the stratified water mass of the outer Hebridean shelf meets the mixed inner shelf water mass) exists to the south-west of Tiree (Ellett, 1979; Simpson *et al.*, 1979).

Inner shelf bottom waters (influenced by the SCC) are typically warmer and less saline than outer shelf bottom waters (Craig, 1958; Ellett, 1979) and though seasonal stratification is common in shelf seas (e.g. Simpson & Hunter, 1974; Pingree &

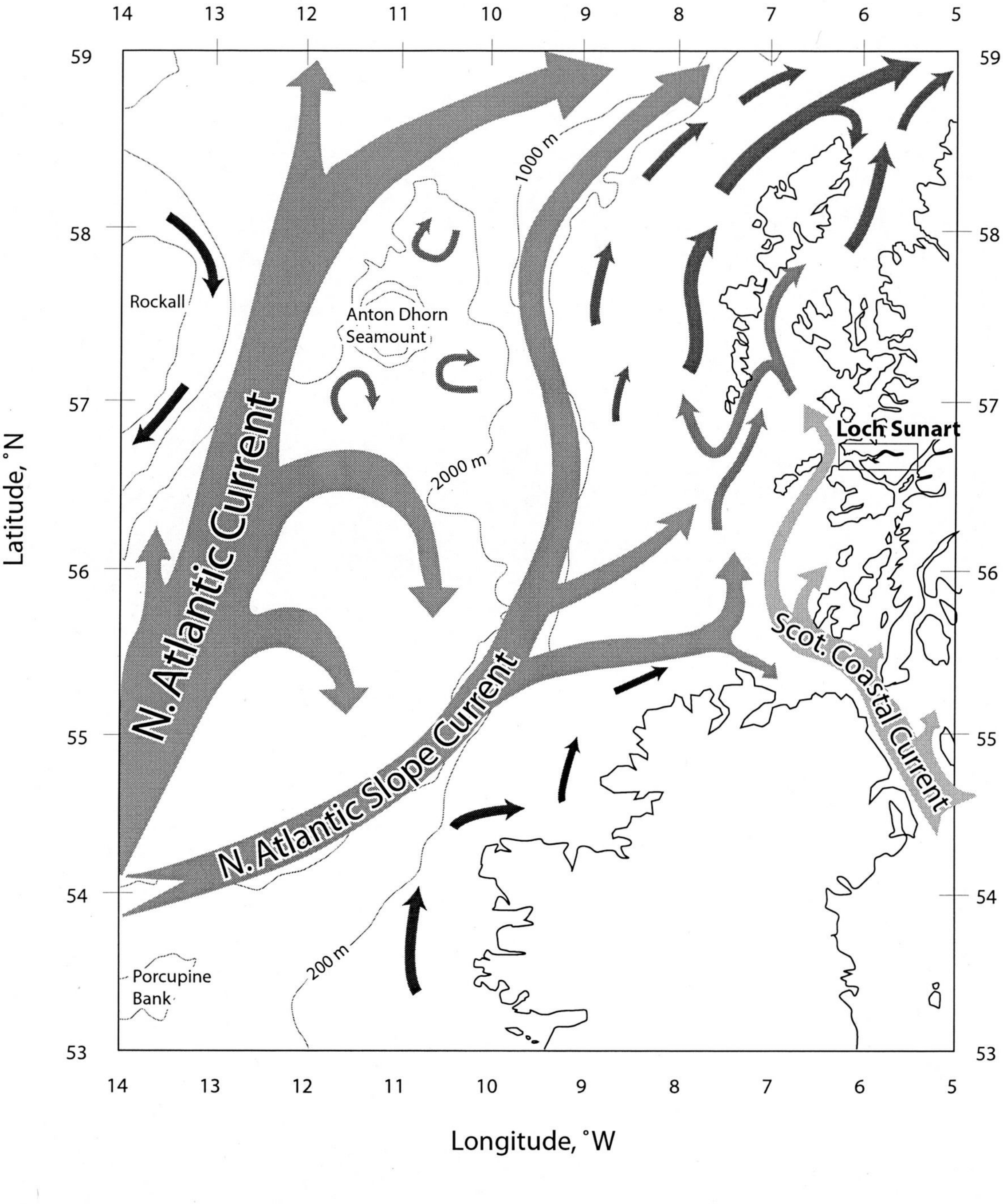

Figure 2.7 Schematic of surface ocean currents to the west of Scotland and Ireland. Also shown is the simplified bathymetry of the area and geographical regions. Loch Sunart is highlighted by a rectangle. Figure re-drawn after Ellet & Blindheim (1992).

Griffiths, 1978; Simpson & Rippeth, 1993; Backhaus, 1996; Scourse & Austin, 2002; Scourse *et al.*, 2002; Scourse *et al.*, 2004) many Inner Hebridean locations often exhibit mixed water columns (Craig, 1958; McKay *et al.*, 1986) due to high tidal currents and rough seabed topography (Ellett & Edwards, 1983). Such a region of mixing is located just outside the mouth of Loch Sunart (McKay *et al.*, 1986).

Despite this tendency towards a well-mixed water column, Hebridean shelf bottom waters show a classical 'lagged' response to the seasonal heating cycle (figure 2.8). Surface waters display a temperature cycle largely in phase with air temperatures, thus exemplifying a strong ocean-atmosphere coupling (e.g. Czaja *et al.*, 2003). Bottom water temperatures (BWT) tend to lag behind air temperatures e.g. maximum BWT occur around November (figure 2.8), only after winter winds mix the heated surface layer down through the water column

2.1.7 Oceanographic response to climate forcing

The ocean-atmosphere coupling and inter-annual variability over the surface NE Atlantic appears to be both complex and poorly understood. However, inter-annual variability in the NE Atlantic Ocean surface currents appear to be strongly linked with climatic forcing mechanisms such as those modulated by the NAO (e.g. Dickson *et al.*, 1988; Dickson *et al.*, 1996; Belkin *et al.*, 1998; Blindheim *et al.*, 2000; Holliday, 2003; Belkin, 2004).

For example; during strongly positive NAO years, the NASC pervading the slope north of Ireland is likely to be of Eastern North Atlantic Central Water (ENAW) origin, i.e. warm and saline (Holliday, 2003), whereas during negative NAO years the water in the Rockall Trough often consists of ENAW, together with the cooler and fresher waters of the Sub-Arctic Intermediate Water (SIAW) and the Western North Atlantic Central Water (WNAW; Holliday, 2003). During a positive NAO phase, mixing of the saline NASC water with the SCC (which may be stronger during NAO positive winters; Kershaw *et al.*, 2004) at the mouth of Loch Sunart (Craig, 1958; Ellett & Edwards, 1983) is likely to result in the coastal bottom waters entering Loch Sunart being more saline in comparison to NAO negative years, even when modified by regional processes such as seasonal heating and freshwater runoff (Ellett &

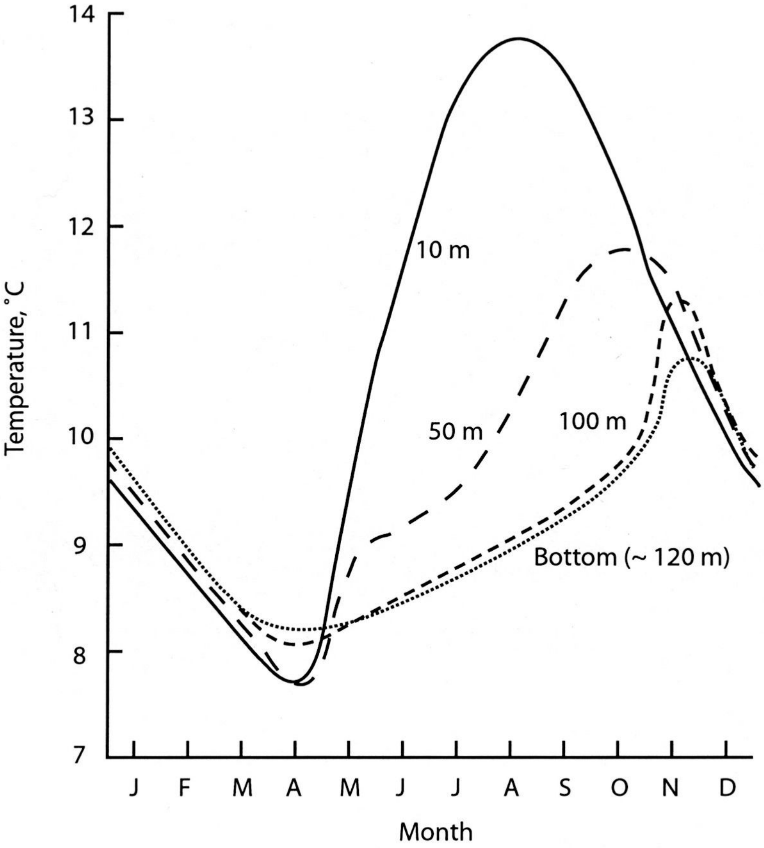

Figure 2.8 Annual temperature cycles taken during 1973-77 from 4 depths on the Hebridean Shelf, west of Barra Head (56°52′ N, 8°22′W). Re-drawn and modified from Ellet (1979).

Edwards, 1983). The NAO is a winter phenomenon (Jones *et al.,* 1997) and whilst the deep or intermediate ocean is likely to demonstrate a 2-4 year lagged response to the NAO (Holliday, 2003), the response of surface waters may be much faster. Gillibrand *et al.*, (2005) showed (via sensitivity analyses) that variations in coastal salinity between 34-34.6 for water depths below 30 m were communicated to both main and inner basin water of Loch Sunart during circulation modelling for extreme NAO years.

2.2 Cruises and Fieldwork

Hydrographic data and sample material were collected through participation on a series of research cruises (see table 2.2). All oceanographic positions on the cruises were obtained using Global Positioning Systems (GPS), and are reported as decimal latitudes and longitudes, i.e. in degrees and decimal minutes N/W. Ordnance Survey (OS) reference points are given for the weather station positions. Sample station details are provided in appendix 1.

2.3 Sampling methods

2.3.1 Sediment core acquisition

Sediment cores were recovered from Loch Sunart during April 2001, from the R.V. *Clupea* (Fisheries Research Services, Aberdeen) and during September 2001, from the R.V. *Calanus* (Dunstaffnage Marine Laboratories).

A Sholkovitch coring device was used to obtain short cores up to 70 cm in length on the April 2001 R.V. *Clupea* cruise. This type of corer is used when an undisturbed short sediment core containing the sediment water interface is required. Due to demands on the equipment and the high water content of the sediment, the Sholkovitch cores were extruded and sliced at 0.5 cm, 1cm and 2cm intervals whilst onboard R.V. *Clupea* by A. G. Cage (AGC), William Austin (WENA) and Niels Norgaard-Pedersen (NNP), stored in plastic bags and refrigerated. Radiocarbon dating was carried out on marine molluscs from the base of each core to provide a reconnaissance age and information on gross accumulation rates before the long cores were obtained.

Table 2.2 Research cruises in Loch Sunart.

Date	Research Vessel	Scientific Party	Aims and objectives for this study
6th – 8th April, 2001	R.V. *Clupea*	PAG, AGC, WENA, NNP	• CTD casts • Surface sediment samples (Craib corer and grab sampler) • Sholkovitch cores (~65-70 cm in length) • Deployed main basin mooring
27th – 29th June, 2001	R.V. *Envoy*	AGC, WENA, NNP, PAG	• Surface sediment samples (grab sampler) • CTD casts • Deployed inner basin mooring
28th – 29th July, 2001	R.V. *Envoy*	RB, AGC, JJ, WENA	• Geophysical surveying and ground truthing work in Loch Sunart and Loch Teacuis (RB & JJ) • Collect water samples from River Strontian for ?^{18}O: salinity mixing line
3rd – 5th September, 2001	R. V. *Calanus*	TS, JH, AGC, NNP	• Long gravity cores • Sholkovitch cores
17th – 22nd June, 2002	R.V. *Envoy*	AGC, WENA, PAG, THS, ERW	• Surface sediment samples (grab sampler) • CTD casts • Recovered inner basin mooring

AGC – Alix Gayle Cage (University of St Andrews)
WENA – Dr. William E. N. Austin (University of St Andrews)
NNP – Dr. Niels Nørgaard-Pedersen (University of St Andrews)
PAG – Dr. Philip A. Gillibrand (FRS Aberdeen, now at SAMS, Oban)
RB – Dr. Richard Bates (University of St Andrews)
JJ – Dr. Jack Jarvis (University of St Andrews)
TS – Dr. Tracy Shimmield (SAMS)
JH – Dr. John Howe (SAMS)
THS – Timothy Hadyn-Smith (University of St Andrews)
ERW – Emilie Wadsworth (University of St Andrews)

T

The longer cores for high resolution palaeoclimate work were recovered during September 2001, from the R.V. *Calanus* using a British Geological Survey (BGS) 3 m cylindrical gravity corer (with PVC liner), approximately 8.4 cm in diameter. Gravity cores are commonly used for obtaining continuous cores, particularly from soft sediments, however this method of coring often results in the 'shortening' of the sediment stratigraphy leading to 'undersampling' of the sedimentary archive (Skinner & McCave, 2003). Two sediment cores were taken at each coring site: the gravity core was used to obtain sediment cores up to 3 m in length and a short Sholkovitch core to capture the sediment water interface which is often 'lost' during gravity coring. The gravity cores were logged by Dr. J. Howe and NNP, and stored at 4 ºC at the Dunstaffnage Marine Laboratory.

Gravity core GC023 (core length 2.89 m) was recovered from the Dun Ghallain Deep, in the main basin of Loch Sunart, (56.6670 ° N, –5.8388 ° W, in decimal degrees; water depth = 120 m; figure 2.9) and was the core selected for palaeoenvironmental study due to a high sediment accumulation rate over the last 2000 years (chapter 8). An accompanying Sholkovitch core SC023 (core length of 0.74 m) was also recovered nearby (56.6659 ºN, –5.8404 ºW; approximate distance from GC023 = 138 m). Subsequent geochemical data (see chapter 8) from the two cores confirms that they can be correlated together, despite being from slightly different positions. The working half of core GC023 and the extruded sliced intervals from SC023 were transported to the School of Geography & Geosciences (University of St Andrews), whereupon GC023 was re-logged and sampled at continuous 1 cm intervals for analyses. All samples were stored at 4ºC, and the gravity core material was covered in cling-film to prevent the core material from drying out. Storing samples at low temperatures is vital, since bacteria contained in sediments can break-down organic matter at high (e.g. room) temperatures.

2.3.2 Surface sediment samples

Thirty-one surface sediment samples were taken from Loch Sunart for benthic foraminiferal analyses and sedimentological analyses (see figure 2.9). The samples were obtained using either a Van Veen grab sampler or a Craib corer (used solely on the April 2001 R.V. *Clupea* cruise). The Craib corer enables the sediment water

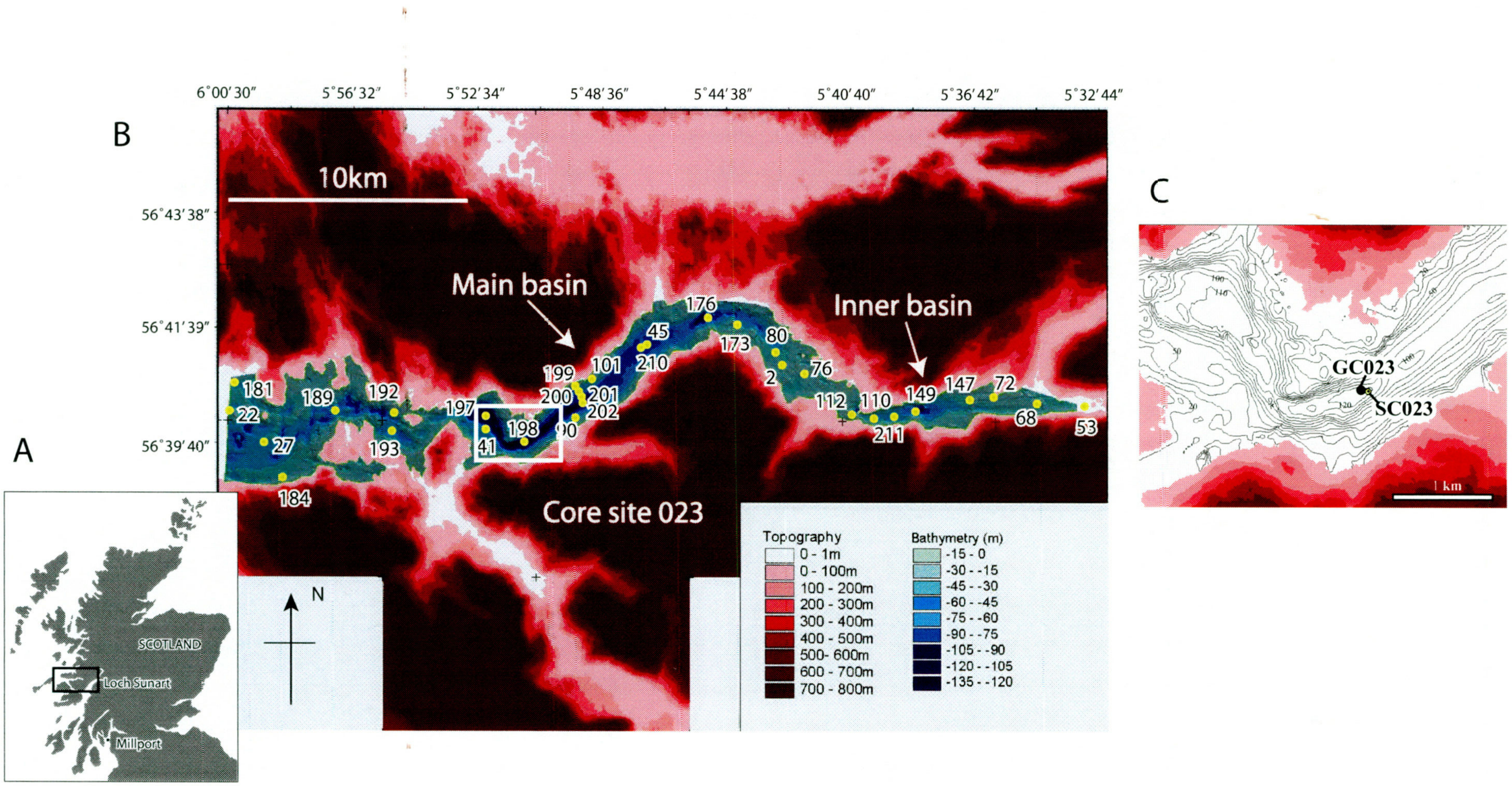

Figure 2.9 A) Location of Loch Sunart on the NW coast of Scotland. B) Location of core site 023 in the Dun Ghallain Deep of the main basin of Loch Sunart. Also shown are the positions of the Loch Sunart surface sediment samples obtained for foraminiferal analyses (yellow dots) along with the sample number. C) Site of gravity core GC023 and Sholkovitch core SC023 in context with surrounding bathymetry (10 m contour intervals).

interface to be captured in most fine-grained sediments, which is advantageous since the benthic foraminifera inhabiting the 'soupy' sediments (due to high water content) at the sediment-water interface may be lost during grab sampling. Unfortunately, the Craib corer was not available for all cruises and was not suitable for all sites; therefore the grab sampler was the main method used to obtain surface samples, particularly coarser sediments.

On recovery, the top 1-2 cm of sediment was scraped off into a container and preserved for subsequent foraminiferal analysis (see section 2.6). The remainder of the sediment was archived in refrigerated (4 °C) or frozen (-20 °C) conditions to be used for grain size, C/N and loss-on-ignition analyses.

2.3.3 CTD measurements

CTD (conductivity, temperature and depth) measurements were carried out during the R.V. *Clupea* April 2001 cruise, the R.V. *Envoy* June 2001 cruise and the R.V. *Envoy* June 2002 cruise.

On the R.V. *Clupea* 2001 cruise, a CTD cast was taken using a CTD maintained and calibrated by FRS Aberdeen at every coring site. CTD casts using a STD Plus 646 instrument with SmartTalk 2.00 software (procured by the School of Geography & Geosciences in 2002) were taken at the majority of the sediment sampling sites during the 2002 and 2003 cruise on R.V. *Envoy*.

Data from the CTD was downloaded using SmartTalk 2.00 software and put into Excel spreadsheets. The bottom water temperatures and salinities (determined using the conductivity data) were read off the cast data for use in isotopic studies and faunal assemblage work. CTD casts were also taken to calibrate the stationary moorings (see section 2.4.1). Full CTD data are presented in appendix 2.

2.4 Observational instruments

2.4.1 Stationary hydrographic mooring

To gain an understanding of the seasonal hydrographic changes in Loch Sunart, two stationary Anderaa RCM-7 current meters complete with temperature and conductivity sensors and a data logger (figure 2.10) were deployed in the inner basin (56.6842 dec. ° N, -5.6211 dec. °W) between 27th June 2001 and the 18th June 2002, and the main basin (56.6660 °N, -5.8434 °W) between 7th April, 2001 until the 17th June 2002. These stationary moorings were suspended approximately 40 m above the sea bed by a configuration of buoys (fig 2.11), well below the influence of the brackish surface layer (Gillibrand *et al.*, 1995). A series of independent CTD casts were taken to calibrate the mooring instruments throughout the deployment. These casts are important, since instruments left in the marine environment for a long period of time often become 'fouled' (i.e. overgrown with weeds and other marine life), and this inhibits conductivity readings causing the instrument to 'drift' i.e. salinity progressively decreases. Unfortunately, the current meters quickly became 'fouled' (figure 2.10) thus no current data is available. Upon recovery of the moorings, the instruments were taken to FRS Aberdeen where Dr P. Gillibrand downloaded the data into Excel files, visually checked the data and corrected the data for instrumental 'drift'. Data presented in appendix 3.

2.4.2 Weather station

2.4.2.1 Site location

The weather station was placed in a field (owned by Mr. & Mrs. Campbell, Ariundle Centre) in Aruindle, approximately 2 km north of Strontian (Ordnance Survey reference NM822633, figure 2.12). The field offered a secure, accessible site which was within the River Strontian catchment area and which was 'open', i.e. not sheltered by trees or buildings and unaffected by varying environmental conditions such as the 'clothesline', 'leading edge' and 'oasis' effect (figure 2.13; Campbell Scientific technical manual, 1999).

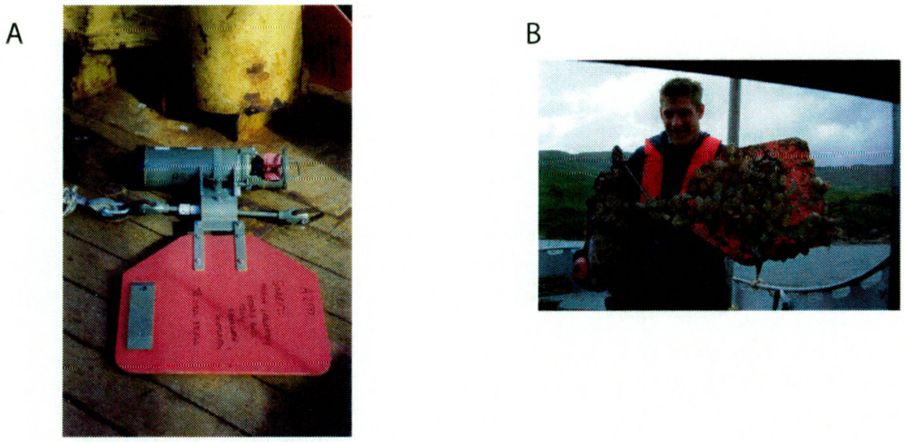

Figure 2.10 A) Anderaa RCM-7 mooring deployed in Loch Sunart's inner and main basin, loaned from and calibrated by Fisheries Research Services, Aberdeen. B) The 'fouled' mooring recovered after 12 months deployment in the inner basin of Loch Sunart. (Timothy Hadyn-Smith for scale on R.V. *Envoy*).

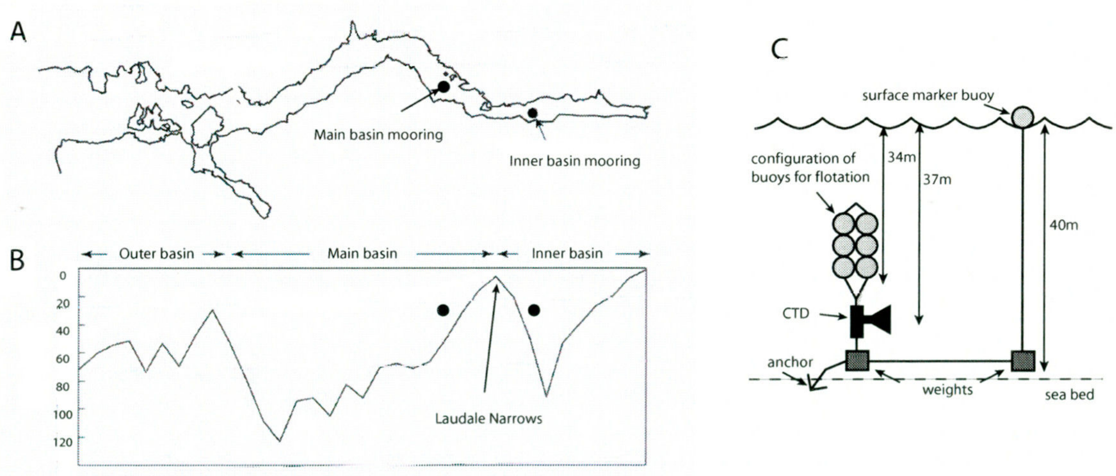

Figure 2.11 A) Mooring positions in the inner and main basin of Loch Sunart. B) Depth (~ 40 m) of moorings with respect to bathymetry. C) Configuration of a mooring.

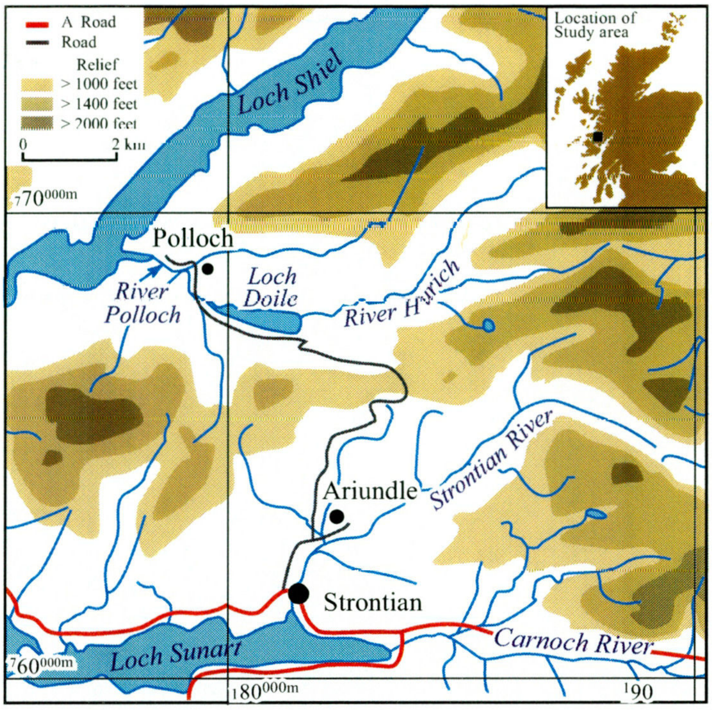

Figure 2.12. The location of the Ariundle weather station in the Loch Sunart catchment. Note also the proximity of Polloch weather station and the River Polloch to Ariundle and the River Strontian catchment area. Temperature, precipitation and mean daily flow data were obtained from the Polloch catchment courtesy of SEPA.

Figure 2.13 The Campbell Scientific 'Basic Weather Station' erected at Ariundle, Strontian. The solar panel is clearly visible on the main body of the weather station. The rain gauge can be seen to the left of the weather station. The buildings in the background and the trees and shelter to the left are the nearest permanent fixtures to the weather station and this picture exemplifies the 'open' location of the site.

2.4.2.2 Instrumentation

Due to demands on equipment use within the School of Geography & Geosciences, two stations were used to collect the meteorological data presented in this thesis. There was an overlap in the deployment of the 2 stations to ensure that the data were directly comparable, however data were lost from the first station whilst trying to retrieve it and therefore the temperature data is displayed as two separate series.

The first station, a Kipp & Zonen station collected temperature, relative humidity and wind speed data, and was used between 23rd April, 2001 and the 28th July, 2001. Data from the 14th August, 2001 to the 4th September, 2003 was collected using the Campbell Scientific 'Basic Weather Station' (see figure 2.13). The weather station was powered by a battery recharged by the SOP5 Solar Panel and comprised of: a 50Y temperature and relative humidity probe contained within a T351-RS Solar radiation shield; a 03001-5 wind sentry collecting wind speed and direction data, and a CR510 data logger. A Young Tipping Bucket Rain Gauge (model 52203 - unheated) was used to collect precipitation data (see appendix 4 for specifications). The prevailing local weather is funneled up from the mouth of the loch towards the head (Gillibrand *et al.*, 1995) and up the Strontian valley (*pers. comm.*, Mr. Campbell, 2001), therefore the rain gauge was placed 3 m upwind from the weather station to ensure a rain shadow effect did not influence the precipitation collection. Data from the weather station was downloaded approximately every 4 months using the PC200W software (Campbell Scientific, 1999) and imported into an Excel spreadsheet. Data presented in appendix 5.

2.4.2.3 Data validation

The Ariundle weather station data was validated against data taken from a Scottish Environmental Protection Agency (SEPA) weather station situated in the Polloch catchment (Ordnance Survey reference NM795687; figure 2.12).

2.5 Laboratory Methods

2.5.1 Bulk sediment geochemical analyses

High-resolution geochemical data for selected elements (see chapter 8) were obtained for core GC023 using the X-Ray fluorescence spectroscopy (XRF) core scanner at Bremen University. This research was carried out by WENA and NNP via an EU PALEOSTUDIES award granted to WENA and NNP. Low-resolution geochemical data was obtained for core GC023 via X-Ray diffraction (XRD) methods on discrete samples. The work was carried out by NNP at the School of Geography & Geosciences, University of St Andrews.

2.5.2 Wet/Dry bulk densities and water content

The working half of core GC023 was sub-sampled for the determination of sediment bulk density. These data were also required to adjust magnetic susceptibility data (Dearing, 1998).

Sediment was extracted from a core interval and placed in a pre-weighed plastic pot of a known volume. Wet bulk density was determined via the following equation;

$\text{Density}_{\text{wet}}$ (g.cm^{-3}) = weight of wet sample / volume of sample *(Eq. 2.1)*

Following the determination of wet bulk density, the sample pots containing the sediment were dried in an oven at 105 °C for at least 24 hours. Once they had cooled (in a dessicator), the dried samples were weighed and the following equation was used to calculate the dry bulk density;

$\text{Density}_{\text{dry}}$ (g.cm^{-3}) = weight of dry sample/ volume of sample *(Eq. 2.2)*

The water content of the sediment sample was calculated via;

Water content (%) = wet weight – dry weight of sample / wet weight of sample * 100 *(Eq. 2.3)*

2.5.3 Grain size analysis

Grain size analyses were carried out using the Coulter LS230 Particle Size Machine at the School of Geography & Geosciences, University of St Andrews using raw (i.e. untreated samples) and digested samples (i.e. organic fraction and calcium carbonate removed, see appendix 6 for procedures). Approximately 1g of sediment was sub-sampled from surface sediment samples and core samples. A paste was formed (using distilled water) and this was added to the machine until the obscurity reading reached 14 %. Three runs were carried out on each sample. The software ran statistical analyses for the mode, median and mean of the measurements and these data were put into Excel spreadsheets.

2.5.4 % Organic matter (% LOI_{550})

The loss on ignition (LOI) technique can be used to determine the % organic matter in a sediment sample. Organic matter combusts at temperatures of 500-550 °C leaving ash and CO_2. The weight lost in a sample during this combustion procedure is roughly equal to the percentage of organic matter in the sample. Heiri *et al.,* (2000) provide a review of the LOI process.

A crucible was labelled and weighed (after drying at 105 °C for one hour) and approximately 5g of sub-sampled sediment (which had been stored in refrigerated conditions) was added to the crucible. The crucible containing the sample was then dried at 105 °C overnight and weighed again once cool. The samples were then combusted at 550 °C in a muffle furnace for 4 hours, after which they were placed in a dessicator to cool, and subsequently weighed.

The % organic matter (i.e. the % LOI_{550}) contained within the sample and expressed as a % of dry sediment weight can be calculated by:

$$\% \text{ organic matter} = ((W_{105} - W_{550}) / W_{105}) * 100 \% \qquad \textit{(Eq. 2.4)}$$

where W_{105} = sample weight after drying at 105 °C

W_{550} = sample weight after combustion at 550 °C

2.5.5 *% Calcium carbonate (% LOI_{950})*

Sequential LOI can also be used as a crude method of determining the % of calcium carbonate ($CaCO_3$) in a sample. The LOI_{550} sample is returned to the muffle furnace (after the final LOI_{550} weigh) and combusted at 950 °C for 1 hour, whereupon CO_2 evolves from the $CaCO_3$ leaving oxide. The LOI_{950} sample is then removed from the oven, placed in a dessicator to cool and weighed. The % $CaCO_3$ can be calculated by;

$$\% \, CaCO_3 = [((W_{550} - W_{950}) / W_{105}) * 100] * 1.36 \qquad \textit{(Eq. 2.5)}$$

where W_{950} = sample weight after combustion at 950 °C

1.36 is a multiplying factor to approximate the original weight of carbonate in the sample (Bengtsson & Enell, 1986 cited by Heiri *et al.*, 2001).

2.5.6 C/N ratios

2.5.6.1 Surface sediment sample C/N ratios

Approximately 100 mg of homogenised sample was placed in a small plastic test-tube (with lid) and weighed on a Mettler AT21 microbalance. A few drops of concentrated HCL (1%) was added to the sample in order to remove carbonate, and the sample was agitated to aid the reaction. Further drops of concentrated HCL were carefully added to the sample, ensuring no material was lost, until there was no further reaction to the acid. Distilled water was added to the tube to remove salt-ions from the reaction and the mixture was centrifuged for approximately 3 minutes. The solution was carefully removed using a pipette (ensuring no sample material was lost). This rinsing procedure (i.e. adding distilled water and centrifuging) was carried out 3 times. After the final rinse, the solution was removed from the test tube, which was then placed in a 50 °C drying oven overnight. The tube was placed in a dessicator to cool and then weighed. The above procedures were performed by AGC at the Sedimentology Laboratory, Department of Earth Sciences, University of Bergen, following their methodology (http://hjs.geol.uib.no/hovedlab/instrument_fisons_cookbook_eng.html).

A Fisons EA1108-CHNS-O (accuracy ± 0.3 %) analyzer (see http://hjs.geol.uib.no/hovedlab/instrument_fisons_start_eng.html for details on the instrument) was used for the C/N analyses. All C/N analyses were carried out by Stig

Monsen, at the Sedimentology Laboratory, Department of Earth Sciences, University of Bergen, through the Marie Curie Training Site pre-doctoral fellowship funding awarded to AGC.

2.5.6.2 Core GC023 C/N ratios

Preparation of samples for C/N analyses from core GC023 were carried out by NNP (at the University of St Andrews), following the procedure outlined in King *et al.*, 1998. Samples were dried at approximately 40 ºC (higher temperatures can cause the breakdown of organic matter in the sediment) for approximately 2 days and homogenised using a Fritsch ball mill. Approximately 30 mg of homogenised sediment was accurately weighed out into pre-combusted tin capsules, and samples were carefully acidified with 100 µl aliquots of 2M HCl until all inorganic carbon has been fully decomposed. This is essential since the determination of organic carbon is dependent on the organic carbon being totally separated from the inorganic carbon (Verardo *et al.*, 1990), and inorganic carbon remaining in the sample would result in the carbon content being overestimated (King *et al.*, 1998). Samples were dried at 40 ºC for ~3 days to ensure no moisture remained in the samples, then carefully formed into small balls and analysed by Mr. Tim Brand at the Dunstaffnage Marine Laboratories.

2.6 Benthic Foraminifera

Foraminifera are microscopic, eukaryotic, single-celled marine protozoa belonging to the Kingdom Protoctista, Phylum Granulorecticulosa, Class Foraminifera (Sen Gupta, 1999). Planktonic foraminfera live suspended within the photic zone of the water column, however these forms rarely inhabit coastal waters (Murray, 1991b). Conversely, benthic foraminifera (which live on or in the sea-floor sediment) are ubiquitous in distribution, allowing ecological studies to be carried out throughout a broad range of marine environments (Murray, 1973a).

The $CaCO_3$ tests of benthic foraminifera are generally well preserved and benthic foraminifera have two key proxy pathways with respect to environmental parameters;

the biological pathway where there is a covariation between the abundance of individuals/assemblage composition or the chemical pathway where elements are incorporated into the shell material (Murray, 2001). This allows transfer functions (using modern analogues) to be applied to fossil records and provides a basis for chemical analyses, such as stable isotope work, AMS radiocarbon dating and trace element geochemistry, all of which provide vital palaeoclimate and palaeoceanographic information. Hence their ubiquity, abundance, species diversity and preservation in marine sediments make them the most widely studied marine microfossils.

These marine protozoa are characterised by a simple or multi-chambered test which is composed of either calcite (rare aragonite forms exist) or agglutinated material cemented with an organic or inorganic substance (Haynes, 1981). Some, so-called naked species possess an organic (or tectin) test (e.g. Gooday, 2002), though these wall types are rarely preserved in sedimentary archives. The organic soft tissue of foraminifera consists of protoplasm and performs many functions. For example, protoplasm containing the nucleus, mitochondria (respiration and energy cells) and ribosomes (protein synthesisers) is contained within and protected by the test (endoplasm). Most of the interchange between benthic foraminifera and their environment occurs across the ectoplasm (protoplasm outwith the test walls), which also maintains the secretion of the test and the ectoplasm pseudopodia also capture food and maintain motility. Since fossil benthic foraminifera are primarily used as palaeoproxies in this study, the biology of living foraminifera will not be covered in any great detail here, however Boltovskoy & Wright (1976), Haynes (1981) and Lee, & Anderson (1991) provide useful reviews.

The complex reproduction cycles of benthic foraminifera, often alternating between asexual and sexual reproduction (see Lee *et al.*, 1991), may be influenced by physio-chemical factors such as bottom water temperature or by food availability arising from phytoplankton blooms (e.g. Gooday, 1988; Gooday & Rathburn, 1999; Gustafsson & Nordberg, 2001). Species do not necessarily reproduce and calcify at the same time throughout the year, as demonstrated by the ‘seasonality effect’ of Scourse *et al.*, (2004), thus the population structure of the community varies throughout the year (e.g. Murray, 1983) and may vary from year to year.

2.6.1. Living habitats of benthic foraminifera

Benthic foraminiferal species maintain living habitats either upon the sea floor sediment (epifaunal) or within the surface sediment (infaunal) and test morphology can often be indicative of microhabitat e.g. Corliss, (1985); Buzas *et al.*, (1993). Epifaunal specimens may live on the sediment surface (epibenthic), on plants (epiphytic) or cling to large sediment grains and rocks (epilithic). Infaunal species live at different depths within the sediment in response to food and oxygen availability, as conceptualised by the 'TROX' model of Jorissen *et al.,* (1995) and Jorissen (1999).

The growth (or ontogeny) of benthic foraminifera is typically fast but then slows as individuals mature and can be influenced by biotic factors such as food availability or physical factors such as temperature and salinity (e.g. Boltovskoy & Wright, 1976; Wefer, 1976; Murray, 1991a). For example, species typically have an optimum, maximum and minimum temperature for survival (Murray, 1973a; Boltovskoy & Wright, 1976) and a preference for certain salinity conditions.

For instance, restricted basins with low salinity basin waters often show a bias towards agglutinated taxa (e.g. Murray, 1973b; Brönnimann & Whittaker, 1988b; Brönnimann & Whittaker, 1990; Alve, 1995; Murray & Alve, 1999; Murray *et al.*, 2003). Hyaline taxa from such stressed and low salinity environments often have thin and etched tests due to low pH or problems with carbonate availability (Murray, 1973a); either process creates a stressful environment for calcareous taxa, which must spend 'considerable energy recalcifying their tests' (Boltovskoy & Wright, 1976). Hyaline taxa inhabiting low salinity waters demonstrate an efficient use of available $CaCO_3$ during test formation (using an organic membrane template) whereas miliolina taxa use a less organised method which requires readily available $CaCO_3$ (Boltovskoy & Wright, 1976) and are unable to maintain pseudopodial reticulum activity in hyposaline waters (Murray, 1973a; Haynes, 1981).

2.6.2 Utilising benthic foraminifera as environmental and palaeoenvironmental proxies

As mentioned previously, the ubiquitous distribution of benthic foraminifera in marine environments together with their sensitivity to changes in living habitat, good preservation in most marine sediments and the range of applications based on their shell geochemistry (e.g. stable isotopes) makes these marine organisms extremely useful proxies for studying environmental or palaeoenvironmental change. Before utilising proxies in palaeoenvironmental reconstructions, it is important to understand how fossil benthic foraminiferal assemblages are influenced by environmental parameters. To do this, we must first ascertain how modern benthic foraminiferal assemblages (a statistical representation of the population) respond to abiotic parameters such as hydrography (e.g. temperature, salinity, currents, oxygen availability) and substrate, as well as to biotic factors such as food availability and inputs of organic matter. These relationships, along with measures of species diversity, abundance and wall types (Murray, 1973a, 1991b) can be used to facilitate the recognition of benthic foraminiferal assemblages characteristic of certain ecological environments.

2.6.2.1 Sample collection

The top 1-2 cm of surface sediment was collected from surface sediment grab samples (section 2.3.2) and placed in a plastic container. The thickness of sample collected was largely determined by the oxygen penetration depth or grain size. Where sediment was coarse (e.g. sand) a thicker portion of sediment was retained for foraminiferal analysis since coarser sediments tend to have low foraminifera numbers and deeper oxygen penetration depths. Fine grained sediments have a propensity for higher foraminifera numbers and at these locations a 1 cm scrape was taken. However, some sample sites yielded fine grained ‘smelly’ sediments (i.e. high in organic matter and H_2S) with a thin oxidised layer, thus a thin surface scrape was obtained in order to avoid collecting sediments which were unlikely to have ‘live’ foraminifera within them.

A mixture of ethanol and rose Bengal was added to preserve and stain ‘live’ organic tissue contained within the sediment (after Walton, 1952; see Boltovskoy & Wright, 1976 for technique). Samples were sieved on return from the field season (approximately 1-2 weeks) hence allowing the stain ample time to 'fix'. Specimens were considered 'live' when at least one chamber was stained bright pink by rose Bengal, however live populations are often over-estimated when using rose Bengal as the protoplasm of recently deceased foraminifera (up to 3 months) can also take up the stain (e.g. Bernhard, 2000). However, given the practicality (i.e. speed and cost) of using rose Bengal (Murray & Bowser, 2000), this stain was used in the present study.

Though cores GC023 and SC023 were sub-sampled every 1cm for benthic foraminiferal analysis, only low resolution assemblage analyses were carried out.

2.6.2.2 Preparation of residue for foraminiferal analysis

In the laboratory, samples were wet-sieved using a 63 μm mesh size sieve and a fine water spray. Samples were sieved until the effluent water ran clear (i.e. no mud present), and given the fine-grain size and high organic matter content of these sediments, each sample took on average approximately 2 hours to sieve. Bounded samples, i.e. those with a high % of clay, or compacted sediments from the gravity core, were soaked overnight in sodium hexametaphosphate to encourage disaggregation. The sieve was thoroughly washed in between samples and submerged in methyl blue solution, which stains calcium carbonate thus allowing contaminant foraminifera specimens to be identified in a sample. The sieved samples were rinsed with distilled water and left to dry at 40 °C. The drying temperature is kept fairly low, since drying at high temperatures can damage foraminiferal tests and may alter the shell geochemistry.

2.6.2.3 Foraminiferal analysis

A weight for the total sieved sample was determined and the 125 μm – 500 μm fraction (or residue) was obtained (using sieving methods) for use in foraminiferal analysis. This weighed fraction was divided using a splitter to yield unbiased sub-sample splits from which a sufficient number of specimens could be obtained. A Zeiss Stemi SV11 stereo microscope was used to pick and identify the foraminifera. The sub-sample split was spread evenly over a brass picking tray and over 300 benthic foraminifera were picked using an artists (grade 0000) paintbrush. Statistical studies show that over 300 specimens are required to ensure that assemblages are representative of the whole sample (e.g. Dennison & Hay, 1967 as cited by Boltovskoy & Wright, 1976 and Buzas, 1990). Specimens were picked from each square of the entire split (preferred method), or from random squares (to avoid biasing towards a certain size of specimen) if the number of foraminifera in a sub-sample split were particularly high. Every specimen within a square was picked before moving onto the next square to avoid biasing results towards larger, more visible individuals.

Benthic foraminifera were identified to species level using the taxonomy of Loeblich & Tappan (1987) and archived in slides. Reference materials used for identifying the benthic foraminifera were Höglund (1947), Feyling-Hanssen *et al.,* (1971), Murray (1971, 1979), Haynes (1973), Brönnimann & Whittaker (1988) and Austin (1991). Few planktonic foraminifera were found in the samples, thus planktonic specimens were not identified to species level.

2.6.3 Benthic foraminiferal transfer functions

Birks (1995) provides an excellent review of the theory and practice of ecological calibration, thus the basic principles are outlined here and illustrated in figure 2.14. Fossil assemblages (Y_0) such as fossil benthic foraminiferal assemblages consisting of *m* taxa and *t* samples, can provide important palaeoenvironmental information on, for example, a variable such as past summer bottom water temperature (X_0) . To estimate X_0, the biological response of a suite of modern assemblages (Y), known as a 'training set' and consisting of *m* taxa and *n* samples, to the modern environmental variable (X) can be modelled numerically. The resulting transfer function is applied to the fossil data (Y_0) to provide a quantitative estimate of the past environmental variable X_0).

Five major assumptions are made when using quantitative palaeoenvironmental reconstructions (taken from Birks, 2003);

1. Taxa in the training set (Y) must be systematically related to the environment in which they live (X).

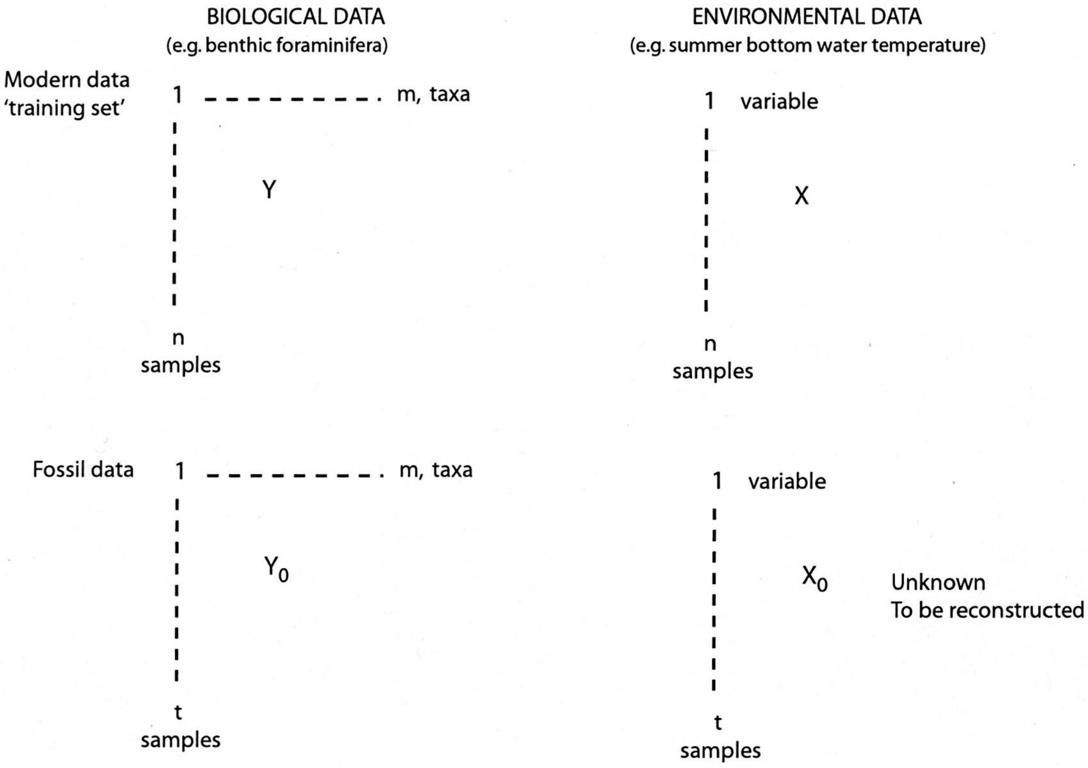

Figure 2.14 The principles of quantitative palaeoenvironmental reconstruction showing X_0, the unknown environment variable (e.g. summer bottom water temperature) to be reconstructed from fossil assemblages Y_0, and the essential role of a modern training set consisting of modern biological (Y) and environmental (X) data. Redrawn from Birks (1995).

2. The environmental variable to be reconstructed is, or is linearly related to, an ecologically important determinant of the system.
3. Taxa in the training set Y are the same biological entities as taxa in the fossil data Y_0 and their response to the environmental variable X must not have changed over the time span of Y_0. The modelled response of modern Y to X over an environmental gradient (created using spatially distributed samples) can be used to reconstruct X_0.
4. Mathematical methods should adequately model the biological response of Y to X and yield transfer functions with sufficient predictive power to allow accurate an unbiased reconstructions of X.
5. Other environmental variables, other than X, should have negligible influence on the biological response or should maintain a joint relationship on taxa distribution over time.

Other requirements state that: fossils must be easily identifiable and well preserved (e.g. benthic foraminifera); fossil data sets should be of comparable taxonomy, quality and sedimentary environment as the training set (e.g. shelf seas); a good independent chronology (e.g. radiocarbon dating) is required for fossil data sets to allow correlations with other proxy records; the training set should be of high quality (ideally > 200 *n* samples) and from the same sedimentary environment (shelf seas), representing the likely range of variables experienced by Y_0; mathematical models should be robust, theorectically sound both ecologically and statistically, critically evaluated and validated and accompanied by sample-specific prediction errors (Birks, 1995).

2.6.3.1 Software

The transfer function work was carried out using the software C2 (Juggins, 2003a). C2 is a Microsoft Windows programme for analysing and visualising palaeoenvionmental data sets and multi-proxy stratigraphic data sets. C2 can be used to develop and apply palaeoecological transfer functions, with choices of: weighted averaging, partial least squares, weighted averaging partial least squares, Imbrie & Kipp factor analysis, correspondence analysis regression, principal component analysis regression, modern analogue technique and maximum likelihood regression and calibration methods; all cross-validated by leave-one-out, bootstrap or n-fold leave out (Juggins, 2003b).

2.6.3.2 Training set

The training set used in the transfer function is the Recent Benthic Foraminifera (RBF) database compiled by the working group of Professor H.P. Sejrup (Sejrup *et al.*, 2004) and access was granted to this data as part of the pre-doctoral fellowship awarded to AGC at the Marie Curie Training Site scheme, University of Bergen. A full description of the transfer function can be found in Sejrup *et al.,* (2004) and the transfer function is discussed further in chapter 7.

The database includes 298 samples from the NW European continental margin and shelf, spanning from Svalbard to the west coast of Ireland. Sejrup *et al.,* (2004) did not include samples from fjordic environments since these environments tend to undergo greater seasonal change than 'open' shelf environments (*pers comm.*, Dr. D. Klitgaard-Kristensen, 2003). However, to extend the environmental gradient of the hydrographic data, and also to add samples similar to the core site, modern Loch Sunart samples were added to the training set (RBF database) following the rules set out in Sejrup *et al.,* (2004), i.e:

1. Only samples from water depths between 50 m and 500 m are included.
2. Samples where '% Other species' exceeds 10% were excluded.
3. Species chosen for inclusion in the training set were the species which frequently constituted to more than 90% of any assemblage.

Unfortunately many of the modern (i.e. surface sediment) benthic foraminifera samples from Loch Sunart could not be included due to the above 'rules', however 3 samples were included (22, 80 and 198). Also, differences in common species between the RBF samples and the Loch Sunart samples were evident, probably due to geographical differences in temperature and salinities. These issues are discussed in further detail in chapter 7.

2.6.4 Stable isotopic compositions in benthic foraminifera

The stable isotopic composition of benthic foraminifera tests are influenced by environmental variables such as temperature, salinity and nutrient availability, often reflecting the properties of the water mass in which they live (Rohling & Cooke, 1999).

2.6.4.1 Stable isotopes from modern benthic foraminifera

Stable oxygen and carbon isotopic analyses were carried out on four benthic foraminifera species: *Ammonia beccarii*, *Cibicides lobatulus, Bulimina marginata* and *Nonionella turgida.* Where possible 'live' specimens were preferentially selected (in the modern study), and where dead or fossil foraminifera were used, only pristine specimens with no visible sign of dissolution or diagenesis were selected. All specimens were selected from the 125-250 μm size fraction.

The appropriate number of benthic foraminifera were picked (using a metal pin) to attain the required weight for the mass spectrometer used (~0.2 mg) . This varied depending on the system requirements and the species used. The isotope sample was weighed and transferred to a small isotope vial, where the foraminifera were gently crushed using a glass rod, and a few drops of methanol were added. The sample was then cleaned via an ultrasonic bath for 1 minute, after which the remaining methanol was carefully decanted using a pipette, ensuring no material was lost. The samples were then placed in a 40 °C oven overnight to dry. After the tops of the glass vials were carefully checked and cleaned for dust, the samples were loaded onto the autosampler of the Kiel Device.

Isotopic analyses were carried out using three different mass spectrometers:

1. A Finnigan MAT 251 with Kiel device at Bremen University (funded through an EU PALEOSTUDIES award granted to WENA and NNP), which had mean errors (shown with standard deviations of 0.035 ± 0.015 ‰ for $\delta^{18}O$ and 0.025 ± 0.011 ‰ for $\delta^{13}C$. The samples were run by WENA and NNP.
2. A Finnigan MAT 251 with Kiel device at the Bjerknes Centre for Climate Change, University of Bergen, with reported $\delta^{18}O$ errors of ±0.07 ‰ and $\delta^{13}C$ errors of ±0.06 ‰. Samples were run by Rune Søraas.

3. A ThermoFinnigan MAT 253 also at the Bjerknes Centre for Climate Change, University of Bergen, with errors of 0.08 ‰ and 0.04 ‰ for $\delta^{18}O$ and $\delta^{13}C$ respectively. Samples were run by Rune Søraas.

Analyses carried out on the latter two mass spectrometers were funded by the EU Marie Curie Training Site Scheme, which hosted AGC for a pre-doctoral fellowship between 3rd March, 2003 to the 1st July, 2003.

2.6.4.2 Isotopic composition of Cibicides lobatulus from cores GC023 and SC023

Cibicides lobatulus specimens were selected from 1cm sample intervals from cores GC023 and SC023 for stable isotope analyses ($\delta^{18}O$ and $\delta^{13}C$). The measurements were carried out at Bremen University (funded through an EU PALEOSTUDIES award granted to WENA and NNP) using a Finnigan MAT 251 with Kiel device.

2.6.4.3 Reporting stable isotope results

Stable isotopic compositions are reported relative to Vienna Pee Dee Belemnite (VPDB) using the NBS-19 standard, and the following equations;

$$\delta^{18}O\ (‰) = [(^{18}O/^{16}O\ \text{sample} / ^{18}O/^{16}O\ \text{standard}) - 1] * 1000 \qquad \textit{(Eq. 2.6)}$$

$$\delta^{13}C\ (‰) = [(^{13}C/^{12}C\ \text{sample} / ^{13}C/^{12}C\ \text{standard}) - 1] * 1000 \qquad \textit{(Eq. 2.7)}$$

2.7 Radiocarbon methods

2.7.1 Principles of radiocarbon dating

Following the seminal publications outlining the determination of the half-life of ^{14}C by Libby *et al.,* (1949; Libby half-life of 5,568±30 years), radiocarbon dating methods have been used to date carbon containing material up to ~45, 000 years old (section 2.7.3). The unstable or radioactive isotope, ^{14}C or radiocarbon, accounts for approximately 1x 10^{-10} % of total carbon present in nature (Bowman, 1990) and is continually produced in the upper atmosphere through the interaction of neutrons (produced by cosmic rays) upon ^{14}N (nitrogen). In the atmosphere, ^{14}C rapidly becomes carbon dioxide, $^{14}CO_2$, and is absorbed by the oceans and enters all living organisms via life processes. Living organisms in the terrestrial biosphere are largely in equilibrium with atmospheric ^{14}C (due to rapid gaseous exchange and replenishment through life processes). The uptake of ^{14}C in marine organisms is more complex, as detailed in section 2.7.2, since marine organisms derive carbon from seawater. Upon death of an organism, the carbon uptake required for life ceases and the system becomes 'closed', and the ^{14}C present in the organism begins to decay. Since the rate of decay of ^{14}C is known (5,568 ± 30 years; Libby, 1955), the approximate year of death can be calculated by measuring the residual ^{14}C activity. See Bowman (1990) for a review of the processes.

The radiometric method of estimating the age of sample material using radiocarbon dating rests on 5 main assumptions (Bowman, 1990; Lowe & Walker, 1997):

1) Radiocarbon is continually produced in the atmosphere, with constant production rates over time.
2) The ^{14}C concentration (i.e. the ^{14}C:^{12}C ratio) is equal in all parts of the biosphere, i.e., there are no vital effects or variance between different species of organisms.
3) The ^{14}C concentration in the biosphere is in equilibrium with the ^{14}C concentration in the atmosphere, therefore assuming rapid mixing between the reservoirs. All living organisms require carbon to construct their skeletons or tissue, and this carbon is derived from carbon dioxide present in the atmosphere or dissolved in water. Therefore, the organism should be in isotopic equilibrium with its reservoir.
4) The decay rate of radiocarbon is known.
5) Radiocarbon exchange between the biosphere and the organism ceases when the organism dies. The system becomes ‘closed’ and since the ^{14}C is no longer replenished, the ^{14}C begins to decay.

These assumptions are vital for applying the methodology of radiocarbon dating, however in reality there are many complications and the assumptions are not strictly correct. For example, *in situ* material can undergo diagenetic alterations and ^{14}C production varies over time (section 2.7.6). Other problems encountered in ^{14}C dating are contamination of the sample by 'old' carbon, such as limestone (often referred to as the *hard water effect*) which contains no active ^{14}C and therefore yields radiocarbon ages much older than expected since the ratio of $^{14}C/^{12}C$ is decreased (e.g. Heier-Nielsen *et al.*, 1995), and contamination by modern ^{14}C, resulting in radiocarbon ages younger than expected (Pilcher, 1991).

2.7.2 Radiocarbon dates from marine organisms

Radiocarbon in the atmosphere is rapidly mixed, and the distribution of atmospheric carbon can be assumed to be relatively homogeneous in comparison to radiocarbon in the oceanic reservoir. Atmospheric radiocarbon can only enter the ocean via mixing across the air-ocean surface, thus the ^{14}C replenishment of the CO_2 dissolved in the oceanic reservoir is severely restricted given the size of the ocean reservoir.

The process of ^{14}C decay and restricted replenishment of ^{14}C in the surface ocean results in a general deficiency of ^{14}C, with the surface ocean displaying a lower specific ^{14}C activity of approximately 0.95 relative to the atmospheric ^{14}C activity of 1 (Olsson, 1984, and Bowman, 1991). Hence the surface ocean appears older than it actually is, i.e. it has an 'apparent age'. Since marine organisms derive carbon from seawater as suggested from the ^{13}C values of their $CaCO_3$ shell (Mook & Vogel, 1968 and Olsson & Osadebe, 1974) they will also display an apparent age, since they exhibit ^{14}C values similar to those in the surrounding ocean reservoir. By comparing measured marine ^{14}C ages with the equivalent atmospheric ^{14}C age, the marine reservoir ^{14}C age, R(t) is determined. The ^{14}C deficiency of a water mass represents R(t) and this age should be applied to conventional radiocarbon dates in order to correct for growth in a given reservoir (Stuiver *et al.*, 1986b). The modelled global reservoir age of the surface ocean is taken to be approximately 400 years (Stuiver & Braziunas, 1993) and the difference in R(t) from the global model curve of the surface ocean defines regional ^{14}C deviations (ΔR), i.e. the marine reservoir age of the sample.

In most regions, the thermocline between the well-mixed shallow surface ocean (0-75 m) and the deep ocean inhibits the exchange of CO_2 between these two reservoirs. Since carbon in the deep ocean has a long residence time and is replenished almost exclusively by ^{14}C from the surface ocean, the deep ocean has, on average, a much lower specific ^{14}C activity than the surface ocean and a greater deficiency in ^{14}C (Olsson, 1984 and Stuiver *et al.*, 1986b), resulting in average R(t) values of ~ 1000 years.

2.7.3 Limits of radiocarbon dating

The limit of the detection of ^{14}C is dependent on the background radiation of the machine and the method used to date the material (e.g. conventional or accelerated mass spectrometry methods; Pilcher, 1991; Gove, 2000). However, the half-life of ^{14}C along with the minute concentration of ^{14}C present in most natural sample material results in the dating method reaching it's limitations by approximately 45,000 years. For example, by 30,000 years and 50,000 years, there is approximately 1% and 0.1%, respectively, of the initial ^{14}C left in the sample.

The detonation of the first nuclear atom bomb in AD 1945 and subsequent nuclear weapons testing, released vast amounts of bomb ^{14}C into the atmosphere, interfering with the natural ^{14}C equilibrium in organisms. The bomb peak was identified in the northern hemispheric atmosphere in 1963 (figure 2.15) with approximately a 100% increase in the $^{14}C/^{12}C$ ratio (Olsson, 1984). However, tree ring archives suggest that atmospheric ^{14}C was influenced by bomb^{14}C enrichment by 1955 (Cain & Suess, 1976), thus AD 1950 is conventionally accepted as the 'youngest' limit at which material can be radiocarbon dated, with ^{14}C dates conventionally reported as years BP, where BP is AD 1950 (Stuiver & Polach, 1977). The serendipitous introduction of bomb-produced radiocarbon into the environment has enhanced the understanding of the global carbon cycle; ^{14}C enrichment acts as a geochemical tracer, improving our knowledge and understanding of atmospheric mixing and oceanic processes (e.g. Levin & Hesshaimer, 2000; Nydal, 2000). The oceanic reservoir showed a lagged response (due to inhibited mixing) to bomb produced ^{14}C, e.g. bomb $\Delta^{14}C$ was first detected in the 1959-1960 band of an *Arctica islandica* shell from the Georges Bank area of the North Atlantic Ocean, whilst the oceanic bomb $\Delta^{14}C$ peak occurred in the1973-1975 band (Weidman & Jones, 1993).

2.7.4 Measuring radiocarbon activity

Radiocarbon age determinations in this thesis were obtained using accelerated mass spectrometry (AMS) dating, primarily since this method requires a small sample size, approximately 50-100 mg of shell material in comparison to 50-100 g of shell material required for conventional dating (i.e. gas proportional counting or liquid scintillation counting; Bowman, 1991)

AMS works by measuring the ratio of carbon isotopes in the sample material (i.e. the number of ^{14}C atoms present with respect to ^{13}C atoms) via the detection of elemental atoms according to their atomic mass (see Linick *et al.*, 1989 and Gove, 2000 for reviews). Sample material is prepared for AMS dating, graphitised and embedded in a cathode which is placed in the machine at the source end (figure 2.16). The graphite target is bombarded with a caesium negative ion sputter source and the resultant carbon negative ion beam is focused into a straight line of travel down the AMS system (using a combination of focusing devices, electrostatic attraction, polarity changes and magnetic deflection) towards the Faraday cup detectors (Linick *et al.*, 1989; Bowman, 1990; Gove, 2000). The measured $^{14}C/^{13}C$ ratio is compared to ratios obtained from the standards and corrected to the $^{13}C/^{12}C$ ratio measured for the same sample, to give a $^{14}C/^{12}C$ ratio to be used in the age determinations.

2.7.5 Calculating and reporting radiocarbon dates

A radiocarbon age determination, t, is based upon;

$$t = [(T / \ln 2)* \ln(I_0 / I)\} \qquad \textit{(Eq. 2.8)}$$

where T is the known ^{14}C half-life, I_0 is the $^{14}C/^{12}C$ of a modern material, ie. a standard and I is the $^{14}C/^{12}C$ ratio of the material to be dated (Nydal, 2000). NBS oxalic acid is typically used as a standard for ^{14}C dating, and is based on the ^{14}C activity in recent wood in 1950 AD. Radiocarbon ages are reported relative to this standard where;

$$\delta^{14}C = [(I - I_0) *1000 / I_0] \qquad \textit{(Eq. 2.9)}$$

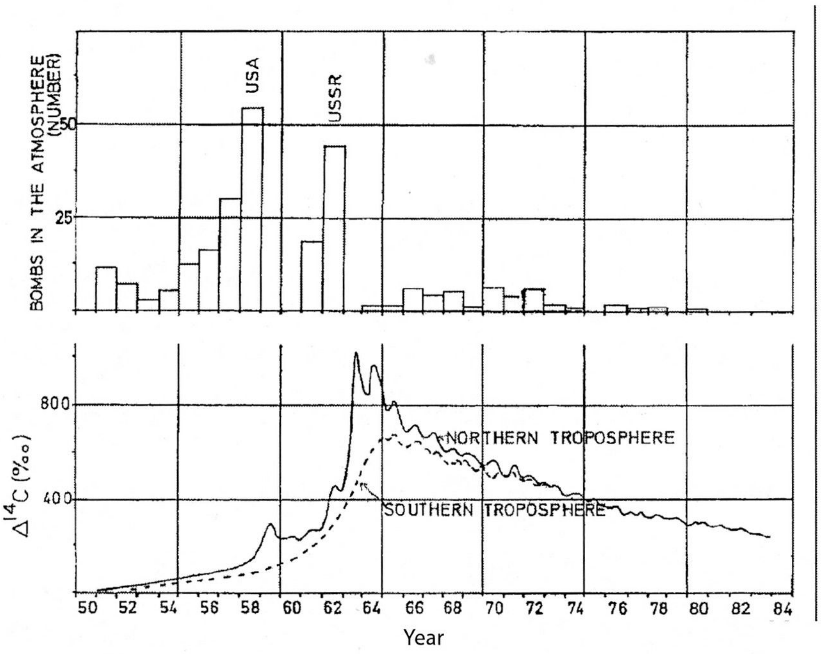

Figure 2.15 Nuclear tests in the atmosphere and the subsequent changes in atmospheric ^{14}C level. Taken from Nydal (2000).

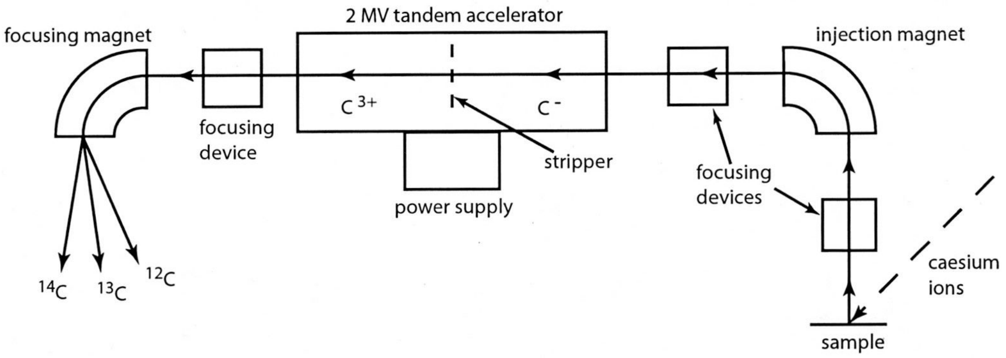

Figure 2.16 A schematic diagram illustrating the basic components of a tandem accelerator used for AMS radiocarbon dating (Bowman, 1990). The carbon ion beam travels through the system right to left, from the source end to the detection end. AMS dating at Aarhus University is centered around the 6 MV HVEC EN type tandem accelerator (http://www.phys.au.dk/ams/snfappl2004condens.pdf). AMS radiocarbon dating of Loch Sunart core matieral was pre-treated at the NERC Radiocarbon Laboratory, East Kilbride and measured on the General Ionex 2.5 MV AMS machine at the University of Arizona.

Though shell material is typically in isotopic equilibrium with the dissolved bicarbonate of the ocean (Mook & Vogel, 1968; Olsson & Osadebe, 1974), the $^{14}C/^{12}C$ ratio measured in shell material must be corrected to account for the fractionation of isotopes during thermodynamic interactions between the organism and its environment (e.g. Craig, 1954; Olsson, 1984). Since ^{14}C decays over time, the $^{14}C/^{12}C$ ratio is corrected using the $\delta^{13}C$ value (section 2.6.4.3, equation 2.6) which is measured independently from the $^{14}C/^{12}C$ ratio. Thus the formula for $\Delta^{14}C$ (Stuiver & Polach, 1977), which includes the correction for isotopic fractionation and represents the 'noramlised' value to the base value of -25 ‰ with respect to the standard carbonate (VPDB; http://www.c14dating.com/agecalc.html), is calculated by;

$$\Delta^{14}C = \delta^{14}C - 2(\delta^{13}C + 25)\ (1 + \delta^{14}C / 1000) \qquad \textit{(Eq. 2.10)}$$

The conventional radiocarbon age, R, is then calculated by;

$$R = -8033 \ln (1 + \Delta^{14}C/1000) \qquad \textit{(Eq. 2.11)}$$

Radiocarbon ages are reported to guidelines stated in Stuiver & Polach (1977), i.e. reported relative to 95% of the activity of the standard NBS oxalic acid in AD 1950, normalised to $\delta^{13}C = -19‰$ with respect to the PDB standard, and accompanied by a standard error of 1 standard deviation and the $\delta^{13}C$ value

2.7.6 Calibrating radiocarbon dates

Calender years and radiocarbon years exhibit a non-linear relationship (Libby *et al.*, 1949) with a curve characterized by high frequency variations superimposed on long-term $\Delta^{14}C$ trends (figure 2.17). These $\Delta^{14}C$ variations are primarily caused by cosmic ray flux, solar activity, variations in ocean ventilation and geomagnetic intensity (e.g. Stuiver *et al.*, 1991; Stuiver & Braziunas, 1993; Goslar *et al.*, 1995; Laj *et al.*, 1996; Druffel, 1997; Bard, 1998; Hughen *et al.*, 2004a). Therefore empirical radiocarbon calibration curves (e.g. IntCal98/Intcal04 and marine98/Marine04; Stuiver & Polach, 1977; Stuiver *et al.*, 1998a; Stuiver *et al.*, 1998b; Hughen *et al.*, 2004b; Reimer *et al.*, 2004a) are used to convert conventional radiocarbon years to calendar years (figure 2.17).

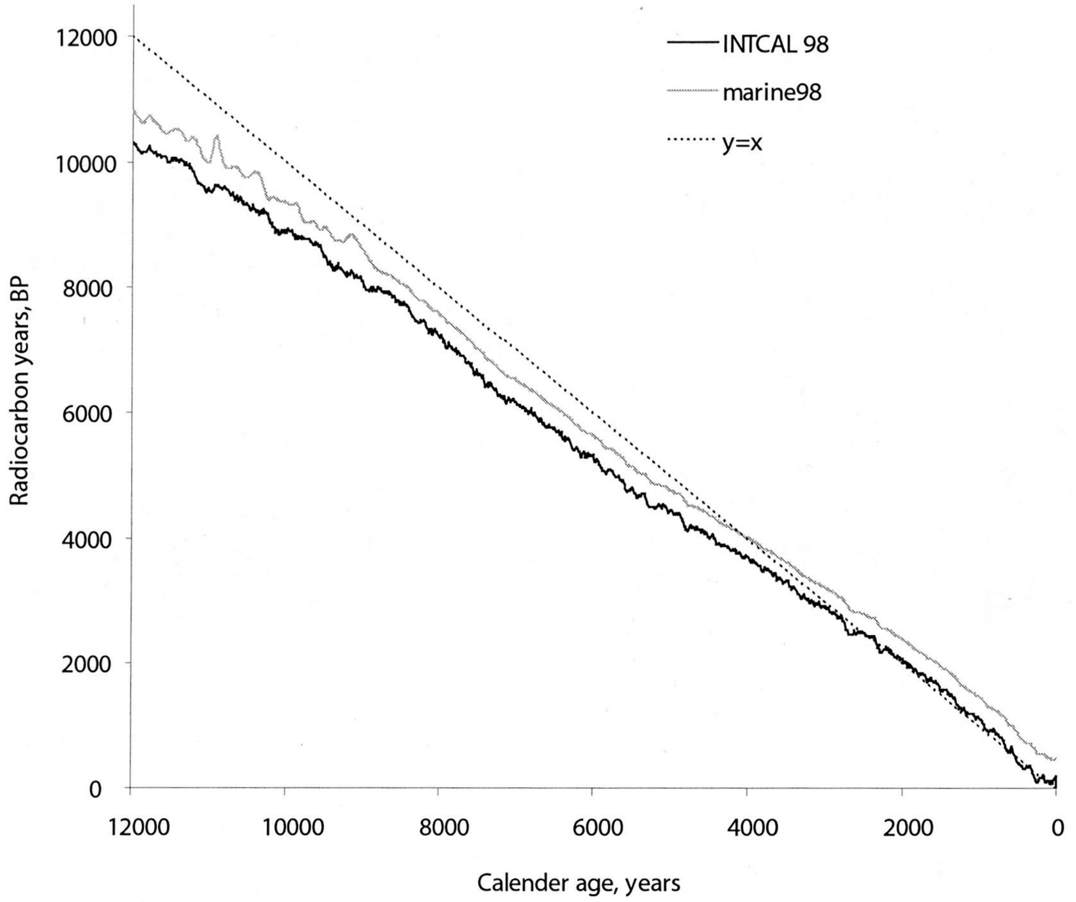

Figure 2.17 Atmospheric (INTCAL 98; solid black line) and marine (marine98; grey solid line) radiocarbon calibration curves from 12,000 cal BP to 0 cal BP (i.e. 1950 AD). Data from Stuiver *et al., (1*998a). Note the deviation of radiocarbon years away from the y=x line exemplifying the monotonic relationship of 1 calendar year = 1 radiocarbon year. The atmospheric calibration curve (INTCAL98) clearly shows a more detailed record than the smoother marine record.

Radiocarbon dates in this thesis were calibrated using the OxCal (v3) program (Bronk Ramsey, 1995, 1998, 2001). This Windows based program utilises a variety of statistical approaches such as intercept or probability methods on the empirical radiocarbon calibration curves of IntCal98 and marine98 (the atmospheric and marine radiocarbon calibration curves respectively; figure 2.17; Stuiver *et al.*, 1998a; Stuiver *et al.*, 1998b). The new calibrations curves; IntCal04 and Marine 04 (Hughen *et al.*, 2004b; Reimer *et al.*, 2004a) were not published at the time ^{14}C ages from the thesis were calibrated.

The surface ocean response to the atmospheric forcing of Δ^{14}C naturally filters the atmospheric data indicative of a 100-200 year moving average (Stuiver *et al.*, 1998a) and the deep ocean exhibits a buffering effect on atmospheric CO_2 (Levin & Hesshaimer, 2000), hence the marine curve is smoother than the atmospheric calibration curve (figure 2.17). Though the modelled global surface ocean reservoir age, *R, is taken to be 400 years (Stuiver & Braziunas, 1993), marine reservoir ages, R(t) can vary geographically and therefore are normally expressed as a deviation (ΔR) from the global average value. Calibration of radiocarbon dates with respect to marine reservoir ages and regional deviations are discussed in detail in chapter 4.

Currently, radiocarbon dates older than ~ 26 kcal BP cannot be calibrated reliably due to the dearth of empirical calibration data ranging from this age to the limitations of radiocarbon dating at ~40,000 years BP (Hughen *et al.*, 2004b; Reimer *et al.*, 2004a), though work continues to extend the limits of calibration (van der Plicht *et al.*, 2004). Material 'younger' than 1950 AD cannot be calibrated via conventional calibration curves due to interference from bomb produced ^{14}C, though a new calibration program CALIBomb (http://calib.qub.ac.uk/CALIBomb/frameset.html) was recently released to calibrate ^{14}C dates by the fraction of modern carbon (F^{14}C) in the sample (Reimer *et al.*, 2004b). Additional problems include the punctuation of the radiocarbon calibration curve by several radiocarbon plateaux of near constant ^{14}C age centred around approximately 12,700, 10, 000 and 9,500 years BP (Lowe & Walker, 1998), and the 'Suess effect'. Suess (1955) reported that the ^{14}C activity in 20th century wood was ~1 % less than the activity for mid-19th century wood (later recalculated to approximate 2.3-3% by Stuiver & Quay, 1981). This secular decrease in activity is attributed to the dilution of the atmospheric ^{14}C/^{12}C ratio by the combustion of ancient fossil fuels during the industrial revolution, which introduced inactive CO_2 (i.e. no ^{14}C) into the atmosphere. Stuiver & Quay (1981) reported a pre-bomb $\Delta^{14}C$ decrease of 20 ± 1.2 ‰ from wood samples obtained in 1949-1951 in comparison to the pre-industrial levels seen in 1855-1864, and indicated that the industrial CO_2 emissions up to 1950 accounted for ~85 % of the $\Delta^{14}C$ decline with the remaining 15% attributed to natural variability. This 'Suess effect' can also be seen in the ocean ^{14}C record (e.g. Sonnerup *et al.*, 1999; Körtzinger *et al.*, 2003) and is manifested by an increase in the reservoir age of the surface and deep ocean between the period 100-0 years BP (AD1850 – 1950; Stuiver *et al.*, 1986a).

2.7.7 Sample acquisition / Laboratory methods for ^{14}C dating of Scottish coastal material

2.7.7.1 Paired dates from a Loch Etive core (GC008) and a Loch Sunart core (SC102)

Gravity cores from Loch Etive along with Sholkovitch and gravity cores from Loch Sunart were inspected for horizons which contained shell material and plant material. There were few horizons with paired marine carbonate-terrestrial organic material, and some of these horizons were unsuitable due to low masses of organic material. Once extracted from the cores, the samples were rinsed with deionised water, dried at 40°C and placed in glass sample bottles.

Esbern Warncke (Biological Institute, University of Bergen, Norway, visiting scientist at the University of Aarhus, Denmark) inspected the terrestrial organic material from the cores. Sample AAR-7491 was identified as wood, possibly a fragment of birch twig, and sample AAR-7493 as oak fragments that are either charred or have been in an acidic environment. To ensure that the source of the organic material was terrigeneous, the C/N ratios of the sample material were determined following the technique of King *et al.,* (1998). The C/N ratios were measured by Mr. T. Brand at the Dunstaffnage Marine Laboratory, Oban.

The remaining organic and carbonate materials were prepared for AMS dating following the methods described in section 2.7.7.2 and analysed at Aarhus University, Denmark.

2.7.7.2 Preparation of historically collected (museum) shells

Ten molluscs collected prior to 1950 were obtained from the National Museum of Scotland, Edinburgh (details presented in chapter 4, table 4.2). The museum archives did not state whether the shells were collected live, but a live collection was assumed for articulated valves (i.e. connected at the hinge) since an unarticulated shell may be indicative of post-mortem disarticulation and possible reworking. Also, some of the specimens had the dried remains of the organism in the articulated shell, which may further suggest that the shell was live at the time of collection.

Two shells were rejected for dating, due to no known collection year. The Loch Creran bivalve (AAR-7489) is not accompanied by a known collection year (see table 4.1), however it was bequeathed to the museum by Alexander Somerville between 1843 – 1907 AD, so it is definitely pre-bomb and expands the data from the sea-loch environment. Additionally, the *Limaria hians* shell from the Clyde, was rejected for two reasons; 1) the shell morphology is such that when alive, the shell cannot be fully articulated, 2) the location was within the Clyde region, which was represented by other samples which came from more restricted marine environments.

The chemical preparation of the historical shell material (for the marine radiocarbon reservoir work) was carried out under the guidance of Prof. Jan Heinemeier, Ann-Berith Jensen and Vibeke Jensen at the AMS ^{14}C Dating Laboratory, University of Aarhus, Denmark.

Approximately 12 mg of carbonate shell material typically yields 1 mg of carbon, however ~40 mg of material was sliced from each sample to prepare for AMS dating, which allows for the potential loss of material during the pre-treatment processes and prepares enough carbon for two AMS dates. The periostracum was scraped off the shells where possible and on the larger scallop shells which are know to live for up to 6 years, the outer growth bands were selected to ensure that the youngest shell material was obtained. Sample material was prepared for AMS dating using the techniques reported in Heier-Nielsen *et al.,* (1995), i.e. cleaned, dried, and acid etched (using 1M HCl) to remove approximately 20-25% of the outer shell surface. The organic component was removed from the sample material by reduction methods (i.e. heating to 80°C for 12 hours in a solution containing $KMnO_4$). After cleaning and drying the sample the mass after chemical preparation was determined. Approximately 14 mg of the prepared sample was then carefully placed in the limb of a double limbed reaction tube. The remainder of the sample was placed in a labelled phial to be used later if necessary. Concentrated phosphoric acid was carefully placed in the other limb of the tube and a vacuum was created in the tubes using a vacuum rig. Once the tubes had been evacuated, the acid was added to the sample material and left overnight in a 25°C water bath, and the following reaction took place to convert the carbonate material into carbon dioxide (CO_2):

$$CaCO_3 + 2H^+ \xrightarrow{25°C} CO_2 + H_2O \qquad \textit{(Eq. 2.12)}$$

The CO_2 samples were then ready to be converted to graphite (since the conventional AMS dating method requires a source of solid carbon) as described in section 2.7.5.3.

For organic samples, carbonate material was removed from a 15 mg sample by adding 1M HCl acid and leaving for 1 hour at 80°C. The acid was removed and 1M NaOH added (left at 80°C for approximately 3 hours or longer with a solution change if necessary) to remove the humic fractions from the sample material. This is an important step as humic acids are highly mobile in terrestrial sedimentary environments and are often younger in age than the sample material itself. Sample SC102-68 was left at room temperature in 1M NaOH, as the material was too fragile for the usual procedure.

The base solution containing the humic fractions was decanted from the solid sample and 1M HCl was added to it, covered and left at 80°C for a few hours. An aliquot of 1M HCl was added to the solid sample and left for 1 hour at room temperature, after which the sample material for dating was rinsed with deionised water and freeze dried. Once dry, the sample was weighed again and approximately 50 % taken for graphitisation. The material for dating was placed in a quartz ampule containing copper oxide, vacuumed and sealed, and combusted at 900°C for on a 1hour cycle in a muffle furnace for the following reaction to take place:

$$C \xrightarrow[900°C]{CuO} CO_2 + Cu \qquad \textit{(Eq. 2.13)}$$

The humic fraction was centrifuged, freeze dried and weighed to determine the percentage of humics in the sample. This fraction was not used in dating and was later discarded.

The vessels containing the prepared carbonate and organic material for dating were attached to the graphitisation machine. For each sample, the necessary volume of CO_2 gas to make 1.1 mg of Carbon was moved across to a reaction tube (containing a small amount of Cobalt powder) after gas had been collected for $\delta^{13}C$ measurements. The required volume of H_2 gas was then added to the reactor tubes for the following reaction to take place;

$$CO_2 + 2H_2 \xrightarrow[700°C]{Co} C + 2H_2O \qquad \textit{(Eq. 2.14)}$$

The 1st reactor tubes were cooled to -35°C to freeze out the water and the 2nd reactor tubes were left at 700°C overnight for the reaction to complete. The resulting graphite material was embedded in a labelled cathode using silver powder and a machine press, and the sample was taken for AMS dating.

All the ^{14}C measurements were carried out using the EN tandem accelerator at the University of Aarhus. The tandem accelerator lacks the sensitivity to measure ^{13}C isotopes precisely, therefore AMS measurements use the ^{14}C /^{12}C ratio measured at Aarhus and the $\delta^{13}C$ values were measured by Dr. Á. E. Sveinbjörnsdóttir, at the Science Institute, Reykjavík, Iceland.

2.7.7.3 Geochronology for Loch Sunart cores GC023 and SC023.

Sample material suitable for AMS radiocarbon dating was collected from gravity core (GC023) and Sholkovitch core (SC023) obtained from Loch Sunart. The sample material was cleaned, dried and sent to the NERC Radiocarbon Laboratory at East Kilbride for pre-treatment and dating.

2.8 Statistical methods

Basic statistics, such as the mean, linear regressions and Pearson's linear correlations (Davis, 2002) were carried out using Minitab v14. Formulas for other statistical methods used in this thesis are provided in the relevant chapters and detailed methodologies can be obtained from Davis (2002).

CHAPTER 3 – INSTRUMENTAL RECORDS FROM NW SCOTLAND: CLIMATE AND HYDROGRAPHY

3.1 Introduction

The proximity of the UK to the Atlantic Ocean and the Gulf Stream typically results in the UK experiencing mild and wet weather (e.g. Bigg, 1996). The climate of NW Europe is heavily influenced by the North Atlantic Oscillation (NAO), which is the dominant mode of atmospheric variability in the Northern Hemisphere (e.g. Hurrell, 1995, 1996), particularly during the winter months (section 1.3). The positive (or high index) phases of the NAO are characterised by the occurrence of a strong high-pressure system over the Azores region along with an intense Icelandic low pressure. During these phases the Atlantic storm track is deflected northwards bringing warm and saturated 'oceanic' air masses to NW Europe (Ruprecht *et al.*, 2002) and results in a mild and wet winter over NW Europe. Conversely, during negative (low) index years, the storm track is deflected towards southern Europe and NW Europe generally experiences cold and dry winters.

The high relief of the Loch Sunart catchment area (figure 2.2), along with it's location on the NW European margin (figure 2.1) results in a high amount of orographic rainfall received from the prevailing westerly weather system, thus the climate of this region is likely to be strongly influenced by the NAO. Hurrell (1995) showed that the correlation coefficients between winter (December-March) precipitation and the NAO index for a number of European stations were stronger for coastal stations (e.g. Bergen: 0.77 and Stornoway: 0.75) than for inland stations (e.g. Oslo: 0.21 and Frankfurt: 0.19). Chandler & Wheater (2002) have also demonstrated the seasonally varying impact of the NAO upon rainfall variability from the west of Ireland. The coastal catchments of NW Scotland receive high mean annual precipitation and are also expected to exhibit high correlation coefficients with the NAO. Thin and poorly developed soils in these mountainous regions, together with generally steep slopes and low soil moisture deficits, translate rainfall rapidly into surface runoff (Black & Cranston, 1995). Therefore, periods of prolonged and heavy rainfall result in a pronounced increase in freshwater input into the fjords.

Given the importance of freshwater inputs in fjordic hydrography (section 1.8.2), the NAO has the potential to impact upon the circulation of Loch Sunart, with positive index years resulting in less frequent deep water renewal events and lower salinity in the upper basins, and vice versa for negative index years. Sedimentary archives obtained from Loch Sunart have the potential to yield palaeoclimatic information on North Atlantic climate and oceanographic variability. There is a dearth of long-term observational data from Scottish sea lochs, so to test whether the NAO does significantly influence the circulation of Loch Sunart, a modeling approach was implemented for an extreme positive NAO year (1988) and an extreme negative year (1996; Jones *et al.*, 1997) using daily wind and freshwater discharge data (from nearby stations) as inputs (Gillibrand *et al.,* 2005).

3.2 Aims and objectives

Climate and oceanographic data from NW Scotland are scarce. A long, monthly marine temperature series is available from Millport from 1953 onwards and the Scottish Environmental Protection Agency (SEPA) has recorded the precipitation and temperature in the nearby Polloch catchment and the mean daily discharge of the River Polloch since 1986 (see figure 3.1 for locations). Jones & Lister (2004) have recently published long (~100 years) regional temperature data for Scotland and Northern Ireland (see section 3.4.1). Thus, the major aims of the study were:

1) To test whether the Loch Sunart catchment experiences similar climate to nearby stations with longer time series. A weather station was placed at Ariundle (in the Loch Sunart catchment area, figure 2.5) to record the prevailing weather at the head of the loch over a 2 year period (see chapter 2). Pearson's linear correlations and regression techniques were used to compare the temperature and precipitation data from the overlap of the Ariundle observations, the recorded data from the Polloch weather station and the longer temperature series of Jones & Lister (2004).
2) To identify how the NAO influences the local climate of NW Scotland using the NAO indices of Jones *et al.,* (1997).
3) To observe the temperature and salinity at 40 m water depth in the inner and main basins of Loch Sunart over an annual cycle using stationary hydrographic moorings (section 2.3.1), and to compare these data with

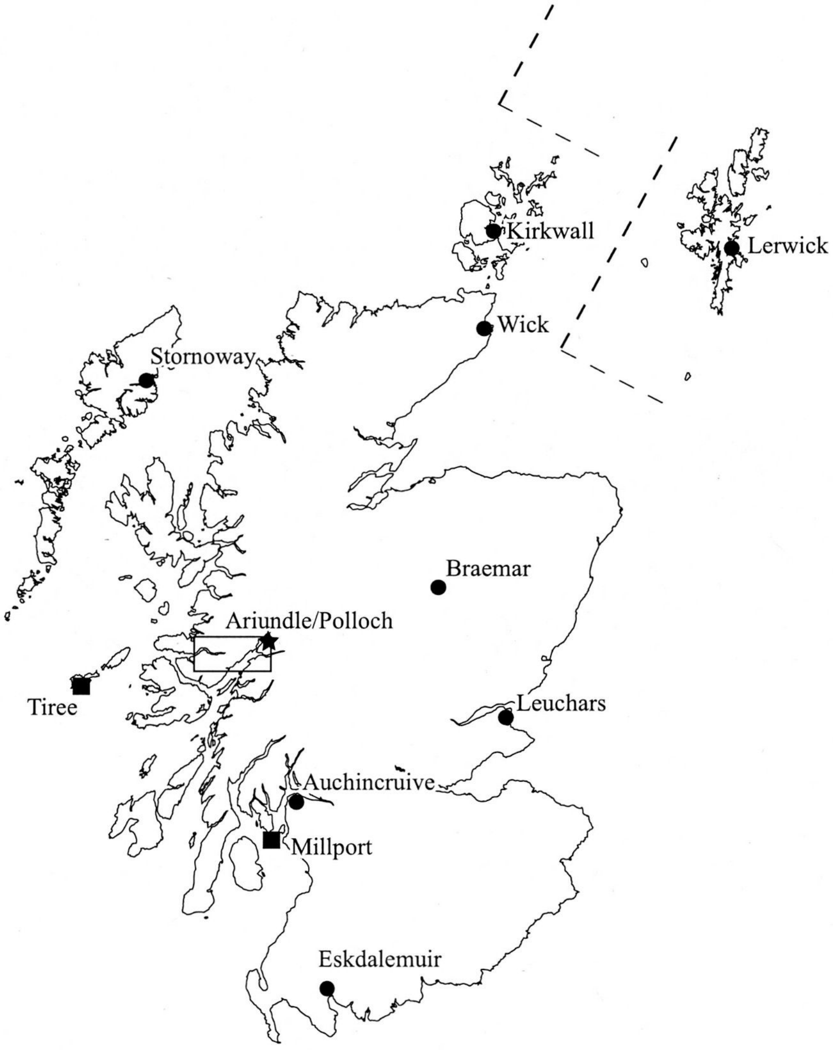

Figure 3.1 Station locations for the Ariundle and Polloch weather stations (star) along with the stations included in the Scottish air temperature series (black circles) from Jones & Lister, 2004. The ScottishIsles temperature (SIT) series consists of data from Stornoway, Kirkwall and Lerwick; the Northern Ireland temperature (NIT) series has data from Armagh only (not shown) and the Scottish Mainland temperature (SMT) series combines data from Wick, Braemar, Leuchars, Auchincruive and Eskdalemuir. Marine temperature series are shown by black squares (Tiree Passage data courtesy of Dr. Mark Inall, DunstaffnageMarine Laboratories, Millport data courtesy of Dr. P. Barnett, University Marine Biological Station, Millport).

catchment climate to identify possible forcing mechanisms of fjordic circulation.

4) To compare Loch Sunart hydrography to other marine temperature series (Millport and Tiree) and compare the marine temperature data with air temperature data from Jones & Lister (2004). If a strong correlation exists, the marine temperature series will be extended back to at least AD 1844 via regression techniques.
5) Investigate the influence of NAO-forced climate on the circulation of the inner basin and main basin of Loch Sunart during extreme positive and negative NAO years using the established circulation model of Elliott *et al.,* (1992) and Gillibrand *et al.,* (1995). See Gillibrand *et al.*, (2005) for details.

3.3. RESULTS OF METEOROLOGICAL DATA

3.3.1. New instrumental data

The observed temperature, wind speed, wind run and precipitation data from the Ariundle weather station over the observed period, 23/04/2001 - 28/07/2001 and the 14/08/2001 - 04/09/2003, are reported in appendix 5. Seasonality in the temperature data is evident (figure 3.2), with warmer temperatures occurring during summer months (June, July, August) and cooler temperatures occurring in the winter months (December, January, February). Clear seasonal signals are not immediately seen in the precipitation, wind run and maximum wind speed, though maximum values do tend to occur in the winter months (figure 3.2). Because wind data is missing from the first Kipp & Zonen weather station deployment (section 2.4.2.2), analyses will focus on data collected from the second Campbell Scientific weather station 14/08/2001 - 04/09/2003.

Histograms in figure 3.3 illustrate the large variability of meteorological data experienced by the Ariundle weather station over the observed time period, and the unimodal spread of the data reflects a strong seasonal forcing. The histograms for maximum daily wind speed (ms^{-1}) and total wind run (km per 24 hours) are similar due to the positive relationship between these two variables (figure 3.4) i.e. during periods of maximum wind speed, more wind passes through the sensor.

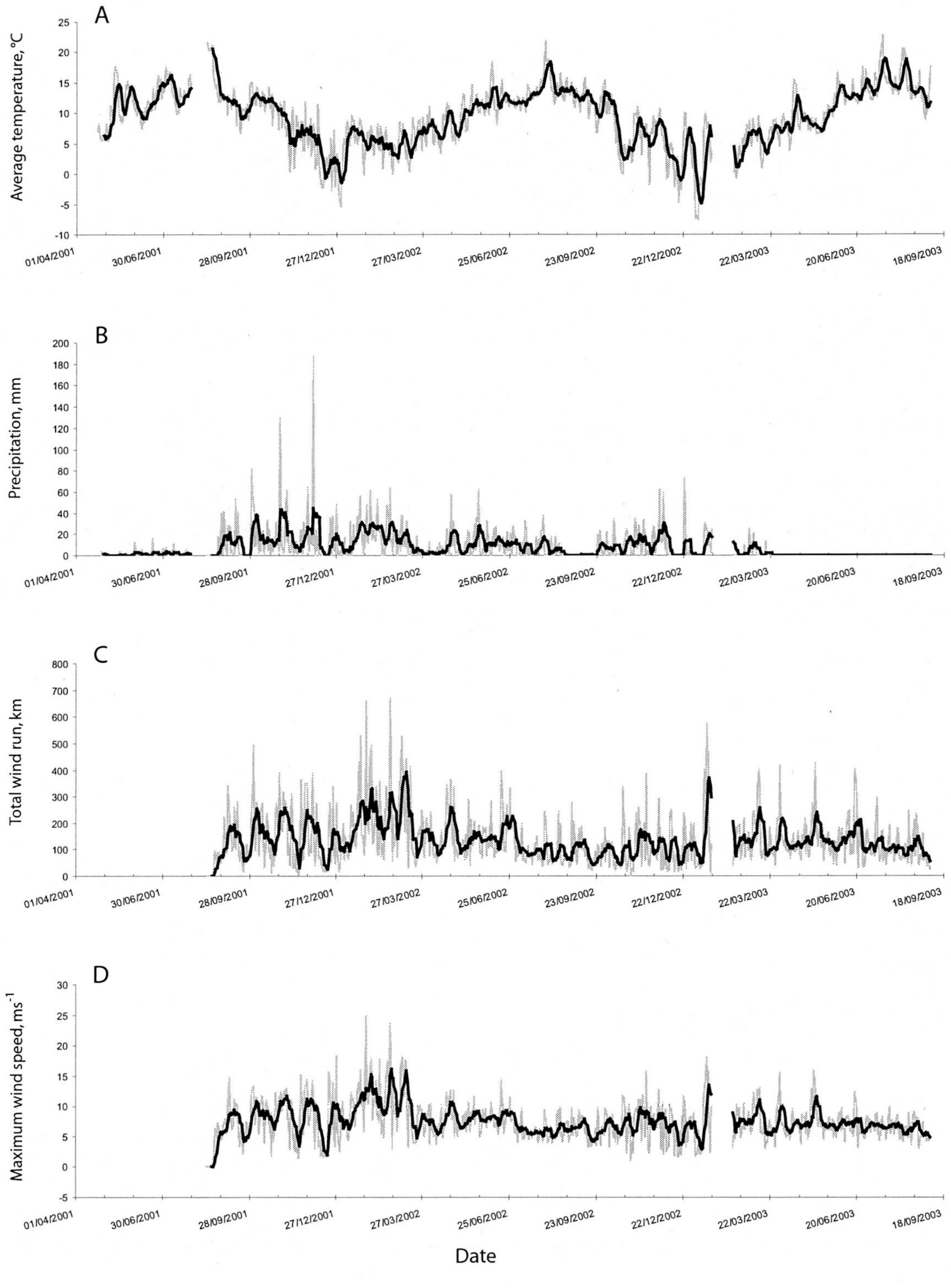

Figure 3.2 Daily data (with a 7 point moving average) from the Ariundle weather station showing: A) average temperature; B) precipitation; C) total wind run over 24 hours and D) maximum wind speed.

3.3.2 *Data quality*

The weather station was left unattended for periods of a few months and during this time it is possible that the rain gauge could have been blocked by organic debris such as leaf litter and bird faeces. However, the internal tipping mechanism was checked during each visit and there were no signs of blockages.

A few problems occurred during the collecting of the data: 1) The first 8 days of data collection (14/08/2001 - 22/08/2001) show zero values for precipitation, wind run and wind speed. Zero precipitation days occur throughout the precipitation data and account for approximately 21% of the data collection period. However, with the exception of the first 8 days, no other days record zero wind speed and wind run suggesting that the zero days do not truly represent the weather conditions at the time of collection and are therefore anomalous measurements. Therefore the measurements from these days are not included in the final data set. There is no explanation as to why data collection begins on the 23/08/01; 2) Data was lost between 21/01/2003 – 11/02/2003 due to overwriting by the data-logger and; 3) Precipitation data is unavailable from the 17/03/2003 onwards due to problems with wildlife (possibly a *Marag fabulosus aurelius*) destroying the electric cables running between the rain gauge and the weather station.

3.3.3 Validation with Polloch temperature and precipitation data

The Ariundle temperature series is in good agreement with the Polloch temperature data (figure 3.5), with a strong positive correlation ($r = 0.93$, $p = 0.0$) and an R^2 value of 0.88. Figure 3.5 shows three obvious anomalies within the Polloch temperature data. These anomalous temperatures occur in May and July; months which are unlikely to have daily mean temperatures of approximately -11 and -5 °C. Removing these data improves the relationship between the 2 variables, giving a regression equation of $y = 0.9688\ x + 0.5092$ ($R^2 = 0.8763$) rather than $y = 0.9182\ x + 1.0224$ ($R^2 = 0.8202$). There are other data points which appear to be anomalous, for example, those lying above the regression line at around 5°C for Polloch temperature and ~13°C for Ariundle temperature. These data points occur within summer months and could be due to local effects experienced at the different weather station locations.

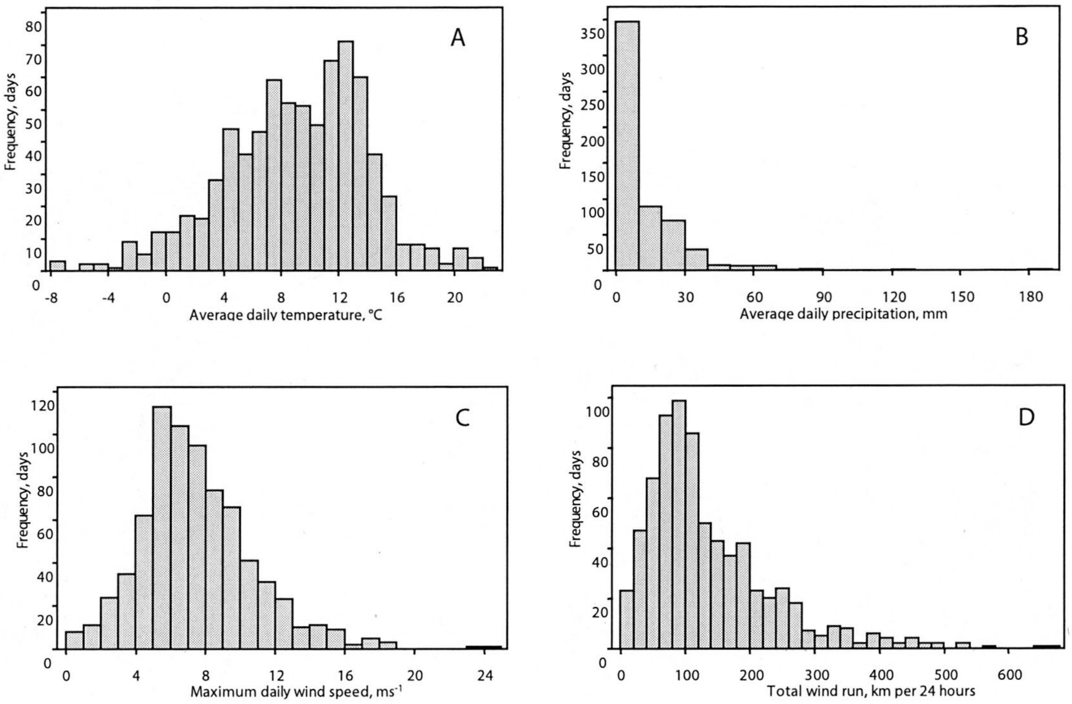

Figure 3.3 Histograms showing the frequency, i.e. number of days of A) average daily temperature (1 bar = 1 °C); B) average daily precipitation (1 bar = 10 mm); C) maximum daily wind speed (1 bar = 1 ms^{-1}) and D) total daily wind run experienced (1 bar = 20 km per 24 hours) at the Ariundle weather station over the collection period 14/08/2001 - 4/09/2003 (14/08/2001 - 17/03/2003 for the precipitation data).

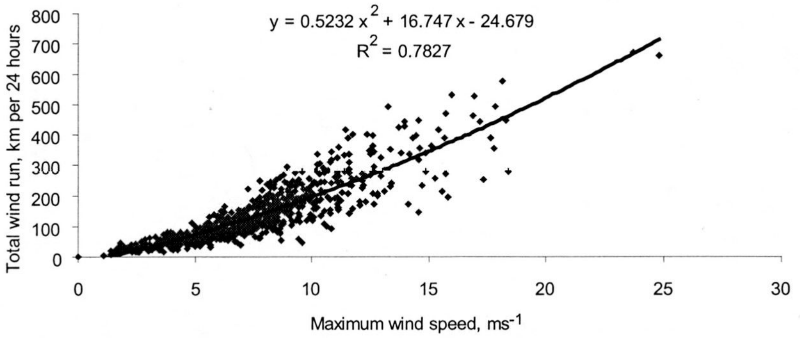

Figure 3.4 The strong positive relationship between maximum daily wind speed and total wind run recorded by the Ariundle weather station for the collection period 23/08/2001 to 4/09/2003.

The gradient from the linear regression equation (Ariundle temperature = 0.9688* Polloch temperature + 0.5092, figure 3.5) suggests the Ariundle weather station experiences similar temperature trends to the Polloch weather station albeit with temperatures being about 0.5 °C warmer. This offset could be due to either local effects experienced due to the different station locations, or by anomalies within the data set.

A fairly strong positive correlation exists between the two data precipitation sets ($r = 0.693$, $p = 0.0$, $R^2 = 0.48$) and figure 3.6 suggests the Ariundle station receives slightly higher levels of precipitation than the Polloch station. The Ariundle-Polloch precipitation relationship is not as strong as the temperature relationship and this is likely to be due to local effects such as topography and rain shadowing, however the two stations clearly exhibit similar precipitation patterns, i.e. experience the same weather systems (figure 3.7). The intensity and occurrence of precipitation varies between the two stations (figure 3.8) with the Polloch station recording more days with zero or light to moderate precipitation (1-15 mm) and the Ariundle station tending towards heavier precipitation days. However, the relationship between the two data sets is much stronger ($r = 0.911$, $p = 0.0$) when the total monthly precipitation data is compared (figure 3.9). This suggests that although precipitation values between the two neighbouring catchments may differ on a day to day basis, the total monthly precipitation received by the catchments is comparable with the Ariundle station receiving higher precipitation per month.

3.3.4 Seasonal and inter-annual differences in Ariundle weather

The NAO is known to affect the winter weather of the UK (see chapter 1). The data obtained from the Ariundle weather station covers two winter periods; 2001/2002 and 2002/2003. NAO indices are ascribed to the latter year of the winter period (since the majority of the monthly pressure data lie in this year), hence these two periods become NAO years of 2002 and 2003. Although both 2002 and 2003 are NAO positive years, the indices differ at +0.79 and +0.4 respectively, thus one would expect the winter of 2002 to be milder and wetter than the winter of 2003.

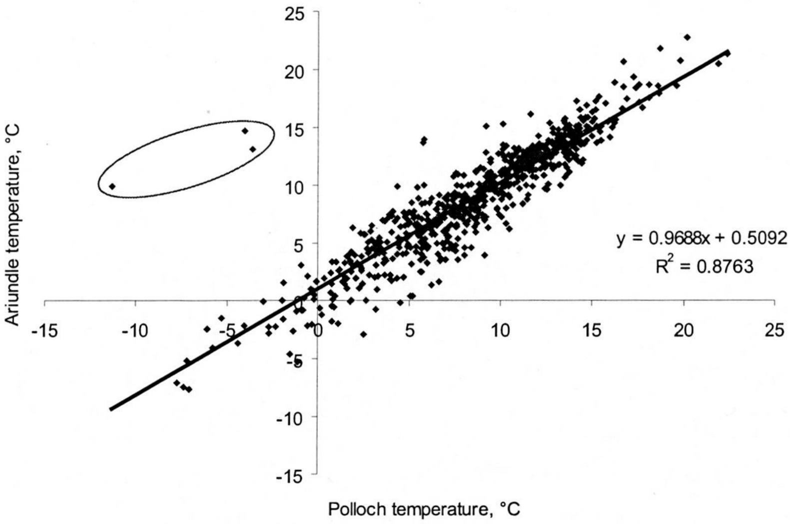

Figure 3.5. Bi-variate regression of the Polloch air temperature (data courtesy of SEPA) and Ariundle air temperature data. Obvious anomalies in the data are highlighted by the ellipse. The regression equation and R^2 value from the linear regression excluding the anomalies are also shown.

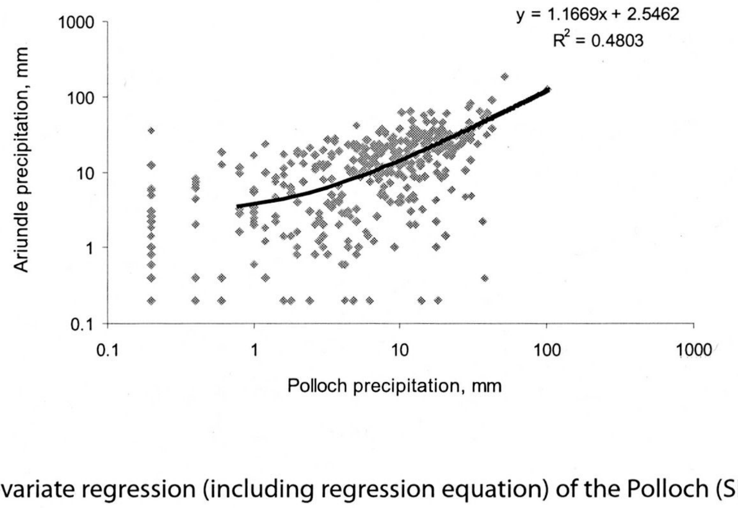

Figure 3.6 Bi-variate regression (including regression equation) of the Polloch (SEPA) and Ariundle daily precipitation.

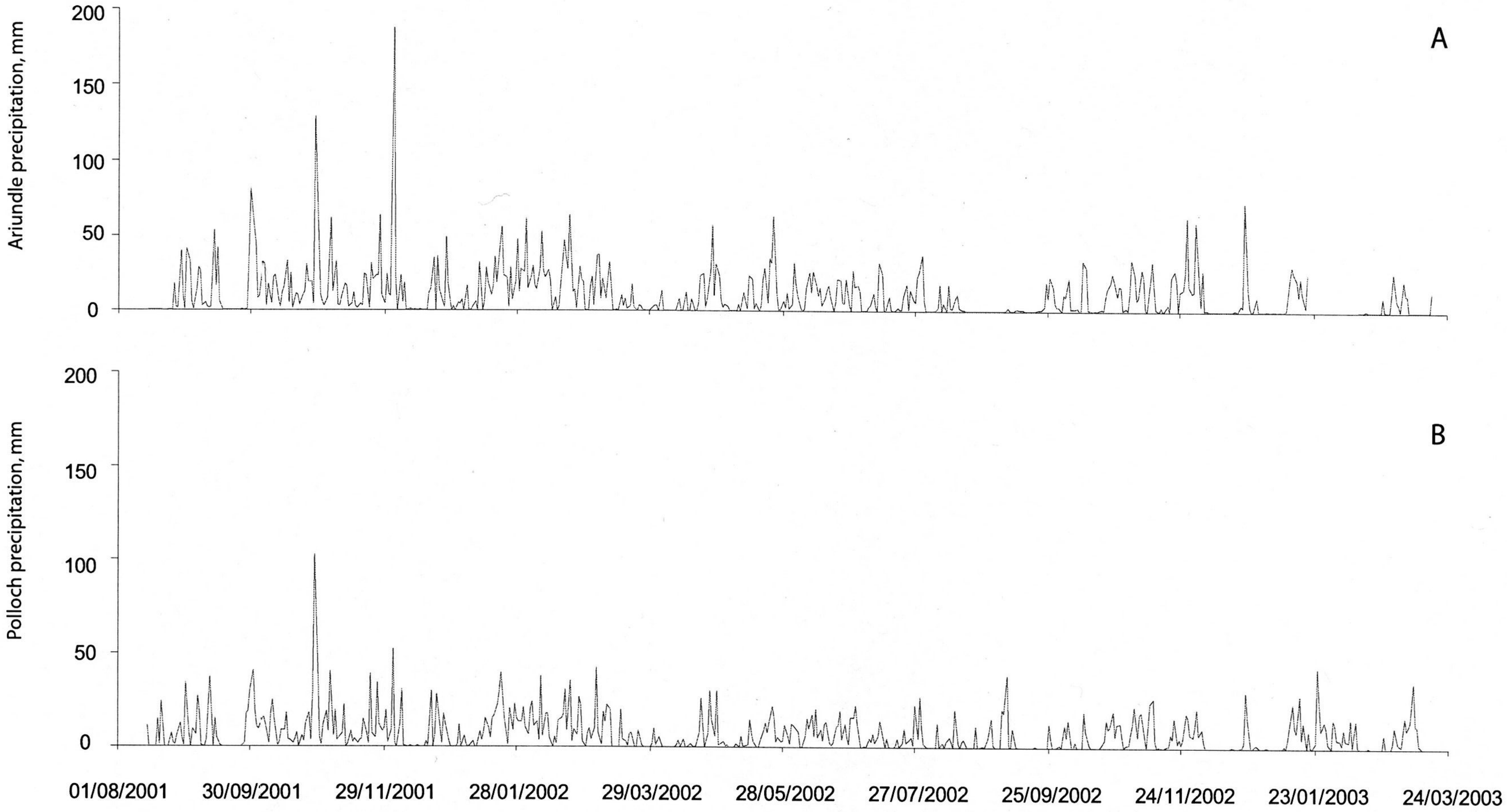

Figure 3.7 Daily precipitation data from the Ariundle weather station (A) collected between 23/08/2001 and the 17/03/2003, and the nearby SEPA Polloch weather station (B). Both stations show similar precipitation trends with the Ariundle station recording higher amounts of precipitation.

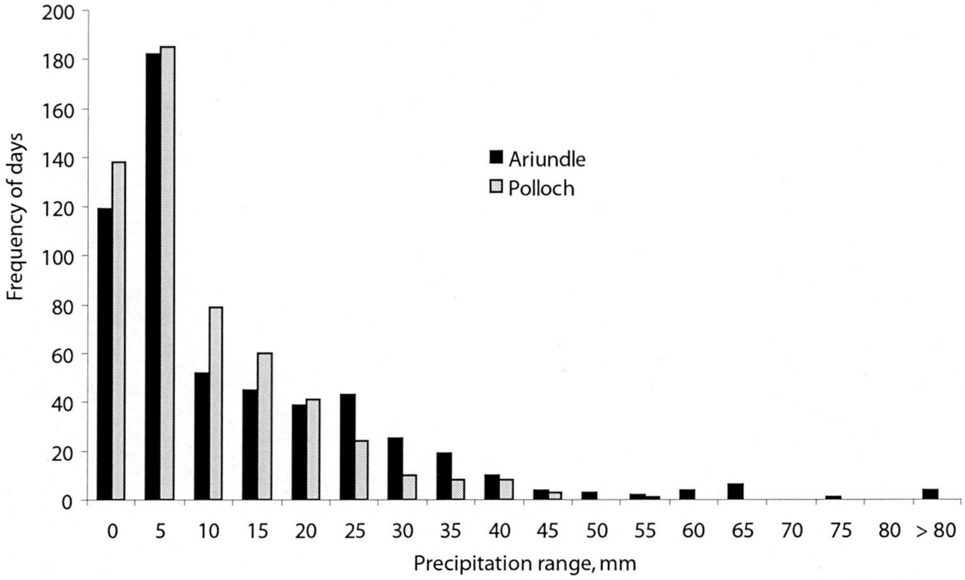

Figure 3.8. Histogram showing the daily precipitation received in the Ariundle (black) catchment in comparison to the daily precipitation recorded at the Polloch station (grey; data from SEPA) between 14/08/2001 and 17/03/2003. The 'bin' size of the histogram is 5 mm.

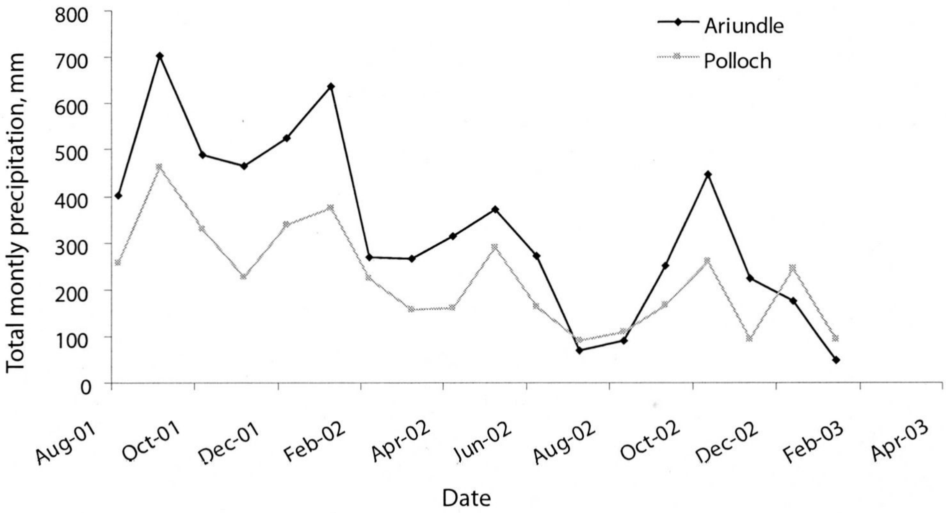

Figure 3.9 Total monthly precipitation from the Ariundle station (black line) and the Polloch station (grey line; data from SEPA) between August 2001 and February 2003. Linear regression between these two data sets gives a regression equation of Polloch precipitation = 1.6068* Ariundle precipitation -26.489 ($R^2 = 0.8298$)

The Ariundle weather data can be averaged over the seasons of the collection period (table 3.1). Winter is taken as December, January and February; Spring as March, April and May; Summer as June, July and August and Autumn as September, October and November. As predicted, during the more positive NAO year (2002), Ariundle experienced a milder and wetter winter than during 2003, with an average temperature of 4.1 °C and an average daily precipitation of 18.1 mm in comparison to the averages of 2.8 °C and 6.5 mm precipitation recorded at Ariundle during the 2003 winter (figure 3.10). The total wind run (i.e. over the season) at Ariundle is also greater in 2002 (15978 km) than in 2003 (8636 km), probably due to the Atlantic storm track being slightly deflected to the south during the less positive NAO year.

3.4 RESULTS OF OCEANOGRAPHIC DATA

3.4.1 CTD data

Temperature and salinity (CTD) profiles taken along the central axis of Loch Sunart all show a distinct thermocline and halocline (typically occurring at similar water depths) demonstrating the stratification typical of fjords (figure 3.11; Farmer & Freeland, 1983). Most profiles (excluding figure 3.11F) show a well-defined surface layer approximately 1-3 m thick with temperatures typically 1-2 °C warmer than the water below and fresher, with salinities reduced by ~ 0.4 in the outer basin, ~ 2 in the main basin and up to 6 in the inner basin (a salinity of 10 was recorded near the Carnoch river inflow). A transitional layer exists beneath the surface layer showing steadily decreasing temperature and increasing salinities. This layer is more prevalent in the temperature profile with salinity typically reaching a near stable value higher up the water column, whilst temperature continues to decrease (e.g. figures 3.11 C and E). Deep basin water typically demonstrates a slighter higher salinity than the transitional layer, with temperatures typically 1-2 °C cooler than the sub-thermocline temperatures (~ 10-11 °C).

An important point to note is that for most profiles, the temperature and salinity at 40m water depth is similar to temperature and salinity at water depths deeper than 40m (e.g. figure 3.11 A and B). This suggests that the annual heating cycle observed by the mooring sensors at ~ 40 m water depth (figure 2.11) is likely to be representative of temperatures in the deeper basin waters, although a 'lag' in the

Table 3.1 Seasonal averages for the Ariundle weather station data. Winter is taken as December, January and February; Spring as March, April and May; Summer as June, July and August and Autumn as September, October and November.

Year	Season	Average temperature, °C	Total precipitation, mm	Average daily precipitation, mm	Maximum wind speed, ms^{-1}	Total wind run per 3 months	Average wind run, km per 24 hrs
2001	Autumn	9.9	1594.2	17.5	8.3	14526.8	159.6
2002	Winter	4.1	1628.6	18.1	9.6	15977.5	177.5
	Spring	8.0	848.4	9.2	8.3	15156.2	164.7
	Summer	13.3	710.8	7.7	6.8	10777.6	117.2
	Autumn	8.7	789.6	8.7	6.9	9112.2	100.1
2003	Winter	2.8	444.8	6.5	6.9	8635.7	127.0
	Spring	8.2	-	-	7.5	12991.7	141.2
	Summer	14.3	-	-	6.6	11039.1	120.0

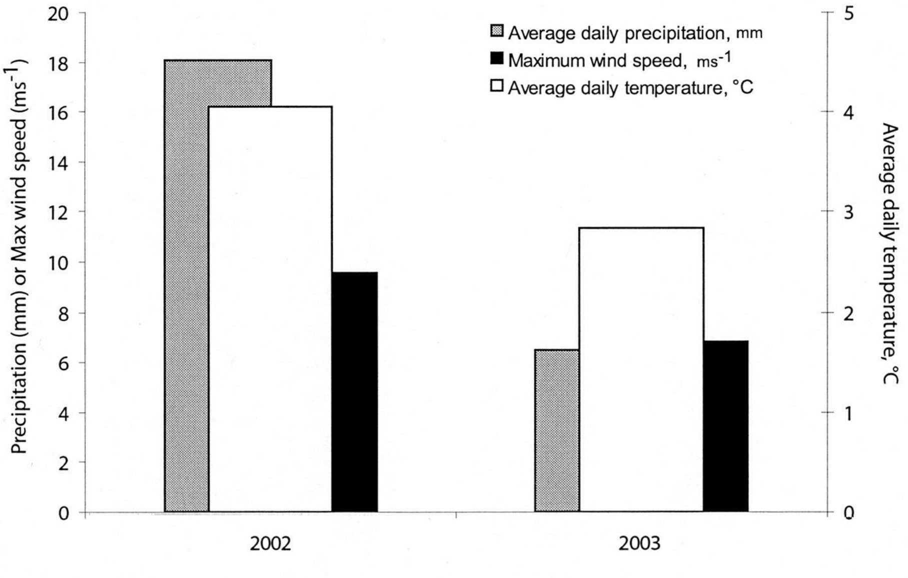

Figure 3.10. Comparison of Ariundle winter weather data for 2002 and 2003, which have positive NAO indices of 0.79 and 0.4 respectively. Temperature, precipitation and wind speed are all greater during the more positive NAO year, 2002. The total wind run is not shown, however there is a strong positive relationship between maximum wind speed and total wind run (figure 3.4), thus the total wind run experienced at Ariundle is likely to be greater during the more positive NAO year of 2002.

Figure 3.11. Salinity (grey line) and temperature (black line) profiles along the central axis of Loch Sunart obtained using an STD Plus 646 CTD instrument measuring conductivity, temperature and depth. Profiles obtained during June 2002. The black arrows in the Sunart catchment indicate major tributaries entering the loch. Profile A is taken from the outer basin, profiles B-D from the main basin and profiles E-H are from the inner basin. Note that vertical scales differ.

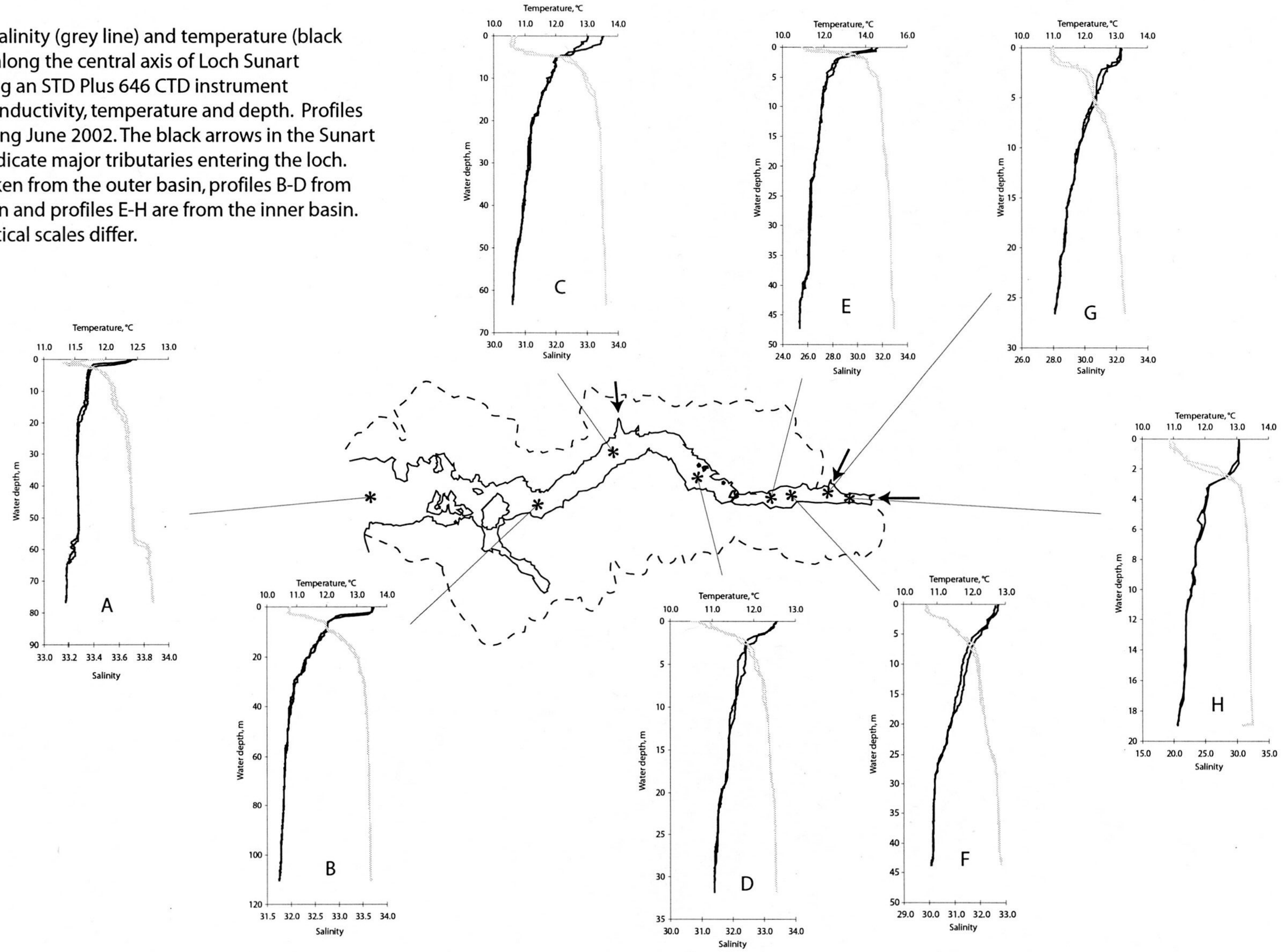

temperature signal may occur in the deeper (> 100 m) waters (e.g. Ellett, 1979, figure 2.8).

3.4.2 Mooring data

Figure 3.12 shows the hourly temperature and salinity readings recorded in the main basin from 7/04/2001 to the 17/6/2002 (yielding 10453 observations) and in the inner basin from 27/6/2001 to the 18/6/2002 (yielding 8541 observations). CTD casts taken to calibrate the moorings agree well with the mooring data (figure 3.12) and although the salinity difference between the mooring and the CTD is ~0.25, the data is valid for use (*pers. comm.,* Dr. P. Gillibrand, 2002).

3.4.2.1 Temperature

The inner and main basins both show strong seasonal trends in bottom water temperature (figure 3.12a). Over the same period of the seasonal cycle, the inner basin has an annual average temperature of 10.79 °C (range 7.70 – 13.46 °C) and whilst the main basin has a cooler minimum and annual average temperature of 6.86 °C and 10.24 °C respectively, the maximum temperature is comparable to the inner basin maximum temperature at 13.47 °C. Although the two bottom water temperature trends are similar for both basins, showing strong seasonal warming and cooling, the main basin temperature record appears to occasionally lag behind the inner basin record. The lag time is not consistent throughout the year, for example, there is about a 2 week difference between the maximum temperature peaks (with the upper basin preceding the main basin), whilst the minimum temperatures occur within approximately 1 week of each other (figure 3.12a). However, from early December to late January, the stepwise decrease in the main basin temperature trend slightly precedes the inner basin trend by 5-7 days and the climbing limb of increasing temperatures after April 2002 shows interchangeable lags between the main and upper basins.

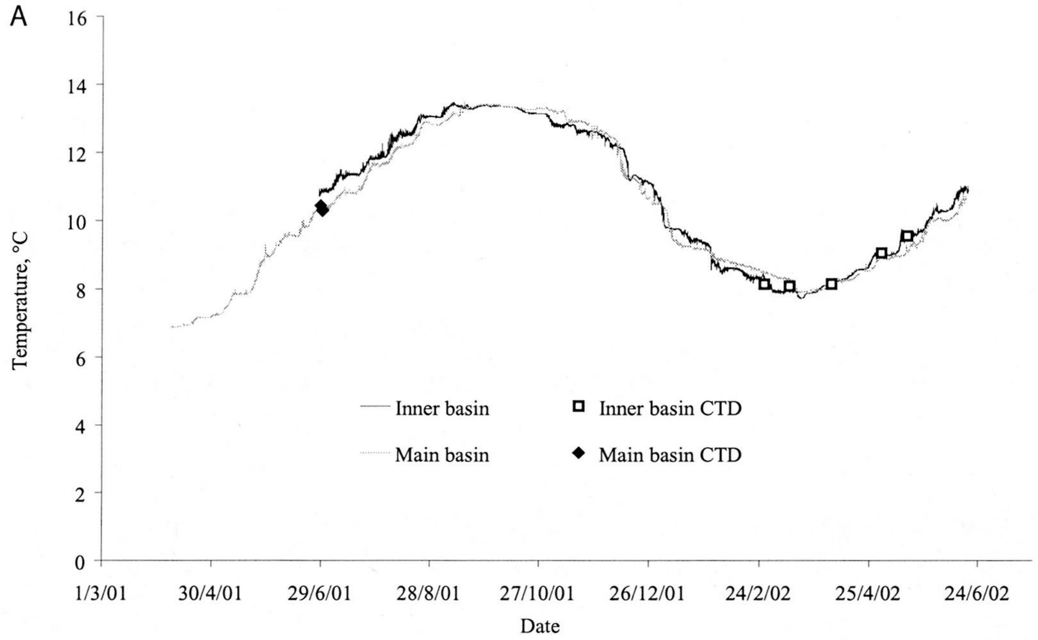

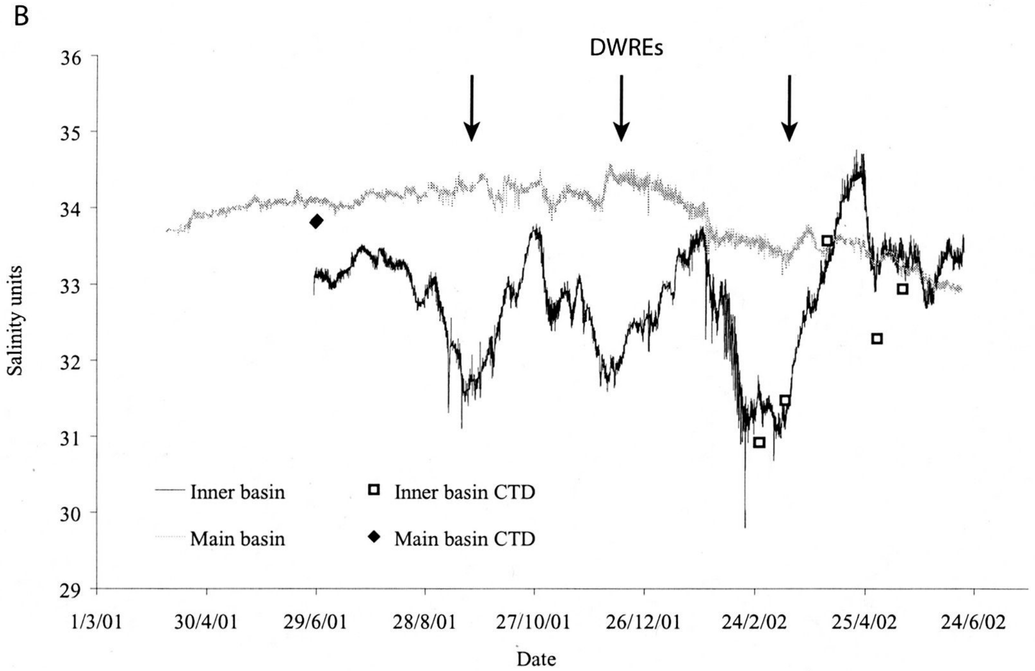

Figure 3.12 Hourly temperature (A) and salinity (B) data from the inner basin mooring (black line) and main basin mooring (grey line) from Loch Sunart. Data courtesy of Dr. P. Gillibrand (Fisheries Research Services, Aberdeen) collected using Anderaa RCM-7 current meters equipped with data loggers and temperature and conductivity sensors. The mooring data were calibrated using CTD casts taken throughout the collection period. Deep water renewal events (DWREs) are indicated by black arrows.

3.4.2.2 *Salinity*

The data from the Loch Sunart moorings show two very different series for the inner and main basins (figure 3.12b). The inner basin is generally less saline than the main basin with average salinities of 32.8 and 33.9 respectively. Both series show high variability on a daily resolution, though the trends in salinity are in no way comparable (figure 3.12b). The salinity of the main basin remains relatively stable at 34, until January 2002 when it decreases to a minimum salinity of 32.9 at the end of the observation period. The inner basin shows far more variability (on a weekly/monthly basis) in salinity than the main basin, with the salinity reaching minimum values of approximately 31 - 31.7 before increasing to salinities of 33.7 – 34, i.e. the occurrence of DWREs (figure 3.12b). From April 2002 onwards, the inner basin waters become more saline, approaching the salinity of the main basin water (figure 3.12b). This is unusual since the inner basin water is typically derived from a mixture of saline main basin water and entrained sill water (which is a mixture of saline and brackish surface water) during deep water renewal events. The CTD casts either side of this high salinity period appear to tie in well with the mooring data, suggesting this is a 'real' event, however the mechanism behind this inner basin high salinity event is unresolved at present (*pers. comm.,* Dr. P. Gillibrand, 2004).

3.5 DISCUSSION

3.5.1 Comparing the Ariundle air temperature series with regional air temperature series

The close correlation of the Ariundle and Polloch temperature and precipitation series suggest the data recorded during the relatively short interval of this study at Ariundle is reliable and suggests both sites experiences the same weather subject to local microclimate effects.

The meteorological data series for the Ariundle weather station is limited in duration. In order to statistically extend the data for this site, the temperature data from Ariundle was compared to long temperature series from the Scottish mainland (SMT), the Scottish Islands (SIT) and Northern Ireland (NIT) obtained from by Phil Jones, University of East Anglia via the HOLSMEER project. The SMT data (figure 3.13) comprised of data from five stations; Auchincruive, Leuchars, Wick (all coastal stations), Braemar and Eskdalemuir (both inland stations). The SIT data is based on data from three stations, Kirkwall, Lerwick and Stornoway and the NIT series represents data from the Armargh station. Station locations are shown in figure 3.1 and further discussion of these data series is presented in Jones & Lister (2004). The Central England Temperature (CET) series (Manley, 1974; Parker *et al.*, 1992) takes the averaged temperatures from stations situated in London, Bristol and Manchester. The CET series spans the longest time frame, extending back to AD 1659, whilst the SMT series spans AD 1800 to AD 2002, the SIT spans AD 1827 to AD 2002 and the NIT series spans from AD 1844 to AD 2002.

There are clear differences in these long temperature series (figure 3.13). Between AD 1844-2002, the mean temperatures are as follows; the CET series has the highest mean temperature at 9.38°C, likely reflecting warmer temperatures from southerly stations; the NIT data has a temperature mean of 8.48°C, and the SIT mean temperature of 7.70°C. The lowest temperature mean (7.03°C) belongs to the SMT series and is likely to be a function of the location of stations used in this data series, e.g. data from inland meteorological stations contribute to this series as do stations in the NE Scotland (such as Leuchars) which may tend towards cooler temperatures than those on the west and north coast. All the data series show a trend towards increasing temperatures towards the 21st Century (table 3.2) with the majority of the warming occuring in the 20th Century, which is consistent with trends found in other studies (Mann *et al.*, 1998; Moberg *et al.*, 2005).

The CET, SMT, SIT and NIT temperature data show very strong positive correlations with Ariundle temperature data (table 3.3), suggesting all localities are affected by the same weather systems. The strongest correlations are with the SMT and NIT data. Like the Ardnamurchan peninsula, Armagh (NIT) is likely to receive the Atlantic weather systems first, i.e. has a strong maritime climate. Three out of the five stations in the SMT data are coastal (west and east coast) thus the data is also likely influenced by a maritime climate, as is the slightly inland Ariundle station. The weakest relationship unexpectedly comes from the SIT data, which have stations relatively near to Sunart (figure 3.1). This could be due to the dampening of the air temperatures by heat transfer from surrounding ocean water (since oceans have higher

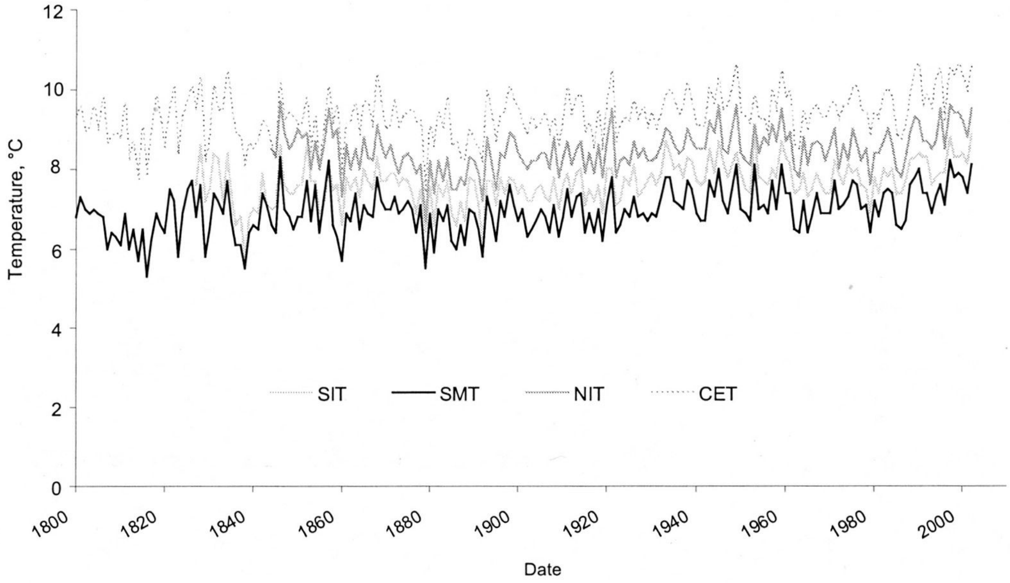

Figure 3.13. Air temperature series (annual averages) from the Scottish mainland (SMT), the Scottish Islands (SIT) and Northern Ireland (NIT) all obtained from Phil Jones, University of East Anglia via the HOLSMEER project (see also Jones & Lister, 2004). The Central England Temperature (CET) data (Manley, 1974 and Parker *et al.*, 1992) was obtained from the website http://www.met-office.gov.uk/research/hadleycentre/obsdata/CET.html.

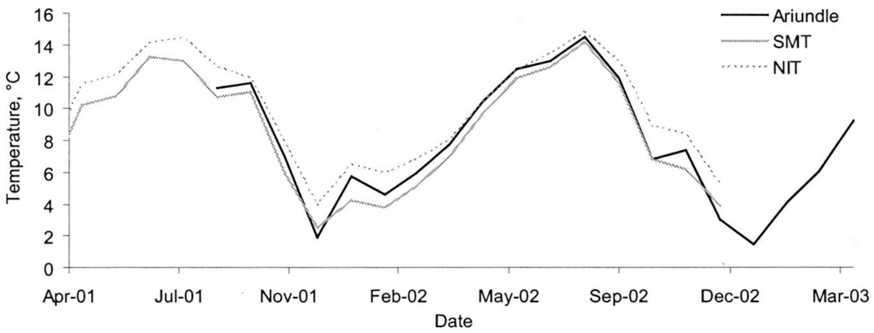

Figure 3.14. Monthly Ariundle temperature reconstructions using the SMT: Ariundle (grey) and NIT: Ariundle (dotted grey line) regression equations (table 3.2). The reconstruction using the SMT regression equation is more realistic than the NIT, with smaller temperature differences occurring throughout the year; the mean anomalies (difference between reconstructed temperature and the observed temperature) are 1.73 °C for the NIT reconstruction and 0.97 °C for the SMT reconstruction.

thermal inertia than land) at the exposed coastal SIT stations along with the influence of the northerly station at Lerwick.

The strong correlations between the temperature data suggests that any one of these long temperature series may be used to reconstruct a longer temperature series for the Loch Sunart area by using the regression equations provided in table 3.2 to extend the Ariundle data. Though the NIT data shows the strongest correlation with the Ariundle data, the SMT correlation is only marginally weaker and the gradient of the regression equation is closer to 1, suggesting a more realistic temperature reconstruction as demonstrated in figure 3.14.

3.5.2 Comparing precipitation records

Though the NW coast of Scotland receives high total annual precipitation (table 2.1), precipitation series from different sites are unlikely to show strong relationships due to rain shadowing and local effects, though they may have similar precipitation series. It is interesting to note that although the correlation between the monthly Ariundle and Polloch precipitation data is much stronger than the relationship between the monthly Ariundle and the monthly England and Wales precipitation (EWP) series (figure 3.15b; data obtained from the Met Office website; http://www.metoffice.gov.uk/research/hadleycentre/CR_data/Monthly/HadEWP_act.txt), the trends in the Ariundle data are equally as comparable to the trends in the EWP as they are to the Polloch data (figure 3.15a). Therefore we can assume that the Ariundle catchment is influenced by the same general weather systems as the EWP stations. The Ariundle station appears to receive a higher total precipitation than the Polloch station (figure 3.15a) probably due to a rain shadow effect on the Polloch station, since the prevailing westerly local weather is funneled up the axis of Loch Sunart into the Strontian catchment (*pers. comm.,* Mr. Campbell, 2001 and Dr. P. Gillibrand, 2004). The Polloch station, by contrast, lies landward and eastward of hilly terrain (figure 2.12). The EWP shows significantly lower total monthly precipitation than both Ariundle and Polloch (figure 3.15), probably due to regional differences in precipitation patterns. The EWP series comprises of 5 regional data sets and is likely to include east coast or inland stations which lie in the rain shadow of the UK, whilst NW Scotland is one of the first parts of the UK to receive the prevailing Atlantic weather systems.

Table 3.2. All UK temperature series show a trend of increasing temperatures towards the 21st Century. The period AD 1800 - AD 1900 shows negligible temperature change, with the majority of warming occurring after AD 1900.

Temperature series	Temperature increase (°C) per century for full series	Temperature increase (°C) per century AD 1800 to AD 1900	Temperature increase (°C) per century after AD 1900
CET	0.23	0.003	0.73
SMT	0.38	0.18	0.66
SIT	0.39	-0.24	0.56
NIT	0.32	Only 50% data available	0.56

Table 3.3. Relationships between monthly air temperature averages from Ariundle and air temperatures from the SMT, SIT, NIT and CET series for the period September 2001 - December 2002 (16 data points). All correlation coefficients are significant with p values > 0.01. Also shown are gradient (m) and intercept (c) values for the regression equation, Ariundle air temperature (˚C) = m* A air temperature series, where A could represent the SMT, SIT, NIT or CET series. Regression equation R^2 values suggest that over 95 % of the variability in the Ariundle data can be attributed to variance in the other data sets.

Data series	Correlation coefficient	Regression equation		
		Gradient (m)	Intercept (c)	R^2
SMT	0.987	1.012	+ 0.405	0.974
SIT	0.972	1.140	-1.587	0.946
NIT	0.988	1.124	-2.094	0.975
CET	0.977	0.903	-0.877	0.954

3.5.3 Influence of the North Atlantic Oscillation on NW Scottish climate

The influence of the North Atlantic Oscillation (NAO) on the climate of Europe is well documented in the literature (see Wanner *et al.*, 2001; Hurrell *et al.*, 2003 for recent reviews) and the coastal stations of NW Europe show clear precipitation responses to the NAO (e.g. Hurrell, 1995; Chandler & Wheater, 2002).

Though the Ariundle data is limited in duration, inter-annual differences in the NAO index appear to influence the weather recorded at the station (figure 3.10), with the more positive year, 2002, yielding higher average winter (DJFM) temperatures, precipitation and maximum wind speed than 2003. A strong correlation (r = 0.802, p = 0.003) also exists between the winter NAO and the total monthly winter (DJFM) precipitation from the Polloch station (for periods 1989-1996 and 2000-2003). Since the Polloch daily precipitation data demonstrates a strong positive correlation with the mean daily flow (MDF) of the River Polloch during the winter months of 1989-1996 (r = 0.779, p = 0.0, n = 2764 for the daily data and r = 0.958, p = 0.0, n = 8 for the DJFM average) one would expect a clear NAO signal in the Polloch MDF. Indeed, figure 3.16 illustrates the influence of the NAO index on the River Polloch averaged winter MDF (r = 0.865, p = 0.0), with the Polloch MDF clearly following trends in the NAO index. By contrast, the winter (DJFM) NAO: precipitation relationship is very weak for the EWP data (r = 0.14, p = 0.06 for the period 1824-2003 and r = 0.286, p = 0.302 for the period 1986-2000), and this is probably due to differences in regional precipitation patterns which have been averaged across a large area (see section 3.5.2).

As mentioned previously, the Ariundle monthly temperature data may be extended using the Ariundle temperature: SMT regression equation, i.e.

Ariundle air temperature (°C) = $1.012 * \mathrm{SMT}_{\mathrm{AIR}} + 0.405$ ($R^2 = 0.974$) *(Eq. 3.1)*

The relationship between the annual average SMT and the NAO is weak (r = 0.313, p = 0.0, $R^2 = 0.1$), however the correlation with winter (DJFM) SMT and the NAO is much stronger (r = 0.687, p = 0.0); the winter SMT and winter NAO series are seen to covary for the majority of the time (figure 3.17). The correlation is expected to be stronger in the winter months, since the NAO is typically a winter phenomenon (chapter 1).

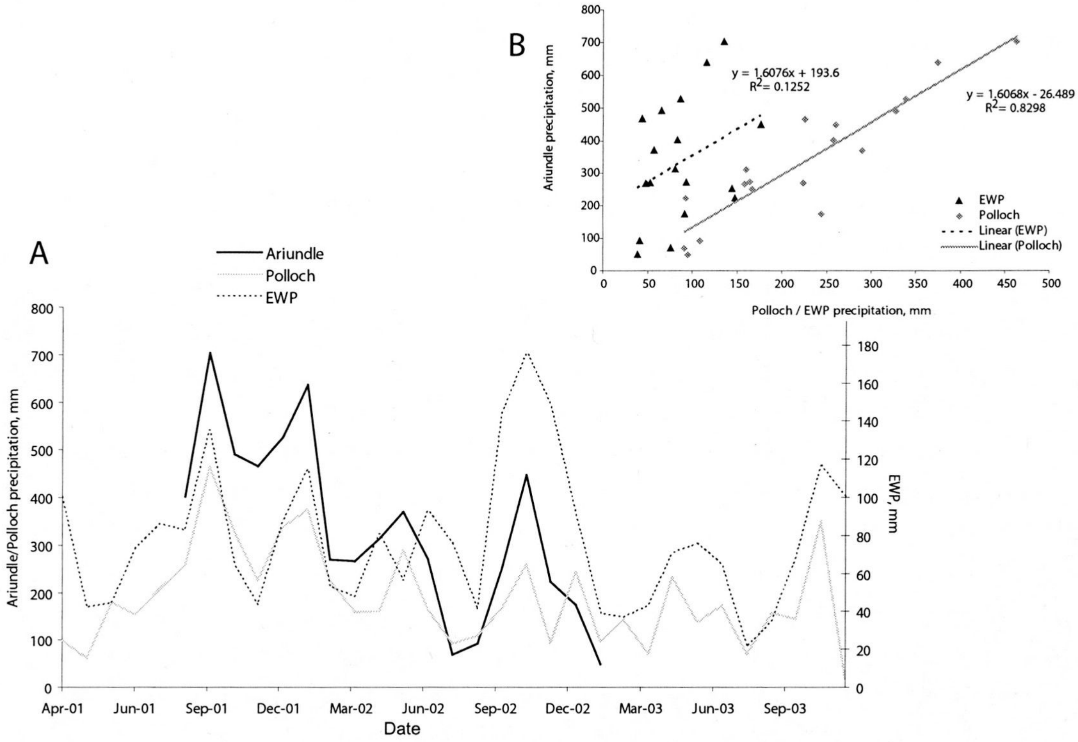

Figure 3.15. (A) Total monthly precipitation from the Ariundle station (black solid line), the Polloch station (grey line; data from SEPA) and the England and Wales precipitation (EWP) series (dotted line; data from http://www.met-office.gov.uk/research/hadleycentre/CR_data/Monthly/HadEWP_act.txt). (B) The Ariundle: Polloch total monthly precipitation relationship is much stronger (grey line) than the Ariundle: EWP relationship (black dotted line).

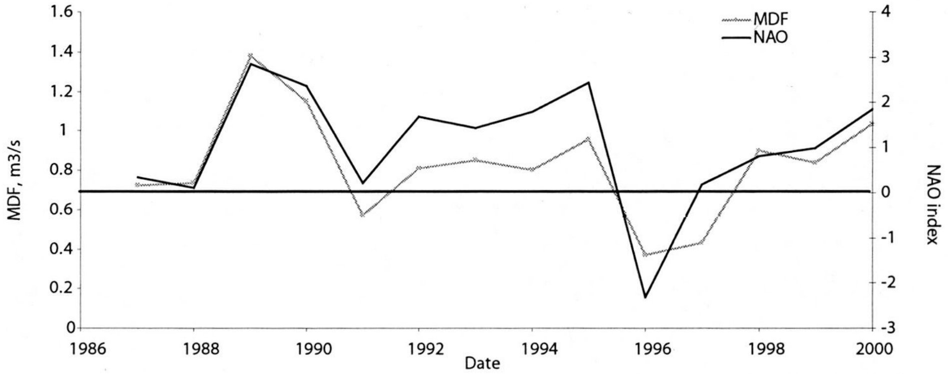

Figure 3.16. Winter (DJFM) NAO index (Jones *et al.,* 1997) and the average winter mean daily flow (MDF) of the River Polloch for the period 1987 - 2000 (data from SEPA) yielding a Pearson's correlation coefficient of r = 0.865 (p = 0.0).

3.5.4 Fjordic hydrography of Loch Sunart

3.5.4.1 Temperature

The seasonal heating cycle observed in Loch Sunart bottom water (figure 3.12) is typical of mid-latitude shelf sea oceanography (chapter 1). Discrete CTD casts obtained from Loch Sunart (data obtained from Dr. P. Gillibrand) show marine temperatures similar to those recorded at both the Tiree and Millport marine stations (figure 3.18), though lags between the data series are evident and this is probably due to the location and exposure of the stations. For example, the Millport temperature series (see section 3.5.5 for more details) is likely to reflect the seasonal heating cycle of surface waters from a sheltered location (the shallow Clyde Sea) along with a strong influence of Irish Sea water (e.g. McKay *et al.*, 1986). In contrast, the Tiree station is situated in an open coastal location (figure 3.1) influenced by both Irish/Clyde Sea water and Atlantic water (McKay *et al.*, 1986), thus the Tiree temperature series probably represents the heating cycle of open coastal waters. Figure 3.18 shows a fairly good agreement between the Tiree and the Loch Sunart temperature data, with the latter appearing to lag the Millport data by ~ 2 months, and like Tiree, Loch Sunart exhibits a smaller annual seasonal temperature range (6.46°C for the inner basin and 6.61°C for the main basin) in comparison to the Millport average seasonal range of 8.2°C. Minimum temperatures at Millport (mean) and Sunart are comparable at ~ 6.8 °C, whilst the Millport mean maximum temperature exceeds the Sunart maximum temperature by approximately 1.6 °C (maximum temperatures of 15.06 °C and 13.4 °C respectively). The varying temperature ranges are likely to reflect seasonal stratification, with enhanced surface layer heating in summer and differences in the water depth of the observations. The Millport data was collected from the surface water layer whilst the Loch Sunart moorings recorded temperature at 40 m water depth which is typically below the thermocline (figure 3.11). Enhanced wind, wave and storm mixing of the water column during the winter months (section 1.8.2) is exemplified by the comparable winter temperatures from Millport and Sunart. The reduced lag time between the Ariundle air temperature series and the Millport marine temperature series suggests the Millport data may more closely reflect air temperature (figure 3.19) whilst temperatures in deeper waters (such as the Loch Sunart series) often show a lagged heating cycle in comparison to surface waters (e.g. Ellett, 1979).

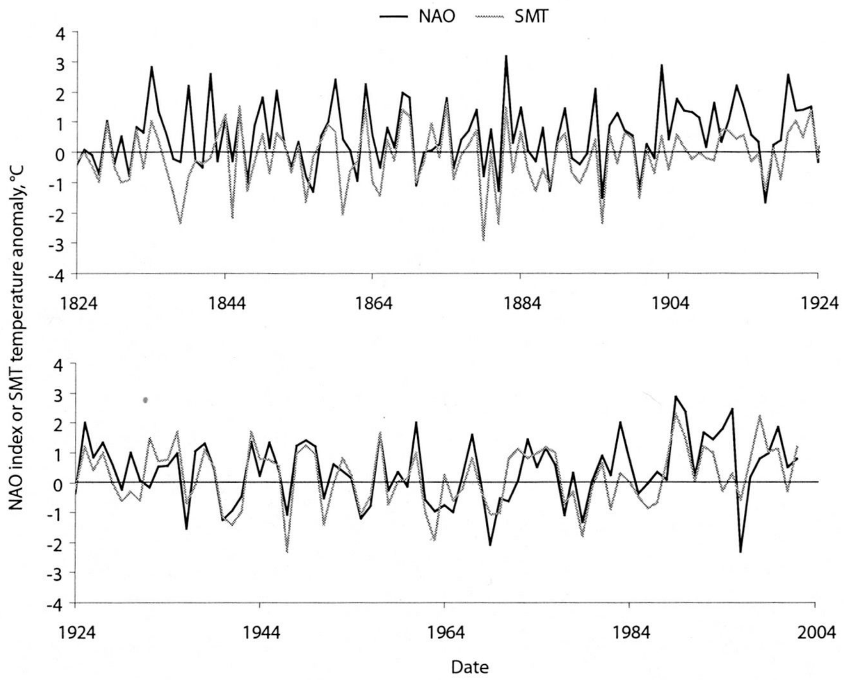

Figure 3.17. The winter NAO index (Jones *et al.*, 1997; black line) and the corresponding winter (DJFM) Scottish mainland temperature (SMT) anomalies (Jones & Lister, 2004; grey line) from AD 1842 to 2002. The two series clearly covary and linear regression of the two data series yields the equation of winter NAO = 0.75*averaged winter SMT - 1.5654 ($R^2 = 0.472$).

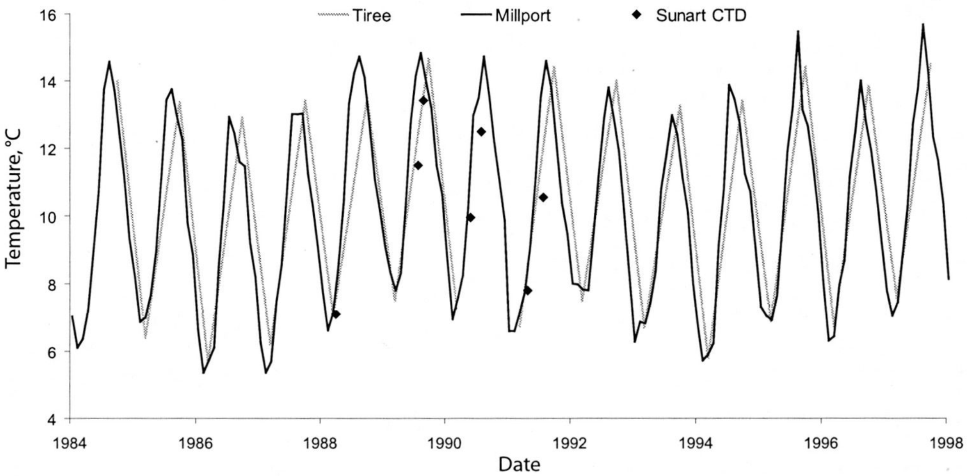

Figure 3.18. Marine temperature series from Tiree (grey line), Millport (black line) and discrete temperature measurements from CTD casts obtained from Loch Sunart (black diamonds).

Though DWREs in sea lochs are driven largely by density changes associated with salinity fluctuations (Gillibrand *et al.*, 1995), temperature changes (positive or negative) may accompany the inflow of coastal waters (e.g. Loch Etive; Austin & Inall, 2002). Gillibrand *et al.,* (1995) observed temperature increases in the inner basin bottom water of Loch Sunart during deep water renewal events in 1989, however it is interesting to note that the observed seasonal heating cycles of the inner and main basins of Loch Sunart are not significantly perturbed by the occurrence of deep water renewal events (e.g. figure 3.11). This suggests that the bottom water temperature of both basins is driven primarily by the coastal water temperature; probably due to the frequency of DWREs which maintain an 'open' connection of the basin waters with coastal waters.

3.5.4.2 Salinity

Periods of low freshwater input are known to be a driving mechanism (along with wind mixing) of fjordic deep water renewal events (DWREs; see chapter 1). Figure 3.20 shows the observed salinity in Loch Sunart with recorded precipitation from the Ariundle station. The main basin salinity shows little response to changes in precipitation, though there is a slight increase in salinity corresponding to the 2nd and 3rd DWRE in the inner basin. The inner basin shows much greater variability in salinity, with salinity increases interpreted as DWREs which appear to occur during periods of low precipitation. The mooring data suggest the time taken for the inner basin to completely renew the deep water (i.e. attain salinity maxima) ranges from 36 to 47 days (figure 3.20), which agrees well with Gillibrand *et al.,* (1995) who suggested DWREs were frequent though irregular in Loch Sunart, probably occurring every 4 weeks. The progressive decrease of salinity is likely due to the wind, tidal and wave mixing (Gade & Edwards, 1980; Farmer & Freeland, 1983; Gillibrand *et al.*, 1995) of less saline surface water into the deeper bottom water, however the rate of salinity change appears to be dependent on the freshwater input. Periods of high rainfall (e.g. from 21/1/2002 - 21/02/2002) result in relatively rapid salinity decreases (30/1/2002 - 20/2/2002) in comparison to slower and sometimes stepwise salinity decreases seen elsewhere in the record (e.g. 30/10/2001 - 1/12/2001). Inner basin salinity also shows significant responses to brief heavy rainfall events, such as those on the 30/9/2001 and 29/10/2001, with noticeable changes in the rate of salinity

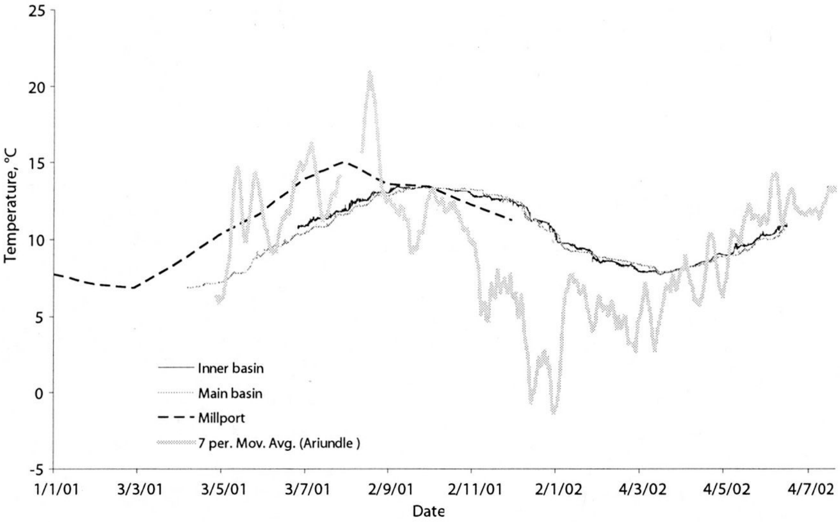

Figure 3.19 Daily bottom water temperatures of Loch Sunart inner basin (black) and main basin (dark grey) lagging approximately 1-2 months behind the monthly Millport marine temperature (dashed line) and the Ariundle air temperature record (7 day running mean).

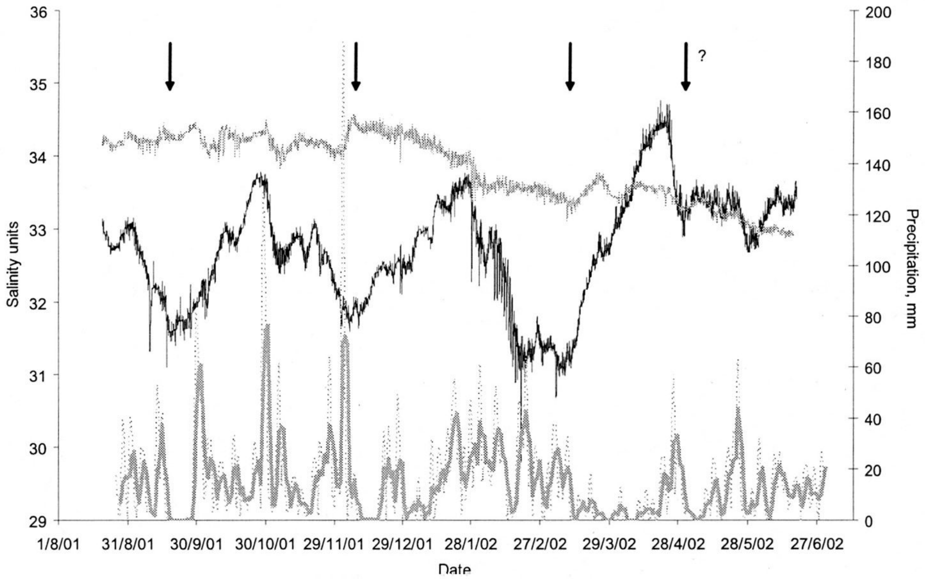

Figure 3.20 Hourly salinity of the inner basin (black line) and main basin (dark grey line) of Loch Sunart recorded at ~40 m water depth between 20/9/2001 and 18/6/2002. Precipitation recorded at the Ariundle weather station (daily data shown by the dotted grey line and the 7 day running mean represented by the thick light grey line). The influence of freshwater inputs into the sea loch (via precipitation in the catchment) is clear in the inner basin salinity, with salinity decreasing following periods of high precipitation and deep water renewal events (black arrows) seemingly triggered when inner basin salinity is low and precipitation is also low. The main basin salinity appears relatively unaffected by the precipitation.

decrease. The sustained period of heavy rainfall between 18/2/2002 and 11/3/2002 appears to have maintained the salinity minimum of the inner basin for much longer than the previous two salinity minima. This minimum also attains the least saline values, which is likely to reflect the delay of the DWRE along with a longer period of freshwater mixing.

The observed salinity changes in the Loch Sunart basins (over the period August 2001 to July 2002) exemplify two important points regarding the circulation of Loch Sunart;

1) Inner basin salinity responds to (and is significantly modified by) freshwater inputs (received as precipitation) from the surrounding catchment.
2) Temperature is not significantly affected by DWREs

3.5.5 Availability of marine temperature records from NW Scottish coastal waters

Palaeoenvironmental proxy reconstructions are more robust when compared and calibrated to historical observations (e.g. Moberg *et al.*, 2005). Given the relatively high resolution of Loch Sunart sedimentary archives (chapter 8), it may be possible to obtain palaeoclimate reconstructions on an annual to decadal resolution, thus a long-term temperature record is essential for comparing proxy temperature data with observed temperature data. However, there is a dearth of long-term marine temperature and salinity records from northern UK coastal waters and the Millport marine temperature series represents the longest continuous sea surface temperature series from the NW coast of Scotland, with nearly continuous monthly temperature observations from AD 1953 to AD 2001.

The Millport marine temperature series shows an annual heating cycle typical of shelf seas, with a mean annual temperature range of ~8 °C, which is similar to the temperature range observed at 40 water depth in Loch Sunart (section 3.5.4). Superimposed upon this seasonal heating cycle is an inter-annual temperature variability, with mean annual temperatures ranging from 8.8 °C to 11.24 °C. The average temperature for May – October coincides with the likely growth period for benthic foraminifera (see chapter 5), and is therefore an important variable when dealing with palaeoenvironmental records (e.g. Scourse *et al.*, 2004). The May-October average temperature (figure 3.21) closely follows the annual average temperature trends with a mean temperature difference of ~ 2 °C. Though the relatively short duration of this temperature series negates the identification of low frequency cycles via spectral analysis, there does appear to be a 15 year cycle occurring in the data which is particularly evident in the May-Oct temperature series (figure 3.21) and of a similar frequency to decadal periodicities reported by O'Sullivan *et al.*, (2002). As with the long-term air temperature series in figure 3.13, the Millport data also shows a trend towards increased modern temperatures, with an overall increase of 0.177°C per decade. This rate of change is slightly greater than the change seen in the SMT temperature series and this could, in part, be due to the short duration of the Millport time series capturing late 20th Century warming.

A long-term (AD 1870 – 1999) record of sea surface temperature anomalies (SSTA) from the grid 55°N - 60°N, 10°W - 05°W is presented in figure 3.22. The May-October SSTA series shows a larger range of anomalies (-0.71 to +1.14 °C) than the annual SSTA (-0.44 to +0.92 °C), though as with the Millport series, the data follow similar long-term trends. Prior to 1925, temperatures generally appear to be cooler than the long-term mean whilst the period between 1925 and 1977 sees consistently positive temperature anomalies. The greatest SSTA variability occurs after 1950 onwards and spectral analysis reveals periodicities of ~ 7.69 years (figure 3.22) which are commonly associated with NAO cyclicity (e.g. O'Sullivan *et al.*, 2002 and references within).

Trends in the SSTA series correspond fairly well with trends in the SMT anomaly data for both the annual average temperature anomalies ($r = 0.664$, $p = 0.0$) and the May-October temperature anomalies ($r = 0.666$, $p = 0.0$), exemplifying the modulation of the UK climate by oceanic heat transfer from the coastal waters (figure 3.23). The SMT anomalies show greater variability than the SST data and this is likely due to the higher thermal intertia of the ocean water and the lower thermal inertia of the land which results in rapid responses of air temperature to atmospheric forcing mechanisms such as the NAO. Sea surface temperature anomaly data from the Faeroe-Shetland Channel also show similar trends to the SMT data (figure 3.24) exemplifying the link

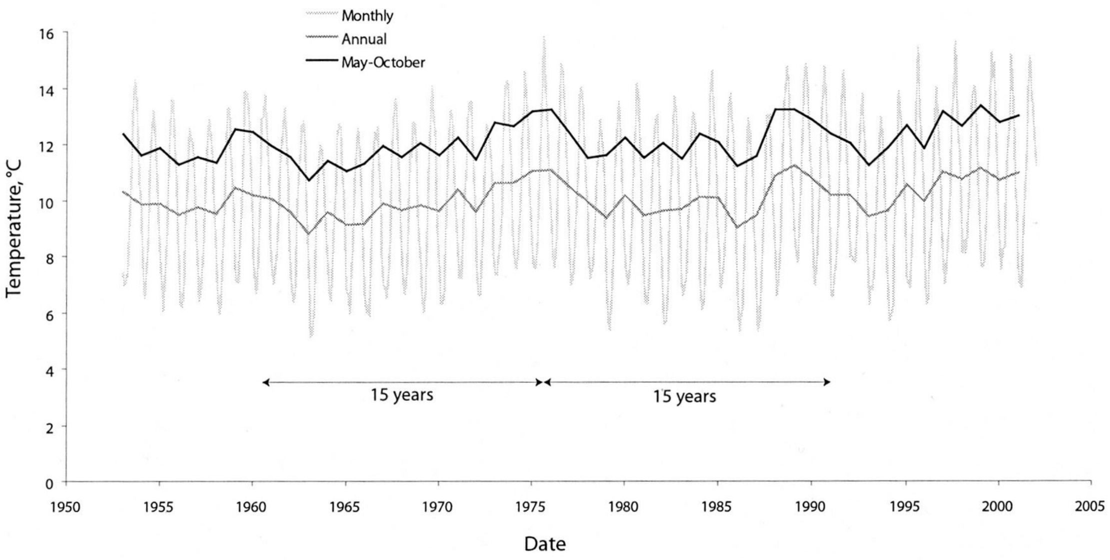

Figure 3.21. Monthly Millport marine temperatures (light grey line) for the period AD 1953 - 2001 (obtained from Dr. P. Barnett, University Marine Biological Station, Millport). Also shown is the inter-annual variability in the Millport temperature series exemplified by the annual average temperature (dark grey line) and the average temperature for May - October (black line) - the typical growing season for benthic foraminifera.

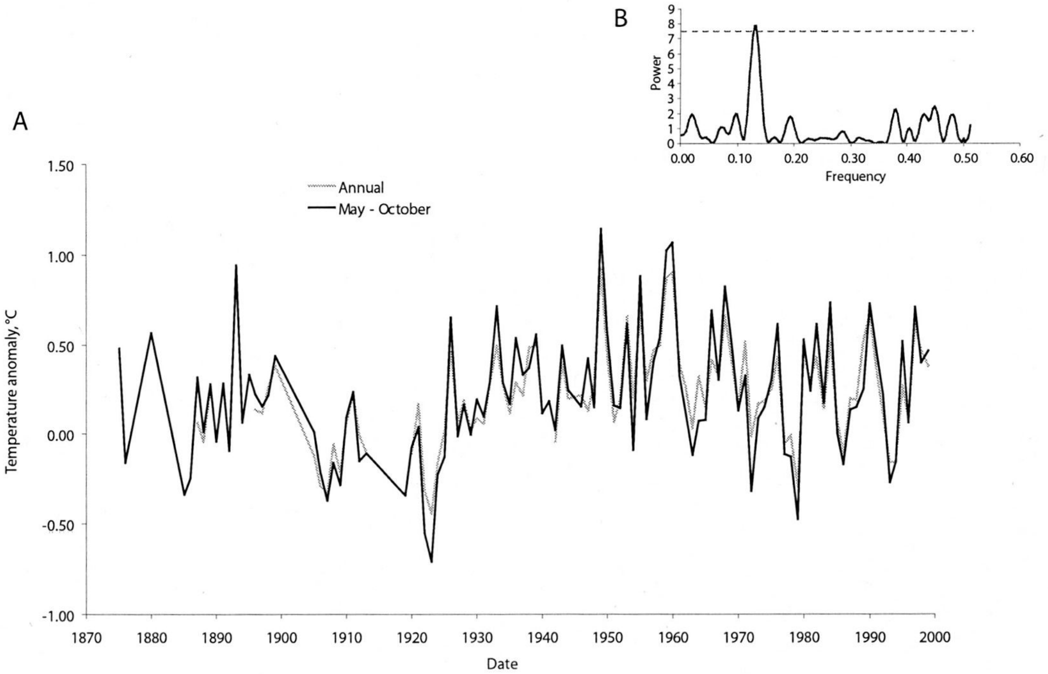

Figure 3.22 (A) Sea surface temperature anomalies for the NW Scotland coastal waters in grid 55°N - 60 °N, 10° W - 5°W (data from Climatic Research Unit, University of East Anglia). The May-October average temperature anomaly series (black line) closely follows the trend of the annual average temperature anomaly. (B) Spectral analysis (using the Lomb Periodogram) of the May - October temperatre anomalies for the period 1950-1999 shows a significant (95 % confidence level) of a cycle at a frequency of 0.13 (inset) equating to cycles with a periodicity of 7.69 years (since frequency is expressed as *1/x unit*).

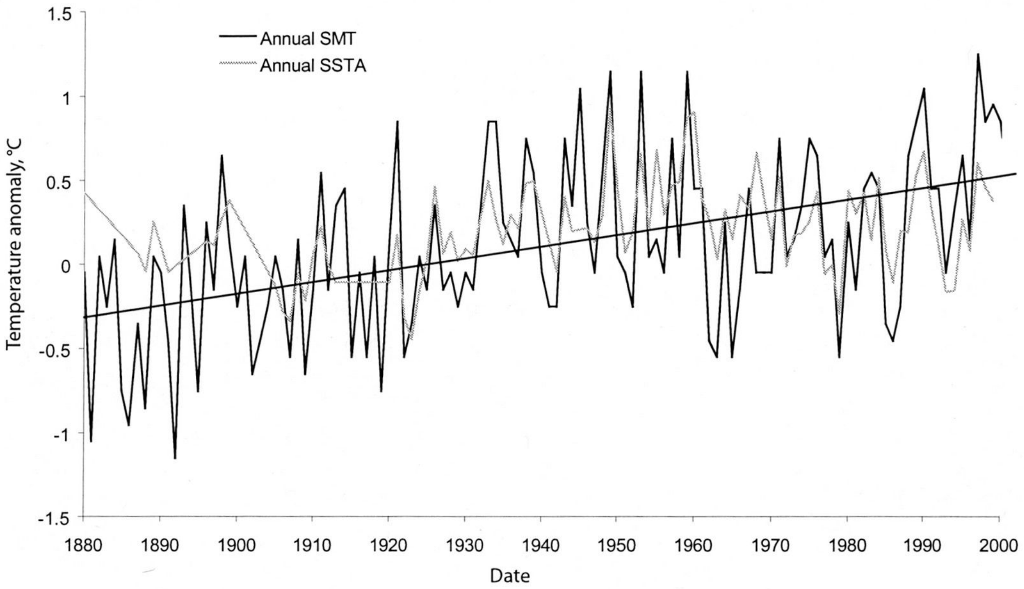

Figure 3.23 Annual average Scottish mainland temperature (SMT) anomalies (black line) and annual average sea surface temperature anomalies (SSTA) from the grid 55°N - 60°N, 10°W - 5°W (data from the Climatic Research Unit (CRU), University of East Anglia, as part of the HOLSMEER programme; http://www.cru.uea.ac.uk/cru/projects/holsmeer). A linear trendline through the SMT data shows an increase of 0.07 °C per decade.

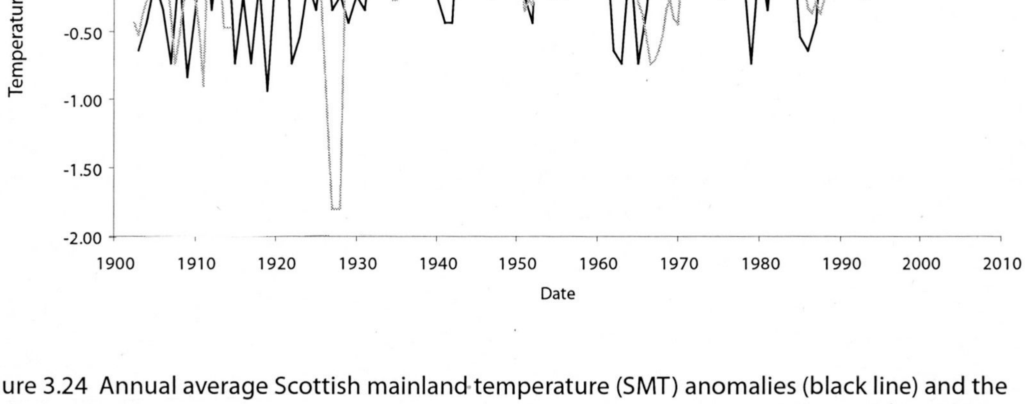

Figure 3.24 Annual average Scottish mainland temperature (SMT) anomalies (black line) and the 2 year running mean temperature anomaly series from the Faeroe-Shetland Channel (data courtesy of Dr. Bill Turrell, Fisheries Research Services, Aberdeen). Despite some periods of anti-phase, the SMT air temperature data coinicdes with the trends in the Faeroe-Shetland Channel marine temperature.

between the climate of NW Scotland and the N Atlantic currents and validating the use of proxies from NW Scotland to investigate past changes in oceanic circulation and climate from the wider NE Atlantic region.

3.5.6 Extending sea surface temperatures from long-term Scottish air temperature data

The strong correlation between the Ariundle temperature record and the long SMT series (section 3.5.1) demonstrates that the SMT series reflects the climate of the Loch Sunart catchment, and the good agreement of the SMT data with sea surface temperature data from Millport, the NW Scotland coastal waters (SSTA) and the Faeroe-Shetland Channel, illustrates the modulation of the climate of NW Scotland by coastal oceanography along with oceanic thermal inertia and heat transfer (section 3.5.5)

Section 3.5.1 showed how linear regression equations can be used to reconstruct and extend a data series. Though the SSTA data spans from AD 1870 – 1999 (with missing monthly data between 1870 and ~ 1919) this data series only shows anomalies from a long-term mean temperature, rather than actual temperature data and represents temperature anomalies from an 'open coastal' location. However, the Millport data series comprises actual temperature data rather than anomalies and likely represents a sheltered location (section 3.5.4) similar to the basin waters of Loch Sunart.

A comparison of the annual average Millport temperatures with the annual average SMT, SIT, NIT and CET series (table 3.4) shows the strongest correlation and best fit between the marine and land temperature series comes from the SMT data set ($r = 0.78$ and $R^2 = 0.609$).

Millport sea surface temperatures typically 'lag' behind the SMT air temperatures (e.g. figure 3.25a) by about 1 month, likely due to the ocean's high thermal inertia and radiative forcing of the ocean's surface layer. When the SMT data is lagged by one month, i.e. the air temperature for January becomes the air temperature for February,

Table 3.4 Pearson linear correlation coefficients (r) and coefficients of determination (R^2) for the comparison of Millport sea surface temperatures and the air temperatures of SMT, SIT, NIT and CET (data from Jones & Lister, 2004; Manley, 1974). All correlations are significant at < p = 0.01.

Air temperature series compared with Millport marine temperature	Annual average		May - October average	
	r	R^2	r	R^2
SMT	0.780	0.609	0.612	0.374
SIT	0.677	0.458	0.598	0.357
NIT	0.650	0.422	0.504	0.254
CET	0.743	0.553	0.599	0.359

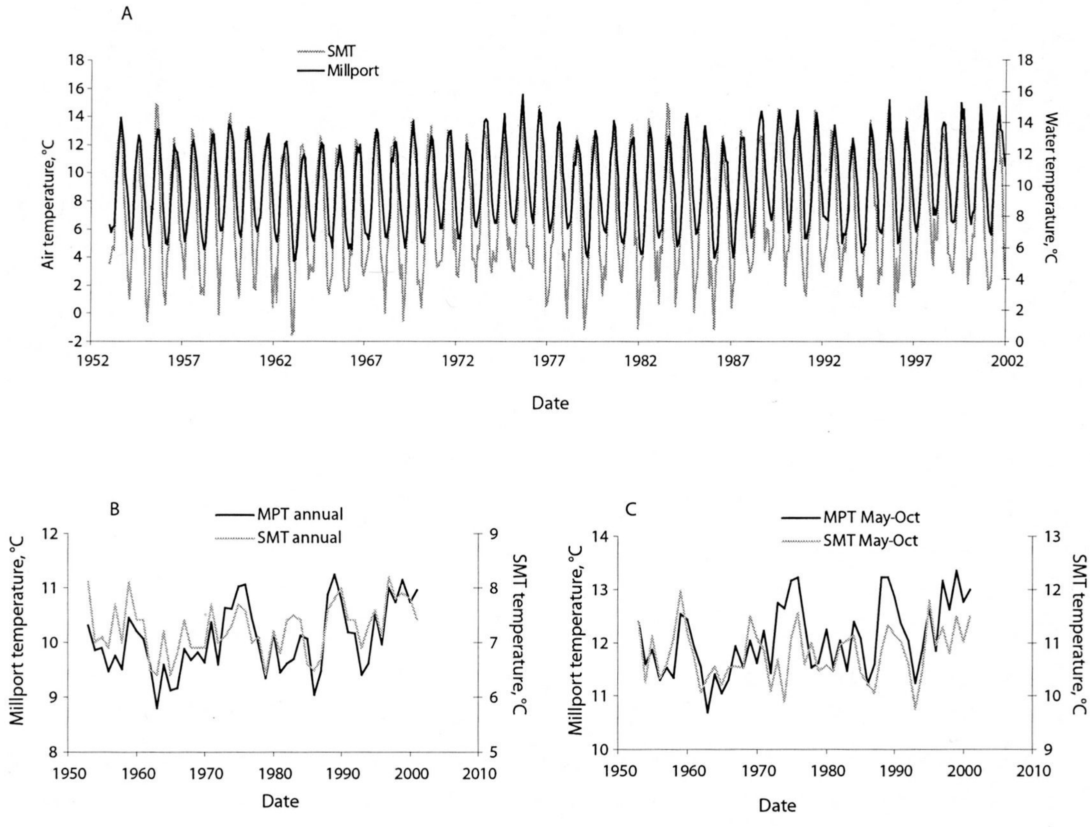

Figure 3.25 Millport marine temperatures (black line) and Scottish mainland temperatures (SMT; grey line) for the period AD 1953 - 2001: A) Monthly averages, B) annual averages C) May - October average.

the correlation coefficient becomes very much stronger at ($r = 0.94$, $p = 0.0$). The regression equation from this 'lagged' relationship for the period AD 1953-2001 is:

$$\text{monthly MPT} = 0.594 * \text{monthly SMT} + 5.750 \quad (R^2 = 0.88) \qquad \textit{(Eq. 3.2)}$$

where monthly MPT = averaged monthly Millport marine temperatures and monthly SMT = averaged monthly Scottish Mainland air temperatures. The reconstructed monthly marine temperature series agrees fairly well with the observed Millport temperature data (figure 3.26). However, for the majority of the annual cycles, the monthly reconstruction either overestimates or under-estimates the marine temperature, resulting in a large error with the mean difference between the reconstructed marine temperature and the observed Millport temperature being $-0.29 \times 10^{-3} \pm 1.41$ °C, i.e. high mean accuracy but low monthly precision. This low precision is likely due to differences in the heat capacity of land and ocean, with the SMT data displaying a large seasonal temperature whilst the marine temperature has small seasonal marine temperature range (figure 3.26). Additionally, there are noticeable inter-annual differences between the reconstructed marine temperature record and the observed Millport record (figure 3.26).

Another method of reconstructing a longer marine temperature series for the Scottish west coast is to use the annual average data. Despite the strengthening of the linear relationship when lagged data is used, correlation coefficients for the monthly SMT and monthly Millport data appear strongest when no lag is applied, i.e. when SMT for June is correlated against the June Millport data (table 3.5). Since the annual average SMT: annual average Millport temperature correlation is also strong (table 3.4), this suggests that a regression equation derived for a yearly average with no lag applied to the data is likely to reproduce a realistic reconstruction of annual sea surface temperatures.

The regression equation derived from the correlation of annual average SMT data and annual average Millport data from AD 1953 to 2001 is given by;

$$\text{RMPT} = 1.01 * \text{Annual average SMT} + 2.75 \quad (R^2 = 0.61) \qquad \textit{(Eq. 3.3)}$$

Table 3.5 Pearson's correlation coefficients of monthly Scottish mainland temperature (SMT) data (columns) and Millport monthly marine temperatures (rows). The top value is the correlation coefficient (r) and the bottom value is the p value. When $p < 0.05$, correlations are significant at a level of 95%. Strong, significant correlations (i.e. $r > 0.5$) are shown by bold italic type.

SMT Millport	JAN	FEB	MAR	APR	MAY	JUN	JUL	AUG	SEP	OCT	NOV	DEC
M - JAN	0.464 0.001	0.235 0.104	0.105 0.474	0.029 0.841	0.336 0.018	-0.014 0.924	0.119 0.417	0.213 0.143	0.074 0.613	0.252 0.081	-0.053 0.716	0.113 0.439
M - FEB	***0.586*** ***0***	***0.586*** ***0***	0.251 0.082	0.058 0.691	0.429 0.002	0.042 0.775	0.137 0.349	0.272 0.058	0.241 0.096	-0.035 0.81	-0.065 0.655	-0.01 0.945
M - MAR	***0.58*** ***0***	***0.614*** ***0***	***0.544*** ***0***	0.003 0.984	0.42 0.003	-0.004 0.981	0.165 0.257	0.291 0.042	0.189 0.193	-0.055 0.706	0.036 0.806	0.13 0.375
M - APR	0.449 0.001	***0.577*** ***0***	0.372 0.008	0.363 0.01	0.336 0.018	-0.105 0.471	0.225 0.12	0.378 0.007	0.15 0.304	0.034 0.815	0.036 0.805	0.133 0.363
M - MAY	0.476 0.001	***0.611*** ***0***	0.358 0.012	0.2 0.169	***0.5*** ***0***	0.008 0.954	0.313 0.029	0.315 0.027	0.183 0.208	0.038 0.796	0.236 0.103	0.129 0.377
M - JUN	0.402 0.004	0.391 0.005	0.279 0.052	0.186 0.202	0.304 0.034	0.352 0.013	0.173 0.235	0.361 0.011	0.09 0.54	0.132 0.365	0.006 0.966	-0.053 0.72
M - JUL	0.266 0.065	0.334 0.019	0.178 0.222	0.14 0.338	0.236 0.103	0.015 0.916	***0.629*** ***0***	0.386 0.006	0.102 0.488	0.09 0.537	0.215 0.137	0.218 0.132
M - AUG	0.34 0.017	0.422 0.003	0.085 0.561	0.173 0.235	0.156 0.285	0.071 0.627	0.51 0	***0.695*** ***0***	0.148 0.31	0.18 0.215	0.209 0.149	0.16 0.272
M - SEP	0.292 0.042	0.481 0	0.167 0.251	0.217 0.133	0.2 0.169	-0.035 0.813	0.43 0.002	***0.565*** ***0***	0.471 0.001	0.005 0.971	0.216 0.136	0.19 0.192
M - OCT	0.26 0.071	0.362 0.011	0.033 0.824	-0.002 0.989	0.307 0.032	0.05 0.733	0.38 0.007	0.441 0.002	0.241 0.096	0.472 0.001	0.127 0.383	0.163 0.262
M - NOV	0.278 0.053	0.339 0.017	0.093 0.523	0.209 0.15	0.206 0.157	-0.014 0.923	***0.518*** ***0***	***0.569*** ***0***	0.237 0.101	0.315 0.028	0.446 0.001	0.123 0.399
M - DEC	0.275 0.056	0.257 0.074	0.092 0.531	-0.002 0.987	0.151 0.3	-0.143 0.328	***0.505*** ***0***	***0.552*** ***0***	0.167 0.251	0.396 0.005	0.427 0.002	0.303 0.034

where RMPT is the annual reconstructed Millport marine temperature series. The intercept of the regression equation accounts for the ~ 2°C difference between the air and marine temperatures.

The resulting reconstructed marine temperature series agrees well with the observed annual average Millport marine temperatures, following the same general temperature trend (figure 3.27a). Although the reconstruction overestimates and underestimates the temperature at times, the mean difference between the observed and reconstructed temperatures is very low at 0.41 x 10^{-5} °C, yielding an error of only 0.38 °C, which is much lower than the error on the monthly data reconstruction.

Though benthic foraminifera typically calcify during May-October, the relationship between Millport sea surface temperatures and the air temperature series over this period are all weaker (table 3.4), thus using a May-October regression equation would produce a poor temperature reconstruction. However as figure 3.25b shows, the annual and May- October Millport temperature data closely follow the same pattern albeit with a 2.02 ± 0.177 °C difference, thus the May-October average temperature could be estimated by adding 2.02 °C onto the reconstructed annual average marine temperature.

A problem in the reconstruction of the Millport temperature data is the long-term trend prevalent in the observed data. The regression equation for the observed Millport data shows a 0.17 °C increase per decade whilst the SMT data for the same period (AD 1953 – 2001) shows only a 0.083 °C warming per decade. This results in a temperature increase of 0.092 °C per decade for the reconstructed marine temperature for AD 1953 – 2001, i.e. the recent (AD 1953-2001) marine temperature trend observed at Millport is dampened of the reconstruction or marine temperature over the same period. However, since the SMT data closely follow trends in both the SSTA (figure 3.23) and Faeroe-Shetland Channel temperature series (figure 3.24), the extended Millport temperature series and reconstruction is still likely to reflect broad changes in the North Atlantic climate (figure 3.27b) albeit with slightly exaggerated temperatures resulting in weaker long term temperature trends.

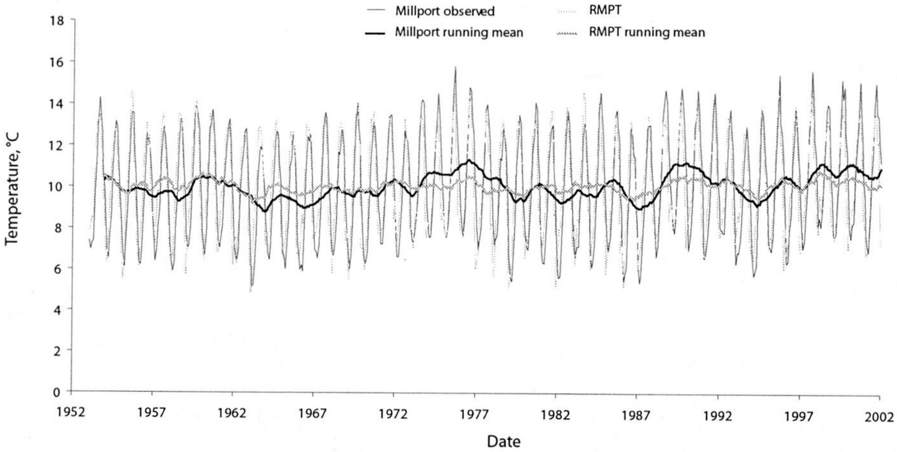

Figure 3.26. Recorded Millport monthly temperature (black line) and 12 month running mean (thick black line) for length of observation period. The reconstructed monthly Millport marine temperature series (RPMT; thin grey line) was obtained using the lagged (1 month lag) linear regression relationship between monthly Millport and Scottish mainland temperature (SMT) data; RMPT = 0.594* monthly SMT + 5.75 (R^2 = 0.88). A 12 month running mean through the reconstructed monthly data is shown by the thick black line.

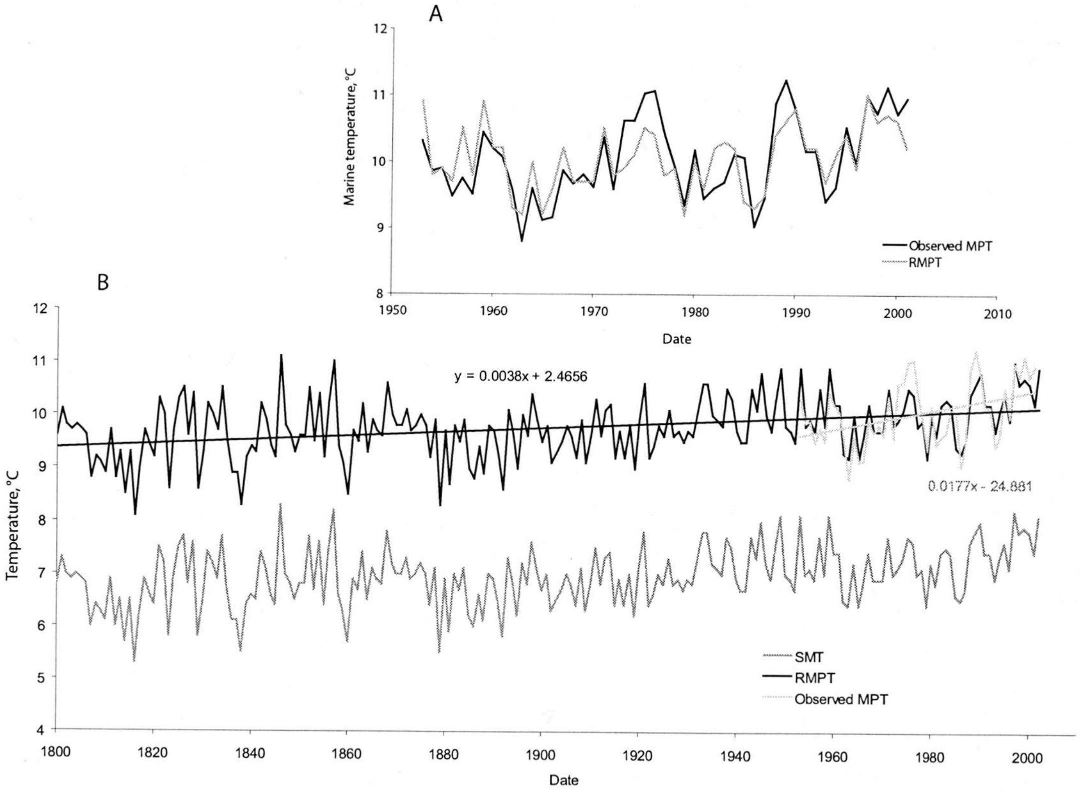

Figure 3.27. (A) Reconstructed annual average marine temperature data (RMPT; grey line) plotted with the observed annual average Millport temperature (MPT; black line) for the period of data collection; AD 1953-2002. (B) Extension of the RMPT (black line) back to the start of the SMT (dark grey line; collection period (AD 1800) via the regression equation; RMPT = 1.01*Annual average SMT + 2.75; R^2 = 0.61). The linear trend line through the long RMPT series shows a temperature increase of 0.038 °C per decade for the period AD 1800 - 2002; a temperature increase of 0.099 °C exists in the RMPT for AD 1953-2002. This is much lower than the temperature trend in observed Millport temperature data (MPT; grey trendline and equation), which suggests a temperature increase of 0.177 °C per decade.

3.5.7 Influence of the North Atlantic Oscillation on sea loch circulation

The influence of the NAO on NW European precipitation is well documented (e.g. Hurrell, 1995; Chandler & Wheater, 2002; Ruprecht *et al.*, 2002; Trigo *et al.*, 2002) and the climate of NW Scotland has been shown to respond to the NAO both on a regional and a local scale (sections 3.3.4 and 3.5.3).

Precipitation falling onto catchment areas is usually subject to the process of infiltration and percolation into the soil, and interception by plants and trees. However, the soils in NW Scotland are relatively thin (particularly on the steep slopes) and poorly developed with mostly sparse vegetation cover. This, together with high annual precipitation (1600-3200 mm average precipitation band; U.K. Meteorological Office data, 1977) results in low soil moisture deficits and the majority of precipitation falling onto the catchment area is therefore usually translated into surface runoff (Black & Cranston, 1995), as exemplified by the strong positive correlation between Polloch precipitation and River Polloch mean daily flow (section 3.5.3). One significant exception to this rule is when precipitation falls as snow and remains in the catchment until the spring melt.

Thus, precipitation from the surrounding catchment is likely to enter Loch Sunart rapidly and the mooring data from Loch Sunart demonstrates both the sensitivity and rapid response of the inner basin salinity to varying inputs of freshwater (e.g. figure 3.20). Although DWREs in Loch Sunart are driven primarily by wind forcing (Gillibrand *et al.*, 1995), high freshwater inputs, by imparting buoyancy to the surface layer, appear to prevent or delay onsets of DWREs (figure 3.20). Therefore one would expect to see different hydrographic responses (particularly in the inner basin) during positive and negative phases of the NAO, with less frequent DWREs occurring during high river discharge years associated with the positive index of the NAO.

3.5.8 Modelling fjordic circulation

To examine this hypothesis Gillibrand *et al.,*, (2005) modelled the fjordic circulation in Loch Sunart during two extreme phases of the NAO; the positive index (+ 2.86) year 1988/89, and the negative index year of 1995/96 (-2.32; Jones *et al.*, 1997).

A two-dimensional laterally-averaged numerical model (which solved the conservation of volume, momentum and salt in an estuary, vertical and eddy viscosity, and diffusivity) with a staggered Cartesian grid using finite difference approximations was used to simulate the circulation in Loch Sunart during the two NAO extremes. The grid used in the model consisted of 19 grid columns and a maximum of 21 grid rows. The model commenced from a specified initial condition and stepped forward in 60 second increments with a 'spin-up' period of 7 days allowing the model to achieve equilibrium. Elliott *et al.,*, (1992) and Gillibrand *et al.,*, (1995) utilised the same model to successfully reproduce observed salinity fields and deep water renewal events in Loch Sunart and further details of the model mechanisms are described in these publications.

3.5.8.1 Model inputs

The model was run for a full year over the two periods; 1) 1st August 1988 – 1st August 1989 and 2) 1st August 1995 – 1st August 1996, to ensure that the winter season (when the NAO is the dominant mode of atmospheric behaviour) was captured.

Inputs to the model included along-channel wind-stress (data from Tiree), river discharge (scaled River Polloch mean daily flow data), surface elevation at the mouth and salt input from the coastal ocean. Surface tidal elevation (data from Tobermory, Mull) was also accounted for (Gillibrand *et al.*, 2005).

There is a general dearth of data for Scottish river catchments and few Scottish catchments less than 50 km^2 are gauged (Black & Cranston, 1995). River discharge data is not available for Loch Sunart, however the SEPA maintains a guage on the River Polloch (in the neighbouring catchment to the north of Loch Sunart) which measures mean daily flow (MDF).

As mentioned previously, the Polloch precipitation: MDF relationship is strong ($r = 0.779$, $p = 0.0$), with periods of higher precipitation accompanied by greater mean daily flows. Since the Ariundle catchment experiences similar precipitation trends to the Polloch catchment (section 3.5.2) a similar precipitation: river discharge relationship to the Polloch catchment (section 3.5.3) is also expected within the Sunart catchment area. It is recognised that differences in the physical characteristics of catchment areas, such as slope, soil development, geology and drainage patterns, would result in varying responses of river discharge to rainfall (Wolf, 1966), however for the purpose of this study, it is assumed that these neighbouring catchments behave identically (*pers. comm.,* Dr. A. Black, 2001).

The Loch Sunart catchment has a total area of 299 km^2 (with numerous sub-catchments) and is much larger than the Polloch catchment area of 7.9 km^2. A simple scaling approach was used to infer the mean daily flows of Sunart sub-catchment rivers. The catchment and sub-catchment areas of Loch Sunart were delineated on an Ordnance Survey map (Sheets 40, 49), and the areas of the sub-catchments were estimated to the nearest 0.1 km^2 (figure 3.28, table 3.6). Assuming no significant precipitation gradient across the Sunart catchment, and similar sub-catchment hydrological responses, the Polloch MDF values were scaled to each sub-catchment, using the following relationship:

$$Q_{ESC} = (Q_{Polloch} / A_{Polloch}) * A_{SC} \qquad \textit{(Eq. 3.4)}$$

where Q_{ESC} represents the estimation of sub-catchment MDF (m^3.s^{-1}), $Q_{Polloch}$ represents the Polloch MDF (m^3.s^{-1}), $A_{Polloch}$ represents the Polloch catchment area (km^2) and A_{SC} represents the area of the sub-catchment (km^2). The mean river flow values during the two simulation periods are shown in table 3.7.

Hourly wind speed and direction data from Tiree was used in the model and the mean wind speed and stress for the NAO extremes can be seen in table 3.7. Coastal salinity was held constant throughout the simulations, though salinity can change due to climatic forcing (e.g. Blindheim *et al.*, 2000). This was partly due to a lack of data (only one CTD profile available for the 12th July 1989) and partially to remove a source of variability from the modelling thereby focusing on hydrographic responses to climatic wind stress and river discharge.

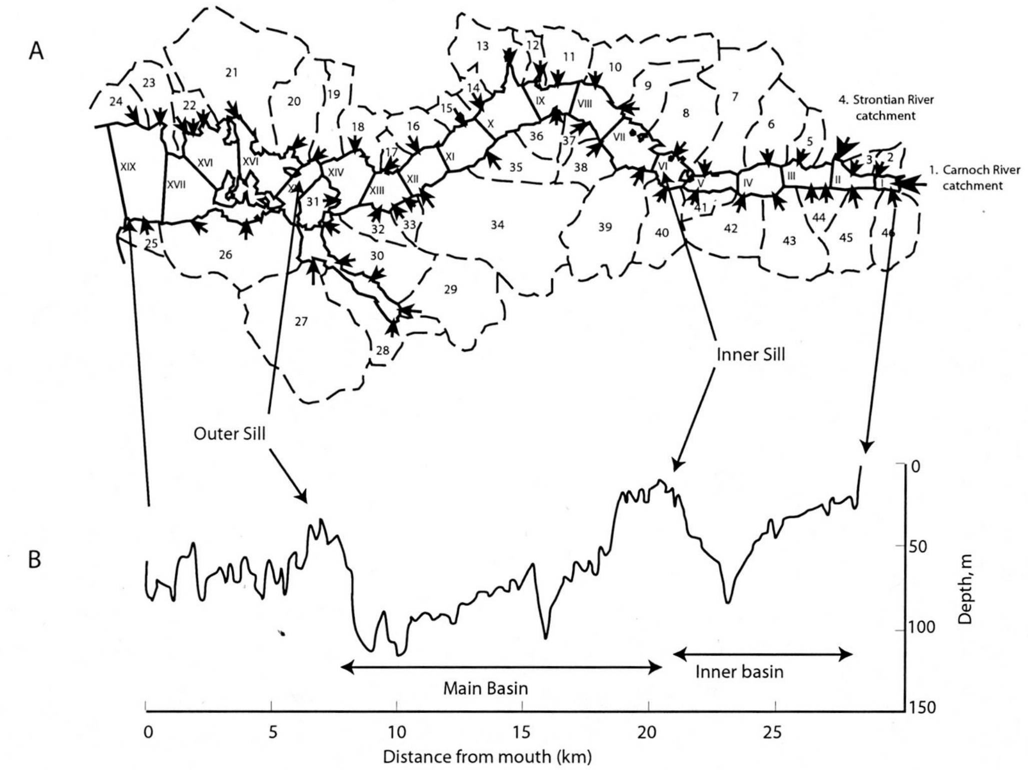

Figure 3.28 A) Sub-catchment areas for streams and rivers discharging into Loch Sunart (A). Areas are given in table 3.6. The across-loch transects represent the columns of the model grid with inner and main basins sills located at transects VI and XIV respectively. B) A depth profile along the central axis of Loch Sunart. Note the catchment areas of the Carnoch and Strontian rivers are too large (table 3.6) to be shown on this map. Black arrows indicate where major sub-catchment tributaries enter the loch. Loch Teacuis is not included in the model grid but provides a significant amount of freshwater into Loch Sunart, thus it's catchments are included here.

Table 3.6 Areas of Loch Sunart sub-catchments delineated in figure 3.28. Also shown is which model transect the sub-catchment freshwater input is attributed to.

Loch Sunart sub-catchment	Area, km^2	Input to transect
1	31.5	I
2	1	I
3	1	II
4	38	II
5	2	III
6	5	IV
7	8.5	V
8	5	VI
9	3.5	VIII
10	6	VIII
11	3.5	IX
12	1	IX
13	5	X
14	1.2	X
15	1.7	XI
16	2.5	XII
17	1	XIII
18	3	XIV
19	3.5	XV
20	5.5	XVI
21	14.5	XVI
22	2	XVII
23	3	XIX
24	2.5	XIX
25	1.7	XIX
26	11.3	XVIII
27	16.5	XIV/XV
28	5	XIV/XV
29	9	XIV/XV
30	7.5	XIV/XV
31	2	XIV
32	2	XIII
33	1.5	XIII
34	21	XII
35	4	XI
36	2	IX
37	1.5	VIII
38	3	VII
39	10	VII
40	5	VI
41	1.5	V
42	5	IV
43	6	IV
44	2	III
45	5	II
46	4.5	I

3.5.8.2 Modelling results

The summary statistics of the modelling results for the two extreme NAO years of 1988-89 and 1995-96 can be seen in table 3.8 and figure 3.29.

The influence of river discharge (mean daily flow, MDF) variations during different NAO phases is exemplified by decreased inner basin salinity following high river discharge events particularly during the NAO negative phase 1995-96 (figure 3.29b), and the occurrence of renewal events following periods of low MDF.

The inner basin salinity demonstrates a significant response to the NAO phase with a salinity range of 0.52 between the positive and negative NAO years and significant changes in the frequency of DWREs (table 3.8), suggesting a strong NAO influence on the inner basin hydrography. Gillibrand *et al.*, (2005) report that the 'influence of the NAO appears to be exerted primarily through the enhanced westerly winds which are prevalent during the positive phase, rather than through the associated increased precipitation and river discharge'. Despite this, renewal events in the inner basin during the NAO positive year (1988-89) appear to occur in periods of low MDF (e.g. the renewal event around day 244 of the 1988-89 run), whilst a prolonged period of higher MDF between days 180 and 240 result in a delayed DWRE (figure 3.29a). This is also seen in the observed salinity record for Loch Sunart (figure 3.20). Additionally, the low discharge from around day 250 of the 1988-89 run results in a long period of relatively high salinity in the inner basin. The 1995-96 negative NAO phase shows a decrease in inner basin salinity during or following periods of relatively high MDF, however the duration of these MDF periods are short in comparison to the periods of low MDF, thus basin water is more regularly replaced, resulting in a higher mean salinity (table 3.8).

Though the inflows into the main basin are very different for the positive and negative NAO phase, the main basin salinity remains fairly constant for the runs during both NAO years, with mean salinities of 34.18 and 34.16 respectively for the 1988/89 and 1995/96 runs (table 3.8). This variation in inflow, along with the increase in frequency of DRWE in the 1995/96 model run suggests a weak relationship between main basin bottom water salinity and the climatic forcing associated with the NAO.

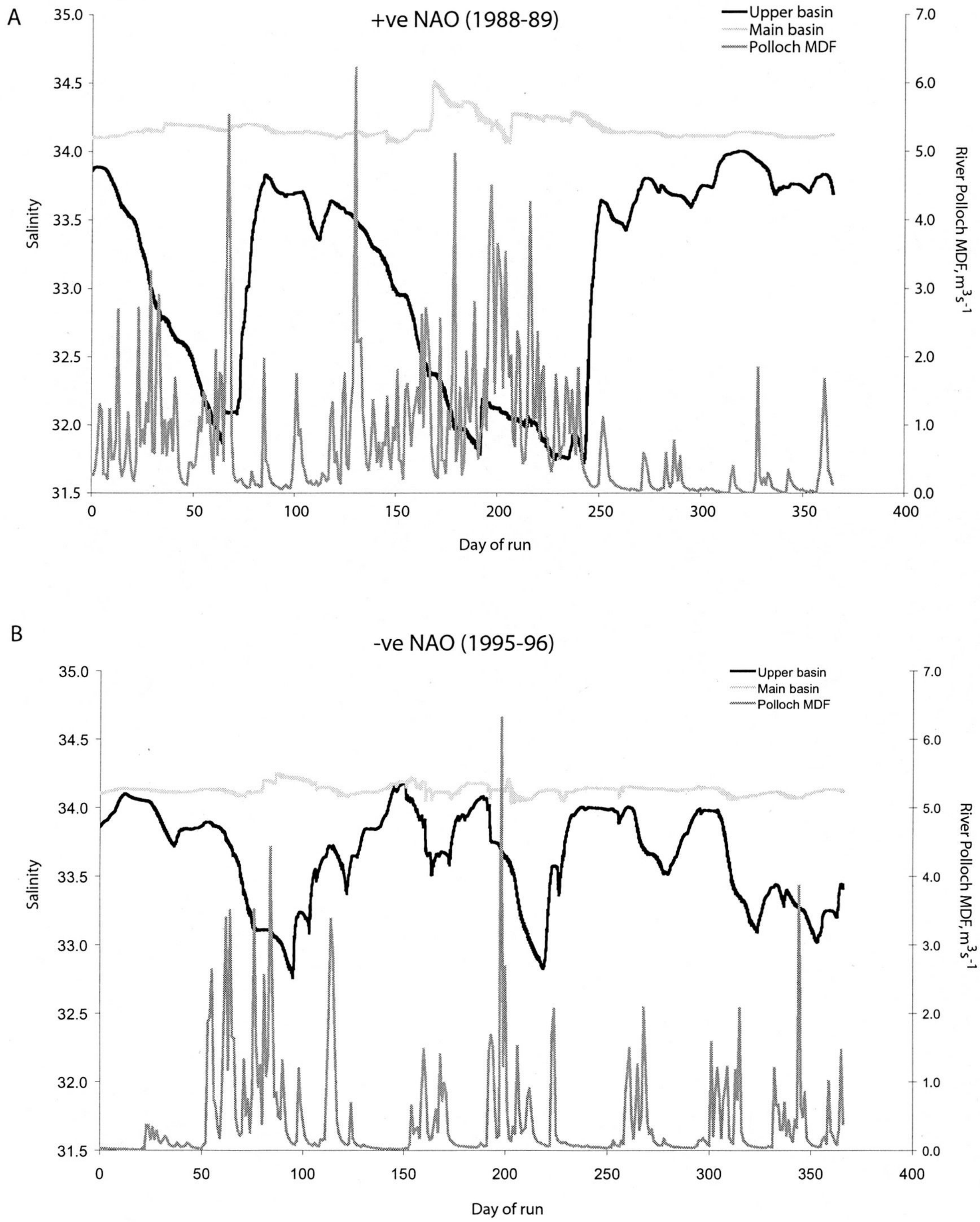

Figure 3.29 Modelling results for the inner basin salinity (black line) and main basin salinity (light grey line) of Loch Sunart during (A) an extreme positive NAO year (1988-89) and (B) an extreme negative NAO year (1995-96). The observed river discharge data (or mean daily flow, MDF) from the River Polloch (data from SEPA; shown in dark grey), scaled according to sub-catchment area, was used as an input into the model, and is included in this figure to illustrate the influence of freshwater input on inner basin salinity.

Gillibrand *et al.,* (2005) point out that the relationships between basin salinity and low frequency (i.e. 30 day running mean) climatic wind stress and river discharge data is much stronger than the relationship between salinity and daily discharge and wind data (table 3.9), particularly during the winter months when the NAO is most dominant. The influence of climatic wind stress or river discharge on inner basin salinity is clearly demonstrated by strong correlations (table 3.9), whilst the much weaker correlations for the main basin salinity support earlier suggestions that climatic wind stress or river discharge has little influence on the salinity in this basin.

The NAO appears to significantly influence the inflow of water into both the main and inner basins of Loch Sunart (table 3.8) however, the differing sensitivity of the basins to the NAO and it's associated weather or inputs is largely due to the differing sill depths of the two basins (figure 3.28). The inner basin sill is very shallow at 8 m water depth, thus inflowing water passing over the inner sill undergoes stronger mixing than water flowing over the outer basin sill (~ 33 m water depth). This results in the bottom water of the inner basin exhibiting characteristics similar to the surface water (which has been mixed at the sill and entrained into the inflowing deep water) whilst the main basin water retains the characteristics of source water seaward of the sill due to less mixing of the surface water layer over the main sill (Gillibrand *et al.,* 2005).

3.5.8.3 Sensitivity analyses

Sensitivity analyses were run on the model output for responses to modified wind stress, freshwater discharge, coastal salinity boundary conditions and low frequency climatic influences (the anomaly produced in the mean strength of wind velocity due to the NAO). A full description and discussion of the sensitivity analyses can be found in Gillibrand *et al.,*, (2005) but a summary is presented here.

Results from the river discharge sensitivity test showed no significant changes (maximum salinity change of 0.03) in main or upper basin salinity even with large modifications, e.g. – 20% and + 35%. As with river discharge, the modification of wind forcing by ± 10% did not significantly alter bottom water salinity, and a ±20%

Table 3.7 Mean and standard deviations for the model forcing parameters for the two NAO simulations. The westerly wind stress, τ_A, is calculated by $\tau_A = \rho_A . C_D . W^2$ where ρ_A is the air density at 1.2 kg m^{-3}, C_D is the drag coefficient at 1.1 x 10^{-3} and W is the westerly component of wind velocity (ms^{-1}). Taken from Gillibrand *et al., (*2005).

Parameter	1988 - 89	1995 - 96
Mean Flow in River Polloch (m^3s^{-1}), catchment = 7.9 km^2	0.76	0.44
Mean Flow into Loch Sunart (m^3s^{-1}), catchment = 299 km^2	28.76	16.65
Westerly Wind Speed - mean (ms^{-1})	2.32	-0.64
Westerly Wind Speed - standard deviation (m^3s^{-1})	5.00	5.73
Westerly Wind Stress - mean (Nm^{-2})	0.025	-0.011
Westerly Wind Stress - standard deviation (Nm^{-2})	0.067	0.082

Table 3.8 Summary statistics of bottom water salinity and inflow from the model simulations during a positive NAO phase (1988-89) and a negative NAO phase (1995-96). Taken from Gillibrand *et al., (*2005).

	1988-89		**1995-96**	
	Salinity	Inflow	Salinity	Inflow
Inner basin				
Mean	33.13	129.6	33.65	203.7
Minimum	31.50	0	32.73	0
Maximum	34.02	1159.5	34.18	1824.7
Standard deviation	0.652	213.4	0.319	278.9
Number of renewal days	108	—	158	—
Main basin				
Mean	34.18	238.8	34.16	694.0
Minimum	34.10	0	34.08	0
Maximum	34.32	2628.9	34.25	7373.6
Standard deviation	0.034	338.4	0.031	974.6
Number of renewal days	120	—	171	—

Table 3.9 Correlation coefficients (r) between the predicted daily mean bottom water salinity and the raw observed daily mean wind stress (τ) and river mean daily flow data (Q) and also the low frequency (running mean) time series (τ_c and Q_c). The values in parentheses are the time lag (days) which give the maximum correlation. All correlations are significant at 95 % except for those italicised. Taken from Gillibrand *et al.,* (2005).

	Inner basin		Main basin	
	1988-89	1995-96	1988-89	1995-96
Q	-0.56 (4)	-0.44 (9)	0.26 (3)	*-0.10 (5)*
τ	-0.51 (7)	-0.31 (17)	0.19 (2)	-0.25 (16)
Q_c	-0.80 (14)	-0.48 (9)	0.22 (6)	*0.06 (4)*
τ_c	-0.89 (15)	-0.39 (18)	0.40 (0)	-0.33 (0)

difference in westerly wind speed resulted in a maximum salinity difference of only 0.07 in the inner basin.

However, DWREs in Loch Sunart are known to be driven by winds with a strong negative westerly component (Gillibrand *et al.*, 1995), and both basins exhibit an increase in mean salinity and a reduction in the number of renewal days when the westerly wind component is reduced. Modified wind stress did have a noticeable effect on the volume inflow with changes of 12% and 33% for the inner and main basins respectively, though these inflows were not marked by salinity changes. The change in volume inflow was probably due to enhanced estuarine circulation in the fjord during increased east-west wind stress component. The climatic wind anomaly sensitivity analysis suggested negligible changes in main basin salinity, with mean salinity variations of less than 0.02 when the low frequency climatic signal was removed. Although the inflow into the main basin appears to respond to changes in this climatic influence, the sensitivity analyses suggest little change in main basin salinity, which agrees well with the model outputs (section 3.5.8.2) and the observed salinity cycle in Loch Sunart (section 3.4.2).

The inner basin on the other hand, shows a significant response to the removal of low frequency climatic signals (both wind stress and river discharge) with salinity increasing by ~ 0.38, the frequency of DWRE increasing by 30 days in the 1988/89 run, whilst the 1995/96 run had a salinity decrease of 0.12 and a decrease of DRWE frequency (16 days).

3.5.8.4 Implications of modelling climatically forced circulation in fjords

Fjordic circulation changes arising from climatic forcing are of particular interest to basin water quality and management issues, since many Scottish sea lochs host fish farms which are a major source of marine pollution (mainly via nutrient enrichment). Knowledge of flushing times and hydrography are essential for monitoring the impact of fish farms on the (often sensitive) sea loch environment (e.g. Gillibrand & Turrell, 1997). For example, Loch Sunart hosts a number fish farms including some in the inner basin; a prolonged period of NAO positive winters may reduce the frequency of DWREs in the inner basin, resulting in less flushing of 'polluted' basin water.

Modelling the response of the Loch Sunart basins to climate forcing provides essential information for the use of Loch Sunart sedimentary archives for palaeoenvironmental reconstruction. Ottersen *et al.,* (2001) show the NAO influences both terrestrial and marine ecology, whilst Nordberg *et al.,* (2000) and Filipsson & Nordberg (2004) report a benthic foraminiferal assemblage response to the prevailing positive NAO phase since the 1970s. Stable oxygen isotopes are often used in palaeoenvironmental reconstructions (chapters 6 and 7) as an indicator of temperature changes. Both temperature and salinity can influence the $\delta^{18}O$ of foraminiferal calcite thus interpretation of $\delta^{18}O$ data can be difficult when an environment experiences both temperature and salinity fluctuations. However, the negligible influence of the NAO on Loch Sunart main basin salinity suggests long $\delta^{18}O$ records from fossil benthic foraminifera are likely to represent temperature changes rather than salinity variations (chapters 6 and 7). This would agree well with Austin & Inall (2002) who used a regional salinity: $\delta^{18}O$ mixing line to calculate (using the palaeotemperature equation of Bemis *et al.*, 1998) the equilibrium calcite from observed Loch Etive temperature and salinity data. They concluded that the small impact of salinity on the $\delta^{18}O$ of water results in the possibility of palaeotemperature reconstructions from the $\delta^{18}O$ of foraminiferal calcite from Loch Etive and other Scottish sea lochs.

3.6 CONCLUSIONS

The climate of the Loch Sunart catchment reflects the climate experienced by the majority of the Scottish mainland, which in turn is strongly influenced by coastal water temperatures via oceanic heat transfer and thermal inertia. These strong relationships allow the Millport marine temperature series to be extended back beyond the period of observation (AD 1953-2001) via the application of a regression equation derived from the period of overlap between the Millport and Scottish mainland temperature (SMT) data. Observed daily temperatures in both the inner and main basin of Loch Sunart (40 m water depth) show a strong seasonal heating cycle, typical of mid-latitude shelf seas, and the agreement of Loch Sunart marine temperatures with Millport marine temperatures advocate the use of the Millport temperature series to hindcast temperatures experienced by Loch Sunart basin waters. The similarity in temperature anomaly trends of the SMT data and the long-term sea surface temperature (SSTA; HOLSMEER data) records suggests the reconstructed and extended Millport marine temperature series is likely to reflect climate variability in the wider North Atlantic region. The extended marine temperature data can be used for direct comparison with the proxy derived palaeotemperature records obtained from Loch Sunart (chapter 8).

NW Scotland temperature and precipitation records show clear responses to the North Atlantic Oscillation, with NAO positive years yielding warmer and wetter winters, whilst cold and dry winters accompany negative NAO years. Given the importance of climatic parameters (such as wind stress and freshwater inputs) to fjord hydrography (e.g. Farmer & Freeland, 1983 and Gillibrand *et al.*, 1995), the circulation of Loch Sunart basins are expected to show a response to the NAO. Salinity observations in Loch Sunart over an annual cycle showed a clear response of inner basin salinity to precipitation received by the catchment (mirrored by freshwater inputs into the sea loch). To test whether the Loch Sunart basin hydrography was significantly modulated by climatic influences during differing phases of the NAO, the circulation of the inner and main basin was modelled using an existing circulation model (Elliott *et al.*, 1992; Gillibrand *et al.*, 1995) with along-channel wind stress, river discharge and surface elevation at the loch mouth as inputs. Modelling results from the inner basin of Loch Sunart showed meteorological forcing during the positive NAO year 1988-89 resulted in less frequent deep water renewal events, greater salinity variability and a lower annual mean salinity (by 0.52) than for the negative NAO year. The NAO appeared to have little influence on main basin salinity, despite significant variations in the inflow of water into the basin. The modelling results agreed well with the observed basin hydrographic responses to freshwater inputs. The implication of negligible inter-annual salinity variations in the main basin of Loch Sunart, along with the report of minor salinity influences on the δ^{18}O of Loch Etive water during renewal events (using the Loch Sunart δ^{18}O: salinity relationship; Austin & Inall, 2002) suggests the main basin of Loch Sunart may provide an ideal location for resolving high resolution palaeotemperature records from fossil benthic foraminiferal δ^{18}O calcite.

CHAPTER 4 - MARINE RESERVOIR AGES IN SCOTTISH COASTAL WATERS

4.1 Introduction

Organisms living in the terrestrial biosphere generally exhibit ^{14}C concentrations which are in equilibrium with the atmospheric ^{14}C due to rapid gaseous exchange during life processes (section 2.7). Conversely, marine organisms typically deposit their carbonate shells in isotopic equilibrium with seawater (Mook & Vogel, 1968), deriving carbon from the surrounding seawater, thus their ^{14}C concentration will reflect the ^{14}C concentration of the seawater in which they live. Restricted replenishment of ^{14}C across the well mixed surface ocean-atmospheric boundary results in ocean water becoming deficient in ^{14}C relative to the atmosphere, therefore marine organisms exhibit an 'apparent age' (section 2.7).

The ^{14}C deficiency of a water mass represents it's reservoir age, R(t), which can be determined by comparing measured marine ^{14}C ages with contemporaneous atmospheric ^{14}C ages (figure 4.1 and section 2.7), and should be applied to conventional marine radiocarbon dates in order to correct for growth in a different carbon reservoir (Stuiver *et al.*, 1986). Though the modelled global surface ocean reservoir age (R*) is taken to be 400 years, with a ΔR equal to zero (Stuiver & Braziunas, 1993), marine reservoir ages can vary geographically (e.g. Berkman & Forman, 1996; Facorellis *et al.*, 1998; Siani *et al.*, 2000; Yoneda *et al.*, 2000). A more accurate way to correct sample ^{14}C ages for regional marine radiocarbon reservoir effects is to subtract ΔR from the measured ^{14}C age prior to using the marine calibration curve for calibration, where ΔR is defined as the difference between a measured marine ^{14}C age and the global model ^{14}C curve of the surface ocean (R, taken from the Marine98 radiocarbon calibrations curve, Stuiver *et al.,* 1998), i.e.:

$$\Delta R = \text{measured } ^{14}\text{C age} - R \qquad \textit{(Eq. 4. 1)}$$

Modern marine reservoir ages may be determined by radiocarbon dating;

i) marine carbonate material obtained live and with a known collection date prior to 1950 AD i.e., pre-bomb samples (e.g.. Mangerud & Gulliksen, 1975; Olsson, 1980 and Heier-Nielsen *et al.*, 1995b)

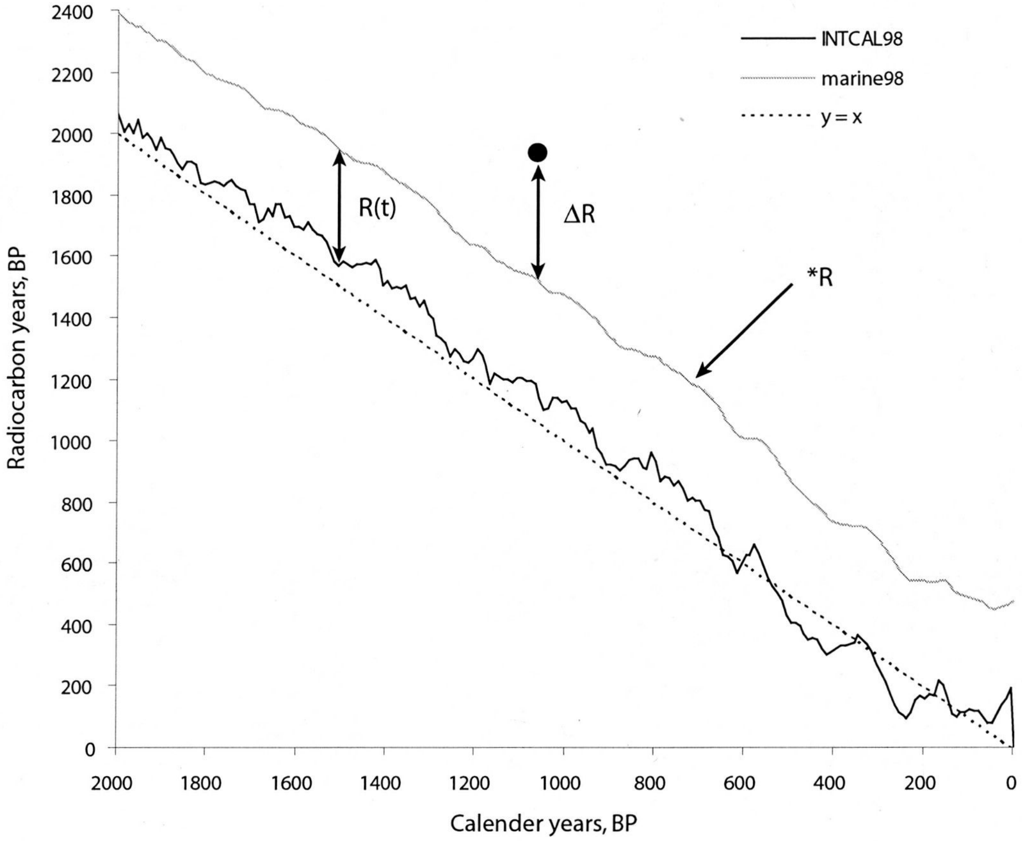

Figure 4.1 Radiocarbon calibration curves for the last 2000 years BP (i.e. before AD 1950). The atmospheric INTCAL 98 curve (solid black line) and marine98 curve (grey solid line) of Stuiver *et al.*, (1998) are shown along with the hypothetical line of y = x. To clarify the terminology appertaining to radiocarbon reservoir ages: i) R(t) = the marine radiocarbon reservoir age which is determined by calculating the difference between the measured ^{14}C age of a marine sample and a contemporaneous terrestrial (wood) sample representing the atmospheric ^{14}C value; ii) R* = the modelled global surface ocean reservoir age applied to all marine radiocarbon ages. This value represent open ocean conditions and equates to ~ 400 years, where ΔR = 0; iii) ΔR = the regional deviation of a marine ^{14}C sample from the model curve (R*) of the surface ocean.

ii) paired marine-terrestrial samples e.g.. wood and shell material, (e.g.. Reimer *et al.,* 2002)

ii) stratigraphic markers such as tephra layers which have a known historical or terrestrial ^{14}C age (e.g.. Austin *et al.,* 1995, Eiríksson *et al.,* 2000).

A synopsis of ΔR determination in the North East Atlantic region is provided in table 4.1.

4.1.2 Regional deviations (ΔR) associated with fjords

Harkness (1983) calculated the reservoir age of UK coastal waters to be 405 ± 40 years, however this data set totalling 14 locations included only 4 from the west coast of Scotland. Since different water masses from the seas surrounding the UK are likely to exhibit difference ΔR tendencies, and ΔR may be affected by a latitudinal effect (e.g. Mangerud, 1975), it is possible that the ΔR value for the west coast of Scotland differs from the regional UK average.

The sea lochs of NW Scotland exhibit fjordic circulation (e.g. chapter 3) i.e. they have a restricted connection with open coastal waters and high freshwater inputs often result in brackish surface waters, which can dilute the salinity of bottom water masses. An important characteristic of fjord circulation are periodic deep water renewal events (DWREs; previously discussed in section 1.8.2 and chapter 3). The ^{14}C/^{12}C ratios of freshwater systems in igneous areas (such as NW Scotland) should be similar to that of the atmosphere (Broecker & Walton, 1959) and are unlikely to be influenced by 'hard water effects' from the surrounding bedrock geology (e.g. Heier-Nielsen *et al.*, 1995b). Additionally, Austin & Inall (2002) exemplified how DWREs could influence the isotopic composition of fjord water and a freshwater influence has been suggested. The significant influence of freshwater in fjordic hydrography suggests that Scottish fjords may exhibit younger marine reservoir ages than the 405 ± 40 years estimated for the coastal waters of the UK (Harkness, 1983). Reimer *et al.,* (2002) report a ΔR value of -33 ± 93 ^{14}C years for the coastal waters of Ireland, Scotland and the Orkney Isles during the mid to late Holocene, whilst Ascough *et al.,* (2004) reported a ΔR of -79 ± 17 ^{14}C years for N and W Scottish coastal waters at approximately 2000 yr BP.

Differences in sea loch bathymetries, i.e. sill and basin depths and freshwater inputs (Edwards & Sharples, 1986), mean that sea lochs typically exhibit varying hydrography. For example, the frequency of DWREs and salinity of basin water (Edwards & Sharples, 1986; Gillibrand *et al.*, 1995; Gillibrand *et al.*, 1996; Allen & Simpson, 1998; Austin & Inall, 2002) will vary and likely show different R(t) responses (e.g. table 4.1). Despite these differences, an average ΔR value for Scottish sea lochs would be useful when constructing chronologies for sedimentary archives from these unique environments.

4.2 Project aims and hypothesis; calculating ΔR values of NW Scottish coastal waters

The 'apparent' age of marine carbonates from sea loch environments could be affected by the following;

a) the degree of exchange with the coastal waters via typical fjordic circulation e.g. DWREs (section 1.8.2). Over longer time-scales, sea-level changes due to the post-glacial isostatic rebound of the land will act to modify these exchange processes because of the critical importance of mixing over the sill regions (section 1.8.2). For example, Shennan *et al.,* (1995) report an isostatic sea level rise of approximately 2 m during the last 2,000 years BP in NW Scotland.

b) Variations in the amount of precipitation and wind strength/direction experienced by the catchment area are also known to impact upon sea loch circulation (chapter 3; Gillibrand *et al.*, 1995; Gillibrand *et al.*, 2005), with more frequent DWRE resulting in more saline bottom waters. Such changes in salinity are likely to affect the ΔR of the sea loch because they reflect the mixing processes between coastal and fjordic water masses.

The hypothesis of variable ΔR values in Scottish sea lochs is tested using two approaches;

1. By radiocarbon dating marine mollusc shells (obtained from the National Museum of Scotland, Edinburgh) collected on known dates prior to 1950 AD (e.g. Mangerud, 1972, Harkness, 1983 and Heier-Nielsen *et al.*, 1995a) to provide a means of determining local reservoir age and regional ΔR of sites

Table 4.1 Determination of regional ΔR values for the North East Atlantic shelf sea region.

Reference	Location	Method	R(t) or ΔR, years BP	Suggested reason for regional R(t), i.e. ΔR
Mangerud (1972)	Norwegian coast and fjords	Pre-bomb shells collected live in known year	R(t) 340 ± 75 to 550 ± 80 Average R(t) 450 ± 40	No significant ΔR deviation Noticed a trend between apparent age and sample water depth – possible brackish water influence
Mangerud & Gulliksen (1975)	Norwegian coast, Spitsbergen and Artic Canada	Pre-bomb shells collected live in known year	R(t) ~ 440 years (Norwegian Coast), 510 ± 30 (Spitsbergen), 750 ± 50 (Artic Canada)	Geographical differences in ΔR reflect the degree of mixing between Atlantic Ocean water and 'older' Artic Ocean water at the sites. Link between increasing R(t) and latitude
Olsson (1980)	Swedish coastal waters	Pre-bomb shells collected in known year and marine mammal bones	R(t) 315 ± 30 years from bones R(t) 335 ± 20 for shells off E Jutland and W Sweden	Reservoir ages likely to have been influenced by the mixing of the brackish Baltic Sea and Atlantic water masses
Harkness (1983)	UK coastal waters	Pre-bomb shells collected in known year	R(t) 405 ± 40 years ΔR = 14 ± 13	The deficiency in ^{14}C reflects the influence of the Atlantic Ocean waters around the coast of the UK. Tentative link between increasing reservoir age with higher latitudes
Heier-Nielsen *et al.*, (1995)	Danish coastal waters, including fjords	Pre-bomb shells collected live in known year	Coastal waters: R(t) 377 ± 16. ΔR=13 ± 16, Fjords: R(t) ~ 634, mean ? R=279	Large variability in the fjordic samples is attributed to the 'hard water effect' i.e. the mixing of North Sea marine waters with groundwater rich in ancient carbon derived from limestone bedrock geology of Denmark.
Reimer *et al.*, (2002)	W coast Ireland, W coast Scotland, Outer Hebrides and the Orkney Islands	Paired dating of marine and terrestrial samples	ΔR = -33 ± 93	ΔR probably constant during the last 2000 years, possibly for the past 6000 years
Ascough *et al.*, (2004)	N and W Scotland	Paired dating of marine and terrestrial samples	ΔR = -73 ± 17	ΔR presented is for the period around 2000 years BP.

around the NW Scottish coast (figure 4.2). Articulated bivalves in pristine condition (periostracum intact and often articulated) from Loch Creran, Loch Fyne, Upper Loch Fyne, Tarbert, and Wemyss Bay were used. There was a dearth of available archived shells from Scottish sea lochs, therefore two shells from Oban were also radiocarbon dated.

Unfortunately, information on the water depth, temperature or salinity did not accompany the shell samples, and knowledge of whether the sample depth is below the typical stratification depth for the sea loch is particularly important. The majority of the mollusc species in this study have reported habitats from littoral to depths of up to 100 m. The preferred substrate tends to be mud or muddy sand suggesting fairly low energy environments of deposition, i.e. water depths below spring low tide and beneath the influence of wave action.

2. By radiocarbon dating paired marine and terrestrial samples obtained from the same horizon in sediment cores from Loch Sunart and Loch Etive (figure 4.2). The difference between the radiocarbon ages for these samples should provide an estimate of local reservoir ages for that period in time, assuming rapid deposition of the terrestrially-derived organic material in the sediment core, i.e. the plant lived contemporaneously with the marine organism (e.g. Siani *et al.*, 2000).

4.3 RESULTS OF THE ^{14}C DATING OF PRE AD 1950 SCOTTISH MARINE BIVALVES FROM MUSEUM COLLECTIONS

All conventional radiocarbon dates are reported as suggested by Stuiver & Polach, 1977), i.e. the Libby half-life of 5568±30 years is used to calculate the decay of ^{14}C, all dates are reported with reference to 95% of the activity in the standard NBS oxalic acid in 1950 AD, and normalised to $\delta^{13}C = -19$ ‰ with respect to the standard PDB.

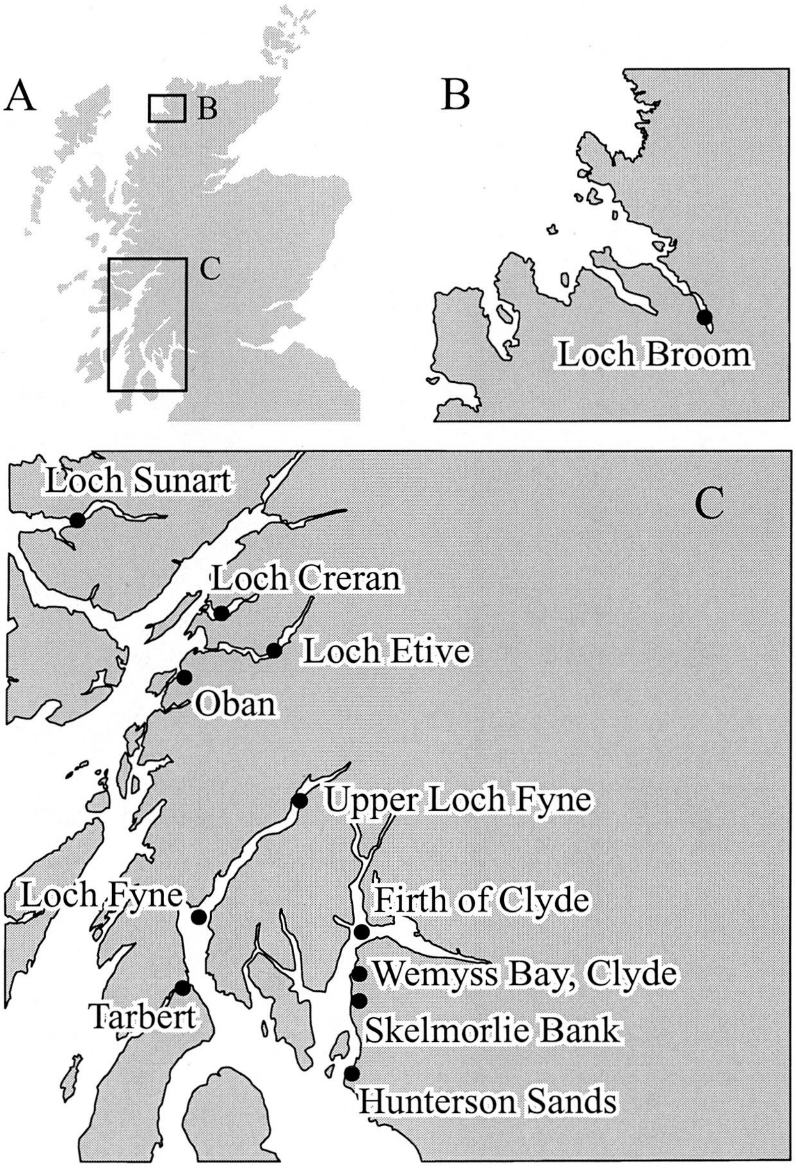

Figure 4.2 - (A) Location map for the radiocarbon reservoir and chronology work, showing the two study areas, which are seen in detail in B and C. The shells used in this study were collected from Loch Creran, Loch Fyne, Upper Loch Fyne, Tarbert, Wemyss Bay, and Oban by Alexander Somerville between 1843 – 1907 AD. Sample material used in Harkness (1983) were collected from Loch Broom, Skelmorlie Bank, Hunterston Sands and the Firth of Clyde.

4.3.1 Radiocarbon data

The results of AMS ^{14}C dating carried out on museum collections of marine bivalves collected 'live' from Scottish west coast waters between AD 1843 and 1935 are presented in table 4.2.

The regional deviation (ΔR) from the mean global surface ocean reservoir age (*R), was calculated by subtracting the (uncalibrated) measured ^{14}C age (R) from the global marine reservoir age (*R where $\Delta R = 0$) taken from the 'marine98' calibration curve of Stuiver *et al.*, 1998b) using equation *4.1.*

Figure 4.3 shows the (uncalibrated) results of the marine radiocarbon reservoir age investigation (with 1 σ error bars). The dates obtained range from 347 ± 39 ^{14}C years BP to 554 ± 35 ^{14}C years BP (table 4.2). Weighted means were used to obtain a more realistic measure of a set of values, since they are skewed towards the mode of the data set rather than the median, and therefore the average will not be 'pulled' by singularly anomalous results;

$$\text{Weighted average, } \varpi = \Sigma\,(x / \sigma^2) / \Sigma\,(1 / \sigma^2) \qquad \textit{(Eq. 4.2)}$$

where x is the ^{14}C age and σ is the ^{14}C age error.

The weighted average radiocarbon age of the samples including the Loch Creran sample (AAR-7489) is 444 ± 14 ^{14}C years BP and 458 ± 15 ^{14}C years when the Loch Creran sample is excluded. Five out of the seven dates fall below the global marine curve, with the 1 σ error bars of only sample AAR-7420 falling within the limits of the global marine radiocarbon curve (from hereon denoted by *R). The error bars of the two older samples showing older dates than *R do not intersect the curve (figure 4.3).

Regional marine radiocarbon reservoir ages are better investigated by exploring the ΔR values, since the data is standardised to $^*R = \Delta R = 0$, i.e. the temporal trend in *R is removed. The results of ΔR are presented in figure 4.4 and are similar to those shown in figure 4.3. Although the Loch Creran sample does not have a specific collection date, the ΔR range has been included to exemplify the extent to which these

Table 4.2 AMS radiocarbon dates from the historical shells obtained from the Scottish Natural History Museum. The AMS ^{14}C measurements were made at Aarhus University, Denmark (AAR) under the guidance of Professor Jan Heinemeir, Ann-Berith Jensen and Vibeke Jensen. Stable isotopic compositions were measured by Dr. Á. E. Sveinbjörnsdóttir, at the Science Institute, Reykjavík, Iceland.

Aarhus reference code	Sample location	Year of collection, AD	Mollusc species	R, ^{14}C years BP	ΔR, years	$\delta^{13}C$, ‰	$\delta^{18}O$ ‰
AAR -7419	Oban	1935	*Musculus discors*	413 ± 36	-49 ± 36	2.02	1.37
AAR -7420	Oban	1935	*Tridonta elliptica*	443 ± 34	-19 ± 34	2.85	2.08
AAR -7421	Upper Loch Fyne	1888	*Pseudamussium septemradiatum*	397 ± 36	-69 ± 36	2.28	1.95
AAR -7422	Loch Fyne	1850	*Aequipecten opercularis*	554 ± 35	67 ± 35	0.75	0.56
AAR -7423	Wemyss Bay, Clyde	1885	*Nucula nucleus*	518 ± 36	49 ± 36	1.97	2.44
AAR -7424	Tarbert, Clyde	1887	*Nucula tenuis*	419 ± 35	-48 ± 35	1.82	2.74
AAR -7489 †	Loch Creran	1843	*Nucula nucleus*	347 ± 39	-143 ± 39	1.29	2.56
		1907	*Nucula nucleus*	347 ± 39	-105 ± 39	1.29	2.56

R is the measured, uncalibrated radiocarbon age of the historical shell. ΔR denotes the deviation from the mean global surface ocean reservoir age, which is calculated by $\Delta R = R - {}^{*}R$, where *R is the global marine reservoir age taken from the 'marine98' calibration curve of Stuiver *et al.,* 1998b).

† The historical age is not known for sample AAR-7489, however it is known that the shell was collected between the 1843 – 1907 AD by Alexander Somerville. Therefore, the two ΔR values for this sample represent the deviation from the marine calibration curve at the oldest possible collection year and the youngest possible collection year. The average ΔR value for the sample is -124 ± 39 years.

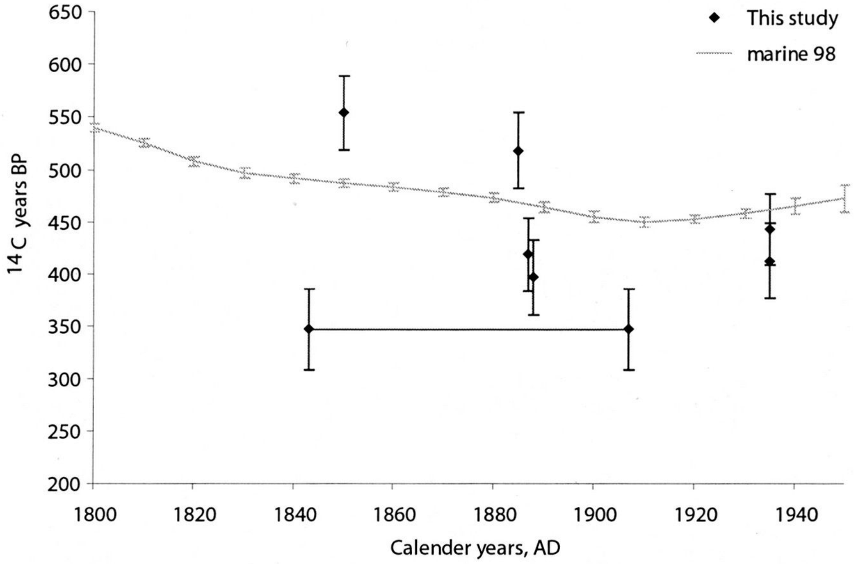

Figure 4.3 The uncalibrated radiocarbon dates (1σ error bars) from this study (black diamonds) and the 'marine98' calibration curve (1σ error bars, grey solid line) representing the global marine radiocarbon reservoir age of the surface ocean (Stuiver *et al.*, 1998b). The potential collection period of the Loch Creran sample (AAR-7489) is shown by the linked dates at 347 ^{14}C years BP.

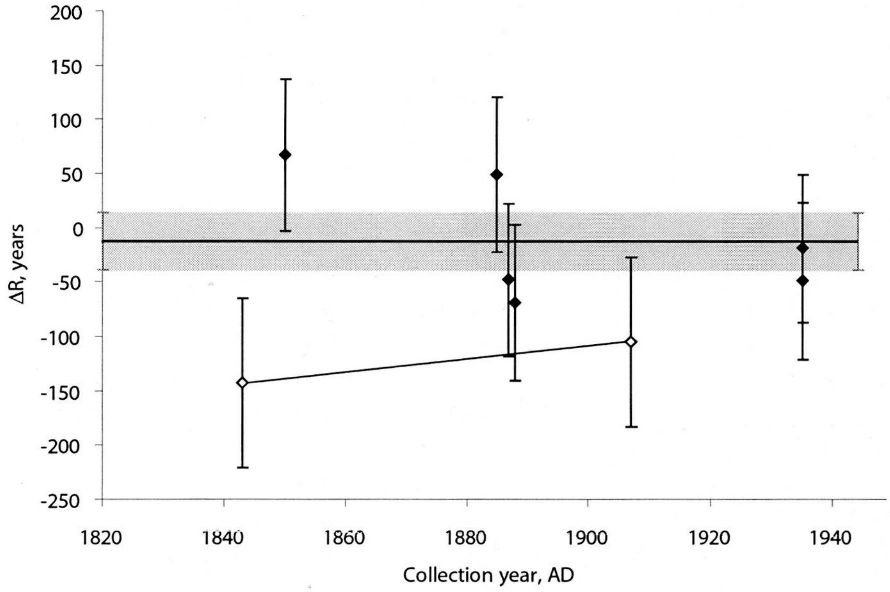

Figure 4.4 The ΔR values of the Scottish west coast shells (filled diamonds) plus the Loch Creran sample (unfilled diamond) with measured ^{14}C age errors of 2 σ (standard deviations). The thick grey line represents the weighted average of the ΔR values (not including the Loch Creran sample) with 2 σ error bars (shaded box).

fjordic environments could deviate from *R. The ΔR values from this study range from a mean value of -124 ± 39 to +67 ± 35 ^{14}C years. The weighted ΔR value for the samples excluding the average ΔR of the Loch Creran sample is -11 ± 14 years, and -25 ± 14 years when an averaged ΔR for the Loch Creran sample is included. Initially there appears to be significant variation between the ΔR values, however figure 4.4 shows that the 2 σ error bars of all samples intersect the 2 σ error bar of the weighted average ΔR = -11 ± 14 years, suggesting that the difference between the data is insignificant (*pers comm.,* Prof. J. Heinemeier, 2001). The fact that the ΔR values fall within the acceptable limits of the weighted average suggests that all data can be included in a regional average (Harkness, 1983).

The mean ^{14}C age of the two samples from Oban (samples AAR-7419 and AAR-7420) fall within the error bars of the dates. A simple statistical method (where Δt is the difference between the two dates and S_t is the combined standard deviation of the mean corresponding to the two dates) shows that $\Delta t < S_t$ and therefore there is no significant difference between the two Oban dates (Nemec, 2003). The lack of same species data negates the possibility of investigating species-specific vital effects, however, the similarity in the dates suggests that vital effects are not a major influence in the uptake of radiocarbon. If this is the case, these data support the suggestion that variance in ΔR values reflect environmental influences, not vital effects (Keith *et al.*, 1964).

4.3.2 Stable isotopic composition of the historically collected shells

The $\delta^{13}C$ and $\delta^{18}O$ measurements for the museum shells are shown in table 4.2 and also in figures 4.8 and 4.9. The $\delta^{13}C$ values range from 0.75 to 2.85 ‰, with a mean value of 1.85 ± 0.68 which is within the range quoted for marine shells (Keith *et al.*, 1964 and Olsson & Osadebe, 1974). The $\delta^{18}O$ values range from 0.56 to 2.74 ‰ with a mean value of 1.96 ± 0.77 ‰. A linear correlation between $\delta^{18}O$ and $\delta^{13}C$ suggests a moderate positive relationship ($r = 0.403$; $R^2 = 16\%$) insignificant at a 95% confidence level ($p = 0.370$), which may be due to the low sample number.

Linear correlations between the ΔR values and the isotope values show:

a) no significant correlation ($r = -0.196$, $p = 0.674$) with respect to $\delta^{13}C$.

b) A moderate correlation (r = -0.506, p = 0.247) with $\delta^{18}O$, significant at 85%. An R^2 value of 0.31 suggests approximately 31% of the variation in ΔR can be explained by variation in $\delta^{18}O$.

The hypothesis presented in section 4.2 proposes that shell carbonate from sea lochs with infrequent DWREs and thus environments of reduced basin water salinity, are likely to exhibit 'younger' marine radiocarbon reservoir ages than *R due to the continuous input of 'new' ^{14}C from precipitation. Therefore, one would expect depleted $\delta^{18}O$ values (reflecting freshwater input) to be accompanied by negative ΔR, i.e. a positive ΔR: $\delta^{18}O$ relationship. However, the negative ΔR: $\delta^{18}O$ relationship for the historically collected museum shell data may be due to a low sample numbers (n = 7) rather than a true representation of basin salinity influence (represented by $\delta^{18}O$) on the ΔR values of marine carbonates from Scottish coastal waters.

4.4 Results from paired ^{14}C dated samples (terrigeneous plant and marine shell material)

Regional ^{14}C deviations (ΔR values) can be calculated by subtracting the ^{14}C date of terrestrial material from the ^{14}C date of contemporaneous marine material (e.g. Siani *et al.*, 2000; Reimer *et al.*, 2002; Ascough *et al.*, 2004). Plant fragments and marine shell material were obtained for AMS dating from the same sediment depth from cores SC102 (Sholkovitch core from Loch Sunart) and GC008 (gravity core from Loch Etive). C/N analyses were carried out on the material prior to dating to ascertain the provenance of the material, i.e. whether it was terrigeneous or marine.

The C/N ratios (table 4.3) and the $\delta^{13}C$ isotope values (table 4.4) of the organic fragments (samples GC008-95 and SC102-68) found in the sea loch sediment cores suggest that they are of terrestrial origin, with C/N ratios falling within the expected range of 17-30 (Middleburg & Nieuwenhuize, 1998). However, the C/N ratios of the fine fraction organic material (from hereon referred to as residues) from samples GC008-26 and GC008-35, suggest a marine provenance for the organic matter (e.g. Thornton & McManus, 1994), hence they are not suitable for investigating reservoir ages.

The ^{14}C measurements of the paired samples are presented in table 4.4. The $\delta^{13}C$ values of samples GC008-95 and SC102-68 fall within the range of land plants (e.g. Middleburg & Nieuwenhuize, 1998), thus confirm the results of the C/N ratios, which suggest a terrestrial origin.

The marine radiocarbon reservoir age, R(t), can be calculated using paired samples by subtracting the calibrated atmospheric radiocarbon age of the plant from the uncalibrated radiocarbon date of the marine carbonate data. The paired samples suggest a R(t) of -1068 ± 111 cal years for Loch Etive and a R(t) of 266 ± 42 cal years for Loch Sunart.

The paired samples from Loch Etive suggest a large negative sign for the radiocarbon reservoir age since the plant sample is older than the marine carbonate sample, therefore they cannot be used to reliably determine the marine reservoir ages. Botanical inspection (by Dr. E. Warncke) of the plant remains suggested no evidence of charring or long-term peat bog residency (*pers. comm.,* Dr. E. Warncke, 2002). Therefore the data may possibly yield information on the input time of terrigeneous material entering the sea loch from the surrounding catchment area, with a possible 'retention' time of approximately 1000 years inferred. Bioturbation is a potential problem which must be considered when dealing with marine sediment cores. Lead and caesium data (chapter 8) suggest some degree of bioturbation in cores GC023 (Sunart) and GC008 (Etive); a process which might act to displace contemporaneous fossil material from its stratigraphic context. However, bottom water in Loch Etive often becomes low in oxygen (due to infrequent deep-water renewals events) and has been known to reach anoxia, therefore the disparity between the data is unlikely to have been caused by bioturbation.

Theoretically, the ΔR value for Loch Sunart can be calculated from the paired samples, since the marine sample has an older (apparent) radiocarbon age than the terrestrial material, and the estimated calendar age of the terrestrial plant sample can be determined through calibration using the 'INTCAL98' curve (Stuiver *et al.*, 1998a). The marine radiocarbon age from the 'marine98' curve for that year is then subtracted from the uncalibrated measured marine radiocarbon date, to give ΔR for that location. The calibrated age of the plant sample is 145 ± 145 cal yr BP (i.e. ~ AD

1805), and the uncalibrated marine radiocarbon age (from the 'marine98' curve) for AD 1805 is 532.7 ± 4 ^{14}C years BP. Therefore, assuming the shell and the plant sample are contemporaneous, the ΔR value for Loch Sunart in this period is approximately -121.7 ± 149 years.

In reality there are serious inherent calibration problems in the case of the Loch Sunart sample. The atmospheric calibration curve suggests that there is a 95.4% probability that the calendar age of the Loch Sunart plant sample is 145 ± 145 cal yr BP, which equates to AD 1805 on the calendar scale. However, the measured radiocarbon age falls with the recent radiocarbon calibration plateau which began at ~AD 1700 extending to the limits of dating, resulting in a multi-modal probability distribution for the calibrated date (figure 4.5). The large error bar for the mean date of 145 ± 145 cal yr BP at 95.4% probability is a function of the large probability distribution under this section of the curve. Within the 68.2% probability calibration range, the mean date of 145 ± 145 cal yr BP (at 95.4% probability) actually falls within a section of the calibration curve with a low (6%) probability. The true calender age cannot be accurately determined for single samples falling within such a radiocarbon plateau.

The calibrated age of sample AAR-7493 is unlikely to be 145 cal yr BP, rather it may fall within the limits of a higher probability mode such as the 25.1% section, corresponding to 230-170 cal BP. Irrespective of this speculation, the nature of the calibration results for the Loch Sunart organic sample (AAR- 7493) implies that these data should not be used to determine marine reservoir ages. Therefore, in the absence of further paired terrestrial marine data, these results will not be discussed further.

4.5 DISCUSSION

4.5.1 Regional ΔR for the West coast of Scotland

The weighted averaged measured radiocarbon age for all the samples including the Loch Creran sample is 444 ± 14 years, and 458 ± 15 years excluding the Loch Creran sample. To improve the spatial coverage of the regional ΔR value and add more sea loch or 'restricted' environments to the relatively small dataset (n = 7) presented in the

Table 4.3 Results of the C/N analysis carried out on the sample material prior to radiocarbon dating in order to ascertain the provenance of the material. All C/N analyses were carried out at Dunstaffnage Marine Laboratories, Oban by Dr T. Brand.

Sample	**Sample material**	**Atomic C/N ratio**	**Wt. % C org**
GC008 - 95	Twig fragment	25.42	26.30
SC102 - 68	Organic fragment	28.58	23.38
GC008 - 26	Organic residue	7.14	19.20
GC008 - 35	Organic residue	5.94	22.43

Table 4.4 AMS radiocarbon dates and stable isotopic compositions of the paired samples (shell and unknown plant species) obtained from sediment cores GC008 (Loch Etive) and SC102 (Loch Sunart). The AMS ^{14}C measurements were made at Aarhus University, Denmark (AAR) under the guidance of Professor Jan Heinemeir, Ann-Berith Jensen and Vibeke Jensen.

Lab reference code	**Sample location**	**Material**	**δ^{13}C, ‰**	**δ^{18}O, ‰**	**^{14}C age years BP**	**Calibrated ^{14}C date, cal yr BP**
AAR -7490	GC008–95	Shell	+ 1.11	+ 1.51	3897 ± 45	3850 ± 130
AAR -7491	GC008 – 95	Plant	- 27.61	- 23.39	4407 ± 49	4965 ± 115
AAR - 7492	SC102–68	Shell	+ 0.74	+ 2.34	411 ± 32	35 ± 64
AAR - 7493	SC102–68	Plant	- 24.22	- 22.85	149 ± 38	145 ± 145

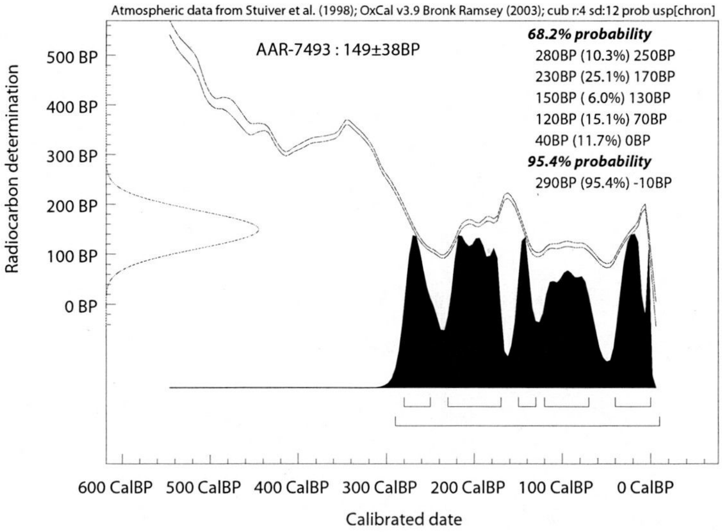

Figure 4.5 Calibration of the Loch Sunart plant sample (AAR-7493) using OxCal3 (Bronk Ramsey, 1995). The Oxcal3 screen dump clearly shows that the sample AAR-7493 falls within the most recent ^{14}C plateau.

previous section, radiocarbon reservoir data from Harkness (1983) were combined with data from this study (table 4.5).

Harkness (1983) determined a marine radiocarbon reservoir age of 405±40 years for UK coastal waters, however this included only four West Scotland sites (seen in table 4.5). Harkness highlighted samples SRR-170 (a+b) and SRR-356(b) as falling outwith the acceptable statistical variance (2σ) for the group's mean apparent age of 405 ±40 years. These samples have not been immediately rejected since the data used here is not from the Harkness (1983) publication but rather the recalculated radiocarbon ages from Reimer (2004; http://radiocarbon.pa.qub.ac.uk/marine/refs/132.html, hereon referred to as Reimer, 2004). The Harkness data from Reimer (2004) shows younger apparent ages than the dates from Harkness (1983) as they have been corrected for isotopic fractionation.

The Harkness weighted reservoir age for the Scottish west coast samples is 460 ± 13 ^{14}C years BP, and individual reservoir ages can be seen along with the data from this study in figure 4.6. Out of the 9 samples, 6 samples show negative ΔR values, with samples SRR-356a, SRR-356b and SRR-357b exhibiting positive ΔR values greater than ~ 70 ± 33 years (table 4.5). Harkness (1983) dated the inner and outer parts of the shell separately, and also dated the periostracum of the *Pinna fragilis* shell (sample SRR-710-c). Keith *et al.*, (1964) obtained a mean δ^{13}C variation of 0.73‰ between the outer and inner shell material (which they attributed to variations in carbon uptake between the shell's internal and external environments) and the mean δ^{13}C variation from the Harkness data agrees well at 0.27 ± 0.22‰.

The ΔR results from the differing shell parts generally fall within the standard deviation limits of each other (table 4.5; figure 4.7), with the exception of the periostracum data (SRR-710-c) and the Loch Broom sample (SRR-356) which are statistically significantly different. The periostracum of sample SRR-710-c has a δ^{13}C value of -16.5‰; 12.7‰ different to the inner/outer shell mean δ^{13}C. Periostracum is an organic layer formed from proteinaceous material, hence it is unlikely to yield δ^{13}C values similar to the inorganic carbon in $CaCO_3$. Results of sample SRR-710-c have been excluded from relationships requiring δ^{13}C as a variable, however the ^{14}C age of this sample has been included in the weighted averages since Harkness (1983) does

Table 4.5 Recalculated measured radiocarbon ages, marine reservoir ages and ΔR values for the Harkness (1983) shells from the Scottish west coast. Data obtained from Reimer, 2004 (http://radiocarbon.pa.qub.ac.uk/marine/refs/132.html, last updated 14th February, 2004 accessed on 19th February, 2004). OS denotes outer shell, IS denotes inner shell and PERI denotes the periostracum. The sample locations can be seen in figure 4.2.

Laboratory ID	Sample location	Sample Material	Historical age	^{14}C age BP	ΔR, years	δ^{13}C, ‰
SRR -357a	Loch Broom	*Dosinia exoleta* - OS	1900	442 ± 29	-12 ± 30	0.5
SRR -357b	Loch Broom	*Dosinia exoleta* - IS	1900	526 ± 34	71 ± 34	0.3
SRR -1822a	Firth of Clyde	*Venus gallina* - IS	1890	400 ± 46	-64 ± 46	-0.2
SRR -1822b	Firth of Clyde,	*Venus gallina* - OS	1890	391 ± 52	-73 ± 52	0
SRR - 710c	Skelmorlie Bank,	*Pinna fragilis* - PERI	1920	426 ± 80	-26 ± 80	-16.5
SRR - 710a	Skelmorlie Bank,	*Pinna fragilis* - OS	1920	343 ± 42	-109 ± 42	3.5
SRR - 710b	Skelmorlie Bank,	*Pinna fragilis* - IS	1920	329 ± 54	-123 ± 54	4.1
SRR -356a	Hunterston Sands	*Cerastoderma edule* - OS	1926	531 ± 38	75 ± 38	1.3
SRR -356b	Hunterston Sands	*Cerastoderma edule* - IS	1926	545 ± 32	89 ± 33	1.4

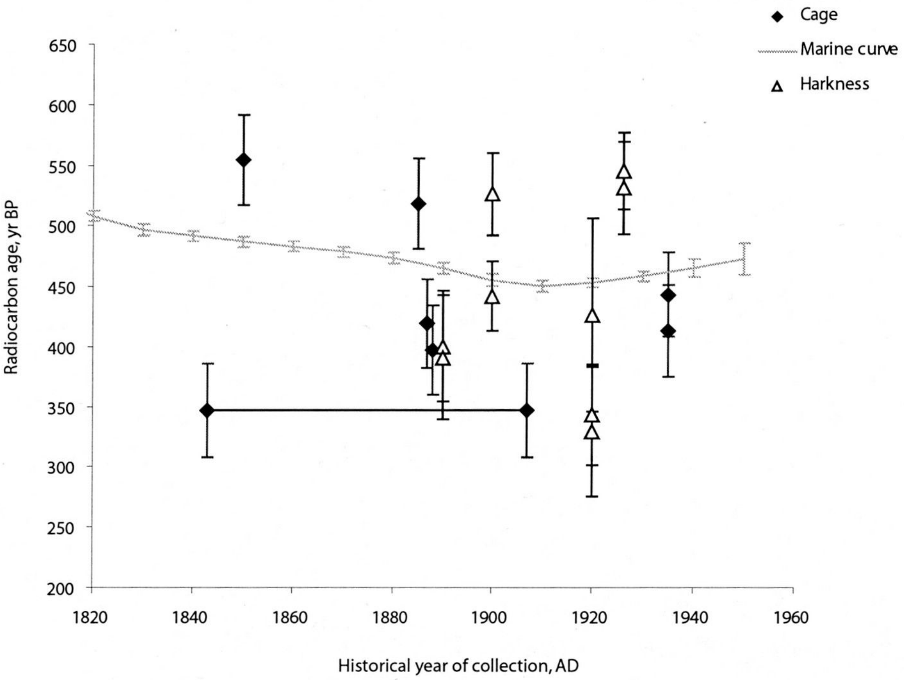

Figure 4.6 Radiocarbon data (plus 2 σ error bars) from this study (Cage, 2005; filled diamonds) plotted with Harkness data (unfilled triangles; from Reimer, 2004) for the west coast of Scotland. The 'marine98' curve (Stuiver *et al.*, 1998) is shown in grey. The two samples joined by a black line represent the limits of the possible collection period for the Loch Creran sample AAR-7489.

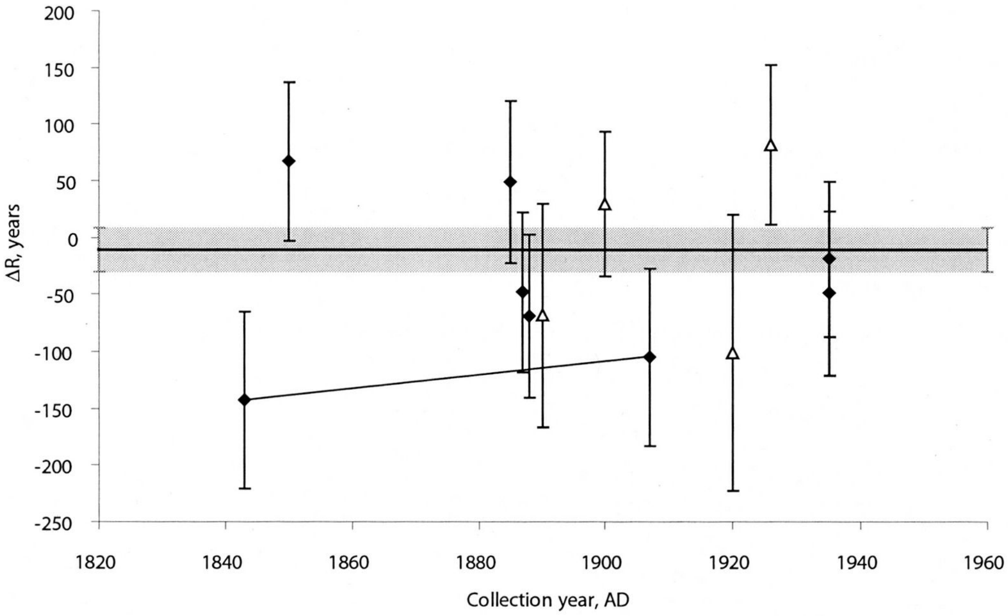

Figure 4.7 Averaged ΔR values (and 2σ error bars) for the Scottish west coast shell samples from this study (black diamonds) and Harkness (Reimer, 2004, unfilled triangles). The weighted average ΔR and 2σ error bars is shown by the grey bar and shaded box.

not specify whether the outer section of the other dated shells included the periostracum. The Loch Broom samples have similar $\delta^{13}C$ values (table 4.5) and one would expect similar ^{14}C concentrations (Craig, 1953). All the shells used in this study and by Harkness (1983) were whole valves with no visual signs of deterioration, such as a powdery surface common as a result of recrystallisation processes (Aitken, 1990). Mangerud (1972) suggests material yielding $\delta^{13}C$ values isotopically lighter than -3‰ should be checked for signs of possible contamination but notes that it is impossible to separate a contamination effect from influence of brackish or freshwater $\delta^{13}C$ at the time of shell formation. Additionally, Harkness (1983) did not mention the Loch Broom samples as being problematic. It is possible that the large difference in ^{14}C ages for the outer and inner fractions of *Dosinia exoleta* could be a species-specific effect related to food availability, shell structure and the isotopic disequilibrium within the organism's internal carbon pool (e.g. Reimer *et al.*, 2002). The Loch Broom sample has been included in the study since the averaged value falls within the acceptable 2σ statistical limits of the weighted average ΔR (figure 4.7).

The averaged Harkness ΔR data for the whole shell are presented along with the data from this study in figure 4.7. The combined Cage and Harkness (hereon denoted by C&H) data show a weighted average ΔR value of -11 ± 10 ^{14}C years, including an averaged ΔR value for the Loch Creran sample. A Student t-test was used to test for significant difference between the mean ΔR found in this study and the mean found from Harkness's data (Davis, 2002). The following variation of the Student t-test function was used since the null hypothesis was accepted in the Snedecor F-test (with S^2 representing the variance of the means);

$$F = S_1^2 \ / \ S_2^2 \qquad \textit{(Eq. 4.3)}$$

$$t = \ x_1 - x_2 \ / \ \surd\, S^2\,(1/n_1 + 1/n_2) \qquad \textit{(Eq. 4.4)}$$

where x is the mean, n is the number of samples and S^2 is the pooled variance of the individual variances of the means being tested, calculated by;

$$S^2 = (n_1 - 1)\, S_1^2 \ + \ (n_2 - 1)\, S_2^2 \ / \ n_1 + n_2 - 2 \qquad \textit{(Eq. 4.5)}$$

The Student t-test shows that the ΔR value (including Loch Creran) of -25 ± 14 years from this study is not statistically different at 95 % confidence to the combined C&H ΔR value but they are different at an 85 % confidence level.

The ΔR value of the C&H data is likely to be pulled more towards 0 by the inclusion of the Hunterson Sands sample (SRR-356) (table 4.5). Hunterston Sands is located near the mouth of the Firth of Clyde (figure 4.2) so one might expect to see less negative ΔR values due to a greater influence of 'older' coastal waters. However, as Harkness (1983) points out, the Hunterston Sands and Skelmorlie Bank samples may have been influenced by pollution, since organic wastes (containing modern ^{14}C and ^{14}C-free residues) were being dumped in the Clyde Sea at the time of the collection period (1920). Since the Hunterston Sands sample (SRR-356) is the only sample to lie outwith the acceptable statistical variance (2σ) of the data's weighted average ΔR (see figure 4.7), and it's validity of truly representing the natural regional ΔR is in doubt, it has been omitted from the west Scottish weighted average. Therefore, the new calculated weighted average of ΔR for C/H is -27 ± 11 years.

The Student t-test (*Eq 4.3*) (with the null hypothesis accepted in the F-test) shows that the C&H ΔR value of -27 ± 11 years is statistically different (at 99.5% confidence) to the ΔR value of 14 ± 13 years quoted by Harkness (1983, data from Reimer, 2000) for UK coastal waters, with the coastal and fjord waters of the Scottish west coast yielding significantly more negative ΔR values. The likelihood that this ΔR value of -27 ± 11 years is a reliable estimate is supported by being statistically similar to the ΔR value of -33 ± 93 years recently quoted by Reimer *et al.*, (2002) for the region encompassing west Ireland, Scotland and the Orkney Islands. However, the ΔR presented here is statistically different to the ΔR of -79 ± 17 years reported by Ascough *et al.*, (2004). This may be due to temporal differences or differences in methods. Bondevik *et al.,* (1999) also reported a marine reservoir age of 380 ± 32 years (ΔR = -20) for the west coast of Norway. Therefore, a correction of ΔR = -27 ± 11 years can be applied to marine radiocarbon ages from the NW coast of Scotland.

4.5.2 Stable isotopes, regional hydrography and ΔR

The sea lochs of NW Scotland exhibit fjordic circulation (e.g. Farmer & Freeland, 1983) i.e. they have a restricted connection with open marine water masses (Atlantic Ocean) and high freshwater inputs often result in brackish surface waters, which can dilute the salinity of bottom water masses. Positive relationships between salinity and the stable isotopic composition ($\delta^{18}O$ and $\delta^{13}C$) of shell material has been reported by many authors (e.g. Lloyd, 1964; Mook & Vogel, 1968; Mook, 1971), with isotopically heavier values occurring in more saline water masses. Spiker (1980) found that $\delta^{13}C$ and $\Delta^{14}C$ in estuarine waters exhibit a conservative mixing relationship between river and ocean water end-members, again with isotopically heavier $\delta^{13}C$ and $\Delta^{14}C$ values occurring in high to mid salinity waters.

Broecker & Walton, 1959 suggested that river-water bicarbonate in igneous areas should have a $^{14}C/^{12}C$ ratio close to that of atmospheric $^{14}C/^{12}C$. The bedrock geology of NW Scotland is predominantly igneous, and the thin and poorly developed soils overlying the steep slopes rapidly translate rainfall into surface runoff (Black & Cranston, 1995). The freshwater inputs into the loch should therefore be relatively unaffected by ^{14}C deficient carbon derived from humus and instead have ^{14}C activities close to that of atmospheric CO_2.

The less saline fjordic waters may 'leak' out into coastal regions where they are readily mixed, and the tendency towards negative ΔR values around the west Scotland coast likely reflects the degree of mixing between 'older' fully marine Atlantic waters and 'younger', slightly less saline coastal waters (Harkness, 1983). Additionally, surface waters in the NE Atlantic tend to be isotopically ($\delta^{13}C$) lighter (by approximately 1 ‰) than expected due to the penetration of anthropogenic CO_2 in this region of deep water formation (Keir *et al.*, 1998). The mixing of 'young' water with 'old' water in this region may also cause negative ΔR values particularly in historical shells collected in the early 1900s (i.e. pre-bomb).

The stable isotope data presented in this study come from different mollusc species. Despite this, Keith *et al.,* (1964), for example, found that major variations in the $\delta^{13}C$ values of marine molluscs were controlled by environmental variables, not by species-specific vital effects. Therefore this study assumes that vital effects between species are minimal, and that ΔR values, like stable isotope values, are influenced by environmental conditions. This inference is supported by the ^{14}C data from Oban which shows statistically similar ^{14}C reservoir ages from two different bivalve species (table 4.2).

Bi-plots of δ^{18}O and δ^{13}C often exhibit positive linear relationships (e.g Mook, 1971) and data from this study also shows a moderate insignificant positive correlation ($r = 0.403$, $p = 0.370$). Positive trends between salinity and the stable isotope composition of shell carbonate (δ^{18}O and δ^{13}C) have been seen in previous studies (e.g. Mook & Vogel, 1968), and Keith *et al.,* (1964) suggest that δ^{13}C variations are not as affected by fractionation process as the temperature dependent oxygen isotopes. Therefore, it is likely that δ^{18}O and δ^{13}C variations in Scottish west coast shells reflect the admixture of isotopically light δ^{13}C and δ^{18}O from freshwater inputs with the relatively isotopically enriched coastal water δ^{13}C and δ^{18}O.

Assuming the shell δ^{13}C (and δ^{18}O) data reflects the degree of mixing between fjord and coastal water around NW Scotland, and given the reported relationships between salinity and ^{14}C observed by Spiker (1980), one may expect to see similar patterns in ΔR from sea lochs. However, the relationship between shell isotopic composition and ΔR must first be examined before relationships between ΔR and hydrography can be investigated any further.

4.5.3 Stable oxygen isotopic composition and ΔR

Salinity mixing lines (eg. Epstein & Mayeda, 1953; Mikalsen & Sejrup, 2000; Austin & Inall, 2002) demonstrate a depletion in $\delta^{18}O_{water}$ with decreasing salinity. This relationship should also be observed in marine shells since they tend to be in isotopic equilibrium with surrounding water (Mook & Vogel, 1968; Olsson & Osadebe, 1974). Both temperature and salinity affect the isotopic composition of calcium carbonate (e.g. Bemis *et al.*, 1998) however, these data are not known for the sample locations or time of collection for the museum shells. The data presented here suggests a moderate negative and insignificant relationship (probably due to low sample numbers; $r = -0.506$, $p = 0.247$) between δ^{18}O and ΔR, with 26 % of the variation in ΔR being explained by variations in δ^{18}O (fig 4.8). Coastal and fjordic waters often have stratified water columns, hence salinity and temperature differences occur with depth and mixing. Since the role of temperature is significant in the fractionation of oxygen isotopes (e.g. Bemis *et al.*, 1998 and references therein), the $\delta^{18}O$ results alone cannot be used to confirm the influence of freshwater mixing upon the shell composition.

4.5.4 Stable carbon isotopic composition and ΔR

The $\delta^{13}C$:salinity relationship is typically positive, i.e. $\delta^{13}C$ becomes isotopically heavier in more saline waters (Lloyd, 1964; Mook & Vogel, 1968; Mook, 1971; Spiker, 1980; Polyak *et al.*, 2003). Marine water bicarbonates typically have $\delta^{13}C$ values from -2 ‰ to +1.5 ‰ (e.g. Keith *et al.*, 1964 and Mook, 1971) with surface marine waters generally showing little variability in $\delta^{13}C$ (Mook & Vogel, 1968). River-water bicarbonate tends to have $\delta^{13}C$ values close to the $\delta^{13}C$ of atmospheric CO_2 (~ -7 ‰) with $\delta^{13}C$ values typically around -8 to -12 ‰ (e.g. Keith *et al.*, 1964, Mook, 1971 Spiker, 1980 and Matson & Brinson, 1990). Inputs of carbon derived from land plants and stable organic residues from peat or humus with isotopically light $\delta^{13}C$ values (~ -25 to -30 ‰) into relatively small freshwater reservoirs such as rivers may further influence river water $\delta^{13}C$ (e.g. Keith & Anderson, 1963). Brackish and 'peaty' surface waters were observed in the upper basin of Loch Sunart during research cruises, and though bottom waters are likely to be more saline (chapter 3), there is a potential for basin water $\delta^{13}C$ to be modified by the isotopically light $\delta^{13}C$ from freshwater inputs (Keith *et al.*, 1964).

Marine molluscs typically deposit their carbonate shell in isotopic equilibrium with the surrounding environment, ie. the $\delta^{13}C_{carbonate}$ reflects $\delta^{13}C_{water}$, (Mook & Vogel, 1968). Shell $\delta^{13}C$ values range from -15.1 ‰ to -2.1 ‰ for freshwater molluscs, and from -1.7 ‰ to +4.2 ‰ for marine environments and intermediate salinity waters (i.e. salinity less than 30) typically show more depleted values (Keith *et al.*, 1964; Mook & Vogel, 1968). The $\delta^{13}C$ values presented here range from -0.2 to 4.1 ‰ (see tables 4.2 and 4.5) suggesting little brackish water influence on the shell isotopic composition during calcification (Keith *et al.*, 1964 and Mook, 1971). Mangerud (1972) reported a similar range of 'typical marine $\delta^{13}C$' values for molluscs from Norwegian fjords. However, a positive relationship between shell $\delta^{13}C$ and depth (where salinity increases due to fjordic circulation) led him to suggest that the isotopically depleted

$\delta^{13}C$ values from shallow water shells do reflect the admixing of freshwater and fjordic water in the surface layers.

It is thought that the metabolic pathway is important in governing $\delta^{13}C$ in mollusc shells (Wilbur, 1960), particularly in the inner nacreous layers which may reflect the internal environments of the shells. Reimer *et al.,* (2002) point out that molluscan feeding habits are important when interpreting $\delta^{13}C$ (and therefore $\Delta^{14}C$) data since this determines how carbon enters the organism. For example filter feeders obtain carbon directly from the seawater in the form of dissolved inorganic carbon (DIC), whereas deposit feeders may utilise old organic carbon from detritus. The shells used in this study were all bivalve filter feeders, hence they should derive their carbon directly from seawater dissolved inorganic carbon (DIC). Carbon may be derived from sources other than the seawater such as CO_2 from benthic respiration (Spiker, 1980) and fermentive muds. Both of these are typically depleted in $\delta^{13}C$ with respect to marine carbonate values (Keith & Anderson, 1963), hence marine organisms calcifying in such environments may not deposit shell material in isotopic equilibrium with the seawater. Sediments from sea lochs can often be quite gaseous (e.g. Howe *et al.*, 2002) and care must be taken when ^{14}C dating shells from such an environment. However, the $\delta^{13}C$ data reported in this study (tables 4.2 and 4.5) suggest that the shell material were not unduly influenced by these external carbon sources, and likely represent the $\delta^{13}C$ of the surrounding environment.

The $\delta^{13}C$: ΔR relationship for data generated from this study was weak and insignificant ($r = -0.196$, $p = 0.674$; section 4.3.2) and the combined C&H $\delta^{13}C$ (excluding sample SRR-356) also delivers a weak and insignificant $\delta^{13}C$: ΔR relationship ($r = -0.413$; $p = 0.16$; figure 4.9), which may be due to the relatively low sample number ($n = 13$). Spiker (1980) reported that $\delta^{13}C$ and $\Delta^{14}C$ in estuarine waters exhibit conservative mixing between the river and ocean water end-members, with isotopically heavier $\delta^{13}C$ in high and mid salinity waters. Assuming the shell $\delta^{13}C$ (and $\delta^{18}O$) data reflects the degree of admixing in fjords and coastal regions around NW Scotland, similar patterns in ΔR are expected elsewhere, i.e. decreasing ΔR in lower salinity fjord environments (figure 4.10). Although we do not see this relationship in figure 4.9, the lack of sample numbers and the lack of information on sample location negate an interpretation of the $\delta^{13}C$: ΔR relationship from these data.

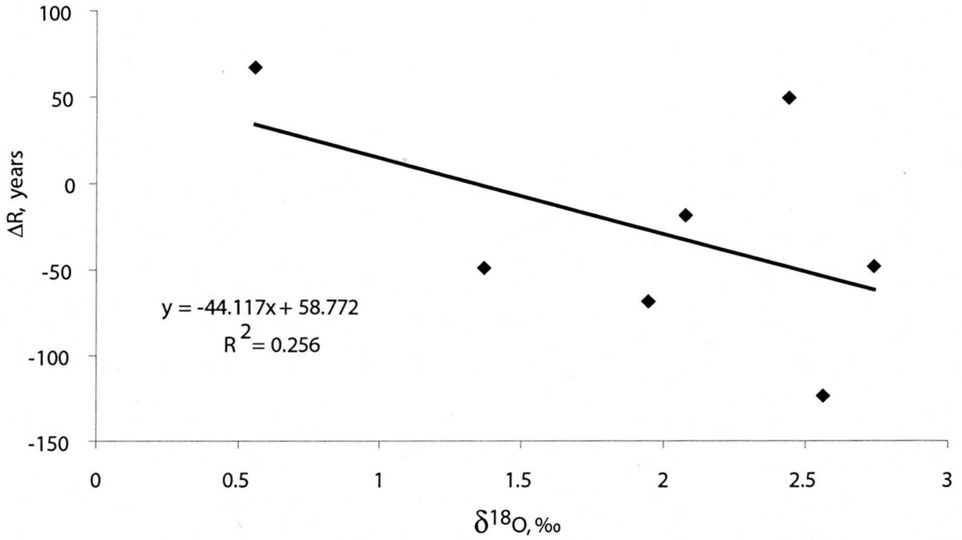

Figure 4.8 Biplot and linear regression equation showing the relationship between ΔR and $\delta^{18}O$ from NW Scottish coastal and fjordic shell samples from this study. Harkness (1983) does not show $\delta^{18}O$ data, therefore the sample size cannot be increased to improve the relationship of r = -0.506, p = 0.247 (n=7).

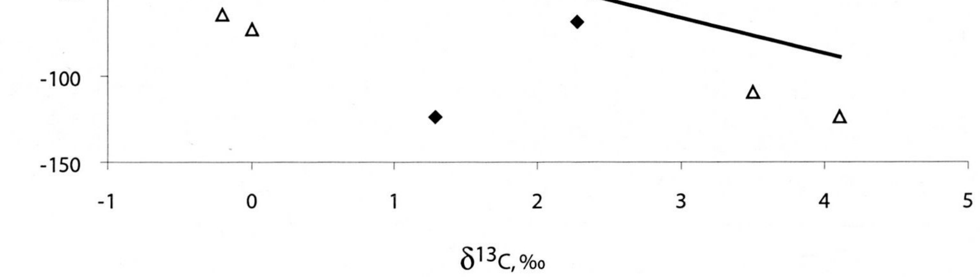

Figure 4.9 Biplot and linear regression equation showing the relationship between ΔR and $\delta^{13}C$ from NW Scottish coastal and fjordic shell samples from this study (black diamonds) and Harkness (1983) using data from Reimer (2004; unfilled triangles).

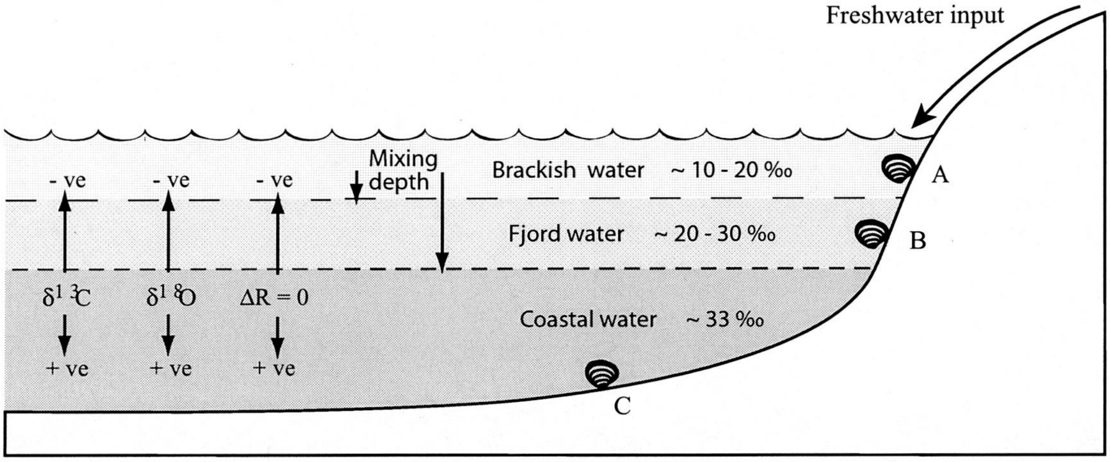

Figure 4.10 The theorectical influence of fjordic hydrogaphy and salinity on shell isotopic composition and ΔR values. Shells lying within lower salinity water (e.g. shells A and B) should exhibit more negative ΔR and depleted $\delta^{13}C$ and $\delta^{18}O$ than those shells lying in deeper, more saline basin waters (shell C).

4.6 CONCLUSIONS

The igneous bedrock geology of NW Scotland, along with the thin and poorly developed soils overlying the steep slopes rapidly translating rainfall into surface runoff (Black & Cranston, 1995), means that the freshwater inputs into sea lochs typically should have an isotopic signal close to atmospheric $^{14}C/^{12}C$ (Broecker & Walton, 1959), i.e. be relatively unaffected by ^{14}C deficient carbon derived from humus. Unfortunately, information on water depth, temperature and salinity was not available for the museum shell samples, thus it is impossible to determine whether the shells were collected from depths below the typical stratification for the sea loch in question. Despite this, a shell collected from a shallow depth in a sea loch with a thick brackish surface layer or large mixing depth (the depth to which freshwater is mixed down the water column; see Edwards & Sharples, 1986) is likely to exhibit isotopically lighter $\delta^{18}O$ and $\delta^{13}C$ (Austin & Inall, 2002; Polyak *et al.*, 2003), and thus a 'younger' marine radiocarbon reservoir age (more negative ΔR value) than a shell obtained from a high salinity water mass (figure 4.10). The shallow mixing depth of Loch Sunart (2 m) and low basin salinity reduction (0.2) means that marine carbonate material from the GC023 core site (120 m water depth) are unlikely to exhibit the large ΔR values measured in the Loch Creran sample (mixing depth of 19 m; 0.4 basin salinity reduction). Nevertheless, the sea lochs and coastal waters of NW Scotland do appear to have negative ΔR and a correction factor of $\Delta R = -27 \pm 11$ years should be applied to marine radiocarbon dates from the NW coast of Scotland. The use of this correction factor to marine radiocarbon dates from the deep basins of Loch Sunart is supported by the use of the Bondevik *et al.,* (1999) ΔR value of -20 in sedimentary archives from Norwegian fjords (Mikalsen *et al.*, 2001).

To conclude, the data presented in this study suggests that

1. Stable carbon and oxygen isotopic compositions from marine organisms living in the coastal and sea loch (fjord) environments of NW Scotland likely reflect the influence of freshwater input and mixing process with coastal waters within fjords.

2. A regional ΔR value of -27 ± 11 years has been determined for the coastal waters and fjordic waters of NW Scotland, which is statistically different

(at a confidence level of 99.5%) to the ΔR value of 14 ± 13 years reported for UK coastal waters (Harkness, 1983) and in good agreement with the -33 ± 93 years reported by Reimer *et al.,* (2002).

3. This negative ΔR value of -27 ± 11 years supports the hypothesis that high freshwater inputs into NW Scottish coastal waters should produce marine radiocarbon reservoir ages, R(t), 'younger' than the global surface ocean radiocarbon reservoir age of R(t) = 400 years, ΔR = 0 (Stuiver & Braziunas, 1993).

4. Is it recommended that a correction factor of ΔR = -27 ± 11 years should be applied to marine radiocarbon dates from the NW coast of Scotland during calibration.

CHAPTER 5 – DISTRIBUTION OF MODERN BENTHIC FORAMINIFERA IN LOCH SUNART SURFACE SEDIMENTS

5.1 Introduction

The high sediment accumulation rate in shelf sea and fjordic environments (chapter 1) offer ideal sedimentary archives for high-temporal resolution palaeoenvironmental studies (e.g. HOLSMEER). Before utilising them in palaeoenvironmental reconstructions, it is important to understand how the sediment proxies are influenced by environmental parameters. To do this, it must first be ascertained how modern benthic foraminifera respond to abiotic parameters such as hydrography (e.g. temperature, salinity, currents) and sedimentology, as well as to biotic factors such as food availability and inputs of organic matter. Finally, the processes by which benthic foraminiferal assemblage distributions are translated into and the preserved in the fossil record, need to be understood.

Whilst the benthic foraminiferal distribution of the NE Atlantic and NW European shelf seas have been relatively well documented (Murray, 1991a; Conradsen, 1993; Corliss & Vanweering, 1993; Conradsen *et al.*, 1994; Bergsten *et al.*, 1996; Alve & Murray, 1997; Austin & Evans, 2000; Hughes *et al.*, 2000; Gooday & Hughes, 2002; Klitgaard-Kristensen *et al.*, 2002; Murray, 2003b; Scott *et al.*, 2003), literature on the benthic foraminifera in NW European fjords is fairly limited. The majority of these studies focus on Scandinavian fjords which tend to be either deep with deep sills, or anoxic (e.g. Höglund, 1947; Thiede *et al.*, 1981; Qvale *et al.*, 1984; Alve & Nagy, 1986a, b, 1988; Alve, 1990; Alve & Nagy, 1990; Austin & Sejrup, 1994; Alve, 1995; Husum & Hald, 1998; Klitgaard-Kristensen & Buhl-Mortensen, 1999; Mikalsen *et al.*, 1999; Gustafsson & Nordberg, 2000, 2001; Murray *et al.*, 2003).

There is a general dearth of data on benthic foraminiferal distribution in the seas around NW Scotland. Heron-Allen & Earland (1916) recorded the distribution of foraminifera around the NW Scottish coast, which included two shallow samples (< 21 m water depth) from Loch Sunart: one from Laga Bay in the main basin, and another from the outer basin. Hannan & Rogerson (1997) studied the benthic foraminiferal distribution in the Clyde Sea, although without reference to species.

Murray *et al.,* (2003) recently investigated the benthic foraminifera distribution in the highly stratified fjord, Loch Etive. Though the Clyde Sea behaves like a sea loch in many respects, it is different enough from a fjord for it to be excluded from the catalogue of Scottish Sea Lochs (*pers. comm.,* A. Edwards, 2003 and Edwards & Sharples, 1986). The hydrography of Loch Etive is also very different to Loch Sunart, with a more restricted exchange with 'open' coastal waters along with a higher freshwater input (Edwards & Sharples, 1986) and high terrestrial organic matter input, resulting in the benthic foraminiferal assemblages being dominated by agglutinated taxa. Murray (2003b) also reported on the benthic foraminifera assemblages from deeps on the Hebridean Shelf, with one station, Muck Deep, being situated to the west of the Ardnamurchan peninsula.

This study aims to document for the first time, the distribution of modern benthic foraminifera from a range of water depths in the significant basins of Loch Sunart: a Scottish sea loch with a relatively good connection (and exchange) with 'open' coastal waters.

5.2 METHODS

Thirty-one surface sediment samples were collected from Loch Sunart using a van Veen grab or Craib corer (April 2001 cruise) and prepared for foraminiferal analysis (chapter 2). The positions and water depths of these samples can be seen in table 5.1 and figure 5.1.

Low numbers of stained specimens in Loch Sunart surface sediments preclude the use of live assemblages in this study and instead, the total assemblage has been used throughout.

The use of dead or total assemblages in ecological studies has been heavily criticised by Murray (1991; 2000) who instead advocates the use of the live assemblage data in ecological interpretations. Since the primary aim of the study is to aid the interpretation of fossil assemblages in Loch Sunart, it is important to gain a sense of how benthic foraminiferal assemblages respond to prevailing (long-term) marine conditions rather than to seasonal 'snapshots' (e.g. Conradsen, 1993; also see section

Table 5.1 Positions of Loch Sunart surface sediment samples selected for foraminiferal analyses. Latitudinal and longitudinal postions are presented as decimalised co-ordinates, and the negative sign preceding longitude reflects the westerley position with regard to the Greenwich meridian, i.e. 0°. Also shown are the recorded bottom water temperature (BWT) and bottom water salinity (BWS) and sedimentological information regarding the samples, e.g. organic matter content and grain size properites. Winter BWS and BWT was not available for some stations.

Station	**Latitude, N**	**Longitude, W**	**Depth (m)**	**Collection date**	**Summer BWT, °C**	**Winter BWT, °C**	**Summer BWS**	**Winter BWS**	**% Organic matter**	**% CaCO3**	**% Clay**	**% Silt**	**% Sand**	**% > 125 microns**	**Mean grain size**	**Median grain size**	**Modal grain size**	**Skewness:**	**Kurtosis:**	**d10:**	**d50:**	**d90:**
53	56.6851	-5.5466	5	Jun-01	12.0		31.0		1.4	3.0	0.0	2.9	97.1	92.5	732.8	605.3	663.9	0.7	-0.5	165.1	605.3	1542.7
68	56.6865	-5.5691	11	Jun-01	12.8	7.3	30.7	32.4	3.8		0.7	23.9	75.5	56.9	290.9	164.7	168.8	2.4	6.0	21.7	164.7	693.9
147	56.6872	-5.5818	16	Jun-02	12.6	7.3	31.1	32.5	7.0	3.2	2.4	56.4	41.2	22.0	93.7	44.4	96.5	4.1	23.2	6.2	44.4	217.4
72	56.6866	-5.5839	30	Jun-01	12.4	7.3	32.5	32.5	3.4	2.4	0.5	18.1	81.5	72.9	648.2	528.3	1162.3	0.6	-0.8	24.5	528.3	1517.3
149	56.6842	-5.6216	59	Jun-02	12.1	7.3	33.0	32.7	18.0	9.7	3.5	78.2	18.3	7.3	42.6	21.1	18.0	3.6	16.6	4.5	21.1	99.8
211	56.6825	-5.6338	93	Jun-02	11.9	7.3	33.1	32.9	6.7	2.2	1.8	26.9	71.3	50.3	285.1	151.8	168.8	2.6	6.0	20.2	151.8	659.8
110	56.6796	-5.6469	53	Jul-01	12.3	7.3	33.1	32.8	2.5	9.5	1.0	17.3	81.7	79.5	625.6	489.2	1026.0	0.7	-0.5	14.2	489.2	1447.7
112	56.6807	-5.6499	45	Jul-01	12.3	7.3	33.1	32.8	2.5	9.5	1.9	31.7	66.3	58.0	261.6	159.5	185.3	2.7	7.9	7.4	159.5	574.5
76	56.6930	-5.6857	12	Jun-01	12.3	7.4	31.4	32.9	4.0	1.8	2.1	40.0	57.9	31.5	136.3	81.8	105.9	2.4	7.1	6.6	81.8	328.9
2	56.6925	-5.7064	64	Jun-00	11.8		33.6		11.8	17.5	2.6	48.4	49.1	34.3	135.0	69.0	254.7	1.6	2.5	6.0	69.0	364.8
80	56.6965	-5.7080	44	Jun-01	11.8	7.3	33.6	33.5	12.1	9.3	2.6	50.0	47.4	30.2	133.2	59.9	234.6	2.0	4.5	5.9	59.9	371.1
173	56.7020	-5.7261	31	Jun-02	11.9	7.4	33.6	33.5	4.5	4.5	5.8	54.9	39.3	23.4	75.3	28.1	116.3	2.1	5.2	3.1	28.1	205.9
176	56.7050	-5.7372	46	Jun-02	11.8	7.4	33.6	33.5	8.3	5.9	7.2	67.3	25.6	14.3	57.5	15.7	9.4	3.4	14.3	2.7	15.7	156.8
45	56.6993	-5.7731	72	Apr-01	11.6	7.3	33.8	33.6	13.8	7.6	2.5	46.7	50.8	38.4	136.7	78.2	274.9	1.1	0.5	6.1	78.2	358.6
210	56.6988	-5.7753	70	Jun-02	11.6	7.3	33.8	33.6	10.1	7.1	6.1	86.2	7.8	3.2	24.2	12.9	13.6	3.9	18.9	3.1	12.9	52.7
101	56.6874	-5.8059	23	Jul-01	12.2	7.4	33.7	33.5	5.3	8.3	3.6	41.5	54.9	42.0	346.1	82.2	1800.7	1.7	1.5	4.9	82.2	1288.7
201	56.6829	-5.8096	68	Jun-02	11.7		33.6		10.9	9.5	7.1	72.3	20.5	8.2	71.2	31.9	45.8	2.6	7.6	3.4	31.9	195.2
202	56.6795	-5.8099	97	Jun-02	11.6	7.4	33.8	33.7	12.0	8.2	7.4	85.4	7.1	2.4	22.1	11.6	11.3	3.8	17.9	2.6	11.6	49.8
200	56.6833	-5.8128	55	Jun-02	11.8	7.5	33.8	33.6	11.3	8.4	6.6	74.6	18.8	6.3	57.9	31.1	41.7	2.9	10.9	3.6	31.1	143.7
90	56.6740	-5.8130	36	Jul-01	12.0	7.5	33.8	33.5	5.3	8.3	7.1	67.1	25.8	14.2	57.4	17.6	9.4	3.2	12.9	2.7	17.6	156.8
199	56.6840	-5.8135	17	Jun-02	12.4	7.4	33.2	33.3	1.5	10.8	3.6	41.5	54.9	42.0	346.1	82.2	1800.7	1.7	1.5	4.9	82.2	1288.7
198	56.6660	-5.8434	121	Jun-02	11.6	7.4	33.8	33.7	6.8	4.3	5.3	66.7	28.1	17.6	61.7	18.7	12.0	2.6	7.9	3.5	18.7	185.1
41	56.6701	-5.8649	65	Apr-01	11.9	7.4	33.9	33.6	6.1	15.8	2.8	46.1	51.2	37.2	81.4	0.7	171.2	3.5	6.2	81.4	372.4	
197	56.6736	-5.8658	111	Jun-02	11.7	7.4	33.9	33.6	6.1	15.8	3.1	32.8	64.1	59.0	646.1	471.0	1909.0	0.6	-1.0	9.0	471.0	1631.0
192	56.6727	-5.9185	90	Jun-02	11.9	7.5	34.0	33.9	4.5	14.5	3.1	32.8	64.1	59.0	646.1	471.0	1909.0	0.6	-1.0	9.0	471.0	1631.0
193	56.6669	-5.9198	51	Jun-02	12.3	7.5	34.1	33.7	3.9	9.5	3.0	29.8	67.3	64.1	307.0	244.2	324.3	1.2	1.3	6.0	244.2	758.6
189	56.6706	-5.9467	75	Jun-02	12.3	7.5	34.2	33.9	3.6	7.4	4.0	35.0	61.0	57.9	323.0	197.5	245.2	1.9	3.2	4.4	197.5	1017.3
184	56.6498	-5.9806	17	Jun-02	12.4	7.5	33.8	33.8	4.3	25.7	1.0	9.9	89.1	83.7	834.5	787.6	1584.0	0.3	-1.2	94.3	787.6	1692.0
27	56.6622	-5.9920	113	Apr-01	12.4	7.5	34.1	33.9	11.1	11.9	3.0	51.0	46.0	30.1	114.3	57.8	208.8	2.2	7.5	5.7	57.8	293.5
181	56.6804	-6.0117	36	Jun-02	12.5	7.5	34.1	33.8	5.5	8.6	7.2	64.0	28.8	20.4	80.5	17.2	9.4	3.0	9.9	2.7	17.2	242.1
22	56.6722	-6.0135	45	Apr-01	12.5	7.5	34.2	34.0	9.4	11.3	3.4	59.1	37.5	19.3	76.9	39.2	74.5	2.0	4.5	5.0	39.2	205.5

Figure 5.1 Positions of the Loch Sunart surface sediment samples obtained for foraminiferal analyses (yellow dots) along with the sample number. These samples have been plotted upon a bathymetry map (created using ArcGIS) to provide a visualisation of sample site water depths. Also shown are the approximate locations of the two Loch Sunart stations (max depth ~ 22 m) sampled by Heron-Allen & Earland (1916; white stars), as estimated by figure provided in the text. It is worth noting that although the text stated specifically that a sample had been obtained from Laga Bay, the figure in Heron-Allen & Earland (1916) shows 2 locations, neither of which are at Laga Bay.

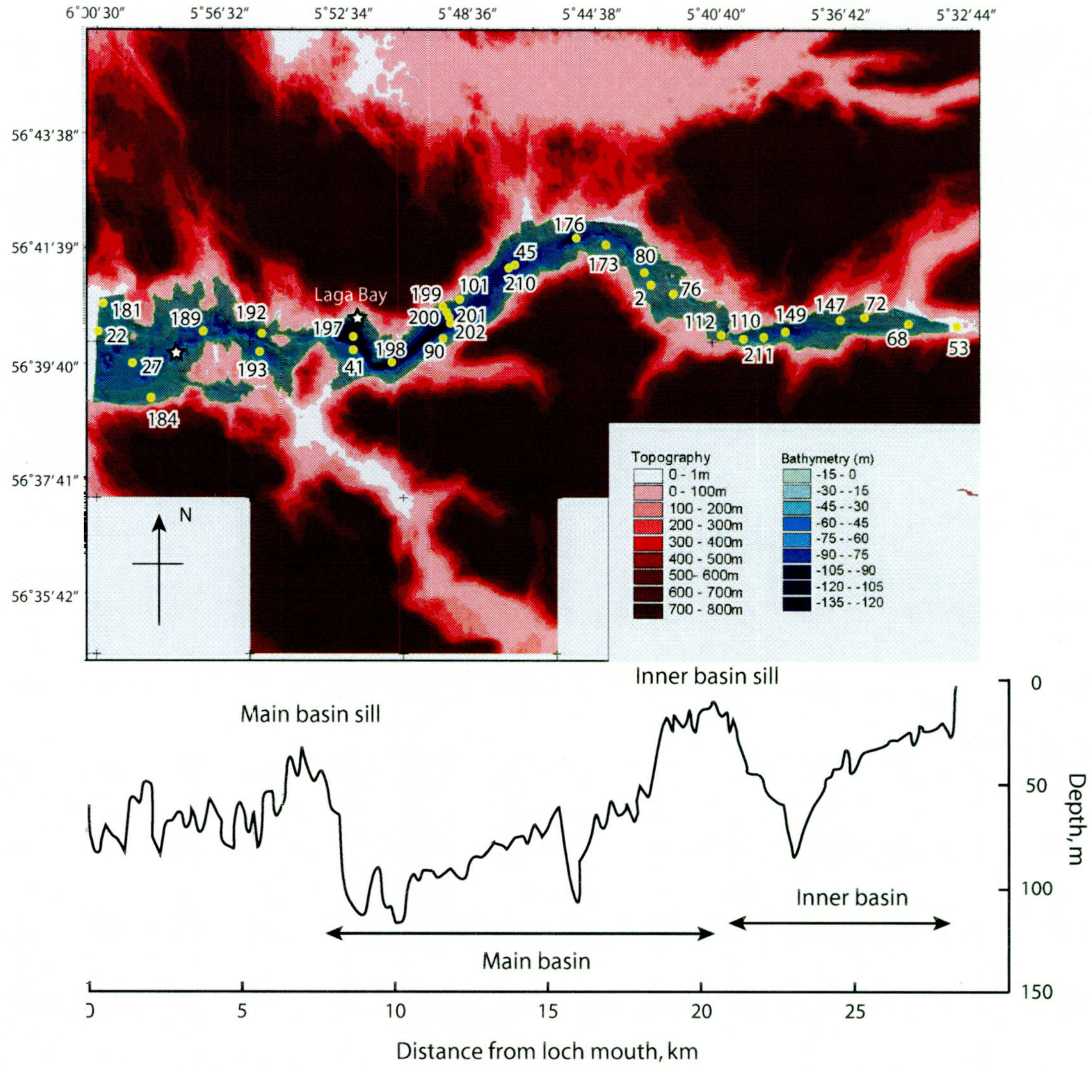

5.4.5). Irrespective of this, the number of live specimens from each assemblage was noted, as were the number of broken tests (presented in table 5.3). The depth, bottom water temperature (BWT) and bottom water salinity (BWS) were noted at the time of sample collection, and where possible grain size, % organic matter and % calcium carbonate analyses were carried out on accompanying sediment samples (see chapter 2).

Data were entered into Microsoft Excel worksheets and formatted for use in the computer programmes PAST (Hammer *et al.*, 2001) and Minitab v14, both of which were used for statistical analyses. Foraminiferal abundance graphs were plotted using the computer programme C2 (Juggins, 2003a, b).

5.2.1 Diversity indices

When determining the diversity of samples, numerical methods must be selected which are not dependent on sample size. For example, it is likely that a greater number of species will be observed in sample counts of say > 400 specimens than ~ 300 specimens. Therefore diversity indices were determined by calculating the Fisher-α species diversity, the heterogeneity (via the Shannon-Weaver index of entropy) and the dominance (using the Simpson index), details of which are provided in appendix 7. Diversities were calculated using the statistical computer package PAST (Hammer *et al.*, 2001).

5.2.2 Multivariate Statistical Analyses

The benthic foraminiferal assemblages from Loch Sunart were subjected to R-mode cluster analysis (using PAST), in order to determine any similarities between sample assemblages. After transforming the data (by square-rooting; Lepš & Šmilauer, 2003) to stabilise variances and reduce the 'signal to noise' ratio (Prentice, 1980), the cluster analysis was carried out using the Bray-Curtis similarity measure (Bray & Curtis, 1957) with the unweighted pair group method with arithmetic averaging (UPGMA) algorithm. The Bray-Curtis similarity measure is commonly used in ecological studies (Lepš & Šmilauer, 2003) and utilises abundance data rather than binary data. The UPGMA algorithm was used in preference to the single linkage or minimum variance clustering (i.e. Ward's method) algorithms since single linkage methods are reported to perform poorly (Parker & Arnold, 1999) and Hammer *et al.*, (2001) suggests Ward's method works best with the Euclidean distance, which itself is not the best similarity measure for community analysis.

The interpretation of hierarchical cluster analysis dendograms must be carried out with care, since the results of this multivariate statistical method are: i) not subject to significance testing and ii) will always produce clusters irrespective of whether or not the data forms distinct groups (Parker & Arnold, 1999). Additionally, while this method clusters 'similar' data together, it gives no ecological information; thus cluster analysis results must be interpreted qualitatively and may give way to subjectivity. Parker & Arnold (1999) suggest additional multivariate analyses should be carried out to verify potential assemblages, and Shi (1993) recommends an integrated multivariate approach to the statistical analyses of ecological data: combining cluster analysis to classify the data into groups, and then ordination techniques to quantify inter-relationships. Therefore, non-metric multidimensional scaling (using the Bray-Curtis similarity measure) was applied to the data using PAST (Hammer *et al.*, 2001) as was simultaneous Q-mode and R-mode factor analysis using Minitab v14 (e.g. Walden & Smith, 1995).

5.3 RESULTS

A total of 149 benthic foraminiferal taxa were recorded in Loch Sunart, comprising of 42 agglutinated taxa, 12 porcelaneous taxa and 95 hyaline taxa. Count data was transformed into percentage abundances (appendix 8) and the most common taxa (i.e. those present in over 20% of the samples) occurring in Loch Sunart are represented in table 5.2. Appendix 9 shows the total recorded taxa and taxa codes used in the study.

Planktonic foraminifera tend to be extremely rare in Loch Sunart, occurring in only 6 assemblages. Sample 27 has the highest abundance of planktonic foraminifera (7.6 %) which is probably due to it's proximity to the 'open' coastal waters. The remaining samples contain rare planktonic foraminifera (< 0.88 %). Given the rarity of planktonic foraminifera in the Loch Sunart samples, individuals were not identified to species level.

Table 5.2 Common benthic foraminiferal species in Loch Sunart sorted by the number of occurrences in samples. There are 31 samples in total, hence the minimum N value of 6 shown here represents 19 % occurrence. Also shown is the maximum abundance in any one sample and the mean abundance of the taxa across all samples.

Species	Occurrence (N)	Max. abundance %	Mean abundance %
Eggerelloides scaber	30	78.5	16.5
Ammonia becarrii	29	31.4	9.2
Cibicides lobatulus	29	49.0	11.5
Spiroplectammina wrightii	28	26.0	9.5
Bulimina marginata	28	43.4	11.1
Nonionella turgida	26	11.9	2.9
Ammoscalaria runiana	25	30.3	3.5
Asterigerinata mamilla	25	49.6	4.2
Elphidium excavatum	25	20.4	4.5
Adercotryma glomeratum	22	5.5	1.2
Rosalina praegeri	22	4.8	1.6
Bolivina spathula	20	3.0	0.5
Recurvoides trochamminiforme	19	3.6	0.6
Rheophax subfusiformis	19	5.3	0.9
Bolivina pseudopunctata	19	4.3	0.7
Stainforthia fusiformis	19	8.6	1.3
Bulimina elongata	18	4.4	0.9
Rhabdammina sp.	17	1.5	0.3
Bulimina gibba	17	2.3	0.4
Spiroplectammina earlandi	16	2.5	0.3
Quinqueloculina seminlum	16	3.3	0.8
Bolivina pseudoplicata	16	4.2	0.7
Elphidium magellanicum	16	1.1	0.3
Hyalinea balthica	15	2.6	0.4
Elphidium gerthi	14	1.1	0.2
Epistominella vitrea	14	4.6	0.5
Trifarina angulosa	14	1.9	0.3
Fissurina lucida	13	0.4	0.1
Melonis barleeanus	13	5.9	0.6
Bolivina variablis	12	4.8	0.4
Fissurina ellipitica	12	1.7	0.2
Rosalina anomala	12	0.8	0.1
Elphidium magarataceum	10	1.2	0.1
Stainforthis loeblichi	10	1.4	0.2
Quinqueloculina sp.	9	1.3	0.2
Buliminella elegantissima	9	0.6	0.1
Cassidulina reniforme	9	1.5	0.2
Elphidium macellum	9	14.6	0.9
Elphidium williamsoni	9	98.2	3.3
Cribrostomoides kosterensis	8	3.2	0.2
Oolina williamsoni	8	0.3	0.1
Millaminna fusca	7	0.9	0.1
Acervulina inhaerens	7	8.8	0.4
Amphicoryna scalaris	7	0.7	0.1
Nonion pauperatum	7	2.5	0.1
Patellina corrugata	7	0.8	0.1
Cornuspira involvens	6	3.4	0.2
Psammosphaera bowmanni	6	0.3	0.0
Quinqueloculina agglutinata	6	0.4	0.1
Cassidulina obtusa	6	2.0	0.2
Guttulina sp.	6	1.5	0.1
Islandiella narcrossi	6	0.5	0.1
Nonionella auricula	6	2.0	0.2
Nonion depressulus	6	2.9	0.2
Planktonic spp.	6	7.6	0.3
Trifarina fluens	6	0.3	0.1

5.3.1 Benthic foraminiferal abundance

Benthic foraminiferal abundance (total) is reported here as the number of benthic foraminifera per cm^3 of sample ($specimens.cm^{-3}$). Benthic foraminiferal abundance per gram of dry residue ($specimens.g^{-1}$) has also been calculated (appendix 7). Though this method does not account for the particle size distribution of the sample, it has been calculated for comparison to other studies (e.g. Alve & Nagy, 1986a).

Benthic foraminiferal abundance varies greatly in Loch Sunart assemblages, ranging from 9 - 1343 $specimens.cm^{-3}$for samples 149 to 176 respectively (table 5.3), with low abundances tending to occur in very shallow water depths (e.g. sample 53). For samples from water depths >16m, the mean abundance is calculated as 406 $specimens.cm^{-3}$.

Factor analysis of benthic foraminiferal abundance values and environmental variables measured in Loch Sunart shows the first two factors account for 59 % of the variance in the data, with summer BWT and grain size parameters such as % silt, % sand and % organic matter plotting against the first factor (figure 5.2). Longitude and % $CaCO_3$ are the most important variables on the second factor axis (figure 5.2). Correlations appertaining to longitude appear negative due to the negative sign preceding the decimalised longitude, however they must be interpreted as being the inverse of this, i.e. positive. Although longitude is a spatial variable rather than a parameter appertaining solely to substrate or hydrography, it is a factor which represents a combination of a multitude of environmental parameters, such as BWS and substrate properties, as well as variables which were not measured (e.g. oxygen availability, quality of organic matter, nutrient loadings etc).

Linear correlation coefficients (table 5.4) of benthic foraminiferal abundance values and environmental variables measured in Loch Sunart show that no significant relationships exist between foraminiferal abundance calculated by $specimens.cm^{-3}$ and environmental variables, and this is also suggested by the short $specimens.cm^{-3}$ line in the factor analysis (figure 5.2). However, the factor analysis shows that Loch Sunart modern benthic foraminiferal abundances ($specimens.cm^{-3}$) are most closely related to longitude (figure 5.2) and the linear correlation coefficient suggests a moderate and marginally insignificant relationship does exist with longitude ($r = -0.366$, $p = 0.051$),

Table 5.3. Loch Sunart samples sorted by the % stained specimens (i.e. 'live' individuals) in a sample. The majority of samples have less than 5 % stained benthic foraminifera. The samples with > 5 % stained specimens (with the exception of sample 53) appear to occur in sediments with a high silt and organic matter content (see also table 5.2).

Station	Longitude	Depth (m)	Collection date	BWT, °C	BWS	% Organic matter	% Silt	% Sand	% Broken specimens	% Stained specimens	Specimens/g	Shannon H	Fisher alpha
53	-5.5466	5	Jun-01	12.0	31.0	1.4	2.9	97.1	3.1	83.4	42	0.1	0.7
202	-5.8099	97	Jun-02	11.6	33.8	12.0	85.4	7.1	30.5	32.5	34600	2.8	11.7
149	-5.6216	59	Jun-02	12.1	33.0	18.0	78.2	18.3	35.0	30.2	2377	1.2	6.1
45	-5.7731	72	Apr-01	7.3	33.6	13.8	46.7	50.8	28.6	24.7	75000	3.1	17.2
197	-5.8658	111	Jun-02	11.7	33.9	6.1	32.8	64.1	28.7	18.9	1878	2.7	13.9
27	-5.9920	113	Apr-01	7.5	33.9	11.1	51.0	46.0	16.0	12.2	82840	3.6	22.6
76	-5.6857	12	Jun-01	12.3	31.4	4.0	40.0	57.9	1.4	11.2	1018	2.2	10.6
211	-5.6338	93	Jun-02	11.9	33.1	6.7	26.9	71.3	24.8	5.2	452	2.0	9.2
201	-5.8096	68	Jun-02	11.7	33.6	10.9	72.3	20.5	25.9	5.0	11475	2.3	11.6
41	-5.8649	65	Apr-01	7.4	33.6	6.1	46.1	51.2	45.7	4.5	14182	2.8	12.6
147	-5.5818	16	Jun-02	12.6	31.1	7.0	56.4	41.2	11.4	4.4	1668	1.0	6.4
112	-5.6499	45	Jul-01	12.3	33.1	2.5	31.7	66.3	36.6	4.3	184	2.5	9.0
192	-5.9185	90	Jun-02	11.9	34.0	4.5	32.8	64.1	40.8	4.0	1804	2.6	12.1
101	-5.8059	23	Jul-01	12.2	33.7	5.3	41.5	54.9	36.5	3.6	6567	2.7	13.1
198	-5.8434	121	Jun-02	11.6	33.8	6.8	66.7	28.1	41.0	3.2	8040	2.3	8.2
80	-5.7080	44	Jun-01	11.8	33.6	12.1	50.0	47.4	33.8	2.7	16400	2.7	12.0
90	-5.8130	36	Jul-01	12.0	33.8	5.3	67.1	25.8	24.4	2.6	195	2.6	14.3
200	-5.8128	55	Jun-02	11.8	33.8	11.3	74.6	18.8	40.1	2.2	61045	2.8	15.1
72	-5.5839	30	Jun-01	12.4	32.5	3.4	18.1	81.5	7.4	2.2	301	1.9	10.0
210	-5.7753	70	Jun-02	11.6	33.8	10.1	86.2	7.8	72.1	1.9	697	2.2	6.1
110	-5.6469	53	Jul-01	12.3	33.1	2.5	17.3	81.7	57.4	1.7	303	2.0	9.0
181	-6.0117	36	Jun-02	12.5	34.1	5.5	64.0	28.8	27.3	1.7	6767	2.8	13.3
199	-5.8135	17	Jun-02	12.4	33.2	1.5	41.5	54.9	66.4	1.7	4229	2.0	10.1
189	-5.9467	75	Jun-02	12.3	34.2	3.6	35.0	61.0	52.8	1.4	1416	2.1	8.3
68	-5.5691	11	Jun-01	12.8	30.7	3.8	23.9	75.5	6.9	0.9	396	1.2	6.7
22	-6.0135	45	Apr-01	7.5	34.0	9.4	59.1	37.5	29.9	0.8	15242	2.3	7.3
176	-5.7372	46	Jun-02	11.8	33.6	8.3	67.3	25.6	46.3	0.8	18143	2.3	11.6
193	-5.9198	51	Jun-02	12.3	34.1	3.9	29.8	67.3	59.5	0.8	1456	2.1	9.3
184	-5.9806	17	Jun-02	12.4	33.8	4.3	9.9	89.1	54.7	0.6	1775	2.2	13.2
173	-5.7261	31	Jun-02	11.9	33.6	4.5	54.9	39.3	47.3	0.5	4072	2.6	9.5

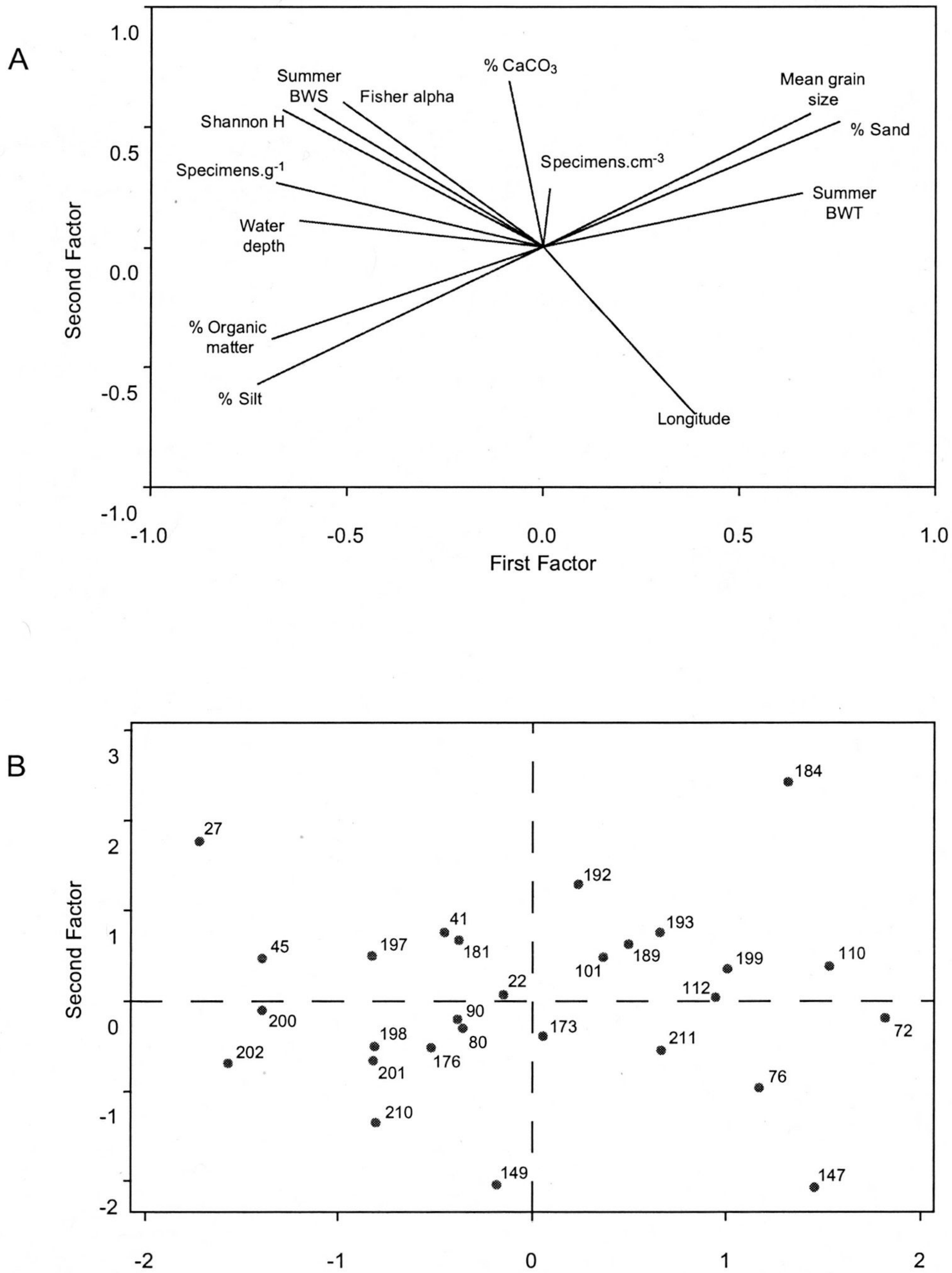

Figure 5.2 Loading plot (A) of the environmental variables influencing the benthic foraminiferal abundance (specimens.cm^{-3}) and % stained specimens in Loch Sunart. The summer BWT and BWS have been used though a seperate analyses using the April BWT and BWS show little variation. Sample 53 is not included in this analysis due to it's very shallow depth. How the Loch Sunart samples relate to the environmental variables, i.e. how they are influenced by parameters in multivariate space, can be seen in the score plot (B). Longitude must be reversed to account for its negative decimalised value.

Table 5.4 Matrix showing Pearson correlation coefficients (r, top value) and p values (bottom value) for Loch Sunart benthic foraminiferal abundances, diversities, % stained specimens and environmental parameters. Correlations which are significant at 95% are shown in bold. Correlations appertaining to longitude must have their signs inversed due to the negative sign preceding the decimalised longitude value, e.g. the correlation between longitude an bottom water salinity (BWS) is actually a positive relationship.

	Longitude	Depth (m)	BWT, ˚C	BWS	% Organic matter	% CaCO3	% Silt	% Sand	Mean grain size,µm	% Stained specimens	Specimens /g	Specimens /cm3	Shannon	Simpson
Depth (m)	-0.31 0.10													
BWT, ˚C	**0.39** **0.03**	**-0.36** **0.05**												
BWS	**-0.74** **0.00**	**0.52** **0.00**	-0.29 0.12											
% Organic matter	0.03 0.88	**0.37** **0.05**	**-0.39** **0.04**	0.19 0.31										
% CaCO3	**-0.51** **0.01**	0.08 0.69	-0.19 0.33	**0.46** **0.01**	0.04 0.84									
% Silt	-0.10 0.60	0.24 0.21	-0.15 0.43	0.24 0.19	**0.66** **0.00**	-0.26 0.17								
% Sand	0.13 0.51	-0.24 0.21	0.13 0.48	-0.27 0.15	**-0.63** **0.00**	0.26 0.18	**-1.00** **0.00**							
Mean grain size, µm	-0.05 0.80	-0.08 0.67	0.29 0.12	-0.01 0.95	**-0.55** **0.00**	**0.42** **0.02**	**-0.83** **0.00**	**0.82** **0.00**						
% Stained specimens	0.10 0.60	**0.41** **0.03**	-0.24 0.20	0.01 0.97	**0.63** **0.00**	0.01 0.94	0.31 0.10	-0.30 0.12	-0.18 0.35					
Specimens /g	-0.26 0.17	**0.36** **0.05**	**-0.65** **0.00**	0.25 0.19	**0.55** **0.00**	0.05 0.80	0.29 0.12	-0.28 0.13	-0.33 0.08	**0.38** **0.04**				
Specimens/cm /cm	**-0.37** **0.05**	-0.11 0.58	0.15 0.43	0.29 0.13	-0.31 0.10	0.01 0.97	0.05 0.81	-0.08 0.70	-0.09 0.65	**-0.39** **0.04**	-0.09 0.66			
Shannon	**-0.52** **0.00**	**0.43** **0.02**	**-0.49** **0.01**	**0.65** **0.00**	0.21 0.26	0.33 0.08	0.15 0.43	-0.17 0.38	-0.14 0.45	0.13 0.50	**0.60** **0.00**	0.09 0.63		
Simpson	**-0.57** **0.00**	**0.50** **0.01**	**-0.38** **0.04**	**0.77** **0.00**	0.05 0.78	0.20 0.29	0.17 0.37	-0.20 0.30	-0.14 0.45	-0.03 0.87	**0.41** **0.03**	0.19 0.34	**0.92** **0.00**	
Fisher alpha	**-0.36** **0.05**	0.28 0.14	**-0.41** **0.03**	**0.38** **0.04**	0.26 0.17	**0.41** **0.03**	0.00 0.98	0.00 0.98	0.00 0.98	0.21 0.28	**0.68** **0.00**	0.00 0.98	**0.84** **0.00**	**0.61** **0.00**

suggesting that BWS (along with sedimentological changes along the fjord axis) is likely to be a major influence on benthic foraminiferal abundance, since longitude and BWS are strongly correlated ($r = -0.75$, $p = 0$). These relationships prevail even when only main basin and outer basin data is used, i.e. the environmental gradient of the BWS is weakened.

Benthic foraminiferal abundance calculated by specimens.g^{-1} appears to be closely related to substrate properties (figure 5.2). The strongest abundance relationship is with the % organic matter of sediment ($r = 0.55$, $p = 0$; table 5.4), though grain size is also important, with foraminiferal abundances decreasing with increasing mean grain size, i.e. higher abundances are found in finer grained sediments. The strong correlation between % silt and % organic matter in sediments ($r = 0.67$, $p = 0.0$) is likely to explain the results of the factor analysis.

5.3.2 Live benthic foraminifera in Loch Sunart surface sediments

Sample 53 has the highest proportion of live specimens, with 83 % of the assemblage comprising of live *E. willamsoni* specimens, however the numbers of 'live' specimens in Loch Sunart benthic foraminiferal assemblages are typically low (table 5.3) with only 8 samples containing between 5-32 % of live specimens.

Since live benthic foraminiferal specimens are rare in Loch Sunart (tables 5.3 and 5.5) and numbers are too low to be statistically significant, little ecological information can be derived from the data. Linear correlations (see table 5.4) point to significant positive correlations between % live specimens and % organic matter ($r =0.63$, $p = 0$) and water depth ($r =0.41$, $p = 0.03$). A negative correlation exists between % live specimens and % sand ($r=-0.377$, $p=0.041$), and although other grain size attributes such as % silt show slightly insignificant (i.e. $0.05 < p < 0.1$) correlations (table 5.4), factor analysis suggests that the % live specimens in a sample is closely correlated with substrate % organic matter and % of silt (figure 5.2).

Table 5.5 Live count data (L) and total count data (T) from Loch Sunart surface sediment samples. The representation of live specimens as a % of the total assemblage is also given.

Station		27	41	45	53	68	72	76	80	90	101	110	112	147	149	173	176	181	189	192	193	197	198	200	202	210	211	Total live	Total Dead	Representation
Adercotryma glomeratum	L	5		16				4	1	2					1			1	2			3			3			38	86	44.2
	T	9		25				12	8	8					2			2	2			3			15					
Ammonia becarrii	L	6	5	5			2	5	2			1	2		7		1	1			2	4		2	4		1	50	539	9.3
	T	24	57	15			16	20	18			19	83		18		36	74			76	28		12	11		32			
Ammoscalaria runiana	L	2	2	20				1					2							1			1		3			32	118	27.1
	T	5	19	26				7					34							8			13		6					
Amphicoryna scalaris	L	1																										1	2	50.0
	T	2																												
Bolivina pseudoplicata	L																								2			2	6	33.3
	T																								6					
Bolivina pseudopunctata	L			1								1													2		1	5	32	15.6
	T			13								1													15		3			
Bolivina spathula	L	2		1																								3	25	12.0
	T	16		9																										
Bolivina striatula	L																					1						1	2	50.0
	T																					2								
Bolivina variablis	L																			2								2	3	66.7
	T																			3										
Bulimina marginata	L	8	5	32						5	3				3	1				1		6		1	44	1		110	756	14.6
	T	42	58	118						107	29				16	96				28		18		120	121	3				
Buliminella elegantissimsa	L					1																						1	1	100.0
	T					1																								
Cassudulina obtusa	L															1												1	2	50.0
	T															2														
Cibicides lobatulus	L	1					1													3					3	2		10	255	3.9
	T	23					7													119					5	101				
Cribrostomoides kosterensis	L												1															1	11	9.1
	T												11																	
Eggerelloides scaber	L	13	5	5			1	15					6	12	80					3				1	3	1	5	150	1218	12.3
	T	26	39	19			189	144					75	249	233					20				25	13	47	139			
Elphidium excavatum	L			3																					2			5	25	20.0
	T			16																					9					
Elphidium magellanicum	L																					1						1	1	100.0
	T																					1								
Elphidium macellum	L																									2		2	61	3.3
	T																									61				
Elphidium margarataceum	L																									1		1	5	20.0
	T																									5				
Elphidium williamsoni	L				133	1																						134	164	81.7
	T				160	4																								
Epistominella vitrea	L			1																		1			1			3	16	18.8
	T			9																		3			4					
Fissurina elliptica	L												1									1						2	7	28.6
	T												2					4				1								
Fissurina lucida	L										1																	1	1	100.0
	T										1																			
Haplophragmoides sp A	L								1		3																	4	10	40.0
	T								6		4																			
Haplophraqmoides bradyi	L																								1			1	9	11.1
	T																								9					
Lagena substriata	L																								1			1	1	100.0
	T																								1					
Melonis barleaanum	L			1																								1	2	50.0
	T			2																										
Miliolina spp.	L																					3						3	5	60.0
	T																					5								
Nonion auricula	L	2																				1						3	12	25.0
	T	10																				2								
Nonion depressulus	L							2																				2	8	25.0
	T							8																						
Nonionella turgida	L	11	2	11			1	2	5		4	2	1				2	6		7		17	10	3	26	1	3	114	267	42.7
	T	32	18	54			3	5	19		5	2	1				14			9		29	13	20	39	1	3			
Parafissurina himatiostoma	L			1																								1	1	100.0
	T			1																										
Psammosphaera bowmanni	L	1		1										1									1				1	5	5	100.0
	T	1		1										1									1				1			
Quinqueloculina seminlum	L																		1						2			3	18	16.7
	T																		9						9					
Recurvoides trochamminforme	L	4		5											2							5			2			18	32	56.3
	T	5		7											2							7			11					
Rhabdammina sp.	L										1	1																2	3	66.7
	T										2	1																		
Rheophax scotti	L																								1		6	7	7	100.0
	T																								1		6			
Rheophax subfusiformis	L	2		1				2				1	1											1			1	9	32	28.1
	T	2		3				8				4	6											5			4			
Rosalina praegeri	L						2						1									6						9	27	33.3
	T						3						11									13								
Spiroplectammina earlandi	L	1													1												1	3	14	21.4
	T	2													3												9			
Spiroplectammina wrightii	L	1	1	4															3			8						17	271	6.3
	T	4	74	18															87			88								
Stainforthia fusiformis	L	1		1		1				1	2						1	1				4	1		10			23	100	23.0
	T	42		1		1				6	7						3	1				8	1		30					
Stainforthia loeblichi	L	1								1						1												3	9	33.3
	T	4								3						2														
Textularia earlandi	L							1																				1	2	50.0
	T							2																						
Trifarina angulosa	L	2																										2	3	66.7
	T	3																												
Trochammina cf. parvus	L																			1								1	1	100.0
	T																			1										
Vernueilla advena	L																				1							1	1	100.0
	T																				1									
Trochammina adaptera	L																					1						1	1	100.0
	T																					1								

5.3.3 Spatial distribution of benthic foraminifera

5.3.3.1 Wall structure

The ternary plot in figure 5.3a shows the characteristic wall structures of the Loch Sunart benthic foraminiferal assemblages (% data in table appendix 8). Porcelaneous taxa have fairly low proportions (<10 %) in all assemblages, particularly in the inner basin (<3.5%), though the proportion of porcelaneous taxa increases towards the outer basin (figure 5.3b).

Inner basin samples are typically dominated by agglutinated species, with proportions often exceeding 80 %. Though shallow sample 53 lies within the inner basin, it yields only hyaline species. The two inner basin samples with lower proportions of agglutinated species (110 and 112) are situated close to the sill region, and it is likely that these sample locations experience relatively saline main basin water. Sample sites located further away from the sill are likely to experience brackish water for the majority of the year.

Main and outer basin assemblages are dominated by relatively high proportions of hyaline taxa, low agglutinated species and low porcelaneous percentage abundances (figure 5.3), with mean ratios of 72: 27: 1 and 77: 20: 3 respectively. A 2-sample T test (Davis, 2002) suggests there is little difference in the proportions of wall types of the main and outer basin (T-value =-1.72 , p = 0.101), though figure 5.3b clearly shows a higher proportion of porcelaneous taxa in the outer basin.

5.3.3.2 Species diversity

Loch Sunart benthic foraminiferal assemblages yield a broad range of diversity values ranging from 0.7 – 22.6 for the Fisher-α index, 0.1 - 3.6 for the Shannon-Weaver index and 0.04 – 0.96 for the Simpson index (table 5.3). The Shannon-Weaver (commonly referred to as the information function) and Simpson indices are strongly correlated ($r = 0.92$, $p = 0$; figure 5.4), thus only the Shannon-Weaver index will be used here.

Samples with a low species diversity (either Fisher-α or Shannon-Weaver values) generally have assemblages with low equitability, that is they have assemblages

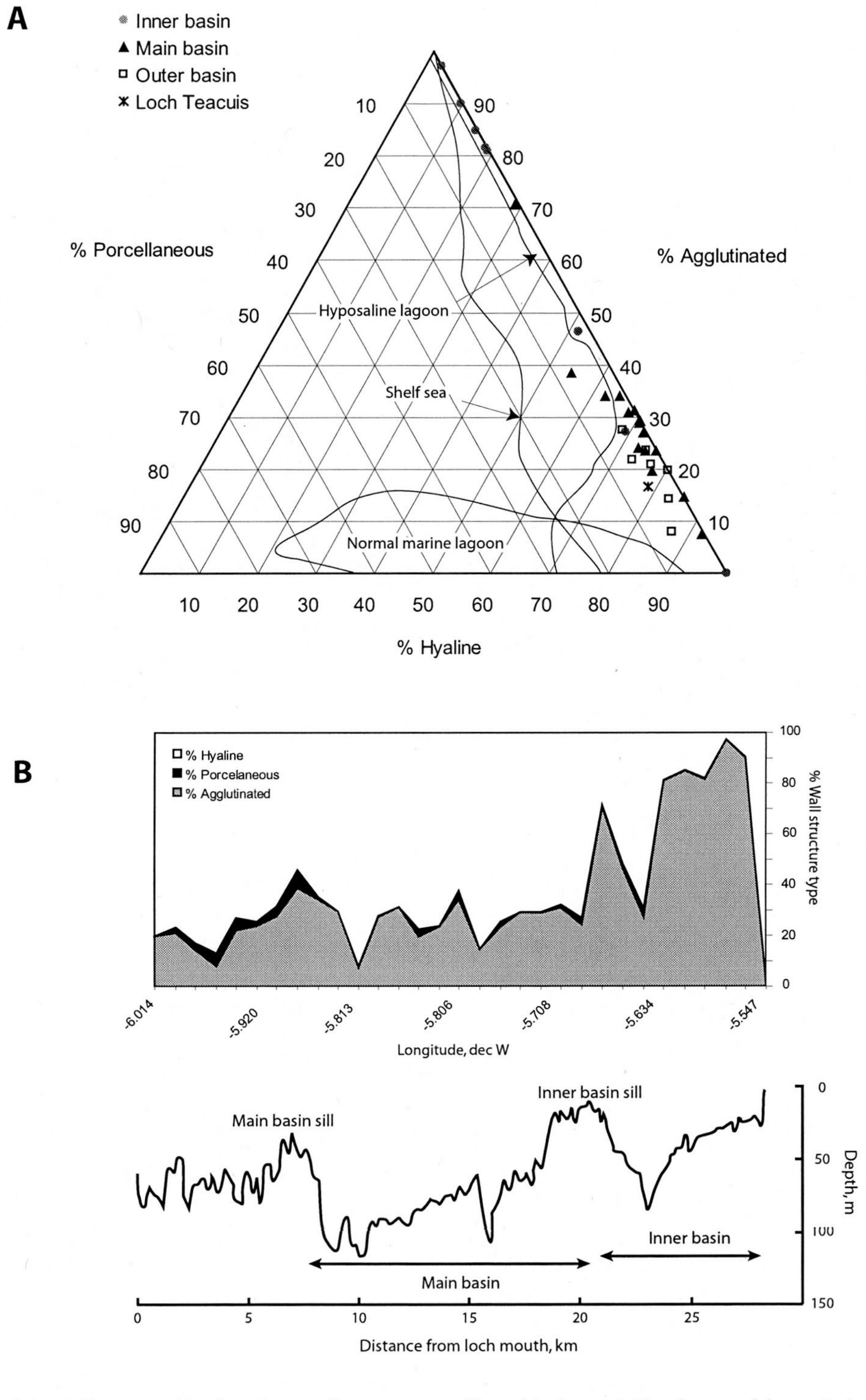

Figure 5.3 A) Ternary plot showing wall structures of benthic foraminiferal assemblages in Loch Sunart, along with Murray's (1973) classification of marine environments. All samples are contained within the 'shelf sea' catergory. The majority of the samples fall into the hyposaline lagoon category, though a few fall outside this envelope and into the 'shelf sea' environment. Since the shelf sea and the hyposaline lagoon environments overlap, it is difficult to establish which of these Loch Sunart most closely resembles. (B) The proportion of porcellaneous and hyaline taxa increase towards the coast, suggesting outer basin assemblages are more indicative of shelf seas than hyposaline lagoons.

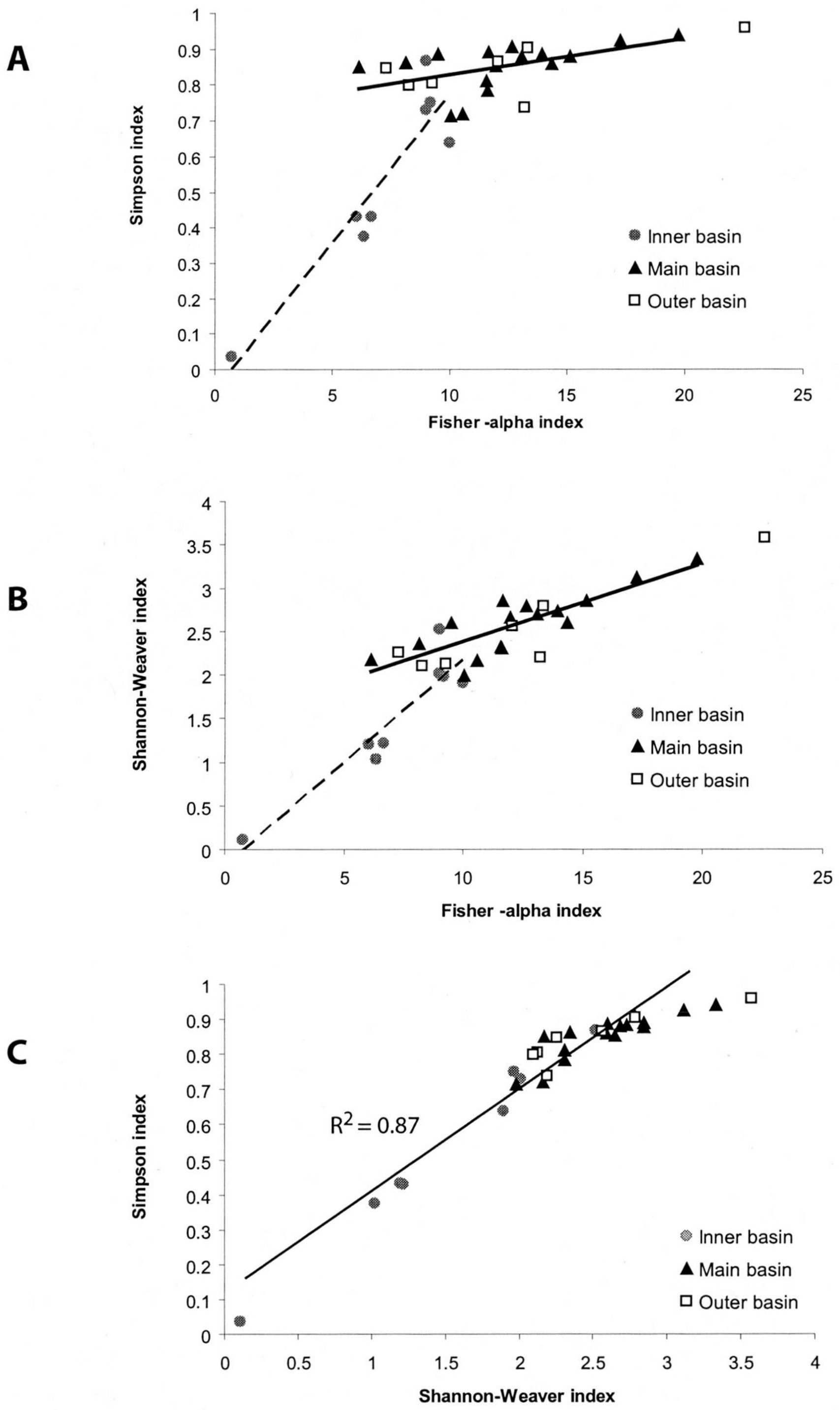

Figure 5.4 Species diversity indices for Loch Sunart benthic foraminiferal assemblages. The Fisher-alpha index represents the species diversity within a sample of *n* individuals and takes rarer species into account. The Simpson index reflects the dominance of taxa within the sample, with assemblages dominated by a few taxa having lower Simpson indices. Assemblages with low species diversity are often dominated by a few taxa (A). The Shannon-Weaver index (often referred to as the information function) represents both species diversity and how the abundances are spread over the species (e.g. equitability). Assemblages with a high species diversity tend to have high equitability, i.e. the abundance is spread evenly over the species present, as shown by plots B and C.

dominated by a few species (figure 5.4). Conversely, samples with high species diversity have higher equitability values and species abundance is more evenly spread over the taxa. Two trendlines can be extracted from the data shown in figure 5.4a and 5.4b, with the inner basin samples having a steeper trend than the main and outer basin trendline. The differences in slope are likely to be salinity differences between the basins with the inner basin waters typically being more hyposaline than the outer and main basin waters.

Inner basin assemblages tend to have the lowest species diversity, and samples appear to be clustered into two groups (with the exception of anomalous sample 53); those with Fisher-α indices of around 6 and Shannon-Weaver values of ~1.2 and those with richer species diversity and equitability (Fisher-α values ~ 9 and Shannon-Weaver values ~2; figure 5.4b). Two of the three low diversity inner basin samples (68 and 147) represent the shallowest samples from the inner basin and are dominated by a few taxa, in this case *Eggerelloides scaber.* Haynes, (1981) suggested that samples with low equitability tend to occur in stressed environments, and the lower salinities (30.7-31.3) in the inner basin shallower water depths are likely to lead to only tolerant species being able to inhabit the environment. Though sample 149 is from deeper water with a higher BWS, the high content of substrate organic matter (18 %) may present a stressed environment for some foraminiferal species. The sample with the lowest species diversity (Fisher-α = 0.7) and lowest equitability (0.08) is sample 53, which is dominated by a single taxon, *Elphidium williamsoni,* with an abundance of ~98%. This sample location has a water depth of only 4.5 m, and given the tidal range in Loch Sunart (~ 4 m), represents the most extreme physical environment of all the assemblages. The dominance of an assemblage by a single taxon is common in stressed environments (Murray, 1973), thus the sample was included in the cluster analysis due to it being a 'true' outlier, i.e. not a product of sampling or analysis failure (Shi, 1993). However, it has been excluded from most of the statistical analyses, since the data from this extreme environment significantly skewed the results.

Main basin assemblages show a large range in species diversity and equitability (figure 5.4), probably due to the wide variability of sample environments within the data set, e.g. different water depths, different substrates etc. Diversity indices tend to be strongly positively correlated with BWS (table 5.4) with species diversity and equitability increasing towards the coast (e.g. figure 5.5). Weak positive correlations between the diversity indices and depth are also apparent (table 5.4), probably due to the inter-correlations between depth, BWT and BWS, % silt and % organic matter in the sediments (table 5.4). Also apparent is a positive and fairly strong correlation between diversity and % $CaCO_3$ present in the sediments, which in turn, is correlated with BWS. This suggests that outer basin samples, which are situated within 'normal marine' water masses (i.e. salinities >34) should show richer species diversities, however outer basin samples typically yield lower diversity assemblages than main basin samples (figure 5.5). This may be due to grain size effects, with coarse grained substrates found in the shallower and more energetic water column of the outer basin. One would therefore expect to see the highest diversities in calm, outer basin environments and this is seen in sample 27, which has the highest foraminiferal abundance, species diversity and equitability and is located in an isolated deep (113 m water depth) of the outer basin (average water depth ~ 70 m).

5.3.3.3 Longitudinal distribution of Loch Sunart benthic foraminifera

The distribution of common benthic foraminiferal species (i.e. those with relative abundances > 2 %) show marked variations along the axis of the loch (figure 5.5), with certain taxa becoming more dominant in specific basins or environmental habitats.

The majority of common agglutinated taxa, e.g. *Ammoscalaria runiana* (grouped with *Ammoscalaria pseudospiralis*), *Cribrostomoides* species, *Spiroplectaminna earlandi* and the *Rheophax* species (comprising primarily of *Rheophax subfusiformis* and *Rheophax scotti*) typically have their maximum abundances within the inner basin of Loch Sunart, though they are present throughout most of the assemblages in reduced abundances. *Eggerelloides scaber* is the dominant taxon in the inner basin, contributing ~ 22-79 % of each assemblage, and though this species becomes less dominant outside the inner basin, the majority of main and outer basin assemblages contain between 1-11% *E. scaber* (table 5.2; figure 5.5). The *Trochamminna* group are present in low abundances (probably due to the fragile nature of the test) throughout the loch, with the maximum abundance in the high diversity outer basin

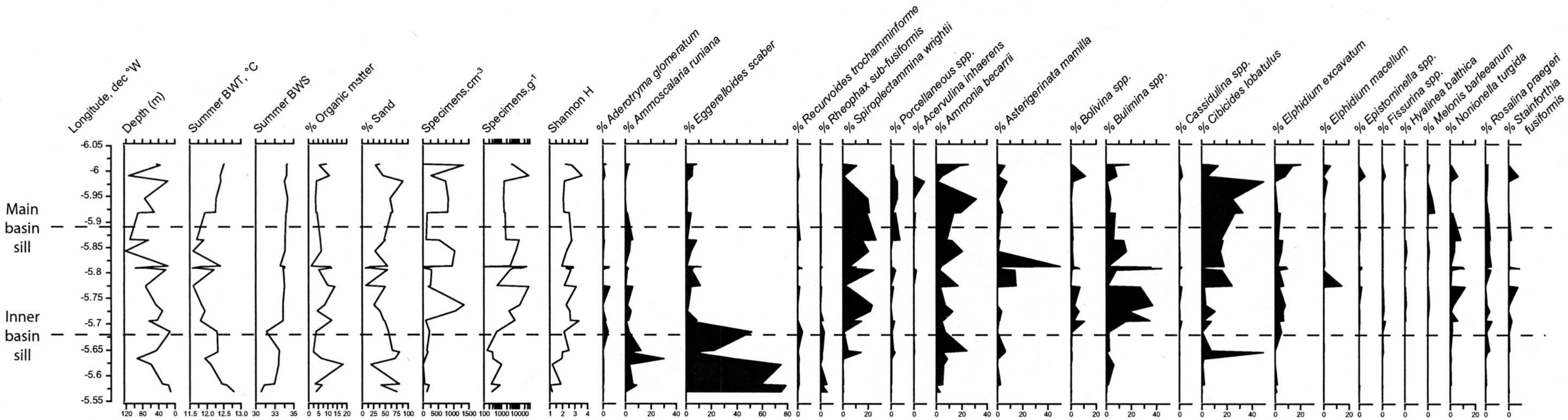

Figure 5.5 The distribution of benthic foraminifera (abundances > 2 %) from Loch Sunart surface sediment samples, plotted against longitude. Sediment sample water depths and the bottom water temperature (BWT) and bottom water salinity (BWS) recorded at the site, are also shown, as are benthic foraminiferal abundance (specimens.cm^{-3} and specimens.g^{-1}), organic matter content and proportion of sand sized particles in the sediment sample. The proportion of sand and silt in a Loch Sunart sediment sample are roughly inversely correlated, thus locations with a high % sand of is likely to have a low % of silt and clay. Only the Shannon-Weaver index (Shannon H) is represented here. High Shannon-Weaver values typically represent high species diversity and high equitability (figure 5.4). Drawn using C2 (Juggins, 2003).

sample 27. The rest of the agglutinated taxa (*Adercotryma glomeratum, Haplophragmoides bradyi, Recurvoides trochamminiforme*) have their maximum abundances within the main basin, which may be due to the relatively calm depositional environment, as interpreted by the fine grained sediments. *Spiroplectammina wrightii* (grouped here with *Textularia bocki*) is rare or absent in inner basin assemblages, prevalent in the main basin and shows maximum abundances in the seaward part of the main basin and within the outer basin (figure 5.5).

Significant abundances of hyaline species typically occur in the main and outer basins (figures 5.3 and 5.5) and may be rarer in inner basin waters due to lowered salinity and increased organic carbon contents (Boltovskoy & Wright, 1976). Maximum abundances of *Bulimina marginata*, *Nonionella turgida, Stainforthia fusiformis*, and the *Bolivina spp.* typically occur in the deeps of the main basin where environmental conditions are likely to be calm. *Fissurina* species and *Epistominella* species are also present in the main basin assemblages, occurring where low abundances of epiphytic taxa (such as *Cibicides lobatulus*) suggest a very calm depositional environment. Rarer taxa (< 2%) present in the main basin include *Haplophragmoides* species A (Haynes), *Elphdium magellanicum, Stainforthia* species (predominantly *Stainforthia. loeblichi*), and *Trifarina* species (mainly *Trifarina angulosa*). Samples from shallower water depths contain taxa indicative of higher energy environments (e.g. *Elphidium excavatum, Asterigerinata mamilla, S. wrightii* and *C. lobatulus*).

Typical outer basin assemblages (e.g. samples 189 and 192) tend to have high abundances of *C. lobatulus, Ammonia beccarii*, *E. excavatum* and *S. wrightii* which reflect the relatively high energy depositional environments at these sites despite the fairly deep water depths (>75 m). The significant increase in the abundance of *Miliolina* species is likely due to the influence of more saline water masses (see section 5.4.1).

5.3.4 Depth distribution of benthic foraminifera

Determining the depth preference of benthic foraminifera species proves difficult for Loch Sunart samples (figure 5.6) since the elongated and narrow bathymetry of the sea loch, along with a large spring tidal range (~4m) results in high energy

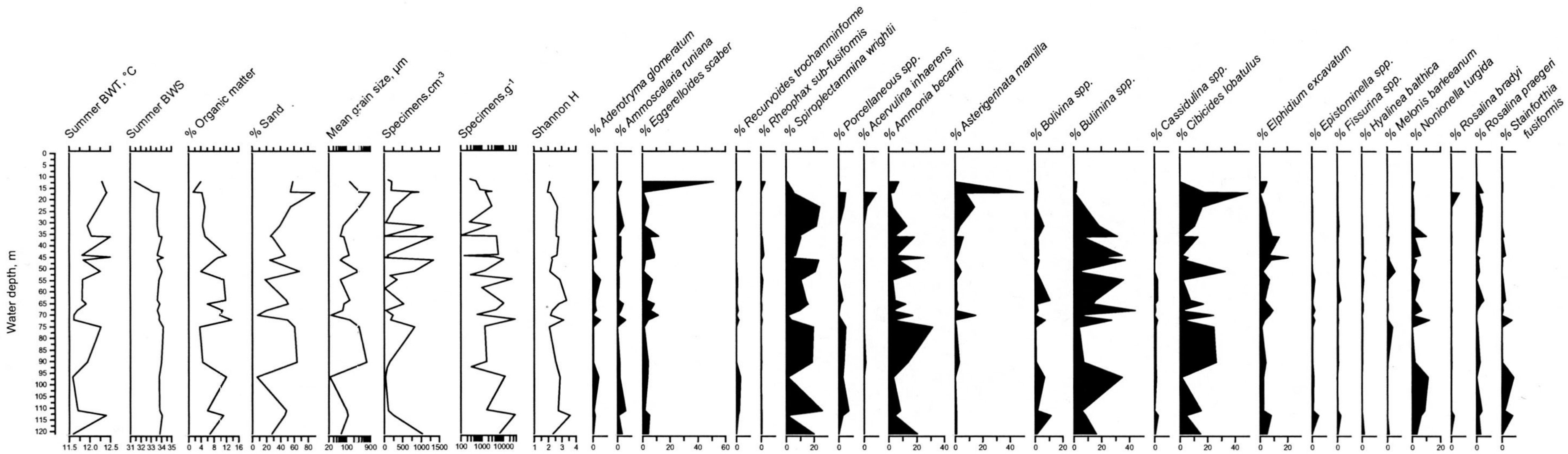

Figure 5.6a The distribution of benthic foraminifera (abundances > 2 %) from Loch Sunart surface sediment samples deeper than 10 m, plotted against water depth. Bottom water temperature (BWT) and bottom water salinity (BWS) recorded at the site are also shown, as are benthic foraminiferal abundance (specimens.cm^{-3} and specimens.g^{-1}), organic matter content and proportion of sand sized particles in the sediment sample. The proportion of sand and silt in a Loch Sunart sediment sample are roughly inversely correlated, thus locations with a high % of sand is likely to have a low % of silt. Both the Shannon-Weaver index (Shannon H) and the Fisher- alpha indices are shown. Drawn using C2 (Juggins, 2003).

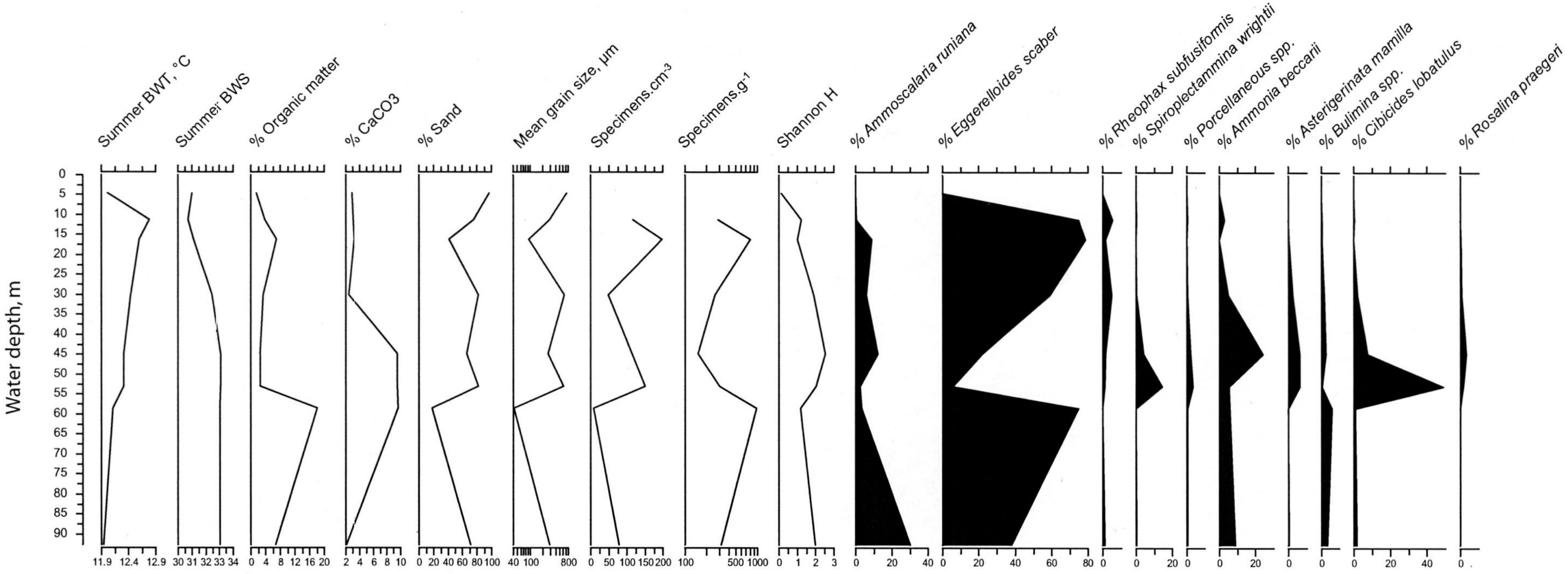

Figure 5.6b The distribution of benthic foraminifera (abundances > 2 %) from the surface sediments (deeper than 10 m) of Loch Sunart's inner basin, plotted against water depth. Bottom water temperature (BWT) and bottom water salinity (BWS) recorded at the site are also shown, as are benthic foraminiferal abundance (specimens.cm^{-3} and specimens.g^{-1}), organic matter content and proportion of sand sized particles in the sediment sample. The proportion of sand and silt in a Loch Sunart sediment sample are roughly inversely correlated, thus locations with a high % of sand is likely to have a low % of silt. Both the Shannon-Weaver index (Shannon H) and the Fisher- alpha indices are shown. The dominanceof *E. scaber* is clearly evident. Drawn using C2 (Juggins, 2003).

depositional environments occurring in deep water (chapter 3), whilst shallower samples can yield fine-grained sediments. However, a single depth transect across the main basin exemplifies that some Loch Sunart taxa do show general trends with water depths (figure 5.7). For example, *R. subfusiformis, E. scabra, A. mamilla,* and *E. willamsoni* abundances all decrease with water depth, whilst *Bolivina spp.*, *Epistominella spp., N. turgida, S. fusiformis* and *A. beccarii* all exhibit a preference for deeper water.

5.3.5 Benthic foraminiferal assemblages

Cluster analysis and non-metric multidimensional scaling identify 4 main benthic assemblage groups (figure 5.8). These groups are also seen in the results of the R-mode and Q-mode factor analysis (figure 5.9). The Q-mode factor analysis (similar to cluster analysis) identifies groups of samples which plot close together in multivariate space and thus (in this case) have similar benthic foraminiferal assemblages and environmental variables (figure 5.9a). R-mode factor analysis shows the correlation between species (and/or environmental variables) with highly correlated variables plotting close in proximity on the loading plot and with the size of the factor loading reflecting the amount of variance of a variable (figure 5.9b; Walden & Smith, 1995). In this case, we can assume that highly correlated species typically occur together in assemblages (e.g. *N. turgida* and *S. fusiformis*), whilst species which plot opposite each other in the loading plot are not usually present in the same assemblage (e.g. *C. lobatulus* and *R. trochamminiforme*).

Sample 53 has a very low similarity (~ 5 %) with respect to the other assemblages (figure 5.8) due to the high dominance of a single taxon, *Elphidium willamsoni* (abundance of 98 %; see section 5.3.3.2), thus this anomalous sample is not included in the assemblage groups.

5.3.5.1 Group A: E. scaber assemblage

This assemblage group primarily consists of inner basin samples containing high proportions of agglutinated taxa (> 70 %) and typically dominated by *E. scaber* with abundances of 38-79 % (appendix 8). Secondary species include *A. runiana* (0.3-30

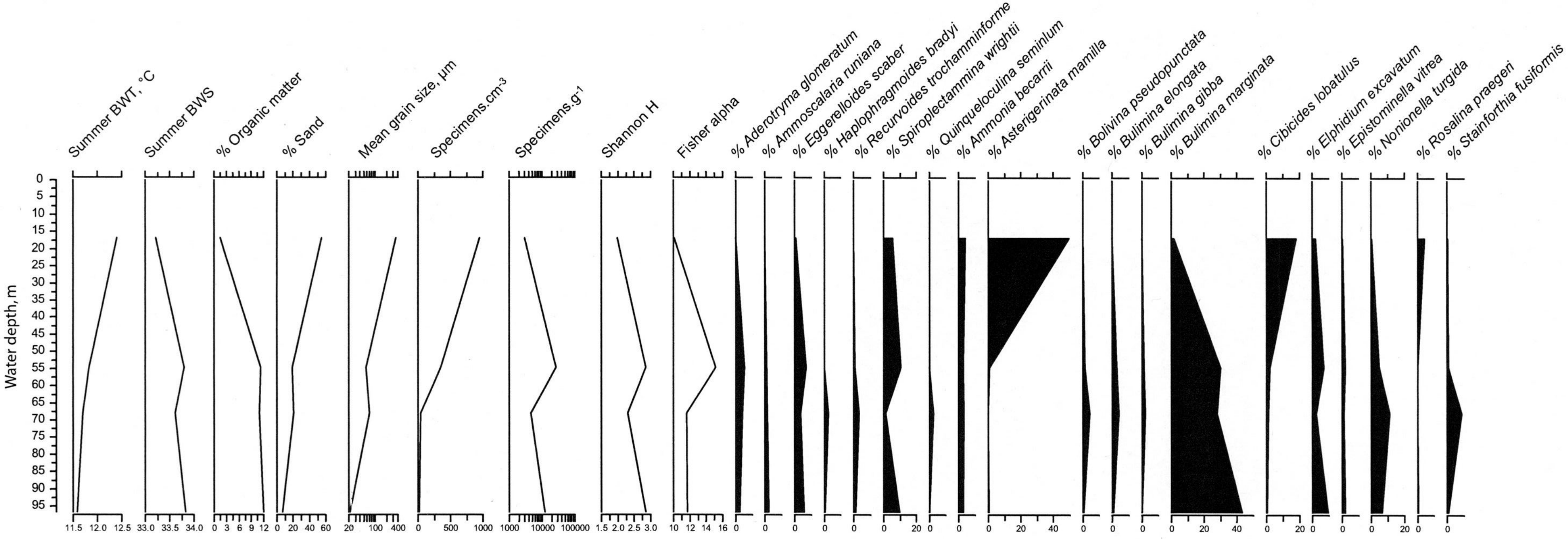

Figure 5.7 The distribution of benthic foraminifera (abundances > 2 %) taken across a depth transect in the main basin of Loch Sunart (samples 199-202) in an area of fairly low current activity. Bottom water temperature (BWT) and bottom water salinity (BWS) recorded at the site are also shown, as are benthic foraminiferal abundance (specimens.cm^{-3} and specimens.g^{-1}), organic matter content and proportion of sand sized particles in the sediment sample. The proportion of sand and silt in a Loch Sunart sediment sample are roughly inversely correlated, thus locations with a high % of sand is likely to have a low % of silt. Both the Shannon-Weaver index (Shannon H) and the Fisher- alpha indices are shown. Drawn using C2 (Juggins, 2003).

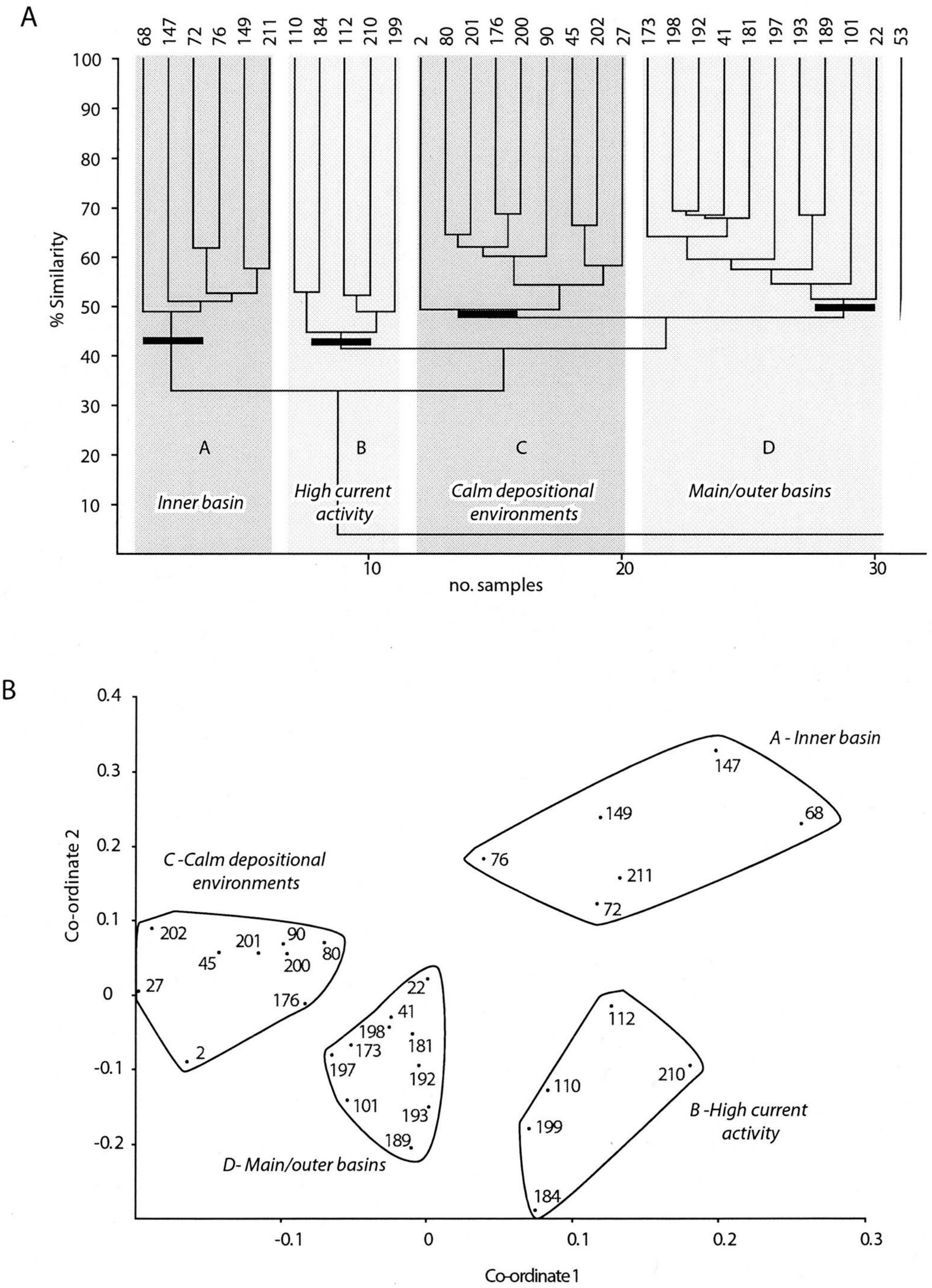

Figure 5.8 Multivariate statistical analyses of Loch Sunart modern benthic foraminiferal abundance data, transformed using the square-root method (Lepš & Šmilauer, 2003) in order to determine foraminiferal assemblages, using PAST (Hammer *et al.*, 2001), and applying the Bray-Curtis similarity index. The cluster analysis (A) identifies 4 broad assemblage groups, grouped with similarities of 45 - 50 %. Validation of the cluster analysis via non-metric Multi Dimensional Scaling (MDS, stress 0.17; Shi, 1993) shows that assemblage groups defined by cluster analysis are replicated in MDS space, hence can be deemed as significant assemblages. Additionally, assemblage groups A and C were reproduced using cluster analyses with different similarity measures (e.g. Euclidean).

Assemblage groups are: A) *E. scaber*; B) *Cibicides lobatulus – Asterigerinata mamilla – Ammonia beccarii;* C) B*ulimina marginata – Nonionella turgida – Stainforthia fusiformis* and D) *Ammonia beccarii – Cibicides lobatulus – Spiroplectammina wrightii.* Further details are given in the text.

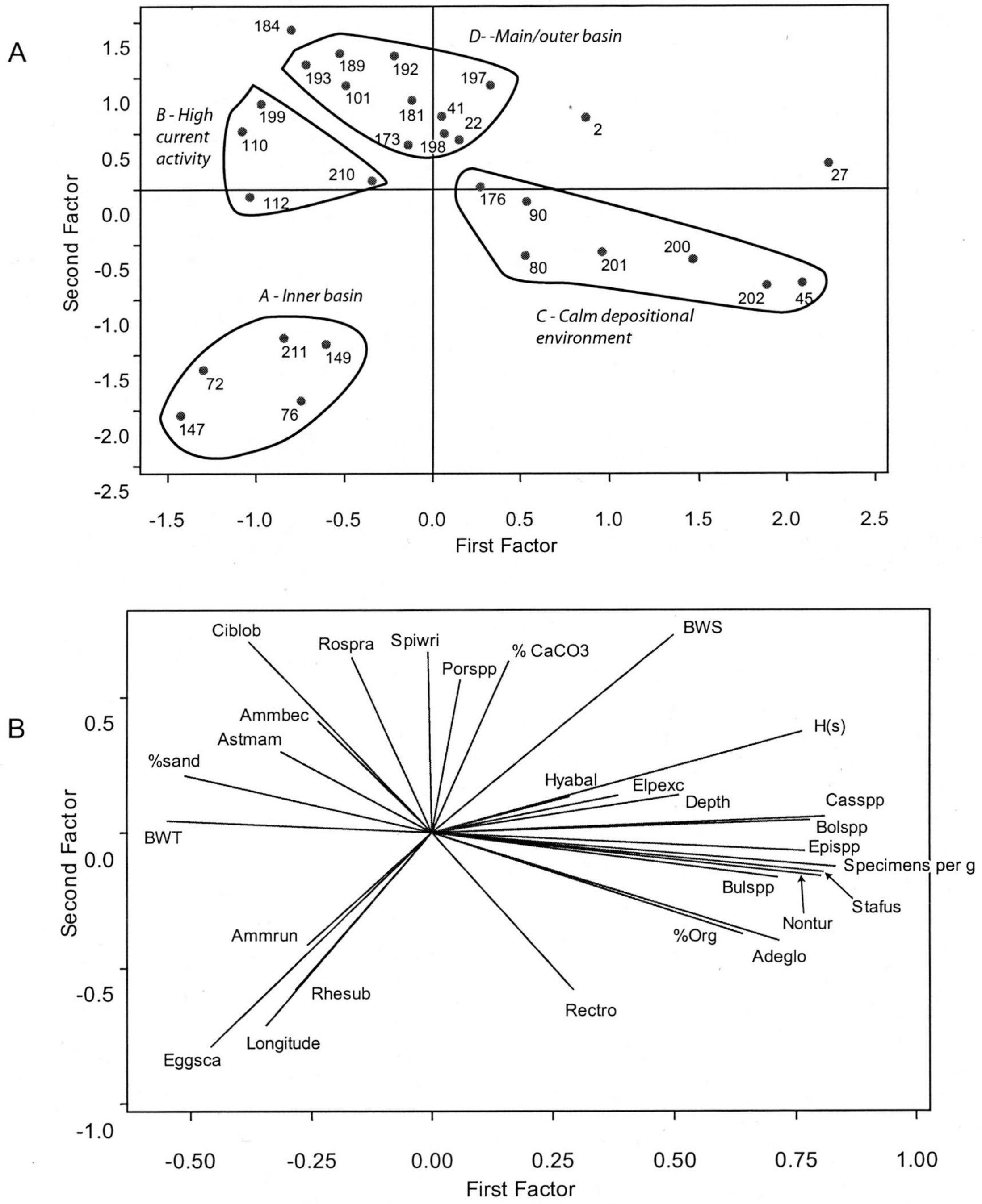

Figure 5.9 Results from the simultaneous R-mode and Q-mode factor analyses (using Minitab v14). The score plot (A) shows how Loch Sunart samples are correlated in multivariate space, and this agrees well with the results of the cluster and non-metric MDS analyses. Samples 2 and 27 (particularly sample 2) are located away from assemblage group C in factor analysis multivariate space, and sample 184 is not included in assemblage B. Since signs of this is also seen in the non-metric MDS analysis (figure 5.8), there are likely to be significant differences in the assemblages. The loading plot (B) shows the relationships between benthic foraminiferal species and environmental variables. Though % silt is not shown here, it is the inverse of % sand and lies close to % Org (organic matter). Taxa codes take the first 3 letters of genus and species and can be seen in full in appendix 9.

%), *A. beccarii* (2.8-8.8 %), *R. subfusiformis* (1.1-5.3 %) and *B. marginata* (0.6-5.1 %). The exception to this group representing solely inner basin samples is sample 76, which lies close to the inner basin sill in the main basin, and has an assemblage dominated by *E. scaber*. Inner basin samples 112 and 110 lie outwith cluster A, and this is likely due to the low abundance of *E. scaber* within the assemblages (< 21 %). Geographically, the sampling locations (112 and 110) come from a similar depth, are close to the sill region, and contain a high proportion of hyaline taxa (> 50%) in comparison to the other inner basins samples (< 19%).

5.3.5.2 Group B: ***Cibicides lobatulus – Asterigerinata mamilla – Ammonia beccarii***

Samples in this group come from all basins, representing a range of water depths and contain a high proportion of hyaline taxa (typically > 85 %) with a fairly high proportion of broken tests (36 – 72 %; table 5.3). Species diversity and equitability is moderate to low (Fisher-α values = 6 - 13; Shannon-Weaver = 2 - 2.5), as are abundances (116 – 945 specimens.cm^{-3}).

The majority of samples are characterised by 'high energy' taxa such as *C. lobatulus* (typically >25 %) and *A. mamilla.* (table 5.6). Other species indicating a high energy environment are *S. wrightii*, *Elphidium macellum* and *Acervulina inhaerens.* All samples have low abundances of *B. marginata* and *N. turgida.* The tolerant species *A. beccarii* is present in all samples except 184.

Though both cluster analysis and non-metric MDS place the inner basin samples 112 and 110 in this group, probably due to abundant *C. lobatulus, A. beccarii* and *A. mamilla* (figure 5.9), the samples differ slightly to the others due to *E. scaber* appearing within the top 3 most abundant taxa (table 5.6). This is probably due to the location of these samples within the inner basin of Loch Sunart.

5.3.5.3 Group C: ***Bulimina marginata – Nonionella turgida – Stainforthia fusiformis***

This assemblage group comprises mainly of main basin samples from depths > 36 m which have some of the lowest % broken specimens (< 46%). Benthic foraminiferal

Table 5.6 The 5 most abundant taxa for each sample in the 4 assemblages groups

A

Species	LS-68	Species	LS-147	Species	LS-72	Species	LS-149	Species	LS-211	Species	LS-76
Eggerelloides scaber	75.1	*Eggerelloides scaber*	78.5	*Eggerelloides scaber*	59.1	*Eggerelloides scaber*	74.9	*Eggerelloides scaber*	38.3	*Eggerelloides scaber*	51.6
Rheophax subfusiformis	5.3	*Ammoscalaria runiana*	8.8	*Ammoscalaria runiana*	5.9	*Ammonia becarrii*	5.8	*Ammoscalaria runiana*	30.3	*Ammonia becarrii*	7.2
Agglutinated Ind	5.0	*Agglutinated sp. Large foram*	2.5	*Rheophax subfusiformis*	5.0	*Bulimina marginata*	5.1	*Ammonia becarrii*	8.8	*Elphidium excavatum*	5.0
Ammonia becarrii	2.8	*Rheophax subfusiformis*	1.6	*Ammonia becarrii*	5.0	*Ammoscalaria runiana*	3.2	*Bulimina marginata*	2.8	*Adercotryma glomeratum*	4.3
Rheophax scotti	1.2	*Agglutinated Ind*	1.0	*Cornuspira involvens*	3.4	*Agglutinated Ind*	1.6	*Agglutinated sp. Large foram*	2.5	*Recurvoides trochamminiforme*	3.6

B

Species	LS-110	Species	LS-112	Species	LS-210	Species	LS-199	Species	LS-184
Cibicides lobatulus	48.7	*Ammonia becarrii*	24.2	*Cibicides lobatulus*	24.3	*Asterigerinata mamilla*	49.6	*Cibicides lobatulus*	49.0
Spiroplectammina wrightii	14.3	*Eggerelloides scaber*	21.9	*Ammonia becarrii*	17.4	*Cibicides lobatulus*	17.9	*Acervulina inhaerens*	8.8
Eggerelloides scaber	6.1	*Ammoscalaria runiana*	9.9	*Asterigerinata mamilla*	15.0	*Spiroplectammina wrightii*	5.4	*Asterigerinata mamilla*	7.8
Asterigerinata mamilla	6.1	*Cibicides lobatulus*	7.6	*Elphidium macellum*	14.6	*Rosalina praegeri*	4.6	*Rosalina cf. bradyi*	6.0
Ammonia becarrii	5.5	*Asterigerinata mamilla*	6.4	*Eggerelloides scaber*	11.2	*Ammonia becarrii*	4.0	*Spiroplectammina wrightii*	5.1

C

Species	LS-2	Species	LS-80	Species	LS-176	Species	LS-45	Species	LS-201	Species	LS-202	Species	LS-200
Spiroplectammina wrightii	14.7	*Bulimina marginata*	34.6	*Bulimina marginata*	34.4	*Bulimina marginata*	19.6	*Bulimina marginata*	43.4	*Bulimina marginata*	27.9	*Bulimina marginata*	30.2
Bulimina marginata	13.9	*Eggerella scabra*	8.9	*Spiroplectammina wrightii*	23.4	*Nonionella turgida*	11.9	*Spiroplectammina wrightii*	9.6	*Nonionella turgida*	11.2	*Spiroplectammina wrightii*	10.6
Cibicides lobatulus	7.6	*Spiroplectammina wrightii*	7.0	*Elphidium excavatum*	8.1	*Stainforthia fusiformis*	7.5	*Elphidium excavatum*	9.6	*Stainforthia fusiformis*	8.6	*Eggerelloides scaber*	7.1
Bolivina variablis	4.8	*Elphidium excavatum*	6.7	*Ammonia becarrii*	7.1	*Ammoscalaria runiana*	5.7	*Nonionella turgida*	6.8	*Adercotryma glomeratum*	4.3	*Elphidium excavatum*	7.1
Rosalina praegeri	4.8	*Nonionella turgida*	5.8	*Cibicides lobatulus*	3.5	*Adercotryma glomeratum*	5.5	*Eggerelloides scaber*	5.9	*Bolivina pseudopunctata*	4.3	*Adercotryma glomeratum*	5.3

Species	LS-90	Species	LS-27
Bulimina marginata	31.5	*Elphidium excavatum*	8.2
Eggerelloides scaber	11.8	*Stainforthia fusiformis*	8.0
Nonionella turgida	10.0	*Bulimina marginata*	6.7
Spiroplectammina wrightii	9.1	*Nonionella turgida*	6.1
Elphidium excavatum	8.8	*Eggerelloides scaber*	4.9

D

Species	LS-173	Species	LS-101	Species	LS-198	Species	LS-41	Species	LS-197	Species	LS-192	Species	LS-193
Ammonia becarrii	20.6	*Cibicides lobatulus*	17.1	*Spiroplectammina wrightii*	26.0	*Cibicides lobatulus*	26.4	*Cibicides lobatulus*	32.6	*Ammonia becarrii*	31.4	*Ammonia becarrii*	18.5
Spiroplectammina wrightii	20.1	*Spiroplectammina wrightii*	15.8	*Cibicides lobatulus*	15.4	*Spiroplectammina wrightii*	19.1	*Spiroplectammina wrightii*	21.1	*Cibicides lobatulus*	24.6	*Elphidium excavatum*	14.0
Bulimina marginata	15.9	*Ammonia becarrii*	12.2	*Nonionella turgida*	8.6	*Ammonia becarrii*	14.0	*Ammonia becarrii*	19.3	*Spiroplectammina wrightii*	19.8	*Cibicides lobatulus*	13.3
Cibicides lobatulus	14.9	*Bulimina marginata*	9.8	*Ammonia becarrii*	8.3	*Bulimina marginata*	6.2	*Melonis barleaanum*	5.9	*Melonis barleaanum*	3.9	*Spiroplectammina wrightii*	10.8
Elphidium excavatum	5.0	*Eggerelloides scaber*	8.3	*Ammoscalaria runiana*	5.9	*Eggerelloides scaber*	4.4	*Asterigerinata mamilla*	4.3	*Miliolina ind*	2.5	*Asterigerinata mamilla*	5.9

Species	LS-189	Species	LS-181	Species	LS-22
Ammonia becarrii	25.4	*Ammonia becarrii*	18.5	*Ammonia becarrii*	25.4
Elphidium excavatum	20.4	*Elphidium excavatum*	14.0	*Elphidium excavatum*	20.4
Bulimina marginata	18.3	*Cibicides lobatulus*	13.3	*Bulimina marginata*	18.3
Eggerelloides scaber	8.5	*Spiroplectammina wrightii*	10.8	*Eggerelloides scaber*	8.5
Cibicides lobatulus	6.1	*Asterigerinata mamilla*	5.9	*Cibicides lobatulus*	6.1

abundances calculated by volume vary, ranging from 15 – 1,342 specimens.cm^{-3} with a mean of 288 specimens.cm^{-3}, though abundances calculated by weight of total dry residue are the highest seen in the Loch Sunart surface samples (4,545 – 35,873 specimens.g^{-1}), as is species diversity and equitability (Fisher-α = 11.6 - 22.6; Shannon-Weaver > 2.3). Samples in this group typically have a moderate proportion of hyaline taxa (69 - 83 %).

With the exception of samples 2 and 27, samples in this group are dominated by *B. marginata* with typical abundances > 20 % (table 5.6) and often contain significant abundances (i.e. > 2%) of secondary diagnostic species, which include *N. turgida* (6 – 12 %), *S. fusiformis* (~ 8 %) and *A. glomeratum* (4 - 5.5 %). *E. scaber* (5 - 12.5 %) and *S. wrightii* (7 – 23 %) are present in most samples, as is *E. excavatum* (7 - 10 %). Samples in this assemblage group typically have low proportions of 'high energy'; taxa such as *C. lobatulus* (<8 %) and the presence of 'delicate' agglutinated taxa, such as *A. glomeratum* and *A. runiana* point to a relatively calm depositional environment (figure 5.9). Additionally, *Bolivina* species such as *Bolivina variablis, B. pseudopunctata, B. pseudoplicata* and *B. spathula* are common in these samples with abundances often > 1% (appendix 7).

5.3.5.4 Group D: Ammonia beccarii – Cibicides lobatulus – Spiroplectammina wrightii

Samples from this assemblage group lie mainly in the main and outer basin of Loch Sunart, from water depths between 23 – 121 m. Broken tests contribute 27 -50 % of the total count. Foraminiferal abundance is variable (23 – 1328 specimens.cm^{-3}, mean 615 specimens.cm^{-3}) and higher than abundances in the group C assemblages, though benthic foraminiferal abundance calculated by specimens.g^{-1} is typically lower (1361 – 10,221 specimens.g^{-1}). This also applies for species diversity and equitability with Fisher-α values from 7-14 and Shannon-Weaver 2.1 – 2.8.

A. beccarii and *C. lobatulus* are present in all samples (abundances of 8-31 % and 6-33 % respectively, and these two species represents the most abundant species in all assemblages (table 5.6) except sample 198 where the *S. wrightii* has the highest abundance (26 %). *S. wrightii* also appears to be an important species in Group D assemblages (table 5.6). It is interesting to note that *S. wrightii* is the secondmost abundant species (16-26 %) in assemblages from the main basin (samples 173, 101, 198, 41 and 197) but typically contributes less (< 11%) to outer basin sample assemblages (table 5.6) with the exception of sample 192 (~20 % *S. wrightii*). Conversely, *E. excavatum* becomes more important in outer basin samples showing the second highest abundance (14 -20 %) after *A. beccarii* (19-31 %) in samples 193, 189, 181 and 22.

Some samples within this assemblage group also contain significant proportions of *B. marginata* (6-18 %), *E. scaber* (4-8 %) and *A. mamilla* (4-6 %). Species typically indicative of 'coastal waters' such as *Miliolina spp.* and *Melonis barleeanum*, are also present in the assemblages of this group (table 5.6; appendix 8).

5.4 DISCUSSION

5.4.1 Environmental information from benthic foraminiferal wall structures

Murray (1991b) suggests that benthic foraminiferal wall structures can provide environmental information and the ternary plots of Loch Sunart benthic foraminiferal wall structures lie in the overlap of hyposaline lagoon and shelf sea segments (figure 5.3), with the inner basin assemblages falling 'nearer' to hyposaline lagoon.

Restricted basins are often dominated by agglutinated taxa, e.g. inner basin assemblages from Loch Sunart typically have >81 % agglutinated specimens, and hyaline specimens from the deep inner basin of Loch Sunart tend to have thin and etched tests. This is likely due to low pH or low calcium carbonate ($CaCO_3$) availability (Boltovskoy & Wright, 1976) and either process creates a stressful environment for calcareous taxa, which must spend 'considerable energy recalcifying their tests' (Boltovskoy & Wright, 1976). The low abundance of porcelaneous species in Loch Sunart assemblages is also typical of fjordic or low salinity environments (e.g. Alve & Nagy, 1990; Austin & Sejrup, 1994; Murray *et al.*, 2003) and Murray (1973) reports that miliolina taxa are unable to maintain pseudopodial reticulum activity in hyposaline waters. Additionally, unlike hyaline taxa which efficiently use available $CaCO_3$ during test formation, porcelaneous taxa are thought to have a less organised method which requires readily available $CaCO_3$ (Boltovskoy & Wright, 1976). This may explain the lack of this wall type in the inner basin which experiences salinities of < 33, i.e. marine brackish waters.

Since miliolina taxa experience life mode problems in restricted basins/hyposaline waters, the increasing proportions of porcelaneous taxa in the seaward Loch Sunart assemblages may be interpreted as indicators of the increasing influence of higher salinity (i.e. 'normal marine') water masses (e.g. figure 5.3). This is also true for hyaline taxa which typically become more abundant with increased availability of $CaCO_3$ (e.g. Christiansen *et al.*, 1996) and likely explains slightly higher proportions of hyaline taxa in outer basin samples.

5.4.2 Loch Sunart benthic foraminiferal abundance with respect to other fjordic environments

Comparison of benthic foraminiferal abundances from similar fjordic environments proves difficult, since fjords are often unique in their hydrography and depositional environments. However, with mean benthic foraminiferal abundances of 409 specimens.cm $^{-3}$ and 6,938 specimens.g^{-1} for fine-grained sediments (i.e. less than 75% sand sized particles), Loch Sunart sediments appear to yield much richer benthic foraminiferal abundances than other fjordic environments with similar substrates. For example, Hannah & Rogerson, (1997) report abundances of 200-400 specimens.cm $^{-3}$ for muddy sediments and 20-50 specimens.cm $^{-3}$ for sandy sediments from the Clyde Sea, NW Scotland, the equivalent to 340-680 specimens.g^{-1} (by applying a factor of 1.7 as described in their paper). The lower foraminiferal abundances in the Clyde could be due to differences in the amount of silt (though no data is given) in the sediments, since the sampling stations are much shallower (< 46m) than the majority of the Loch Sunart stations. Also, it is not clear whether the Clyde Sea foraminiferal abundance is for live or total data. If reported abundance data represent live specimens only, samples with the highest foraminiferal abundances consists ~ 45 % live specimens (Hannah & Rogerson, 1997), thus Clyde Sea samples would have a total foraminiferal abundance of around 1500 specimens.g^{-1}. Murray *et al.,* (2003) reported low benthic foraminiferal abundances of 5-65 dead specimens.cm $^{-3}$ for the brackish Loch Etive surface sediments, and this is likely due to the stressed environment as suggested by the dominance of the assemblage by agglutinated taxa and the tendency towards dissolution of calcareous test in the organic-rich surface sediments of Loch Etive (*pers. comm.,* WENA, 2005).

The Sandebukta branch of the Oslo fjord shows lower (total) foraminiferal abundances than Loch Sunart, with abundances of 200-800 specimens.g^{-1} for sediments from water depths of ~ 10-50 m (Alve & Nagy, 1986a). Austin & Sejrup, (1994) report total abundances of 2.5-52 specimens.cm^{-3} in the Syslakvåg tributary of the Spjeldnesosen basin (Lurefjord) and 0.3-258 specimens.cm^{-3} from the Fensfjord, near Håvarden. Though the stations from this study were fairly shallow with respect to Loch Sunart (< 40 m water depth), the sediment properties appear similar. Benthic foraminiferal abundances (unstained) to the equivalent of 76 specimens.cm^{-3} (3800 specimens/50 cc) are found in the inner basin of the Fensfjord, increasing to 380 specimens.cm^{-3} for the outer fjord area (Klitgaard-Kristensen & Buhl-Mortensen, 1999). Calcareous benthic foraminiferal abundances (total) from the Sognefjord (NW Norway) appear to be fairly similar to calcareous abundances.cm^{-3} determined for Loch Sunart, with abundances ranging from 4.9-1512 calcareous specimens.cm^{-3}, with ~50 % of samples yielding abundances >100 calcareous specimens.cm^{-3} (Mikalsen *et al.*, 1999). The slightly higher abundances from these deep samples (water depths > 121m) may be explained by the finer grained sediments (90% finer than 63 μm) and high salinity water masses (~ 35) in this environment.

Like many other studies (e.g. Alve & Nagy, 1990; Austin & Sejrup, 1994; Hannah & Rogerson, 1997; Klitgaard-Kristensen & Buhl-Mortensen, 1999), the abundance of benthic foraminifera in Loch Sunart surface sediments is influenced by increases in BWS and silt content (figure 5.2). The inner basin assemblages typically have much lower foraminiferal abundances than the outer or main basin assemblages, however the majority of the maximum foraminiferal abundances (specimens.cm^{-3}) occur in outer basin samples and likely reflect competition in normal marine conditions (Alve & Nagy, 1990). High benthic foraminiferal abundance also occur in samples where the substrates have high percentages of silt, e.g. in the deep basins. Sample 181, with a high BWS (34.11) and high silt proportion (64%) in the outer has the highest abundance (1327 specimens.cm^{-3}), whilst the high abundance of sample 27 (35,873 specimens.g^{-1}) is likely due to the strong influence of marine waters and it's location in an isolated deep in the outer basin (e.g. Murray, 2003a).

Thus, the steady and gradual trend of increasing foraminiferal abundance from the inner fjord to the outer fjord of Fensfjord (Klitgaard-Kristensen & Buhl-Mortensen, 1999) is not seen in Loch Sunart. Since % silt and % organic matter are inextricably linked, it is likely that relationships correlated with silt are also responding to the availability of organic matter in the sediment (Scott *et al.*, 2003). Typically, C/N ratios decrease from a terrigeneous influence in the inner fjord to a more marine organic matter influence in the outer fjord area in the Fensjfjord region (Klitgaard-Kristensen & Buhl-Mortensen, 1999). Though C/N ratios from bulk sediment samples are not available in this study, it is plausible that a similar trend exists in Loch Sunart, with organic matter in the inner basin generally being of low quality (i.e. refractory and derived from terrigeneous inputs from the catchment) whilst main and outer basin organic matter is of higher quality and derived primarily from phytodetritus.

5.4.3 Loch Sunart species diversity with respect to other fjordic environments

Spatial comparisons of benthic foraminiferal abundances and diversities can be influenced by patchiness (Murray, 1973), particularly if there has been a recent reproduction event (e.g. samples 53 and 202) and 'live' foraminiferal abundance or diversity determined for a sample location could be grossly misrepresentative of that area. Additionally, the sampling method can significantly influence benthic foraminiferal abundance or taxa representation since fine sediment and epifaunal specimens are easily lost when sampling using a van Veen grab. The 4 samples obtained using the Craib corer (which captures the sediment-water interface), samples 45, 27, 41 and 22, exhibit relatively high abundances, though this is likely to be due to a recent population explosion rather than a sampling artefact (table 5.3). This study uses the total assemblages, likely representative of 1-2 years, thus patchiness should not significantly influence the results. Also, since it cannot be determined whether foraminiferal specimens were lost during sampling, it will be assumed that foraminiferal taxa and abundances present in sample residues are wholly representative of in-situ sediment at the sampling location.

The low species diversity and high dominance of the Loch Sunart inner basin assemblages (Fisher-α = 6-10, Shannon-Weaver = 1-2.2) is typical of stressed environments (Haynes, 1981 and Murray, 1991a), and the tendency towards hyposaline waters in the inner basin means that the majority of calcifying foraminifera will have difficulty growing or surviving in these waters (e.g. Boltovskoy & Wright, 1976; see section 5.4.1). Murray *et al.,* (2003) report similar Fisher-α diversities of 1.5 – 7 and information function values of 1.23 – 1.85 for agglutinate-dominated assemblages from Loch Etive; a sea loch with an environment tending towards hyposalinity, anoxia and high inputs of organic matter.

Loch Sunart main and outer basin benthic foraminiferal assemblages typically have a higher diversity than the majority of other fjordic (total) assemblages, with around 80% of the 28 samples having Fisher-α values between 10-22 (Shannon-Weaver indices between 2.1 to 3.6). Austin & Sejrup (1994) report Fisher-α values of 2-11 for NW Norwegian fjords, whilst Sandebukta yields diversities of Fisher-α values of 1-9 and information function (or Shannon-Weaver) values ranging from 0.7 – 2.6 (Alve & Nagy, 1990). Murray (2003b) reported Fisher-α values of 12.5 – 13.5 for dead assemblages from the Muck Deep (Hebridean Shelf), which is similar to the majority of diversities in Loch Sunart (figure 5.4). Klitgaard-Kristensen & Buhl-Mortensen (1999) report Shannon-Weaver values of 3-4 from the Fensfjord, suggesting greater species diversity and equitability than for the Loch Sunart samples, which is probably due to a greater influence of 'open' marine (high salinity) water and finer-grained sediments in these deep fjordic sites.

Marine calcareous forms can become more competitive under increasing normal marine conditions (Alve & Nagy, 1990). High species diversities in Loch Sunart typically occur in assemblages with high specimen abundances, thus likely reflecting optimal growing conditions for the benthic foraminifera. However, Klitgaard-Kristensen & Buhl-Mortensen (1999) report no change in species diversity along an offshore – inner fjord transect, despite a propensity for higher foraminiferal abundances in more saline waters. Species diversities in Loch Sunart have strong and significant positive correlations to BWS (even when inner basin samples are removed, table 5.4). Inner basin assemblage diversities are typically low, though samples 110 and 112 which are located near the sill area are likely to have a 'marine' salinity influence. Interestingly, the majority of the outer basin assemblages have similar or lower species diversities than some main basin assemblages. This is likely due to finer sediments in the main basin which are indicative of calmer and more stable depositional environments. Fine grained sediments in Loch Sunart also typically have high % of organic matter (table 6.2) and substrates with high organic contents also tend to have greater species diversity (Murray, 1991).

A rich diversity of benthic foraminifera is likely accompanied by high diversities of other organisms and probably results in a wide selection of food for predators. The rich species diversity of benthic foraminifera in Loch Sunart surface sediments in comparison to other fjordic environments, and also to local shelf areas, such as the inner Hebridean shelf, exemplifies the importance of protecting Loch Sunart as a designated Site of Special Scientific Interest (SSSI).

5.4.4 Planktonic foraminifera

Planktonic foraminifera do not typically inhabit shelf sea regions (Arnold & Parker, 1999) thus juvenile tests found in shelf sea sediments have usually been transported into the environment (Murray, 1991b). This explains the relative absence of planktonic foraminifera in Loch Sunart sediments and evidence of etching and infilling of the small, dead specimens suggests these tests have been transported into the loch. Sample 27 has the highest abundance of planktonic foraminifera, probably due to it's proximity to the open coastal water with the possibility of winter storms transporting planktonic forms into the loch.

5.4.5 Distribution of 'live' benthic foraminifera in Loch Sunart: a possible response to food availability?

Murray (1991b, 2000) suggested 'live' assemblages should be used to determine ecological preferences of benthic foraminiferal species. Though the low numbers of 'live' specimens in Loch Sunart surface sediments (table 5.4) negates a statistical analysis of ecological influences on Loch Sunart benthic foraminiferal population dynamics, samples with relatively high 'live' abundances are typically from water depths > 60 m with a relatively high organic matter content (> 4%; table 5.4), suggesting a possible benthic foraminiferal response to food availability (e.g. Gooday & Rathburn, 1999; Gustafsson & Nordberg, 2001; Heinz *et al.*, 2001).

Food availability or substrate?

However, maximum 'live' abundances typically occur in fine-grained sediments (negative correlation with % sand; table 5.4) particulary in the fine-grained sediment of the deep basins of Loch Sunart. This fine sediment, possibly accompanied by lower bottom water dissolved oxygen concentrations (e.g. Gillibrand *et al.*, 1996), is likely to result in a shallower redox boundary than found in the shallow-water coarse sediments. Thus taxa which normally exhibit a deep infaunal depth habitat (such as *N. turgida*) may migrate to a shallow infaunal life mode for optimal growth conditions (Alve & Bernhard, 1995) as suggested by the conceptual 'TROX' model (Jorissen *et al.*, 1995). Therefore, more foraminiferal specimens and taxa are likely to be included in a 1-2 cm surface sediment benthic foraminifera scrape (chapter 2) from the fine sediments of deep basins rather the coarser sediments of shallower site; increasing the potential for 'live' specimens to be observed. However, fine-grained substrates typically have high organic matter contents (Bordovskiy, 1965) and it's difficult to ascertain whether the 'live' benthic foraminiferal distribution seen in Loch Sunart is reflecting food availability or substrate grain size (table 5.4); indeed it is likely that they reflect both.

Seasonal response to food availability

High abundances of 'live' specimens (24.7 % and 12.2 % respectively) from samples 45 and 27 collected in April, may reflect the benthic foraminiferal response to the spring phytoplankton bloom (Gooday & Rathburn, 1999). Such a response is common in seasonally stratified shelf seas (e.g. Murray, 1983; Murray, 1991b) and locally, in the Clyde Sea, Hannah & Rogerson, (1997) showed maximum abundances of juvenile tests (suggesting a recent reproduction phase, Murray, 1973) occurred around April. A slight increase in Clyde Sea juvenile tests also occurred during the autumn (October-November) phytoplankton bloom and this is typically when the benthic foraminifera in NW Norwegian fjords tend to reproduce (*pers. comm.*, Dr. G. Mikalsen, 2004). Additionally, Scourse *et al.,* (2004) demonstrated that benthic foraminifera in shelf sea environments typically calcify at different periods throughout the year. Thus, low abundances of 'live' specimens in Loch Sunart could reflect the timing of sample collection (June).

5.4.6 Validating the use of the total assemblage in Loch Sunart

The tenuous possibility of a 'seasonal' benthic foraminiferal response to food availability in Loch Sunart may validate the use of total assemblages in this seasonally stratified fjord. Since sampling is infrequent and essentially restricted to one month (June), using solely the 'live' benthic foraminifera assemblage will only give a seasonal 'snapshot' of the ecological influences upon particular benthic foraminiferal species and may not be representative of long-term marine conditions. Conversely, the total assemblage (representing 1-2 years sedimentation) is likely to reflect the prevailing conditions in the loch, which is the primary variable of interest in palaeoenvironmental reconstructions (due to typically sub-decadal resolution of records).

5.4.7 Taphonomic processes - dissolution and transport

A problem of using total assemblages is that post-mortem taphonomic processes are not accounted for, i.e. where a species is found 'live', taphonomic processes occurring after the death of the individuals may result in dissolution or transport of that individual away from the site. Murray & Alve, (1999b) regard taxa which are found dead but not 'live' in the Skagerrak-Kattegat, as 'exotic' and allochthonous to the site, however they stress that comparative studies of 'live' and dead assemblages must be carried out frequently over period of at least 1 year before conclusions regarding the taphonomic processes influencing benthic foraminiferal assemblages can be made. Given the 'snapshot' sampling of Loch Sunart surface sediments and the known seasonal variability of 'live' benthic foraminifera occurrences (e.g. Scourse *et al.*, 2004), marking species out as allochthonous may be misrepresentative of the 'real' distribution of benthic foraminifera.

However, many of the assemblages do show signs of taphonomic processes. There is evidence of reworking in the Loch Sunart surface sediments, for example sample 189 shows a high percentage of broken or etched tests (53 %) along with 3 broken individuals of *Elphidium arctica* and *Elphidium asklundi* which are both arctic species, likely reworked from pre-Holocene sediments. A weak insignificant positive correlation exists between the % of broken tests in a sample and the % of sand >125 μm for samples from the main and outer basin ($r = 0.280$, $p = 0.206$). Using figure 4 in Murray (1984), the proportion of broken tests in these sediments point to a winnowed lag deposit which is typical of areas experiencing modest current activity on continental shelves or channels in lagoons or estuaries, and the general lack of small benthic foraminifera observed in these assemblages (e.g. sample 193) supports this hypothesis.

Calcareous taxa in the inner basin of Loch Sunart are likely to live in a stressful environment due to the high organic matter contents of sediments and low salinities (Boltovskoy & Wright, 1976), and this is exemplified by the low proportion of hyaline specimens in the 'typical' inner basin assemblages (figure 5.3). Where calcareous taxa are found, live specimens often make up > 50 % of a hyaline species' total abundance (table 5.5), pointing to a propensity for the post-mortem dissolution of calcareous tests.

The pH of marine waters is usually ~ 8, however high amounts of decomposing organic material can significantly lower the pH of restricted basins. The dissolution of calcareous tests usually occurs at pH values of < 7.8 (Boltovskoy & Wright, 1976). Murray (1968 *cf.* Boltovskoy & Wright, 1976) reported that hyaline tests tend to become opaque fairly rapidly at pH values of ~7 and specimens of *A. beccarii* found in Loch Sunart's inner basin usually have opaque white tests suggesting clear signs of etching and dissolution or low availability of calcium carbonate (review in Murray & Alve, 1999a).

Hyaline species which host symbiotic algae (or sequester chloroplasts), such as *A. beccarii* and *N. turgida,* are thought to be able to tolerate more stressful environments, and counteract the effects of low pH (Alve & Nagy, 1990) and this may explain the ability of these species to live in such stressful conditions. Despite this, calcareous taxa living in the inner basin of Loch Sunart appear to experience a stressful environment, likely spending energy recalcifying their tests, which upon death probably undergo dissolution.

5.4.8 Distribution of benthic foraminifera in Loch Sunart

Loch Sunart differs from the fjords of Scandinavia in that both the sills and basins are generally much shallower, creating grain size distributions governed by current activity rather than depth (e.g. figure 2.5). For example, sediment from sample 192, obtained from a water depth of 90 m, contains 64 % sand, whilst sample 181 from 36 m, contains only 29 % sand. Additionally, basin water exchange is typically more restricted in Scottish fjords, and less likely to be influenced by 'open' coastal waters, thus salinities may be lower.

Multivariate statistical analyses identified 4 major benthic foraminiferal assemblages for Loch Sunart. Prior to the discussion of the environmental significance of these assemblages, it is important to understand each taxon of significant abundance or interest and this will be discussed using the following criteria: distribution of benthic foraminiferal species (abundances > 2%) plotted against longitude in order to identify possible distributions influenced by BWS and quality of organic matter (figure 5.5); species abundances > 2 % with depth, with the inner basin and main/outer basin treated separately (figure 5.6); a single depth transect taken across the main basin to eliminate the influence of the spatial variations on environmental parameters (figure 5.7); and the correlation of environmental parameters and grouped taxa using factor analysis (figure 5.9).

5.4.8.1 Taxonomic notes on benthic foraminiferal species common in Loch Sunart

Life modes for the following benthic foraminiferal species have largely been taken from Murray (1991), and have been found living in Loch Sunart, unless stated otherwise.

PORCELANEOUS TAXA

Abundance of porcelaneous taxa in Loch Sunart is typically low (section 5.4.1). However, the positive relationship between BWS (figure 5.5 and 5.9) and the abundance of porcelaneous taxa suggests increasing proportions of this wall type may be used an as indicator for the increasing influence of higher salinity coastal waters (e.g. Christiansen *et al.*, 1996). ***Quinqueloculina seminulum*** is the most common and abundant species (< 3.3 %): other common species include ***Milionella***

subrotunda, Spiroloculina rotunda, Quinqueloculina stalkeri, Quinqueloculina bicornis **and** ***Triloculina trihedra*.**

AGGLUTINATED TAXA

A. glomeratum is an epifaunal species which appears throughout Loch Sunart with abundances of less than 5.5%. Thiede *et al.,* (1981) suggested the distribution of this taxon is restricted by salinity, i.e. it is stenohaline, which may explain the low abundances (< 0.6 %) in the inner basin assemblages. Factor analysis suggests that this taxon is strongly correlated to the % of silt and organic matter in the substrate (figure 5.9) which agrees well with the findings of Alve & Nagy (1986a). As with the Celtic Sea assemblages (Scott *et al.*, 2003), *A. glomeratum* is negatively correlated with BWT and this species appears to have a preference for low temperatures (Murray, 1991).

In this study, ***Ammoscalaria runiana*** has been grouped with *A. pseudospiralis* since broken specimens have resulted in difficulties identifying between the two. *A. runiana* appears throughout the Loch Sunart samples, with maximum abundances (>10 %) occurring in the inner basin. Factor analysis shows this species is inversely correlated to BWS and commonly occurs with *E. scabra* and *R. subfusiformis* (figure 6.10). Thiede *et al.,* (1981) reported occurrences of living specimens in the shallow waters (3-20 m) of the Oslofjord, whilst dead individuals were found down to 200 m, however *A. runiana* has been found 'live' at the deepest parts of Loch Sunart, both within and outwith the inner basin. Murray (2003a) found *A. pseudospiralis* alive at depths of 218 m in the Muck Deep and suggests this species may be infaunal (Murray, 1991).

Eggerelloides scaber is an infaunal species; known to be tolerant of a wide range of environmental variables, and found living in water masses with salinities > 20, temperatures between 1-20 °C, low oxygen levels, pollutions sources and substrates ranging from mud to sandy mud (e.g. Conradsen, 1993 and references within). Hence, it is often found in most fjordic environments (e.g. Höglund, 1947; Alve & Nagy, 1986a; Murray *et al.*, 2003). Few live or dead *E. scaber* are found on the Hebridean shelf (Murray, 2003b; Murray, 2003a) or the Celtic Sea (Scott *et al.*, 2003). However, high abundances of *E. scaber* are found in Loch Sunart surface sediments, particularly in the inner basin, where *E. scaber* dominates the assemblages. This is likely due to the high tolerance of this species, which along with the organic cement of the test, means it can live in low salinity/low oxygen environments (e.g. Haynes, 1981). Thiede *et al.,* (1981) reported maximum abundances of *E. scaber* between 10-20 m, with no specimens observed below 60 m. However, specimens of *E. scaber* were found living in all water depths of Loch Sunart (maximum 113 m) and Murray *et al.,* (2003) found *E. scaber* living at depths greater than 50 m in Loch Etive. The low abundance of *E. scaber* in the restricted deep basins of Lurefjorden and Masfjorden is likely due to the water depth of the samples (> 300 m; Klitgaard-Kristensen & Buhl-Mortensen, 1999) rather than location, since Austin & Sejrup (1994) report abundant *E. scaber* in shallower samples. Scott *et al.,* (2003) report a strong correlation between *E. scabra* and % sand, however only a weak correlation is seen in Loch Sunart (figure 5.9) and many other studies report no substrate preference (e.g. Conradsen, 1993; Murray, 1991b). Murray (2003a) suggested an affinity between organic carbon content and *E. medius* (a close relation to *E. scaber*) and high % organic matter are normally found in fine sediments, whilst *E. scaber* typically exhibits a positive correlation with organic content in Skagerrak sediments (Conradsen, 1993; Conradsen *et al.*, 1994). In Loch Sunart, *E. scaber* has the strongest correlation with longitude, which likely reflects the variation in BWS, as well as oxygen levels and organic content and quality (figure 5.9).

Heron-Allen & Earland (1916) reported ***Psammosphaera bowmanni*** occurring in NW Scottish sites, and Höglund (1947) reported occurrences of this species in the shallow waters (< 40m) of the Gullmar Fjord. *Psammosphaera bowmanni* was found living in rare abundances (1 individual per sample) in Loch Sunart mainly at depths > 72 m, in substrates with sand contents varying between 28-71 %. This species is extremely fragile (Höglund, 1947) and as with many agglutinated species, the drying and sieving process may have broken other *P. bowmanni* prior to identification. However, given that most of the specimens found in Loch Sunart are live, and hence represent the total assemblage of *P. bowmanni*, we may interpret it's presence as an indicator of fairly low energy environments. This is also true for other fragile taxa such as *Rheophax scotti* and *Textularia earlandi.* The fragility of these taxa tests limit their use in palaeostudies due to the likely possibility of destructive post-mortem taphonomic processes.

Recurvoides trochamminiforme is present in low abundances (<3.2 %) throughout Loch Sunart and the fjords of NW Norway (Austin & Sejrup, 1994; Klitgaard-Kristensen & Buhl-Mortensen, 1999), though it is common in Sandebukta, particularly within the *Verneuilina media* assemblage which occurs in deep waters under 'normal' marine conditions (Alve & Nagy, 1986a) and also in the Gullmar fjord (Höglund, 1947). It has recently been found living on the Hebridean Shelf (Murray, 2003b), and Murray & Alve (2000) report common occurrences at water depths >80 m where seasonal stratification occurs. In Loch Sunart, maximum abundances of *R. trochamminiforme* occur in the deep waters of the main basin and is closely associated with *A. glomeratum* and % organic matter (figure 5.9). The negative correlation of *R. trochamminiforme* with 'high energy' taxa such as *C. lobatulus* (figure 5.9) suggests a preference for calm depositional environments. Where live specimens are recorded in Loch Sunart, they typically make up at least 71 % of the total species abundance pointing to post-mortem taphonomic processes.

Maximum abundances of the infaunal species ***Rheophax subfusiformis*** typically occur in Loch Sunart water depths shallower than ~ 60 m (though it is present at 121 m), where the % organic matter is low and the substrate is fairly sandy (>60 % sand). Höglund (1947) finds this species in abundance in the Gullmar Fjord, whilst Heron-Allen & Earland (1916) record rare occurrences in their Loch Sunart stations. Though *R. subfusiformis* is reported to prefer normal salinities and sandy/muddy sand substrates in Loch Etive (Murray *et al.*, 2003), *R. subfusiformis* in Loch Sunart correlates with *E. scaber* and longitude, which is related to BWS (figure 5.9). This correlation with longitude may reflect the high tolerance of *R. subfusiformis* to environmental stress and the ability of this species, with it's simple wall structure, to survive and grow in hyposaline waters.

Spiroplectaminna wrightii is a common epifaunal species on the Hebridean shelf (e.g. Heron-Allen & Earland, 1930; Murray, 2003b; Murray, 2003a) and Heron-Allen & Earland, 1930 reported it as 'very common' at their Loch Sunart stations. In this study, *S. wrightii* has been grouped together with *Textularia bocki*, based on the advice of Professor Knudsen (*pers. comm.,* 2001) and Scott *et al.,* (2003) show the distributions of these two taxa to be very similar in the Celtic Sea. *S. wrightii* is found throughout the main and outer basins of Loch Sunart, and is strongly associated with 'high energy' taxa such as *C. lobatulus* and *R. praegeri*. This agrees well with other studies showing this epifaunal/epiphytic taxon has an affinity with coarse grained sediments (e.g. Murray, 1991; Conradsen, 1993; Klitgaard-Kristensen & Buhl-Mortensen, 1999; Scott *et al.*, 2003). The low abundances of *S. wrightii* in inner basin assemblages may be due to low carbonate availability and difficulties in test formation, since this agglutinated species has a calcium carbonate cement (Haynes, 1981), and likely explains it's positive correlation with BWS (figure 5.9). The often low abundance of *S. wrightii* in other fjords (e.g. Höglund, 1947; Austin & Sejrup, 1994; Klitgaard-Kristensen & Buhl-Mortensen, 1999) may be due to the fine-grained sediments which are typically found in these deep silled fjords.

HYALINE TAXA

Asterigerinata mamilla is an epifaunal, inner shelf species, and in Loch Sunart, is found (dead) to be most abundant at shallow water depths (<30 m) with sandy substrates. This substrate preference, along with it's association with *C. lobatulus* and *R. praegeri* (figure 5.9) suggests this species thrives in higher energy environments (Murray, 1979). This preference for high energy environments is supported by the correlation of dead Celtic Sea *A. mamilla* with sediments which are skewed towards coarse sediment and have a high % of gravel (Scott *et al.*, 2003).

Ammonia beccarii is an infaunal species with a cosmopolitan distribution and is known to tolerate a wide range of temperatures (0-30 °C) and salinities (e.g. Murray, 1991b), as exemplified by it's abundance in the inner basin assemblages of Loch Sunart (e.g. figure 5.5). Difficulties in identifying variants of *Ammonia* in Loch Sunart (e.g. Hayward *et al.*, 2004) lead to all *Ammonia* specimens being grouped as *A. beccarii* (*pers. comm.*, Dr. P. Kristensen, 2001). *A. beccarii* is common and abundant throughout the surface sediments of Loch Sunart (table 5.6), particularly those with a high % of sand, and it's close association with taxa such as *C. lobatulus* and *A. mamilla* (figure 5.9) suggests a propensity towards higher energy environments. This agrees well with other studies which also link *A. beccarii* with shallow water depths (e.g. Austin & Sejrup, 1994; Scott *et al.*, 2003). An *A. beccarii* depth trend is not seen in Loch Sunart (figure 5.6), probably due to high current activities often propagating to deep water (section 2.13) , though the preference of *A. beccarii* for high energy environments may explain the rare abundances in the deep (frequently > 350m) NW

Norwegian fjords (Mikalsen *et al.*, 1999 and Klitgaard-Kristensen & Buhl-Mortensen, 1999). The abundance of *A. beccarii* closely follows summer BWT (figures 5.5. and 5.9) and optimum temperatures for growth and reproduction of *A. beccarii* fall between 15-20 °C (Boltovskoy & Wright, 1976). This may explain the maximum abundances of *A. beccarii* in the outer basin of Loch Sunart or in shallower areas, where temperatures are typically warmer (table 5.3). Murray (2003b) recently extended the northern limit of the warmer water *A. beccarii* variant *Ammonia falsobeccarii*; a variant identified in the Loch Sunart assemblages and which may explain the higher abundances of *A. beccarii* at higher BWT.

Maximum abundances of ***Bolivina*** species (mainly ***B. pseudopuntata, B. pseudoplicata*** and ***B. spathula***) typically occur at deep sites in Loch Sunart, which have fine grained sediments, fairly high organic matter and high species diversity and equitability (figure 5.9). Though Haynes (1981) suggests *Bolivina* can tolerate oxygen levels as low as 0.1 ml/l, species of *Bolivina* are commonly associated with well oxygenated water masses of normal shelf salinity (e.g. Thiede *et al.*, 1981; Klitgaard-Kristensen & Buhl-Mortensen, 1999), and Alve & Nagy (1990) find high abundances of *B. skagerrakensis* in the deep, stable and high salinity waters of the Oslofjord. The *Bolivina* group occurs with *S. fusiformis*, *B. marginata* and *N. turgida* in Loch Sunart (figure 5.9), and given the affinity of these taxa for stratified waters (e.g. Scott *et al.*, 2003) suggests the presence of these taxa reflect stratified water masses overlying a calm depositional environment.

Bulimina marginata is present throughout Loch Sunart (table 5.2) though as with all calcareous taxa, minimum abundances occur in the inner basin samples. *B. marginata* is thought to be an infaunal species (Murray, 1991), though Mackensen *et al.,* (2000) suggests *Bulimina spp.* may migrate in the sediment to seek optimal growth and survival conditions. *B. marginata* becomes more abundant across the main basin depth transect (figure 5.7), agreeing with Thiede *et al.,* (1981) who reported high abundances of *B. marginata* between 20-100 m in the Oslo fjord. *B. marginata* typically exhibits a preference for fairly high BWS between 33-35 and BWT around 10-14 °C (Thiede *et al.*, 1981) and maximum abundances typically occur in Norwegian fjordic sites with stable, high salinity water masses (Austin & Sejrup, 1994) or in the intermediate layer, where the seasonal surface layer and deep stable water masses meet (Alve & Nagy, 1990). Maximum abundances of *B. marginata* occur in the main basin in sediments with a low sand content and high organic matter (figure 5.9). A similar association between *B. marginata* abundance and % organic matter has been reported for Hebridean shelf sites (Murray, 2003a) and the Skagerrak (Conradsen, 1993) and Klitgaard-Kristensen & Buhl-Mortensen (1999) suggest *B. marginata* may thrive in fjordic environments rather than offshore sites due to differences in the refractory carbon source, i.e. the ability to use low quality (high C:N ratio) food. However, some studies report no correlation between *B. marginata* and total organic carbon (Mikalsen *et al.*, 1999; Klitgaard-Kristensen *et al.*, 2002). Mikalsen *et al.,* (1999) found higher abundances of *B. marginata* in the deeper parts of the fjords and suggested *B. marginata* thrives under stratified water masses which may have low oxygen concentrations, and both Klitgaard-Kristensen *et al.,* (2002) and Scott *et al.,* (2003) linked high abundances of *B. marginata* with areas of stratification. The occurrence of *B. marginata* with other 'stratification' indicators such as *S. fusiformis* and *N. turgida* suggest this may also be in the case in Loch Sunart (figure 5.9). Though Höglund (1947) reports *B. marginata* in similar abundances as *S. fusiformis* in the Gullmar Fjord and though *B. marginata* is closely associated with *S. fusiformis* (figure 5.9), *B. marginata* is much more abundant than *S. fusiformis* in Loch Sunart (e.g. figure 5.5).

Cibicides lobatulus is an epifaunal species with a preference for sandy sediments and high energy environments (Murray, 1991). *C. reflugens* (a close relative to *C. lobatulus*) is very rare in Sandebukta (Alve & Nagy, 1986a) and low abundances of *C. lobatulus* in the Sognefjord may be due to the fine grained substrate with dead specimens suggesting reworking (Mikalsen *et al.*, 1999), whilst Klitgaard-Kristensen & Buhl-Mortensen (1999) attribute the poor-sorting of sediments for the high abundance of *C. lobatulus* in the Fensfjord/Lurefjord. Though few live specimens (table 5.5) are found in Loch Sunart, abundances are typically high (>20%), particularly in areas where % sand is high and grain sizes are skewed towards coarser sediments, suggesting an environment with high current activity, for example, at the sill regions (sample 110; figure 5.5) or in shallower waters of the outer basin. Conradsen *et al.,* (1994) suggest the patchy distribution of *C. lobatulus* is a response to localised conditions and substrate, and this is certainly true in Loch Sunart. Scott *et al.,* (2003) suggest *C. lobatulus* in the Celtic Sea is an indicator of a well mixed water column (i.e. not stratified), which corroborates the ecological preference of the taxa for fully oxygenated, high energy conditions and accompanying coarse substrates as found in other studies (e.g. Austin & Sejrup, 1994; Conradsen, 1993; Klitgaard-Kristensen *et al.*, 2002). Additionally, Klitgaard-Kristensen *et al.,* (2002) identify a Scottish coastal current assemblage characterised by *C. lobatulus* and *Rosalina* spp. and dead *C. lobatulus* are common on the Hebridean shelf (Murray, 2003b), thus the high abundances of *C. lobatulus* in the outer basin samples may reflect transport of *C. lobatulus* from the shelf and into the loch.

Elphidium excavatum is an infaunal inner shelf species (Murray, 1971) known to be extremely tolerant to low salinities and a variable environment. It is found in extremely low abundances (dead) in Muck Deep (Murray, 2003b) and the deep waters of west Norwegian fjords (Mikalsen *et al.*, 1999) and found both live and dead in Loch Etive (Murray *et al.*, 2003). In Loch Sunart, *E. excavatum* is strongly correlated with depth (figure 5.9), with maximum abundances typically occurring between 30-70 m water depth (figure 5.6). Austin & Sejrup (1994) found maximum occurrences of *E. excavatum* at 15m depth, whilst Conradsen (1993) reports *E. excavatum* assemblages are likely to reflect variable halocline conditions in the Skagerrak.

Elphdium williamsoni is the dominant species at 5 m water depth at the head of Loch Sunart. The high proportion of sand at this site (97 %) reflects the extremely high energy of this environment, which lies close to the inter-tidal range (2-4m) and also within the brackish surface layer where BWS can be < 30. Alve & Nagy (1990) also show *E. willamsoni* to be most frequent at depths of 1-5 m, and suggest that the symbiotic algae frequently hosted by species of *Elphidium* likely supply oxygen to the foraminifera and counteracts the low pH found in these hyposaline waters. Loch Sunart *E. williamsoni* showed a propensity for green colouration, suggesting symbiosis with algae.

The epifaunal ***Hyalinea balthica*** are found dead in low abundances (<2.6 %) in Loch Sunart; particularly in the deep basins which have fine-grained, organic-rich sediments and a propensity for high species diversity and equitability (figure 5.9). High abundances of *H. balthica* are common in NW Norwegian fjords and have been linked to a preference for low dissolved oxygen levels (Mikalsen *et al.*, 1999) or high levels of the low quality (i.e. refractory) organic carbon usually found in fjordic sediments (Klitgaard-Kristensen & Buhl-Mortensen, 1999). Loch Sunart *H. balthica* also shows a negative correlation with BWT; a trend also seen in the Celtic Sea where it is attributed to stratification processes (Scott *et al.*, 2003).

Nonionella turgida is typically a deep infaunal taxon which occurs live and dead in most Loch Sunart samples and Heron-Allen & Earland, (1916) found *N. turgida* to be common at both of their Loch Sunart stations. *N. turgida* were found living in the Sognefjord (Mikalsen *et al.*, 1999), however it is usually absent or rare in Norwegian fjords (e.g. Austin & Sejrup, 1994; Klitgaard-Kristensen & Buhl-Mortensen, 1999) and instead *N. labradoricum* (a close relation with an Arctic affinity) is the more common species, preferring cool (< 7°C) stable water masses with high BWS (e.g. Alve & Nagy, 1986a). The affinity of this species for fine-grained, organic rich sediments has been recorded in the Celtic Sea (Scott *et al.*, 2003), the Kattegat-Skagerrak (Conradsen, 1993; Conradsen *et al.*, 1994) and the Hebridean shelf (Murray, 2003b; Murray, 2003a) and maximum abundances of *N. turgida* typically occur in the deep waters of the Loch Sunart main basin (figures 5.5) which typically have fine grained, organic rich sediments (figure 5.9). *N. turgida* in Loch Sunart appears in assemblages containing *B. marginata*, *S. fusiformis* and *Epistominella*; taxa with known preferences for higher salinity, stable deep water masses with a typically high organic matter input associated with areas of stratification.

Rosalina praegeri in Loch Sunart shows a strong association with *C. lobatulus*, *A. beccarii*, *A. mamilla* and *S. wrightii* (figure 5.9) suggesting a preference for fairly high energy environments. *R. praegeri* is common in relatively low abundances in Loch Sunart (table 5.2) and low numbers of live specimens are found in samples from the inner basin sill and outer basin regions (table 5.5), and interestingly, on a scallop shell attached to the inner basin mooring at 40 m water depth, suggesting the propensity for juveniles of this species to be transported up into the water column (e.g. Alve, 1999). Abundances of dead *R. praegeri* (none are found live) are common at Hebridean shelf sites (Murray, 2003b; Murray, 2003a) and both live and dead *R. praegeri* are reported in the Celtic Sea (Scott *et al.*, 2003) and in the Skagerrak (Conradsen, 1993). Low abundances of *R. praegeri* in other fjord environments (e.g. Austin & Sejrup, 1994;

Klitgaard-Kristensen & Buhl-Mortensen, 1999) are probably due to the fine-grained sediments.

The infaunal species, ***Stainforthia fusiformis*** is known to be an opportunistic species and Alve (2003) provides an excellent review of this species. *S. fusiformis* is common in fjordic environments (e.g. Höglund, 1947; Alve & Nagy, 1990; Austin & Sejrup, 1994; Klitgaard-Kristensen & Buhl-Mortensen, 1999; Mikalsen *et al.*, 1999; Gustafsson & Nordberg, 2000; Nordberg *et al.*, 2000; Gustafsson & Nordberg, 2001; Alve, 2003; Filipsson *et al.*, 2004) as well as some NW European shelf seas (e.g. Conradsen *et al.*, 1994; Murray, 2003b; Murray, 2003a; Scott *et al.*, 2003). The rare occurrence of *S. fusiformis* in Loch Etive (Murray *et al.*, 2003) is likely due to the brackish nature of the water column, as with the Baltic Sea (Alve, 2003). In Loch Sunart, maximum abundances of *S. fusiformis* occur in the deeps of the main and outer basins (figures 5.5 and 5.6) indicating a preference for substrates with a high % silt and % organic matter (figure 5.9). This agrees well with other studies which suggest *S. fusiformis* typically shows a clear response to food availability (e.g. Alve & Murray, 1997; Gustafsson & Nordberg, 2000, 2001), particularly at stratification fronts (Scott *et al.*, 2003). However, many authors suggest *S. fusiformis* has a preference for sediments with a high proportion of fine sands (e.g. Conradsen, 1993, Klitgaard-Kristensen *et al.*, 2002 and Alve, 2003), and Scott *et al.*,, 2003 suggested locations where *S. fusiformis* is correlated with fine-grained sediments more likely reflects an affinity to the organic matter in the sediments, since fine-grained sediments tend to yield high organic matter contents. In Loch Sunart, *S. fusiformis* is closely associated with *B. marginata*, *N. turgida* and *A. glomeratum* (figure 5.9); all taxa associated with stable conditions and high organic inputs likely to arise from long-periods of water column stratification.

This study has grouped the ***Cassidulina*** species together, though different species have different ecologies. In Loch Sunart, ***C. laevigata*** are typically found in the fairly coarse sediments of the outer basin, suggesting a preference for high BWS, high oxygen levels and a relatively energertic environment, which agrees well with other studies (e.g. Klitgaard-Kristensen & Buhl-Mortensen, 1999; Mikalsen *et al.*, 1999; Klitgaard-Kristensen *et al.*, 2002; Murray, 2003a). Associations of ***C. obtusa*** are common in high salinity, probably well oxygenated bottom waters (Murray, 1991;

Mikalsen *et al.,*, 1999) and *C. obtusa* in Loch Sunart is most abundant in the main basin deeps, and is closely correlated with % silt and *Epistominella* and *Bolivina* species (figure 5.9). A single live individual of the typically small *C. obtusa* species was found in Loch Sunart (sample 173) and low abundances of live *C. obtusa* is common in Sognefjorden (Mikalsen *et al.*, 1999) whilst significant live abundances reported for Hebridean shelf sediments, may be due to the fine mesh used in the study (63 μm; Murray, 2003a).

This brings us to low abundances of dead ***Cassidulina reniforme*** in the deep basins of Loch Sunart. Specimens are typically small and it is possible that some individuals have been misidentified, since *C. reniforme* classically has an Arctic affinity. Austin & Sejrup (1994) question whether *C. reniforme* in the fjords of W Norway is due to 'modern occurrence' or re-working of pre-Holocene sediments. The presence of 4 individuals of the Arctic species *Elphidium arctica* and *Elphdium asklundi* in sample 189, demonstrates that Loch Sunart sediments can be significantly reworked, and small *C. reniforme* could be transported into the main basin, though equally, the presence of dead *C. reniforme* in the deep, cool bottom water of the main basin could also be a 'real' occurrence (e.g. Austin & Sejrup, 1994). Additionally, 3 individuals of another Arctic species, *Bolivina albatrossi*, occur dead and well preserved in sample 90. This good preservation along with the relatively fine grain size of the sediment (table 5.3) suggests a possibility that the *B. albatrossi* are *in situ*. Given the paucity of 'live' benthic foraminiferal recordings in Loch Sunart (table 5.5), the fact that *C. reniforme* has not been found live in Loch Sunart does not preclude the fact that they could live there, i.e. absence of evidence is not evidence of absence. Loch Sunart's main basin water is strongly stratified in summer (chapter 3) with BWTs typically around 10-11 °C (chapter 3) in June; probably becoming warmer towards late autumn (Ellett, 1979) when winter mixing of the water column occurs. Craig (1958) suggests 'pockets' of cold bottom water (< 8 °C) can be isolated in the main basin of Loch Sunart during the seasonal summer warming, only losing their identity with winter mixing (a hypothesis also supported by Ellett & Edwards, 1983). This highlights the variability in inter-annual bottom water temperatures and points to the possibility that Loch Sunart main basin BWT may reach a temperature where arctic benthic foraminiferal can sustain growth and possibly, reproduction. If this is the case, then this will be the first recording of *C. reniforme* in Loch Sunart, and will extend its southern distribution.

5.4.9 Loch Sunart benthic foraminiferal assemblages: environmental information

Multivariate statistical analyses on benthic foraminifera identified 4 major assemblages in Loch Sunart (section 5.3.5; figures 5.9 and 5.10).

5.4.9.1 E. scaber assemblage: Inner basins

E. scaber dominates the inner basin assemblages of Loch Sunart (abundances typically > 51 %, figure 5.10) where basin water BWS is variable (due to DWREs) and often brackish (≤ 33), whilst the seasonal change in BWT is large (summer BWT between 11.9-12.8 °C; winter BWT ~ 7 °C; chapter 3). Organic matter content in the substrate can be variable (7.2 ± 5.5 %), as can the grain size composition of the sediment (1.8 ± 1.1 % clay; 40.6 ± 23 % silt; 57.6 ± 24 % sand).

The domination of the assemblage by a single taxon and subsequent low species diversity and equitability, along with significant proportions of agglutinated taxa with simple wall structures such as *A. runiana* (> 3%) and *R. subfusiformis* (1-5%), suggest a depositional environment experiencing variable and likely environmentally stressed conditions. Hyaline taxa, porcelaneous taxa and aggluintated taxa with a calcareous cement, are present in low abundances, probably due to the low availability of $CaCO_3$ or the low pH of this hyposaline environment, resulting in post-mortem dissolution (Murray & Alve, 1999c; Murray & Alve, 1999a).

Benthic foraminifera species in this assemblage all show high tolerance of fluctuations in their environment (e.g. *A. beccarii* is the dominant hyaline taxon), which is important given the frequent occurrence of deep water renewals in the inner basin (Gillibrand *et al.*, 1995), which greatly alters basin water salinity. Low abundances of *C. lobatulus* along with the presence of *B. marginata*, *N. turgida* and *S. fusiformis* suggests a low-energy environment with a propensity for low dissolved oxygen levels and high organic matter of low quality (i.e. refractory).

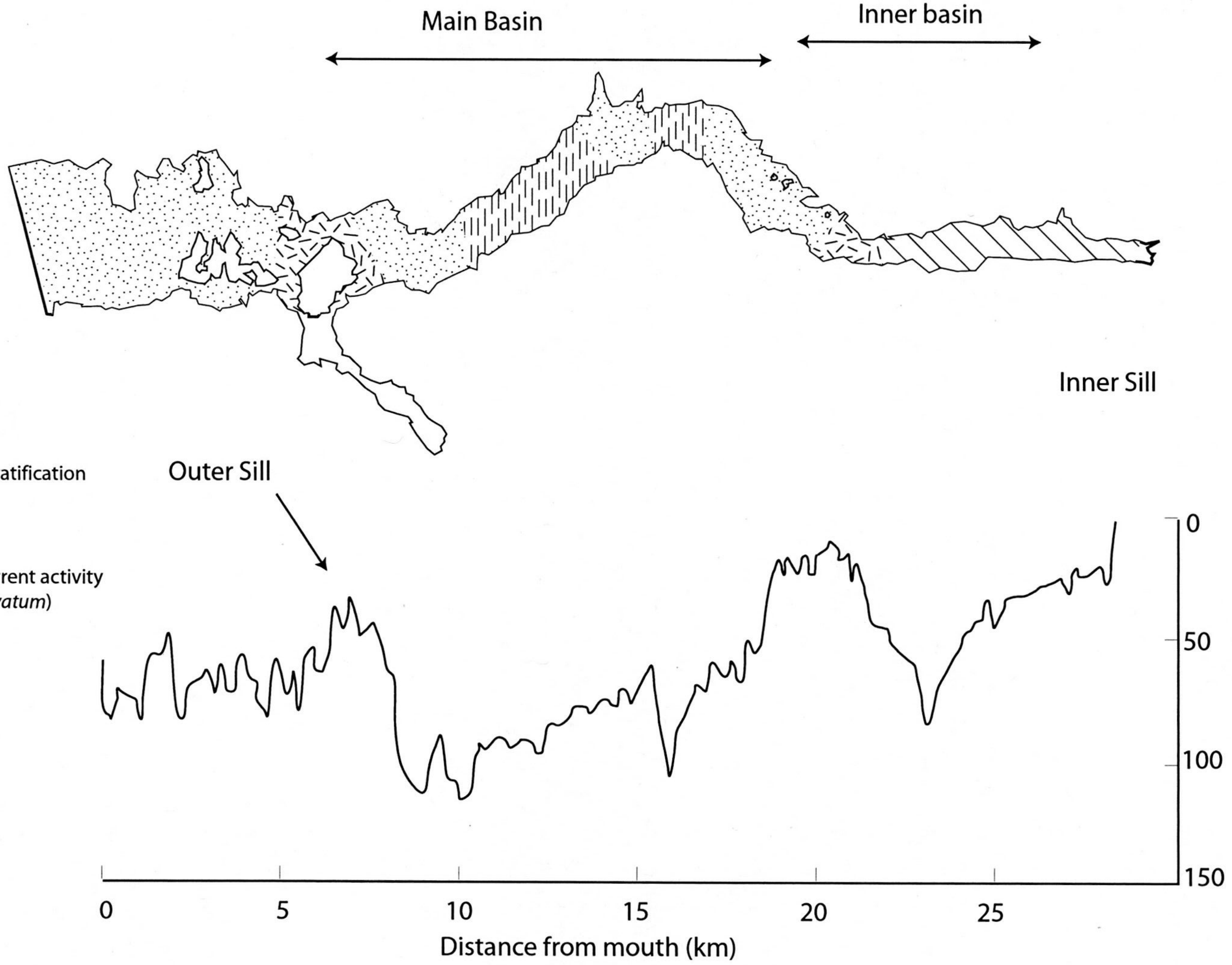

Figure 5.10 Distribution of the benthic foraminiferal assemblages identified in Loch Sunart by multivariate analyses;

▨ Inner basin - restricted exchange with coastal waters (*E. scaber*)

▨ High current activity (*C. lobatulus - A. mamilla – A. beccarii*)

▥ Calm depositional environment - possible stratification (*B. marginata – N.turgida – S. fusiformis*)

░ Main/outer basin - mild /episodic coastal current activity (*A. beccarii – C. lobatulus – S. wrightii – E. excavatum*)

Thus, sample locations within Loch Sunart exhibiting an assemblage similar to the *E. scaber* assemblage are likely to be regions of varying BWS with a propensity towards brackish salinities (<33) or locations of high 'low-quality' organic matter contents which are likely to create a 'stressful environment' for most taxa, particularly hyaline taxa. Though the applicability of agglutinated dominated assemblages in palaeoenvironmental reconstructions is generally thought to be limited due to problematic preservation at 'open' marine sites, agglutinated taxa may provide important palaeoecological information (Alve & Murray, 1995; Murray & Alve, 1999c, 2000), particularly in locations of carbonate dissolution.

5.4.9.2 C. lobatulus - A. mamilla – A. beccarii assemblage: High current activity

Samples within this assemblage group are characterized by large abundances of 'high energy' taxa such as *C. lobatulus*, *A. mamilla, E. macellum* and *A. beccarii* and low abundances of taxa with an affinity for calm, stable environments (e.g. *N. turgida* and *S. fusiformis*; figure 5.9).

Since this assemblage group is observed in all basins, at a range of water depths, it is unlikely that BWT or BWS are major controls on the assemblage. All samples (except 210) have low organic matter content (4.2 ± 3.4 %) which may be due to the typically coarse grain size of the sediments (% clay< 2.7%; 37.3 ± 30 % silt; 60 ± 30 % sand) since organic matter is typically contained in fine sediment.

This coarse grain size composition, together with high proportions of broken or etched tests, point to a very energetic environment with high current activity. The shallow water depth (17 m) of samples 184 and 199 explains the 'high energy' assemblage for these samples. However, samples 110, 112 and 210 are from water depths between 45 – 70 m, i.e. well below the depth at which wind or current mixing is likely to influence the sediments. The geographic location of these samples at sill areas (figure 5.1) suggest that these assemblages found at water depths deeper than ~ 25 m are likely to reflect very high current activity, possibly due to DWREs. Thus, changes in the abundance of the 'high energy' taxa (such as *C. lobatulus*) may reflect varying current activity at a site.

5.4.9.3 *B. marginata – N.turgida – S. fusiformis*: Calm depositional environment

This assemblage group is predominantly located within main and outer basin 'deeps' (> 36 m; figure 5.1) which typically have fine grained substrates (5.1 ± 2.3 % clay; 62.5 ± 13.9 % silt and 32.3 ± 16 % sand), rich in organic matter (10.7 ± 2.5 %). Typical summer BWS recorded for these deep basin locations range from 33.5 to 33.8 and 34.1 for the outer basin sample, 27. Summer BWTs are typically cooler (~11.8 °C) in the main basin than the inner or outer basin (≥ 12.1°C), probably due to a combination of water depth and seasonal stratification which likely inhibits the mixing down of warmer surface waters (chapter 3). High species diversity (Fisher-α = 11.6-22.6; Shannon-Weaver > 2.3) and foraminiferal abundance of assemblages contained in this group likely reflect calm depositional environment and greater competition in the higher salinity waters (Alve & Nagy, 1990).

This assemblage group is characterised by high proportions of taxa with affinities for high, stable BWS and fine grained, organic rich sediment, e.g. *B. marginata, N. turgida, S. fusiformis, A. glomeratum, E. scaber* and *Bolivina* species (see section 5.4.8.1 and figure 5.9). Low proportions of 'high energy; taxa such as *C. lobatulus* (< 8 %) along with the presence of 'delicate' agglutinated taxa, such as *A. glomeratum* and *A. runiana* point to a relatively calm depositional environment. Similar associations of benthic foraminiferal taxa are found under stratified settings (section 5.8.4.1 and e.g. Mikalsen *et al.*, 1999; Scott *et al.*, 2003).

Therefore, Loch Sunart fossil assemblages showing similarities to this assemblage are likely to reflect calm depositional environments with little current activity. This assemblage is also likely to represent sites underlying a stratified water column, probably accompanied by a high organic matter flux and stable deep basin bottom waters which are typically cool and more saline than the intermediate fjordic layer.

5.4.9.4 *A. beccarii – C. lobatulus – S. wrightii – E.excavatum*: Main/outer basin

Samples contributing to this assemblage group are from a range of water depths (23 – 121 m) in the main and outer basin of Loch Sunart (figure 5.1). Typical hydrography recorded at the time of sampling suggests these sites are well ventilated and likely to experience the influence of coastal waters, e.g. BWT of 11.6 – 12.5 °C and BWS of 33.6 – 34.2.

The presence of taxa such as *B. marginata*, *S. fusiformis* and *N. turgida* (albeit in low abundances) which typically reflect stratified water masses and calm depositional environments, alongside significant abundances of taxa with a known affinity for fairly energetic environments (e.g. *A. beccarii*, *C. lobatulus* and *S. wrightii*; section 5.4.8.1), suggests this assemblage group is indicative of environments experiencing episodic or mild current activity. This propensity for mild or epidisoic current activity is also reflected in sediment grain size composition, which has fairly equal proportions of silt and sand (50 % sand, 46 % silt and 4 % silt) and a moderate organic content (mean 5.6 ± 1.7 %).

The relative importance of *S. wrightii* and *E. excavatum* within specific assemblages of this group is likely to be related to basin water or substrate organic content quality. For example, *S. wrightii* comprises either the highest abundance or the second highest abundance, in samples from the main basin (173, 101, 198, 41 and 197), whilst taxa with the highest abundances in the outer basin samples are *A. beccarii* and *E. excavatum.* Thus increases in *E. excavatum* and *A. beccarii* at a core site may reflect a stronger marine influence. Additionally, this assemblage group contains taxa which are likely indicative of 'coastal waters' such as *Miliolina spp.* and *Melonis barleeanum* (table 5.6; appendix 8).

5.5 CONCLUSIONS

Multivariate statistical methods (cluster analysis, non-metric multi-dimensional scaling and factor analysis) have been applied to a suite of spatially distributed Loch Sunart benthic foraminiferal assemblages. Four benthic foraminiferal assemblages have been identified, reflecting: A) a restricted and stressed environment (found in the inner basin); B) high current activity; C) a calm depositional environment with possible stratification of the water column; D) main and outer basin reflecting coastal water influence (figure 5.10). Though the benthic foraminiferal species recorded in Loch Sunart are similar to those found in other Scandinavian fjords, the shallow depth of Loch Sunart, along with the frequent exchange with coastal waters, provides a unique benthic foraminiferal distribution which is very different to other fjordic distributions. Species diversity and abundance are typically higher in Loch Sunart than at nearby shelf sites (Murray, 2003b) and many NW European fjord sites, one reason why Loch Sunart has been designated as a Site of Special Scientific Interest.

Agglutinated species indicative of low salinity and stressed environments (e.g. *E. scaber* and *R. subfusiformis*) were found in abundance in inner basin assemblages, and the good preservation of these taxa, along with signs of carbonate dissolution, points to the possibility of obtaining palaeoenvironmental information (e.g. basin salinity) from these restricted basins (e.g. Alve & Murray, 1995; Murray & Alve, 1999c, 2000).

C. lobatulus is common throughout Loch Sunart benthic foraminiferal assemblages (table 5.2), however the highest abundances of *C. lobatulus* occur with other 'high energy' and robust taxa such as *S. wrightii*, *A. beccarii*, *A. mamilla, Rosalina spp,* and *E. macellum* at either shallow water depths (>20 m) or areas of intense current activity, such as the inner basin sill region (Elliott *et al.*, 1992). Thus, an increase in *C. lobatulus* in core assemblages is likely to reflect an increase in current activity at the site.

B. marginata, *N. turgida* and *S. fusiformis* all demonstrated positive relationship with sediment organic matter content, thus typically occur in assemblages where fine grained sediments point to a calm depositional environment, i.e. deep basins. Additionally, 'cool' water species such as *A. glomeratum, C. reniforme,* and *Epistominella* spp. suggest the overlying water columns of these deep basins are likely to be stratified and the presence of *S. fusiformis* and *Bolivina* spp. may reflect lowered dissolved oxygen concentration in the bottom waters of these deep basins. Thus where similar assemblages or significant abundances of specific taxa (such as *A. glomeratum*) are found, conditions may be interpreted as being more stable due to enhanced stratification.

The last assemblage, D, encompasses most of the outer basin and main basin from samples. The fairly high abundances of *C. lobatulus, A. beccarii, S. wrightii*, together with lower abundances of taxa typically found in calm depositional environments (e.g.

B. marginata and *N. turgida*) suggests that locations yielding these assemblages experience either mild current activity or episodic current activity, as seen during DWREs. The increasing prevalence of *E. excavatum* towards the outer basin of Loch Sunart, points to the possibility that this taxon could be used as an indicator for increasing salinities in Loch Sunart fossil assemblages. This is also true for porcelaneous taxa which are typically rare in Loch Sunart surface sediments.

The typical fjordic bathymetry of Loch Sunart (i.e. deep basins and shallow sills) presents two potential areas for future palaeoclimatic research. The calm depositional environment of the main basin deep presents well preserved, high diversity benthic foraminiferal assemblages. These assemblages are likely to respond to inter-annual changes in seasonal stratification, organic input and temperature (e.g. Mikalsen *et al.*, 2001; Scourse *et al.*, 2002); changes which may be reflected in test composition (Austin & Inall, 2002; Allison & Austin, 2003) and possible reconstructed using qualitative and quantitative approaches (chapter 7).

Although taphonomic processes such as the post-mortem dissolution of calcareous tests, are likely to result in problems with generating an isotope record, recent studies focusing on agglutinated benthic foraminiferal taxa from marginal marine environments suggest agglutinated dominated assemblages may provide useful palaeoenvironmental information (Alve & Murray, 1995; Murray & Alve, 2000; Murray *et al.*, 2003). Inner basin benthic foraminiferal assemblages are likely to be hugely influenced by salinity changes and terrestrial organic matter input, thus sedimentary archives from this area may provide useful palaeorecords of environmental change in the catchment, such as inter-annual or sub-decadal changes in precipitation (depending on core resolution).

CHAPTER 6 - STABLE ISOTOPIC COMPOSITIONS OF MODERN BENTHIC FORAMINIFERA FROM LOCH SUNART

6.1 Introduction

The stable isotopic composition of benthic foraminiferal tests are influenced by environmental variables such as temperature, salinity and nutrient availability, often reflecting the properties of the water mass in which they live (see Rohling & Cooke, 1999 of a review). Many studies have focused on modern benthic foraminifera to ascertain which taxa are the most reliable recorders of water mass properties (e.g. Duplessy *et al.*, 1970; Vinot-Bertouille & Duplessy, 1973; Shackleton, 1974; Woodruff *et al.*, 1980; Belanger *et al.*, 1981; Graham *et al.*, 1981; Vincent *et al.*, 1981; Grossman, 1984b, a, 1987; McCorkle *et al.*, 1990; Wilson-Finelli *et al.*, 1998; Mackensen & Bickert, 1999; Mackensen *et al.*, 2000; Tachikawa & Elderfield, 2002; Schmiedl *et al.*, 2004). However, most of these studies focused on deep-sea benthic foraminifera; few studies have investigated shelf-sea benthic foraminifera (Erez, 1978; Bauch *et al.*, 2004; Scourse *et al.*, 2004) and no such investigations have been reported from Scottish sea lochs. Before isotopic compositions from benthic foraminiferal species can be used to reconstruct palaeoceanographic conditions, it is important to determine whether they are in isotopic equilibrium with the surrounding seawater in which their tests calcified.

6.1.1 Environmental influences on test isotopic composition

6.1.1.1 Oxygen isotopic compositions

Stable oxygen isotopic fractionation is heavily temperature dependent and since the seminal publication of Urey (1947) much work has been undertaken to refine and improve the temperature: $\delta^{18}O$ relationship (e.g. McCrea, 1950; Epstein *et al.*, 1953; Craig, 1965; O'Neil *et al.*, 1969; Emrich *et al.*, 1970; Kim & O'Neil, 1997; Bemis *et al.*, 1998; Lynch-Stieglitz *et al.*, 1999). Recent palaeotemperature work carried out by Bemis *et al.*, (1998) on Planktonic foraminifera yielded the following empirical relationship:

$$T\ (^\circ C) = a + b(\delta_c - \delta_w) \qquad \textit{(Eq. 6.1)}$$

Where: a and b are constants at 16.5 and -4.8 respectively; δ_c is the isotopic composition of calcite and δ_w is the isotopic composition of seawater.

A relationship between salinity and oxygen isotopic composition of seawater also exists and atmospheric processes which act upon the isotopic composition of precipitation determine the slope of salinity:$\delta^{18}O$ mixing lines in coastal waters (e.g. Craig & Gordon, 1965; Israelson & Buchardt, 1991; Mikalsen & Sejrup, 2000). The salinity:$\delta^{18}O$ mixing line for Loch Sunart has been established by Austin & Inall, (2002) as:

$$\delta^{18}O_{\text{seawater}} = 0.18 * \text{salinity} - 6 \qquad (R^2 = 0.998) \qquad \textit{(Eq. 6.2)}$$

6.1.1.2 Carbon isotopic compositions

Marine phytoplankton preferentially take up lighter $^{12}CO_2$ during photosynthesis, resulting in surface waters being relatively enriched in ^{13}C (Rohling & Cooke, 1999). Upon death, phytoplankton accumulate and sink to the sea bed as particulate organic matter, where it decomposes and releases ^{12}C, causing lighter $\delta^{13}C$ values in bottom waters. Thus stable carbon isotopic compositions in benthic foraminifera often reflect productivity, circulation and the ventilation of water masses (e.g. Mackensen & Bickert, 1999; Rohling & Cooke, 1999; Mackensen *et al.*, 2000 and references within).

6.1.2 Equilibrium calcite

Since marine organisms tend to calcify in isotopic equilibrium with seawater (e.g. Mook, 1968), foraminiferal $\delta^{18}O$ should reflect the $\delta^{18}O$ of the seawater, hence the salinity or the temperature of the water mass. Similarly, stable carbon isotopes from foraminiferal tests ($\delta^{13}C$) should reflect the $\delta^{13}C$ of the dissolved inorganic carbon ($\delta^{13}C_{DIC}$) of seawater. However, vital effects (section 6.1.2.1) are common in benthic foraminifera (e.g. Grossman, 1987 and references therein), often resulting in stable isotopic compositions which differ from those expected, i.e. the organism is in isotopic disequilibrium with the surrounding environment. Thus it is important to determine whether a benthic foraminiferal species is in isotopic equilibrium with the surrounding seawater before it is used to reconstruct palaeoceanographic conditions.

6.1.2.1 Vital effects in benthic foraminifera

Vital effects in benthic foraminifera were first reported by Duplessy *et al.*, (1970) who noted that although the isotopic curves of *Pyrgo, Planulina wuellerstorfi* and mixed species from a deep-sea site were parallel, they were offset by 1‰ or more. Since then, much focus has been awarded to vital effects in benthic foraminifera (e.g. Vinot-Bertouille & Duplessy, 1973; Erez, 1978; Woodruff *et al.*, 1980; Graham *et al.*, 1981; Vincent *et al.*, 1981; Grossman, 1984b, a). Grossman, (1987) provides an excellent review of vital effects in modern benthic foraminifera.

The physiological processes responsible for vital effects fall into two categories. The first is kinetic isotopic fractionation, which is thought to be caused by the preferential uptake of the lighter isotopes of carbon and oxygen during the hydration and hydroxylation of CO_2 (e.g. McConnaughey, 1989a, b), and is often associated with calcification rates (e.g. Erez, 1978, McConnaughey, 1989a; Owen *et al.*, 2002). Isotopic variations in foraminiferal carbonate due to ontogenic effects have been reported in some species of planktonic foraminifera (e.g. Rohling & Cooke, 1999 and references therein). No such trends have been reported in deep-sea benthic foraminifera (e.g. Vincent *et al.*, 1981; Grossman, 1984b and Tachikawa & Elderfield, 2002) until recently by Schmiedl *et al.*, (2004), who reported positive logarithmic correlations between the test size of *Uvigerina mediterranea* from the Mediterranean Sea and stable isotopic compositions. Spero *et al.*, (1997) recently showed that foraminiferal $\delta^{18}O$ and $\delta^{13}C$ is also influenced by seawater carbonate ion concentration.

The second is metabolic isotopic fractionation which is demonstrated by $\delta^{13}C$ deviations from strict kinetic behaviour and results primarily from changing $\delta^{13}C$ available to the organism to incorporate into the shell. Metabolic effects are influenced by respiration and photosynthetic processes, resulting in the ^{13}C depletion or enrichment of the organism's internal DIC pool, respectively (McConnaughey, 1989a; McConnaughey *et al.*, 1997). Shell $\delta^{13}C$ tends to reflect the isotopic mixing of metabolic $\delta^{13}C$ with environmental $\delta^{13}C$ (e.g. $\delta^{13}C_{seawater}$) as demonstrated by the isotopic mixing line seen of McConnaughey *et al.*, (1997).

6.1.3 Oxygen isotopic equilibrium

The relationships of temperature and salinity with oxygen isotopic composition (equations 6.1 and 6.2) can be used to calculate the theoretical isotopic composition of a carbonate (equilibrium calcite) calcifying at a given temperature and salinity. Since $\delta^{18}O_{seawater}$ measurements are determined relative to the standard Vienna Standard Mean Ocean Water (VSMOW) and $\delta^{18}O_{CaCO3}$ is determined relative to the standard Vienna Peedee Belemnite (VPDB), the $\delta^{18}O_{seawater}$ must be corrected by -0.27 ‰ to convert it to the VPDB scale (Hut, 1987), i.e.

$$\delta^{18}O_{seawater\,(VPDB)} = \delta^{18}O_{seawater\,(VSMOW)} - 0.27 \qquad \textit{(Eq. 6.3)}$$

The equation for equilibrium calcite ($\delta^{18}O_{Eq.CaCO3}$) using the Bemis *et al.,* (1998) temperature:$\delta^{18}O$ equation and the Austin & Inall (2002) salinity:$\delta^{18}O$ equation can therefore can be defined as;

$$\delta^{18}O_{Eq.CaCO3} = [\{T - 16.5 - (4.8 * [(S*0.18) - 6]-0.27)\} / -4.8] \qquad \textit{(Eq. 6.4)}$$

where T is the bottom water temperature (°C) and S is the bottom water salinity in which the test calcified.

To test whether a marine organism calcifies in isotopic equilibrium with its surrounding water mass, the measured $\delta^{18}O_{foram}$ can be compared (i.e. $\Delta\delta^{18}O$) with the expected oxygen isotopic composition ($\delta^{18}O_{Eq.CaCO3}$), given that the temperature and salinity of the sample site is known.

$$\Delta\delta^{18}O = \delta^{18}O_{foram} - \delta^{18}O_{Eq.CaCO3} \qquad \textit{(Eq 6.5)}$$

Few benthic foraminifera calcify in isotopic equilibrium with seawater, however several taxa calcify close to isotopic equilibrium (e.g. Grossman, 1987). Porewater $\delta^{18}O$ depletion with respect to bottom water $\delta^{18}O$ has been attributed to low porewater pH and a decrease in carbonate ion concentrations with sediment depth (Bemis *et al.*, 1998), and is thought to influence the negative $\delta^{13}C:\delta^{18}O$ correlation observed in benthic foraminiferal tests (Belanger *et al.*, 1981). Grossman, (1984b) and McCorkle *et al.*, (1990) demonstrated that species living in low oxygen sediments (i.e. deep dwelling species) tended to be closer to oxygen isotopic equilibrium than shallow infaunal taxa.

6.1.4 Carbon isotopic equilibrium

Again, since marine organisms calcify in isotopic equilibrium with seawater, stable carbon isotopes should reflect the $\delta^{13}C$ of the dissolved inorganic carbon (DIC) of seawater (assuming negligible metabolic effects).

Temperature exhibits little influence on stable carbon isotopic composition (e.g. Grossman, 1984a; Romanek *et al.*, 1992), whilst salinity influences $\delta^{13}C$ of carbonates only in areas of freshwater and seawater admixing (e.g. Mook, 1971; Spiker, 1980; Lubinski *et al.*, 2001; Bauch *et al.*, 2004). Theoretical $\delta^{13}C_{Eq.CaCO3}$ must therefore be determined through direct measurements of $\delta^{13}C_{DIC}$, i.e.

$$\Delta\delta^{13}C = \delta^{13}C_{foram} - \delta^{13}C_{DIC} \qquad \textit{(Eq 6.6)}$$

Metabolic effects influenced by respiration and photosynthetic processes can result in ^{13}C depletion or enrichment of the organism's internal DIC pool respectively (McConnaughey, 1989a; McConnaughey *et al.*, 1997), resulting in 'vital effects' (section 6.1.2.1). Thus test $\delta^{13}C$ often reflects the isotopic mixing of internal metabolic $\delta^{13}C$ with $\delta^{13}C_{DIC}$ of seawater.

6.1.5 Environmental influences on benthic foraminiferal test $\delta^{13}C$

Kroopnick, (1985) demonstrated that a strong negative linear correlation between $\delta^{13}C$ of total CO_2 ($\delta^{13}C_{TCO2}$) and apparent oxygen utilisation (AOU) existed throughout the global oceans, with $\delta^{13}C_{DIC}$ in the water column closely following nutrient (phosphate) availability. Since the epifaunal taxa *Cibicidoides* typically calcifies close to isotopic equilibrium with $\delta^{13}C_{DIC}$ (e.g. Belanger *et al.*, 1981; Graham *et al.*, 1981; Mackensen *et al.*, 1993), stable carbon isotopes from this benthic foraminiferal group can often yield information on organic carbon accumulation, productivity (e.g. Zahn *et al.*, 1986; Schmiedl *et al.*, 2004) and water mass circulation (e.g. Mackensen & Bickert, 1999 and references therein). Unfortunately, no water column or sediment $\delta^{13}C$ profiles are available for Loch Sunart or indeed any Scottish fjords at present (H. Kennedey, pers.comm 2004), hence the carbon isotopic equilibrium of Loch Sunart benthic foraminifera cannot be established. Surface waters of the North Atlantic (<500 m at ~60 °N) typically have $\delta^{13}C$ values around ~ 1–1.5 ‰ (Kroopnick, 1985; Keir *et al.*, 1998). Whilst the $\delta^{13}C_{DIC}$ in anoxic fjords tends to be depleted (e.g. -10 ‰ at 40 m, Velinsky & Fogel, 1999; Gustafsson & Nordberg, 2000), Loch Sunart is well ventilated (Gillibrand *et al.*, 1995) hence is likely to show main basin bottom water $\delta^{13}C_{DIC}$ values similar to the $\delta^{13}C_{DIC}$ of coastal waters (e.g. Hellings *et al.*, 1999).

6.1.5.1 Depth habitat as suggested by $\delta^{13}C$

Microhabitat effects are the primary influence on the $\delta^{13}C$ of infaunal benthic foraminifera with shell $\delta^{13}C$ reflecting porewater $\delta^{13}C$ (e.g. Woodruff *et al.*, 1980; Belanger *et al.*, 1981; Grossman, 1984b; Corliss, 1985a; Sauter *et al.*, 2001). The decomposition of organic matter (rained down from surface ocean productivity) within the sediments consumes oxygen, releasing isotopically light CO_2 and thus depleted $\delta^{13}C$ into the porewaters (McCorkle *et al.*, 1985). The $\delta^{13}C$ of sediment porewater is similar to the $\delta^{13}C$:AOU relationship observed in the water column (Kroopnick, 1985), with $\delta^{13}C$ values becoming isotopically lighter with increasing oxygen utilisation. Since infaunal benthic foraminifera species derive CO_2 for test calcification from the surrounding porewater, the $\delta^{13}C_{foram}$ reflects porewater $\delta^{13}C_{DIC}$ and taxa living in a deep infaunal habitat generally have more depleted $\delta^{13}C$ values than those species living in a shallow infaunal habitat (e.g. McCorkle *et al.*, 1990; Buzas *et al.*, 1993; McCorkle *et al.*, 1997; Mackensen *et al.*, 2000; Tachikawa & Elderfield, 2002; Schmiedl *et al.*, 2004). This is known as a microhabitat effect.

Porewater $\delta^{13}C$ gradients are site specific and primarily dependent on the carbon rain rate and the sediment depth at which organic matter decomposes (McCorkle *et al.*, 1985). Depletions of up to (and at times exceeding) 1‰ cm^{-1} are common for deep-sea sites (e.g. McCorkle *et al.*, 1985; McCorkle & Emerson, 1988; Martin *et al.*, 2000;

Tachikawa & Elderfield, 2002), and steeper gradients are often seen in reducing environments due to shallower O_2 penetration into the sediments (McCorkle & Emerson, 1988). Oxygen penetration depth is of importance to the porewater $\delta^{13}C$ profile (McCorkle & Emerson, 1988) and has been found to have a close relationship to organic carbon flux rate. In deep sea environments, the flux rate of organic carbon (C_{org}) to the sea floor (Altenbach *et al.*, 1999) and the rate of C_{org} degradation decreases with increasing water depth, with sediments receiving low C_{org} generally having deeper oxygen penetration (Sauter *et al.*, 2001).

6.1.6 Use of benthic foraminiferal stable isotopes in palaeoceanography

Cibicides wuellerstorfi and *Uvigerina peregrina* are two benthic foraminifera species commonly used to construct palaeoceanographic records (e.g. Zahn *et al.*, 1986), since the first is thought to calcify close to isotopic equilibrium with the $\delta^{13}C_{DIC}$ of seawater and the latter species calcifies close to seawater $\delta^{18}O$ (Shackleton, 1974). Neither species were found to be present in Loch Sunart sediments (see chapter 5), thus the abundant epifaunal species *Cibicides lobatulus* was selected to obtain Loch Sunart palaeoisotope records (chapter 8).

Although *C. wuellerstorfi* is commonly accepted as calcifying close to isotopic equilibrium with the seawater $\delta^{13}C_{DIC}$ (e.g. Woodruff *et al.*, 1980; Belanger *et al.*, 1981; Graham *et al.*, 1981; Grossman, 1984a; Wilson-Finelli *et al.*, 1998; Tachikawa & Elderfield, 2002), studies show deviations (both enriched and depleted with respect to equilibrium $\delta^{13}C_{DIC}$) of as much as 1 ‰ from isotopic equilibrium for other species of *Cibicides* (e.g. McCorkle *et al.*, 1997; Mackensen *et al.*, 2000; Schmiedl *et al.*, 2004), and it is possible that Loch Sunart *C. lobatulus* may display a $\delta^{13}C$ offset.

A number of studies report a tendency for *Cibicidoides* species to calcify in isotopic disequilibrium with respect to theoretical equilibrium $\delta^{18}O$ calcite, exhibiting consistently negative $\Delta\delta^{18}O$ values of up to -1‰, i.e. depleted $\delta^{18}O$ with respect to equilibrium calcite (e.g. Woodruff *et al.*, 1980; Belanger *et al.*, 1981; Graham *et al.*, 1981; Vilks & Deonarine, 1988; Rathburn *et al.*, 1996; McCorkle *et al.*, 1997; Scott *et al.*, 1998; Schmiedl *et al.*, 2004; Scourse *et al.*, 2004). Despite the test morphology of *Cibicides* (plano-convex) suggesting an epibenthic habitat (Corliss, 1985a) and observations of *Cibicides* species living in true epibenthic habitats (i.e. epilithic or epiphytic), Bornmalm *et al.*, (1997) observed a preference for a very shallow infaunal habitat for *C. pachyderma* in laboratory experiments, with individuals forming 'cysts' within the sediment around them. McCorkle *et al.*, (1990) found specimens of *C. lobatulus* from the deep-sea had $\Delta\delta^{18}O$ of around -0.7 ‰ and McCorkle *et al.*, (1997) suggested the isotopic composition of *C. lobatulus* from the California continental margin was likely influenced by 'vital effects' and questioned whether the species is truly epibenthic. Rathburn *et al.*, (1996) also attributed isotopic differences between deep-sea *Cibicidoides* species and *Cibicides bradyi* to a transitional (0-4cm) habitat depth for *C. bradyi.* Conversely, Bemis *et al.*, (1998) recently demonstrated that deep-sea core-top *Cibicidoides* from the Atlantic, Pacific and Indian Oceans and the Arabian Sea and Gulf of Mexico appeared to calcify close to oxygen equilibrium calcite, and Lynch-Stieglitz *et al.,* (1999) showed *Cibicidoides* specimens calcified close to isotopic equilibrium in temperatures of 5-27 ºC. Few studies have explored isotopic compositions of modern mid-latitude shelf/fjord benthic foraminifera (e.g. Scourse *et al.*, 2004), and it is particularly important to ascertain the degree of oxygen isotope disequilibria in taxa used to obtain palaeoisotope records. For instance, applying a 0.2 ‰ correction to account for an apparent 'vital effect' which may actually derive from the palaeotemperature used (e.g. the difference in $\Delta\delta^{18}O$ when applying the O'Neil *et al.*, 1969 and Bemis *et al.*, 1998 equations), may produce an erroneous temperature offset of ~ 1 °C.

6.2 Aims and methods

This chapter aims to investigate the stable isotopic compositions of modern benthic foraminifera from the surface sediments of Loch Sunart in order to:

i) determine major ecological influences (i.e. temperature, salinity or depth habitat) on test composition of common species found in Loch Sunart;

ii) establish the degree of isotopic disequilibria in modern *Cibicides lobatulus* from Loch Sunart. This is important because *C. lobatulus* is used to provide the palaeoisotope record for cores GC023 and SC023.

Oxygen and carbon isotopic analyses were carried out on four benthic foraminifer species; *Ammonia beccarii, Cibicides lobatulus, Bulimina marginata* and *Noniella turgida.* These species were chosen because they are: a) abundant throughout the sea loch surface sediments; b) represent the species with the greatest number of 'live' individuals; and c) represent a range of reported depth habitats i.e. epifaunal, shallow infaunal and deep infaunal (see chapter 4). Additionally, *C. lobatulus* was used to obtain the isotope record from Loch Sunart cores GC023 and SC023, hence an understanding of factors affecting the isotopic composition of this species in the surface sediments of Loch Sunart should aid the interpretation of down-core isotope records.

6.3 RESULTS

All stable isotope results are reported relative to Vienna Pee Dee Belemnite (VPDB) using the NBS-19 standard, and the following equations;

$$\delta^{18}O\ (‰) = [(^{18}O/^{16}O\ \text{sample} / ^{18}O/^{16}O\ \text{standard}) - 1] * 1000 \qquad \textit{(Eq. 2.6)}$$

$$\delta^{13}C\ (‰) = [(^{13}C/^{12}C\ \text{sample} / ^{13}C/^{12}C\ \text{standard}) - 1] * 1000 \qquad \textit{(Eq. 2.7)}$$

6.3.1 Isotopes from modern foraminifera

The isotopic compositions for all 4 species of benthic foraminifera studied are presented in table 6.1. Specimens which were categorised as 'live' are denoted by 'L', and specimens which were 'dead' are represented by 'D'. The life status of specimens in the first sample batch (run at Bremen) were unspecified, thus these specimens could be 'dead' or 'live' and are denoted by 'U'. All samples are accompanied by data on: collection date, station co-ordinates, water depth, bottom water temperature (BWT) and bottom water salinity (BWS).

Ammonia beccarii

$\delta^{18}O$ values for all *A. beccarii* samples (i.e. live, dead and 'unspecified') are enriched in ^{18}O relative to the $\delta^{18}O$ of VPDB, and range from 0.73 ‰ to 1.66 ‰ with a mean $\delta^{18}O$ value of 1.32 ± 0.20 ‰. Carbon isotopic compositions of all the *A. beccarii*

Table 6.1. a) Oxygen and carbon isotopic compositions of *Ammonia beccarii* selected from the 150-250µm fraction of the uppermost 1-2 cm of Loch Sunart surface sediments. Live samples are represented by 'L', and dead samples by 'D'. The samples were run on three different mass spectrometers: 1) A Finnigan MAT 251 with Kiel device at Bremen; 2) A Finnigan MAT 251 with Kiel device at Bergen; 3) A ThermoFinnigan MAT 253 at Bergen. Bottom water temperature (BWT) and salinity (BWS) are given for each sample location. Theoretical equilibrium $\delta^{18}O$ calcite, $\delta^{18}O_{Eq.CaCO3}$ (section 6.1.3), is also calculated for each sample location and the difference ($\Delta\ \delta^{18}O$) between the $\delta^{18}O_{Eq.CaCO3}$ and measured $\delta^{18}O$ is represented by ? $\delta^{18}O$.

Sample	System	Collection date	Live or Dead?	Latitude,	Longitude	Water depth, m	BWT, °C	BWS	$\delta^{13}C$, ‰	$\delta^{18}O$, ‰	$\delta^{18}O_{Eq.CaCO3}$ ‰	$\Delta\ \delta^{18}O$, ‰
25	1	4.01	U	56.6605	-6.0118	67	7.88	34.16	-1.21	1.42	1.674	0.250
27	3	4.01	L	56.6622	-5.9920	65	7.88	34.16	-1.41	1.04	1.674	0.634
27	3	4.01	L	56.6622	-5.9920	65	7.88	34.16	-1.37	1.34	1.674	0.334
27	3	4.01	L	56.6622	-5.9920	65	7.88	34.16	-1.61	1.42	1.674	0.254
30	1	4.01	U	56.6562	-5.9657	41	7.87	34.07	-1.08	1.07	1.661	0.588
34	1	4.01	U	56.6704	-5.9468	71	7.88	34.12	-1.42	0.92	1.669	0.747
41	1	4.01	U	56.6701	-5.8649	58	7.73	33.74	-1.12	1.25	1.631	0.382
44	3	4.01	L	56.6755	-5.8202	90	8.13	33.84	-1.38	1.12	1.565	0.445
45	3	4.01	L	56.6993	-5.7731	70	7.54	33.65	-1.29	1.16	1.653	0.493
68	2	6.01	D	56.6865	-5.5691	11.2	11.10	32.87	-0.82	0.83	0.770	-0.060
72	2	6.01	L	56.6866	-5.5839	30.0	10.87	32.82	-1.44	1.33	0.810	-0.520
75	1	6.01	U	56.6855	-5.6159	43	10.99	33.39	-1.29	1.44	0.888	-0.556
76	2	6.01	L	56.6930	-5.6857	12.0	10.91	33.49	-0.93	1.36	0.923	-0.437
110	1	7.01	U	56.6796	-5.6469	52.9	10.95	33.05	-0.06	1.39	0.836	-0.556
112	1	7.01	L	56.6807	-5.6499	44.7	10.87	33.11	-0.50	1.44	0.863	-0.573
145	1	6.02	U	56.6848	-5.5811	25.7	10.97	32.13	-1.29	1.31	0.666	-0.648
147	2	6.02	D	56.6873	-5.5835	14	11.37	32.07	-0.99	1.07	0.571	-0.499
149	1	6.02	D	56.6848	-5.6231	58.5	10.78	32.98	-1.32	1.37	0.859	-0.511
155	3	6.02	L	56.6776	-5.6283	26.6	11.00	32.94	-1.06	1.24	0.806	-0.434
160	1	6.02	U	56.6849	-5.6732	11.7	10.91	33.49	-0.34	1.45	0.923	-0.524
162	1	6.02	U	56.6846	-5.6830	12.8	10.91	33.49	0.54	1.16	0.923	-0.239
173	3	6.02	L	56.7020	-5.7261	31.2	10.67	33.73	-1.2	1.25	1.015	-0.235
180	1	6.02	U	56.6824	-5.9885	21.4	11.75	33.89	-0.21	1.48	0.820	-0.664

Sample	System	Collection date	Live or Dead?	Latitude,	Longitude	Water depth, m	BWT, °C	BWS, psu	$\delta^{13}C$, ‰	$\delta^{18}O$, ‰	Eq.calcite, ‰	$\Delta\delta^{18}O$, ‰
181	1	6.02	U	56.6804	-6.0117	36.1	11.54	33.69	-0.24	1.66	0.828	-0.832
182	2	6.02	L	56.6706	-6.0026	46	11.03	33.86	-1.26	1.42	0.964	-0.456
183	2	6.02	L	56.6631	-5.9972	75.5	12.14	34.05	-1.43	1.42	0.767	-0.653
183	1	6.02	L	56.6637	-5.9966	75.5	12.14	34.05	-1.44	1.61	0.767	-0.845
183	3	6.02	L	56.6631	-5.9972	75.5	12.14	34.05	-1.61	1.51	0.767	-0.743
183	3	6.02	L	56.6631	-5.9972	75.5	12.14	34.05	-1.44	1.48	0.767	-0.713
189	2	6.02	D	56.6706	-5.9467	75	10.91	33.87	0.14	1.32	0.992	-0.328
192	2	6.02	D	56.6727	-5.9185	90.2	11.39	33.67	-0.58	1.21	0.855	-0.355
193	2	6.02	D	56.6669	-5.9198	51.1	11.39	33.60	-0.37	1.61	0.843	-0.767
197	2	6.02	L	56.6736	-5.8658	111	10.41	33.67	-1.3	1.33	1.059	-0.271
198	1	6.02	U	56.6654	-5.8405	121	10.40	33.66	-0.33	1.58	1.060	-0.522
199	2	6.02	D	56.6840	-5.8135	16.7	11.24	33.44	-0.76	1.32	0.845	-0.475
200	2	6.02	D	56.6833	-5.8128	54.7	10.58	33.70	-0.88	1.5	1.029	-0.471
200	3	6.02	L	56.6833	-5.8128	54.7	10.58	33.70	-1.23	1.52	1.029	-0.491
201	2	6.02	L	56.6829	-5.8096	68	10.44	33.77	-1.25	1.27	1.071	-0.199
201	3	6.02	L	56.6829	-5.8096	68	10.44	33.77	-1.41	1.5	1.071	-0.429
206	1	6.02	U	56.6316	-5.8412	12.8	10.16	33.80	-1.28	1.42	1.135	-0.287
207	2	6.02	U	56.6348	-5.8520	29.6	12.40	32.56	0.26	1.45	0.445	-1.005
207	1	6.02	D	56.6349	-5.8523	29.6	12.36	32.56	0.38	1.39	0.453	-0.932
208	2	6.02	D	56.6474	-5.8831	25.6	12.36	32.56	-0.77	1.17	0.453	-0.717
210	2	6.02	D	56.6988	-5.7753	70	11.77	33.13	-0.44	1.15	0.679	-0.471
210	2	6.02	D	56.6988	-5.7753	70	10.59	33.60	0.44	0.73	1.009	0.279
211	3	6.02	L	56.6825	-5.6338	92.6	10.69	33.33	-1.58	1.42	0.940	-0.480

n = 46
Mean $\delta^{13}C = -0.895 \pm 0.605$ ‰. Mean $\delta^{18}O = 1.323 \pm 0.200$ ‰. Mean $\Delta\delta^{18}O = 0.212 \pm 0.453$ ‰ *(live samples only)*

Table 6.1 b). Oxygen and carbon isotopic compositions of *Cibicides lobatulus* (dead) selected from the 150-250μm fraction of the uppermost 1-2 cm of Loch Sunart surface sediments. Live samples are represented by 'L', and dead samples by 'D'. The samples were run on three different mass spectrometers: 1) A Finnigan MAT 251 with Kiel device at Bremen; 2) A Finnigan MAT 251 with Kiel device at Bergen; 3) A ThermoFinnigan MAT 253 at Bergen. Bottom water temperature (BWT) and salinity (BWS) are given for each sample location. Theoretical equilibrium $\delta^{18}O$ calcite, $\delta^{18}O_{Eq.CaCO3}$ (section 6.1.3), is also calculated for each sample location and the difference ($\Delta\delta^{18}O$) between the $\delta^{18}O_{Eq.CaCO3}$ and measured $\delta^{18}O$ is represented by $\Delta\delta^{18}O$.

Sample	System	Collection date	Live or dead?	Latitude,	Longitude	Water depth, m	BWT, °C	BWS, psu	$\delta^{13}C$, ‰	$\delta^{18}O$, ‰	$\delta^{18}O_{Eq.CaCO3}$ ‰	$\Delta\delta^{18}O$, ‰
25	1	4.01	U	56.6605	-6.0118	67	7.88	34.16	1.53	0.96	1.674	0.713
30	1	4.01	U	56.6562	-5.9657	41	7.87	34.07	1.39	0.87	1.661	0.793
34	1	4.01	U	56.6704	-5.9468	71	7.88	34.12	0.46	0.50	1.669	1.168
41	1	4.01	U	56.6701	-5.8649	58	7.73	33.74	1.33	0.89	1.631	0.738
44	3	4.01	L	56.6755	-5.8202	90	8.13	33.84	0.96	0.97	1.565	0.595
72	3	6.01	D	56.6866	-5.5839	30.0	10.87	32.82	1.28	0.73	0.810	0.080
110	1	7.01	U	56.6796	-5.6469	52.9	10.95	33.05	1.15	0.61	0.836	0.226
112	1	7.01	U	56.6807	-5.6499	44.7	10.87	33.11	1.43	0.96	0.863	-0.101
162	1	6.02	U	56.6846	-5.6830	12.8	10.91	33.49	0.79	0.98	0.923	-0.055
173	2	6.02	D	56.7020	-5.7261	31.2	10.67	33.73	1.66	0.95	1.015	0.065
180	1	6.02	U	56.6824	-5.9885	21.4	11.75	33.89	1.31	0.58	0.820	0.239
181	1	6.02	U	56.6804	-6.0117	36.1	11.54	33.69	1.48	0.93	0.828	-0.098
182	2	6.02	U	56.6706	-6.0026	46	11.03	33.86	1.2	0.91	0.964	0.054
183a	1	6.02	U	56.6637	-5.9966	75.5	12.14	34.05	1.36	0.84	0.767	-0.075
183b	2	6.02	D	56.6631	-5.9972	75.5	12.14	34.05	1.24	0.71	0.767	0.057
189	2	6.02	D	56.6706	-5.9467	75	10.91	33.87	1.58	0.85	0.992	0.142
192	2	6.02	D	56.6727	-5.9185	90.2	11.39	33.67	0.68	0.59	0.855	0.265
193	2	6.02	D	56.6669	-5.9198	51.1	11.39	33.60	1.55	0.62	0.843	0.223
197	2	6.02	D	56.6736	-5.8658	111	10.41	33.67	0.39	0.83	1.059	0.229
198a	1	6.02	U	56.6654	-5.8405	121	10.40	33.66	1.27	0.63	1.060	0.425
198b	1	6.02	U	56.6654	-5.8405	121	10.40	33.66	1.51	0.83	1.060	0.234
199	2	6.02	D	56.6840	-5.8135	16.7	11.24	33.44	1.76	0.79	0.845	0.055

Sample	System	Collection date	Live or dead?	Latitude,	Longitude	Water depth, m	BWT, °C	BWS, psu	$\delta^{13}C$, ‰	$\delta^{18}O$, ‰	Eq.calcite, ‰	$\Delta \delta^{18}O$, ‰
200	3	6.02	D	56.6833	-5.8128	54.7	10.58	33.70	1.67	1.14	1.029	-0.111
201	3	6.02	D	56.6829	-5.8096	68	10.44	33.77	1.67	0.93	1.071	0.141
206	1	6.02	U	56.6316	-5.8412	12.8	12.40	32.56	0.50	0.40	0.445	0.046
207a	1	6.02	U	56.6349	-5.8523	29.6	12.36	32.56	0.99	0.49	0.453	-0.041
207b	2	6.02	D	56.6348	-5.8520	29.6	12.36	32.56	0.92	0.61	0.453	-0.157
208	2	6.02	D	56.6474	-5.8831	25.6	11.77	33.13	1.14	0.62	0.679	0.059
210a	2	6.02	D	56.6988	-5.7753	70	10.59	33.60	1.09	0.82	1.009	0.189
210b	2	6.02	D	56.6988	-5.7753	70	10.59	33.60	1.15	0.5	1.009	0.509
210c	2	6.02	D	56.6988	-5.7753	70	10.59	33.60	1.64	0.63	1.009	0.379
InMoor§	2	6.02	L	56.685	-5.623	40	10.86	32.76	0.37	0.78	0.802	-0.023

n = 32
Mean $\delta^{13}C = 1.201 \pm 0.398$ ‰ Mean $\delta^{18}O = 0.759 \pm 0.20$ ‰ Mean $\Delta\delta^{18}O = -0.111 \pm 0.170$ ‰ *(not including verified 'dead' samples)*

§ This sample was obtained from 'live' *C. lobatulus* living on a scallop shell found attached to the inner basin mooring equipment, thus a depth of ~ 40 m is likely.

Table 6.1 c). Oxygen and carbon isotopic compositions of ‘live’ *Bulimina marginata* selected from the 150-250µm fraction of the uppermost 1-2 cm of Loch Sunart surface sediments. The samples were run on three different mass spectrometers: 1) A Finnigan MAT 251 with Kiel device at Bremen; 2) A Finnigan MAT 251 with Kiel device at Bergen; 3) A ThermoFinnigan MAT 253 at Bergen. Bottom water temperature (BWT) and salinity (BWS) are given for each sample location. Theoretical equilibrium $\delta^{18}O$ calcite, $\delta^{18}O_{Eq.CaCO3}$ (section 6.1.3), is also calculated for each sample location and the difference ($\Delta\delta^{18}O$) between the $\delta^{18}O_{Eq.CaCO3}$ and measured $\delta^{18}O$ is represented by $\Delta\ \delta^{18}O$.

Sample	**System**	**Collection date**	**Latitude,**	**Longitude**	**Water depth, m**	**BWT, °C**	**BWS, psu**	**$\delta^{13}C$, ‰**	**$\delta^{18}O$, ‰**	**$\delta^{18}O_{Eq.CaCO3}$, ‰**	**$\Delta\ \delta^{18}O$, ‰**
27	3	4.01	56.6622	-5.9920	65	7.88	34.16	-0.84	1.47	1.674	0.204
44	3	4.01	56.6755	-5.8202	90	8.13	33.84	-0.52	1.75	1.565	-0.185
76	2	6.01	56.6930	-5.6857	12.0	10.91	33.49	-0.56	1.52	0.923	-0.597
173	3	6.02	56.7020	-5.7261	31.2	10.67	33.73	-0.07	1.67	1.015	-0.655
182	2	6.02	56.6706	-6.0026	46	11.03	33.86	-0.08	1.67	0.964	-0.706
183	3	6.02	56.6631	-5.9972	75.5	12.14	34.05	-0.68	1.62	0.767	-0.853
197	3	6.02	56.6736	-5.8658	111	10.41	33.67	-0.89	1.67	1.059	-0.611
200	3	6.02	56.6833	-5.8128	54.7	10.58	33.70	-0.49	1.89	1.029	-0.861
201	3	6.02	56.6829	-5.8096	68	10.44	33.77	-0.81	1.79	1.071	-0.719
202	2	6.02	56.6795	-5.8099	96.6	10.16	33.80	-0.99	1.65	1.135	-0.515

n = 9

Mean $\delta^{13}C = -0.593 \pm 0.319$ ‰. Mean $\delta^{18}O = 1.670 \pm 0.122$ ‰. Mean $\Delta\ \delta^{18}O = -0.550 \pm 0.327$ ‰

Table 6.1 d). Oxygen and carbon isotopic compositions of 'live' *Noniella turgida* selected from the 150-250μm fraction of the uppermost 1-2 cm of Loch Sunart surface sediments. The samples were run on three different mass spectrometers: 1) A Finnigan MAT 251 with Kiel device at Bremen; 2) A Finnigan MAT 251 with Kiel device at Bergen; 3) A ThermoFinnigan MAT 253 at Bergen. Bottom water temperature (BWT) and salinity (BWS) are given for each sample location. Theoretical equilibrium $\delta^{18}O$ calcite, $\delta^{18}O_{Eq.CaCO3}$ (section 6.1.3), is also calculated for each sample location and the difference ($\Delta\ \delta^{18}O$) between the $\delta^{18}O_{Eq.CaCO3}$ and measured $\delta^{18}O$ is represented by $\Delta\delta^{18}O$.

Sample	System	Collection date	Latitude,	Longitude	Water depth, m	BWT, °C	BWS, psu	$\delta^{13}C$, ‰	$\delta^{18}O$, ‰	$\delta^{18}O_{Eq.CaCO3}$, ‰	$\Delta\ \delta^{18}O$, ‰
27	3	4.01	56.66222	-5.992	65	7.880	34.157	-1.79	1.31	1.674	0.364
44	3	4.01	56.67553	-5.82022	90	8.130	33.840	-1.79	1.36	1.565	0.205
72	3	6.01	56.68663	-5.58385	30.0	10.870	32.819	-1.82	1.15	0.810	-0.340
183	3	6.02	56.66312	-5.99723	75.5	12.140	34.047	-2.04	1.4	0.767	-0.633
197	3	6.02	56.67357	-5.86577	111	10.410	33.670	-1.96	1.12	1.059	-0.061
200	3	6.02	56.68328	-5.81282	54.7	10.576	33.695	-1.75	1.45	1.029	-0.421
201	3	6.02	56.68293	-5.80957	68	10.435	33.766	-1.88	1.33	1.071	-0.259
202	3	6.02	56.6795	-5.8099	96.6	10.160	33.800	-2.01	1.38	1.135	-0.245
211	3	6.02	56.68253	-5.6338	92.6	10.693	33.333	-1.62	1.09	0.940	-0.150

n = 9

Mean $\delta^{13}C$ = -1.851 ± 0.135 ‰. Mean $\delta^{18}O$ = 1.288 ± 0.133 ‰. Mean $\Delta\delta^{18}O$ = -0.171 ± 0.308 ‰

samples tend to be depleted in ^{13}C relative to VPDB with $\delta^{13}C$ values ranging from -1.61 ‰ to 0.537 ‰ with a mean of -0.895 ± 0.605 ‰.

The mean values and data range for 'live', 'dead' and 'unspecified' *A. beccarii* are shown in table 6.1a. A 2-sample T-test (using Minitab v14; Davis, 2002) shows there is no difference between the stable oxygen isotopic compositions for 'live' and 'dead' specimens, which have mean $\delta^{18}O$ values of 1.354 ± 0.136 ‰ and 1.231 ± 0.25 ‰ respectively. However, there is a significant difference between the mean $\delta^{13}C$ values for 'live' (mean $\delta^{13}C$ of -1.298 ± 0.261 ‰) and 'dead' (mean $\delta^{13}C$ of -0.565 ± 0.556 ‰) *A. beccarii.*

There appears to be no relationship between $\delta^{18}O$ and $\delta^{13}C$ for *A. beccarii* (figure 6.1) as suggested by a Pearson correlation coefficient (table 6.2). Mean $\delta^{18}O$ and $\delta^{13}C$ values for the 'unspecified' *A. beccarii* samples are 1.366 ± 0.209 ‰ and -0.656 ± 0.692 ‰ respectively.

Cibicides lobatulus

Stable oxygen isotope compositions of all *C. lobatulus* samples (i.e. 'live', 'dead' and 'unspecified' status) show enriched $\delta^{18}O$ relative to the $\delta^{18}O$ of VPDB and range from 0.399 ‰ to 1.14 ‰ with a mean $\delta^{18}O$ value of 0.759 ± 0.20 ‰ (table 6.1b). Carbon isotopic compositions for 'live' and 'dead' *C. lobatulus* also tend to be enriched in ^{13}C relative to VPDB with $\delta^{13}C$ values ranging from 0.371 ‰ to 1.76 ‰ with a mean of 1.201 ± 0.398 ‰.

The Loch Sunart data set includes only 2 known 'live' *C. lobatulus,* which have a mean $\delta^{18}O$ value of 0.875 ± 0.134 ‰ and a mean $\delta^{13}C$ value of 0.665 ± 0.417 ‰. The mean $\delta^{18}O$ value for the 'live' samples is similar to the $\delta^{18}O$ mean for the 'dead' samples (0.764 ± 0.180 ‰), however the mean $\delta^{13}C$ values differ between the 'live' and 'dead' samples, with values of 0.655 ± 0.417 ‰ and 1.295 ± 0.407 ‰ respectively. The full ('live', 'dead' and 'unspecified') and the 'unspecified' samples of *C. lobatulus* show moderate significant ($p < 0.05$) positive $\delta^{18}O:\delta^{13}C$ relationships (fig. 6.2), whilst the 'dead' *C. lobatulus* samples show an insignificant positive relationship, probably due to the larger range of isotope values (table 6.2).

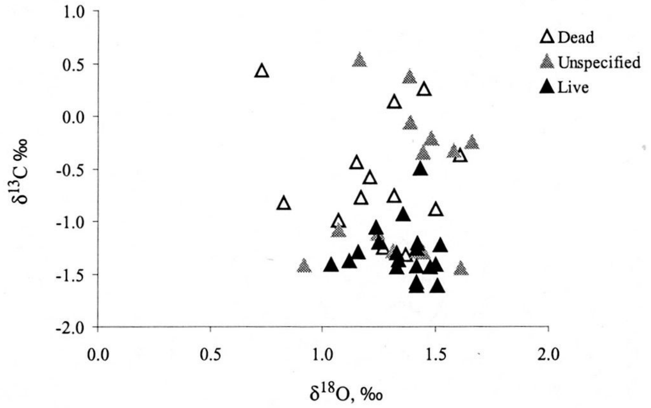

Figure 6.1. Stable isotopic compositions for dead (white triangles), live (black triangles) and 'unspecified life status' (grey triangles) *Ammonia beccarii* from Loch Sunart surface sediments collected in April 2001 and June 2002.

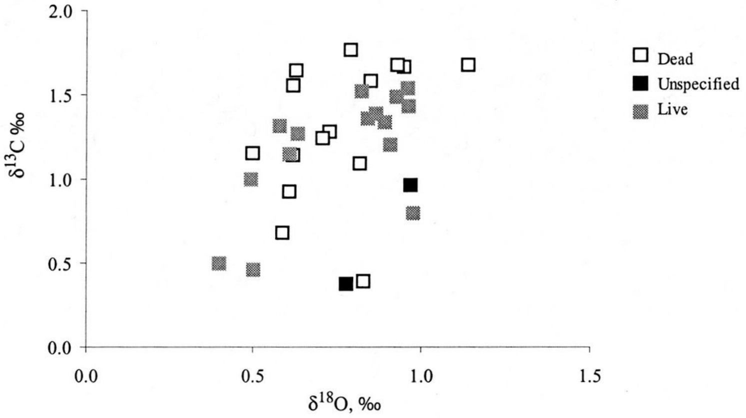

Figure 6.2 Stable isotopic compositions for 'dead' (white squares), 'live' (black squares) and 'unspecified' life status' (grey squares) *Cibicides lobatulus* from Loch Sunart surface sediments collected in April 2001 and June 2002.

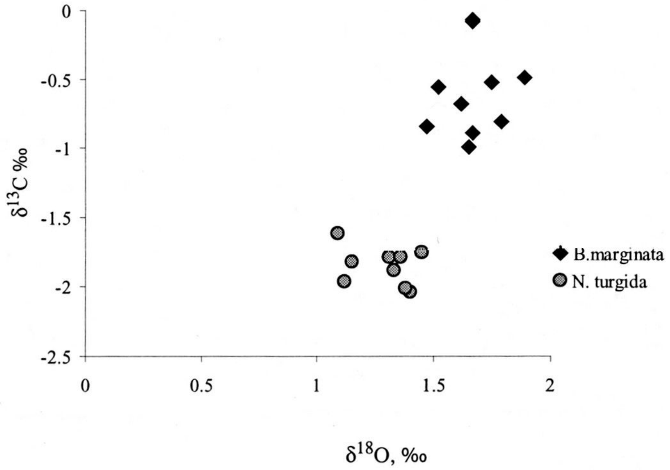

Figure 6.3 Stable isotopic compositions for 'live' *Bulimina marginata* (black diamonds) and 'live' *Nonionella turgida* from Loch Sunart surface sediments collected in April 2001 and June 2002.

Table 6.2 Pearson correlation coefficients (r; second column, top row) and corresponding p values (second column; bottom row) for the $\delta^{18}O$ and $\delta^{13}C$ relationship of the Loch Sunart benthic foraminifera used it this study. Correlation coefficients are given for; (A) the full data set, including 'live', 'dead' and 'unspecified' life status samples; (B) 'Live' specimens; (C) 'Dead' specimens and (D) those samples which have an 'unspecified' life status (U). The number of samples included in each correlation is given in the first column.

Species Data set	***Ammonia beccarii***		***Cibicides lobatulus***		***Bulimina marginata***		***Noniella turgida***	
Full (A)	46	-0.075 0.622	32	0.420 0.017	10	0.169 0.641	9	-0.325 0.393
Live (B)	19	-0.148 0.629	2	N/A	10	0.169 0.641	9	-0.325 0.393
Dead (C)	13	-0.032 0.897	15	0.394 0.146	N/A		N/A	
Unknown life status (U)	14	0.185 0.529	15	0.639 0.01				

Table 6.3 Stable isotopic compositions of Loch Sunart samples containing differing numbers of 'live' (L) or 'dead' (D) *Ammonia beccarii* and *Cibicides lobatulus* specimens. In general, samples with a high ratio of specimens per μg comprise of more juvenile specimens than samples containing single or a few specimens (low ratio samples). All samples were collected in June 2002 with the exception of sample 27 (April 2001).

Sample	**Species**	**Life status**	**No. of specimens**	**Sample mass (μg)**	**No. specimens per μg**	**$\delta^{13}C$, ‰**	**$\delta^{18}O$, ‰**
183a	Ab	L	5	37	0.1351	-1.61	1.51
183b	Ab	L	4	39	0.1026	-1.44	1.48
183c	Ab	L	14	81	0.1728	-1.43	1.42
200a	Ab	D	1	76	0.0132	-0.88	1.5
200b	Ab	L	1	35	0.0286	-1.23	1.52
201a	Ab	D	9	79	0.1139	-1.25	1.27
201b	Ab	L	4	27	0.1481	-1.41	1.5
210a	Ab	D	1	73	0.0137	-0.44	1.15
210b	Ab	D	3	82	0.0366	0.44	0.73
27a	Ab	L	3	47	0.0638	-1.41	1.04
27b	Ab	L	4	47	0.0851	-1.37	1.34
27c	Ab	L	4	41	0.0976	-1.61	1.42
210c	Cl	D	1	72	0.0139	1.09	0.82
210d	Cl	D	6	82	0.0732	1.15	0.5
210e	Cl	D	20	77	0.2597	1.64	0.63

Bulimina marginata

All isotopic data for *B. marginata* are for 'live' specimens (table 6.1c). Stable oxygen isotope compositions are enriched in ^{18}O relative to VPDB, with a mean $\delta^{18}O$ of 1.67 ± 0.122 ‰ (ranging from 1.47 ‰ to 1.89 ‰). The $\delta^{13}C$ values show more variation ranging from -0.99 ‰ to -0.07 ‰ with a mean $\delta^{13}C$ value of -0.593 ± 0.319 ‰ (figure 6.3). There appears to be no significant correlation between $\delta^{18}O$ and $\delta^{13}C$ (table 6.2).

Noniella turgida

All isotopic data for *N. turgida* are for 'live' specimens (table 6.1d and fig. 6.3). Stable oxygen isotope compositions are enriched in ^{18}O relative to VPDB, with a mean $\delta^{18}O$ of 1.288 ± 0.133 ‰ (ranging from 1.09 ‰ to 1.45 ‰). The $\delta^{13}C$ values are depleted in ^{13}C with respect to the standard and range from -2.04 ‰ to -1.62 ‰ with a mean $\delta^{13}C$ value of –1.851 ± 0.135 ‰. There appears to be no significant correlation between $\delta^{18}O$ and $\delta^{13}C$ for *N. turgida* from Loch Sunart surface samples (table 6.2).

6.3.2 Stable isotopic composition and specimen size

To test whether isotopic compositions of Loch Sunart benthic foraminifera show a relationship with growth, a number of isotopic analyses were carried out using sample masses containing differing numbers of *A. beccarii* and *C. lobatulus* specimens from the same sample site, i.e. calcifying under the same environmental conditions. Individuals were not measured prior to analyses, therefore specimen size was crudely estimated using the ratio of the number of specimens per sample mass (μg), i.e.

$$\text{Specimen size ratio} = \text{number specimens} / \text{sample mass } (\mu g) \qquad \textit{(Eq. 6.7)}$$

Samples with a high specimen size ratio contain a greater number of individuals and are likely to contain more juvenile specimens, whereas low ratio samples (few large tests) are more likely to contain specimens at 'adult' stages. Similar sized specimens were used to 'create' the samples, hence a sample with a high ratio should represent small tests, not a mixture of large and small tests. The results seen in table 6.3 are a subset taken from tables 6.1a and 6.1b.

No significant relationships occur between test size and $\delta^{18}O$ for either species (table 6.4). *C. lobatulus* shows a moderate positive and marginally insignificant relationship between test size and both $\delta^{18}O$ ($r = 0.419$, $p = 0.094$) and $\delta^{13}C$ ($r = 0.424$, $p = 0.09$), which is likely to be influenced by the strong $\delta^{18}O$:$\delta^{13}C$ relationships seen in table 6.2. Variations in $\delta^{18}O$ and $\delta^{13}C$ for *A. beccarii* samples (live and dead) containing different test sizes (i.e. different growth stages) range from 0.09 to 0.38 ‰ and 0.18 ‰ to 1 ‰ respectively. This agrees well with Vincent et al., (1981) who reported intraspecific $\delta^{13}C$ and $\delta^{18}O$ ranges in the order of several tenths of 1 ‰ for this taxon.

A. beccarii shows a strong specimen size:$\delta^{13}C$ logarithmic relationship with an R^2 value of 0.72 (figure 6.4) and a strong significant correlation coefficient of -0.715 ($p = 0.013$, table 6.3). As expected, this relationship weakens to a moderate positive relationship ($r = -0.554$, $p = 0.003$) when more samples (live and dead) are included. Interestingly, the relationship breaks down completely when only live samples are included (see table 6.3).

6.3.3 Environmental influences on stable isotopic composition

Table 6.5 show the Pearson correlation coefficients (r) and p-values for the influence of environmental variables upon the stable isotopic composition of *A. beccarii*, *C. lobatulus*, *B. marginata* and *N. turgida*. For the majority of samples, bottom water temperature (BWT) and bottom water salinity (BWS) were obtained at the time of sample collection. For those samples without accompanying hydrographic data, BWT and BWS were interpolated from other stations. Nutrient (phosphate, ammonia, nitrate and silicate) data and dissolved oxygen data were obtained from hydrographic surveys taken on the 25/5/90, 24-25/7/90, 30/4/91 – 1/6/91, 28/6/91 – 3/7/91 and 5-15/6/91 (data obtained from Fisheries Research Services, Aberdeen). This nutrient data is only a 'snapshot' view of nutrient values in Loch Sunart bottom waters at a certain period, hence although they give an idea of 'typical' values, they are not necessarily indicative of the nutrients in the water column during the lifetime of the foraminifera. Similarly, bottom water temperatures (BWT) and salinities (BWS) and % organic matter assigned to 'dead' (or even 'live') samples may not be comparable to the conditions experienced during calcification. Thus, the most accurate relationships should be obtained from correlations with 'live' samples. A point to

Table 6.4 Pearson correlation coefficients (r) and p-values for the relationship of benthic foraminifera specimen size (represented by the ratio of the number of individuals in a sample per μg of sample mass) and the stable isotopic composition of the tests for samples collected from Loch Sunart in April 2001 and June 2002. The number of samples in each correlation is shown by 'n'. *Ammonia beccarii* has 3 sets of correlations; (A) the samples included in table 7.3, which show 11 isotopic analyses from 5 sample sites; (B) all samples ('live' and 'dead') which have specimens per μg information; (C) all 'live' samples with specimens per μg information.

Species / Variable		*Ammonia beccarii* (A)	*Ammonia beccarii* (B)	*Ammonia beccarii* (C)	*Cibicides lobatulus*	*Bulimina marginata*	*Nonionella turgida*
n		11	26	17 (live)	17(1 live)	10 (live)	9 (live)
$\delta^{18}O$	r	-0.274	0.192	0.022	0.419	0.138	0.237
	p	0.416	0.347	0.932	0.094	0.704	0.540
$\delta^{13}C$	r	-0.715	-0.554	0.054	0.424	-0.312	0.415
	p	0.013	0.003	0.836	0.090	0.380	0.267

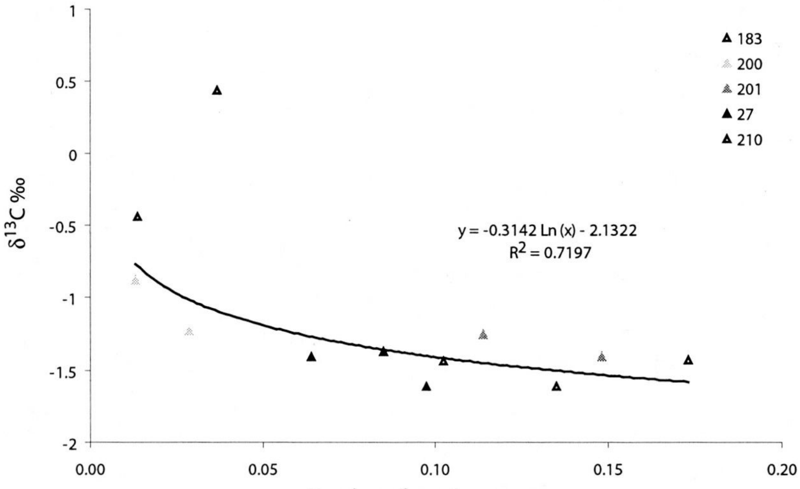

Figure 6.4. Influence of specimen size (number of specimens per μg) on the $\delta^{13}C$ of *Ammonia beccarii* from different sample stations (see legend). The *A. beccarii* with the positive $\delta^{13}C$ value from station 210 has been excluded from the logarithmic trendline due to it's anomalous value.

Table 6.5 Pearson correlation coefficients, r, (top) and corresponding p-values (bottom of cell) for selected environmental variables and A) benthic foraminiferal test $\delta^{18}O$ and B) benthic foraminiferal test $\delta^{13}C$. The same number of samples (shown in A) were used for both $\delta^{18}O$ and $\delta^{13}C$. Only samples collected in June months are used to limit strong correlations due to seasonal differences in bottom water temperature (BWT) and bottom water salinity (BWS). Correlations utilise data from 'live' specimens, with the exception of *C. lobatulus* where specimens with no specified life status were used (i.e. not identified as 'dead'). Cell shading represents the significance the correlations; dark shading shows 95% probability ($p < 0.05$), medium shaded cells show marginal insignificance ($0.05 < p < 0.075$). Cells with no shading indicated weak or insignificant relationships.

A - $\delta^{18}O$

Species Variable	*Ammonia beccarri*	*Cibicides lobatulus*	*Bulimina marginata*	*Nonionella turgida*
Sample number, n	11	8	10	9
Longitude	-0.141 0.679	-0.079 0.852	0.208 0.563	-0.563 0.114
Water depth	-0.053 0.878	-0.040 0.925	0.236 0.512	-0.155 0.691
BWT	0.747 0.008	-0.396 0.332	0.145 0.689	-0.099 0.799
BWS	-0.036 0.917	0.374 0.362	-0.298 0.404	0.636 0.066
% Organic matter	0.062 0.857	*0.609 0.109	0.375 0.286	0.777 0.014
% $CaCO^3$	0.132 0.698	0.476 0.233	0.276 0.440	0.853 0.003

B- $\delta^{13}C$

Species Variable	*Ammonia beccarri*	*Cibicides lobatulus*	*Bulimina marginata*	*Nonionella turgida*
Longitude	0.104 0.761	0.223 0.595	0.080 0.826	0.516 0.155
Water depth	-0.563 0.072	-0.722 0.043	-0.630 0.051	-0.245 0.524
BWT	0.169 0.619	0.262 0.531	0.240 0.504	-0.336 0.377
BWS	0.006 0.987	0.007 0.987	-0.164 0.650	-0.363 0.337
% Organic matter	-0.146 0.668	0.054 0.899	-0.377 0.282	-0.143 0.713
% $CaCO^3$	-0.191 0.574	0.101 0.813	-0.345 0.329	-0.309 0.418

bear in mind is that fjords experience seasonal changes in temperature (see chapter 3) and the hydrography (particularly in the upper basin) can change rapidly (i.e. during a deep water renewal event, DWRE). Therefore, hydrographic data obtained at the time of sample collection may also be a 'snapshot' of conditions of that day and not necessarily representative of long-term conditions.

Ammonia beccarii

Due to the large proportion of 'live' *A. beccarii* (19 out of the total 46 samples, only 'live' samples have been used in the correlations. Two significant moderate relationships emerge when 'live' *A. beccarii* data is used in correlations. $\delta^{18}O$ has a significant moderate positive relationship with BWT ($r = 0.557$, $p = 0.013$), whilst $\delta^{13}C$ shows a significant moderate negative correlation with water depth ($r = -0.521$, $p = 0.022$). *A. beccarii* $\delta^{13}C$ also shows a significant moderate negative relationship with BWS ($r = -0.462$, $p = 0.046$) whilst a positive moderate insignificant relationship also exists between longitude and $\delta^{13}C$ for live *A. beccarii* (table 6.5). Fjordic hydrography and sedimentary characteristics generally change with distance from the fjord mouth as it penetrates inland (see chapter 3), for example, salinity becomes fresher towards the head of Loch Sunart, whilst temperatures can show a slight decrease. Ammonia, phosphate concentrations and % organic matter typically increase towards the head of the loch, whilst oxygen concentration and saturation decreases (see figure 6.5). Therefore, the relationship between stable isotopic composition of the test and longitude is likely to reflect organic inputs and productivity in the fjord, as well as the mixing between the inner basin water (which have a $\delta^{13}C_{DIC}$ reflecting the remineralisation of terrestrial organic matter) and coastal water DIC.

Cibicides lobatulus

Low numbers of available 'live' *C. lobatulus* in the Loch Sunart samples (chapter 5) meant the majority of isotopic analyses were run on 'live' ($n = 2$), 'dead' and specimens with no life status given. This low number of 'live' *C. lobatulus* isotopic data may explain the lack of significant correlations with environmental variables (table 6.5), since a large proportion of samples are accompanied by 'snapshot' BWT

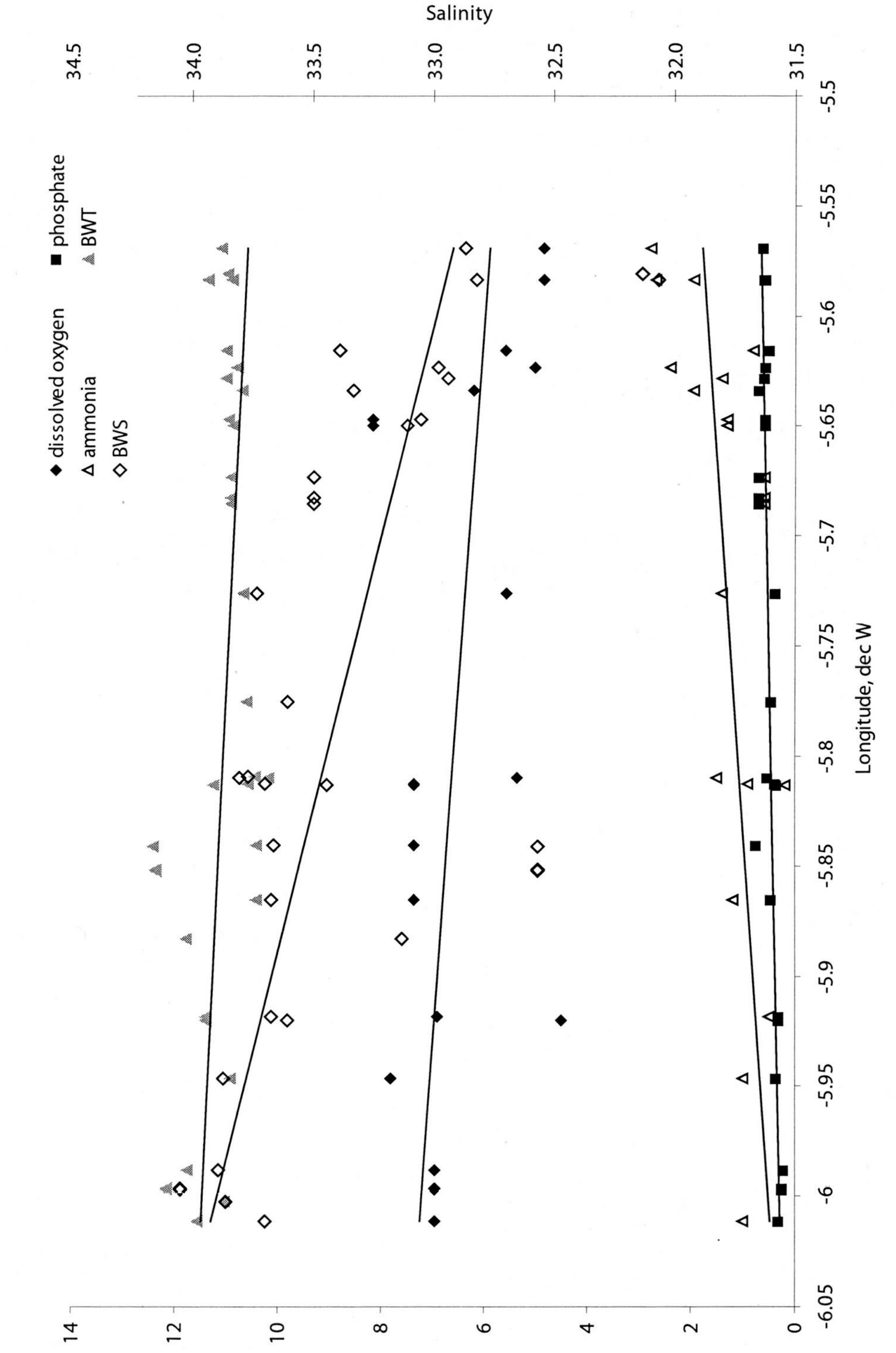

Figure 6.5 Differences in the quality of Loch Sunart bottom waters across all 3 basins from the head of the sea loch (-5.5 dec W) to the mouth (-6 dec W). Sill regions occur at approximately -5.66 dec W, separating the inner basin from the main basin, and at ~ -5.89 dec W, separating the main and outer basins of Loch Sunart. Bottom water salinity (BWS; white diamonds), bottom water temperature (BWT; grey triangles) and dissolved oxygen concentrations(black diamonds) all show a trend of increasing values towards the fjord mouth, i.e. with increasing coastal water influence. The concentration of phosphate (black squares) and ammonia (white trianlges) in the bottom waters appears highest in the inner basin, typically decreasing towards the mouth of Loch Sunart. Data from Fisheries Research Services, Aberdeen, collected during 1990 to 1991.

and BWS which may not represent prevailing conditions experienced by the benthic foraminifera during test calcification.

Nevertheless, the total (live, dead and uncertain) data for *C. lobatulus* show two significant correlations with $\delta^{18}O$; a fairly moderate negative relationship with BWT ($r = -0.354$, $p = 0.047$), and a moderate positive relationship with BWS ($r = 0.404$, $p = 0.022$). The similarity in the strength of these correlations and likely inter-play of BWS and BWT on $\delta^{18}O$ may be problematic in the interpretation of palaeo-isotope records.

A marginally insignificant relationship occurs between $\delta^{13}C$ for total *C. lobatulus* and BWS ($r = 0.343$, $p = 0.055$), pointing to a strong possibility that the $\delta^{13}C$ of *C. lobatulus* can be used to reconstruct BWS, with enriched $\delta^{13}C$ typically occurring with higher BWS.

As expected, the dead only *C. lobatulus* samples have no significant relationships, though 2 marginally insignificant relationships occur between $\delta^{18}O$ and BWT ($r = -0.473$, $p = 0.075$) and water depth and $\delta^{13}C$ ($r = -0.497$, $p = 0.060$).

Bulimina marginata* and *Noniella turgida

Since only 'live' specimens were analysed, one would expect strong relationships to occur between isotopic composition and environmental variables, since environmental data collected at the time of sampling should be representative of conditions experienced by the benthic foraminifera during calcification. This is not true for nutrient concentration data or dissolved oxygen data which was collected ~ 10 years prior to this study.

The $\delta^{18}O$ values from *B. marginata* show no significant relationships with environmental variables (table 6.5), however a strong negative correlation ($r = -0.645$, $p = 0.044$) exists between *B. marginata* $\delta^{13}C$ and water depth.

The $\delta^{18}O$ of Loch Sunart *N. turgida* tests appear to be significantly influenced by % organic matter in the sediment ($r = 0.777$, $p = 0.014$) and a fairly strong yet marginally insignificant correlation exists between $\delta^{13}C$ and phosphate concentration ($r = 0.669$, $p = 0.070$). *N. turgida* $\delta^{18}O$ also shows a moderate and marginally insignificant relationship with BWS (($r = 0.636$, $p = 0.066$). The statistical significance of these relationships could be vastly improved by gaining more data and the $\delta^{13}C$ of *N. turgida* has potential for investigating palaeoproductivity.

6.3.4 Equilibrium calcite (Eq.$CaCO_3$)

Theoretical equilibrium calcite values ($\delta^{18}O_{Eq.CaCO3}$) were calculated from observed temperature and salinity at the site using the regional $\delta^{18}O$: salinity mixing line (Austin & Inall, 2002) and the Bemis *et al.* (1998) palaeotemperature equation (equation 5.4), along with the O'Neil *et al.* (1969) and Lynch-Stieglitz *et al.* (1999) palaeotemperature equations for comparison. The deviation ($\Delta\delta^{18}O$) of measured $\delta^{18}O$ from equilibrium calcite ($\delta^{18}O_{Eq.CaCO3}$) was determined using equation 5.5.

Generally, *A. beccarii* showed enriched $\delta^{18}O$ values with respect to $\delta^{18}O_{Eq.CaCO3}$ with dead and 'unspecified' data showing more variability than in the 'live' data (figure 6.6a), which may be expected due to 'snapshot' temperature and salinity data. Assuming the temperature and salinity data accompanying the 'live' data is representative of the calcifying conditions, 'live' *A. beccarii* ($n = 19$) shows a mean enrichment of $\Delta\delta^{18}O$ of 0.212 ± 0.453 ‰ with respect to $\delta^{18}O_{Eq.CaCO3.}$

'Live' *C. lobatulus* data ($n = 2$) show a mean $\Delta\delta^{18}O$ of -0.309 ± 0.404 ‰. To boost the sample numbers, the uncertain data was added to the live samples to give a mean $\Delta\delta^{18}O$ of -0.278 ± 0.354 ‰ ($n = 17$). Thus, measured $\delta^{18}O$ values of *C. lobatulus* are consistently depleted in ^{18}O with respect to $\delta^{18}O_{Eq.CaCO3}$ (figure 6.6b). *B. marginata* show a mean $\Delta\delta^{18}O$ of 0.55 ± 0.327 ‰ ($n = 10$), indicating that measured $\delta^{18}O$ is isotopically heavier than $\delta^{18}O_{Eq.CaCO3}$ and *N. turgida* appears to calcify nearest to $\delta^{18}O_{Eq.CaCO3}$ with a mean $\Delta\delta^{18}O$ of 0.171 ± 0.308 ‰ (figure 6.6c).

All the taxa have 'live' specimens collected in April, when BWT is at it's minimum and approximately 5°C cooler than during the warm autumn (August-November) months (see chapter 3). These April data fall below theoretical $\delta^{18}O_{Eq.CaCO3}$,

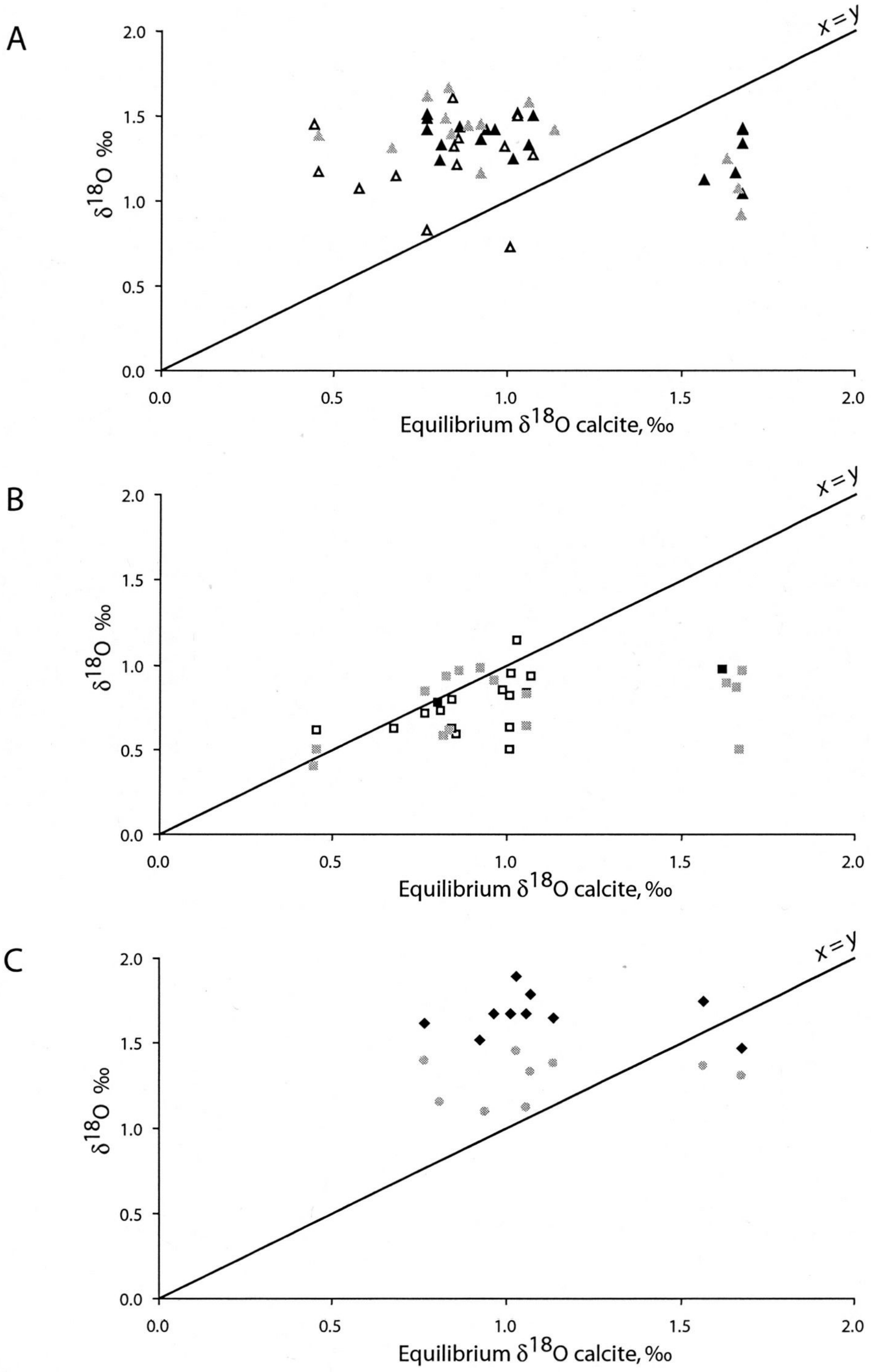

Figure 6.6 Equilibrium $\delta^{18}O$ calcite (calculated using observed bottom water salinity and temperature) determined using the Austin & Inall (2002) regional $\delta^{18}O$: salinity mixing line and the Bemis *et al.,* (1998) palaeotemperature equation, and the measured $\delta^{18}O$ values for (A) *Ammonia beccarii,* (B) *Cibicides lobatulus,* (C) 'live' *Bulimina marginata* (black diamonds) and 'live' *Noniella turgida* (grey circles). In graphs A and B, 'live' specimens are denoted by black shapes, 'dead' specimens unfilled shapes and specimens with 'unspecified' life status are shown by grey shapes. The relationship of $x = y$ is also shown (black line).

displaying negative $\Delta\delta^{18}O$ values, even for *A. beccarii*, *B. marginata* and *N. turgida* which tend to be isotopically enriched in ^{18}O with respect to $\delta^{18}O_{Eq.CaCO3}$. When these April data are excluded (except for 'live' specimens) the mean $\Delta\delta^{18}O$ changes for each species. *C. lobatulus* has a mean $\Delta\delta^{18}O$ of -0.111 ± 0.170 ‰ (n = 27), *A. beccarii* has a mean $\Delta\delta^{18}O$ of 0.495 ± 0.15 ‰ for live samples only (n = 13) and a mean $\Delta\delta^{18}O$ of 0.544 ± 0.188 ‰ for live and uncertain samples. *B. marginata* has a mean $\Delta\delta^{18}O$ of 0.690 ± 0.122 ‰ (n = 8). A 2-sample t-test shows there is no statistical difference between the 'winter' and 'summer' data for *N. turgida* (t = 0.16, p = 0.89), suggesting *N. turgida* calcifies relatively close to oxygen isotopic equilibrium throughout the year.

6.3.5 Determining depth habitats from stable carbon isotopic compositions of 'live' benthic foraminifera

Comparison of stable carbon isotopic compositions of 'live' benthic foraminifera can yield important information on the depth habitat of taxa (e.g. McCorkle *et al.,* (1990). Table 6.8 shows both oxygen and carbon stable isotope compositions for live benthic foraminifera taken from the same Loch Sunart surface sediment samples with corresponding environmental data. The $\delta^{18}O$ of benthic foraminifera are influenced by vital effects (section 6.3.4), hence although there may be some relationship between $\delta^{18}O$ and depth habitat (figure 6.7 and Bemis *et al.* 1998) it is too complex to be addressed in this study. Conversely, the relationship between habitat depth and $\delta^{13}C$ is well documented (section 6.1.5.1), thus only $\delta^{13}C$ will be discussed here.

Carbon isotopic compositions (along with the mean values) for all four species can be seen in figure 6.8. There are large intraspecific variations in the range of $\delta^{13}C$ isotope values, with *C. lobatulus* showing the largest range (1.28 ‰) and *N. turgida* the smallest range (0.42 ‰). *A. beccarii, B. marginata* and *N. turigda* all have negative $\delta^{13}C$ values, with means of -1.31 ± 0.19 ‰, -0.59 ± 0.32 ‰ and -1.85 ± 0.14 ‰ respectively, whilst *C. lobatulus* is the only species with enriched (positive) $\delta^{13}C$ values ranging from 0.39 to 1.67 ‰, with a mean $\delta^{13}C$ value of 1.27 ± 0.44 ‰.

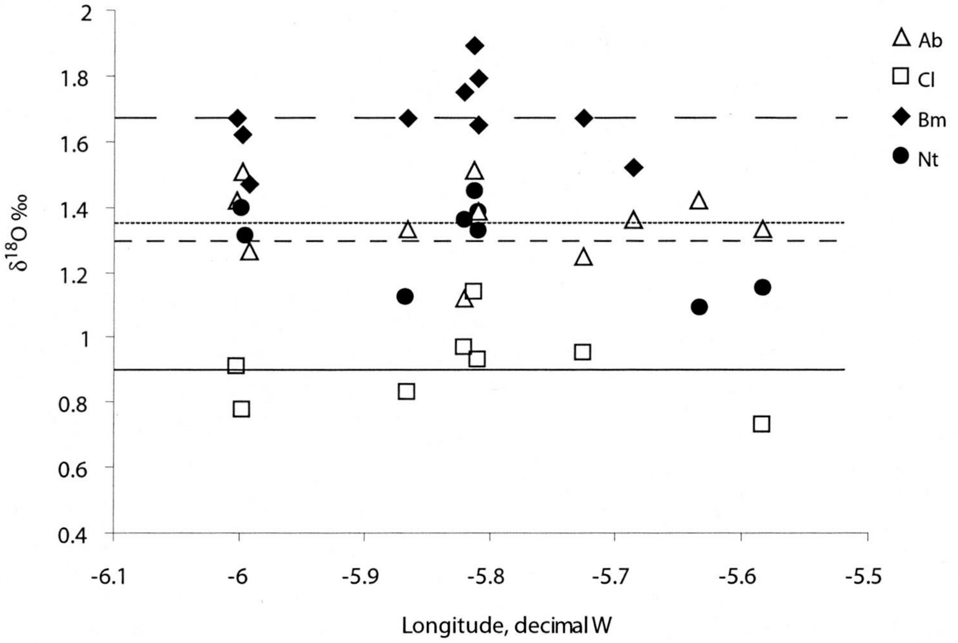

Figure 6.7 Measured $\delta^{18}O$ (symbols) and mean values (lines) of 'live' *Ammonia beccarii* (unfilled triangles and dotted line), 'live and unspecified life status' (i.e. not identified as dead) *Cibicides lobatulus* (white squares, solid line), 'live' *Bulimina marginata* (black diamonds, long dashed line) and 'live' *Nonionella turgida* (black circles, short dashed line) from Loch Sunart surface sediments collected in June 2001/2002. Samples are arranged by longitudinal position.

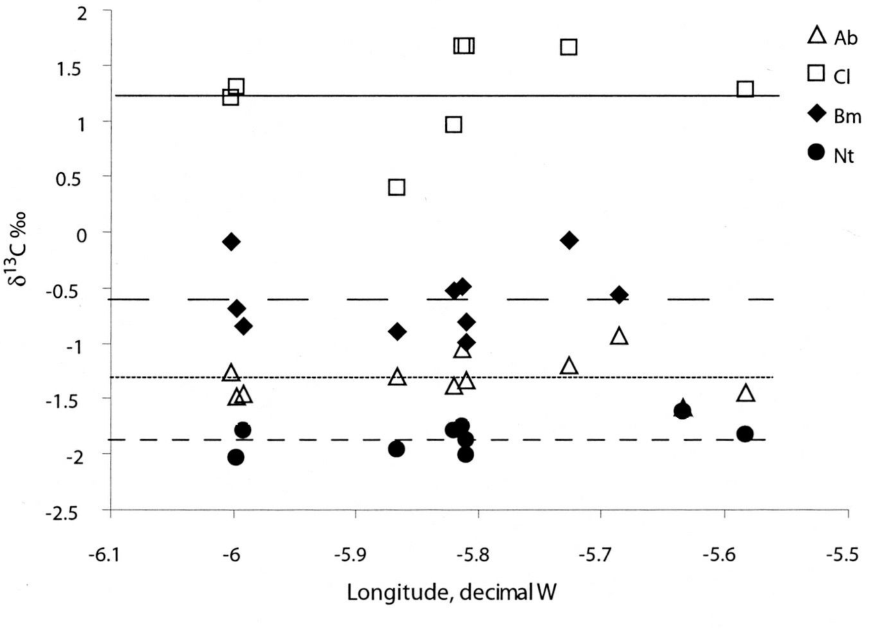

Figure 6.8 Measured $\delta^{13}C$ (symbols) and mean values (lines) of 'live' *Ammonia beccarii* (unfilled triangles and dotted line), 'live and unspecified life status' (i.e. not identified as dead) *Cibicides lobatulus* (white squares, solid line), 'live' *Bulimina marginata* (black diamonds, long dashed line) and 'live' *Nonionella turgida* (black circles, short dashed line) from Loch Sunart surface sediments collected in June 2001/2002. Samples are arranged by longitudinal position.

6.4 DISCUSSION

6.4.1 Ontogenetic influence on test composition or 'seasonal effect'?

Significant negative relationships between $\delta^{13}C$ and number of specimens per µg for modern Loch Sunart *A. beccarii* (figure 6.4) suggests a trend of isotopically enriched $\delta^{13}C$ values with larger specimens. This is in good agreement with Schmiedl *et al.*, (2004), who reported positive logarithmic correlations between the test size of deep-sea *Uvigerina mediterranea* (from the Western Mediterranean Sea) and stable isotopic compositions, which they attributed the enrichment to a slow-down of metabolic activity in later life stages, as seen in planktonic foraminifera (e.g. Spero & Lea 1996). Growth in benthic foraminifera tends to slow down after the rapid calcification rates during the juvenile life stage (Murray 1991), and it is likely that kinetic isotopic fractionation affects test composition (McConnaughey 1989a). The lack of a significant $\delta^{13}C$: test size relationship for 'live' *A. beccarii* is likely due to the paucity of 'small ratios' in the data, i.e. samples containing a few large tests rather than a physiological process. Despite the establishment of a definite size influence on the stable isotopic composition of benthic foraminifera from Loch Sunart being hindered by the paucity of data, it is also possible that the geochemical composition of foraminiferal tests reflect a 'seasonal effect' rather than an ontogenetic effect (section 6.4.1.1), and to clearly separate the two influences on test isotopic composition is likely to be difficult.

However, large isotopic variations seen between single specimens and multiple specimen analyses in this study agree with previous suggestions (e.g. Vinot-Bertouille & Duplessy 1973; Boyle 1995) that isotopic analyses are best carried out on samples containing either more than one individual or from a homogenised sample in order to generate an 'average' value. Intraspecific isotopic compositions from benthic foraminifera can vary by as much as 2 ‰ (Vinot-Bertouille & Duplessy 1973; Vincent *et al.*, (1981), highlighting a need for caution when selecting benthic foraminifera specimens for isotopic analysis. For instance, the 0.32 ‰ difference between *C. lobatulus* $\delta^{18}O$ data using 1 specimen and 6 specimens from sample 210 (table 7.3), equates to a temperature difference of ~ 1.5 °C (Bemis *et al.* 1998), whilst the 0.13 ‰ $\delta^{18}O$ difference between 6 and 20 *C. lobatulus* specimens yields a smaller potential temperature error of 0.62 °C. The down-core isotope record for cores GC023 and SC023 were obtained using > 5 *C. lobatulus* specimens, thus variations in $\delta^{18}O$ are more likely to reflect changes in environmental conditions rather than possible ontogenic or 'seasonal' effects.

Shelf-seas, notably in the mid to high latitudes, typically experience seasonal heating cycles (chapter 3) and since benthic foraminifera may live from a few months up to a few years (e.g. Lee *et al.*, 1991), it is possible that the stable isotopic compositions of shelf sea benthic foraminifera record different parts of the seasonal temperature cycle (e.g. Allison & Austin, 2003). This may explain the disparity of results between shelf sea benthic foraminifera (e.g. the Mediterranean and Loch Sunart) appearing to show ontogenic effects on isotopic composition, whereas deep-sea taxa living in stable oceanographic conditions do not. For example, small *A. beccarii* captured 'live' in June are likely to have grown following spring reproduction (chapter 5), thereby recording isotopically enriched $\delta^{18}O$ associated with cooler BWT (chapter 3). Large 'live' *A. beccarii* on the other hand, may have grown following reproduction during warmer autumn BWT the year before collection. Refer to section 8.4.6 for a discussion on the 'seasonal effect' in benthic foraminifera.

6.4.2 Environmental influences of isotopic composition

When exploring abiotic influences on shell chemistry, it is advantageous to use 'live' specimens, since these should be calcifying in the water mass from which hyrdographic data may be collected. The dearth of 'live' specimens in Loch Sunart surface sediments (chapter 5) hinders the interpretation of isotope values and correlations with environmental variables. Additionally, Loch Sunart shows a seasonal temperature cycle (chapter 3) and fjordic hydrography may change quickly (e.g. deep water renewal events), therefore temperature and salinity measurements are often a 'snapshot' of possible conditions in which 'live' foraminifera may have calcified (section 6.3.3). For example 'dead' deep-sea benthic foraminifera living in stable environmental conditions have been shown to have isotopic compositions similar to 'live' specimens from the same sample (e.g. McCorkle *et al.*, 1990), however shelf sea benthic foraminifera tend to show more variability (Scourse *et al.*, 2004) with $\delta^{18}O$ of 'live' specimens often isotopically heavier than dead specimens.

6.4.2.1 Temperature and Salinity

Since *C. lobatulus* is used to generate the fossil isotope records from Loch Sunart, the discussion will focus on this species. As mentioned previously, low numbers of 'live' *C. lobatulus* in the data set prohibits the correlation of 'live only' isotopic compositions and environmental factors, thus all the data presented here uses the full, larger data sets comprising of 'dead' specimens and specimens which have no specified life status.

C. lobatulus conforms to expected temperature dependent oxygen isotopic fractionation (e.g. Bemis *et al.* 1998), i.e. isotopic enrichment with cooler BWT, displaying a moderate negative correlation between $\delta^{18}O$ and BWT ($r = -0.354$, $p = 0.047$). A number of samples which may not have been collected live in April have low BWTs associated with them, and when these April data are removed (the 'live' April sample remains) the $\delta^{18}O$:BWT strengthens and becomes more significant ($r = -0.565$, $p = 0.006$), as does the $\delta^{18}O$: BWS relationship ($r = 0.452$, $p = 0.016$). The similar magnitude of these correlation coefficients along with their opposite trends exemplifies how the inter-play of $\delta^{18}O$ isotopic fraction due to temperature and salinity may potentially pose problems regarding the interpretation of palaeoisotope records.

If the fossil *C. lobatulus* $\delta^{18}O$ isotope record is to be used to reconstruct temperatures, then this 'interplay' must be unravelled. The 0.62 ‰ range in $\delta^{18}O$ measured in fossil *C. lobatulus* from core GC023 (chapter 8) reflects either a ~ 3 °C variation in temperature (Bemis *et al.,* 1998) or a salinity change of around 3.4 (Austin & Inall, 2002) or a combination of both. Since BWS appears to remain relatively stable at the main basin core site (chapter 3), irrespective of DWREs in the inner basin (Gillibrand *et al.,* 1995), or extreme climatic forcing (Gillibrand *et al.,* 2005), it is extremely unlikely that main basin BWS would fluctuate by nearly 3.4.

On the other hand, the long-term Millport marine temperature series, which the seasonal temperature cycle recorded in Loch Sunart is strongly coupled with (chapter 3), exhibits an inter-annual May-October (typical period of test calcification) temperature range of 2.66 °C (10.7 – 13.35 °C). This demonstrates that the $\delta^{18}O$ of fossil *C. lobatulus* in Loch Sunart are likely to reflect temperature changes rather than salinity changes. The hypothesis that foraminiferal calcite from Loch Sunart likely reflects temperature changes rather than salinity changes is illustrated in figure 6.9, which clearly shows how the seasonal heating cycle of Loch Sunart basin water translates into seasonality in the theoretical $\delta^{18}O_{Eq.CaCO3}$ curve, and also how inter-annual temperature differences can impact upon $\delta^{18}O_{Eq.CaCO3}$. The higher variability in inner basin $\delta^{18}O_{Eq.CaCO3}$ highlights the significance of salinity changes associated with freshwater inputs and DWREs; since the inner and main basin of Loch Sunart show similar seasonal heating cycles, the gradient between main basin $\delta^{18}O$ and inner basin $\delta^{18}O$ could potentially be used to examine past environmental change and palaeocirculation of the inner basin due to climatic forcing.

6.4.3 $\delta^{18}O$:$\delta^{13}C$ relationship in *C. lobatulus*

C. lobatulus is the only species presented here with a significant positive $\delta^{18}O$:$\delta^{13}C$ relationship ($r = 0.420$, $p = 0.017$, $n = 32$), suggesting kinetic fractionation (rather than metabolic fractionation) dominates during calcification (McConnaughey 1989c), thus the species is more likely to calcifiy towards isotopic equilibrium with both $\delta^{18}O$ water and $\delta^{13}C$ DIC (McConnaughey et al. 1997). This positive $\delta^{18}O$:$\delta^{13}C$ relationship agrees with those previously reported for shelf sea benthic foraminifera (Vinot-Bertouille and Duplessy 1973). Linear positive $\delta^{18}O$:$\delta^{13}C$ correlations are thought to reflect incomplete isotopic fractionation largely due to fast growth rates (Vincent et al. 1981), suggesting shelf sea benthic foraminifera grow faster than deep-sea benthic foraminifera, which typically tend towards negative $\delta^{18}O$:$\delta^{13}C$ correlations (e.g. Woodruff et al. 1980). This may explain why the isotopic relationships presented here do not agree with those previously reported for deep-sea benthic foraminifera, and also exemplifies the potential of obtaining 'seasonal' records from large, mature foraminifera (e.g. Allison & Austin, 2003).

6.4.4 Equilibrium calcite

The majority of isotope studies have been carried out on deep-sea benthic foraminifera (see chapter 1), and since *C. lobatulus* is predominantly a shelf sea species, little literature exists on the isotopic equilibrium of this species.

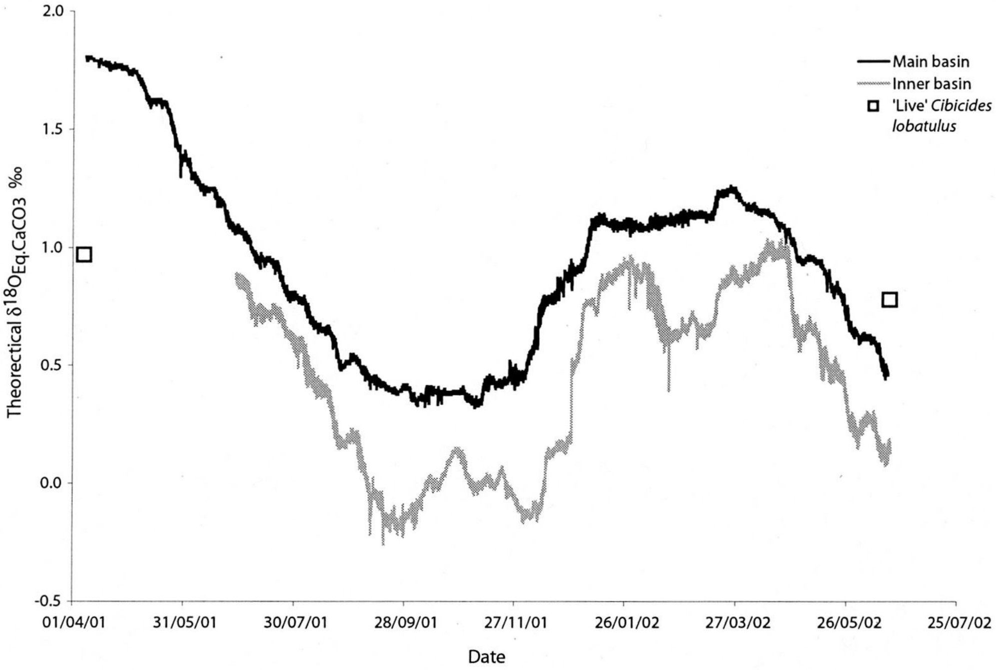

Figure 6.9 The theoretical range of equilibrium $\delta^{18}O$ calcite ($\delta^{18}O_{Eq.CaCO3}$) in Loch Sunart for the inner basin (grey line) and the main basin (black line) calculated using equations 5.2 to 5.5 (Hut, 1987; Bemis *et al.*,1998; Austin & Inall, 2002) and using the temperature and salinity data from moorings located at 40 m water depth in the main and inner basin (chapter 3). The effect of the seasonal heating cycle (chapter 3) on the $\delta^{18}O_{Eq.CaCO3}$ range can be clearly observed. The difference between the main basin and inner basin $\delta^{18}O_{Eq.CaCO3}$ reflects the differences in BWT and BWS, with respective values of 10.79 ± 1.93 °C and 32.8 ± 0.7 for the inner basin, and 10.69 ± 2 °C and 33.86 ± 0.44 for the main basin. The measured $\delta^{18}O$ o.f the two 'live' *Cibicides lobatulus* specimens from Loch Sunart are also shown (white squares). The specimen collected live in June lies close to the theoretical range of equilibrium $\delta^{18}O$ calcite ($\delta^{18}O_{Eq.CaCO3}$) whilst the live specimen collected in April exhibits $\delta^{18}O$ depleted with respect to $\delta^{18}O_{Eq.CaCO3}$, suggesting the majority of the test calcified in warmer bottom waters.

6.4.4.1 Stable carbon isotopes

Generally, the *Cibicidoides* family is considered to calcify close to isotopic equilibrium with $\delta^{13}C_{DIC}$ of seawater (e.g. Woodruff *et al.* 1980; Belanger *et al.* 1981; Wilson-Finelli *et al.* 1998), hence it is likely that *C. lobatulus* from Loch Sunart reflects bottom water $\delta^{13}C_{DIC}$. Unfortunately, data does not exist to compare Loch Sunart *C. lobatulus* $\delta^{13}C$ to observed δ13C$_{DIC}$, however the mean $\delta^{13}C$ of Loch Sunart *C. lobatulus* is 1.20 ± 0.4 ‰, and this is similar to 'typical' $\delta^{13}C$ values of 1-1.5 ‰ reported for North Atlantic (60 °N) surface waters (<500m). This similarity supports the notion that *C. lobatulus* (both modern and fossil) from Loch Sunart represents the $\delta^{13}C_{DIC}$ of the bottom water, albeit with the possibility of underestimating the values by up to approximately 0.5-0.7 ‰ (Mackensen *et al.*, 2000)

6.4.4.2 Stable oxygen isotopes

Grossman (1984b) and McCorkle *et al.*, (1990) demonstrated that species living in low oxygen sediments (i.e. deep dwelling infaunal species) tended to be closer to oxygen isotopic equilibrium than shallow infaunal taxa. The data shown in figure 6.10 agrees with this hypothesis, with the deep infaunal *N. turgida* showing $\delta^{18}O$ values closer to isotopic equilibrium than the shallower dwelling taxa, i.e. *A. beccarii* and *B. marginata*. The exception is the relatively small disequilibria displayed by the epifaunal species *C. lobatulus*.

Data from Loch Sunart benthic foraminifera were expected to resemble results from the Celtic Sea (shelf sea) rather than data from deep-sea environments. Scourse *et al.*, (2004) reported a large oxygen isotopic disequilibria for 'live' Celtic Sea *C. lobatulus* (mean $\Delta\delta^{18}O$ of -0.92 ± 0.56 ‰) and found 'live' *A. batavus* (a close relation to *A. beccarii*) to calcify close to isotopic equilibrium with $\delta^{18}O_{water}$ ($\Delta\delta^{18}O = -0.05 \pm 0.22$ ‰). Conversely, *A. beccarii* from Loch Sunart show a large oxygen isotopic disequilibria with a mean $\Delta\delta^{18}O$ of 0.495 ± 0.15 ‰ (which is in good agreement with Vinot-Bertouille and Duplessy 1973), whilst *C. lobatulus* (live and dead) from Loch Sunart appear to calcify close to isotopic equilibrium with a mean $\Delta\delta^{18}O$ of -0.111 ± 0.170 ‰ (for warm BWT). This $\Delta\delta^{18}O$ value for *C. lobatulus* lies much closer to isotopic equilibrium with $\delta^{18}O_{Eq.CaCO3}$ than previously suggested, thereby agreeing well with the findings of Bemis *et al.*. (1998) and Lynch-Steiglitz *et al.*, (1999). The difference in calculated $\Delta\delta^{18}O$ for these two species is due to the palaeotemperature equation used to calculate equilibrium calcite.

When the Bemis *et al.,* (1998) equation is applied to the Celtic Sea *C. lobatulus* data, the $\Delta\delta^{18}O$ values move closer to isotopic equilibrium, with $\Delta\delta^{18}O$ of -0.63 ± 0.56 ‰. Scourse *et al.,* (2004) include, within the calculation of mean average $\Delta\delta^{18}O$, two *C. lobatulus* samples (one live and one dead) with negative $\delta^{18}O$ and $\delta^{13}C$ values, however *Cibicidoides* usually show enriched isotopic compositions relative to VPDB (e.g. figure 6.2). The calculated temperature for this sample is ~ 19.5 ± 0.1 °C (using both the O'Neil *et al.,* 1969 and the Bemis *et al.,* (1998) equation), which is anomalously high given the quoted observed maximum temperature of 14.2 °C for the sample water depth of 75m in the St Georges Channel. The authors saw no reason to exclude these samples (*pers comm.*, Prof. J. Scourse, 2004), however given the wealth of data showing positive stable isotope values (particularly with $\delta^{18}O$) for *C. lobatulus,* along with the unrealistically high calculated temperature from the samples, these data are likely to be anomalous and could be excluded. Although this does not bring the mean $\Delta\delta^{18}O$ as close to isotopic equilibrium as the Loch Sunart *C. lobatulus* data, it does shift the Celtic Sea $\Delta\delta^{18}O$ to -0.4 ± 0.29 ‰ (using the Bemis *et al.,* 1998 equation).

6.4.5 Which palaeotemperature equation to use for *C. lobatulus*?

The differences between the published $\Delta\delta^{18}O$ for *Cibicidoides* spp (and *A. beccarii*) and the $\Delta\delta^{18}O$ found in this study are influenced by the palaeotemperature equation used. Woodruff *et al.,* (1980), Belanger *et al.,* (1981), Graham *et al.,* (1981), Vilks & Deonarine (1988), McCorkle *et al.,* (1990); Rathburn *et al.,* (1996); McCorkle *et al.,* (1997), Schmiedl *et al.,* (2004) and Scourse *et al.,* (2004) all use the palaeotemperature equation given by O'Neil *et al.*, (1969) to calculate equilibrium $\delta^{18}O$ calcite:

$$T\ (^\circ C) = 16.9 - 4.38(\delta^{18}O_{\text{foram}} - \delta^{18}O_{\text{water}}) + 0.1(\delta^{18}O_{\text{foram}} - \delta^{18}O_{\text{water}})^2 \qquad (Eq\ 6.8)$$

This equation used synthetic carbonates precipitated at temperatures of 0-500°C (largely in water super-saturated with respect to CO_3^-) to derive a palaeotemperature equation. Shackleton (1974) modified this equation and calibrated it to the $\delta^{18}O$ of the deep infaunal species *Uvigerina peregrina.* The palaeotemperature equation derived by Bemis *et al.,* (1998) on the other hand was obtained through laboratory and field studies on planktonic foraminifera (using filtered seawater), hence is likely to be more 'realistic'. Bemis *et al.,* (1998) reported that core-top (deep-sea) *Cibicidoides* agreed well with the low-light equation (seen in equation 7.4) in temperatures <10°C, whereas the data from the deep infaunal species *Uvigerina peregrina* agreed more with the palaeotemperature equations of Shackleton (1974) and Erez & Luz (1983). This explains some of the discrepancy found in the comparison of data from Loch Sunart and the Celtic Sea data, since Scourse *et al.,* (2004) use the O'Neil *et al.,* (1969) equation, thus the infaunal *A. beccarii* from the Celtic Sea appears to be close to isotopic equilibrium whilst *C. lobatulus* has high disequilibria. Lynch-Stieglitz *et al.*, (1999) provide the most recent regression palaetotemperature equation from modern *Cibicidoides* and *Planulina,* which is statistically similar to the laboratory 'fractionation' derived palaeotemperature equations of Kim & O'Neil (1997) and the Bemis *et al.,* (1998). The calibration of a palaeotemperature equation to empirical data often results in 'offsets' occurring over a given temperature range (e.g. table 1 in Bemis *et al.,* 1998) and these offsets must be taken into account when comparing palaeotemperature equations (*pers comm.,* Dr. U. Ninneman, 2004).

The difference between the Bemis *et al.,* (1998) and O'Neil *et al.,* (1969) equations and their respective calculations of isotopic equilibria for the infaunal and epifaunal species is likely to be due to a carbonate ion effect down the sediment profile (Bemis *et al.,* 1998). This appears plausible especially since $\delta^{13}C$ compositions of benthic foraminifera show that infaunal taxa calcify in different porewater chemistry than epifaunal taxa (e.g. McCorkle *et al.,* 1997). Spero *et al.*, (1997) demonstrate a carbonate ion (pH) effect on planktonic foraminiferal test isotopic composition, and pH has seen to be important in the isotopic fractionation of deep-sea corals (Adkins *et al.,* 2003). Sediment porewater pH profiles do not exist for Scottish fjords, however Hanson & Donaghay 1998 show porewater pH profiles in a North American stratified coastal fjord typically decrease with sediment depth. Since a 0.2 increase in pH is thought to equate to a $\delta^{18}O$ depletion of ~0.22 ‰ (Zeebe, 1999), one would expect the $\delta^{18}O$ of deep infaunal taxa to differ from the $\delta^{18}O$ of epifaunal benthic foraminifera. Therefore, using the same palaeotemperature equation to determine the oxygen isotopic equilibrium of both infaunal and epifaunal taxa which calcify in such different environments is likely to be unrealistic, and could introduce significant errors into palaeotemperature reconstructions, since 0.22 ‰ approximately reflects a 1 °C change. However, few studies have focussed upon the carbonate ion effect in benthic foraminifera and to do so was beyond the means and scope of this project; future work could expand empirical data in this relatively neglected area.

Given the similarity of the palaeotemperature equations of Kim *et al.,* (1997), Bemis *et al.,* (1998) and the Lynch-Stieglitz *et al.,* (1999) and the demonstration by the latter two that the *Cibicidoides* group calcifies close to isotopic equilibrium with the $\delta^{18}O$ of seawater, we may assume that *C. lobatulus* from Loch Sunart reliably records the $\delta^{18}O$ signal of the bottom water. The Lynch-Stieglitz *et al.,* (1999) equation rather than the Bemis *et al.,* (1998) equation is used in this study as the BWT range experienced in Loch Sunart falls within the studied temperature range (5-27 °C) of Lynch-Stieglitz *et al.,* (1999), and this equation yields the smallest difference between observed temperature and predicted temperature for *C. lobatulus* (figure 6.11).

The demonstrated low disequilibria of *Cibicidoides group* using species specific palaeotemperature equations such as Bemis *et al.,* (1998) and Lynch-Stieglitz *et al.,* (1999) has implications for future isotopic work on benthic foraminifera. The near-isotopic equilibrium of this species to both theoretical $\delta^{18}O_{Eq.CaCO3}$ and $\delta^{13}C_{DIC}$ would enable a complete 'view' (or reconstruction) of bottom water geochemistry to be gained, rather than relying on taxa living within the porewater environment. Additionally, future laboratory and research costs could be significantly reduced since only one species, *Cibicidoides,* could be used to obtain both the $\delta^{18}O$ and a $\delta^{13}C$ isotope record, which additionally, is measured simultaneously on the mass spectrometer.

6.4.6 Seasonal effect in benthic foraminifera

Scourse *et al,* (2004) reported a seasonal effect in isotopic data from Celtic Sea benthic foraminifera, with foraminifera typically calcifying during periods of the year with warmer bottom waters. For example, Celtic Sea *C. lobatulus* and *B. marginata* both tend to calcify during the warm bottom water temperatures of peak late summer,

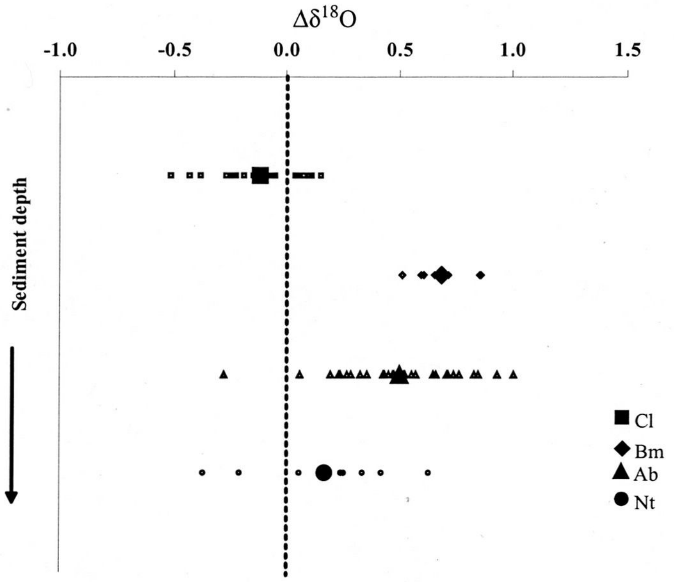

Figure 6.10 Mean (large symbols) deviations $\Delta\delta^{18}O$ away from equilibrium calcite for 'live' and 'dead' *Ammonia beccarii* (triangles), *Cibicides lobatulus* (squares), *Bulimina marginata* (diamonds) and *Nonionella turgida* (circles). Small symbols show individual measurements collected in June/July 2001 and June 2002. Since it is likely that taxa calcify during the warm BWT of summer, winter (April) data has been excluded. The data has been plotted against the depth habitat within the sediment as suggested by the $\delta^{13}C$ for each species. Refer to section 6.4.5.2.

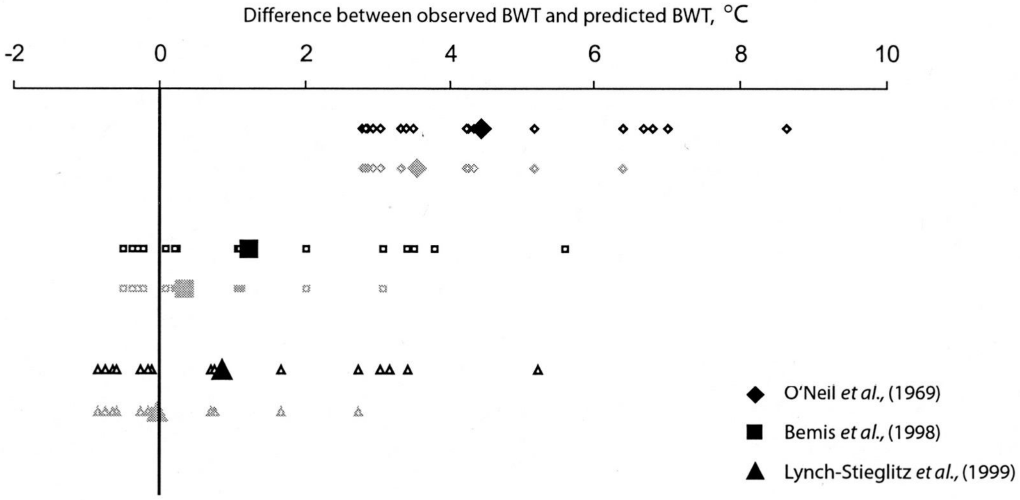

Figure 6.11 Mean (large symbols) differences between observed temperature and predicted temperature for live or unspecified life status, *Cibicides lobatulus* using the palaeotemperature equations of O'Neil *et al.*, (1969), Bemis *et al.*, (1998) and Lynch-Stieglitz *et al.*, (1999). Small symbols show individual measurements. The black symbols show values for all live specimens including April samples. The grey symbols show values excluding April samples (with the exception of the one 'live' April sample), since it is likely that taxa calcify during the warm BWT of summer.

whereas *A. batavus* calcifies in late spring (cooler BWT) in mixed water masses and late summer (warmer BWT) in stratified water columns, probably as a response to phytodetrital food inputs.

In Loch Sunart's main basin, higher $\delta^{18}O_{Eq.CaCO3}$ values occur with cool BWT during the winter months (i.e. January to May), whilst the maximum BWT occurring in late summer/early autumn (late September to October) yield low $\delta^{18}O_{Eq.CaCO3}$ of around 0.5 ‰ (figure 6.9). Figure 6.12 shows the difference between observed BWT (recorded during the collection of the largely 'live benthic foraminiferal specimens) and predicted BWT (using the Lynch-Stieglitz, *et al.,* 1999 and Austin & Inall, 2002 equations).

The statistical similarity between the mean BWT for summer and winter *N. turgida* $\delta^{18}O$ data suggests this species calcifies close to isotopic equilibrium throughout the year (figures 6.10 and 6.12). However, the predicted BWT derived from the $\delta^{18}O$ of live 'winter' samples from *A. beccarii* and *C. lobatulus* (and possibly *B. marginata*) all have higher BWT, i.e. measured $\delta^{18}O$ values lying well below the expected $\delta^{18}O_{Eq.CaCO3}$ (figures 6.6 and 6.12). The similarity of the predicted winter BWT (or $\Delta\delta^{18}O$) to the predicted summer BWT for these taxa, point to a possibility that 'live' tests collected in the 'winter' months with cool BWT actually calcified during warmer BWT. For example, large 'live' *A. beccarii* samples collected in April (during minimum BWT) clearly yield calculated temperatures indicative of summer BWT (figure 6.12). Cytoplasm from benthic foraminifera living in infaunal habitats have been shown to retain rose Bengal staining several months following death, with cytoplasm generally decomposing at a slower rate in low oxygen conditions (Jorissen *et al.*, 1995), however this is unlikely to explain the temperature differences seen in figure 6.12. Owen *et al.,* (2002) report decreased growth rates in the *Pecten maximus* scallop during minimum BWT, and it may be possible that benthic foraminifera also experience inhibited calcification during cooler BWT, thereby remaining 'live' over winter yet preserving test $\delta^{18}O$ values representing 'summer' BWT.

Predicted BWT calculated from measured $\delta^{18}O$ of 'live' taxa collected during the winter months from Loch Sunart often display calculated BWTs much higher than those observed in Loch Sunart during the summer (June/July) collection periods

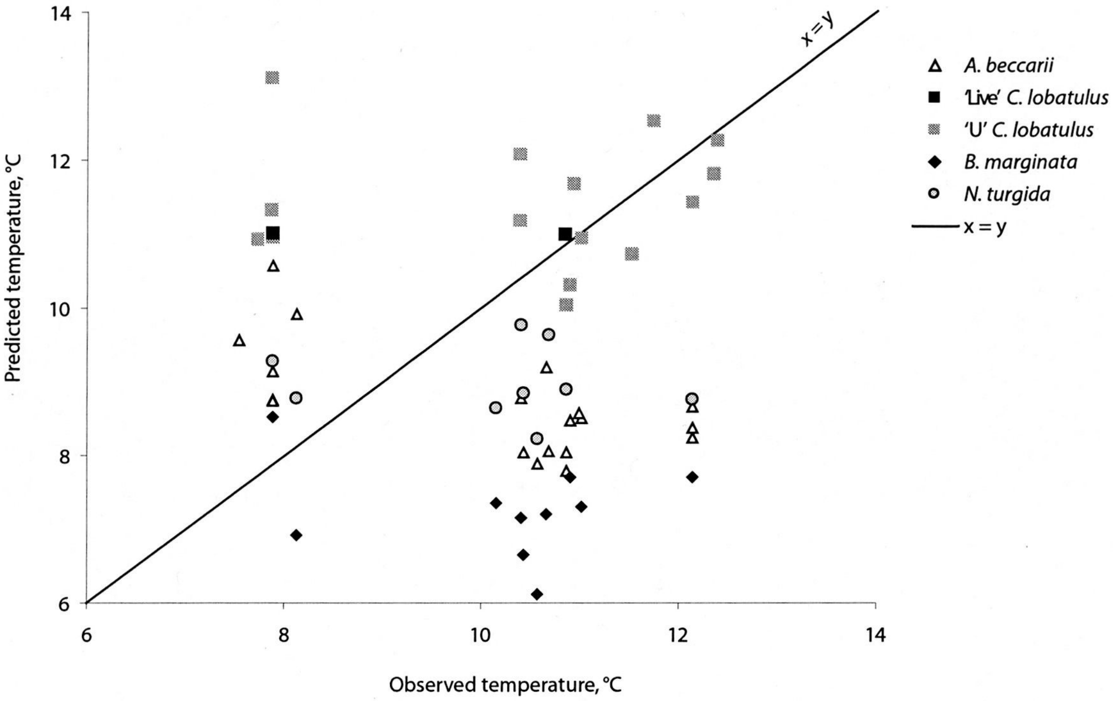

Figure 6.12 . Observed temperatures and calculated temperatures (using the Lynch-Steiglitz *et al.*, 1999 and Austin & Inall, 2002 equations) for live *Ammonia beccarii* (unfilled triangles), *Cibicides lobatulus* (squares), 'live' *Bulimina marginata* (diamonds) and 'live' *Nonionella turgida* (circles). Since the *Cibicides lobatulus* data for Loch Sunart includes only two live samples (black squares), specimens which have unspecified life status (i.e. possibly collected 'live'; grey squares) have also been included. The straight line represents x = y, i.e. calcification of benthic foraminiferal test in isotopic equilibrium with the theoretical equilibrium stable oxygen isotopic composition of seawater.

(figure 6.12). For example, the measured $\delta^{18}O$ of *C. lobatulus* from sample 34, collected from a BWT of 7.88 °C at 70 m water depth in April, 2001, yields a predicted BWT of 13.45 °C and this agrees well with the maximum temperature of 13.36 °C recorded at 40 m water depth (likely reflecting BWT throughout; chapter 3) in Loch Sunart during October, 2002. This suggests benthic foraminifera from Loch Sunart tend to calcify during peak BWT in October/November/December, which agrees well with the findings of Scourse *et al.,* (2004). Benthic foraminifera from Norwegian fjords have also been found to calcify around November (*pers. comm.,* Dr. G. Mikalesen, 2004).

6.4.7 Gaining information from benthic foraminifera test $\delta^{13}C$

Porewater $\delta^{13}C$ profiles and the $\delta^{13}C$ of test carbonate can be used to estimate the calcification depths of selected benthic foraminifera species (e.g. McCorkle *et al.,* 1990). Porewater $\delta^{13}C$ gradients are site specific and primarily dependent on the carbon rain rate and the sediment depth at which organic matter decomposes (McCorkle *et al.,* 1985). Unfortunately, no water column or sediment $\delta^{13}C$ profiles are available from Scottish sea lochs at present (*pers. comm.,* Dr. H. Kennedy, 2004).

6.4.7.1 Relative living depths of Loch Sunart benthic foraminifera

Figure 6.13 shows the potential microhabitat depths of the studied benthic foraminifera species, using the well established porewater $\delta^{13}C$: $\delta^{13}C_{CaCO3}$ relationship (e.g. McCorkle *et al.,* 1990). The porewater profile is from a station CH90-BC5 (McCorkle et al. 1997), a deepwater site (1477m) on the NE American continental margin. It is acknowledged that $\delta^{13}C$ porewater gradients are likely to differ in fjordic environments (section 6.1.5); this profile was used due to the bottom water $\delta^{13}C$ being comparable to that suggested for Loch Sunart (via the mean $\delta^{13}C$ from *C. lobatulus*). Although a fjordic $\delta^{13}C$ porewater profile may be steeper, the mean $\delta^{13}C$ from Loch Sunart benthic foraminifera fit well on the curve with respect to species reported living depths (chapter 5) and the depth of the sediment layer obtained for sampling (1-1.5 cm).

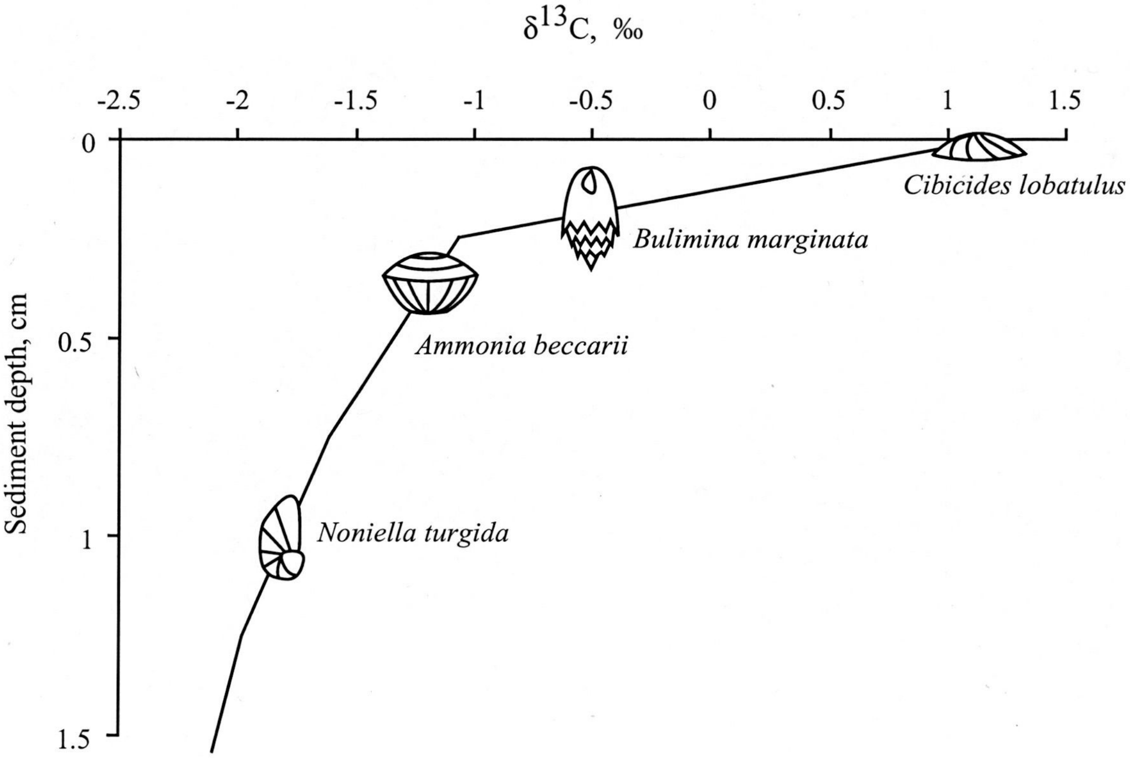

Figure 6.13. Hypothesised living depths of *Ammonia beccarii, Bulimina marginata, Cibicides lobatulus* and *Nonionella turgida*, as estimated from the intersection of their mean $\delta^{13}C$ values with the $\delta^{13}C$ porewater profile (solid line) taken from station CH90-BC5 (McCorkle et al. 1997), a deepwater site (1477m) on the NE American continental margin.

Cibicides lobatulus

Cibicidoides taxa are generally regarded as having an epifaunal life mode (Corliss 1985), although there is some debate around this (e.g. Bornmalm *et al.*, 1997; McCorkle *et al.,* 1997). The *C. lobatulus* specimens from Loch Sunart have the most positive (enriched) $\delta^{13}C$ values (mean $\delta^{13}C$ of 1.27 ± 0.44 ‰) of the benthic species studied here, suggesting the shallowest habitat depth (figure 6.13). Since the $\delta^{13}C$ of *Cibicidoides* taxa is likely to reflect the $\delta^{13}C$ of bottom water (sections 6.1.5 and 6.4.5.1), this suggests Loch Sunart bottom waters are likely to have an average $\delta^{13}C_{DIC}$ of 1.27 ± 0.44 ‰.

Bulimina marginata

The mean $\delta^{13}C$ value of *Bulimina marginata* points to a relatively shallow habitat depth (figure 6.13), which agrees well with Buzas *et al.*, (1993) and Gustafsson & Nordberg (2001), who placed *B. marginata* as a shallow infaunal species living at the sediment-water interface. Mackensen *et al.*, (2000), suggested *Bulimina aculeata* (and possibly other *Bulimina* taxa) are extremely mobile within sediments, seeking optimal micro-environmental conditions. McCorkle *et al.*, (1997) suggested that near-constant $\delta^{13}C$ isotopic signal seen with sediment depth for species such as *B. aculeata* may reflect calcification in a small sub-zone of the microhabitat range. Hence, although the $\delta^{13}C$ values presented here for *B. marginata* suggest a shallow infaunal habitat (figure 6.13), this may represent the calcification depth of the species and not necessarily the living depth.

Ammonia beccarii

Buzas *et al.,* (1993) showed a summary of the sediment depths at which *A. beccarii* and *A. batavus* have been found living and due to the wide range of depths, they concluded that a definite microhabitat for this taxa could not be established. Loch Sunart *A. beccarii* has $\delta^{13}C$ values with a mean of -1.31 ± 0.19 ‰, suggesting an intermediate infaunal habitat (figure 6.13).

Noniella turgida

N. turgida has an average $\delta^{13}C$ value of -1.85 ± 0.14 ‰ representing the most depleted carbon isotopic composition of the 4 taxa, hence the deepest living habitat (figure 6.13). *N. turgida* tests are often coloured yellow, which may be indicative of chloroplast husbandry and Bernhard & Bowser (1999) showed that *Noniella labrodorica* and *N. stellata* (close relations to *N. turgida*) sequestered chloroplasts in oxygen depleted environments. Gustafsson & Nordberg (2001) also found a significant positive moderate correlation between *N. turgida* populations and chlorophyll *a*. Phytoplankton tend to have depleted $\delta^{13}C$ values (~ -20 ‰) due to the preferential uptake of the lighter $^{12}CO_2$ during photosynthesis (Rohling and Cooke 1999). If *N. turgida* in Loch Sunart surface sediments are indeed sequestering chloroplasts, then the depleted $\delta^{13}C$ values seen in the test carbonate could be influenced by the assimilation of isotopically light $\delta^{13}C$ from the phytoplankton, hence the $\delta^{13}C$ values may not be reflecting true microhabitat depth but rather influences of metabolic isotopic fractionation.

6.4.7.2 Estimating porewater $\delta^{13}C$ gradients for Loch Sunart

If *C. lobatulus* reflects the $\delta^{13}C$ of the bottom water and *N. turgida* is the deepest dwelling taxon, then the observed bottom water – porewater $\delta^{13}C$ difference ($\Delta\delta^{13}C$) can be calculated for the top 1 – 1.5 cm of Loch Sunart surface sediments by;

$$\Delta\delta^{13}C = \text{mean } \delta^{13}C_{\text{Cibicides lobatulus}} - \delta^{13}C_{\text{Noniella turgida}} \qquad (Eq\ 6.9)$$

This gives a mean $\Delta\delta^{13}C$ of ~ 3.12 ‰, which is steeper than the majority of deep-sea open ocean sites (see above), but comparable to sites from the western North Atlantic with similar bottom water compositions and shallow oxygen penetration (McCorkle & Emerson 1988).

All the Loch Sunart benthic foraminiferal taxa in this study exhibit negative correlations between $\delta^{13}C$ and water depth (table 5.5), particularly *C. lobatulus* ($r = -0.722$, $p = 0.043$), thus porewater $\Delta\delta^{13}C$ gradients should decrease with increasing water depth (see figure 6.14). This relationship of depleted $\delta^{13}C_{C.\ lobatulus}$ and thus decreasing $\Delta\delta^{13}C$, with increasing water depth is likely due to increasing apparent oxygen utilisation (AOU) from benthos respiration and organic matter remineralisation (e.g. Belanger *et al.,* 1981; Graham *et al.,* 1981 and Kroopnick, 1985). On the other hand, organic carbon (C_{org}) flux rate and degradation typically decreases with increasing water depth, resulting in less depleted $\delta^{13}C$ being released into sediment porewater via decomposing organic matter (Altenbach et al. 1999; Sauter et al. 2001). However, given the strength of the *C. wuellerstorfi* δ^{13}C: AOU relationship, the probability that *C. lobatulus* from Loch Sunart is in isotopic equilibrium with δ^{13}C DIC, and the strength of the $\delta13C_{C.lobatulus}$: water depth relationship, it is likely that the δ^{13}C of *C. lobatulus* is reflecting the increased AOU at water depth, with increased AOU occurring during times of high marine productivity.

6.4.8 Implications for palaeoreconstructions

6.4.8.1 Reconstructing past bottom water oxygen concentrations

Whilst Loch Sunart experiences regular renewal of basin water with coastal waters (Gillibrand *et al.*, 1995), the water column is likely to show slightly depleted δ^{13}C values with respect to coastal waters due to the consumption of oxygen in this relatively restricted coastal environment (see above). For example, Gillibrand *et al.*, (1996) demonstrated the depletion of bottom water oxygen concentration during a stagnant period in Loch Ailort, with oxygen replenishment occurring during renewal events. The main basin of Loch Sunart appears to be less responsive than the inner basin to climatic forcing (Gillibrand *et al.*, 2005) and there is little seasonal difference in dissolved oxygen content and AOU around the west coast of Scotland (Boyer *et al.*, 1999), hence the δ^{13}C of *C. lobatulus* is likely to reflect $\delta^{13}C_{DIC}$ arising from the admixture of the fjord waters and open ocean waters of the Atlantic

McCorkle *et al.*, (1990) suggested that the $\Delta\delta^{13}$C gradient between *C. wuellerstorfi* and the deep infaunal *Globobulimina affinis* may provide an estimate of past bottom water oxygen concentrations. Although the exact microhabitat of *N. turgida* and it's relation to oxygen penetration cannot be verified for Loch Sunart, McCorkle *et al.,* (1990) suggest deep-sea *Noniella* have a microhabitat similar to *G. affinis* (i.e. inhabits the zone where oxygen concentration = 0), and the δ^{13}C values for Loch Sunart *N. turgida* do suggest a deeper infaunal habitat than for instance, *B. marginata* (figure 6.13). Future comparison of the $\Delta\delta^{13}$C between *C. lobatulus* and *N. turigda* may provide a means of investigating past bottom water oxygen concentrations in Loch Sunart throughout time. This may be invaluable to understanding the natural ventilation of the loch, it's link to climate change (e.g. Gillibrand *et al.,* 2005) or response to anthropogenic forcing, given the economic dependence of fish farms on such fjordic environments (e.g. Gillibrand & Turrell, 1997).

6.4.8.2 *$\Delta\delta^{13}C$ and the potential for reconstructing palaeoproductivity*

Organic carbon from deep-sea environments tends to degrade within the top few mm's (Sauter *et al.*, 2001). *B. marginata* appears to inhabit a depth close to the sediment-water interface (figure 6.13) and likely reflects the net rate of diagenetic carbon release to the porewater from organic matter decomposition (McCorkle *et al.*, 1997). Zahn *et al.* (1986) reported a relationship between accumulation rates of organic carbon in NE Atlantic sediments and the $\Delta\delta^{13}C$ of the epifaunal *C. wuellerstorfi* and the shallow infaunal *Uvigerina peregrina.* Mackensen *et al.* (2000) also suggested that $\Delta\delta^{13}C$ gradients between epibenthic species such as *Cibicidoides* species and *Bulimina* species could act as a proxy for palaeoproductivity, with porewater $\delta^{13}C$ becoming isotopically depleted at localities with fresh phytodetritus accumulations (Mackensen *et al.*. 1993), i.e. the 'Mackensen Effect'. *B. marginata* and *C. lobatulus* are common throughout Loch Sunart surface sediments and are preserved well within sedimentary archives (see chapter 5). Paired isotopic analyses of these species may provide a record of palaeoproductivity in Loch Sunart, and although this was not achievable within the scope of this project, preliminary data shows an insignificant (probably due to low sample number) strong positive relationship between $\Delta\delta^{13}C$ *C. lobatulus* : *B. marginata* and % organic carbon (figure 6.15). Future work could improve upon this calibration by expanding the empirical data set and including more samples sites to extend the use of the palaeoproductivity to other shelf sea records.

6.5 CONCLUSIONS

The comparison of $\delta^{13}C$ data from Loch Sunart *C. lobatulus*, *B. marginata*, *A. beccarii* and *N. turgida* with the $\delta^{13}C$ porewater profile from a similar N Atlantic site supports the previously reported epifaunal habitat for *C. lobatulus*, and assigns infaunal life modes for the other taxa; from the shallow infaunal *B. marginata* and *A. beccarii* to the deeper dwelling *N. turgida*. The difference in $\delta^{13}C$ *C. lobatulus* and *N. turgida*

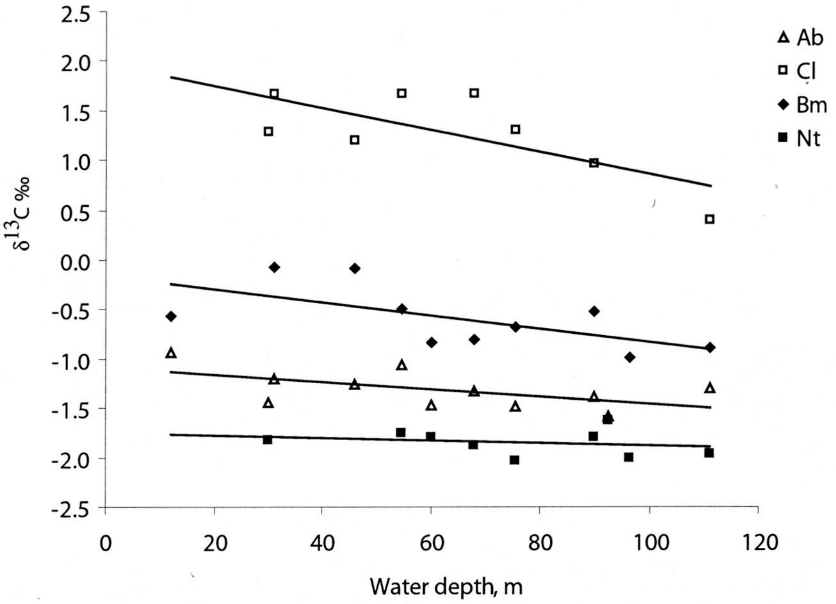

Figure 6.14. Carbon isotopic compositions of 'live *Ammonia beccarii* (triangles), *Cibicides lobatulus* (either live or dead; squares), 'live' *Bulimina marginata* (diamonds) and 'live' *Noniella turgida* (circles) with water depth. Samples obtained from Loch Sunart during April 2001/June 2002.

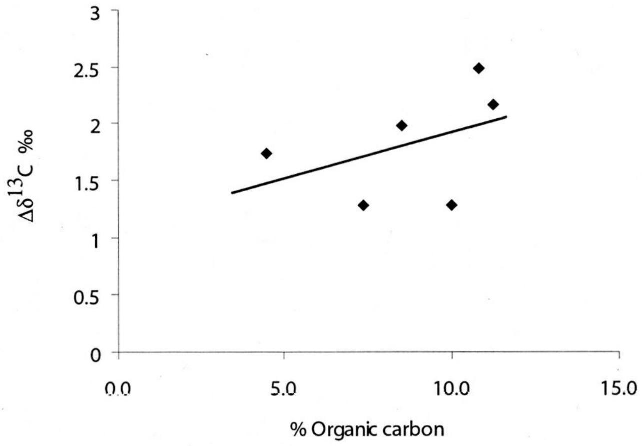

Figure 6.15 The positive relationship ($r = 0.689$, $p = 0.199$) between % organic carbon in Loch Sunart surface sediments and the $\Delta\delta^{13}c$ gradient between the epibenthic *Cibicides lobatulus* and the shallow infaunal species *Bulimina marginata*. The insignificant p value for the relationship is likely to be due to low sample numbers ($n = 6$).

suggests a porewater gradient ($\Delta\delta^{13}C$) of ~ 3.12 ‰ for an average sediment depth of 1.5 cm.

With these depth habitats in mind, measured $\delta^{18}O$ from *A. beccarii*, *B. marginata*, *N. turgida* and *C. lobatulus* were compared to the $\delta^{18}O$ of equilibrium calcite to determine the degree of isotopic disequilibria ($\Delta\delta^{18}O$) from the theoretical equilibrium $\delta^{18}O$ calcite for seawater ($\delta^{18}O_{Eq.CaCO3}$) for each species, with the focus being on *C. lobatulus*, since this species was used to obtain the palaeoisotope records from Loch Sunart cores GC023 and SC023. By using palaeotemperature equations calibrated with empirical $\delta^{18}O$ data from epifaunal *Cibicidoides* taxa (Bemis *et al.,* 1998 and Lynch-Stieglitz *et al.,* 1999) rather than infaunal taxa, *C. lobatulus* from Loch Sunart was found to calcify much closer to $\delta^{18}O_{Eq.CaCO3}$ than previously reported (e.g. Scourse *et al.*, 2004) with a $\Delta\delta^{18}O$ of -0.11 ± 0.17 ‰. *N. turgida* also calcified fairly close to isotopic equilibrium (using the Bemis *et al.,* 1998 equation) with a $\Delta\delta^{18}O$ of 0.17 ± 0.3 ‰, whilst both *A. beccarii* and *B. marginata* displayed large $\Delta\delta^{18}O$ disequilibria with $\delta^{18}O_{Eq.CaCO3}$ with $\Delta\delta^{18}O$ of 0.5 ± 0.15 ‰ and 0.69 ± 0.12 ‰ respectively. An explanation for the disparity between the relatively small *C. lobatulus* $\Delta\delta^{18}O$ presented here and the large disequilibria reported in other studies, is likely due to the palaeotemperature equation used. Studies reporting a large $\Delta\delta^{18}O$ typically use the O'Neil *et al.,* (1969) equation calibrated using infaunal taxa, and changes in porewater chemistry, e.g. pH, are likely to impact upon test $\delta^{18}O$ of infaunal benthic foraminiferal species (e.g. Spero *et al.,* 1997 and Zeebe, 1999). Thus this study has exemplified the need for authors to take care when selecting a $\delta^{18}O$: temperature equation to derive palaeotemperature from fossil benthic foraminifera. Additionally, the small oxygen and carbon isotopic disequilibria reported here for *C. lobatulus* (or *Cibicidoides* spp.) has implications on future project costings, since the estimation of bottom water $\delta^{18}O_{SMOW}$ and $\delta^{13}C_{DIC}$ can be determined from only one species, thus significantly reducing laboratory costs.

Loch Sunart *C. lobatulus* $\delta^{18}O$ typically display a negative correlation with BWT and a positive correlation with BWS. The 0.62 ‰ $\delta^{18}O$ range in fossil *C. lobatulus* from Loch Sunart core GC023 (chapter 8) reflects either a ~ 3 °C variation in temperature (Bemis *et al.,* 1998) or a salinity change of around 3.4 (Austin & Inall, 2002). Salinity variations of this magnitude are extremely unlikely to occur in Loch Sunart, even due to climatic forcing such as the NAO (chapter 3), however the observed Millport marine temperature series (chapter 3) displays an inter-annual range of 2.66 °C for May-October averaged temperature. Thus *C. lobatulus* $\delta^{18}O$ from Loch Sunart is likely to reflect BWT rather than BWS; an important relationship to determine before a palaeo-$\delta^{18}O$ isotope record is interpreted. Additionally, differences in predicted (calculated using the Lynch-Stieglitz *et al.,* 1999 palaeotemperature equation) and observed bottom water temperatures (BWT) for *C. lobatulus* specimens likely collected 'live' in winter, exhibit predicted BWT 3-5°C higher than recorded at the site during sampling. This suggests that *C. lobatulus* in Loch Sunart exhibit a 'seasonal effect' (Scourse *et al.,* 2004), possibly calcifying in the warm BWT during October/November; a period when benthic foraminifera from NW Norwegian fjords typically reproduce (*pers. comm.,* Dr. G. Mikalsen, 2004). Thus palaeotemperature derived from *C. lobatulus* will reflect summer BWT; the variable reconstructed using the transfer function approach of Sejrup *et al.,* (2004).

CHAPTER 7 – A BENTHIC FORAMINIFERAL TRANSFER FUNCTION APPROACH TO RECONSTRUCT SCOTTISH WEST COAST FJORDIC PALAEOENVIRONMENTS

7.1 Introduction

A major aim of palaeoenvironmental research is to reconstruct past climate or environmental conditions from proxies (e.g. fossils or sediments) and as palaeoenvironmental research techniques progress and develop, there is a growing need for the quantitative reconstruction of palaeoenvironmental variables rather than qualitative interpretations (Birks, 2003). Quantitative data are required for input into general circulation models and for the implementation of climate policies. Quantitative palaeoenvironmental reconstructions can be obtained through the understanding of present ecological responses of a biological proxy to environmental variables via statistical techniques, followed by the creation of a statistical mathematical model (such as a transfer function) which can reliably reconstruct the desired environmental variable. Such methods are discussed in chapter 2; useful reviews of quantitative environmental palaeoecological techniques are provided by ter Braak (1995) and Birks (1995; 2003).

Since the inception of the transfer function method for palaeoenvironmental reconstruction by Imbrie & Kipp (1971) the technique has developed, becoming more sophisticated in it's construction and diversifying both in the type of proxy used and the range of applications (e.g. Malmgreen *et al.*, 2001). The ubiquitous distribution of benthic foraminifera in marine sediments, along with the generally good preservation of fossil benthic foraminifera, makes this protozoan an excellent proxy for palaeoenvironmental reconstructions using transfer function techniques (Birks, 1995). Benthic foraminiferal transfer function techniques have been used to reconstruct palaeoproductivity (e.g. Loubere *et al.*, 2003), palaeodepth (Hohenegger, 2005) and sea-level change (e.g. Gehrels, 2000; Gehrels *et al.*, 2002; Edwards *et al.*, 2004; Horton & Edwards, 2005). Palaeoenvironmental reconstructions of ocean salinity or temperature have, until recently, largely been restricted to marine diatoms and planktonic foraminifera (e.g. Koc¸ & Jansen, 1994; Birks & Koc, 2002; de Vernal *et al.*, 2002; Jiang *et al.*, 2002; Jiang & Eiriksson, 2005; Kucera *et al.*, 2005). However, Sejrup *et al.*, (2004) recently published a benthic foraminiferal transfer function to reconstruct bottom water temperature (BWT) and bottom water salinity (BWS). This transfer function uses the Recent Benthic Foraminifera database (RBF); a training set from the NW European continental margin (figure 7.1). This transfer function has been shown to reconstruct summer (July, August and September) BWT and BWS for two eastern North Sea sediment cores fairly well in comparison to the planktonic foraminifera $\delta^{18}O$ record from the same cores.

7.1.2 Aims and objectives

A basic requirement of using transfer functions to reconstruct palaeoenvironmental conditions is that the training set must include modern surface samples and associated data which cover the range of environmental variables experienced at the core site in the past (Birks, 1995). The glacial limit of the Younger Dryas cold event extended into the upper basin of Loch Sunart (Benn, 1997), thus the main basin core site is likely to have experienced post-glacial BWTs much colder than can be found in Loch Sunart today. Applying a transfer function using a training set comprising of solely modern Loch Sunart benthic foraminiferal assemblages will result in inaccurate BWT reconstructions since the lowest BWT able to be reconstructed is constrained by the coldest BWT (11.6 °C) in the modern training set. Therefore there is a clear advantage to using the Serjup *et al.,* (2004) RBF training, which has long environmental gradients for both summer BWT and summer BWS (table 7.1)

However, applying the Sejrup *et al.,* (2004) transfer function to reconstruct bottom water temperature (BWT) and bottom water salinity (BWS) from Loch Sunart fossil benthic foraminiferal assemblages poses two major problems;

1) The minimum salinity in the Sejrup *et al.,* (2004) RBF training set is 33.6 (recorded at the Kattegat sites) which is similar to salinities observed in Loch Sunart main basin bottom waters (table 7.1 and chapter 3). However, the environmental gradient of summer bottom water temperatures (T_S) must be extended since the maximum T_S of the Sejrup *et al.,* (2004) RBF training set is 11.99 °C, and summer bottom water temperatures in Loch Sunart can often reach > 12 °C (chapter 3).

2) Sejrup *et al.,* (2004) excluded fjordic samples to try and minimise variance in the data, since fjordic hydrography differs to coastal hydrography due to localised

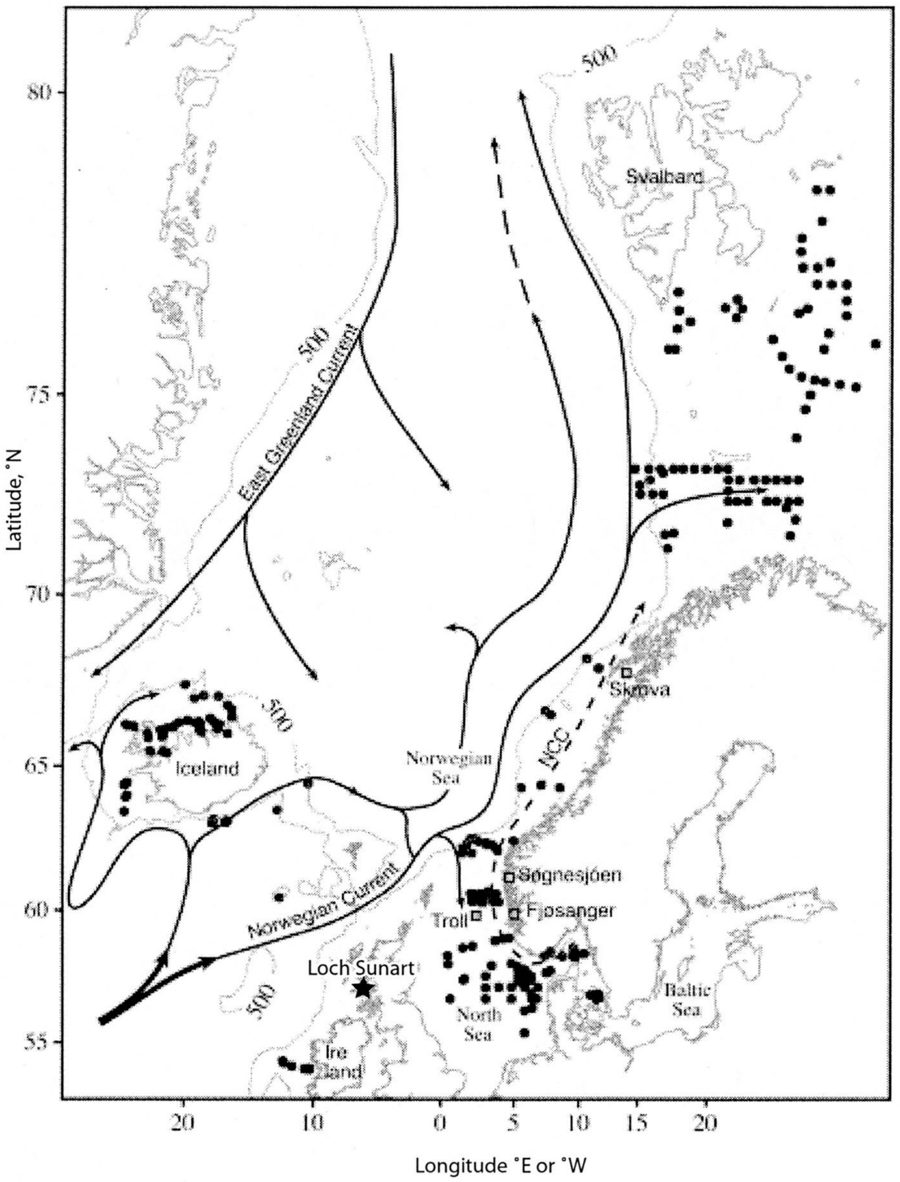

Figure 7.1. Sample locations included in the Recent Benthic Foraminifera (RBF) database of Sejrup *et al.,* (2004) along with the present day surface ocean circulation (the Norwegian Coastal Current is the extension of the Atlantic and slope current in figure 2.7). Locations of the Fjøsanger and Troll 8903/28-03 cores used to test the transfer functions and sites with instrumental time series (Skrova and Sognesjøen) are also shown. The location of Loch Sunart is indicated (black star) though Loch Sunart samples were not included in the original training set of Sejrup *et al.,* 2004 . Modified from Sejrup *et al.,* (2004).

Table 7.1 Summary statistics for the weighted averaging partial least squares (WA-PLS) transfer-function models based on leave-one-out (jacknife) cross-validation for bottom water temperature (Ts, ˚C) and salinity (Ss). Ts Sejrup and Ss Sejrup represents the models published in Sejrup *et al.,* (2004). Models Ts1, Ts2, Ts3 and Ss1 all include the recent benthic foraminifera database (RBF) of Sejrup *et al.,* (2004) plus 3 Loch Sunart (LS) samples; LS-22, LS-80 and LS-198. Ts1 is the full RBF of n = 260 plus the 3 LS samples, Ts2 is Ts Sejrup plus 3 LS samples and Ts3 is Ts2 omitting 3 outliers. Ss1 is the Ss Sejrup model plus 3 LS samples. Transfer function models used in reconstructions are shown in bold italic type. Descriptive statistics of the environmental variable in question are also given for each model.

Prediction models	WA-PLS Component	Ts Sejrup (n = 253)	Ts1 (n = 263)	Ts2 (n = 256)	Ts3 (n = 253)	Ss Sejrup (n = 260)	Ss1 (n = 263)
R2 jack	1	0.85	0.83	0.85	0.85	0.73	0.74
	2	0.88	0.86	0.88	0.89	***0.79***	0.80
	3	***0.89***	0.86	0.89	***0.90***	0.79	***0.80***
	4	0.89	0.87	0.89	0.90	0.80	0.80
	5	0.89	0.87	0.89	0.90	0.79	0.79
Max bias jack	1	2.17	2.17	2.24	2.24	0.45	0.46
	2	1.33	1.37	1.18	1.06	***0.24***	0.33
	3	***1.32***	1.54	1.15	***1.09***	0.25	***0.28***
	4	1.17	1.43	0.89	0.83	0.21	0.31
	5	1.32	1.45	1.07	0.99	0.21	0.30
RMSEP	1	1.22	1.32	1.25	1.23	0.19	0.19
	2	1.09	1.22	1.12	1.08	***0.17***	0.17
	3	***1.06***	1.20	1.09	***1.03***	0.17	***0.17***
	4	1.05	1.18	1.08	1.01	0.17	0.17
	5	1.04	1.18	1.09	1.02	0.17	0.18
Environmental variables	Minimum	-0.68	-0.68	-0.68	-0.68	33.58	33.58
	Maximum	11.99	12.51	12.51	12.51	35.47	35.47
	Mean	5.57	5.64	5.60	5.62	34.95	34.94
	Median	6.59	6.64	6.66	6.73	35.05	35.05
	Standard deviation	3.18	3.24	3.22	3.23	0.37	0.38

influences from the surrounding catchment (e.g. Gade & Edwards, 1980; Farmer & Freeland, 1983). Thus benthic foraminiferal assemblages from fjords may have different water mass characteristics and ecological responses from other RBF samples which are typically influenced by the oceanic currents in the North Eastern Atlantic region (figure 7.1; *pers. comm..,* Dr. D. Klitgaard-Kristensen, 2003). Before the transfer function can be confidently used in Loch Sunart palaeoenvironmental studies, reconstructions must first be compared to modern regional instrumental data to ascertain whether the fossil benthic foraminiferal assemblages of Loch Sunart are responding to the same North Atlantic oceanic climate which influences assemblages in the RBF.

To address these problems, suitable modern benthic foraminiferal assemblages from Loch Sunart surface sediment samples were added to the recent benthic foraminiferal (RBF) database of Sejrup *et al.,* (2004), in order to extend the environmental gradient of the RBF training set. The transfer function was then applied to assemblages from the upper section (0-13 cm) of Loch Sunart core SC023 (section 2.3.1) which has a resolution of 1.2 years.cm (see section 8.3.2.2 for geochemical data and section 8.4.1.1 for a discussion on the age models). This allowed the transfer function reconstructions to be tested via a direct comparison of reconstructed summer BWS and BWT with instrumental marine temperature and salinity records from the coastal waters of NW Scotland (chapter 3).

7.2 METHODS

7.2.1 Reproducing the transfer function of Sejrup *et al.,* (2004)

The full RBF database (n=634, 65 taxa) was acquired by AGC whilst a pre-doctoral fellow at the Bergen MCTS (see Sejrup *et al.*, 2004 for data). Samples without data were removed and the database was manipulated following the 'rules' stated in Sejrup *et al.*, 2004 (and after personal communication with Dr. D. Klitgaard-Kristensen), that is all samples from water depths shallower than 30 m and deeper than 500 m were removed, as were assemblages with more than 10 % 'Other Species' and samples from fjordic environments. This left the 260 samples included in the published RBF training set of Sejrup *et al.,* (2004). Sejrup *et al.,* (2004) removed taxa with less than 10 occurences in the database (leaving a reported 55 taxa), however, the prediction statistics and graphical models could not be reproduced when these taxa were excluded and the models used here include all taxa (appendix 10).

In order to select a transfer function method, detrended correspondence analysis (DCA) and detrended canonical correspondence analysis (DCCA) should be applied to the training set in order to gain an estimate of gradient length of the environmental variable to be reconstructed, and determine whether linear or unimodal transfer functions techniques should be used (Birks, 1995). Sejrup *et al.,* (2004) reported gradient lengths > 2 standard deviations (SD) for DCA axes 1 and 2, which had strong and significant ($p < 0.001$) relationships with summer bottom water temperature (T_S) and summer bottom water salinity (S_S) respectively. DCCA showed similar patterns to the DCA axes and suggested that T_S and S_S explained 16% and 9% of the variance in the biological data respectively, thus capturing the major gradients of variation in the modern benthic foraminiferal data (Sejrup *et al.*, 2004). The majority of the taxa with > 10 occurrences in the training set ($n = 55$) showed a statistically significant relationship with T_S with most taxa ($n = 36$) having a unimodal biological response, whilst 49 taxa showed a statistically significant mostly unimodal ($n = 40$) response to S_S (Sejrup *et al.*, 2004). The statistical method of weighted averaging partial least squares (e.g. ter Braak & Juggins, 1993; ter Braak *et al.*, 1993) was selected since gradient lengths exceeded 2 SD, the majority of taxa showed unimodal responses to the environmental gradients of interest, i.e. T_S and S_S (Birks, 1995) and the modern data '*conformed to the numerical assumptions of the method and its underlying model*' (Sejrup *et al.*, 2004).

7.2.2 Adding benthic foraminiferal assemblages from Loch Sunart

In order to extend the bottom water temperature gradient (section 7.1.2), three of the thirty-one benthic foraminiferal assemblages from Loch Sunart (chapter 5) were added to the RBF database. These samples were LS-22 (outer basin), LS-80 (upper main basin), LS-198 (GC023 core site); all from water depths > 30 m. Though the Sejrup *et al.,* (2004) training set did not exclude samples with indications of reworking, many of the deep sites of Loch Sunart have coarse sediment suggesting high current activity, thus the potential for reworking of the sediments (chapter 5); samples LS-22, LS-80 and LS-198 were primarily selected due to fairly low sand contents suggesting deposition in a relatively calm environment. The rich diversity of Loch Sunart benthic foraminiferal assemblages (chapter 5) means that the majority of the samples had to be excluded since assemblages (particularly those from the 'calm' depositional environments of the deep basins) typically exceeded the 10 % 'Other species' cut-off (i.e. species not included in the main taxonomic groups of the training set; Sejrup *et al.*, 2004) by at least 5-10%. The three samples selected for inclusion into the RBF database were samples with a low percentage of 'Other species'; these were percentages of 11.8 %, 6.3 % and 4.0 % for samples LS-198, LS-80 and LS-22 respectively. Out the 55 benthic foraminiferal taxa included in the RBF of Sejrup *et al.,* (2004), 52 were shown to be responsive to T_s and 49 taxa demonstrated a relationship with S_s, fulfilling a criterion of the transfer function approach to palaeoenvironmental reconstructions. Including Loch Sunart samples with a high % 'Other species' could significantly influence the transfer function model (both the estimates and the predictive power) since these taxa may not respond to T_s or $S_{s.}$ Additionally, these samples are representative of the main and outer basin of Loch Sunart; inner basin samples were not included because of the restricted connection of the inner basin water with the coastal water (chapter 3) along with the high proportion of agglutinated taxa (chapter 5). Loch Sunart assemblage counts (chapter 5) include aggultinated taxa thus assemblage percentage abundances were recalculated to represent only porcelaneous and hyaline taxa. However, the low proportion of agglutinated taxa within these samples (chapter 5) meant counts were typically n > 300 for all samples, i.e. deemed to be statistically representative of the environment (Buzas, 1990).

7.2.3 Potential problems faced when applying a transfer function model

A problem inherent in collaborations between many working groups of researchers is taxonomic determination (section 2.6.3) and Sejrup *et al.,* 2004 approached such problems by using a reduced number of taxa, grouping species into generic groups (e.g. *Lagena* spp.), using *Elphidium excavatum* (rather than different ecophenotypes) and using *Cassidulina laevigata* (rather than *Cassidulina teretis*) to avoid regional misidentifications. *E. excavatum* has been grouped together in this study and since *C. laevigata* is rare in Loch Sunart surface sediments (chapter 5), this taxonomic problem is unlikely to affect Loch Sunart reconstructions. *Gavlenopsis prageri* in the training set of Sejrup *et al.,* (2004) was identified as *Rosalina prageri* in chapter 6, and has been called *G. prageri* in this chapter.

Percentage abundance data can often produce constrainment problems in ecological statistics (Prentice, 1980), thus, as with Sejrup *et al.,* (2004), species percentage abundance data were transformed to square roots to account for this and also to stabilise variances and minimise signal-to-noise ratios.

7.3 RESULTS

7.3.1 Modifying the Sejrup *et al.,* (2004) transfer function model

The addition of the 3 Loch Sunart samples in the RBF database has extended the temperature gradient of the original RBF database from 11.99°C to 12.51°C (figure 7.2a), shifting the mean from 5.57 °C to 5.62 °C (table 7.1). The salinity gradient has not been extended (figure 7.2b), however mean salinity has shifted slightly from 34.95 to 34.94 (table 7.1).

7.3.1.1 Temperature

The prediction statistics for the WA-PLS models are shown in table 7.1. Model Ts1 (where T_s represents summer bottom water temperature; July-August-September averaged BWT) is the full RBF database (n = 260) plus the 3 Loch Sunart (LS) samples and the prediction statistics show a fairly poor model with a high $\text{RMSEP}_{\text{jack}}$ of 1.2 °C and a high maximum bias (1.54 °C) in comparison to the Sejrup *et al.,* (2004; Ts Sejrup) model (table 7.1). Outliers were identified as samples having residuals greater than the standard deviation of the environmental gradient (Birks, 1995; Sejrup *et al.*, 2004). However, Sejrup *et al.,* (2004) omit sample B997-320 with a residual (-3.0) which is less than the standard deviation of 3.18 °C. Samples identified as outliers in Ts1 were very similar to the outliers omitted by Sejrup *et al.,* (2004). Given that Sejrup *et al.,* (2004) ran additional statistical tests on 'rogue' samples, the published transfer model of Sejrup *et al.,* (2004), where n = 253, was used as a base for the creation of a modified transfer function model. Therefore Ts2 represents T_s Sejrup *et al.,* (2004) plus the 3 Loch Sunart samples (n = 256).

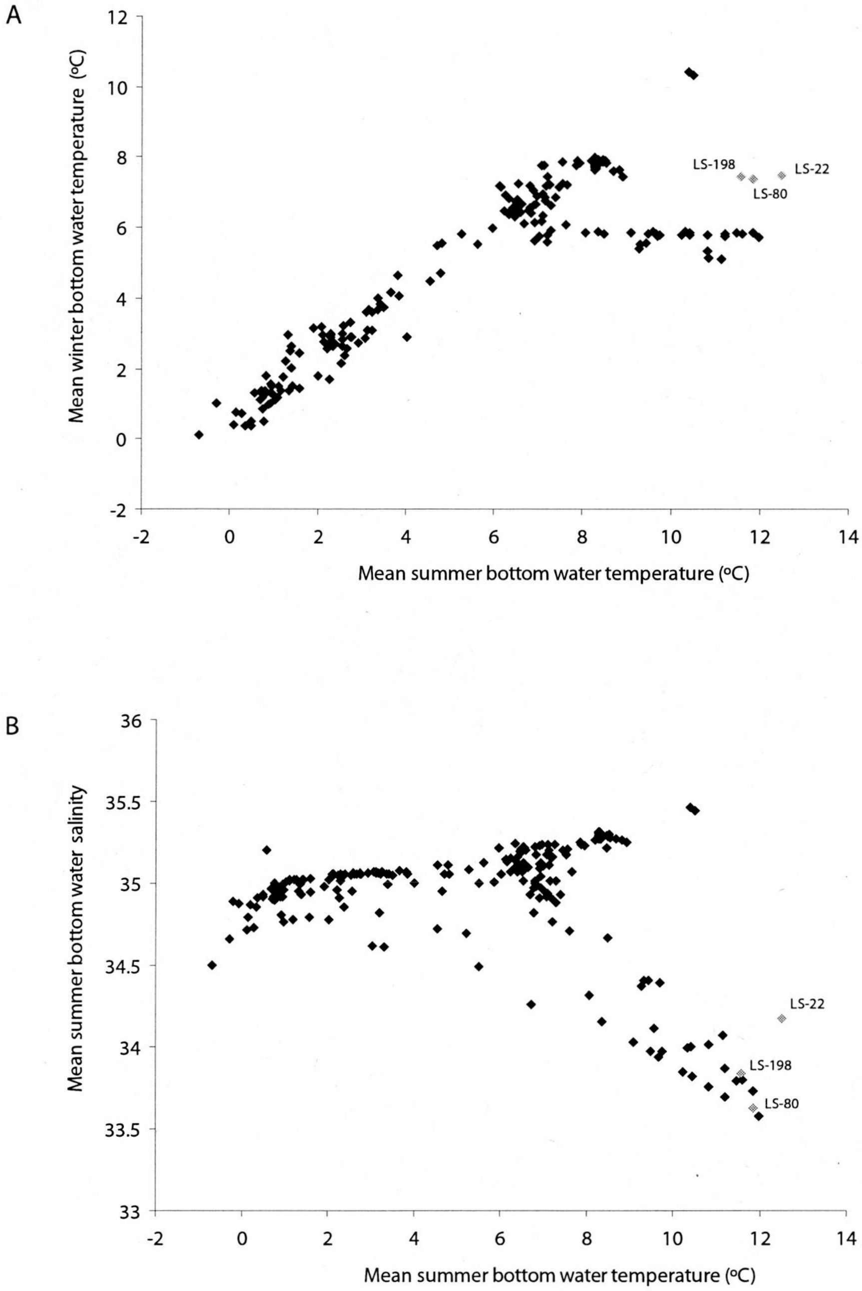

Figure 7.2 Biplots showing (A) mean summer bottom water temperature and mean winter bottom water temperature and (B) mean summer bottom water temperature and salinity for samples included in the recent benthic foraminifera database (RBF) of Sejrup *et al.*, 2004 (black diamonds). Also shown are samples from Loch Sunart (grey diamonds) which have been added to the RBF database in this study. Figure modified after Sejrup *et al., (*2004) .

WA-PLS component 3 was selected from Ts2 as this component has the lowest $\mathrm{RMSEP_{jack}}$ (1.09 °C) and the lowest maximum bias (1.15 °C) for the least number of components (table 7.1; ter Braak & Juggins, 1993; Sejrup *et al.*, 2004). Three outliers (samples HM 101-93-1, 9009 and B997-325) were visually identified in the model (figure 7.3a and b) and upon inspection, the residuals (observed temperature – predicted temperature) of these samples were greater than the Ts2 standard deviation of 3.22 °C, thus these samples were omitted (Birks, 1995). The prediction statistics of the subsequent model, Ts3 (n = 253) appear to perform slightly better than the published Sejrup *et al.,* (2004) model (Ts Sejrup) with an $\mathrm{RMSEP_{jack}}$ of 1.03 °C and a maximum bias of 1.09 °C (table 7.1). This may be due to the lengthening of the temperature gradient through the inclusion of the Loch Sunart samples and the placement of LS-198 on the line of best fit (figure 7.3 c and d).

7.3.1.2 Salinity

Sejrup *et al.,* (2004) presented a summer bottom water salinity (Ss) transfer function using 260 samples and a 2 component model (table 7.1). No outliers were omitted despite many samples having residuals greater than the standard deviation of salinity (figure 7.4 and b; Birks, 1995) and although Sejrup *et al.,* (2004) do not fully discuss this, the samples with high residuals were probably included due to their significant influence on the model and good DCCA relationship with bottom water salinity.

Therefore the salinity transfer function presented here (Ss1) includes all 260 samples from the RBF database plus the 3 Loch Sunart samples (n = 263). Loch Sunart samples sit at the lower end of the salinity gradient (figures 7.2b and 7.4a). Prediction statistics suggest a three component WA-PLS model for 263 samples performs slightly better than the two component mode used by Sejrup *et al.,* (2004; table 7.1) and the range of residuals appears to be smaller (figure 7.4b). As with Sejrup *et al.,* (2004), no outliers were omitted from the model.

7.3.2 Applying the transfer function to fossil benthic foraminiferal assemblages

Benthic foraminiferal assemblages from cores SC023 and GC023 are dominated by *Bulimina marginata*, *Cibicides lobatulus*, *Elphidium excavatum, Ammonia beccarii, Nonionella turigda* and *Stainforthia fusiformis*, with secondary species (abundances >

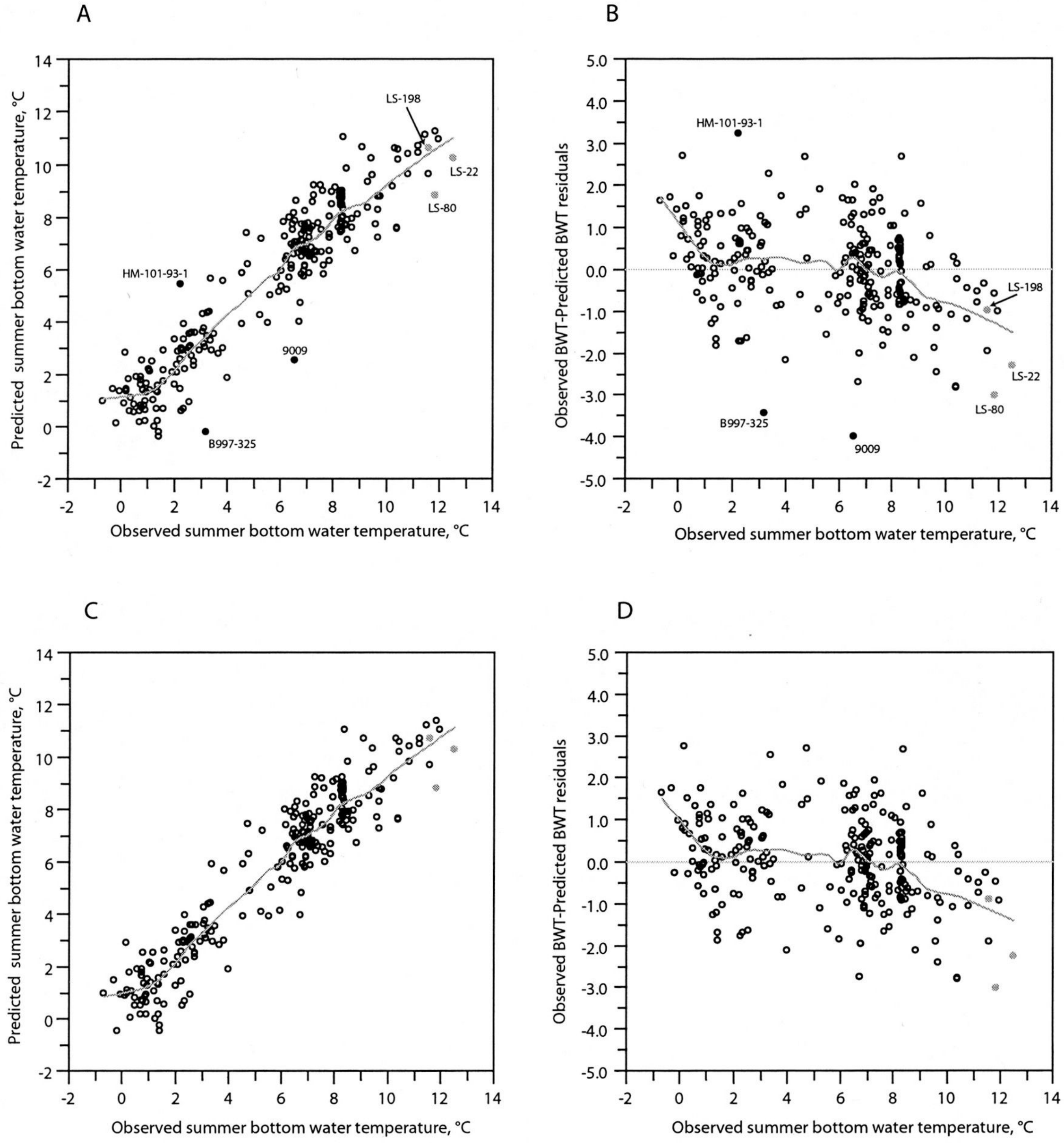

Figure 7. 3 A) Observed and predicted summer bottom water temperatures (and residuals) biplots for the leave-one-out (jack-knife) cross validation weighted averaging partial least squares (WA-PLS) regression transfer function model obtained using the C2 programme (Juggins, 2003). Dark grey lines show the lines of fit using locally weighted plot smoothers (span = 0.25, order = 2).

A) Observed and predicted summer bottom water temperatures and residuals (***B***) from component 3 of the WA-PLS model Ts2, i.e. the published Sejrup *et al.,* (2004) transfer function model consisting of 253 samples from the recent benthic foraminifera database (RBF) plus 3 Loch Sunart samples (LS-22, LS-80 and LS-198; indicated by grey filled circles). Outliers are labelled and indicated by filled black circles.

C) Observed and predicted summer bottom water temperatures and residuals (***D***) from component 3 of the WA-PLS model Ts3; the same model as Ts2 but with the outliers omitted. Ts3 is the transfer function model used to reconstruct summer bottom water temperatures in Loch Sunart.

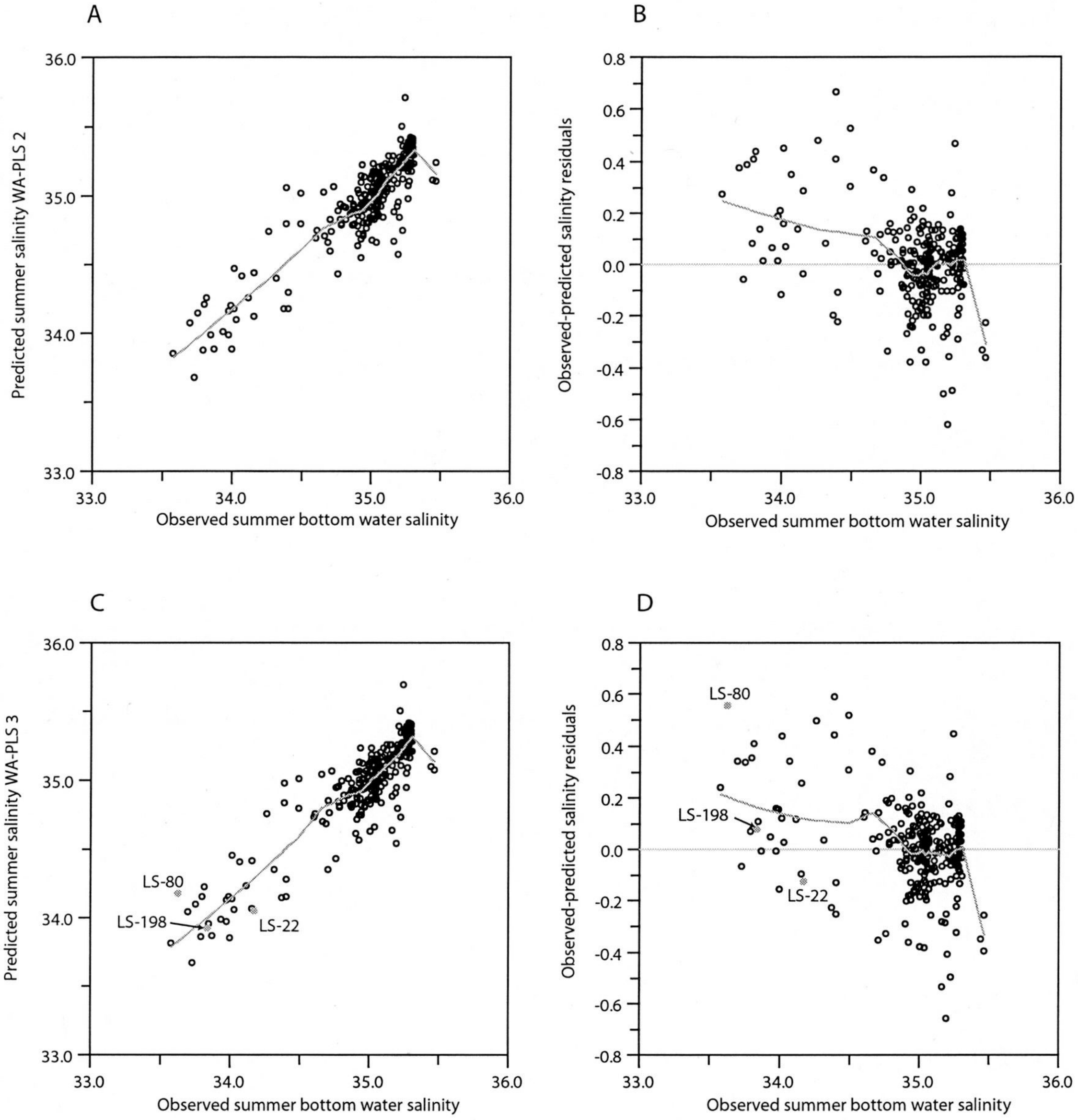

Figure 7.4 Observed and predicted summer (July-August-September) bottom water salinity (and residuals) biplots for the jacknife cross validation weighted averaging partial least squares (WA-PLS) regression models carried out using the C2 programme (Juggins, 2003).

A) The WA-PLS component 2 model published in Sejrup *et al.*, 2004 including all 260 samples of the recent benthic foraminifera (RBF) database (n = 260). ***B)*** shows the residuals (observed salinity -predicted salinity) for model A.

C) The WA-PLS component 3 model using the RBF database (n = 260) plus 3 Loch Sunart samples (labelled and shown as grey circles) as a training set (n = 263). ***D)*** shows the residuals for model C. Dark grey lines shows the lines of fit using locally weighted plot smoothers (span = 0.25, order = 2).

2%) including *Gavlenopsis praegeri*, *Hyalinea balthica* and *Epistominella vitrea* for core SC023 (figure 7.5) and *G. praegeri*, *Epistominella vitrea* and *Quinqueloculina seminulum* for core GC023 (figure 7.6). These taxa are commonly found in modern Loch Sunart benthic foraminiferal assemblages (chapter 5); an important requirement when dealing with quantitative palaeoenvironmental reconstructions (section 2.6.3).

7.3.2.1 SC023

Reconstructed summer bottom water temperature (RBWT) for site SC023 ranges from 9.01 – 10.03 °C, with temperatures typically varying by 0.2-0.5 °C and showing a general trend of increasing summer BWT towards the top of the core (figure 7.5). Reconstructed BWT using the Sejrup *et al.,* (2004) model (Ts Sejrup) shows the same trend but with lower temperatures (mean difference of 0.63 °C between Ts3 and Ts Sejrup; figure 7.5). The error on the reconstruction is given by the $\text{RMSEP}_{\text{jack}}$ and is 1.03 °C for Ts3 (figure 7.5) and 1.06 °C for Ts Sejrup.

The reconstructed summer bottom water salinity (RBWS) ranges from the maximum salinity of 34.22 near the base of the core, gradually decreasing (with some inter-annual variability) to less saline waters at the top of the core (34.02; figure 7.5). The minimum salinity (33.99) occurs at 3.25 cm, thus the range of reconstructed salinity for SC023 is 0.22, with an error of 0.17. Again, the Sejrup *et al.,* (2004) model reconstructed salinity (Ss Sejrup) shows the same salinity trends but slightly higher salinities (by up to 0.099).

A strong negative correlation exists between RBWT and RBWS (-0.892, p = 0) with cooler temperatures occurring in higher salinity waters and vice versa (figure 7.5).

7.3.2.2 GC023

The RBWT for core GC023 has a larger temperature range than the RBWT for SC023 (2.98 °C and 1.02 °C respectively). With the exception of the basal assemblage (290.5 cm) which produces a cool temperature of 9.11 °C, temperatures between 80.5 – 280.5 cm vary between 10.33 – 11.63 °C (figure 7.6), with the maximum temperature of 11.63 °C occurring at 180.5 cm, followed by a temperature of 9.86 °C

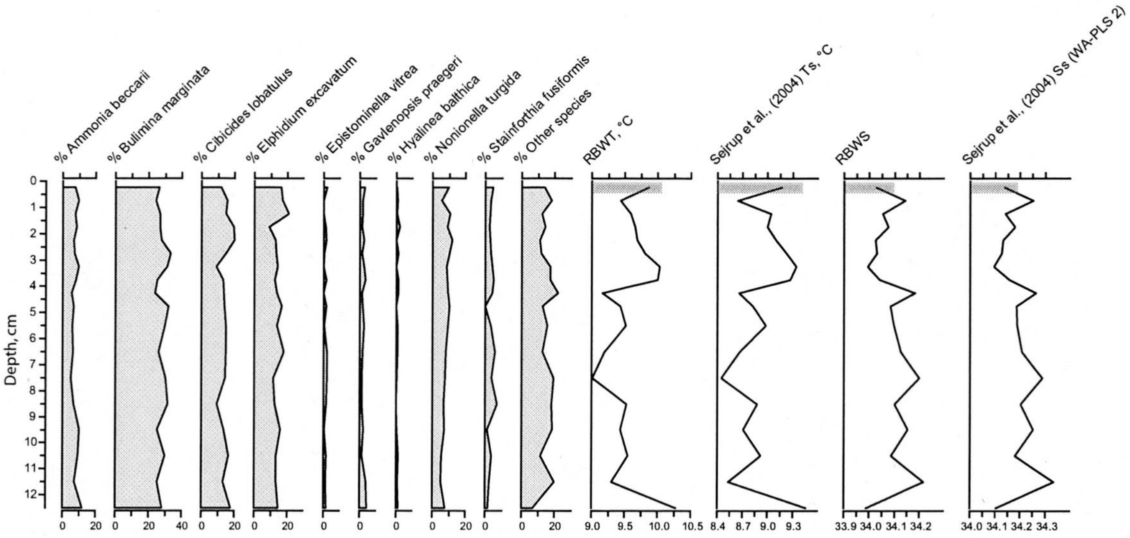

Figure 7.5. Reconstructed summer bottom water temperature (RBWT) and salinity (RBWS) for core SC023 using the WA-PLS jacknifed transfer function models Ts3 and Ss1 shown in figures 7.3 and 7.4. All reconstructions use the 3rd WA-PLS component unless otherwise stated. Statisical errors on the reconstructions (determined by $\text{RMSEP}_{\text{jack}}$) are indicated by grey bars. Also shown are taxa present in the assemblages with over 2% abundance and reconstructions using the Sejrup et al., (2004) transfer functions. The C2 programme (Juggins, 2003) was used to create the transfer function model, determine the reconstructions and draw the stratigraphic plots.

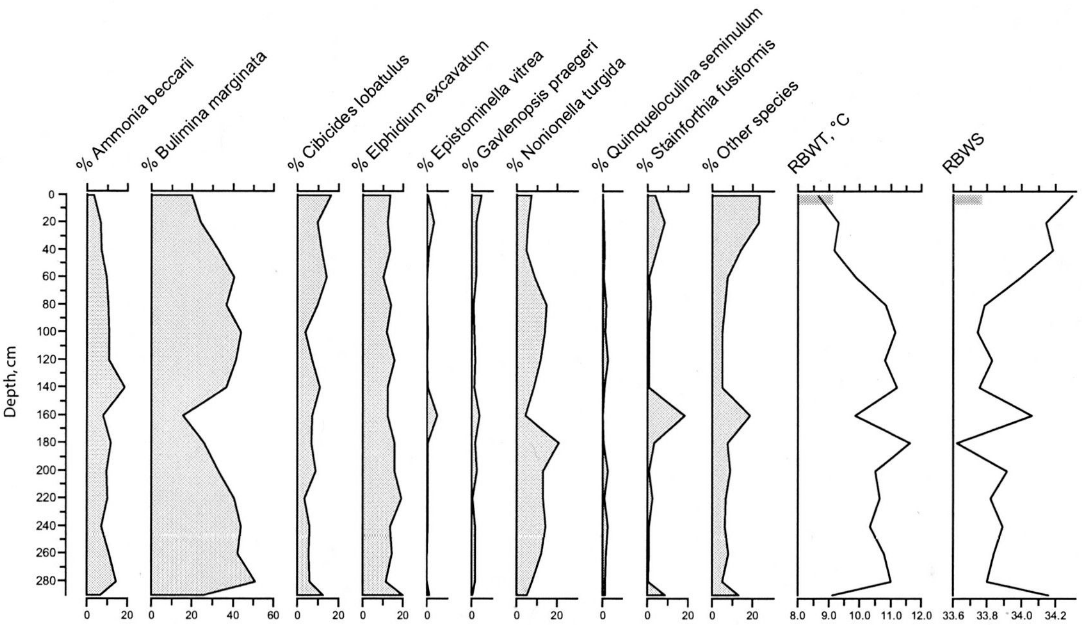

Figure 7.6 Reconstructed summer bottom water temperature (RBWT) and salinity (RBWS) for core GC023 using the WA-PLS jacknifed transfer function models Ts3 and Ss1 shown in figures 7.3 and 7.4. All reconstructions use the 3rd WA-PLS component. Statisical errors on the reconstructions (determined by $\text{RMSEP}_{\text{jack}}$) are indicated by grey bars. Also shown are taxa present in the assemblages with over 2% abundance. The C2 programme (Juggins, 2003) was used to create the transfer function model, determine the reconstructions and draw the stratigraphic plots.

at 160.5 cm. Above 80.5 cm, the temperature steadily decreases to a minimum of 8.65 °C at the core top (figure 7.6). This is closer to the temperatures seen in core SC023 (figure 7.5) but not identical, suggesting a potential loss of core top for GC023 (chapter 8).

RBWS from core GC023 has a stronger negative correlation to RBWT ($r = -0.992$, $p = 0$) than in SC023, so that RBWS inversely covaries with RBWT (figure 7.6). Thus, the cool temperature of the basal sample (290.5 cm) is accompanied by a fairly high salinity (34.16) whilst the lower part of the core (80.5 – 280.5) shows fairly low salinities varying around 33.8. Salinity begins to increase from 34.00 at 60.5 cm to the maximum salinity of 34.30 at the core top (0.5 cm). As with SC023, the Sejrup *et al.,* (2004) transfer functions reconstructed temperatures are approximately 0.7 °C cooler than Ts3 (figure 7.7) and salinities approximately 0.11 greater than Ss1 (figure 7.8).

A fairly rapid shift towards a cooler temperature and increased salinity is observed at 160.5 cm depth in core GC023. This is likely due to the fairly low % abundance of *B. marginata* at this depth, along with the peak in % *E. vitrea*, % *S. fusiformis* and % 'Other species'.

7.4 DISCUSSION

7.4.1 Applicability of transfer function approach in Loch Sunart

The majority of samples in the RBF database are mostly from shelf regions which are directly influenced by 'open' marine water masses and NE Atlantic ocean currents (figure 7.1). Given that fjordic hydrography is significantly influenced by catchment processes (chapter 3), the applicability of using a transfer function based upon the Sejrup *et al.,* (2004) training set was tested through direct comparison with observed temperature data from Millport (chapter 3). Unfortunately, recorded salinity data for the coastal waters of NW Scotland are currently unavailable (*pers. comm.,* Dr. M. Inall, 2005), and sea surface salinity data from the Faroe-Shetland Channel (chapter 3) cannot be used to represent inter-annual changes in the BWS of Loch Sunart (*pers.*

comm., Dr. B. Turrell, 2005). The reconstruction of bottom water temperature and salinity for GC023 will be discussed in a wider context in chapter 8.

7.4.2 Summer bottom water temperature reconstructions

The transfer function appears to reconstruct Loch Sunart summer bottom water temperature (RBWT) well, with temperature trends following the Millport summer (JAS) temperature series (figure 7.7).

7.4.2.1 Accounting for error

The error associated with the method is 1.03 °C, i.e. similar to the reconstructed temperature range (figure 7.7). The $\text{RMSEP}_{\text{jack}}$ error of Sejrup *et al.,* (2004) is approximately 3.9 % of the temperature gradient length suggesting a robust transfer function model when compared to other proxies used to reconstruct summer temperature which typically have errors of 8-20 % of the gradient. Thus, although the error is large in comparison to the predicted temperature range, the good agreement between observed Millport and predicted temperature suggests the transfer function reliably reconstructs trends in the summer bottom water temperature of the coastal waters of NW Scotland.

7.4.2.2 Differences in temperature range

The RBWT has a smaller inter-annual temperature range (~ 1°C) than the observed Millport temperature range of ~ 2.5 °C (figure 7.7). This, in part, is probably due to the different responses of surface waters (Millport) and deeper waters (Loch Sunart) to the seasonal heating cycle, with deeper waters typically showing a lagged response and a much reduced temperature range in comparison to surface waters (figure 2.8; Ellett, 1979). This also explains the difference in mean RBWT and Millport temperatures (9.5 ± 0.3 °C and 13.8 ± 0.7 °C respectively) since the core site lies at 120 m water depth and the Millport data represents sea surface temperatures (chapter 3).

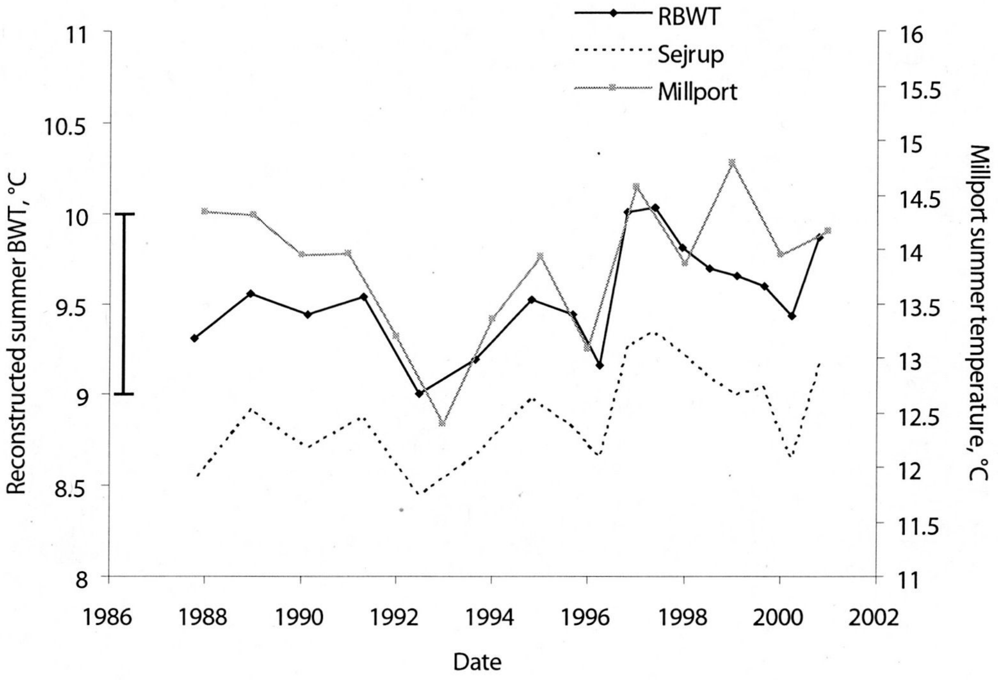

Figure 7.7 Reconstructed summer (July-August-September) bottom water temperature (RBWT) from core SC023 using the 3 component WA-PLS transfer function (Ts3) model shown in figure 7.3 (solid black line) and July-August-September averaged sea surface temperature from Millport (grey line). The age model is produced using a combined lead-caesium chronology (see section 8.3.2.2 for geochemical data and section 8.4.1.1 for a discussion on the age model). The transfer function of Sejrup *et al.*, (2004; black dotted line) is also shown. The $\mathrm{RMSEP}_{\mathrm{jack}}$ determined error of 1.03 °C is represented by the black bar; the Sejrup *et al.*, (2004) RBWT has a similar error of 1.06 °C.

The transfer function reconstructs a summer bottom water temperature (Ts) of 9.86 °C for the SC023 core top (~AD 2001) which is similar to the summer BWT (~9 °C) measured between 1973-77 at 120 m water depth at a site west of Barra Head on the Hebridean shelf Ellett, 1979). This is cooler than 10.4 °C observed at the core site in June 2002, though June lies on the rising limb of the heating cycle and summer BWT during the later summer months are likely to have been ~0.5 °C higher (Ellett, 1979). However the Scottish mainland air temperature (SMT) series shows that the summer (JAS) of 2001 was slightly cooler than 2002, thus Loch Sunart BWT may have also been cooler (chapter 3). Additionally, measured July BWT from the main basin of Loch Sunart varied by 1.82 °C from 1990 to 1991 (CTD cast data from Dr. P. Gillibrand, FRS) exemplifying the significant inter-annual variability of summer temperature in Loch Sunart main basin bottom waters. The transfer function appears to be reliably recording trends in summer bottom water temperatures in Loch Sunart, albeit potentially underestimating BWT by approximately ~ 0.25 – 0.5 °C.

7.4.2.3 Inherent problems in the training set

An additional influence on reconstructed Loch Sunart summer BWT may be the environmental gradient of the training set. The inclusion of Loch Sunart samples in the Sejrup *et al.,* (2004) training set does extend the temperature gradient towards slightly warmer temperatures (table 7.1), however only 21 out of the 253 samples (largely from the Kattegat/Skaggerak and the North Sea) used in the transfer function model have summer BWTs greater than 10 °C (figure 7.2a). A major requirement of a training set is that it is representative of the likely range of past environmental variables (section 2.6.3; Birks, 1995) thus the position of the modern Loch Sunart samples at the end of the temperature gradient (figure 7.3) along with the general under-representation of warm (>10 °C) samples may hinder the reconstruction of Loch Sunart temperatures since inverse methods (such as WA-PLS) typically perform better when unknown (i.e. fossil) samples are from a large central part of the training set distribution (ter Braak, 1995). Ideally, to estimate the optima and tolerances of species, the optima of the taxa should lie well within the range of environmental values (e.g. ter Braak & Looman, 1986) otherwise 'shrinking' of the environmental gradient can occur (Marchetto, 1994). A few of the dominant taxa (such as *A.*

beccarii) in Loch Sunart benthic foraminiferal assemblages exemplify this problem, since maximum abundances appear to correlate with higher BWT (chapter 5; figure 5.9). However, since the transfer function reconstructs higher temperatures (~11 °C) for GC023, it is likely that the lower RBWT of SC023 is a function of changing hydrography rather than constraints of the model. Also, the WA-PLS method accounts for this problem via a deshrinking regression step (ter Braak & Juggins, 1993), thus 'shrinking' of the environmental gradient shouldn't be a major problem.

7.4.2.4 Basin water response to climatic forcing

Though the transfer function model Ts3 may slightly under estimate summer bottom water temperature, and is accompanied by an error similar to the range of temperature variation, the good agreement with the observed Millport temperature data and thus coastal sea surface temperature data (chapter 3), suggests that fossil benthic foraminiferal assemblages in Loch Sunart are recording the summer marine temperatures of the NE Atlantic coastal waters.

The North Atlantic Oscillation significantly influences NE Atlantic climate and oceanography (chapter 3 and Blindheim *et al.*, 2000; Holliday, 2003) and observed bottom water temperatures at two coastal stations on the Norwegian coast show a strong relationship with the NAO (figure 7.1; Sejrup *et al.,* 2004). Hence it is likely that the summer bottom water temperature of Loch Sunart also responds to NAO forcing (chapter 3), and it may be possible to resolve NAO-influenced palaeoproxy records from the high resolution palaeoenvironmental reconstructions of Loch Sunart.

7.4.3 Salinity

7.4.3.1 Overestimating summer bottom water salinity

Reconstructed summer bottom water salinities (RBWS) are mostly greater than 34 (figure 7.8), however CTD casts taken at the core site in June/July of 1990, 1991, 2000 and 2002 show salinities of 33.85 – 33.96, i.e. RBWS is typically overestimated by ~ 0.1 – 0.3. Seasonal salinity in sea loch environments is typically more variable than temperature (chapter 3), though it is unlikely that the reconstructed - observed main basin salinity differences are an artefact of the sampling periods, since main

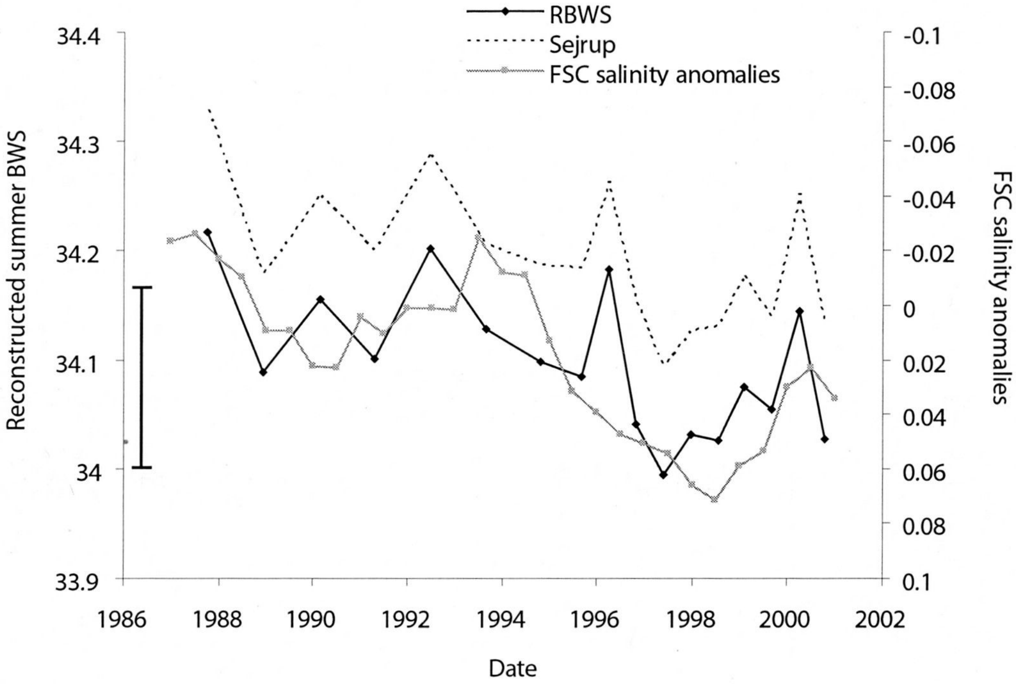

Figure 7.8 Reconstructed summer (July-August-September) bottom water salinity (RBWS) for core SC023 using the 3 component WA-PLS transfer function (Ss1) model shown in figure 7.4 (black solid line) and salinity anomaly data (grey line) from the Faeroe-Shetland Channel (FSC; data from Dr. W. Turrell, FRS). The age model is produced using a combined lead-caesium chronology (see section 8.3.2.2 for geochemical data and section 8.4.1.1 for a discussion on the age model). Note that FSC salinity anomalies cannot be used to represent likely inter-annual BWS experienced in the deep basins of Loch Sunart (*pers. comm.*, Dr. B. Turrell, 2005), however, some similarity exists between inverted F-S salinity anomalies (right hand axis; see text for discussion). The transfer function of Sejrup *et al.*, (2004;black dotted line) is also shown. The $RMSEP_{jack}$ determined salinity error (for both Ss1 and Sejrup *et al., (*2004) transfer function model of 0.17 is represented by the black bar.

basin salinity appears to remain relatively constant, even when extreme NAO climatic forcing is taken into account (Gillibrand *et al.*, 2005). As with RBWT, the overestimation of RBWS may be due to disparity in the distribution of training set samples along the salinity gradient (figure 7.4) with only 19 samples (out of 263) having salinities < 34, thus the likely range of Loch Sunart summer bottom water salinities is under-represented in the training set (see above discussion on problems of temperature reconstructions at the limits of an environmental gradient in a training set).

7.4.3.2 Comparison of reconstructed BWS with observed BWS

The lack of observational salinity data for Scotland's coastal waters (chapter 3) makes comparison with the Loch Sunart reconstructed summer bottom water salinity (RBWS) difficult. The trend of decreasing RBWS (figure 7.5 and figure 7.8) is concurrent with recent reports of decreasing salinity in North Atlantic waters (e.g. Blindheim *et al.*, 2000; Hansen *et al.*, 2001) and it is interesting to note that the trends in the RBWS appear to covary with Faroe-Shetland Channel (FSC) salinity anomalies (from 800 dbar) when the axes of the latter are inverted (figure 7.8). Though the FSC data shows shifts towards positive anomalies, these are superimposed on a general long-term freshening trend (Turrell *et al.*, 1996), hence the inversion of the axes to represent similar surface ocean freshening as reported in Blindheim *et al.,* (2000). Incidently, recent positive salinity anomalies in the FSC may occur due to enhanced current activity in the North Atlantic region in response to the NAO (e.g. Blindheim *et al.*, 2000; Holliday, 2003). Comparison of Loch Sunart salinity and FSC data is further complicated due to the differences in observational water depth (FSC data obtained from 800dbars ~ 800 m) and sampling locations. Freshwater inputs from the surrounding catchment play an important role in determining fjordic salinity (e.g. Farmer & Freeland, 1983; Gillibrand *et al.*, 1995). The prolonged positive NAO phase since the early 1990s dominates North Atlantic climate (chapter 3) and increased precipitation falling over NW Europe (e.g. Ruprecht *et al.*, 2002) along with changes in wind strength and direction, may manifest itself in slightly lower main basin salinities (chapter 3). Bottom water salinity variations, influenced by climatic forcing have implications for interpreting stable isotopic compositions from benthic foraminifera, because both temperature and salinity can be significant influences (chapter 6).

7.4.4 Comparison of SC023 reconstructions with fossil stable isotope records

7.4.4.1 Stable oxygen isotope compositions

The $\delta^{18}O$ record of fossil foraminifera is often used as an indicator for bottom water temperature or salinity characteristics, with lighter $\delta^{18}O$ (i.e. depleted in ^{18}O) signifying warmer temperatures and/or 'fresher' salinities and heavier $\delta^{18}O$ (enriched in ^{18}O) typically occurring in cooler or more saline waters (chapter 6).

Whilst RBWT from core SC023 agrees well with Millport temperature (figure 7.7), the $\delta^{18}O$ measurements from fossil *C. lobatulus* obtained from the same sample levels (chapter 8) appear at times to be in anti-phase with RBWT, Millport temperature and RBWS (figures 7.9 and 7.10). Anti-phasing between the $\delta^{18}O$ record and the Millport temperature series could be attributed to problems in core chronology, however $\delta^{18}O$ and RBWT are derived from the same benthic foraminiferal assemblages, thus problematic chronology is not likely the reason for the anti-phasing.

It is possible that the SC023 $\delta^{18}O$ record is representing salinity variations rather shifts in temperature with the lighter $\delta^{18}O$ indicating decreased salinity (figure 7.10). However, a 0.33 ‰ $\delta^{18}O$ shift from 0.78 ‰ in 1993 to 1.11 ‰ in 1995 would require a change in salinity of ~ 1.8 (Austin & Inall, 2002) and a salinity shift of this magnitude in the main basin is unlikely to occur, even during extreme climatic events (Gillibrand *et al.*, 2005). For example, during the 'Great Salinity Anomalies' events, observed salinities off Ardmore Point (Sound of Mull), the Rockall Trough and North Sea varied by less than 0.15 (Ellett & Edwards, 1983 and Belkin *et al.*, 1998) and modelled Loch Sunart main basin salinity varies by only 0.02 between two recent extreme NAO years (Gillibrand *et al.*, 2005), though it is acknowledged that the open ocean and fjordic regimes are very different. Therefore, while *C. lobatulus* $\delta^{18}O$ undoubtedly reflects the interplay of temperature and salinity influence (chapter 6), it is extremely unlikely that the *C. lobatulus* $\delta^{18}O$ record of Loch Sunart *C. lobatulus* solely records changes in bottom water salinity.

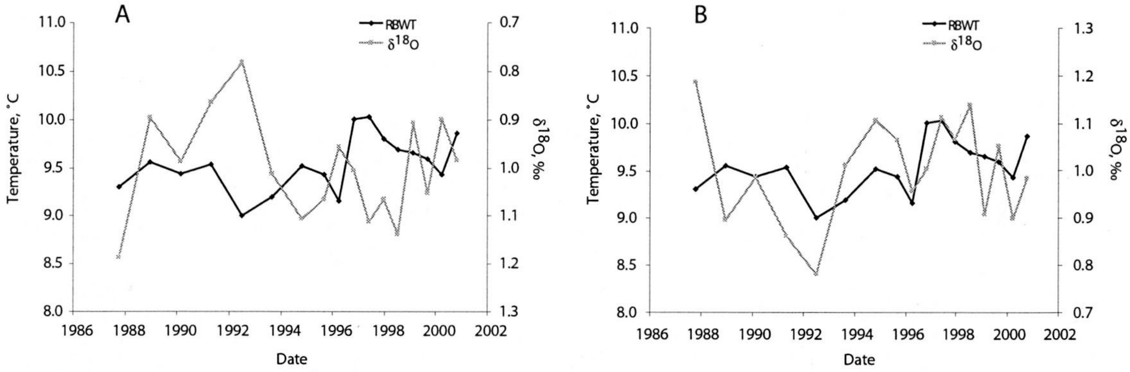

Figure 7.9 (A) Reconstructed summer (July-August-September) bottom water temperature (RBWT) for core SC023 (black line) using the 3 component WA-PLS transfer function model (Ts3) shown in figure 7.3 and created using the C2 programme (Juggins, 2003), plotted with the stable oxygen isotopic compositions ($\delta^{18}O$) of *Cibicides lobatulus* taken from the same sample depths (grey line). (B) with the $\delta^{18}O$ axis inverted. The age model is produced using a combined lead-caesium chronology (see section 8.3.2.2 for geochemical data and section 8.4.1.1 for a discussion on the age model).

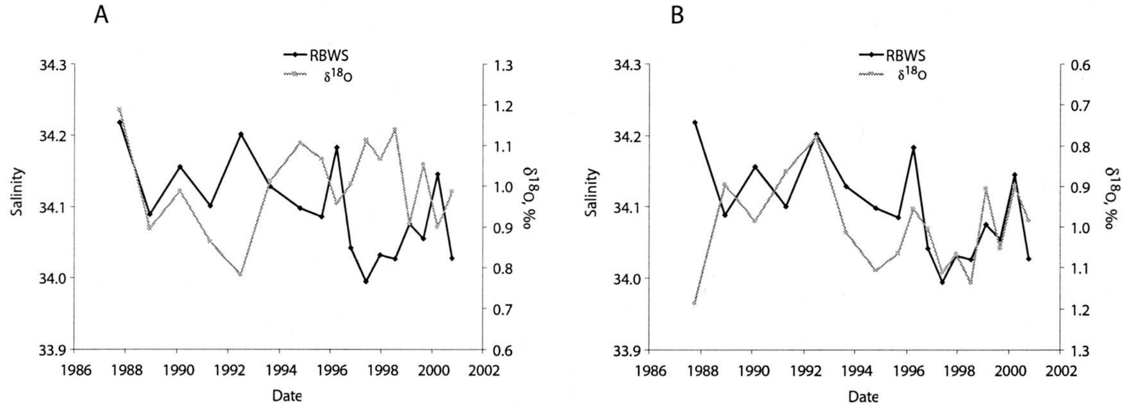

Figure 7.10 (A) Reconstructed summer (July-August-September) bottom water salinity (RBWS) for core SC023 (black line) using the 3 component WA-PLS transfer function model (Ss1) shown in figure 7.4 and created using the C2 programme (Juggins, 2003), plotted with the stable oxygen isotopic compositions ($\delta^{18}O$) of *Cibicides lobatulus* taken from the same sample depths (grey line). (B) As with A but with the $\delta^{18}O$ axis inverted. The age model is produced using a combined lead-caesium chronology (see section 8.3.2.2 for geochemical data and section 8.4.1.1 for a discussion on the age model).

Conversely, the same 0.33 ‰ shift points to a temperature variation of ~ 1.5 °C (assuming a relationship of 1°C per 0.21 ‰; Bemis *et al.*, 1998) which is similar to temperature changes observed in the Millport data for the same period (1993 – 1995; figure 7.7). This suggests that it is more likely that the *C. lobatulus* $\delta^{18}O$ is responding to changes in bottom water temperature at the core site since the $\delta^{18}O$ variations reflect the magnitude of observed temperature changes, though the interaction may be complex (figure 7.9).

7.4.4.2 Reasons for $\delta^{18}O$ anti-phasing

The main difficulty arising from the hypothesis that $\delta^{18}O$ reflects temperature variations rather than shifts in salinity is that measured $\delta^{18}O$ is often heavier, rather than lighter, during warmer summers (figure 7.9). From 1991 onwards, the correlation between SC023 $\delta^{18}O$ and RBWT appears tighter when the $\delta^{18}O$ axis is inverted; a pattern also seen in the comparison of measured $\delta^{18}O$ and theoretical equilibrium calcite (figure 7.11). *C. lobatulus* is a species which probably calcifies in late summer–early autumn (chapter 6), hence the $\delta^{18}O$ inversion is not likely to be due calcification during a different phase of the seasonal heating cycle (e.g. Scourse *et al.*, 2004).

This $\delta^{18}O$ anti-phasing with BWT is not constant throughout time. Between AD 1986-1991, SC023 *C. lobatulus* $\delta^{18}O$ displays the conventional $\delta^{18}O$:temperature relationship of enriched $\delta^{18}O$ with cooler water temperatures (chapter 6) and this 'in-phase' $\delta^{18}O$: temperature correlation is also seen for core GC023 *C. lobatulus* $\delta^{18}O$ and RWBT (chapter 8). Extending the RBWT further back would provide more information on the $\delta^{18}O$: RBWT relationship; however, problems in obtaining lead-caesium data for the cores during the project inhibited this extended data collection.

Ocean: atmosphere coupling is typically strong in the N Atlantic (chapters 1 & 3) and the recent prolonged positive NAO phase is likely to have significantly influenced coastal water salinity (Holliday, 2003) and sea surface temperatures (chapter 3). Inter-annual variability in the NE Atlantic Ocean currents has been linked to climatic forcing such as the NAO (chapter 1; Dickson *et al.*, 1996; Blindheim *et al.*, 2000; Holliday, 2003) and the response of NW Scottish coastal hydrography to the NAO is

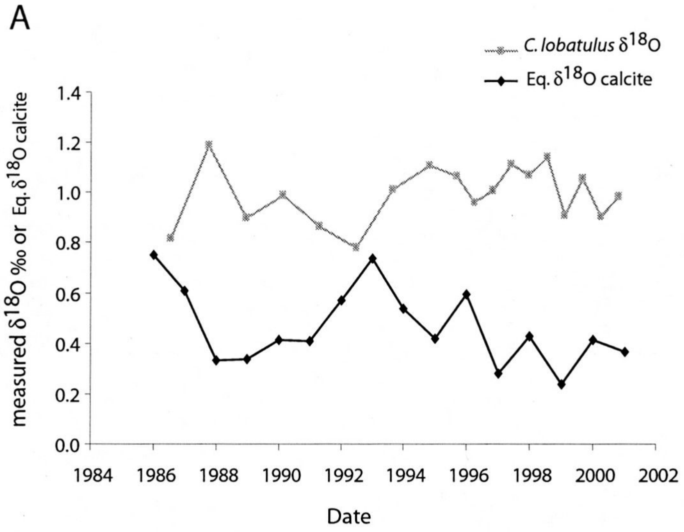

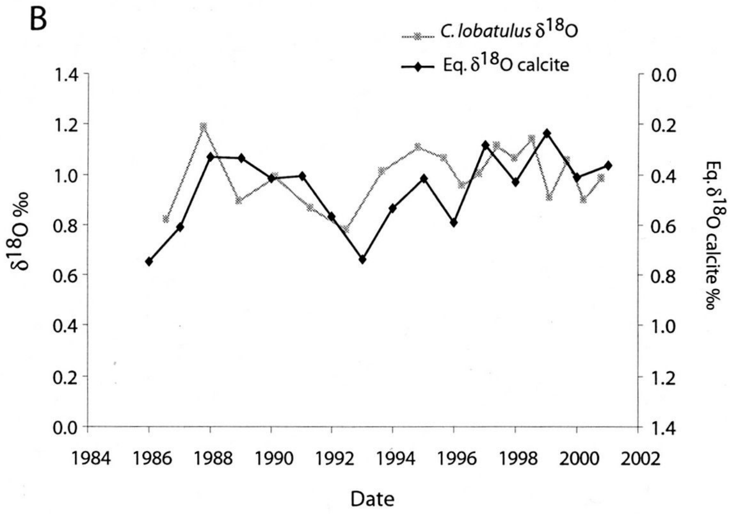

Figure 7.11 ***(A)*** Measured $\delta^{18}O$ from fossil *Cibicides lobatulus* from core SC023 (grey line) and theorectical equilibrium $\delta^{18}O$ calcite (Eq. $\delta^{18}O$ calcite) calculated from the observed Millport sea surface temperature series using the equations of Bemis *et al., (*1998) and Austin & Inall (2002) and assuming a constant salinity of 34.17 (averaged main basin salinity from Gillibrand *et al.,* 2005). ***(B)*** As for A, but with the Eq. $\delta^{18}O$ calcite axis inverted. The age model is produced using a combined lead-caesium chronology (see section 8.3.2.2 for geochemical data and section 8.4.1.1 for a discussion on the age model).

discussed in section 2.16 and 2.17. Recent *C. lobatulus* $\delta^{18}O$ may reflect an increase in fjordic stratification due to the prolonged positive NAO phase. For example, higher freshwater inputs (Ruprecht *et al.*, 2002) and surface ocean warming (as seen in the Millport sea surface temperature series) associated with positive NAO phases may lead to enhanced fjordic stratification (section 1.8.2.2). An increase in the stability of the thermocline (and halocline) in high index NAO phases, may lead to less down-mixing of the warm brackish surface layer, hence slightly cooler BWT, more saline BWS and thus enriched $\delta^{18}O$ in benthic foraminiferal tests and vice versa for negative NAO phases.

Additionally, strongly positive NAO (winter) years are typically accompanied by stronger North Atlantic slope currents (NASC), bringing warmer and more saline waters of Eastern North Atlantic Central Water (ENACW) origin into the Rockall trough, whereas during lower NAO index years, the Rockall trough water mass consists of ENAW and the cooler and fresher waters of the Sub-Arctic Intermediate Water (SIAW) and the Western North Atlantic Central Water (WNAW; Holliday, 2003). Thus, during strongly positive NAO years, the mixing of the warm, saline NASC water with the SCC (which also may be stronger during NAO positive winters; Kershaw *et al.*, 2004) at locations of vertical mixing on the Hebridean shelf (Craig, 1958) is likely to result in the coastal bottom waters entering Loch Sunart being more saline in comparison to NAO negative years (figure 7.12); even when modified by regional processes such as seasonal heating and freshwater runoff (Ellett & Edwards, 1983). This may work to further strengthen fjordic stratification and Loch Sunart main basin salinity may slightly increase during NAO positive years due to enhanced estuarine circulation (Gillibrand *et al.*, 2005). But if stratification is the dominant process here, then how is the good agreement of reconstructed BWT and the Millport marine temperature series explained?

Though seasonal stratification is common in shelf seas, locations with high tidal currents can have a mixed water column depending on seabed topography (Ellett & Edwards, 1983); one such region of mixing is located outside the mouth of Loch Sunart (Craig, 1958). Loch Sunart basin waters display similar seasonal heating cycles to other marine temperatures from the coastal waters of NW Scotland, thus the benthic foraminiferal assemblages are likely to record inter-annual variations in

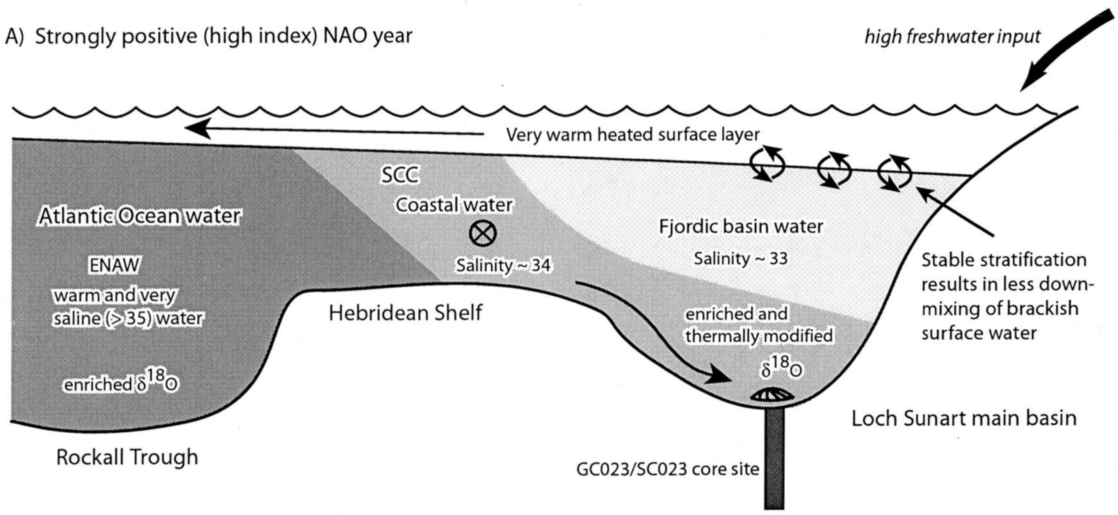

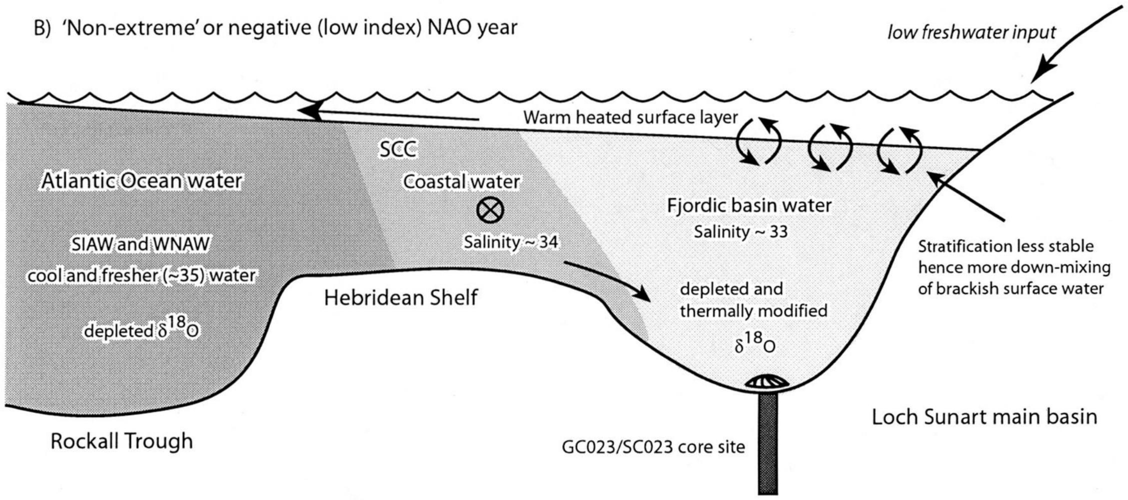

Figure 7.12 A) During strongly positive NAO years, the Rockall Trough water mass typically consists of Eastern North Central Atlantic Water (ENCAW) which is warm and salty (Holliday, 2003). Mixing of this salty ENCAW with the fresher and warm Scottish Coastal Current (SCC) is likely to lead to a fairly saline coastal water mass. Increased stability of the stratified surface layer likely results in increased estuarine circulation, which may 'pull' coastal waters into the main basin. Loch Sunart basin water displays a similar seasonal heating cycle to other marine temperature series from NW Scottish coastal waters. Therefore, although the benthic foraminiferal assemblage record a warm year, higher salinity bottom water is reflected in *Cibicides lobatulus* δ^{18}O from core SC023 or GC023, suggesting cooler, more saline bottom waters.

B) During negative NAO years and possibly 'non-extreme positive NAO years, Rockall Trough waters originates from the Sub-Arctic Intermediate Water (SIAW) and Western North Atlantic Central Water (WNAW) which are cooler and fresher than the ENAW, thus after mixing with the SCC, coastal waters are also likely to be fresher. Weak fjordic stratification along with fresher coastal waters are likely to result in lower salinity fjordic water dominating the main basin of Loch Sunart. Therefore, although the benthic foraminiferal assemblage record a cool year, lower salinity bottom water is reflected in *Cibicides lobatulus* δ^{18}O from core SC023 or GC023 suggesting warmer, fresher bottom waters.

bottom water temperatures. The $\delta^{18}O$ anti-phasing with RBWT in core SC023 is likely caused by stratification processes and the thermal modification of coastal water masses of different origins and thus salinities, entering the main basin (figure 7.12). Disparity between the measured $\delta^{18}O$ and reconstructed BWT could also be a function of differing habitat depths of the benthic foraminifera, since the majority of benthic foraminiferal taxa used in the reconstruction are likely to have infaunal habitats differing by at least approximately 0.25 cm to the epifaunal *C. lobatulus* (chapter 6).

RBWT and $\delta^{18}O$ from the top of core GC023 shows the opposite $\delta^{18}O$:temperature relationship to core SC023, with isotopically depleted *C. lobatulus* $\delta^{18}O$ accompanying higher RBWT. The two cores have different sampling resolutions, however this is unlikely to explain the differences in the $\delta^{18}O$: temperature relationships. Given that the transfer function appears to reconstruct SC023 summer BWT well (figure 7.9), the notation that light $\delta^{18}O$ signifies warm temperatures will be used to interpret the $\delta^{18}O$ values of core GC023.

7.4.5 Stable carbon isotopic composition and Loch Sunart bottom waters

The reconstructed salinity record poses an additional problem to the interpretation of foraminiferal $\delta^{18}O$. The salinity: $\delta^{13}C$ relationship is typically positive with more saline waters accompanied by enriched $\delta^{13}C$ values (e.g. Spiker, 1980 and Polyak *et al.*, 2003). Though questions have been raised about the accuracy of the reconstructed SC023 RBWT (section 7.5.3), trends in $\delta^{13}C$ values from *C. lobatulus* agree fairly well with RBWS (figure 7.13), with enriched $\delta^{13}C$ accompanying more saline RBWS. Between 1992 – 1996, *C. lobatulus* $\delta^{13}C$ appears to be isotopically enriched during lower RBWS; this may reflect the coastal salinity changes associated with the 1990s North Atlantic 'great salinity anomaly' which likely arrived in the Rockall Trough region around 1993-1996 (Belkin, 2004).

7.5 CONCLUSIONS

The Recent Benthic Foraminifera (RBF) training set and transfer functions of Sejrup *et al.,* (2004) can be modified by adding modern Loch Sunart benthic foraminifera assemblages from samples which adhere to the 'rules' outline in Sejrup *et al.,* 2004:

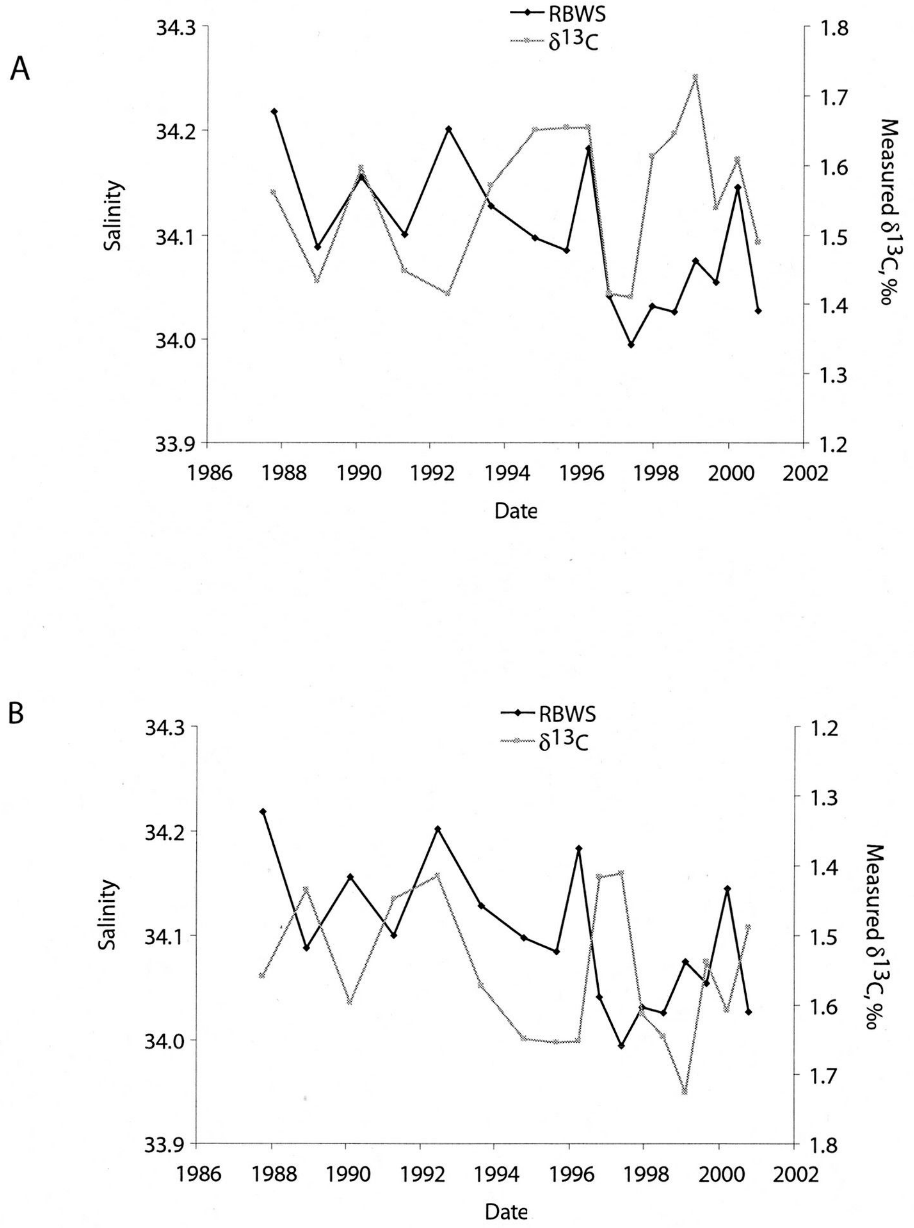

Figure 7.13 (A) Reconstructed summer bottom water salinity (Ss; black line) using the 3 component WA-PLS transfer function model (Ss1) shown in figure 7.4 and created using the C2 programme (Juggins, 2003) and measured stable carbon isotopic compositions ($\delta^{13}C$; black line) of *Cibicides lobatulus* taken from the same sample depths as the benthic foraminiferal assemblages used in the reconstruction.(B) As with A but with the $\delta^{13}C$ axis inverted. The age model is produced using a combined lead-caesium chronology (see section 8.3.2.2 for geochemical data and section 8.4.1.1 for a discussion on the age model).

i.e. samples must have associated bottom water temperature (BWT) and salinity (BWS) data; be from water depths deeper than 30 m, and at least 90 % of the assemblage taxa must be represented in the RBF. The addition of 3 Loch Sunart samples (22, 80 and 198) from the main and outer basin extended the upper limit of the summer (July-August-September) BWT environmental gradient from 11.99 °C to 12.51 °C, and increased the mean summer BWT from 5.57 °C to 5.62 °C. Though the addition of the Loch Sunart samples did not extend the lower limit of the summer BWS environmental gradient (already at 33.58), mean summer BWS did decrease from 34.95 to 34.94.

The computer program C2 (Juggins, 2003a, b) was used to create weighted-averaging partial least squares (WA-PLS) transfer function models for summer BWT (Ts3) and BWS (Ss1), using the RBF plus the 3 Loch Sunart samples; n = 253 and validated using the 'leave-one-out' (or jack-knife) method. For both the T_s and S_s transfer function models, the 3 component WA-PLS model yielded the lowest (and therefore best) maximum $\text{bias}_{\text{jack}}$ and lowest root mean square error of prediction ($\text{RMSEP}_{\text{jack}}$). The Ts3 model yielded a max $\text{bias}_{\text{jack}}$ of 1.09 °C and a $\text{RMSEP}_{\text{jack}}$ of 1.03 °C; these are improvements on the max $\text{bias}_{\text{jack}}$ of 1.32 °C and $\text{RMSEP}_{\text{jack}}$ of 1.06 °C reported in Sejrup *et al.,* (2004), and may arise from the extension of the environmental gradient. The Ss1 gave a higher max $\text{bias}_{\text{jack}}$ than the 2 component WA-PLS S_s of Sejrup *et al.,* (2004) with max $\text{bias}_{\text{jack}}$ values of 0.28 and 0.24 respectively. $\text{RMSEP}_{\text{jack}}$ values were equal at 0.17. However, a criterion of the transfer function approach to quantitative palaeoenvironmental reconstruction is that the likely range of variables experienced by the fossil data set should be covered by the environmental gradient of the training set, thus since there are few data at the lower end of the summer salinity gradient of the S_s model (figure 7.2), the model Ss1 was preferred.

The application of Ts3 to the fossil benthic foraminiferal assemblages of core SC023 (obtained from the main basin of Loch Sunart) reconstructed a summer (July-August-September) temperature series that is in good agreement with the observed summer marine temperatures of NW Scottish coastal waters between AD 1986 – 2000. The Millport sea surface temperature series displayed inter-annual temperatures ranging between 12.4 – 14.8 °C whilst the reconstructed summer bottom water temperature (RBWT) yielded a temperature range of 9.0 – 10.1 °C; the differences in the temperature range is likely due to a 'dampened' seasonal heating cycle signal in the deep water (120 m) of the core site (e.g. Ellett, 1979). Given the strong relationship between reconstructed NW Scottish marine temperatures, air temperatures and the NAO (chapter 3) along with the reported oceanic response to climate forcing (e.g. Holliday, 2003), Loch Sunart palaeoproxies derived from benthic foraminifera are likely to reflect the climate of the North Eastern Atlantic region. The RBWS and *C. lobatulus* $\delta^{18}O$ from core SC023 appear, at times, to be in anti-phase with each other, despite RBWS generally following NW Scottish coastal marine temperatures. The mechanism for this anti-phasing is likely to be intricate, given the complexity of regional coastal hydrography (e.g. Hill *et al.*, 1997; Holliday, 2003) and fjordic basin water exchange (Gillibrand *et al.*, 2005), however a stratification process is outlined as a possible cause, though the anti-phasing could also reflect the faunal depth habitats. Irrespective of this, the *C. lobatulus* $\delta^{18}O$ changes are unlikely to reflect solely BWS variations since the 0.33 ‰ $\delta^{18}O$ shift between 1993-1995 would require a change in salinity of ~ 1.8 (Austin & Inall, 2002), which is highly unlikely to occur in Loch Sunart, even during extremes of NAO climatic forcing (Gillibrand *et al.,* (2005). The same shift of 0.33 ‰ equates to a temperature change of around 1.5 °C (Bemis *et al.,* 1998) and this is similar to the inter-annual temperature variations seen in the Millport temperature series. Therefore, a direct *C. lobatulus* $\delta^{18}O$: salinity relationship is likely to be overprinted by a stronger inter-annual temperature effect but is possible that benthic $\delta^{18}O$ are influenced by underlying inter-annual salinity variations caused by climatically forced regional circulation changes.

Reconstructed summer BWS (RBWS) ranges from 33.99 to 34.22. Observed BWS at the core site is typically ~ 33.6, suggesting the transfer function model Ss1consistently over-estimates BWS at the Loch Sunart core site, and this may be due to the under-representation of benthic foraminiferal assemblages with similar BWS in the RBF. The inter-annual salinity variations in the RBWS cannot be compared to an observed BWS series, however, the $\delta^{13}C$ from the epifaunal species *C. lobatulus* suggests isotopically depleted $\delta^{13}C$ typically occurs with fresher salinities; a relationship also reported by Polyak *et al.,* (2003). Additionally, the trend towards decreasing salinity towards the core top is consistent with reports of freshening in the N Atlantic region and could reflect the influence of the prolonged positive NAO phase (e.g. Blindheim *et al.,* 2000).

CHAPTER 8 – LATE HOLOCENE PALAEOENVIRONMENTAL HISTORY OF LOCH SUNART

8.1 Introduction

Recent studies have shown that Holocene climate is not as stable as once thought (chapter 1) with 4 marked climatic phases occurring within the past 2000 years; the Roman Warm Period (RWP), the Dark Ages Cold Period (DACP), the Medieval Warm Period (MWP) and the Little Ice Age (LIA). The latter climatic event, the LIA, is particularly important since it: coincides with the Maunder Minimum of solar activity (Reid, 1997; Luterbacher *et al.*, 2001; Shindell *et al.*, 2001); occurs during a phase of sluggish current activity in the NE Atlantic (Bianchi & McCave, 1999b); and is thought to be linked to the 1-2 kyr climate cycles which pervade late Quaternary palaoerecords (Bond *et al.*, 1999). Additionally, the LIA provides a good test of palaeo-data, since it has a small but defined signal relative to the deglaciation signal (Jennings *et al.*, 2001) and is covered relatively well by instrumental data.

Despite this, marine palaeoclimate records from the Holocene often stop short of the last 2000 years (e.g. Austin & Kroon, 2001; Birks and Koc, 2002; Husum & Hald, 2004a), probably due to a lack of resolution or the loss of core tope material in these deep sea or shelf sedimentary records (*pers comm.*, Dr. W. Austin, 2005). Since fjords (or sea lochs) act as natural sediment traps, it is possible to obtain high resolution palaeoclimatic archives for the last 11000 years from these marginal environments (chapter 1). Additionally, the strong influence of the surrounding catchment upon fjordic hydrography and sedimentology provides the potential to study interlinking terrestrial and marine environmental change in the sediment core (chapter 1).

The westerly location of Loch Sunart on the European N Atlantic seaboard (figure 2.7) results in a strong relationship with North Atlantic driven weather systems and marine climate (chapter 3; Hurrell, 1995), demonstrating the potential sensitivity of this region to millennial and centennial scale climate and oceanic variability (e.g. Oliver *et al.*, 1997; Baker *et al.*, 1999; Bianchi & McCave, 1999b; Cooper *et al.*, 2000; Kroon *et al.*, 2000; Proctor *et al.*, 2000; Austin & Kroon, 2001; O'Sullivan *et* *al.*, 2002; Proctor *et al.*, 2002; Dawson *et al.*, 2004; Hall *et al.*, 2004; Lozano *et al.*, 2004; Gillibrand *et al.*, 2005).

8.1.1 Aims and objectives

Though palaeoclimatic and palaeoenvironmental studies have been carried out in many Scandinavian fjordic environments, particularly during the past decade (e.g. Alve, 1995; Kristensen *et al.*, 1995; Kelly *et al.*, 1999; Nordberg *et al.*, 2000; Mikalsen *et al.*, 2001; Nordberg *et al.*, 2001; Sejrup *et al.*, 2001; Gustafsson & Nordberg, 2002; Howe *et al.*, 2002; Plassen & Vorren, 2002; Hald *et al.*, 2003; Filipsson & Nordberg, 2004; Husum & Hald, 2004a; Kristensen *et al.*, 2004; Lysa *et al.*, 2004; Smittenberg *et al.*, 2005), few studies have addressed palaeoenvironmental change in Scottish sea lochs (Dix & Duck, 2000; Howe *et al.*, 2002; Murray *et al.*, 2003) and none in Loch Sunart. Therefore, presented here is the first multi-proxy late Holocene palaeoenvironmental record from Loch Sunart.

In order to interpret palaeoenvironmental data it is essential to understand the modern processes occurring in the environment, i.e. employ the principles of uniformitarianism, where the present is the key to the past. Palaeoenvironmental work in the fjords of NW Scotland have focused upon depositional regimes across the Late Glacial – Interglacial Transition (Dix & Duck, 2000; Howe *et al.*, 2002) or recent (last 200 years) environmental change in the near-anoxic Loch Etive (Murray *et al.*, 2003) which is not comparable to the well ventilated Loch Sunart (chapter 1). Modern studies in Loch Sunart or other sea lochs have primarily been concerned with circulation processes (Elliott *et al.*, 1992; Gillibrand *et al.*, 1995; Gillibrand *et al.*, 2005) or fishery studies (Treasurer, 2001; McKenzie *et al.*, 2004). Previous chapters, therefore, have explored elements of the modern environment of Loch Sunart which have implications for the interpretation of palaeorecords. For instance; exploring the impact of N Atlantic climate systems on observed temperature series from Loch Sunart via comparison with long instrumental records (chapter 3) and determining the sensitivity of Loch Sunart circulation to climatic forcing (Gillibrand *et al.*, 2005); investigating marine radiocarbon reservoir ages in NW Scottish fjords to improve the geochronology of cores obtained from these environments (chapter 4); determining the modern distribution of benthic foraminifera in Loch Sunart (chapter 5) and calibrating recent proxies to instrumental records (chapter 6 & 7).

The main aim of this chapter is to use the environmental and ecological data collated in the previous chapters to aid the interpretation of a 3 m gravity core GC023 obtained from the main basin of Loch Sunart via a multi-proxy approach. The suitability of utilising sedimentary archives from Scottish sea lochs will be discussed and the palaeoenvironmental record from core GC023 will be placed into a broader context of NE Atlantic palaeoclimate via comparison to other records.

8.2 METHODS

Gravity core GC023 (core length 2.89 m) was recovered from the main basin of Loch Sunart; the Dun Ghallain Deep (56.6670° N,–5.8388 °W' figure 2.9), from a water depth of 120 m. An accompanying Sholkovitch core, SC023 (0.74m length) was also recovered (56.6659 °N, –5.8404 °W; approximate distance from GC023 = 138 m) to capture the sediment-water interface, since the core top can often be lost during gravity coring (chapter 2). The lithology of the core was noted (figure 8.1) and marine molluscan material was removed for radiocarbon dating. Grain size analyses were carried out at a 1 cm resolution for raw sediments samples and at a 10 cm increments for digested samples (i.e. with organic and calcium carbonate content removed; see methods chapter). High resolution (at 1cm increments) geochemical trace element data was obtained via an XRF core scanner and low resolution geochemical data (approximately every 30 cm) was obtained using XRD methods (chapter 2). Stable oxygen and carbon isotopic compositions were measured on approximately 20 specimens of the benthic foraminifera *Cibicides lobatulus* (via stable isotope mass spectrometry) at a 1 cm sampling resolution.

The geochronology for cores GC023 and SC023 was constructed using a combination of radiocarbon dating and bulk sediment geochemical methods using lead and caesium (data from Dr. T. Shimmeild, SAMS; see Appleby & Oldfield, 1992; Appleby, 1997 for methodology). The conventional radiocarbon dates for the geochronology of GC023 and SC023 were calibrated using OxCal3 (Ramsey, 1995, 2001), which uses the marine radiocarbon curve ('marine98') of Stuiver *et al.,* (1998), after a regional ΔR correction of -27 ± 11 was applied (see section chapter 4).

8.3 RESULTS

The majority of data are presented diagrammatically; raw data can be found in the appendices.

Sedimentology

8.3.1 GC023 core log

Gravity core GC023 is comprised of clayey silt from the base (290.5 cm) to approximately 70cm, and silt from 70 cm to the top of the core (figure 8.1). The core appears to be moderately bioturbated throughout and contains a significant number of bivalve shells, some of which were used for radiocarbon dating (figure 8.1). Additionally a number of plant fragments were also logged within the core, demonstrating the significance of inputs (particularly organic matter) from the surrounding catchment.

Sholkovitch core SC023 consists of silt from 70 cm to the core top, thus agreeing well with the sedimentology of core GC023. Additionally, the magnetic susceptibility (MS) and grain size > 63 μm of core SC023 agrees fairly well with GC023, pointing to little, if any, loss of the GC023 core top (figure 8.1).

8.3.2 Geochronology for core GC023

8.3.2.1 Radiocarbon chronology

The measured radiocarbon results and the calibrated radiocarbon ages (for ΔR = 0 and ΔR = -27 ± 11) can be seen in table 8.1. Shell material from the base of core GC023 gives a calibrated age of 2055 ± 55 years BP. The uppermost shell dates at 27 and 30 cm core depth show 'modern' calibrated ages, (i.e. post-bomb) suggesting material above this depth has accumulated within the last ~50 years (after AD 1950). The calibration peak of sample AA-51569 occurs before AD 1950 at around AD 1910 (figure 8.2) indicating a small probability that the date is pre-1950. This pre-1950 peak in the calibrated dates is also seen in the historical shells collected during the late

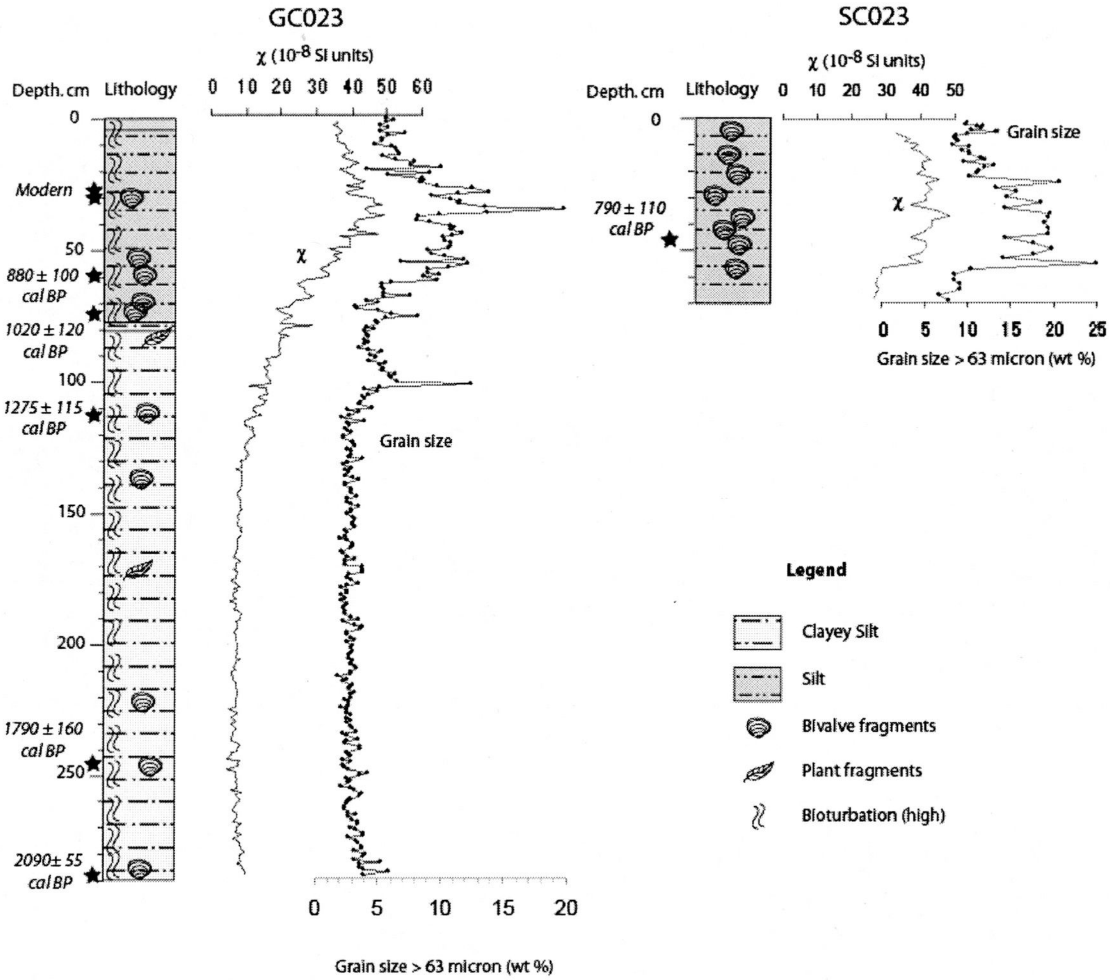

Figure 8.1 Gravity core GC023 (290.5 cm sediment recovered) and Sholkovitch core SC023 (69.5 cm sediment recovered) obtained from the main basin of Loch Sunart (56.6670° N,–5.8388 °W')from a depth of 121 m. See figure 2.7 for core location. Shown for both cores are magnetic susceptibility (χ ; thin black line) and raw sediment grain size > 63 μm (thick black line with symbols). The black stars represent calibrated radiocarbon dates using the OxCal 3programme (Bronk Ramsey, 1995) and are reported according to Stuiver & Polach (1977).

Table 8.1 Measured radiocarbon ages and calibrated (using OxCal 3) radiocarbon ages from mollusc material obtained from Loch Sunart cores, GC023 and SC023. The SC023 date was not included in the age model. † - The modern dates were excluded from polynomial trend line. ‡ - These inverted dates were not included in the ^{14}C age model.

Core	Lab code	Depth, cm	^{14}C years, BP	^{14}C cal BP ΔR = 0	^{14}C cal BP ΔR = -27 ± 11
GC023	† SUERC - 675	27	MODERN	n/a	n/a
	† AA -51569	30	340 ± 60	MODERN	MODERN
	SUERC - 677	58	1322 ± 43	855 ± 95	880 ± 100
	‡ SUERC - 678	73	1180 ± 41	730 ± 90	755 ± 95
	AA -51570	73	1430 ± 55	990 ± 120	1020 ±120
	SUERC - 679	111.5	1695 ± 57	1235 ± 115	1275 ±115
	‡ AA -51571	247	2450 ± 60	2110 ± 170	2140 ± 160
	SUERC - 680	250	2180 ± 61	1760 ± 150	1790 ± 160
	CAMS - 82821	286	2425 ± 40	2050 ± 100	2090 ± 120
SC023	† SUERC - 681	49	1215 ± 47	772 ± 105	790 ± 110

Marine data from Stuiver et al. (1998); Delta_R -27±11;OxCal v3.9 Bronk Ramsey (2003); cub r:4 sd:12 prob usp[chron]

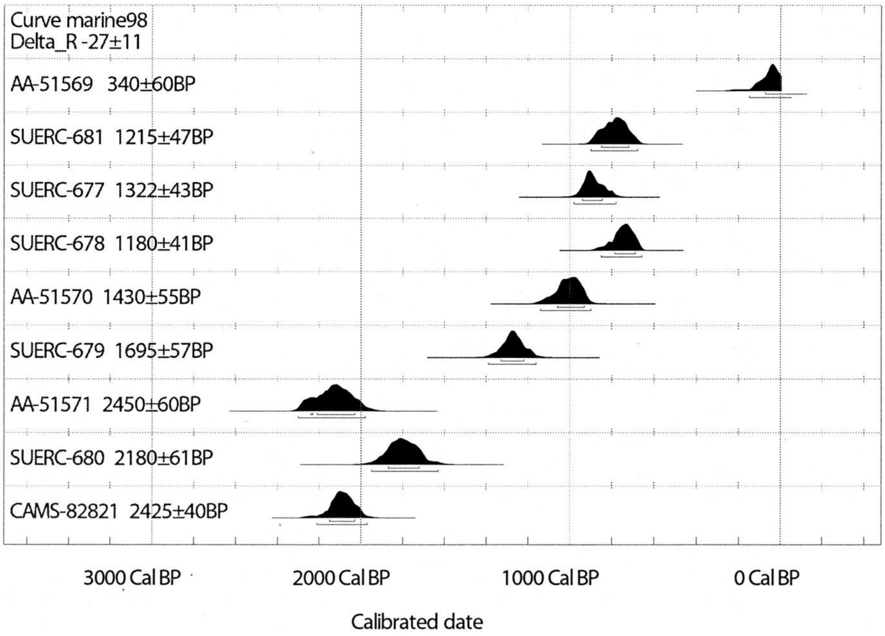

Figure 8.2 The calibration of GC023 and SC023 ^{14}C dates using OxCal 3 (Bronk Ramsey, 1995) and the regional ΔR value of -27 ± 11 years. Sample AA-51571 has a clear age inversion with respect to the rest of the data, thus was omitted from the age GC023 model.

1890's / early 1900's. The stratigraphic order and similarity of ^{14}C dates from SC023 (SUERC-681) and GC023 (SUERC-677) suggest that these cores are reconcilable with respect to ^{14}C and that a negligible amount of core-top was lost from GC023.

Two samples (SUERC-678 and AA-51571) show stratigraphic age inversions (figure 8.3) and hence were not included in the constructed radiocarbon age model (figure 8.4).

A 3rd order polynomial line gives the best fit through the GC023 ^{14}C data between 58-290 cm (i.e. excluding the modern dates at 27 and 30 cm, and the SC023 date) with an R^2 value of 1 and an equation of;

$$y = 0.000199357475088383\, x^3 - 0.102712965102871\, x^2 + 20.359343157428\, x + 4.93973935608025 \qquad \textit{(Eq. 8.1)}$$

(N.B. Values of equation 8.1 have been shown to ~ 18 decimal places since rounded values, i.e. up to 4 decimal points, can cause significant deviations in the constructed geochronology when such power functions are employed.

The ^{14}C data in figure 8.4 suggests that the sediment accumulation rate (SAR) has varied during the last 2 millennia. The sediment accumulation rate appears to be relatively steady from the bottom of the core (with a possibly slower SAR up to 250 cm) to approximately 111 cm, from where it slightly decreases until ~ 49 cm. The presence of the two modern dates around 30 cm gives an extremely slow sedimentation rate (~ 0.016 $cm.yr^{-1}$) for the section between 30-49 cm, and a rapid sedimentation rate of ~ 0.6 $cm.yr^{-1}$ from 30 cm to the core top.

8.3.2.2 Geochemical chronology

Excess ^{210}Pb ($xs^{210}Pb$), ^{137}Cs and $^{206}Pb/^{207}Pb$ measurements were carried out on cores GC023 and SC023 by T. Shimmield at Dunstaffnage Marine Laboratories, Oban (funded by the EU Framework V project: HOLSMEER), the results of which are presented in figure 8.5.

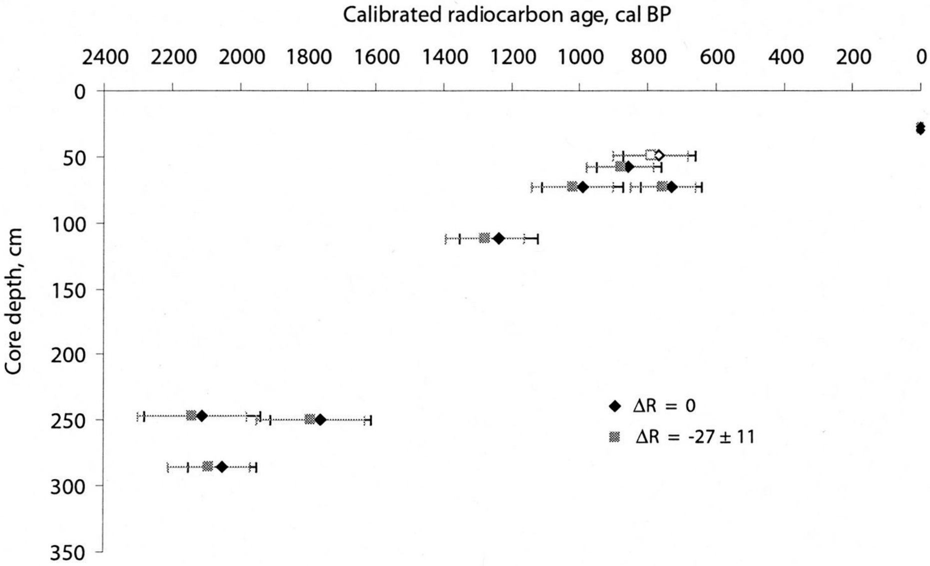

Figure 8.3 Calibrated radiocarbon dates for GC023 (filled symbols) and SC023 (unfilled symbols) when ΔR = 0 (black diamonds) and when ΔR = -27 ± 11 (regional correction calculated from this study, grey squares).

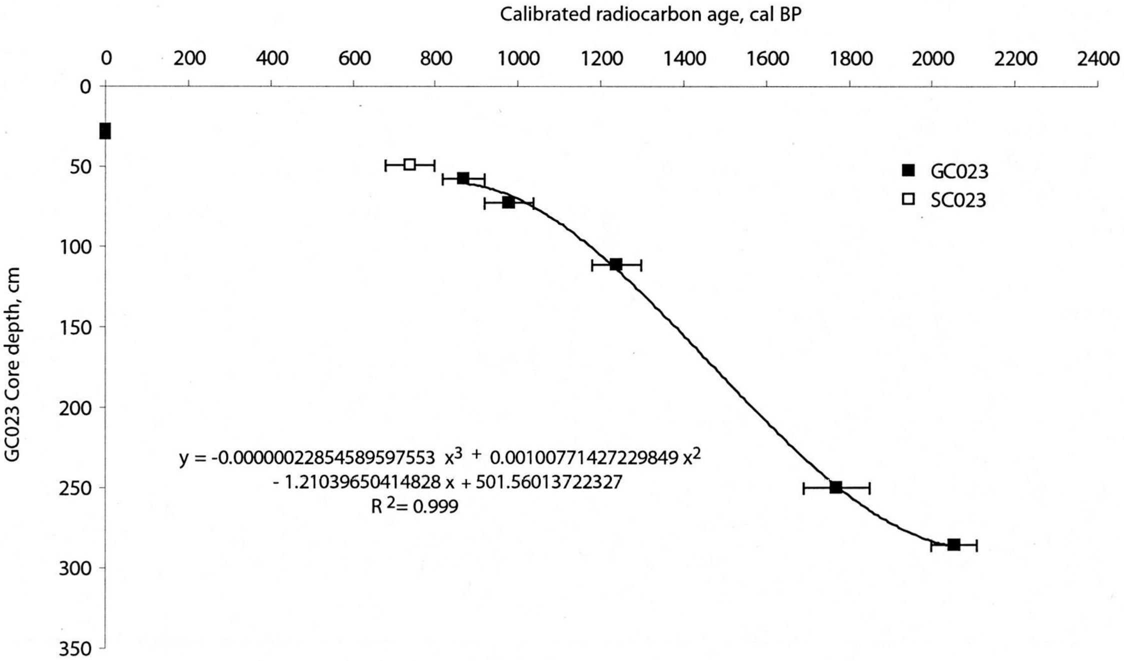

Figure 8.4 Radiocarbon chronology of calibrated radiocarbon dates (using OxCal 3; Bronk Ramsey, 1995, and a regional ΔR of -27 ± 11) from core GC023 (black squares). The basal date from the SC023 core (unfilled square) suggests a good correlation with GC023.

The excess ^{210}Pb decreases with sediment depth as expected, except for the peak between 14-20 cm which has been attributed to bioturbation advecting high excess ^{210}Pb to depth. This section of core SC023 has been removed from any interpretation of the chronology. The peak in ^{137}Cs (figure 8.5) at ~ 22 cm reflects the 1975 Sellafield discharge arriving in Loch Sunart in 1976 (Begg, 1992) and provides a valuable age-control point. The shift towards depleted ^{206}Pb/^{207}Pb ratios (figure 8.5) around 70 cm depth shows the commencement of leaded fuel use in the 1920's (*pers. comm.*, Prof. G. Shimmield, 2004). The historical occurrence of the latter two proxies provide two 'tie-points' for constructing the geochronology.

Chronologies were derived for ^{210}Pb (applying the Constant Initial Concentration model, Appleby & Oldfield, 1983) and ^{137}Cs using dry bulk densities and cumulative mass converted to years. When plotted against the ^{206}Pb/^{207}Pb data, it is clear that the ^{137}Cs chronology provides the best age model, with the decrease in ^{206}Pb/^{207}Pb occurring at around AD 1920 (fig 8.6), the reported time period for which anthropogenic Pb from internal combustion engines first significantly impacted the UK (Farmer *et al.*, 1997). The difference in chronologies is most likely due to the perturbation of xs^{210}Pb by the burrows, and therefore the ^{137}Cs chronology is preferred. Alternatively, the two chronologies can be combined and averaged (*pers. comm.*, Prof. G. Shimmield, 2004), and this is the age model which will be used in this study. All results are shown in table 8.2.

Despite ^{206}Pb/^{207}Pb measurements from GC023 being somewhat 'spikier' than those from SC023 the depths at which the ^{206}Pb/^{207}Pb ratio decreases is similar, suggesting that the top 60 cm of the two cores are reconcilable and that the GC023 core top was captured (*pers. comm.,* Dr. T. Shimmeild, 2004).

8.3.3 Grain size analyses

8.3.3.1 Raw sediment grain size > 63 um

From the base of GC023 to approximately 115 cm, untreated (i.e. raw) grain size > 63 μm (from hereon grain size) shifts from a mean of 4.10 ± 0.8 % for the bottom 10 cm (16 samples) to a fairly constant of around 2.85 ± 0.5 % (165 samples).

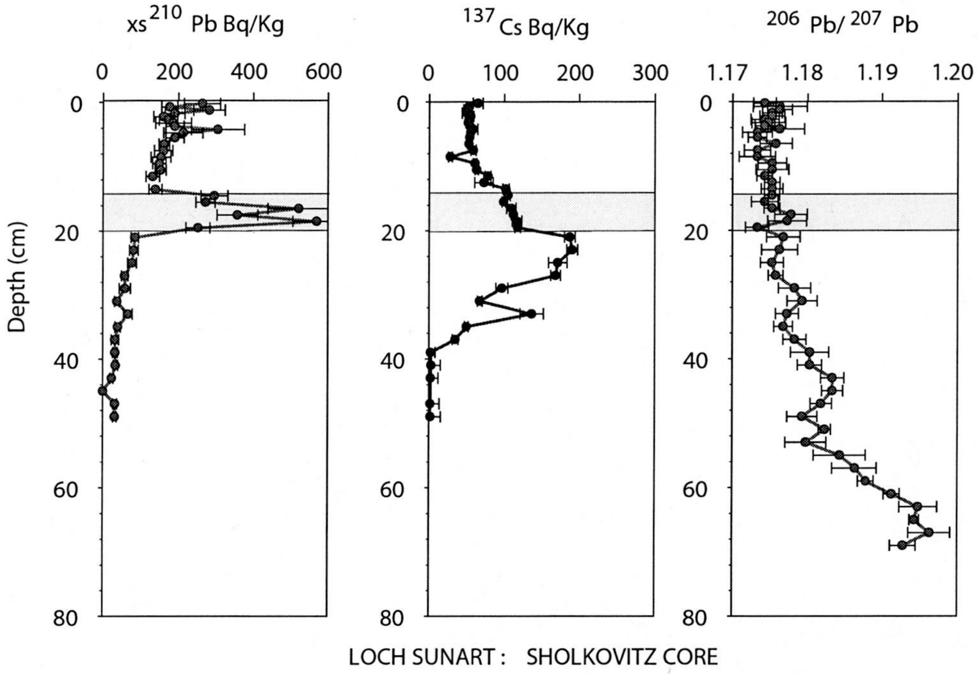

Figure 8.5 Excess ^{210} Pb (xs ^{210} Pb), ^{137}Cs and ^{206} Pb/^{207} Pb measurements from the Loch Sunart Sholkovitz core, SC023. The grey shaded bar represents possible bioturbation as suggested by the peak in xs^{210} Pb.

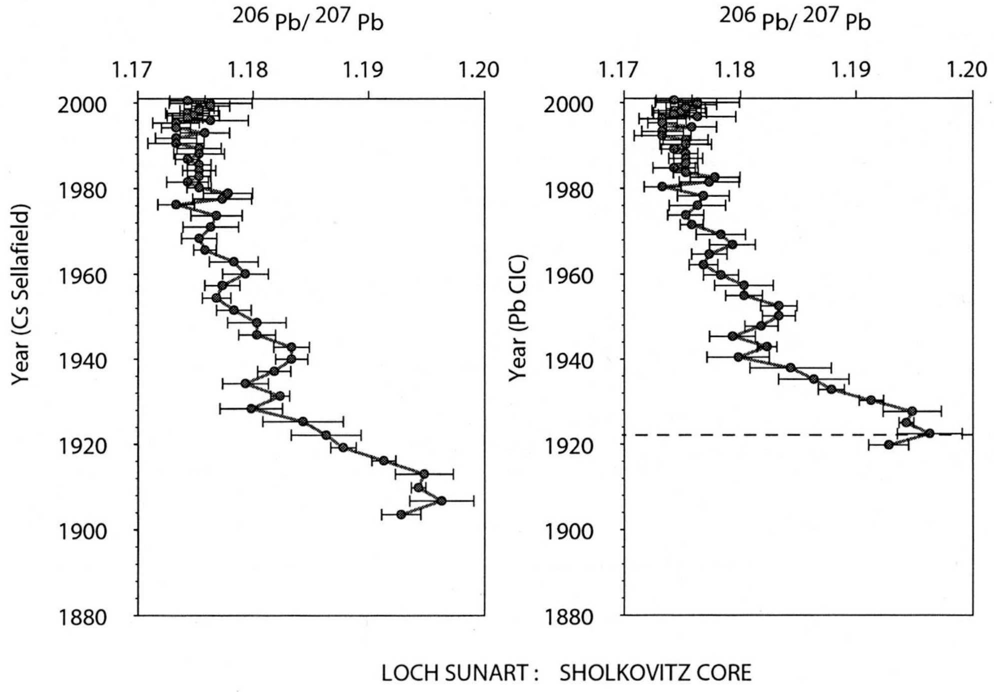

Figure 8.6. ^{206} Pb/^{207} Pb ratios plotted against a) the excess ^{210}Pb chronology and b) the ^{137}Cs chronology. The

Table 8.2 Chronologies (years AD) for core SC023. The excess ^{210}Pb chronology was derived using a Constant Initial Concentration model and an activity of 0.29gcm-2. The ^{137}Cs age model assumed an activity of 0.35g/cm^{2}. The combined chronology shows the averaged Pb CIC and ^{137}Cs age models.

Sediment depth, cm	g/cm^2	Pb CIC	^{137}Cs Sellafiel d	Combined chronology
0.25	0.2	2000.5	2000.6	2000.55
0.75	0.3	1999.9	2000.1	2000
1.25	0.5	1999.2	1999.5	1999.35
1.75	0.7	1998.7	1999.1	1998.9
2.25	0.8	1998.1	1998.6	1998.35
2.75	1	1997.5	1998.1	1997.8
3.25	1.2	1997	1997.6	1997.3
3.75	1.3	1996.4	1997.2	1996.8
4.25	1.5	1995.9	1996.7	1996.3
4.75	1.7	1995.3	1996.2	1995.75
5.5	2	1994.2	1995.3	1994.75
6.5	2.3	1993	1994.3	1993.65
7.5	2.7	1991.8	1993.3	1992.55
8.5	3	1990.5	1992.3	1991.4
9.5	3.4	1989.3	1991.3	1990.3
10.5	3.8	1988.1	1990.2	1989.15
11.5	4.1	1986.8	1989.1	1987.95
12.5	4.5	1985.5	1988.1	1986.8
13.5	4.9	1984.2	1987	1985.6
14.5	5.3	1982.8	1985.8	1984.3
15.5	5.7	1981.5	1984.8	1983.15
16.5	6.1	1980.2	1983.6	1981.9
17.5	6.4	1978.9	1982.5	1980.7
18.5	6.8	1977.6	1981.4	1979.5
19.5	7.2	1976.2	1980.4	1978.3
21	8	1973.7	1978.2	1975.95
23	8.7	1971	1976	1973.5
25	9.5	1968.3	1973.8	1971.05
27	10.3	1965.6	1971.5	1968.55
29	11.1	1962.9	1969.2	1966.05
31	11.9	1960	1966.8	1963.4
33	12.7	1957.3	1964.6	1960.95
35	13.6	1954.4	1962.1	1958.25
37	14.4	1951.5	1959.7	1955.6
39	15.3	1948.6	1957.3	1952.95
41	16.1	1945.7	1954.9	1950.3
43	16.9	1942.8	1952.5	1947.65
45	17.8	1940	1950.1	1945.05
47	18.6	1937.1	1947.7	1942.4
49	19.4	1934.2	1945.3	1939.75
51	20.3	1931.3	1942.9	1937.1
53	21.1	1928.3	1940.4	1934.35
55	22	1925.3	1937.9	1931.6
57	23	1922.1	1935.2	1928.65
59	23.8	1919.2	1932.8	1926
61	24.7	1916.1	1930.2	1923.15
63	25.6	1913	1927.6	1920.3
65	26.5	1909.8	1925	1917.4
67	27.4	1906.7	1922.4	1914.55
69	28.4	1903.6	1919.8	1911.7

At 115 cm, a change in the depositional regime appears to occur with a shift to increased grain size (figure 8.7) and two distinctive peaks occur; the first between 105.5 cm and 90.5 cm with grain sizes typically >5.5 % and a maximum grain size peak of 12.5 % at 102.5 cm; the second peak occurs between 62.5 – 26.5 cm with a mean grain size of 10.7± 2.17 % and a maximum grain size of 19.7 % occurring at 35.5 cm. Grain size begins to decrease from around 26.5 cm to reach a grain size of 5.6 ± 0.64 % for the top 10 cm of core GC023. Data presented in appendix 11.

8.3.3.2 Treated sediment grain size > 63 μm

Grain size > 63 μm for the digested and de-calcified (from hereon referred to as 'treated') sediment samples shows similar trends to the raw grain size record, that the grain size is finer below 115 cm and coarser above, with the peak grain size occurring around 36 cm (figure 8.2). However, treated sediment samples show coarser grain sizes than the raw samples (typically greater than 6 vol-% in the lower section and > 10 vol-% in the upper section of the core).

The treated samples appear to uncover more variability in grain size > 63 μm than the raw sediment samples, e.g. the lower section has two peaks where grain size % nearly doubles, a feature not seen in the raw sample series (figure 8.2). This suggests that the grain size of the raw sediment sample series may at times be dominated by the finer particles of organic material or carbonate present in the sediment, rather than minerogenic sediment.

8.3.4 Magnetic Susceptibility

Low frequency and high frequency magnetic susceptibility (χ) readings for core GC023 show good agreement (appendix 12), though at times lower values in the high MS indicate the presence of fine-grained magnetic particles (Dearing, 1998).

Magnetic susceptibility varies around a mean of 7.56 ± 0.97 SI units from the base of the core up to 135 cm, though slightly higher χ (>9) is common between the base and 279 cm. At 135 cm, χ gradually begins to increase, peaking at 48.9 SI units at 38 cm core depth. This gradual increase is punctuated by a small χ peak of 28.5 SI units at 80 cm core depth. After ~34 cm, χ begins to decrease to a value of 35.2 SI units at the core top (figure 8.7).

A strong χ: grain size relationship exists for core GC023 ($r = 0.86$, $p = 0.0$) with higher χ values typically occurring with coarser grain sizes (figure 8.8).

8.3.5 Water content and dry bulk density

The dry bulk density and water content of GC023 sediments were primarily determined for the purpose of calculating mass specific magnetic susceptibility since water is diamagnetic (Dearing, 1998).

The sediments of core GC023 typically have high water contents, with all samples retaining > 40% water (figure 8.7; appendix 13). Water content is greater at the top of the core (~ 58 %) than at the bottom of the core (41 %) probably due to the dewatering of the sediment through compression from the overlying sediments.

There is a gradual decrease in the dry bulk density of the sediments from ~ 0.94 g/cm^3 at the base of the core to 0.57 g/cm^3 at the core top. Again this is likely due to compression effects of overlying sediments.

8.3.6 Bulk sediment geochemical data

8.3.6.1 Total carbon content (C_{total})

The % total carbon (C_{total}) remains fairly stable at 3.3 ± 0.05 % from the base of the core to 125 cm. Apart from the isolated peak of 4.16 % C_{total} at 110 cm, the % C_{total} increases (with some variability) towards the top of the core, reaching a maximum C_{total} (excluding the peak) of 4% (figure 8.7) at 0 cm. Data presented in appendix 14.

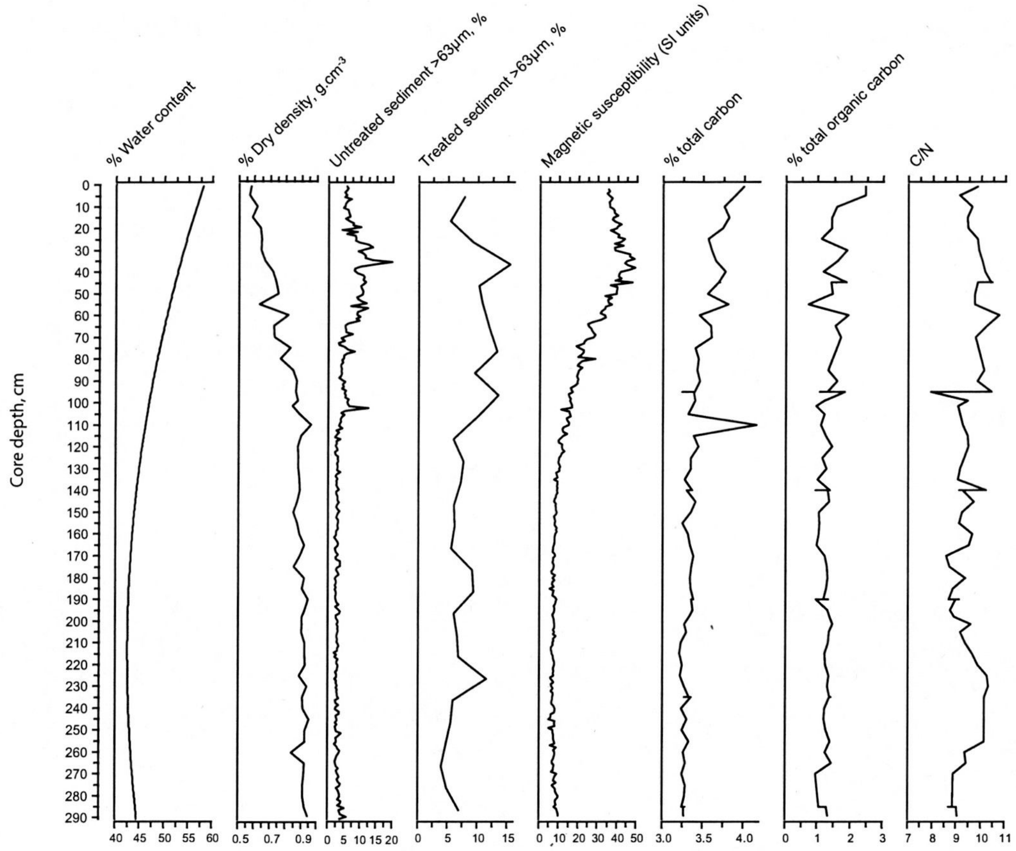

Figure 8.7 Sedimentological properities of core GC023. Units are displayed on the top axis.

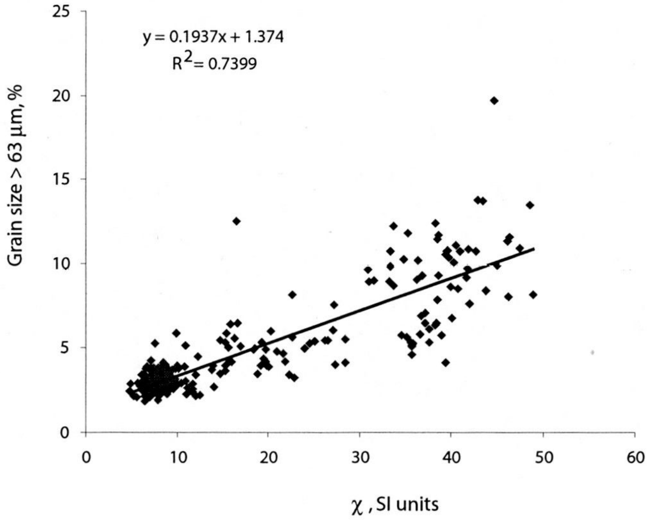

Figure 8.8 Biplot of magnetic susceptibility (χ) and grain size > 63 μm for Loch Sunart core GC023. The linear regression equation and R^2 are also shown.

8.3.6.2 Total Organic Carbon content (TOC)

With the exception of lower % total organic carbon (TOC) between 280-275 cm, % TOC remains fairly stable between 289 – 170 cm with a mean of 1.27 ± 0.12 %, largely following the C_{total} trends (figure 8.7). TOC decreases slightly at 165 cm, from where it increases (with great variability) to 1.93 % at 60 cm, and rapidly drops to 0.7 % TOC at 55 cm. TOC then increases towards the core top demonstrating relatively large shifts (~0.8%) in TOC until the maximum TOC of 2.6% at 1 cm.

8.3.6.3 C/N ratio

GC023 C/N ratios vary around a mean of 9.49 ± 0.55 and there appear to be 3 main C/N events in the core (figure 8.7; appendix 14). A high ratio (> 10) period occurs between 255 – 220 cm, followed by C/N ratios (~ 9.2) indicating a more marine influence at the core site between 205 cm and 99 cm. The top 95 cm of the core sees C/N ratios fluctuating between 9.74 and the maximum C/N ratio of 10.73, before the C/N ratio gradually decreases to ratio of around 9.86 at the core top. A similar range of C/N ratios is seen in a nearby core from Loch Sunart's main basin (*pers. comm.*, Greg Anton, 2005). Sample repeats taken at 95 cm show 3 very different C/N ratios of 7.93, 9.47 and 10.45; this is likely to demonstrate the heterogeneous nature of sediment within the core rather than analytical error.

8.3.6.4 High resolution XRF trace element data.

Trace element geochemistry from core GC023 shows high frequency variability for all elements (figure 8.9). However, the low frequency trends and shifts seen in the data are thought to be due to the dewatering of these high water content sediments at the core breaks (i.e. where the core has been split into 3 lengths; *pers. comm.* Dr. W. Austin, 2005), with maximum counts typically occurring towards the breaks (figure 8.4). Since the dewatering effects cannot be separated from natural variability, these geochemical data unfortunately cannot be interpreted with confidence.

It is also difficult to separate environmental variability from noise when counts per second measurements are low counts, i.e. < 50 counts per second (*pers. comm.* Dr. W. Austin, 2005), as is the case for (Cu), strontium (Sr), vanadium (V), chromium (Cr),

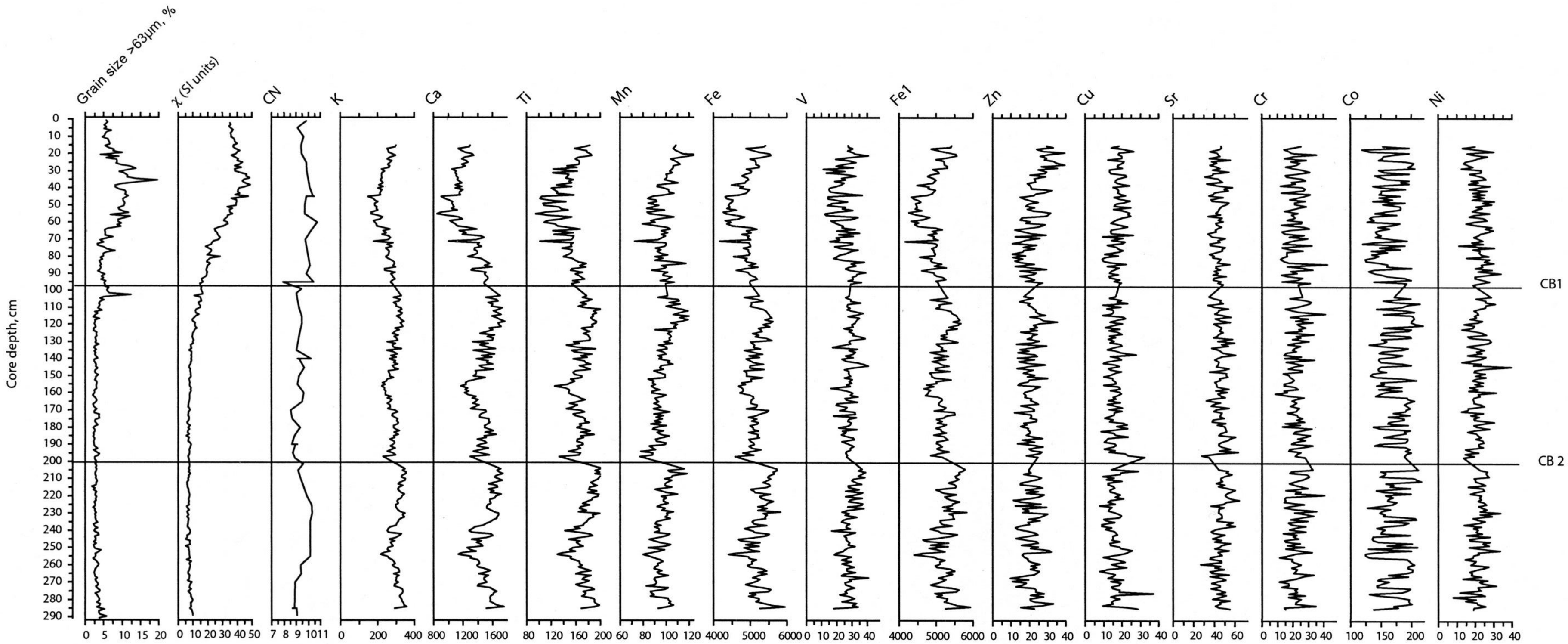

Figure 8.9 High resolution XRF geochemical data from Loch Sunart core GC023. Units for grain size > 63 μm and magnetic susceptibility (χ) are shown on the top axis. Element data is in units of counts per second. Fe1 represents the oxidised state of iron. Core breaks (CB1 and CB2) are indicated by a black line. Grain size, magnetic susceptibility (χ) and CN ratios are shown for comparison to figure 8.1 and 8.4. Data obtained by WENA and NNP at the University of Bremen via the EU Palaeostudies programme.

nickel (Ni) and zinc (Zn). Though data for cobalt (Co) fluctuates between ~125 – 200 counts per second, this data is also too noisy to interpret. Potassium (K), calcium (Ca), titanium (Ti) and iron (Fe) all show a slight decrease towards the core top and have similar trends as indicated by strong positive correlation coefficients ($r > 0.78$, $p = 0$) Manganese (Mn) has a weaker relationship with K, Ca, Ti and Fe ($0.36 < r < 0.58$, $p = 0$) and appears to increase slightly towards the core top.

Despite concerns relating to the feasibility of using the high resolution geochemical data from GC023 due to dewatering effects and at times, low counts, Zn appears to show little variability around the core breaks but a definite increase from around 70 cm. Data presented in appendix 15.

8.3.6.5 Low resolution XRD data

To aid the interpretation of the high resolution XRF geochemical data and distinguish any underlying trends from dewatering effects, discrete bulk sediment samples were analysed via XRD measurements (appendix 15).

Sodium oxide (Na_2O), chloride (Cl) and iron oxide (Fe_2O_3) all show a gradual increase from the core bottom towards the core top, whilst potassium oxide (K_2O), silicon oxide (SiO_2), aluminium oxide (Al_2O_3) and magnesium oxide (MgO) all decreased towards the core top (figure 8.10). Phosphorous oxide (P_2O_5) percentage abundance is highest at the core top and bottom, whilst % sulphur oxide (SO_3) is lowest at the core top and bottom. Manganese oxide (MnO) displays a very distinct step at 160-185 cm, with higher values in the core top. Titanium oxide (TiO_2) shows fluctuating % abundance in the bottom half of the core with a significant decrease from 160 cm to 20 cm, where TiO_2 shift towards increasing values at the core top.

Many of the geochemical data show a marked decrease in concentration during the coarse grain size event (in the untreated sediment grain size record) around 40 cm core depth (figures 8.10) and fluctuations occurring in the lower half of the core; where 'treated' sediment grain size points to coarser grain size composition (figure 8.10).

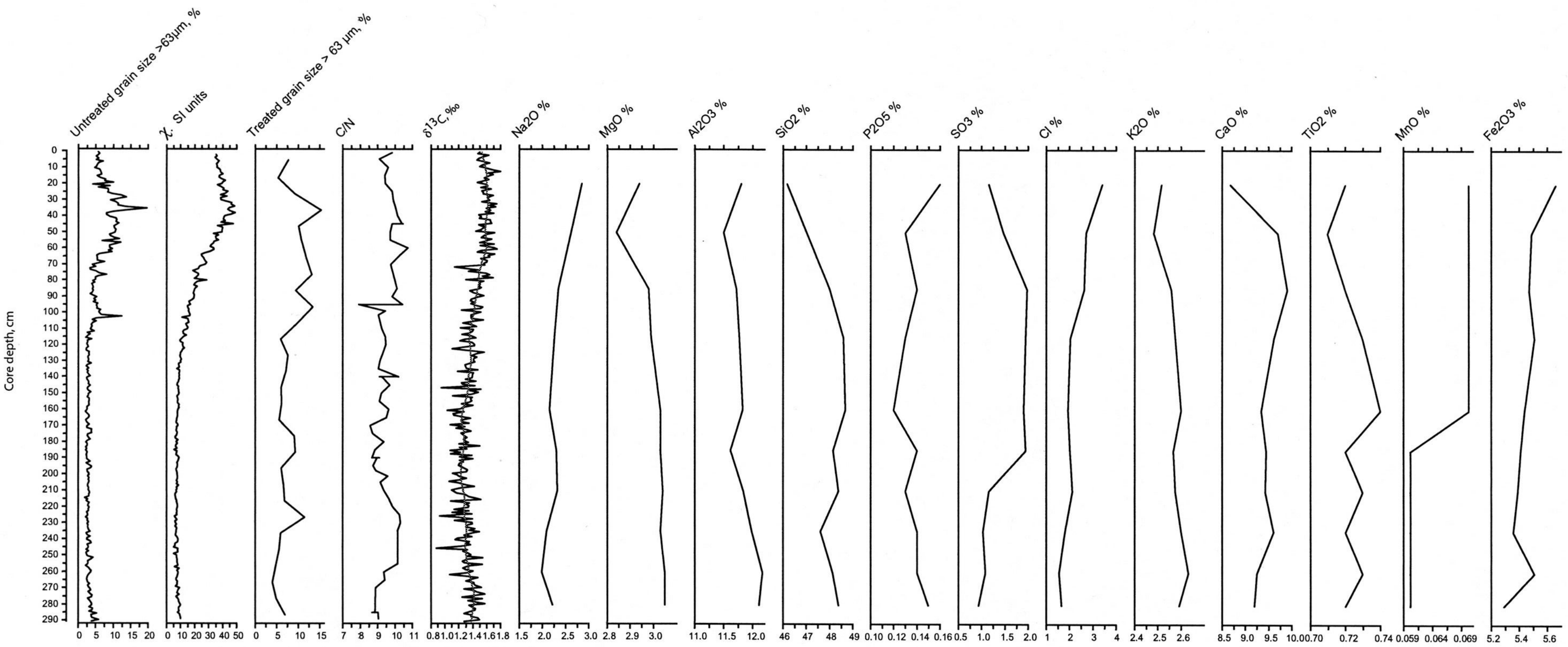

Figure 8.10 Low resolution XRD data (in %) from Loch Sunart core GC023. Grain size, magnetic susceptibiity (χ), CN ratio and the $\delta^{13}C$ record from *Cibicides lobatulus* (with a 0.1 LOWESS smoother) are also shown.

8.3.7 Benthic foraminiferal stratigraphy

8.3.7.1 Benthic foraminiferal abundance and diversity

Low-resolution data (every 20 cm) from core GC023 show clear variations in benthic foraminiferal abundance and diversity (figure 8.11). Since species diversity determined using the Shannon-Weaver and Fisher-α indices typically show linear relationships with each other and with the equitability of the assemblage (chapter 5), only the Shannon-Weaver index has been shown in figure 8.11 for diagrammatical reasons. Fisher-α are indicated in the text for comparison to other studies (e.g. Murray, 1973, 1991). Diversities range from 2.06 to 3.196 for the Shannon-Weaver index and from 6.7 to 18.4 for the Fisher-α index. As with the modern surface samples (chapter 5), richer species diversity and higher equitability typically occur in samples with a higher benthic foraminiferal abundance per gram (chapter 5), and the Shannon-Weaver index and benthic foraminiferal abundance are well correlated ($r = 0.707$, $p = 0.002$).

From the base of the core, benthic foraminiferal abundance decreases from 2741 specimens.g^{-1} to 778 specimens.g^{-1} at 140.5 cm, with a large increase in abundance (3887 specimens.g^{-1}) occuring at 160.5 cm. After this, abundance steadily increases from 1363 specimens.g^{-1} at 120.5 cm to 1601 specimens.g^{-1} at 80.5 cm and shows a large increase in abundance from 60.5 cm to the maximum benthic foraminiferal abundance of 5693 specimens.g^{-1} at 20.5 cm. Abundance increases slightly towards the core top. Benthic foraminiferal abundances have been calculated via specimens.g^{-1} rather than volume due to potential problems with the compaction of sediment in the core (*pers comm.*, Dr. Austin, 2005). Though species diversity also shows a pronounced peak (Shannon-Weaver = 3.06, Fisher-α = 13.5) at 160.5 cm, the diversity curve differs from the abundance curve in that species diversity is more pronounced in the basal assemblage and the core top assemblages (0-60 cm). The basal assemblage has a Shannon-Weaver diversity of 2.68 (Fisher-α = 10.9), decreasing to 2.06 (Fisher-α = 6.09) at 280.5 cm, increasing to 3.2 at the core top (Fisher-α = 17.6).

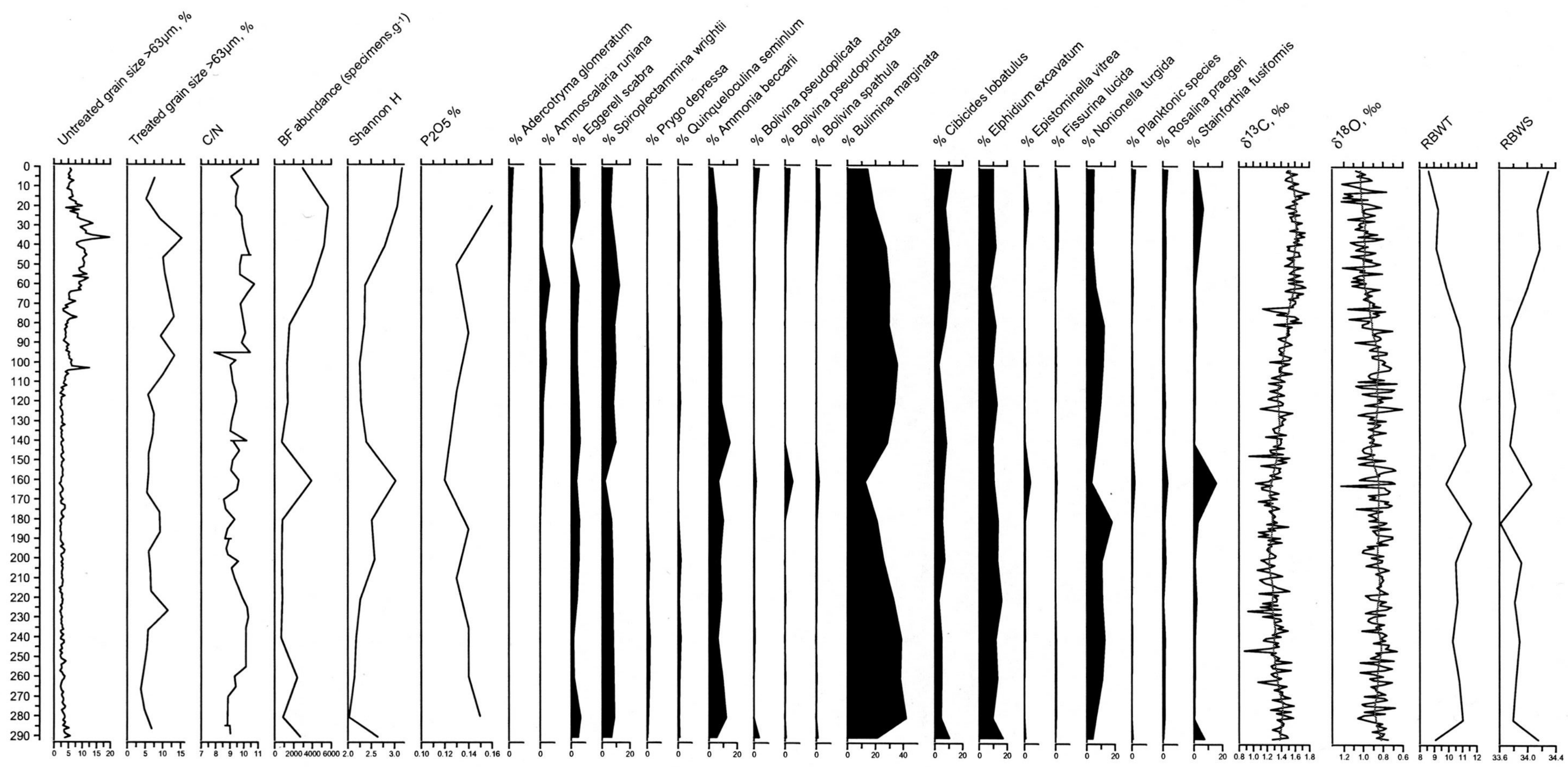

Figure 8.11 Benthic foraminiferal taxa with percent abundances > 2% along with benthic foraminiferal abundance (BF) and benthic foraminiferal species diversity (Shannon H), and the reconstructed bottom water temperature (RBWT) and reconstructed bottom water salinity (RBWS; using the modified weighted-average partial least squares transfer function model outlined in chapter 7) for Loch Sunart core GC023. Also shown are the stable oxygen and carbon compositions from the benthic species *Cibicides lobatulus* (which typically have associated errors of 0.03 ‰) and LOWESS smoothers with a span of 0.1. Sediment grain size, C/N ratios and phosphorous concentration (P_2O_5 %) are shown for comparison.

8.3.7.2 Benthic foraminiferal assemblages

Sediment samples from core GC023 are primarily dominated by *Bulimina marginata* with samples commonly having abundances between 20-40 %. Secondary species with abundances between 10 – 20 % include *Spiroplectaminna wrightii, Ammonia beccarii, Cibicides lobatulus* and *Nonionella turgida.*

The benthic foraminiferal basal assemblage (at 290.5 cm) is similar to the assemblage at 160.5 cm, with reduced *A. beccarii*, *B. marginata* and *S. wrightii* abundance, and increased *Bolivina* species, *Epistominella vitrea* and *S. fusiformis* abundance. However, a noticeable difference in the two assemblages is that the basal assemblage also displays a significant increase in *C. lobatulus* and *Elphidium exavatum* abundances (figure 8.11).

Elphidium excavatum appears to decreases slightly towards the top of the core whilst *Gavelinopsis praegeri* and *C. lobatulus* increases (figure 8.11). *E. scabra* shows a definite response to the grain size peak at around 35.5 cm, decreasing from ~ 6% to 0%. *Ammoscalaria runiana* appears at 160.5 cm, increasing to ~ 6% abundance before decreasing again towards the top of the core. *Adercotryma glomeratum* is largely absent from the core, only appearing at 40.5 cm and then increasing towards the top of the core.

The most significant changes in the benthic foraminiferal assemblages are the peaks and troughs in taxon abundances at 160.5 cm (figure 8.11) with notable decreases of *A. beccarii*, *B. marginata* and *S. wrightii* abundance. The most significant increases in the assemblages are the peaks in abundance of *Bolivina pseudopunctata, Epsitominella vitrea,* and *S. fusiformis* at 160.5 cm. These peaks coincide with a trough in *B. marginata* (12.7 %), and though this is likely to be an artefact of the increasing proportions of other species, as shown by the increase in the Shannon-Weaver diversity index, *B. marginata* abundance was already decreasing from 240.5 cm. Additionally, the benthic foraminiferal abundance peaks at this point. An interesting point to note is that the *N. turgida* abundance at 180.5 cm precedes the taxa abundance changes at 160.5 cm.

8.3.8 GC023 stable isotopic compositions

8.3.8.1 GC023 $\delta^{18}O$

$\delta^{18}O$ values from core GC023 range from 0.61 ‰ to 1.23 ‰ (appendix 16). The record shows high frequency oscillations regularly reaching around 0.4 ‰, superimposed on long term isotopic shifts. A LOWESS smoother through the $\delta^{18}O$ data points to long-term shifts in the record (figure 8.11). The $\delta^{18}O$ record (figure 8.12) frequently displays high frequency isotopic shifts of around 0.4 ‰, which is the equivalent of 2 °C (chapter 7 and Bemis *et al.*, 1998) and has 4 distinct low frequency periods: 1) the relatively stable period from the core bottom to approximately 150 cm core depth, with $\delta^{18}O$ varying between 0.8 - 0.9 ‰; 2) the discrete extreme positive $\delta^{18}O$ value of 1.23 ‰ at 161.5 cm; 3) the brief phase of more positive values between 152 – 138 cm; 3) the shift towards more enriched $\delta^{18}O$ from 102 cm towards the core top.

The $\delta^{13}C$ record shows higher frequency change with isotopic shifts typically around 0.4 ‰. The long-term (i.e. low frequency) trends shows less variability than the $\delta^{18}O$ record, with heavier $\delta^{13}C$ at the base of the core becoming gradually lighter between 250 – 160 cm. At 160 cm there appears to be a shift towards heavier $\delta^{13}C$ until ~ 64 cm, where the long-term $\delta^{13}C$ trend remains fairly stable before shifting towards lighter $\delta^{13}C$ in the top 10 cm.

8.3.8.2 GC023 $\delta^{13}C$

The $\delta^{13}C$ record for GC023 shows similar high-frequency oscillations to $\delta^{18}O$, however the amplitude change of these oscillations frequently appears to be less than 0.2 ‰ (figure 8.12). The long-term shift in the record is clearly visible and appears to be less variable than the $\delta^{18}O$ record. $\delta^{13}C$ values are around 1.45 ‰ at the base of the core and this shift towards isotopically lighter $\delta^{13}C$ values of around 1.20 ‰ at 212 cm, where the $\delta^{13}C$ record remains relatively stable up to 164 cm (figure 8.12). From 164 cm to ~ 68 cm, $\delta^{13}C$ values become progressively enriched in ^{13}C, shifting from a mean of around 1.20 ‰ to 1.6 ‰ and fluctuating between 1.55 - 1.65 ‰, before moving towards slightly more depleted $\delta^{13}C$ values in the top 10 cm of the core.

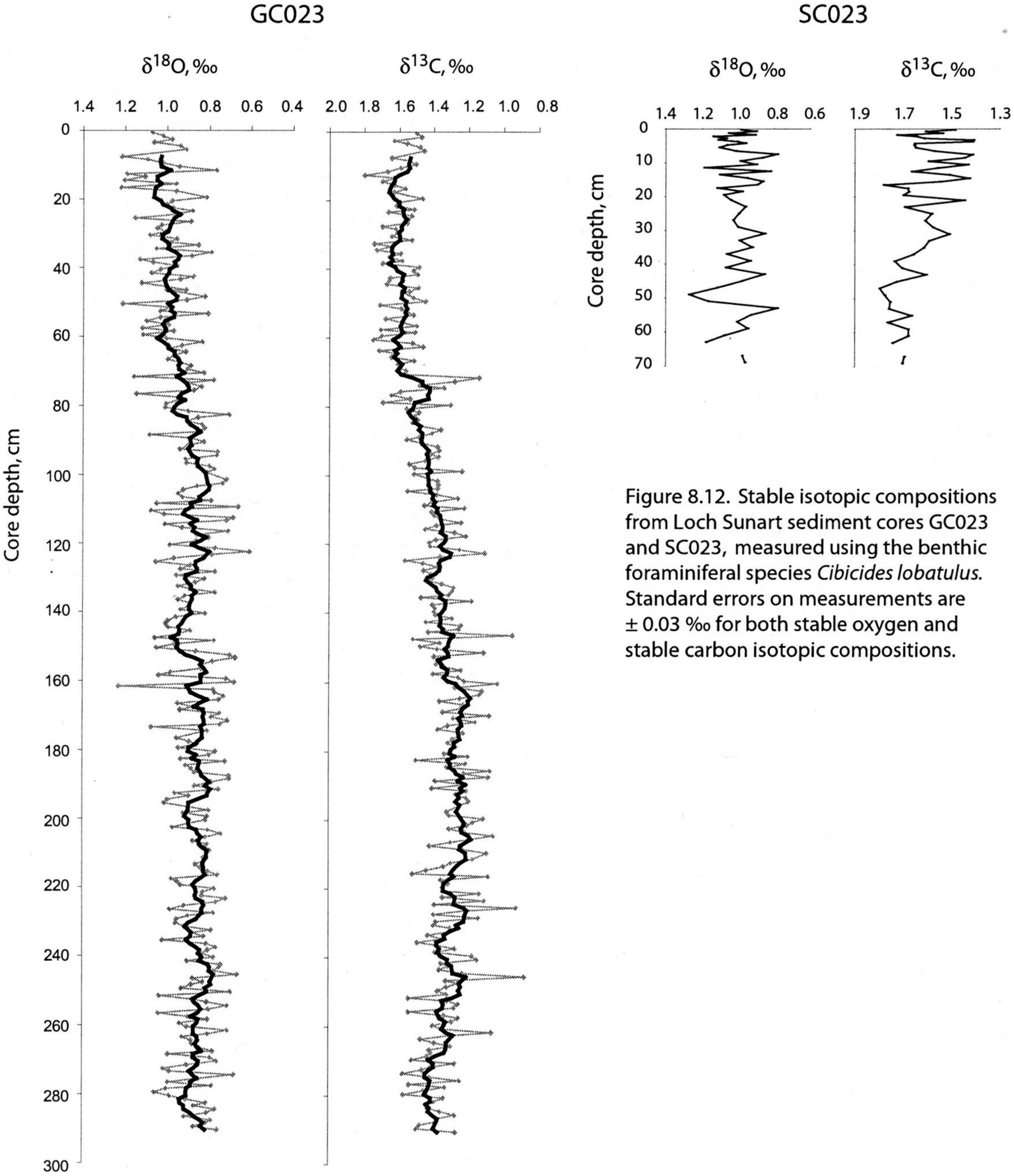

Figure 8.12. Stable isotopic compositions from Loch Sunart sediment cores GC023 and SC023, measured using the benthic foraminiferal species *Cibicides lobatulus*. Standard errors on measurements are ± 0.03 ‰ for both stable oxygen and stable carbon isotopic compositions.

A significant moderate positive $\delta^{18}O:\delta^{13}C$ relationship exists for GC023, with a Pearson's correlation coefficient (r) of 0.518 (p = 0.000), and the magnitude of this correlation is similar to the $\delta^{18}O:\delta^{13}C$ relationships found for modern *C. lobatulus* from Loch Sunart surface sediments.

8.3.9 SC023

8.3.9.1 SC023 $\delta^{18}O$

The $\delta^{18}O$ record in core SC023 is pervaded by frequent isotopic shifts ranging from 0.92 ‰ to 1.41 ‰ with the largest shift (0.51 ‰) occurring between 53 and 49 cm (figure 8.12). There is a slight long-term trend (y = 0.0004x + 1.1281, figure 8.12) towards depleted $\delta^{18}O$ at the top of the core. From the bottom of the core to 43 cm, the $\delta^{18}O$ shows large isotopic shifts after which the $\delta^{18}O$ record is fairly stable with fairly low amplitude (~ 0.2 ‰) $\delta^{18}O$ fluctuations until ~17cm. The amplitude of the isotopic oscillations appear to increase and there is a general move towards isotopically lighter $\delta^{18}O$ values between 17.5 – 7.5 cm, and a period of enriched $\delta^{18}O$ between 6.5 – 2 cm before returning to isotopically lighter $\delta^{18}O$ to the top of the core.

8.3.9.2 SC023 $\delta^{13}C$

Overall, the $\delta^{13}C$ record for SC023 shows a linear trend (y = 0.003x + 1.5457, figure 8.12) from relatively isotopically heavy $\delta^{13}C$ values around 1.7 ‰ at the base of the core, towards lighter $\delta^{13}C$ approximating 1.54 ‰ at the top of the core. Like $\delta^{13}C$ from GC023, the SC023 $\delta^{13}C$ record appears to be 'smoother', with less oscillations than the $\delta^{18}O$ record.

The lack of significant correlation (r = 0.223, p = 0.124) between the $\delta^{18}O$ and $\delta^{13}C$ measurements in core SC023, suggests the $\delta^{18}O$ and $\delta^{13}C$ from this record typically do not covary as much as in GC023, though this could be due to lower sample numbers in SC023 (n = 49).

Stable isotopic compositions of SC023 *C. lobatulus* and GC023 *C. lobatulus* from similar core depths do not match exactly (figure 8.12) but the similarity in the *C. lobatulus* $\delta^{18}O$ trends for the two cores suggests little of the core top was lost during recovery of gravity core GC023. The *C. lobatulus* $\delta^{13}C$ record of SC023 and GC023 also follow similar trends from 0-45 cm; from where the SC023 $\delta^{13}C$ appears to shift towards isotopically enriched $\delta^{13}C$ in comparison to GC023 $\delta^{13}C$ (figure 8.12). This likely reflects a small-scale change in the environmental conditions at the two sites, which are ~ 138 m apart.

8.4 DISCUSSION

8.4.1 Problematic geochronology

The stratigraphic order and similarity of ^{14}C dates from SC023 (SUERC-681) and GC023 (SUERC-677; figure 8.4) suggest these cores are reconcilable with a calculated sediment accumulation rate (SAR) of 0.068 $cm.yr^{-1}$ (for 0-58 cm core depth); similar to those derived from ^{14}C dates in Norwegian fjords (Mikalsen *et al.*, 2001). The two modern ^{14}C dates point to a rapid SAR of 0.6 $cm.yr^{-1}$ from 30 cm to the core top; agreeing well with the anthropogenic influenced high SARs reported from similar depositional environments (e.g. Howe *et al.*, 2002).

However, the rapid slow-down of sedimentation between 30-49 cm (SAR ~ 0.024 $cm.yr^{-1}$) points to potential problems in the geochronology and when the Pb-Cs chronology is plotted alongside the ^{14}C chronology (figure 8.13), the problems of reconciling the two chronological methods are obvious. The combined Pb-Cs chronology suggests that the top 69 cm of sediment at the Loch Sunart core site SC023 was deposited since AD 1920, giving a SAR of 0.78 $cm.yr^{-1}$. This is similar to reported SARs (using Pb) from other fjordic environments, e.g. Howe *et al.,* (2002) reported a SAR of ~ 0.7$cmyr^{-1}$ in Loch Etive, whilst SARs of approximately 0.15$cmyr^{-1}$ and 0.68$cmyr^{-1}$ have been reported for NW Norwegian fjords (Kristensen *et al.*, 2004) and Gullmar Fjord, Sweden (Nordberg *et al.*, 2000). The two modern radiocarbon dates around 30 cm in the GC023 core agree well with the Pb-Cs chronology (figure 8.13) suggesting that the geochronology for the top 30 cm of both GC023 and SC023 can be assumed to be robust.

The agreement between the two chronological methods breaks down at ~ 30-49 cm depth, with the radiocarbon chronology appearing to be offset by 755 ± 95 cal years. Offsets of this magnitude are often seen in Danish fjords which are influenced by old

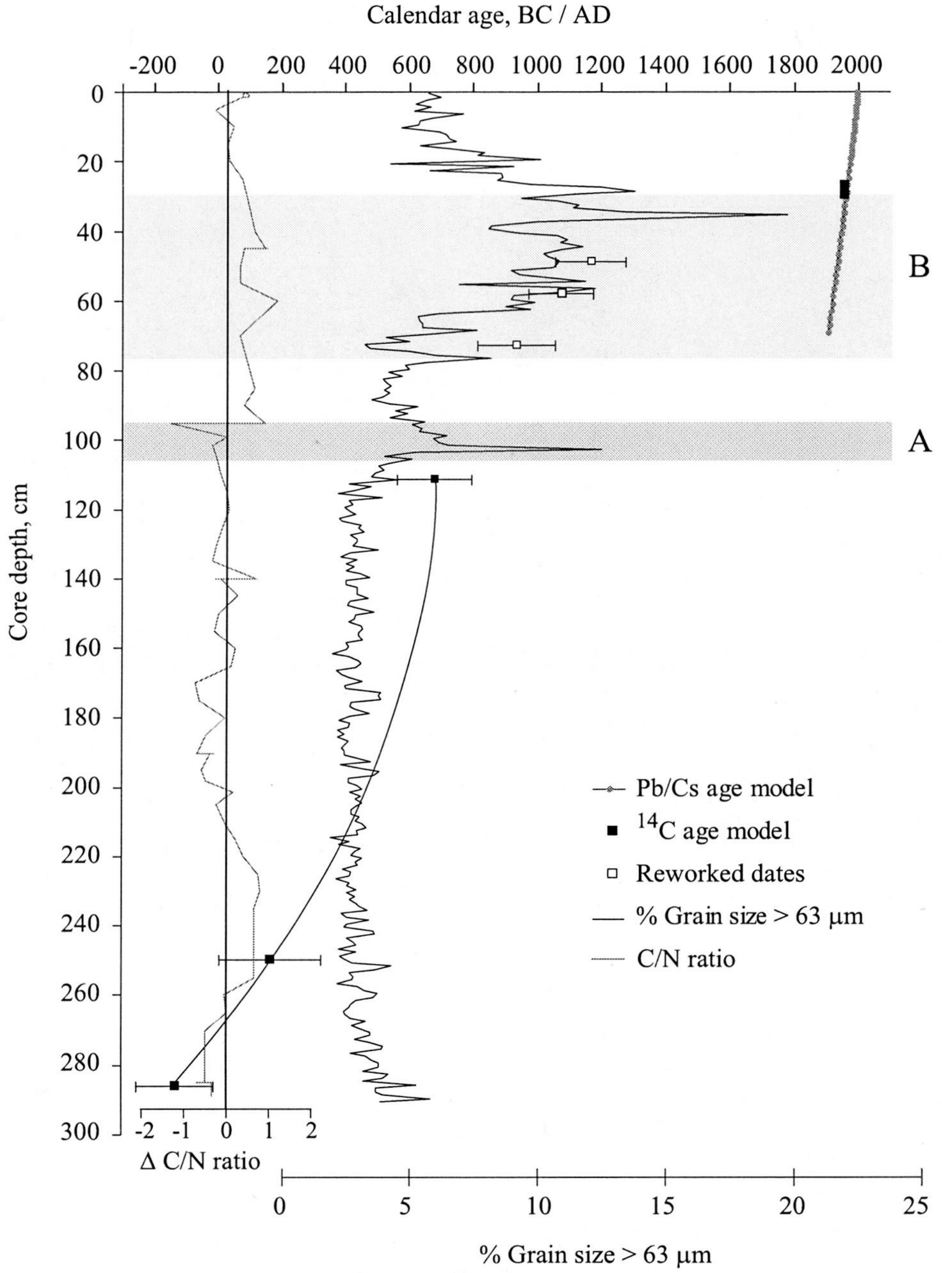

Figure 8.13 The problems of reconciling the radiocarbon (^{14}C) chronology of core GC023 with the lead-caesium (Pb/Cs) chronology from core SC023. The dates in the lower part of the core (black squares) were used to construct the ^{14}C age model (black squares). The sharp increase in % grain size > 63 μm at 113 cm depth and the subsequent decrease in sedimentation rate points to a period of winnowing or scouring of the sediments (A), probably by strong bottom currents. This is supported by a negative ΔC/N (normalised to the mean) shift towards more marine C/N values. The disparity between Pb/Cs chronology and the 14C dates (unfilled squares) lying within the high (>5%) grain size values suggests that these ^{14}C dates are likely to be reworked, thus they are omitted from the 14C age model. The ΔC/N ratio suggests increased terrigeneous inputs at this time (B). The modern dates agrees well with the Pb/Cs data and may have calcified during a time of negligible winnowing and decreased input from the catchment.

carbon from the limestone bedrock geology (chapter 2; Heier-Nielsen *et al.*, 1995). The predominantly igneous/metamorphic geology of Loch Sunart will not contribute a 'hard water' effect to Loch Sunart ^{14}C measurement, though inwash of 'old carbon' in the form of stable organic residues from eroding peat and mor humus in the catchment (Appleby *et al.*, 1985) could significantly influence the $^{14}C/^{12}C$ ratio, and GC023 C/N ratios point to increased input from the surrounding catchment (figure 8.13).

Presently, the main basin water of Loch Sunart is frequently exchanged with coastal waters (Gillibrand *et al.,* 1995) and any 'old carbon' signal is likely to be greatly diluted by the $^{14}C/^{12}C$ signal of the coastal waters. GC023 *C. lobatulus* $\delta^{13}C$ (a proxy for bottom water salinity; BWS) from 80 cm upwards is fairly enriched in ^{13}C, suggesting coastal waters are a significant influence in main basin water during this period. Radiocarbon curves over the past 2 millenia exhibit a ^{14}C plateau (section 2.7.9). The plateau in the marine radiocarbon curve is much 'smoother' than the atmospheric curve (Stuiver *et al.,* 1998) and though ^{14}C dates from fjordic environments are likely to display a ^{14}C age influenced by atmospheric ^{14}C, it is unlikely that the ^{14}C plateau explains the observed ^{14}C: Pb-Cs disparity.

The large gap between the calibrated ^{14}C date of 725 ± 60 AD at 111.5 cm (SUERC-679) and the Pb-Cs date of AD 1920 at ~ 70 cm points to a SAR of 0.034 $cmyr^{-1}$; fairly low for a fjordic environment in comparison to other studies. Grain size and magnetic susceptibility data both point to a dynamic change in either sedimentation or hydrography taking place at ~ 102 cm depth in GC023, the section of the age model which displays a SAR decrease (fig. 8.13). The core site is landward of a sill and the steep-sided bathymetry of the Dun Ghallain Deep (figure 2.9) is likely to funnel and accelerate tidal currents (which can propagate to the floor of Loch Sunart; Gillibrand *et al.*, 1996) and currents associated with deep water renewal events, over the core site. Therefore, the sharp increase in grain size and the slow SAR likely represents winnowing of the sediment as bottom water current strength increases (e.g. Bianchi & McCave, 1999a; Mikalsen *et al.*, 2001). The hypothesis of sediment winnowing or removal in deep basins of Loch Sunart; basins which are usually thought to hold thick sediment packages due to sediment focussing; is supported by the seismic profile shown in figure 8.14, which demonstrates that the Holocene sediment package at ~

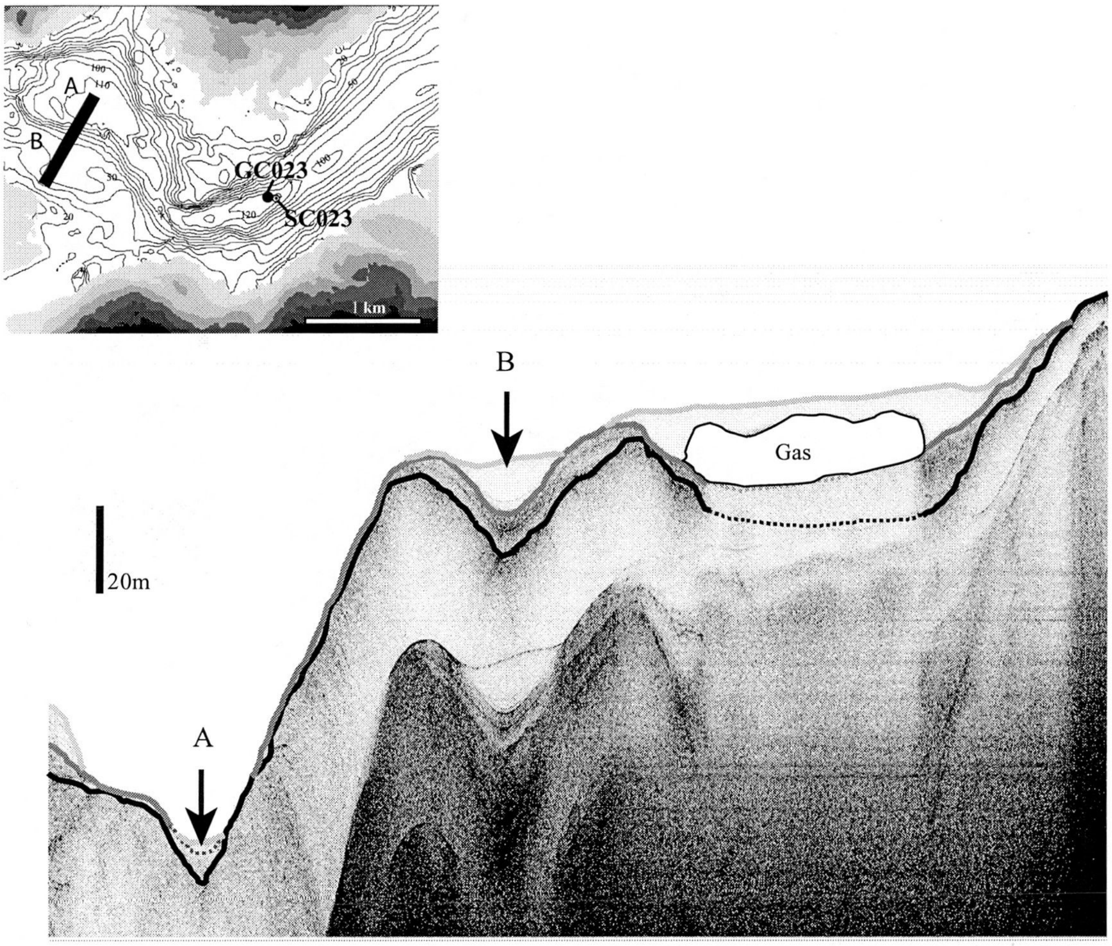

Figure 8.14 Seismic profile of the deep basin in Loch Sunart, near Laga, maximum water depth approximately 111 m. The inset shows the location of the seismic profile near the GC023 core site in the Dun Ghallain Deep. Seismic characteristics suggest the black line is possibly bedrock, the dark grey line is the upper boundary of the Late-Glacial/Younger Dryas sediment package and the light grey line represents the modern day sediment surface, i.e. the surface of the Holocene sediment package. The sediment package at on the shelf (B) is clearly thicker than the sediment package in the deep at A, which one may expect to be thicker due to sediment focussing, supporting the hypothesis of winnowing of sediments in Loch Sunart's deepest basin. Data obtained from Dr. C. R. Bates.

111 m water depth is substantially thinner than the Holocene sediment package at ~ 50 m water depth. These seismic data were not available at the time of coring.

If the sharp increase in grain size at ~ 102 cm depth is due to winnowing, then the ^{14}C data above this depth are likely to be from reworked shell material and therefore will not be used in the age model (figure 8.13). Molluscs used to obtain the ^{14}C dates below 102 cm (SUERC-679, SUERC-680 and CAMS-82821) were obtained from clayey-silt sediment and are likely *in situ*; thus the chronology between ~300 cm and ~102 cm is assumed to be reliable (figure 8.13).

However, the grain size record of GC023 is unlikely to be caused solely by winnowing since the geochemical chronology points to rapid sedimentation from approximately AD 1920 onwards (i.e. from 69cm to the core top); a period which displays the coarsest grain size composition. An increase in magnetic susceptibility from ~ 100 cm core depth and a shift from typical marine C/N ratios to high ratios point to an increased input from the catchment coinciding with this phase of increased sediment accumulation. The steady shift back towards more 'marine' C/N ratio from around 35 cm core depth coincides with the shift towards finer grain sizes and decreased magnetic susceptibility (fig 8.13), suggesting either a change in catchment erosion or a decrease in bottom current influence i.e. reduced winnowing. A switch back to sedimentation without a winnowing influence would explain the good agreement of the two modern dates (SUERC-675 and AA-51569) with the Pb-Cs chronology, since the bivalves used for dating would have been *in situ* within the sediment (figure 8.13). Interestingly, Appleby *et al.,* (1985) suggest peak sedimentation rates in a core recovered from Loch Frisa (a freshwater loch on Mull) occur in the early 19th century, with a small decline around AD 1950.

8.4.1.1 Age models

The apparent winnowing of sediment at core site GC023 results in the top and bottom section of the core being irreconcilable. A 200-year difference between ^{14}C and Pb-Cs can also be seen in core HM122-10BC from Ranafjorden (Kristensen *et al.*, 2004). Kristensen *et al.,* (2004) exclude this date from the age-model and construct a geochronology from the basal ^{14}C date and the Pb-Cs age model. However, the differences in geochronology with depth for core GC023, along with large changes in sedimentology and geophysical evidence of thin sediment packages in deep basins, demonstrate that sediment removal and winnowing processes occur in the deep basins of Loch Sunart, and most probably, other fjordic environments. It has also highlighted the potential problems of obtaining few age control points for constructing geochronologies, as SARs can vary over time, and although the number of ^{14}C dates from GC023 has complicated the interpretation of sedimentation in these fjords, it has also pointed to potential hiatuses.

Though erroneous ^{14}C dates in stratigraphy can occur with bioturbation, to 'force' an age model from the basal ^{14}C of GC023 to the beginning of the Pb-Cs data (as Kristensen *et al.,* 2004 did), particularly given independent data pointing to sediment removal from the site, would result in an extremely unrealistic core geochronology.

Thus two age models are used in this study. The first (Pb-Cs age model) is constructed from the Pb-Cs data (table 8.2) and is applied to the top 69 cm of core GC023. The Pb-Cs age model has an average SAR of 0.78 $cm.yr^{-1}$, and can be calculated using the 3rd order polynomial equation ($R^2 = 1$) which reproduces the measured Pb-Cs chronology with maximum errors of ± 0.24 years

$$y = -0.0000102350300784856 * x^3 + 0.0031776057627003 * x^2 + 1.12265137883038 * x - 51.078992155376 \qquad (Eq.\ 8.2)$$

The second age model (^{14}C age model) differs from the age model given by equation 8.1, in that it is constructed using the calibrated (ΔR corrected) ^{14}C dates of SUERC-679, SUERC-680 and CAMS-82821, i.e. it excludes the possibly reworked dates from SUERC-677 and AA-51570. The age model is calculated from the 3rd order polynomial equation (where $R^2 = 1$);

$$y = 0.026446543157518 * x^2 - 5.84201379909619 * x + 1597.59450242915 \qquad (Eg.\ 8.3)$$

This ^{14}C age model is applied to GC023 core depths below 105 cm, yeilding an average SAR of 0.2045 $cm.yr^{-1}$.

The high SARs calculated for each age model demonstrate the potential of obtaining high resolution studies from the fjordic environments of NW Scotland, and thick packages on the shelf areas in Loch Sunart (e.g. figure 8.13) are likely to yield high resolution palaeorecords, possibly spanning the Holocene. The problematic geochronology of core GC023 highlights two important issues: a) the need to understand modern processes influencing the site, i.e. current activity and sediment deposition, and b) the importance of reconnaissance geophysical surveys prior to coring. Despite the construction of the two age models, the chronology of core GC023 is questionable, and therefore, changes in the palaeoenvironmental proxies obtained from GC023 will be first be discussed with relation to depth.

8.4.2 Changes in fjordic circulation during the past 2000 years: evidence of increasing marine coastal water influence at the core site

8.4.2.1 Bulk sediment geochemical data

The clearest sign of a change in bottom water conditions is the significant shift in manganese (MnO) concentration at ~ 185 cm (figure 8.10). This shift signifies a major change in the redox boundary (Chester, 1990), pointing to better ventilation and oxygenated conditions from 185 cm to present, as seen by the frequency of present day main basin water exchange (chapter 3). Vanadium (V) concentration tends to be enriched in anoxic conditions (Morford & Emerson, 1999; Yarincik *et al.*, 2000) and although there are problems with the high resolution geochemical data, V does appear to be enriched in the bottom half of the core (figure 8.9). The occurrence of the MnO shift and $\delta^{13}C$ shift (though small) at around the same time (figure 8.15) may point to a major regime change in ocean or atmospheric climate forcing of fjord circulation around this time.

Sodium and chloride are typical seawater elements (Open University, 1995) but are also present in igneous and metamorphic rocks, with sodium oxide (NaO) constituting a significant component (~5%) of the rock geochemistry. However chloride (Cl) is typically a trace component in these rocks (*pers comm.*, Dr. W. Stephens, 2005), thus the increase of Cl (and most probably NaO) towards the top of GC023 is likely to reflect the increasing influence of coastal saline waters rather than detrital inputs eroded from the local geology.

8.4.2.2 Stable carbon isotopes – a signal of marine influence at the core site?

Cibicides lobatulus is thought to calcify close to the isotopic equilibrium of $\delta^{13}C$ dissolved inorganic carbon ($\delta^{13}C_{DIC}$) in seawater (chapter 6; Mackensen *et al.*, 1993), thus *C. lobatulus* $\delta^{13}C$ from GC023 should reflect changes in the $\delta^{13}C_{DIC}$ of the overlying water masses at the core site. Unlike $\delta^{18}O$, temperature exhibits little influence on stable carbon isotopic composition (e.g. Grossman, 1984; Romanek *et al.*, 1992), however salinity does affect $\delta^{13}C_{DIC}$ (e.g. Mook, 1971; Spiker, 1980; Lubinski *et al.*, 2001; Bauch *et al.*, 2004). Since *C. lobatulus* $\delta^{13}C$ probably calcifies close to the seawater $\delta^{13}C_{DIC}$ (chapter 6), it is likely that GC023 *C. lobatulus* $\delta^{13}C$ traces changes in the origin of source water at the core site, i.e. the admixing of fjordic $\delta^{13}C_{DIC}$ and coastal water $\delta^{13}C_{DIC}$, and thus likely reflects salinity variations with isotopically enriched *C. lobatulus* $\delta^{13}C$ representing a stronger influence of 'marine' coastal waters in the main basin of Loch Sunart (e.g. Mackensen & Bickert, 1999). This hypothesis is supported by the fairly strong relationship between the *C. lobatulus* $\delta^{13}C$ and grain size > 63 μm ($r = 0.630$, $p = 0.0$, $n = 285$) with enriched $\delta^{13}C$ (suggesting a 'marine' signal) typically co-occurring with coarser sediments (figure 8.16). The strength of the grain size: $\delta^{13}C$ relationship thus points to enhanced current activity and basin exchange significantly influencing the grain size record of GC023, particularly within the upper core.

Therefore, the shift towards enriched $\delta^{13}C$ at 160.5 cm suggests increased ventilation and influence of marine coastal waters at the core site, a hypothesis which is consistent with other proxies such as the redox potential of the sediments, concentration of seawater elements and benthic foraminiferal response (figure 8.15), and suggests a long-term change in fjordic circulation driven by either ocean circulation or atmospheric climate.

High frequency variability in the $\delta^{13}C$ record exemplifies the sensitivity of Loch Sunart sedimentary archives to environmental change. The large and brief light $\delta^{13}C$ events (e.g. at 245.5 cm, 224.5 cm, 146.5 cm and 71.5 cm) demonstrate that rapid changes in conditions can be captured in these high resolution records (e.g. figure

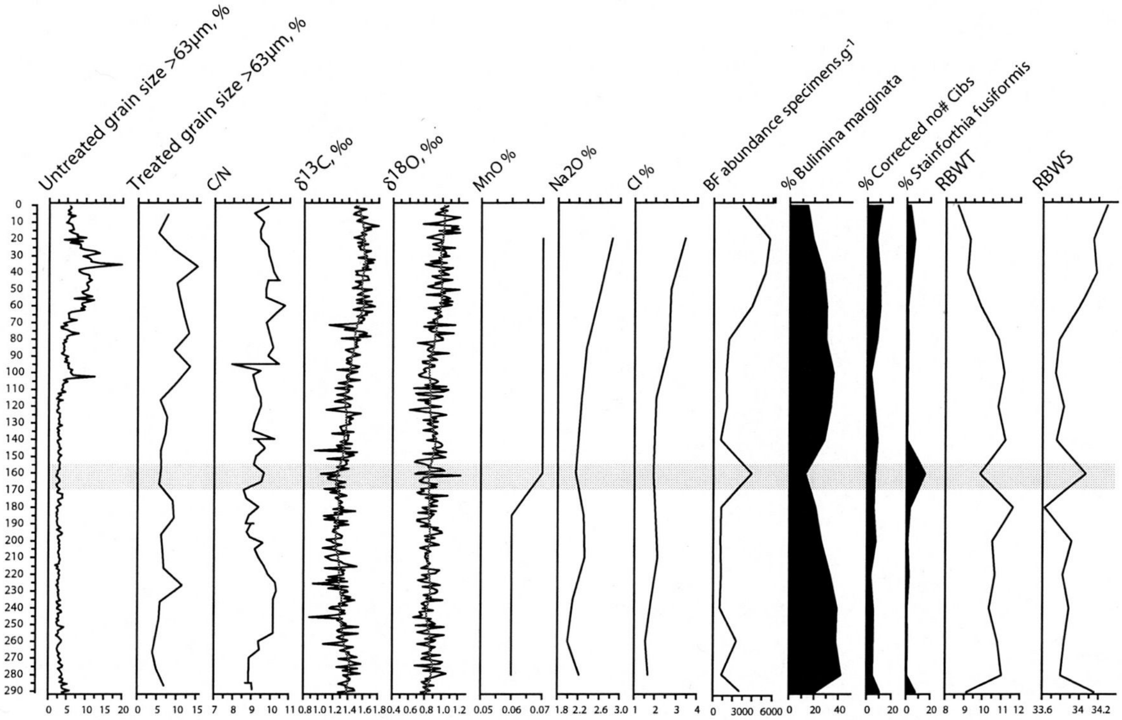

Figure 8.15 Sediment and foraminiferal proxies from GC023 pointing to the increasing influence of saline coastal waters at the core site and the onset of oxygenated conditions in the main basin (shaded grey bar).

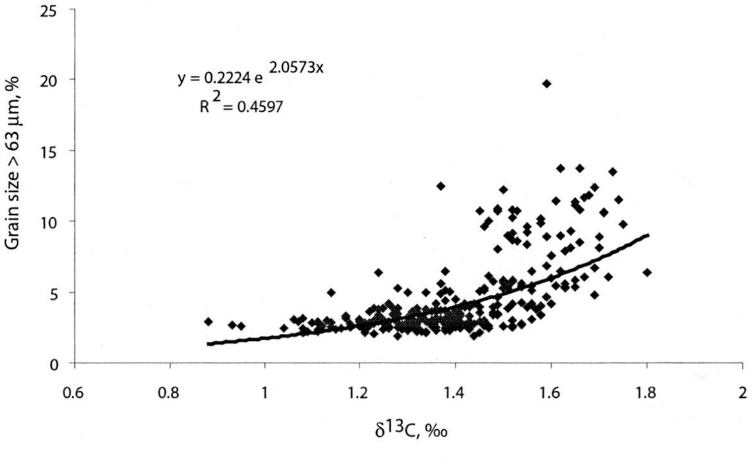

Figure 8.16 Exponential relationship between the $\delta^{13}C$ *Cibicides lobatulus* and untreated (raw) grain size (weight % > 63 µm) from Loch Sunart core GC023. Linear Pearson's correlation coefficients yeild a significant relationship of r = 0.630 (p = 0.0, n = 285).

8.11). These incursions are possibly periods during which fjordic basin was extremely brackish and exemplify the sensitivity of Loch Sunart sedimentary archives to environmental change.

8.4.3 Response of benthic foraminiferal assemblages to environmental change

Whilst the sedimentological properties of core GC023 are likely to contain a mixture of catchment derived and autochthonous inputs, the benthic foraminiferal assemblages of core GC023 should provide a clearer picture of marine environmental conditions over the last 2 millennia. Zones were not applied to the data since the low sampling resolution and known problems with the core's chronology are likely to lead to the construction of inaccurate zone boundaries (*pers. comm.* Prof. G. Whittington, 2005).

8.4.3.1 Benthic foraminiferal population response to increased marine influence and marine productivity

Modern Loch Sunart surface sediment samples with a strong marine influence typically have high benthic foraminiferal abundances and richer species diversity and equitability (chapter 5; Haynes, 1981). Periods of high foraminiferal abundance and species diversity in GC023 occur where C/N ratios, $\delta^{13}C$ and reconstructed bottom water temperature and salinity point to an increased influence of cool, saline coastal waters at the core site (figure 8.15). Phosphorus (shown as P_2O_5 in figure 8.11) concentration in marine sediments is strongly linked to primary productivity and organic carbon flux to the seabed (Delaney, 1998; Anderson *et al.*, 2001), thus the phosphorus concentration variability in GC023 probably reflects varying marine productivity over the last 2 millenia (figure 8.11) with higher productivity typically occurring during periods of high coastal water influence. These inferred increased productivity periods likely explain increases in benthic foraminiferal abundance and species diversity in GC023 (figure 8.11), since benthic foraminifera typically respond to food availability (e.g. Jorissen *et al.*, 1995; Gooday & Rathburn, 1999), particularly when food availability is limited by seasonality (i.e. spring and autumn phytoplankton blooms; Hannah & Rogerson, 1997).

The brief increase in diversity and abundance at ~ 160.5 cm coincides with the onset of the low frequency $\delta^{13}C$ trend and shift to higher MnO_2 concentrations, both suggesting more oxygenated conditions commenced at this level (figure 8.15), thus likely reflecting competitive colonization of this newly ventilated environment. Additionally, sea loch basins typically exhibit high oxygen consumption rates (Gillibrand *et al.*, 1996) and a shift in faunal activity is likely to significantly influence oxygen utilisation (Glud *et al.*, 2003) which in turn can affect the MnO gradient in sediments.

8.4.3.2 Indicators of stratification conditions and a calm depositional environment

Modern assembles with a high proportion of *B. marginata* typically occur at sites with relatively fine sediment, high inputs of organic matter and stratified conditions (e.g. chapter 5 and Mikalsen *et al.*, 1999; Klitgaard-Kristensen *et al.*, 2002; Scott *et al.*, 2003; Husum & Hald, 2004a). The abundance of *B. marginata* in GC023 does not display a direct response to organic carbon content (Conradsen, 1993; Mikalsen *et al.*, 1999; Klitgaard-Kristensen *et al.*, 2002; Murray, 2003a). However, *B. marginata* likely thrives on refractory carbon typically occurring in fjordic environments (Klitgaard-Kristensen & Buhl-Mortensen, 1999) and the abundance decrease of *B. marginata* coinciding with the inferred influx of coastal water likely reflects improved food quality and increased competition, as suggested by the richer species diversity (figure 8.15; section 5.4.8.1).

The increase of taxa such as *Bolivina* species*, Cassudulina* species, *Epistominella vitrea*, *Fissurina lucida* and *S. fusiformis* during higher benthic foraminiferal abundance phases (figure 8.11) suggest periods of higher salinity and probably better oxygenated water (chapter 5; Thiede *et al.*, 1981; Alve & Nagy, 1990; Klitgaard-Kristensen & Buhl-Mortensen, 1999). The hypothesis of increased coastal water influence during these periods is also supported by the increased abundance of planktonic specimens which themselves, are not autochthonous to coastal waters and are likely to have been transported into the loch (chapter 5, e.g. Murray, 1991). Thus, whilst *B. marginata* may prefer high salinity conditions in some environments (e.g. Austin & Sejrup, 1994), high *B. marginata* abundance at core site GC023 is likely to reflect slightly lower salinities, less oxygenated conditions (Mikalsen *et al.*, 1999) and low competition which typically occur with reduced inflow into the main basin.

N. turgida typically shows a strong affinity for fine grained organic rich sediments (chapter 5) though the decreasing abundance of this delicate species in the upper 80 cm is probably due to enhanced bottom water current activity (figure 8.11). Additionally, *N. turgida* shows an affinity for warmer waters in Loch Sunart (chapter 6) and abundance appears to reduce during periods of low reconstructed summer bottom water temperature (RBWT; figure 8.11). The increase in *N. turgida* abundance at 180.5cm is interesting; other taxa show do not show a similar response (figure 8.11), however the ~ 7% abundance increase in *N. turgida* most likely is a response to increased BWT as reconstructed by the transfer function in figure 8.11.

The distribution of *S. fusiformis* in Loch Sunart modern surface sediments demonstrates it's affinity for fine-grained sediments with high organic matter content within fjordic environments (chapter 5 and Alve & Murray, 1997; Gustafsson & Nordberg, 2001). However, the observed association of *S. fusiformis* with *B. marginata*, *N. turgida* and *A. glomeratum* in the modern samples is not seen here (chapter 5; figure 8.11). The sudden peak in *S. fusiformis* abundance from values of around 3% to 15.6 % at 160.5 cm occurs within the same horizon as the isolated δ^{18}O spike, the onset of the low frequency δ^{13}C shift and the change in redox conditions (figure 8.15). *S. fusiformis* is known to be a highly opportunistic species with a fast response to rapid environmental change (Alve, 2003) and it may be that this usually low abundance species in GC023 had little competition during this regime shift.

8.4.3.3 Bottom current activity at core site GC023

Benthic foraminifera living in the main basin of Loch Sunart will experience variable bottom water conditions due to the seasonal heating cycle and stratification processes and deep water renewal events. This explains the high abundance of *B. marginata,* which is common in seasonally variable fjordic water masses (e.g. Alve & Nagy, 1990; Husum & Hald, 2004b) and the fairly constant abundance of tolerant taxa such as *Elphidium excavatum* (Murray, 1971; Mikalsen *et al.*, 1999; Klitgaard-Kristensen *et al.*, 2002; Murray, 2003b; Murray, 2003a; Murray *et al.*, 2003) and *A. beccarii* (Murray, 1991).

Modern distributions of *S. wrightii* and particularly *C. lobatulus* in Loch Sunart suggest a preference for depositional sites experiencing high current activity and well oxygenated, saline waters (chapter 5), hence the moderate abundance of these taxa in GC023 points to episodic and/or mild current activity at the core site. Additionally, an increase in abundance of the 'attached' epifaunal species, *C. lobatulus* and *Gavelinopsis praegeri* towards the core top, suggests an increase in current activity. At present, tidal currents may permeate to the sea bed of Loch Sunart (Gillibrand *et al.*, 1996) and the location of the core site landward of a bathymetric 'canyon' likely results in this site being sensitive to changes in current activity which occur during deep water renewal events (Gillibrand *et al.*, 1995). Therefore, increased abundances of 'high energy' taxa probably point to periods of frequent basin water exchange, i.e. frequent deep water renewal events (DWRE).

8.4.4 Quantitative bottom water reconstructions: fact or fiction?

8.4.4.1 Salinity

In chapter 7, concerns were raised about the applicability of the transfer function model of Sejrup *et al.,* (2004) to reconstruct summer bottom water salinity (RBWS) in the main basin of Loch Sunart. There is a dearth of salinity data available for the coastal waters off NW Scotland (chapter 7). Therefore, at present, RBWS from GC023 cannot be tested against instrumental data, but future work hopes to address this problem (*pers comm.*, Dr. M. Inall, 2005). Though this is by no means a robust comparison, the general long-term trend of RBWS bears a similarity to the *C. lobatulus* $\delta^{13}C$ (a possible proxy for BWS), with lower RBWS and depleted $\delta^{13}C$ occurring between ~ 275 – 80 cm (figure 8.15).

8.4.4.2 Temperature reconstruction

Reconstructed summer bottom water temperature (RBWT; chapter 7) appears to agree well with both inter-annual and long-term trends in instrumental marine temperature records from the west coast of Scotland, hence the RBWT for GC023 (figure 8.15) likely reflects summer bottom water temperatures at the core site.

Both RBWT and *C. lobatulus* $\delta^{18}O$ from GC023 suggests cooling towards the top of the core (figure 8.11), however this is not consistent with recent observations of increasing air and marine temperatures in the North Atlantic (chapter 3). In modern assemblages, *A. beccarii* typically shows a clear positive response to BWT, with increasing abundances of *A. beccarii* in warmer waters (chapter 6). Loch Sunart *A. beccarii* also has a propensity towards higher energy environments (chapter 6; Austin & Sejrup, 1994; Scott *et al.*, 2003), however a decrease in the abundance of *A. beccarii* towards the top of the core (< 80 cm) coincides with an increase in 'high energy' taxa such as *C. lobatulus* and *G. praegeri.* Therefore it may be that the decrease in abundance of *A. beccarii* is reflecting a drop in BWT rather than a decrease in bottom current activity. This hypothesis is supported by the increasing presence of *A. glomeratum*; a taxon with an affinity for cooler waters (though also a propensity towards taphonomic processes; chapter 5 and Murray, 1991) and *Cassudulina reniforme*, which typically has an Arctic distribution (Austin & Sejrup, 1994; Husum & Hald, 2004a) and is found in modern Loch Sunart benthic foraminiferal assemblages with cool BWT (appendix 8).

8.4.4.3 High resolution temperature signals from benthic foraminiferal isotopes

Isotopic measurements on modern *C. lobatulus* demonstrate that this species is likely to calcify close to isotopic equilibrium with seawater $\delta^{18}O$ (e.g. chapter 7), thus *C. lobatulus* $\delta^{18}O$ from core GC023 should reflect changes in the stable isotopic composition of the overlying bottom water masses at the core site.

As discussed in chapters 6 and 7, BWS variations alone of over 2 would be required to drive the typical $\delta^{18}O$ signal in core GC023 (Austin & Inall, 2002); salinity changes which are unlikely to occur, even with extreme climatic forcing (chapter 3 and Gillibrand *et al.*, 2005). Therefore, the high frequency $\delta^{18}O$ shifts in GC023 are likely to be recording inter-annual temperature changes of around 2 °C (Bemis *et al.*, 1998) rather than solely inter-annual salinity variations, or perhaps a combination of both BWT and BWS.

The comparison of estimated bottom water temperature (converted from GC023 *C. lobatulus* $\delta^{18}O$ using the Lynch-Stieglitz *et al.*, 1999 palaeotemperature equation and $\delta^{18}O$: salinity mixing line of Austin & Inall, 2002) with the reconstructed Millport series for the period 1800 – 2000 AD agrees fairly well (figure 8.17). Inter-annual differences between the data series are likely to reflect problems with the geochronology rather than climatic 'lags' (e.g. the deviation between RBWT and instrument BWT at ~1811 AD), since NW Scottish coastal water temperatures tend to be strongly coupled with regional air temperatures and both sites should therefore respond to the same climate forcing signal (chapter 3). Estimated BWT often displays higher temperatures than the reconstructed Millport series which is probably due to calibration problems identified in chapter 3 or the timing of seasonal calcification of *C. lobatulus* (chapter 6).

Irrespective of this, the good agreement of the $\delta^{18}O$-derived palaoetemperature record for GC023 and the reconstructed Millport marine temperature record (figure 8.17) demonstrates that Loch Sunart sediments appear to record a coherent N Atlantic climate signal and exemplifies the potential of obtaining high resolution palaeotemperature records from Loch Sunart sediment records. It also lends support to the hypothesis that high frequency *C. lobatulus* $\delta^{18}O$ shifts are recording inter-annual temperature variations rather than salinity variations and the amplitudes of the observed and reconstructed BWT are similar (figure 8.17).

The long term $\delta^{18}O$ shift of 0.096 ‰ between 0.5-102.5 cm (mean $\delta^{18}O = 0.956 \pm 0.12$ ‰) and 102.5-290.5 cm (mean $\delta^{18}O = 0.86 \pm 0.10$ ‰) suggests either a BWT decrease of 0.46 °C or a salinity increase of ~ 0.53. This $\delta^{18}O$ shift likely reflects the interplay of temperature and salinity on the $\delta^{18}O$ of *C. lobatulus* since the 0.096 ‰ shift is an underestimation of RBWT (mean decrease of 0.75 °C) and an overestimation of RBWS (mean salinity increase of 0.16) for the core section 0.5 – 102.5 cm. However, it is interesting to note that the $\delta^{18}O$ derived 0.53 salinity deviation is similar to the 0.52 RBWS increase between 80.5 – 0 cm (the comparable RBWT decrease is 2.1 °C). This suggests that whilst the high frequency $\delta^{18}O$ is reflecting inter-annual BWT variations, the long-term $\delta^{18}O$ shift may be indicative of an increase in BWS; a hypothesis supported by more 'marine' $\delta^{13}C$ and a benthic foraminiferal response (figure 8.11). Additionally, linear regression lines through the

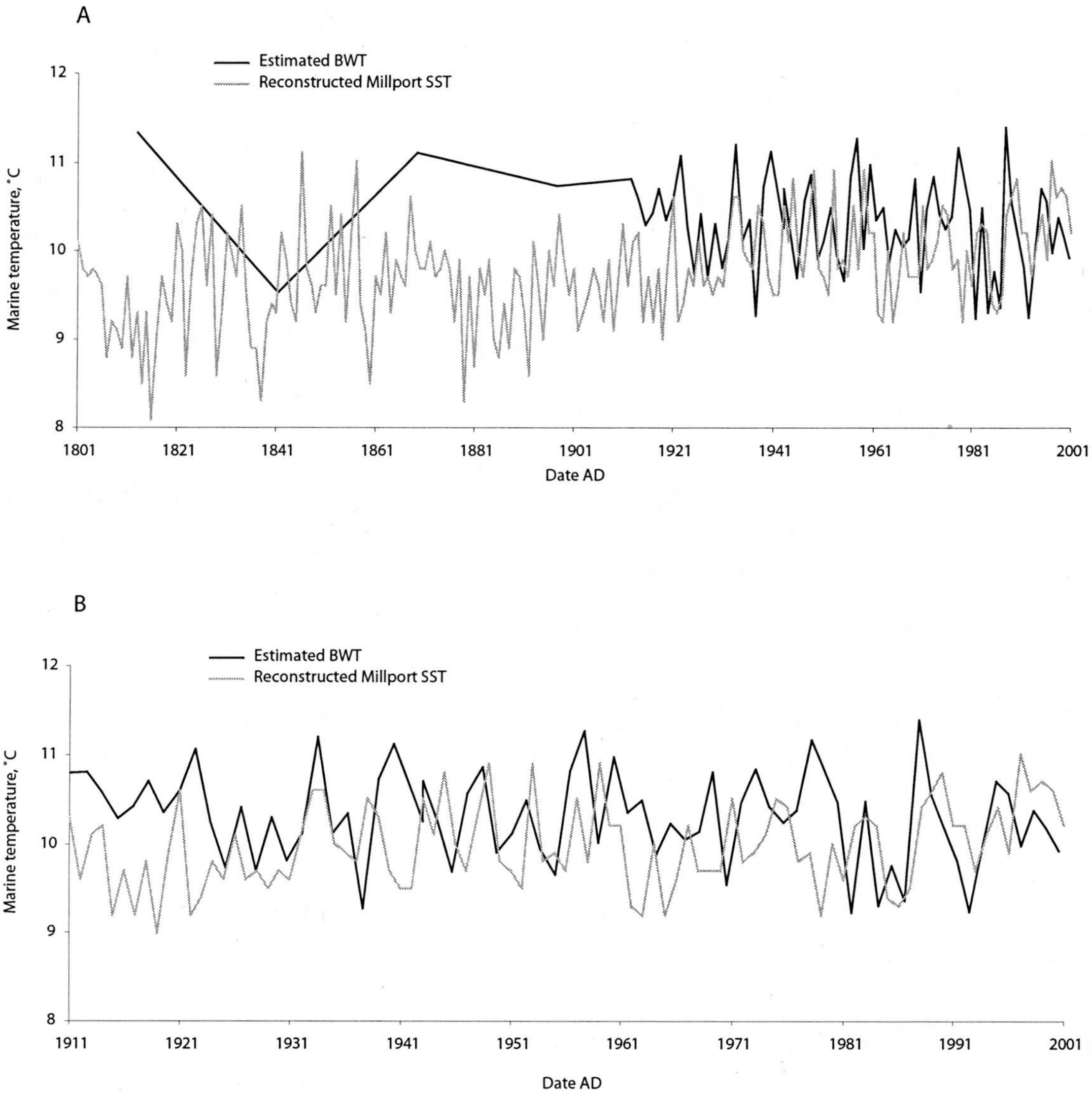

Figure 8.17 **(A)** Estimated bottom water temperature (BWT; black line) at the Loch Sunart GC023 core site and reconstructed annual Millport temperature (grey line) for the period of overlap for the two series (~1810 - 2001) and **(B)** for the period AD 1911-2001. Estimated BWT was calculated using the $\delta^{18}O$ values from GC023 and the Lynch-Steigliz *et al.,* (1999), assuming a constant bottom water salinity of 33.6 (as measured at the core site in June 2002). Also shown is the reconstructed annual Millport temperature series (grey line) determined via calibration of the Millport annual temperature series and the Scottish mainland temperature series for the period 1953-1999 (method and data sources outlined in chapter 3).

estimated BWT show a long-term decrease from 1920 onwards whilst the instrumental data shows a long term increase, suggesting a slight salinity influence on *C. lobatulus* $\delta^{18}O$.

The 0.5 ‰ 'spike' towards enriched $\delta^{18}O$ at 161.5 cm points to a rapid temperature decrease of around 2.3 °C; a temperature drop which is replicated by a 1.7 °C decrease in the RBWT record (figure 8.15). This exemplifies two important points: that rapid and short-lived climatic events are likely to be recorded in the stable isotopic composition of *C. lobatulus* and that benthic foraminiferal assemblages in Loch Sunart can respond quickly to brief fluctuations in main basin bottom water conditions.

8.4.5 Magnetic susceptibility and grain size – catchment derived inputs or enhanced current activity?

The upper section of core of GC023 (0-105 cm) is characterised by relatively coarse grain sizes (more than 4% > 63 μm) and higher magnetic susceptibility (χ; figure 8.7) and such increases in χ are usually interpreted as signals of increased input from the surrounding catchment due to weathering or anthropogenically influenced erosion (e.g. Appleby *et al.*, 1985; Andrews *et al.*, 2001; Mikalsen *et al.*, 2001; Sejrup *et al.*, 2001). However, core GC023 also exhibits a moderate and significant $\delta^{13}C$: grain size relationship (figure 8.16); suggesting catchment derived inputs are not solely the cause of the coarse sediment and exemplifying the important role current activity is likely to play during this period. The predominantly igneous and metamorphic geology of the Loch Sunart catchment (chapter 2) is likely to contain rocks with a significant proportion of the highly magnetic iron (Fe) minerals, such as magnetite (Fe_3O_4) and maghaemite (Fe_2O_3; Dearing, 1998) as exemplified by the high concentrations of Fe and Fe_2O_3 in core GC023, with the latter increasing towards the core top (figure 8.10). Thus the high χ seen at the top of the core likely signifies erosional inputs from the surrounding catchment. The catchment χ signal in the bottom half of the core may have been 'diluted' by paramagnetic or diamagnetic bulk sediment components such as clay or organic matter (figure 8.1and table 4.5 in Dearing, 1998), though it is more likely that catchment inputs were not significant during this period.

8.4.6 Separating catchment erosion from climatically forced current activity

Grain size peaks in the treated sediment samples are not always apparent in the untreated (raw) sediment grain size record (figure 8.7) suggesting the latter may be masked by either an organic or calcium carbonate signal. 'Treated' grain size records potentially allow catchment derived grain size variations to be separated from current-driven grain size variations (e.g. Bianchi & McCave, 1999) and may explain other proxy records. For instance, the treated sediment grain size peak at ~180 cm was likely to have been masked by increased calcium carbonate from the coinciding peak in benthic foraminiferal abundance (figure 8.15) or by marine particulate organic matter as suggested by the 'marine' C/N ratio (figure 8.15); both of which point to a period of enhanced current activity and coastal water influence in the main basin of Loch Sunart. On the other hand, treated sediment grain size from 54.5 cm upwards follows the raw sediment grain size, pointing towards transportation of fine particles away from the site through stronger current activity, i.e. winnowing, and/or domination of the grain size record by minerogenic inputs, though winnowing is more probable.

The isolated grain size peak at 102.5 cm is accompanied by a sharp, brief drop in χ (figure 8.7) thus is unlikely to be due to a turbidite or a rapid catchment derived input (Sejrup *et al.*, 2001). The treated sediment grain size curve also peaks near this interval, pointing to the possibility of enhanced current activity and thus increased marine influence on bottom waters, which may explain the small increase in benthic foraminiferal abundance (figure 8.15). In the N Atlantic, stronger current activity in the bottom water is linked to processes of deep convection and is often indicative of warmer climates (Bianchi & McCave, 1999); the relatively stable and depleted $\delta^{18}O$ around this level also may reflect climatic forcing in the N Atlantic region.

Given the strong grain size relationships for both χ and $\delta^{13}C$, it is likely that the grain size signal in core GC023 records both climatically forced current activity and catchment derived inputs, influenced by anthropogenic activity and climate driven erosion.

8.4.7 Catchment derived geochemical signals

As discussed previously, sodium oxide and chloride are likely to reflect the deposition of marine salts in the sediments. Decreasing aluminium oxide (AlO_3) towards the core top is consistent with a change the lithology from mainly clay (typically aluminium bearing) to clayey silt (figure 8.1 and 8.10).

Increased concentrations of titanium (TiO) in marine sediments from the Cariaco basin likely signify periods of wet climate and high fluvial input (Haug *et al.*, 2003 and Vlag *et al.*, 2004) since Ti is largely a terrigeneous detrital input. Titanium oxide (TiO%) concentrations in core GC023 are generally higher below 85 cm and fairly low between 85 – 20 cm, a pattern also seen in the high resolution XRF data (figure 8.9 and 8.10). If the Ti records in GC023 reflect climatically-driven changes in terrestrial runoff, then this suggests a drier and variable climate between 208-185 cm, moving to wetter climate peaking at 160cm, with a gradual shift to a drier climate coinciding with the grain size peak at 50 cm (figure 8.10). TiO% shifts towards slightly higher values at the core top, pointing to a wetter climate and higher detrital input to the site, though XRD data is not available for the core top. It is interesting to note that the peak in TiO% at 160 cm coincides with a peak in benthic foraminiferal abundance, which may (tenuously) reflect a link to climate and productivity (e.g. Kryc & Murray, 2003).

8.4.8 Sediment carbon signals – catchment derived or a reflection of marine productivity?

The increase of C_{total} and shift towards 'marine' C/N ratios towards the core top points to increasing marine productivity thus increased marine organic matter input, as represented by P concentration (figure 8.7). The C_{total} peak at 110 cm is not accompanied by a TOC or C/N ratio response suggesting the C_{total} peak probably reflects an inorganic carbon input such as foraminiferal tests.

Increasing TOC towards the core top is consistent with an increase in catchment derived inputs as inferred from the χ record (figure 8.7). Marine and estuarine environments typically show C/N ratios around 8 (e.g. Middleburg & Nieuwenhuize,

1998) and terrigeneous material displays C/N ratios ranging from 17-30 (e.g. Andrews *et al.*, 1998; Middleburg & Nieuwenhuize, 1998), though estuarine sediments rarely show strongly terrigeneous (i.e. near 20) C/N ratio signals (Shultz & Calder, 1976). The C/N ratios in core GC023 fluctuate around a mean ratio of 9.49 ± 0.55 with a C/N ratio range of 7.93 – 10.73, suggesting a combination of marine and terrestrial organic matter at the site with occasional periods of increased and decreased organic inputs from the catchment. Loch Sunart C/N ratios are slightly higher than the C/N ratio range of the deeper Lustrafjorden (Mikalsen *et al.*, 1999), probably due to the shallow sill restricting exchange with coastal waters. Higher C/N ratios coincide with increased grain size (raw and digested) from around 0-100 cm in core GC023 (figure 8.7). This is unexpected since organic matter is usually contained in the finer sediment fractions (Bordovskiy, 1965) and NW Norwegian fjordic records with coarse grain sizes typically show low organic content (Mikalsen *et al.*, 2001). However, the high C/N ratios in GC023 point to a significant terrigenous input during this period which agrees with the χ record.

8.4.9 Palaeoenvironmental record from GC023 in context with other climatic or environmental records.

As mentioned previously, problems with geochronology severely hinder the interpretation of palaeoenvironmental conditions from core GC023, and sample resolution is low between ~ AD 700 - 1900 (1250 cal BP – 50 cal BP; figure 8.18). However, the data does show the potential of high resolution reconstructions from these sea loch archives, with sampling resolutions (excluding the 'core gap') of 1 cm per year for the top half of the core (using Pb-Cs chronology) and 1 cm per 4-10 years for the bottom half of the core (> 105 cm).

8.4.9.1 Cool temperatures during the Roman Warm Period?

Proxies from the base of GC023 (*C. lobatulus* abundance, grain size > 63 μm and enriched $\delta^{13}C$) point to slightly increased current activity between 200 – 85 BC. Enhanced current activity typically suggests warmer temperatures (e.g. Bianchi & McCave, 1999b), however RBWT is cooler during this period which agrees well with

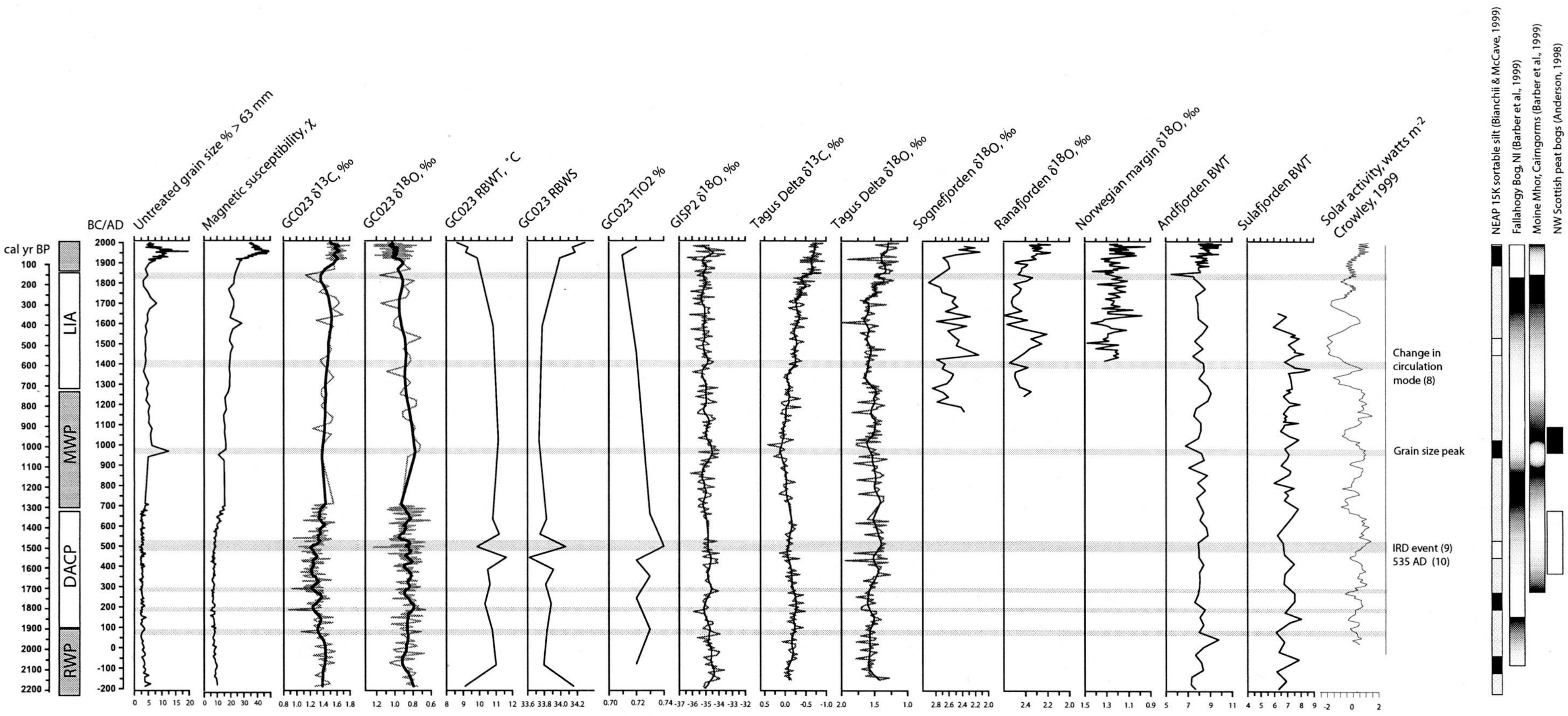

Figure 8.18 Major proxies from Loch Sunart core GC023 plotted by age (AD). Also shown are: **1)** $\delta^{18}O$ from the GISP2 ice core (http://www.ncdc.noaa.gov/paleo/icecore/greenland/ summit/document/gispisot.htm; **2)** $\delta^{18}O$ and $\delta^{13}C$ from Tagus Delta *Uvigerina sp.* (data obtained from Dr. Helga Bára Bartels Jónsdóttir); **3)** $\delta^{18}O$ from Sognefjorden (*Uvigerina meditteranaea*), Ranafjorden (*Cassudulina laevigata)* and Norwegian margin (*N. pachyderma d.)* - data from Dr. D. Kiltgaard-Kristensen; **4)** estimated bottom water temperatures (BWT) from Andfjorden and Sulafjorden (data from Dr. G. Mikalsen); **5)** solar activity record (Crowley, 1999 - data from http://www.cru.uea.ac.uk/cru/data/paleo/jonesmann04). **6)** Bianchi & McCave (1999) sortable silt data - fast/slow phases represented by black/white shading respectively.; **7)** Reconstructed precipitation data from peat bogs show transitions between dry periods (white) and wet periods (black); **8)** Timing of the change in atmospheric circulation over the North Atlantic (Meeker & Mayewski, 2002); **9)** the 1400 cal BP IRD event of Bond *et al.*, (1997) and **10)** the 535 AD 'nuclear winter' (Wohletz, 2000). Events **A-D** represent periods of extremely depleted $\delta^{13}C$ in core GC023. Event **E** identifies the timing of the fjordic circulation shift to more oxygenated conditions and inferred increased marine influence.

evidence of climatic deterioration in Malangenfjord (Husum & Hald, 2004a), Sulafjorden and Andfjorden (Dr. G . Mikalsen, pers. comm., 2004). Conversely, GC023 δ^{18}O appears to be depleted (figure 8.18); this may reflect lower salinity basin water but is consistent with other records showing evidence of warmer temperatures during this period, e.g. the depleted δ^{18}O from the Tagus Delta (data from Dr. H. B. Bartels; Abrantes *et al.*, *in press*) and the GISP 2 ice core (figure 8.18).

8.4.9.2 Changes in fjordic circulation at AD 500?

The long-term shift of δ^{13}C along with indicators of increased oxygenation such as Mn at 160.5 cm point to a major change in fjordic hydrography at approximately AD 500 (1450 BP or 160.5 cm). Once again, it is important to remember that the problematic geochronology greatly hinders the reconstruction of palaeoenvironmental conditions in Loch Sunart over the past 2 millennia. Therefore, following section explores the potential mechanisms driving this circulation change, though only tenuous links between the GC023 record and other palaeoclimatic records can be resolved.

8.4.9.2i Regional sea level change?

Loch Sunart is likely to have experienced a long-term isostatic sea level drop of ~ 2m during the last 2000 years (Shennan *et al.*, 1995) with sea level being around 1.45 m higher at AD 500 than at present (Shennan & Horton, 2002). Isostatic rebound of shallow-silled Scandinavian fjords, for example, has led to anoxic conditions in some basins (Gustafsson & Nordberg, 2002). However, the main basin sill depth (~ 35 m) of Loch Sunart lies well below (~ 15 m) the present day halocline and brackish intermediate layer and Loch Sunart is regularly flushed by deep water renewal events (Gillibrand *et al.*, 1995). It is possible that the 1.45 m decrease in sea level has crossed some circulation threshold, increasing the vigour of coastal-basin exchange and resulting in increased marine coastal water reaching the bottom water of the core site and presently, both tidal and current activity influences main basin bottom water in Loch Sunart (*pers. comm.,* Dr. P Gillibrand, 2004) thus bottom water is rarely stagnant.

8.4.9.2ii Changes in open Atlantic conditions

An ice rafted detritus (IRD) event, similar to a glacial Heinrich event (Andrews, 1998), occurred in the NE Atlantic around AD 550 (1400 cal BP) and these IRD events are typically accompanied by injections of cooler and fresher water (probably from the Greenland Sea) into the core of the North Atlantic Current (Bond *et al.*, 1997). Two distinct $\delta^{18}O$ events occur in core GC023 around this time. The first is the isolated 0.5 ‰ enrichment of $\delta^{18}O$ at ~ AD 496 (1454 cal BP; 161.5 cm) suggesting a temperature change of 2.3°C (figure 8.18). This inferred temperature reduction is of similar magnitude to the 1.7 °C cooling in the reconstructed summer bottom water temperature record (figure 8.18) and similar to the extent of surface ocean cooling postulated for this period by Bond *et al.*, (1997) and Marchitto & deMenocal (2003). However, these IRD events are likely to have lasted a few 100 years and given the high resolution of GC023, it is unlikely to reflect the whole IRD event. GC023 $\delta^{18}O$ shows a period of relatively enriched $\delta^{18}O$ between AD 525–600 (1422 – 1350 cal BP), suggesting a cooling of around 0.5 °C which may reflect cooler temperatures during an IRD event at this time. The low variability in $\delta^{18}O$ during this interval (given the usually high frequency) points to a possible change in local circulation or local climate regime which may have been driven by changes in the North Atlantic climate regime.

The cool RBWT correlates with a period known as the Dark Ages Cold Period (DACP; figure 8.18) which has also been recorded in speleothem $\delta^{18}O$ from SW Ireland (McDermott *et al.*, 2001) and sortable silt records from the NE Atlantic (Bianchi & McCave, 1999). Reconstructed bottom water temperature for Sulafjorden is also cool around AD 560 (*pers comm.,* Dr. G Mikalsen, 2004; figure 8.18), and *Bolivina skaggerakensis* (a benthic foraminiferal taxa often associated with climatic deterioration; Husum & Hald, 2004a) appears in the Voldafjorden around AD 500 with a cooling of BWT occurring around AD 650 (HOLSMEER report, 2004). Given the circulation of the NE Atlantic (chapter 1), it is likely that these temperature changes are being driven by the same process driving the Sunart temperature change.

The foraminiferal $\delta^{13}C$ during the DACP interval is relatively enriched considering IRD events are typically accompanied by fluxes of freshwater into the Atlantic (chapter 1), causing reduced thermohaline circulation (Bond *et al.*, 1999) and regional cooling (Bond *et al.*, 1997). Climate regime change in the North Atlantic is likely to influence the regime in the local catchment around Loch Sunart. However, McDermott *et al.*, (2001) suggest the IRD event at 1400 cal BP may not have caused a huge salinity change in the N Atlantic. Grain size in core GC023 is relatively fine-grained, and this may be linked to sluggish circulation of the NE Atlantic waters (figure 8.18; Bianchi & McCave, 1999). The AD 500 IRD event correlates with a period of high Na^+ in the GISP2 ice core; an indicator of storminess in the North Atlantic (O' Brien *et al.*, 1995; Bond *et al.*, 1997) and increased precipitation during this time may have resulted in enhanced stratification and enhanced circulation. Regionally, peat bogs suggest that the period between AD 400-850 was fairly dry (figure 8.18; Anderson, 1998 and Barber *et al.*, 1999), though Anderson, 1998 points out that reconstructions from other British peat bogs indicated a wet climate at this time.

8.4.9.2iii Volcanically forced climate?

It may be possible that the $\delta^{18}O$ spike at ~ AD 500 represents the nuclear winter of ~ AD 536, forced by the eruption of Krakatoa (Wohletz, 2000) during the DACP. Poor chronology and uncertainty in calibrated radiocarbon ages make it impossible to tie-down such events in the GC023 record.

8.4.9.2iv The onset of the Medieval Warm Period?

The grain size peak at ~ 102.5 cm has an estimated age of ~ AD 1000, bearing in mind the uncertainty in the geochronology of core GC023, this age may not be accurate. Regionally, the Medieval Warm Period (MWP) has been recorded in speleothem $\delta^{18}O$ and dated as being centred about 1000 ± 200 cal BP (McDermott *et al.*, 2001). Sortable silt records from a deep water NE Atlantic core suggest more vigorous activity accompanies warmer climatic periods such as the MWP and Roman Warm Period, indicating the importance of thermohaline circulation variability to millennial and centennial scale climatic variability of the NE Atlantic region during the Holocene (Bianchi & McCave, 1999). A short period of high frequency $\delta^{18}O$ oscillations occurs just prior to the accepted onset of the Medieval Warm Period, between AD 650-700 and may represent a reorganisation of circulation or climate regime, similar to those seen in other records (e.g. Hall *et al.*, 2004). The slight $\delta^{18}O$ depletion in core GC023 around AD 1000 suggests either warmer temperatures, as recorded in the GISP2 ice core record (figure 8.10) and N Atlantic sortable silt records (Bianchi & McCave, 1999) or a period of fresher salinity from an increased runoff from the wet climate of the catchment (Anderson, 1998; Barber *et al.*, 1999; figure 8.18). Though titanium can indicate periods of wet climate (e.g. Haug *et al.*, 2003), the environmental controls on titanium concentration in the sediments of Scottish fjords has not been established, and GC023 shows no agreement with regional precipitation records (figure 8.18).

The long term $\delta^{13}C$ shift in Loch Sunart suggests an onset of fjordic circulation changes at ~ AD 540, yet the long-term shift towards enriched $\delta^{18}O$ values begins around AD 940 pointing to either a decrease in BWT or a slight increase in BWS. Many of the regional studies associated with the HOLSMEER project showed significant changes at ~ AD 1000 (HOLSMEER report, 2004). Though NE Atlantic circulation appeared to become more vigorous during this time (Bianchi & McCave, 1999) as also suggested by treated sediment grain size for GC023, weaker bottom currents are inferred for the Icelandic shelf, increasing *B. skaggerakensis* and decreasing *Cassidulina laevigata* abundances point to climatic deterioration in Voldafjorden and a shift towards enriched $\delta^{13}C$ of *Uvigerina mediterranea* points to weaker turbulence, lower salinity and restricted upwelling (HOLSMEER report, 2004).

8.4.9.3 Long term cooling trend from ~ AD 1000 to the 19th Century

The grain size peak at AD 1000 occurs within a section of geochronological uncertainity and may tenuously reflect winnowing linked to faster bottom water activity in the N Atlantic (Bianchi & McCave, 1999; figure 8.18). Coarse sediments in GC023 from around AD 1000 to 1900, suggests enhanced current activity and the winnowing of sediments at the core site during this time means that climatic periods within this interval, i.e. the LIA and MWP, cannot be fully resolved.

A period of relatively enriched $\delta^{18}O$ and inferred cooler BWT between ~ AD 1531-1700 agrees well with temperature records from Ranafjorden (figure 8.18). However, $\delta^{18}O$ becomes more enriched towards the top of the core (figures 8.12 and 8.18), during a period where both global and marine temperatures are known to be higher (chapters 1 and 3). More apparent is the depleted δ^{13}C between AD 1700-1841, which points to fresher salinities or reduced fjordic circulation (figure 8.18) and agrees well with proxy records of precipitation from Scottish peat bogs (Anderson, 1998; Barber *et al.*, 1999).

8.4.9.4 Environmental records from the AD 1900 to present.

The cooling of Loch Sunart BWT from ~ AD 1920 is not consistent with global air temperature records or NW Scottish marine temperature series which typically show warming from around AD 1920 (e.g. Mann *et al.*, 1998 and chapter 3). Andrews *et al.*, (2001) report a shift to more arctic conditions (decreasing temperature and salinity) in N Iceland fjords. Temperature and δ^{18}O records from the Norwegian fjords (which should experience similar climate systems to NW Scotland) typically show a warming trend (figure 8.19 and Kristensen *et al.*, 2004). The difference in the long-term bottom water trend from Loch Sunart may reflect the impact of changes in the N Atlantic circulation and climate upon the hydrography of the fjord.

The late 19th and 20th century has been characterised by storminess in the N Atlantic, which has a complex relationship with the NAO index (Dawson *et al.*, 2002). Enhanced mixing of the coastal shelf seas during recent periods of high NAO (i.e. post AD 1920) along with increased stratification in Loch Sunart (due to increased precipitation) may have resulted in enhanced estuarine circulation (chapter 3 and Gillibrand *et al.*, 2005) leading to more saline and cooler coastal bottom water entering the main basin of Loch Sunart, despite increasing temperature records elsewhere (chapter 1). This hypothesis is supported by relatively enriched δ^{13}C and δ^{18}O values and the increasing presence of benthic foraminiferal taxa with an affinity for 'cooler saline' waters, e.g. *A. glomeratum, Bolivina* spp. and *E. vitrea* (figure 8.6 and chapter 6). Additionally, depleted GC023 *C. lobatulus* δ^{18}O appears to correlate with higher annual precipitation for England and Wales (figure 8.19), once again pointing to enhanced estuarine circulation during the recent warm period.

Not all warm periods are accompanied by NAO-like behaviour and our current climate is much stormier than during the MWP (Dawson *et al.*, 2004) and chemical

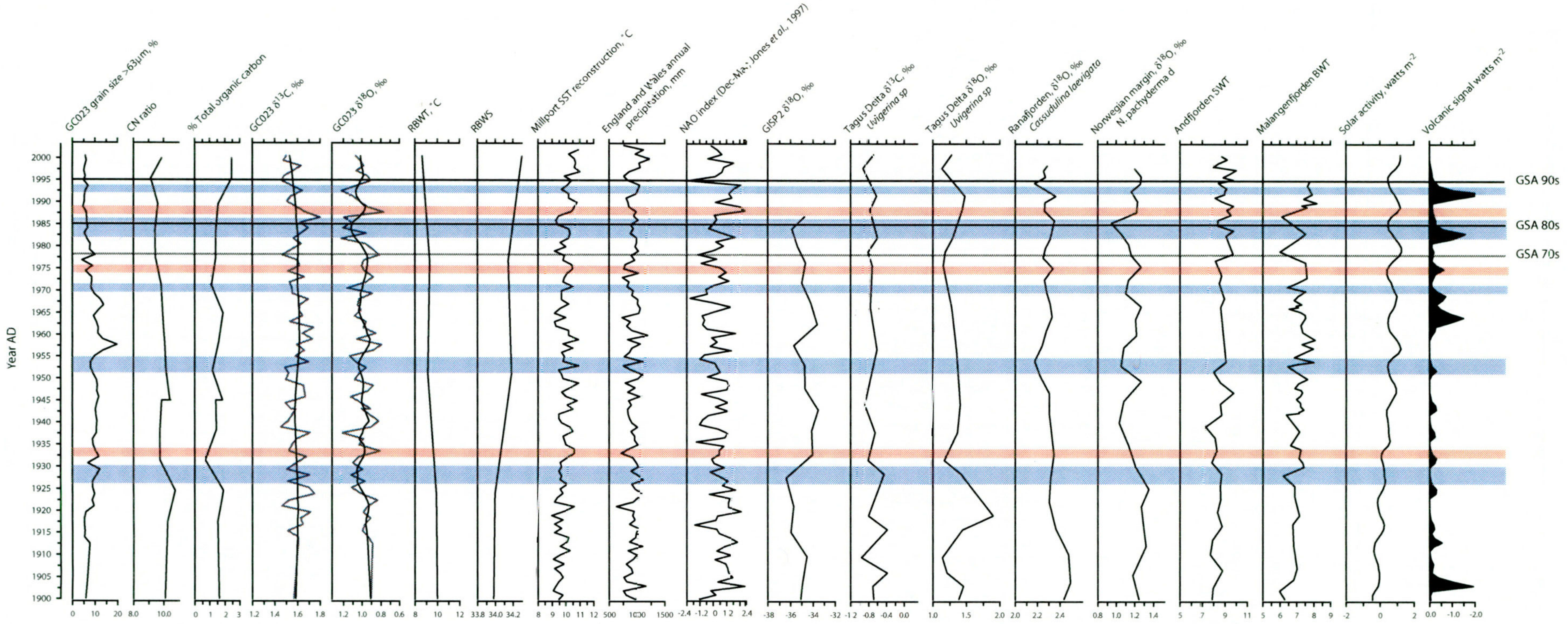

Figure 8.19 Loch Sunart core GC023 proxies for AD 1900 - 2000. The change in core geochronology is visible at ~ AD 1912. Also shown are: **1)** the reconstructed Millport marine temperature series (see chapter 3 and figure 8.9); **2)** the England and Wales precipitation series (data from http://www.cru.uea.ac.uk/~mikeh/datasets/uk/engwales.htm); **3)** the GISP2 δ18O record; **4)** stable isotope data from the Tagus Delta (Portugal; data obtained from Dr. H. Bára Bartels Jónsdóttir); **5)** δ18O data from Ranafjorden and the Norwegian Margin (Kristensen *et al.*, 2004; data obtained from Dr. D. Kiltgaard-Kristensen); **6)** bottom water temperature from Andfjorden and Malangenfjorden (data from Dr. G. Mikalsen); **7)** solar activity and volcanic signals (Crowley, 1999; data obtained from http://www.cru.uea.ac.uk/cru/data/paleo/jonesmann04) and **8)** N. Atlantic Great Salinity Anomalies (GSA, Belkin *et al.*, 1998 andBelkin, 2004).

Periods within GC023 where δ18O correlates with warm phases in other records are shown by red bars; blue bars point to cool periods.

changes in the GISP2 ice core suggest the mode of atmospheric circulation over the North Atlantic region switched around AD 1400 (Meeker & Mayewski, 2002). This may explain why GC023 proxies during the MWP do not display the same enhanced stratification/coastal mixing as proxies from the past 100 years and the Roman Warm Period (figure 8.19).

The recent shift towards depleted $\delta^{13}C$ at around AD 1985 may reflect a reduction in current activity with less influence of coastal waters to the core site as suggested by the decrease in grain size (figure 8.19). Hansen *et al.*, (2001) report a decrease in the Faroe-Shetland overflow since 1950 and postulate a possible decrease in Atlantic water inflow (i.e. reduced thermohaline circulation) which may result in less 'marine' water to the coastal hydrography outside Loch Sunart and thus the fjord itself. However, given the propensity for North Atlantic storminess and increased wave height associated with the high index NAO phase during this time (Dawson *et al.*, 2002), one may also expect vigorous current activity and enhanced circulation in Loch Sunart (Gillibrand *et al.*, 2005). Additionally, during high index NAO years, hydrography in the Rockall trough (and likely the Hebridean shelf) is typically warmer and more saline (figure 7.12 and Holliday, 2003) thus one may expect $\delta^{13}C$ values typical of 'marine' waters in Loch Sunart bottom waters.

Despite differences in the long-term BWT trends, periods of cool and warm BWT inferred from GC023 $\delta^{18}O$ agree well with other instrumental and palaeoclimate records of the last 100 years (figure 8.19). The best agreement is with the Malangenfjord and Andfjorden BWT record which show similar climatic trends to the reconstructed Millport temperature series, thus exemplifying the sensitivity of these NW European fjord records to N Atlantic climate.

8.4.10 Signals from the catchment – climate driven or anthropogenic?

The magnetic susceptibility (χ) curve of GC023 is typical of many other fjordic or lacustrine records; increasing towards the core top before shifting to decreased values in recent times e.g. Andrews *et al.*, (2001); Mikalsen *et al.*, (2001) and Husum & Hald (2004a). However, the onset of higher χ in these records typically occur before ~600

BC (~2500 cal BP) whereas the gradual increase in Loch Sunart commences around ~ AD 700 (~1250 cal BP) with the rapid and large increase beginning at ~ AD 1900 (figure 8.18). Whether this is due to the shorter time span of GC023 (~2050 cal BP), problems in geochronology or differences in settlement times and anthropogenic activity (such as woodland clearance) is difficult to identify. Certainly Anderson (1998) finds evidence of human activity at ~ 3300 cal BP in Wester Ross, and Macklin *et al.*, (2000) found that anthropogenic activities began to impact on the Oban environment around 1000 BP. Andrews *et al.*, (2001) suggested that the increase in χ around 1000 cal BP in a marine sediment core from Reykjarfjördur (Iceland) was associated with a climatically influenced decrease in carbonate in the sediments rather than an anthropogenic signal. However, the increase in total organic carbon and shift to slightly higher C/N ratios during the χ peak suggests that χ in Loch Sunart is primarily a catchment derived signal, potentially modified by enhanced bottom current activity and increased runoof from the catchment. The intensive forest management of the Sunart oakswoods peaked during the 18th and 19th centuries (www.sunartoakwoods.org.uk) and this agrees well with the onset of increased χ as a catchment signal, and χ could also be influenced by heather burning since χ is massively increased in burnt top soil (Smith, 1998).

Given the strength of the grain size:$\delta^{13}C$ and grain size: χ relationships, it is likely that the χ and grain size signals in GC023 record both climatically induced and anthropogenically influenced erosion from the catchment. The influence of catchment derived inputs to the core site could be further explored by the 'unmixing' of mineral magnetic signatures to identify the 'source' (e.g. Lees, 1998) and by looking at pollen in the marine records (e.g. Scourse *et al.*, *in press*).

8.4.11 Anthropogenic signals of pollution

Another possible explanation for the trend towards depleted $\delta^{13}C$ is the influence of anthropogenic carbon in the North Atlantic, commonly termed the 'oceanic Suess effect' (e.g. Sonnerup *et al.*, 1999; Körtzinger *et al.*, 2003). The uptake of isotopically light anthropogenic CO_2 into the ocean via air-sea interactions and deep water production in the North Atlantic (Kroopnick, 1985) has seen a mean global $\delta^{13}C$

change of -0.16 ± 0.02 ‰ per decade between 1970 and 1990 (Quay *et al.*, 2003) and anomalous $\delta^{13}C$ has been recorded in surface waters around the NE Atlantic (Keir *et al.*, 1998). However, if the shift towards depleted $\delta^{13}C$ at AD 1985 is due to the influence of anthropogenic CO_2 then it is surprising, given the rapid exchange between atmospheric CO_2 and freshwater (Broecker & Walton, 1959; Spiker, 1980), that an anthropogenic $\delta^{13}C$ signal is not seen earlier in the GC023 record.

Despite concerns regarding the feasibility of using the high resolution XRF geochemical data, zinc appears to show a significant increase beginning around AD 1900, which is similar to the distinct anthropogenic zinc signal commencing around AD 1850 in Loch Chon, Central Scotland (Roberts, 1998). Additionally, the predominantly marine signal accompanying the sharp rise in TOC input at ~ AD 1995 is not accompanied by catchment or climatically driven grain size variations and may reflect enhanced organic carbon input from the most recent phase of anthropogenic activity, i.e. fish farming in Loch Sunart (Gillibrand *et al.*, 1996).

8.4.12 Climate forcing during the last 2000 years

Spectral analysis (using PAST; Hammer *et al.*, 2001) on the two core sections where geochronology is most secure (0-69.5 cm and 104.5 – 290 cm) suggests no significant cycles exist in the GC023 $\delta^{18}O$ records. The highest powered $\delta^{18}O$ cycles are 16 years (P = 6.33, when P significant at 95 % = 8.89), 26 years (P = 5.05), 12 years (P=4.91) and 11 year cycles (P = 4.39) and were present in only the lower half of the core. Cycles lasting 25-27 years have been found in the Central England Temperature (CET) series and the Koch sea ice index respectively and a cycle lasting 29 years has been reported for the GISP2 $\delta^{18}O$ record (references contained in O'Sullivan *et al.*, 2002). Similarly, 11-12 year cycles are common in both instrumental and palaeoclimatic records (references in O'Sullivan *et al.*, 2002) and are consistent with the 11 year Schwabe sun spot cycle, pointing to the possibility that the *C. lobatulus* $\delta^{18}O$ of Loch Sunart responds to solar forced climate variability in the NE Atlantic (e.g. Mikalsen & Sejrup, 1999; Bond *et al.*, 2001).

The NAO is a major influence on N Atlantic climate (chapter 1), however the relationship between oceanic circulation and particularly the coastal hydrography of

NW Scotland and the NAO is complex (chapter 1; Holliday, 2003) as figure 8.19 shows. Some prolonged periods of enriched $\delta^{18}O$ occur during low solar activity and high volcanic signal (figure 8.19) supporting the hypothesis that Loch Sunart palaeorecords could be recording solar variability, as reported for other palaeoclimatic records from NW Scotland (e.g. Baker *et al.*, 1999; Mikalsen & Sejrup, 1999; Cooper *et al.*, 2000; O'Sullivan *et al.*, 2002) or solar forced NAO fluctuations (Boberg & Lundstedt, 2002).

The lower section of GC023 shows a significant $\delta^{13}C$ cycle at 800 years ($P = 15.05$ when $P_{95} = 8.89$), however this peak must be interpreted with care, since only 1 cycle exists in the given chronology for the GC023 section (899 cal years). Though 800 year cycles have been reported for N British peat bogs (Barber *et al.*, 1994 and Oliver *et al.*, 1997), cycles of this periodicity are fairly uncommon (e.g. Chambers & Blackford, 2001; O'Sullivan *et al.*, 2002). The closest reported cycle is the 720 and 951 year atmospheric Δ^{14} cycles of Stuiver & Braziunas (1996), though it is possible that the 800 year cycle may be connected with the N Atlantic 1500 year cycle (references in O'Sullivan *et al.*, 2002). Interpretation of GC023 palaeoenvironmental proxies and possible cyclicity must be approached with caution due to poor chronology. Futher work on high resolution sediment cores from Loch Sunart spanning over a longer time scale would improve the identification of possible climatically forced periodicity.

8.5. CONCLUSION

Palaeoenvironmental reconstructions from Loch Sunart suggest that these high resolution sedimentary archives have the potential to resolve inter-annual marine climate variability and capture an integrated record of changes in the catchment and marine environment. Various proxies point to a change in fjordic circulation around AD 500, the cause of which is not clear. Possibilities include a threshold change in fjordic circulation due to isostatic sea level fall or changes in open N Atlantic conditions. *C. lobatulus* $\delta^{13}C$ likely records the $\delta^{13}C_{DIC}$ of main basin bottom water and points to an increasing influence of coastal water at the core site during the last 2000 years, also starting around AD 500. Carefully evaluated age-control data highlights problematic geochronology which makes it impossible to resolve climate and environmental change during the Medieval Warm Period and Little Ice Age, and inhibits the interpretation of the development of the fjordic circulation change continuously through the last 2000 years.

Comparison of the *C. lobatulus* $\delta^{18}O$ record with a long reconstructed marine temperature series demonstrates that the test chemistry of *C. lobatulus* from the main basin records inter-annual variations in bottom water temperature of a similar magnitude to instrumental data. Additionally, the agreement of *C. lobatulus* $\delta^{18}O$ and RBWT point to cooler bottom water temperatures and/or higher salinities during the 20th century warm period and also during the Roman Warm Period. This is likely due to increased stratification leading to enhanced estuarine circulation 'pulling' cooler and more saline coastal waters to the core site.

The problematic geochronology for core GC023 along with it's relatively short time span, negates the identification of millennial scale climate cycles often seen in recent late Holocene records (e.g. Bond *et al.*, 1997; Cooper *et al.*, 2000; Keigwin & Boyle, 2000; Wunsch, 2000; Battarbee *et al.*, 2001; Bond *et al.*, 2001; O'Sullivan *et al.*, 2002; Clemens, 2005). However, the good agreement of GC023 palaeoclimate proxies with other N Atlantic records exemplifies the sensitivity of these marginal environments to regional circulation and climate forcing mechanisms. The strong catchment signal suggests the possibility of obtaining high resolution records of linked palaeoenvironmental changes in terrestrial and marine climate and demonstrates the sensitivity of these environments to anthropogenic influences.

CHAPTER 9 – CONCLUSIONS AND FURTHER WORK

Recently, millennial-scale climate changes have been observed in marine sedimentary archives and high resolution ice core records covering the last glacial period and continuing into the Holocene, suggesting Holocene climate is not as stable as once thought (e.g. Mayewski *et al.*, 2004). Initially this millennial-scale variability was attributed to changes in the global thermohaline circulation (THC; Broecker *et al.*, 1990); however the recent identification of centennial and decadal-scale variability in palaeoclimatic records (e.g. Hall *et al.*, 2004; Andresen *et al.*, 2005) suggests factors other than the rate and location of deep ocean ventilation, such as solar variability or an Atlantic multi-decadal oscillation are also likely to be causal factors in long-term climate change (Kerr, 2000).

Shelf sea areas, such as sea lochs or fjords, are sensitive to climatic processes, typically yield high sediment accumulation rates (~ 0.5 cm yr^{-1}) and have the potential to capture land-ocean interactions (Scourse & Austin, 2002). The west coast of Scotland lies in a climatically sensitive region of the North Atlantic (e.g. Holliday, 2003), thus it is likely that Scottish sea loch sediments also capture North Atlantic climatic variability, possibly with sub-decadal resolution. Few studies have utilized palaeoenvironmental archives from Scottish sea lochs and those that have, focused on either the deglacial period (Dix & Duck, 2000; Howe *et al.*, 2002) or on recent (last 200 years) records from the restricted basins of Loch Etive (Murray *et al.*, 2003).

Therefore, the primary aim of this study was to investigate the potential of obtaining high resolution palaeoenvironmental records from Loch Sunart, a fjord on the NW coast of Scotland. In order to achieve reliable palaeoenvironmental reconstructions, there was a clear requirement to understand how modern processes influence the study site. To accomplish these objectives, a ~3 m sediment core (GC023) with a sedimentation rate of approximately 0.1 cm yr^{-1} back to 2090 ± 120 years BP was recovered from the Dun Ghallain Deep in the main basin of Loch Sunart, and a suite of surface sediment samples and accompanying hydrographic data were obtained during a series of research cruises in Loch Sunart between April 2001 and June 2002. Additionally, the marine radiocarbon reservoir age of NW Scottish coastal waters was determined using museum acquired, historically collected marine bivalve shells. Given the broad spectrum of subjects covered by this thesis, chapters were split into themes, each chapter focusing on the specific objectives to be investigated (section 1.10) and containing detailed conclusions. A synopsis of chapter conclusions are presented here in order to provide an over-view of the main findings.

9.1 CONCLUSIONS TO MODERN PROCESSES: PHYSICAL ENVIRONMENT

9.1.1. Can regional indices of long-term climate explain the weather experienced by the Loch Sunart catchment and is there a link between regional coastal water temperatures and air temperatures which is coherent with indices of inter-annual climatic variability such as the North Atlantic Oscillation (NAO)?

Air temperature recorded in the Loch Sunart catchment over a 2 year period (AD 2000-2002) reflect the climate experienced by the majority of the Scottish mainland, which in turn is strongly influenced by coastal water temperatures via oceanic heat transfer and thermal inertia. Scottish air temperatures correlate well with sea surface temperatures from Millport (MPT) on the Scottish west coast. Therefore, the MPT series was extended beyond the period of observation (AD 1953-2001) to AD 1800 via the application of a regression equation derived from the period of overlap between the Millport and Scottish mainland temperature (SMT) data. Additionally, the inner and main basin of Loch Sunart (at 40 m water depth) show a strong seasonal heating cycle, typical of mid-latitude shelf seas, which agrees well with MPT data, further advocating the value of the reconstructed Millport sea surface temperature series (RMPT) to hindcast temperatures experienced by Loch Sunart basin waters. Similarity between long-term SMT and 'open' coastal sea surface temperature (SSTA; HOLSMEER data) records, and also between SMT and winter NAO indices (Jones *et al.*, 1997), suggests the reconstructed and extended Millport marine temperature series reflects long-term climate variability in the wider North Atlantic region. Thus, the extended marine temperature series can be used for direct comparison with the proxy derived palaeotemperature records obtained from Loch Sunart.

Detailed data and discussion can be found in ***chapters 3 and 8.***

9.1.2 Is the fjordic circulation of Loch Sunart influenced by extreme states of atmospheric forcing mechanisms?

Given the importance of climatic parameters (such as wind stress and freshwater inputs) to fjordic hydrography, the circulation of Loch Sunart basins were expected to show a response to the NAO. To test whether the Loch Sunart basin hydrography was significantly modulated by climatic influences during differing phases of the NAO, the circulation of the inner and main basin was modelled using an existing circulation model (Elliott *et al.*, 1992; Gillibrand *et al.*, 1995) with along-channel wind stress, river discharge and surface elevation at the loch mouth as inputs. Modelling results from the inner basin of Loch Sunart showed meteorological forcing during the positive NAO year of 1988-89 resulted in less frequent deep water renewal events (DWREs), greater salinity variability and a lower annual mean salinity (by 0.52) than for the negative NAO year of 1995-96. The NAO appeared to have little influence on main basin salinity (salinity difference of 0.02), despite significant variations in the number of renewal days and inflow of water into the basin (negative NAO year = 171 renewal days and a mean inflow of 694 m^3s^{-1}; positive NAO year = 120 renewal days and a mean inflow of ~239 m^3s^{-1}). The modelling results agreed well with the observed basin water temperature and salinity response (recorded hourly by stationary moorings placed at 40 m water depth in the main basin between 7/04/01 to 17/6/02, and in the inner basin between 27/6/01 to 18/6/02) to precipitation recorded in the Loch Sunart catchment. These data demonstrated a clear response of inner basin hydrography to freshwater inputs, with DWREs typically occurring during periods of low precipitation in the catchment, i.e. probable periods of low freshwater input into the inner basin, whilst main basin salinity remained relatively stable throughout the year. Salinity variations showed negligible impact on the steadily evolving seasonal heating cycle. The main basin temperature cycle (maximum and minimum temperatures of 13.4 °C and 7.9 °C respectively) lagged behind the inner basin temperature (maximum and minimum temperatures of 13.4 °C and 7.7 °C respectively) by about 10 days. This lag likely exemplifies the stronger coupling of the inner basin hydrography to atmospheric processes.

Detailed data and discussion can be found in ***chapter 3.*** This work was carried out in collaboration with Dr. P. A. Gillibrand and Dr. W. E. N. Austin and published in Continental Shelf Research, volume 25, in 2005.

9.1.3 Does the high freshwater input into NW Scottish coastal waters and restricted exchange of fjord water with coastal waters contribute to regionally 'younger' marine radiocarbon reservoir ages, i.e. a negative ΔR value with respect to the global surface ocean reservoir age of 400 years?

Freshwater typically exhibits an isotopic signal close to atmospheric $^{14}C/^{12}C$ (Broecker & Walton, 1959) and the igneous geology of NW Scotland, together with steep-sloped catchments, generally cause the high annual amount of rainfall (primarily orographic) to be rapidly translated to surface runoff and freshwater inputs into the sea loch (Black & Cranston, 1995). Harkness (1983) radiocarbon dated historically collected marine molluscs shells and determined a marine radiocarbon reservoir age of 405 years for UK coastal waters. Given a conservative mixing relationship, fjordic waters are likely to have 'younger' apparent ages than the global average surface ocean radiocarbon reservoir age of R(t) = 400 years, ΔR = 0 (Stuiver & Braziunas, 1993). Accelerator mass spectrometry (AMS) radiocarbon dating of museum shells with a known year of collection (pre-bomb, i.e. pre-1950) yielded a regional ΔR value of -27 ± 11 years, which is statistically different (at a confidence level of 99.5%) to the ΔR value of 14 ± 13 years reported for UK coastal waters (Harkness, 1983) and in good agreement with the -33 ± 93 years reported by Reimer *et al.*, (2002). This regional ΔR value was used to correct radiocarbon dates obtained from cores GC023 and SC023 and it is recommended that a correction factor of ΔR = -27 ± 11 years should be applied to marine radiocarbon dates from the NW coast of Scotland during the calibration process.

Detailed data and discussion can be found in ***chapter 4.***

9.1.4 Can the modern benthic foraminiferal distribution in Loch Sunart surface sediments be related to environmental controls?

The modern distribution of Loch Sunart benthic foraminifera (> 125 μm) was determined from a suite of 31 spatially distributed samples representing a range of water depths (5-121 m). Loch Sunart surface sediments typically yield higher benthic foraminiferal species diversities and abundances than reported for nearby shelf sites (Murray, 2003) or for many NW European fjord sites; possible due to the relatively shallow basin depths and frequent DWREs. Multivariate statistical methods (cluster analysis, non-metric multi-dimensional scaling and factor analysis) identified 4 benthic foraminiferal assemblages reflecting; A) a restricted and stressed environment (found in the inner basin); B) high current activity; C) stratification and a calm depositional environment; D) coastal water influence.

Assemblage group A comprises of samples primarily obtained from the inner basin of Loch Sunart and is dominated by agglutinated taxa (> 70%), in particular, *Eggerelloides scaber.* This dominance by a single species, along with the presence of hyaline taxa such as *A. beccarii*, *E. excavatum* and *B. marginata* (which are known to be tolerant to variable conditions), likely reflects the stressed environment experienced by inner basin benthic foraminifera due to low salinities (≤ 33), variable seasonal conditions (i.e. a strong heating cycle) and high organic matter inputs (7.2 ± 5.5 %). Low proportions of hyaline taxa (often with 'etched' tests) and the near-absence of benthic foraminifera with a porcelaneous wall structure, point to low availability of dissolved carbonate in the brackish inner basin waters and post-mortem carbonate dissolution.

Assemblage group B is dominated by 'high energy' taxa such as *Cibicides lobatulus, Ammonia beccarii, Asterigerinata mamilla* and *Spiroplectaminna wrightii*, with at least two of these species usually accounting for > 50 % of the total assemblage. Since this benthic foraminiferal assemblage group comprises samples taken from either shallow water depths (<20 m) or sill areas, typically with a coarse substrate (60 ± 30 % sand), assemblage group B is likely indicative of locations with very high bottom water current activity.

Assemblage group C (*Bulimina marginata – Nonionella turgida – Stainforthia fusiformis*) consists of sediment samples predominantly obtained from the deeps of the main and outer basin, where the substrate is fine grained (62.5 ± 13.9 % silt), suggesting a calm depositional environment. Species such as *Adercotryman glomeratum* and *Cassidulina reniforme*, along with recorded June BWTs of around 11.8 °C, suggests bottom water conditions at these sites are typically cool for long periods of the year. This, along with the high organic matter content (10.7 ±2.5 %) of the fine-grained sediment and high species diversity and equitablity, suggests benthic foraminifera from this assemblage group are living in relatively stable conditions under a strongly stratified water column.

Assemblage group D (*A. beccarii – C. lobatulus – S. wrightii – E. excavatum*) encompasses outer basin and main basin samples from water depths of 31 – 121 m and from BWS and BWT of 33.6-34.2 and 11.6-12.5 °C, respectively. Fairly high abundances of *C. lobatulus, A. beccarii* and *S. wrightii* in these moderately coarse sediments (50 % sand), with low abundances of 'calm depositional' taxa such as *B. marginata* and *N. turgida*, suggest that locations yielding these assemblages experience either mild current activity or episodic current activity, as seen during DWREs. The increasing abundance of porcelaneous taxa towards the outer basin suggests abundances of foraminifera with this wall structure could be used as a BWS indicator.

Detailed data and discussion can be found in ***chapter 5.***

9.1.5 What influences the modern stable carbon isotopic compositions of benthic foraminifera in Loch Sunart?

The stable isotopic compositions of four benthic foraminifera species; *Ammonia beccarii, Bulimina marginata, Nonionella turgida* and *Cibicides lobatulus* were measured and compared to environmental data collected at the sampling site. The stable isotopic compositions were used to indicate relative living depths for each species, with *C. lobatulus* exhibiting $\delta^{13}C$ values typical of an epifaunal habitat and thus likely recording the $\delta^{13}C$ of seawater dissolved inorganic carbon. The $\delta^{13}C$ of the other species pointed to infaunal living habitats with *B. marginata* appearing to occupy a shallow infaunal habitat, *A. beccarii* living at an intermediate infaunal depth and *N. turgida* yielding the most depleted $\delta^{13}C$, suggesting a deep infaunal habitat. The difference between $\delta^{13}C_{\textit{Cibicides lobatulus}}$ and $\delta^{13}C_{\textit{Nonionella turgida}}$ was used to estimate a pore water $\delta^{13}C$ gradient of ~ 3 ‰, which is steeper than the majority of deep-sea open ocean sites but comparable to sites from the western North Atlantic with similar bottom water compositions and shallow oxygen penetration (McCorkle & Emerson, 1988).

Stable oxygen isotopic compositions from *A. beccarii*, *B. marginata*, and *C. lobatulus* point to a possible 'seasonal effect' in benthic foraminiferal isotopic compositions from shelf seas with a strong seasonal heating cycle, though *N. turgida* appears to calcify close to $\delta^{18}O$ of seawater throughout the year. Comparison of measured $\delta^{18}O$ with theoretical equilibrium $\delta^{18}O$ calcite, calculated using bottom water temperature (BWT) and bottom water salinity (BWS) recorded at the time of collection, suggests *C. lobatulus*, *A. beccarii* and *B. marginata* in Loch Sunart calcify during peak BWT in October/November/December; trends seen in other shelf sea areas (Scourse *et al.*, 2004, *pers. comm.*, Dr. Gaute Mikalesen, 2004).

Detailed data and discussion can be found in ***chapter 6.***

9.1.6 Does the benthic foraminifera Cibicides lobatulus calcify close to the theoretical equilibrium $\delta^{18}O$ calcite of seawater?

Measured $\delta^{18}O$ from *A. beccarii*, *B. marginata*, *N. turgida* and *C. lobatulus* was compared to the $\delta^{18}O$ of equilibrium calcite to determine the degree of isotopic disequilibrium for each species ($\Delta\delta^{18}O$), with the focus being on *C. lobatulus*, since this species was used to obtain the stratigraphic records of $\delta^{18}O$ from Loch Sunart cores GC023 and SC023. Many studies have reported *Cibicidoides* spp. calcifying with pronounced $\delta^{18}O$ disequilibria (e.g. Celtic Sea $\Delta\delta^{18}O_{Cibicides\ lobatulus} = -0.92 \pm 0.56$ ‰; Scourse *et al.*, 2004) whilst infaunal taxa, such as *Uvigerina* (Shackleton, 1974) or *A. beccarii* (Scourse *et al.*, 2004), typically calcify close to isotopic equilibrium. However, Loch Sunart *C. lobatulus* appears to calcify close to oxygen isotopic equilibrium ($\Delta\delta^{18}O = -0.11 \pm 0.17$ ‰) when the Bemis *et al.*, (1998) or Lynch-Stieglitz *et al.*, (1999) palaeotemperature equations (equations calibrated with the epifaunal *Cibicidoides* group), are applied to the data. The disparity between the small *C. lobatulus* $\Delta\delta^{18}O$ presented here and the large $\Delta\delta^{18}O$ disequilibria of *Cibicidoides* reported in other studies, highlights the importance of establishing which palaoetemperature equation to use for a benthic foraminiferal species. It is recommended that a $\delta^{18}O$:temperature equation calibrated to the epifaunal group *Cibicidoides* is used to derive palaeotemperature from measured *C. lobatulus* $\delta^{18}O$ data.

The implication of negligible inter-annual salinity variations in the main basin of Loch Sunart, along with the report of minor salinity influences on the $\delta^{18}O$ of Loch Etive water (Austin & Inall, 2002) suggests the main basin of Loch Sunart may provide an ideal location for resolving high resolution palaeotemperature records from fossil benthic foraminiferal $\delta^{18}O$ calcite. The 0.62 ‰ inter-annual range in *C. lobatulus* $\delta^{18}O$ from core SC023 requires a BWS change of ~ 3, and since a BWS change of this magnitude in Loch Sunart is extremely unlikely to occur, *C. lobatulus* $\delta^{18}O$ does not solely reflect BWS in Loch Sunart. The same 0.62 ‰ variation requires a BWT change of ~ 2.4 °C and since the inter-annual summer sea surface temperature at Millport varies by ~ 2.66 °C (between 1953-2000), the $\delta^{18}O$ *C. lobatulus* is assumed to reflect changes in BWT.

Detailed data and discussion can be found in ***chapter 6.***

9.2 CONCLUSIONS TO PALAEOENVIRONMENTAL RECONSTRUCTIONS

9.2.1 Can an independent proxy of palaeotemperature from Loch Sunart be generated using a benthic foraminiferal transfer function model ?

The Recent Benthic Foraminifera (RBF) training set of Sejrup *et al.,* (2004, n = 260) was modified by adding 3 modern benthic foraminifera assemblages (22, 80 and 198) from the main and outer basin of Loch Sunart. This extended the summer (July-August-September) BWT environmental gradient from 11.99 °C to 12.51 °C (increasing mean summer BWT from 5.57 °C to 5.62 °C) and shifted the mean summer BWS environmental gradient (already at 33.58) from 34.95 to 34.94.

A weighted-averaging partial least squares (WA-PLS), 3 component transfer function model (Ts3) was created for summer (July-August-Setpember) BWT using a training set of n = 253 (including the 3 Loch Sunart samples). A 'leave-one-out' validation of the model yielded a root mean square error of prediction ($RMSEP_{jack}$) of 1.03 °C; a 0.03 °C improvement on the 1.06 °C $RMSEP_{jack}$ of Sejrup *et al.,* (2004). Comparison of the reconstructed summer BWT (RBWT) from SC023 benthic foraminiferal assemblages with the observed May-October Millport sea surface temperature series between 1986-2000, demonstrated that inter-annual trends in RBWT from the main basin of Loch Sunart agree well with trends in the Millport series. The Ts3 model RBWT ranged between 9 – 10.1 °C whereas Millport sea surface temperatures range from 12.4 – 14.8 °C; this difference probably reflects the 'dampened' and lagged response of deep waters to the seasonal heating cycle. Given the strong relationship between reconstructed NW Scottish marine temperatures, air temperatures and the NAO (chapter 3) along with the reported oceanic response to climate forcing (e.g. Holliday, 2003), Loch Sunart palaeoproxies derived from benthic foraminifera are likely to reflect the climate of the NE Atlantic region.

A 3 component, jack-knifed WA-PLS transfer function model for summer (July-August-September) BWS (Ss1) yielded an $\text{RMSEP}_{\text{jack}}$ of 0.17; identical to the 2 component, jack-knifed WA-PLS transfer function model of Sejrup *et al.,* (2004). The model gave SC023 reconstructed summer BWS (RBWS) ranging from 33.99 to 34.22. Observed BWS at the Loch Sunart core site is typically ~ 33.6, suggesting Ss1 over-estimates BWS by ~ 0.4 – 0.8 at the Loch Sunart core site and this may be due to the under-representation of benthic foraminiferal assemblages with similar recorded BWS in the RBF. Unfortunately, the RBWS could not be calibrated with regional salinity series because these do not exist. However, the $\delta^{13}C$ from the epifaunal species *C. lobatulus*, often used as a proxy for BWS changes, suggests isotopically depleted $\delta^{13}C$ typically occurs with fresher salinities. Additionally, the trend towards decreasing salinity towards the core top of SC023 is consistent with reports of freshening in the N Atlantic region and could reflect the influence of the prolonged positive NAO phase (e.g. Blindheim *et al.,* 2000).

Detailed data and discussion can be found in ***chapter 7.***

9.2.2 Can high resolution palaeoenvironmental reconstructions be obtained from Loch Sunart sedimentary archives?

A preliminary radiocarbon date close to the base of the ~ 3 m gravity core GC023, obtained from the Dun Ghallain Deep, in the main basin of Loch Sunart, initially suggested a core resolution of ~ 7 years.cm^{-1}. However, the combined ^{14}C and lead-caesium age model for GC023 suggests a large hiatus of around 1000 years. This hiatus occurred sometime between ~ AD 900 and AD 1900, negating the interpretation of paleonvironmental conditions through the Medieval Warm Period and Little Ice Age. The large increase in grain size during this period, points to the possibility of winnowing or scouring of sediment at this site, which is likely due to strong bottom water current activity influenced by the steep narrow bathymetry seaward of the core site. This hypothesis of winnowing is supported by a seismic profile from a nearby main basin deep which reveals a thin Holocene sediment package in the deep (111 m) and a thick package on the fairly shallow (~ 50 m) flat shelf region, and exemplifies the need to carry out a reconnaissance survey of sites prior to coring to ensure that a continuous high resolution sedimentary archive is recovered.

Carefully evaluated age-control data highlight the problematic geochronology for core GC023 and along with it's relatively short time span, negates the identification of millennial scale climate cycles often seen in recent late Holocene records. The age-model also makes it impossible to resolve climate and environmental change during the Medieval Warm Period and Little Ice Age, and inhibits the interpretation of the development of the fjordic circulation change continuously through the last 2000 years. Despite this geochronology problem, palaeoenvironmental reconstructions from Loch Sunart suggest that these high resolution sedimentary archives have the potential to resolve inter-annual marine climate variability and capture an integrated record of changes in the catchment and marine environment.

Various proxies (such as the redox boundary and *C. lobatulus* $\delta^{13}C$) point to a change in fjordic circulation around AD 500, with a shift to increased coast water influence at the core site. The cause of circulation change is not clear, but possibilities include a threshold change in fjordic circulation due to isostatic sea level fall or changes in open N Atlantic conditions.

Comparison of the *C. lobatulus* $\delta^{18}O$ record with a long reconstructed marine temperature series demonstrates that the test chemistry of *C. lobatulus* from the main basin records inter-annual variations in bottom water temperature of a similar magnitude to instrumental data (i.e. ~ 2 °C). The agreement of *C. lobatulus* $\delta^{18}O$ and RBWT suggests BWT at the site were cooler and BWS were higher during the 20th century warm period and possibly during the Roman Warm Period, and this is likely to be due to increased stratification and enhanced estuarine circulation at this time. A 'spike' of enriched $\delta^{18}O$ around AD 500 (0.5 ‰ heavier than other $\delta^{18}O$ from that core section) equates to a temperature change of ~ 2.3 °C; similar to the RBWT cooling of 1.7 °C at the same level. Two major events occur around AD 500; an IRD event in the North Atlantic and the 'nuclear winter' of AD 535 and though problematic age control makes it impossible to attribute causal factors to shifts in palaeoenvironmental conditions in GC023, such 'extreme' and isolated events likely exemplify the sensitivity and rapid response of palaeoproxies in the Loch Sunart main basin.

The high frequency and large amplitude shifts in *C. lobatulus* isotopic compositions from GC023 exemplifies the sensitivity of these marginal environments to regional circulation and N Atlantic climate forcing mechanisms and illustrates the potential to resolve inter-annual marine climate variability and capture changes in the catchment environment or climate.

Detailed data and discussion can be found in ***chapter 8.***

9.3. FURTHER WORK

The preliminary work presented in this thesis has established the potential to resolve inter-annual climatic variability from sedimentary archives from Loch Sunart and highlighted the following areas for further work which will hopefully improve the understanding of processes influencing palaeoenvironmental proxies in Loch Sunart and achieve more accurate palaeoenvironmental reconstructions from these newly exploited environments:

Chapter 3: Presently, the model used for investigating the climatically forced circulation of Loch Sunart (Elliott *et al.*, 1992; Gillibrand *et al.*, 1995; Gillibrand *et al.*, 2005) only models salinity. However, bottom water temperature variability may also accompany deep water renewal events and this would have implications for palaeoclimatic reconstructions utilising $\delta^{18}O$ of foraminiferal calcite (Austin & Inall, 2002). Proposals have been implemented to extend this modelling work to include temperature as a model output (*pers. comm.,* Dr. P Gillibrand, 2004).

Chapter 4: Sample material from a marine bivalve *Arctica islandica* obtained from Loch Creran in 1969 by Professor John Gage (Dunstaffnage Marine Laboratories, Oban) and since stored at the Scottish Natural History Museum, has been submitted to NERC East Kilbride AMS Laboratory for radiocarbon AMS dating (allocation number 941.1001). Unfortunately, the ^{14}C data were not available at the time of submission.

The shell was alive at the time of collection and scelerochronological methods suggests that the shell was approximately 90 years old, hence spawned around AD 1878. It is hoped that ^{14}C data from this *A. islandica* will provide a record of the ΔR changes over the lifetime of the shell, which are likely to be influenced by climatic variability such as the NAO (e.g. Druffell 1997; Gillibrand *et al.*, 2005) and use bomb produced ^{14}C detected in the shell material as a tracer to investigate the circulation of Loch Creran (e.g. Weidman & Jones, 1993).

Future research cruises in Loch Sunart will continue to try and obtain 'live' *A. islandia.*

Chapter 5: The typical fjordic bathymetry of Loch Sunart (i.e. deep basins and shallow sills) presents two potential areas for future palaeoclimatic research. Fossil benthic foraminifera from the calm depositional environment of the main basin deep appear to document inter-annual bottom water temperature changes (in both assemblage structure and test geochemistry), whilst the inner basin, with it's restricted connection to coastal water and strong response to freshwater inputs (chapter 3) has the potential to provide records of atmospheric climatic forcing through fossil assemblages. Benthic foraminiferal analyses on long sediment cores recovered from both the main basin and the inner basin (between 2001 to 2004), could provide an insight into the environmental gradient of the loch.

Chapter 6: There is a paucity of stable isotope data from NE Atlantic shelf sea benthic foraminifera (Austin *et al., in progress*), and more empirical data is required from living benthic foraminifera from these environments in order to better understand the 'seasonal effect' and controls on test geochemistry, for example, how changes in porewater geochemistry, such as pH, affect the $\delta^{18}O$ of infaunal benthic foraminifera.

Relationships between the $\delta^{13}C$ of epifaunal and deep infaunal taxa and variables such as water depth and substrate organic matter point to possible proxies for past bottom water dissolved oxygen concentrations and palaeoproductivity. The small sample number of paired $\delta^{13}C$ data presented here probably explains the marginally insignificant relationships and the addition of more $\delta^{13}C$ data is likely to improve the statistical significance of the correlations and possibly strengthen the relationship.

Chapter 7: This study illustrates that the shelf sea Recent Benthic Foraminifera training set (plus 3 Loch Sunart samples) of Sejrup *et al.,* (2004) can be used to create a WA-PLS transfer function model that reconstructs a summer bottom water temperature series which is independent of $\delta^{18}O$ derived temperature and agrees well with an observed marine temperature series, even when the fossil samples are at the extreme of the environmental gradient. The training set could be extended to include more samples from sites on the west coast of the UK which are directly influenced by the North Eastern Atlantic circulation but have a more southerly location thus lengthening the temperature gradient. Samples from other sea lochs which display a lower basin salinity but have deep sills and thus are not 'restricted' basins could be included to provide regionally representative samples and extend the lower limit of the BWS gradient. Extended quantitative palaeoenvironmental reconstruction work on core SC023 may provide more information on the relationship between reconstructed summer bottom water temperature and stable isotopic compositions.

Chapter 8: Palaeoenvironmental reconstructions from GC023 clearly illustrate the potential of obtaining high-resolution marine sedimentary archives from these marginal marine environments. These records are likely to resolve inter-annual marine climate variability and capture changes in the catchment environment or climate, thus providing an opportunity to study land-ocean interactions.

Following a seismic survey, a 20 m long core (MD04-2831) from a shallow shelf area, near to the site of core GC023 the Loch Sunart basin was recovered during a recent (2004) R.V. *Marion Dusfresne* cruise and preliminary range finder radiocarbon dates suggests an age of 1,956 ± 19 ^{14}C yrs BP (i.e. uncalibrated and uncorrected for ΔR) at 470 cm. Future work plans to document the palaeoproxies in this core in order to reconstruct the palaeoenvironmental conditions in the main basin of Loch Sunart, during the past 1000 years (the EU project MILLENIUM) and also possibly since the de-glacial period. This will hopefully provide new insights into the evolution of sea loch circulation throughout the Holocene.

REFERENCES

Aarseth, I., 1997. Western Norwegian fjord sediments; age, volume, stratigraphy, and role as temporary depository during glacial cycles. *Coldseis,* **143** (1-4): 39-53.

Abrantes, F., Lebreiro, S., Rodrigues, T., Gil, I., Bartels-Jonsdottir, H., Oliveir, P., Kissel, C. and Grimalt, J.O., *in press.* Shallow-marine sediment cores record climate variability and earthquake activity off Lisbon (Portugal) for the last 2000 years. *Quaternary Science Reviews,*

Adkins, J.F., Boyle, E.A., Curry, W.B. and Lutringer, A., 2003. Stable isotopes in deep-sea corals and a new mechanism for "vital effects". *Geochimica Et Cosmochimica Acta,* **67** (6): 1129-1143.

Aitken, M.J., 1990. *Science-based dating in archaeology.* Longman, London. pp.

Allen, G.L. and Simpson, J.H., 1998. Deep water inflows to Upper Loch Linnhe. *Estuarine Coastal and Shelf Science,* **47** (4): 487-498.

Alley, R.B., 1998. Icing the North Atlantic. *Nature,* **392** 335-336.

Alley, R.B., 2000. Ice-core evidence of abrupt climate changes. *Proceedings of the National Academy of Sciences of the United States of America,* **97** (4): 1331-1334.

Alley, R.B., Clark, P.U., Keigwin, L.D. and Webb, R.S., 1999. Making sense of millennial-scale climate change. in *Mechanisms of Global Climate Change at Millennial Time Scales,* Geophysical Monograph, **112,** P. U. Clark, R. S. Webb and L. D. Keigwin (eds). American Geophysical Union, Washington, DC. 385-394.

Alley, R.B., Mayewski, P.A., Sowers, T., Stuiver, M., Taylor, K.C. and Clark, P.U., 1997. Holocene climatic instability: a prominent widespread event 8200 years ago. *Geology,* **25** 483–486.

Allison, N. and Austin, W.E.N., 2003. The potential of ion microprobe analysis in detecting geochemical variations across individual foraminifera tests. *Geochemistry Geophysics Geosystems,* **4** art. no.-8403.

Altenbach, A.V., Pflaumann, U., Schiebel, R., Thies, A., Timm, S. and Trauth, M., 1999. Scaling percentages and distributional patterns of benthic foraminifera with flux rates of organic carbon. *Journal of Foraminiferal Research,* **29** (3): 173-185.

Altenbach, A.V. and Sarnthein, M., 1989. Productivity Record in Benthic Foraminifera. in *Productivity of the Ocean: Present and Past,* W. H. Berger, V. S. Smetacek and G. Wefer (eds). John Wiley & Sons Limited, 255-269.

Altenbach, A.V. and Struck, U., 2001. On the coherence of organic carbon flux and benthic foraminiferal biomass. *Journal of Foraminiferal Research,* **31** (2): 79-85.

Alve, E., 1990. Variations in estuarine foraminiferal biofacies with diminishing oxygen conditions in Drammensfjord, SE Norway. in *Paleoecology, biostratigraphy, paleoceanography and taxonomy of agglutinated foraminifera,* **327,** C. Hemleben, M. A. Kaminski, W. Kuhnt and D. B. Scott (eds). D. Reidel Publishing Company, 661-694.

Alve, E., 1999. Colonization of new habitats by benthic foraminifera: a review. *Earth-Science Reviews,* **46** (1-4): 167-185.

Alve, E., 2003. A common opportunistic foraminiferal species as an indicator of rapidly changing conditions in a range of environments. *Estuarine, Coastal and Shelf Science,* **57** (3): 501-514.

Alve, E. and Bernhard, J.M., 1995. Vertical Migratory Response of Benthic Foraminifera to Controlled Oxygen Concentrations in an Experimental Mesocosm. *Marine Ecology-Progress Series,* **116** (1-3): 137-151.

Alve, E. and Goldstein, S.T., 2002. Resting stage in benthic foraminiferal propagules: a key feature for dispersal? Evidence from two shallow-water species. *Journal of Micropalaeontology,* **21** 95-96.

Alve, E. and Murray, J.W., 1995. Experiments to determine the origin and palaeoenvironmental significance of agglutinated foraminiferal assemblages. in *Proceedings of the Fourth International Workshop on Agglutinated Foraminifera, Kraków Poland, September 12-19, 1993,* **3,** M. A. Kaminski, S. Geroch and M. A. Gasinski (eds). Grzybowski Foundation Special Publication, 1-11.

Alve, E. and Murray, J.W., 1997. High benthic fertility and taphonomy of foraminifera: a case study of the Skagerrak, North Sea. *Marine Micropaleontology,* **31** (3-4): 157-175.

Alve, E. and Nagy, J., 1986a. Estuarine foraminiferal distribution in Sandebukta, a branch of the Oslo Fjord. *Journal of Foraminiferal Research,* **16** (4): 261-284.

Alve, E. and Nagy, J., 1986b. Pollution induced and changes in estuarine foraminiferal distribution in the Oslo Fjord. in *Second international workshop on Agglutinated foraminifera,* **2,** F. Roegl (eds). University of Vienna Institute of Paleontology, 10.

Alve, E. and Nagy, J., 1990. Main features of foraminiferal distribution reflecting estuarine hydrography in Oslo Fjord. *Marine Micropaleontology,* **16** (3-4): 181-206.

Andersen, K.K., Azuma, N., Barnola, J.-M., Bigler, M., Biscaye, P., Caillon, N., Chappellaz, J., Clausen, H.B., Dahl-Jensen, D., Fischer, H., Fluckiger, J., Fritzsche, D., Fujii, Y., Goto-Azuma, K., Gronvold, K., Gundestrup, N., Hansson, M., Huber, C., Hvidberg, C.S., Johnsen, S.J., Jonsell, U., Jouzel, J., Kipfstuhl, S., Landais, A., Leuenberger, M., Lorrain, R., Masson-Delmotte, V., Miller, H., Motoyama, H., Narita, H., Popp, T., Rasmussen, S.O., Raynaud, D., Rothlisberger, R., Ruth, U., Samyn, D., Schwander, J., Shoji, H., Siggard-Andersen, M.-L., Steffensen, J.P., Stocker, T., Sveinbjornsdottir, A.E., Svensson, A., Takata, M., TISON, J.-L., Thorsteinsson, T., Watanabe, O., Wilhelms, F. and White, J.W.C., 2004. High-resolution record of Northern Hemisphere climate extending into the last interglacial period. *Nature,* **431** (7005): 147-151.

Anderson, D.E., 1998. A reconstruction of Holocene climatic changes from peat bogs in north-west Scotland. *Boreas,* **27** (3): 208-224.

Anderson, L.D., Delaney, M.L. and Faul, K.L., 2001. Carbon to phosphorus ratios in sediments: Implications for nutrient cycling. *Global Biogeochemical Cycles,* **15** (1): 65-80.

Anderson, N.J. and Leng, M.J., 2004. Increased aridity during the early Holocene in West Greenland inferred from stable isotopes in laminated-lake sediments. *Quaternary Science Reviews,* **23** (7-8): 841-849.

Andresen, C.S., Bond, G., Kuijpers, A., Knutz, P.C. and Bjorck, S., 2005. Holocene climate variability at multidecadal time scales detected by sedimentological indicators in a shelf core NW off Iceland. *Marine Geology,* **214** (4): 323-338.

Andrews, J.E., Greenaway, A.M. and Dennis, P.F., 1998. Combined Carbon Isotope and C/N Ratios as Indicators of Source and Fate of Organic Matter in a Poorly Flushed, Tropical Estuary: Hunts Bay, Kingston Harbour, Jamaica. *Estuarine, Coastal and Shelf Science,* **46** (5): 743-756.

Andrews, J.T., 1998. Abrupt changes (Heinrich events) in late Quaternary North Atlantic marine environments: a history and review of data and concepts. *Journal of Quaternary Science,* **13** (1): 3-16.

Andrews, J.T., Caseldine, C., Weiner, N.J. and Hatton, J., 2001. Late Holocene (ca. 4 ka) marine and terrestrial environmental change in Reykjarfjördur, north Iceland: climate and/or settlement? *Journal of Quaternary Science,* **16** (2): 133 - 143.

Appenzeller, C., Stocker, T.F. and Anklin, M., 1998. North Atlantic oscillation dynamics recorded in Greenland ice cores. *Science,* **282** (5388): 446-449.

Appleby, P.G., 1997. Sediment records of fallout radionuclides and their application to studies of sediment-water interactions. *Water, Air and Soil Pollution,* **99** 573-586.

Appleby, P.G., Dearing, J.A. and Oldfield, F., 1985. Magnetic Studies of Erosion in a Scottish Lake Catchment .1. Core Chronology and Correlation. *Limnology and Oceanography,* **30** (6): 1144-1153.

Appleby, P.G. and Oldfield, F., 1983. The Assessment of Pb-210 Data from Sites with Varying Sediment Accumulation Rates. *Hydrobiologia,* **103** (JUL): 29-35.

Appleby, P.G. and Oldfield, F., 1992. Application of lead-210 to sedimentation studies. in *Uranium-series disequilibrium; applications to Earth, marine, and environmental sciences,* M. Ivanovich and R. S. Harmon (eds). Clarendon Press, Oxford. 731-778.

Arneborg, L., 2004. Turnover times for the water above sill level in Gullmar Fjord. *Continental Shelf Research,* **24** 443–460.

Arnold, A.J. and Parker, W.C., 1999. Biogeography of planktonic foraminifera. in *Modern Foraminifera,* B. K. S. Gupta (eds). Kluwer Academic Publishers, 103-122.

Arz, H.W., Gerhardt, S., Patzold, J. and Rohl, U., 2001. Millennial-scale changes of surface- and deep-water flow in the western tropical Atlantic linked to Northern Hemisphere high-latitude climate during the Holocene. *Geology,* **29** (3): 239-242.

Ascough, P.L., Cook, G.T., Dugmore, A.J., Barber, J., Higney, E. and Scott, E.M., 2004. Holocene variations in the Scottish marine radiocarbon reservoir effect. *Radiocarbon,* **46** (2): 611-620.

Aure, J., Molvaer, J. and Stigebrandt, A., 1996. Observations of inshore water exchange forced by a fluctuating offshore density field. *Marine Pollution Bulletin,* **33** (1-6): 112-119.

Austin, W.E.N., 1991. *Late Quaternary benthonic foraminiferal stratigraphy of the western U.K. continental shelf.* Doctoral thesis. University College of North Wales, Bangor. pp. 554.

Austin, W.E.N. and Evans, J.R., 2000a. Benthic foraminifera and sediment grain size variability at intermediate water depths in the Northeast Atlantic during the late Pliocene-early Pleistocene. *Marine Geology,* **170** (3-4): 423-441.

Austin, W.E.N. and Evans, J.R., 2000b. NE Atlantic benthic foraminifera: modern distribution patterns and palaeoecological significance. *Journal of the Geological Society,* **157** 679-691.

Austin, W.E.N. and Inall, M.E., 2002. Deep-water renewal in a Scottish fjord: temperature, salinity and oxygen isotopes. *Polar Research,* **21** (2): 251-257.

Austin, W.E.N. and Kroon, D., 2001. Deep sea ventilation of the northeastern Atlantic during the last 15,000 years. *Global and Planetary Change,* **30** (1-2): 13-31.

Austin, W.E.N. and Sejrup, H.P., 1994. Recent shallow water benthic foraminifera from western Norway: ecology and palaeoecological significance. in *Cushman Foundation for Foraminiferal Research. Special Publication,* **32,** H. P. Sejrup and K. L. Knudsen (eds). 103-125.

Backhaus, J.O., 1989. The North Sea and the climate. *Dana,* **8** 69-82.

Backhaus, J.O., 1990. On the Atmospherically induced Variability of the Circulation of the NW-European Shelf Sea and related Phenomena. in *Modelling Marine Systems,* **1,** A. M. Davies (eds). 93-134.

Backhaus, J.O., 1996. Climate-sensitivity of European marginal seas, derived from the interpretation of modelling studies. *Journal of Marine Systems,* **7** (2-4): 361-382.

Baker, A., Caseldine, C.J., Gilmour, M.A., Charman, D., Proctor, C.J., Hawkesworth, C.J. and Phillips, N., 1999. Stalagmite luminescence and peat humification records of palaeomoisture for the last 2500 years. *Earth and Planetary Science Letters,* **165** (1): 157-162.

Barber, D.C., Dyke, A., Hillaire-Marcel, C., Jennings, A.E., Andrews, J.T., Kerwin, M.W., Bilodeau, G., McNeely, R., Southon, J., Morehead, M.D. and Gagnonk, J.-M., 1999a. Forcing of the cold event of 8,200 years ago by catastrophic drainage of Laurentide lakes. *Nature,* **400** 344-348.

Barber, K.E., Battarbee, R.W., Brooks, S.J., Eglinton, G., Haworth, E.Y., Oldfield, F., Stevenson, A.C., Thompson, R., Appleby, P.G., Austin, W.E.N., Cameron, N.G., Ficken, K.J., Golding, P., Harkness, D.D., Holmes, J.A., Hutchinson, R., Lishman, J.P., Maddy, D., Pinder, L.C.V., Rose, N.L. and Stoneman, R.E., 1999b. Proxy records of climate change in the UK over the last two millennia: documented change and sedimentary records from lakes and bogs. *Journal of the Geological Society,* **156** 369-380.

Barber, K.E., Chambers, F.M., Maddy, D., Stoneman, R.S. and Brew, J., 1994. A sensitive high-resolution record of late Holocene climatic change from a raised bog in northern England. *The Holocene,* **4** 198-205.

Bard, E., 1998. Geochemical and geophysical implications of the radiocarbon calibration. *Geochimica Et Cosmochimica Acta,* **62** (12): 2025-2038.

Bard, E., 2001. Paleoclimate - Extending the calibrated radiocarbon record. *Science,* **292** (5526): 2443-2444.

Barlow, L.K., 2001. The Time Period A.D. 1400-1980 in Central Greenland Ice Cores in Relation to the North Atlantic Sector. *Climatic Change,* **48** (1): 110-119.

Barmawidjaja, D.M., Vanderzwaan, G.J., Jorissen, F.J. and Puskaric, S., 1995. 150 Years of Eutrophication in the Northern Adriatic Sea - Evidence from a Benthic Foraminiferal Record. *Marine Geology,* **122** (4): 367-384.

Bates, C.R., Moore, C. and Harries, D., 2002. *Marine Biotope Research Survey, Loch Sunart, 2002.*

Battarbee, R.W., Cameron, N.G., Golding, P., Brooks, S.J., Switsur, R., Harkness, D., Appleby, P., Oldfield, F., Thompson, R., Monteith, D.T. and McGovern, A., 2001. Evidence for Holocene climate variability from the sediments of a Scottish remote mountain lake. *Journal of Quaternary Science,* **16** (4): 339-346.

Bauch, H.A., Erlenkeuser, H., Bauch, D., Mueller-Lupp, T. and Taldenkova, E., 2004. Stable oxygen and carbon isotopes in modern benthic foraminifera from the Laptev Sea shelf: implications for reconstructing proglacial and profluvial environments in the Arctic. *Marine Micropaleontology,* **51** (3-4): 285-300.

Beck, J.W., Richards, D.A., Edwards, R.L., Silverman, B.W., Smart, P.L., Donahue, D.J., Hererra-Osterheld, S., Burr, G.S., Calsoyas, L., Jull, T.A.J. and Biddulph, D., 2001. Extremely Large Variations of Atmospheric ^{14}C Concentration During the Last Glacial Period. *Science,* **292** (5526): 2453-2458.

Beer, J., Mende, W. and Stellmacher, R., 2000. The role of the sun in climate forcing. *Quaternary Science Reviews,* **19** (1-5): 403-415.

Begg, F.H., 1992. *Anthropogenic ^{14}C in the natural (aquatic) environment.* Ph.D. thesis. University of Glasgow, pp.

Begg, F.H., Cook, G.T., Baxter, M.S., Scott, E.M. and McCartney, M., 1992. Anthropogenic Radiocarbon in the Eastern Irish Sea and Scottish Coastal Waters. *Radiocarbon,* **34** (3): 707-716.

Belanger, P.E., Curry, W.B. and Matthews, R.K., 1981. Core-Top Evaluation of Benthic Foraminiferal Isotopic-Ratios for Paleo-Oceanographic Interpretations. *Palaeogeography Palaeoclimatology Palaeoecology,* **33** (1-3): 205-220.

Belkin, I.M., 2004. Propagation of the "Great Salinity Anomaly" of the 1990s around the northern North Atlantic. *Geophysical Research Letters,* **31** (L08306): doi:10.1029/2003GL019334.

Belkin, I.M., Levitus, S., Antonov, J.I. and Malmberg, S.A., 1998. "Great Salinity Anomalies" in the North Atlantic. *Progress In Oceanography,* **41** (1): 1-68.

Bemis, B.E., Spero, H.J., Bijma, J. and Lea, D.W., 1998. Re-evaluation of the oxygen isotopic composition of planktonic foraminifera: Experimental results and revised paleotemperature equations. *Paleoceanography,* **13** (2): 150-160.

Bengtsson, L. and Enell, M., 1986. Chemical analysis. in *Handbook of Palaeoecology and Palaeohydrology,* B. E. Berglund (eds). John Wiley & Sons, Ltd., Chichester. 423-451.

Berger, W.H., Fisher, K., Lai, C. and Wu, G., 1989. Ocean productivity and paleoproductivity: an overview. in *Productivity of the ocean: present and past,* W. H. Berger, V. S. Smetacek and G. Wefer (eds). Wiley, Chichester. 1-37.

Bergsten, H., Nordberg, K. and Malmgren, B., 1996. Recent benthic foraminifera as tracers of water masses along a transect in the Skagerrak, north-eastern North Sea. *Journal of Sea Research,* **35** (1-3): 111-121.

Berkman, P.A. and Forman, S.L., 1996. Pre-bomb radiocarbon and the reservoir correction for calcareous marine species in the Southern Ocean. *Geophysical Research Letters,* **23** (4): 363-366.

Bernhard, J.M., 2000. Distinguishing live from dead foraminifera: Methods review and proper applications. *Micropaleontology,* **46** (supplement 1):

Bernhard, J.M. and Bowser, S.S., 1999. Benthic foraminifera of dysoxic sediments: chloroplast sequestration and functional morphology. *Earth-Science Reviews,* **46** (1-4): 149-165.

Bernhard, J.M. and Sen Gupta, B.K., 1999. Foraminifera of oxygen-depleted environments. in *Modern Foraminifera,* B. K. Sen Gupta (eds). Kluwer Academic Publishers, 201-216.

Berstad, I.M., Sejrup, H.P., Klitgaard-Kristensen, D. and Haflidason, H., 2003. Variability in temperature and geometry of the Norwegian Current over the past 600 yr; stable isotope and grain size evidence from the Norwegian margin. *Journal of Quaternary Science,* **18** (7): 591-602.

Bianchi, G.G. and McCave, I.N., 1999. Holocene periodicity in North Atlantic climate and deep-ocean flow south of Iceland. *Nature,* **397** (6719): 515-517.

Bigg, G.R., 2003. *The Oceans and Climate.* Cambridge University Press, Cambridge. pp. 273.

Bird, M.I. and Grocke, D.R., 1997. Determination of the abundance and carbon isotope composition of elemental carbon in sediments. *Geochimica et Cosmochimica Acta,* **61** (16): 3413-3423.

Birks, C.J.A. and Koc, N., 2002. A high-resolution diatom record of late-Quaternary sea-surface temperatures and oceanographic conditions from the eastern Norwegian Sea. *Boreas,* **31** (4): 323-344.

Birks, H.J.B., 1995. Quantitative Palaeoenvironmental Reconstructions. in *Statistical Modelling of Quaternary Science Data,* D. Maddy and J. S. Brew (eds). Quaternary Research Association, Cambridge. 161-254.

Birks, H.J.B., 2003. Quantitative Palaeoenvironmental Reconstructions from Holocene Biological Data. in *Global Change in the Holocene,* A. Mackay, R. W. Battarbee, J. Birks and F. Oldfield (eds). Arnold, London. 528.

Blindheim, J., Borovkov, V., Hansen, B., Malmberg, S.A., Turrell, W.R. and Osterhus, S., 2000. Upper layer cooling and freshening in the Norwegian Sea in relation to atmospheric forcing. *Deep-Sea Research Part I-Oceanographic Research Papers,* **47** (4): 655-680.

Boberg, F. and Lundstedt, H., 2002. Solar wind variations related to fluctuations of the North Atlantic Oscillation. *Geophysical Research Letters,* **29** (15): art. no.-1718.

Bock, M.T., Miller, B.S. and Bowman, A.W., 1999. Assessment of eutrophication in the Firth of Clyde: Analysis of coastal water data from 1982 to 1996. *Marine Pollution Bulletin,* **38** (3): 222-231.

Boltovskoy, E. and Wright, R., 1976. *Recent Foraminifera.* Junk, W., The Hague. pp. 515.

Bond, G., Kromer, B., Beer, J., Muscheler, R., Evans, M.N., Showers, W., Hoffmann, S., Lotti-Bond, R., Hajdas, I. and Bonani, G., 2001. Persistent solar influence on north Atlantic climate during the Holocene. *Science,* **294** (5549): 2130-2136.

Bond, G., Showers, W., Cheseby, M., Lotti, R., Almasi, P., deMenocal, P., Priore, P., Cullen, H., Hajdas, I. and Bonani, G., 1997. A Pervasive Millennial-Scale Cycle in North Atlantic Holocene and Glacial Climates. *Science,* **278** (5341): 1257-1266.

Bond, G., Showers, W., Elliot, M., Evans, M., Lotti, R., Hajdas, I., Bonani, G. and Johnson, S., 1999. The North Atlantic's 1-2 kyr Climate Rhythm: Relation to Heinrich Events, Dansgaard/Oeschger Cycles and the Little Ice Age. in *Mechanisms of Global Change at Millenial Time Scales,* **Geophysical Monograph 112,** P. U. Clark, R. S. Webb and L. D. Keigwin (eds). American Geophysical Union,

Bond, G.C., Broecker, W., Johnsen, S., McManus, J., Labeyrie, L., Jouzel, J. and Bonani, G., 1993. Correlations between climate records from North Atlantic sediments and Greenland ice. *Nature,* **365** 143-147.

Bond, G.C., Heinrich, H., Broecker, W., Labeyrie, L., McManus, J., Andrews, J., Huon, S., Jantschik, R., Clasen, S., Simet, C., Tedesco, K., Klas, M., Bonani, G. and Ivy, S., 1992. Evidence for massive discharges of icebergs into the North Atlantic ocean during the last glacial. *Nature,* **360** 245-249.

Bond, G.C. and Lotti, R., 1995. Iceberg Discharges into the North-Atlantic on Millennial Time Scales During the Last Glaciation. *Science,* **267** (5200): 1005-1010.

Bondevik, S., Birks, H.H., Gulliksen, S. and Mangerud, J., 1999. Late Weichselian marine C-14 reservoir ages at the western coast of Norway. *Quaternary Research,* **52** (1): 104-114.

Bondevik, S., Mangerud, J. and Gulliksen, S., 2001. The marine C-14 age of the Vedde Ash Bed along the west coast of Norway. *Journal of Quaternary Science,* **16** (1): 3-+.

Bordovskiy, O.K., 1965. Accumulation of organic matter in bottom sediments. *Marine Geology,* **3** 33-82.

Bornmalm, L., Corliss, B.H. and Tedesco, K., 1997. Laboratory observations of rates and patterns of movement of continental margin benthic foraminifera. *Marine Micropaleontology,* **29** (3-4): 175-184.

Bowman, S., 1990. *Interpreting the past: radiocarbon dating.* British Museum Publications, London. pp. 64.

Boyer, T., Conkright, M.E. and Levitus, S., 1999. Seasonal variability of dissolved oxygen, percent oxygen saturation, and apparent oxygen utilization in the Atlantic and Pacific Oceans. *Deep Sea Research Part I: Oceanographic Research Papers,* **46** (9): 1593-1613.

Boyle, E.A., 1995. Limits on Benthic Foraminiferal Chemical-Analyses as Precise Measures of Environmental Properties. *Journal of Foraminiferal Research,* **25** (1): 4-13.

Bradley, R., 2003. Climate forcing during the Holocene. in *Global Change in the Holocene,* A. Mackay, R. W. Battarbee, H. J. B. Birks and F. Oldfield (eds). Arnold, 10-19.

Bray, J.R. and Curtis, J.T., 1957. An ordination of the upland forest communities of Southern Wisconsin. *Ecological Monograph,* **27** 325-349.

British Geological Survey, 1977. *Geological Survey Ten Mile Map of the United Kingdom: North Sheet (Quaternary)* (Quaternary), 1st, 1:625,000.

British Geological Survey, 1979. *Geological Survey Ten Mile Map of the United Kingdom: North Sheet (Solid)* 3rd, 1:625,000.

Broecker, W., 1997. Thermohaline Circulation, the Achilles Heel of Our Climate System: Will Man-Made CO2 Upset the Current Balance? *Science,* **278** 1582-1588.

Broecker, W.S., 2000a. Abrupt climate change: causal constraints provided by the paleoclimate record. *Earth-Science Reviews,* **51** (1-4): 137-154.

Broecker, W.S., 2000b. Was a change in thermohaline circulation responsible for the Little Ice Age? *Proceedings of the National Academy of Sciences of the United States of America,* **97** (4): 1339-1342.

Broecker, W.S., 2003. Does the trigger for abrupt climate change reside in the ocean or in the atmosphere? *Science,* **300** (5625): 1519-1522.

Broecker, W.S., Bond, G., Klas, M., Bonani, G. and Wolfli, W., 1990. A salt oscillator in the glacial North Atlantic: 1. The concept. *Paleoceanography,* **5** 469–477.

Broecker, W.S., Peng, T.H., Ostlund, G. and Stuiver, M., 1985. The Distribution of Bomb Radiocarbon in the Ocean. *Journal of Geophysical Research-Oceans,* **90** (NC4): 6953-6970.

Broecker, W.S. and Walton, A., 1959. The geochemistry of ^{14}C in fresh water systems. *Geochimica et Cosmochimica Acta,* **16** 15-38.

Bronk Ramsey, C., 1995. Radiocarbon calibration and analysis of stratigraphy: The OxCal program. *Radiocarbon,* **37** (2): 425-430.

Bronk Ramsey, C., 1998. Probability and dating. *Radiocarbon,* **40** (1): 461-474.

Bronk Ramsey, C., 2001. Development of the radiocarbon calibration program. *Radiocarbon,* **43** (2A): 355-363.

Brönnimann, P. and Whittaker, J.E., 1988a. *The Trochamminacea of the Discovery Reports. A Review of the Trochamminacea (Protozoa: Foraminiferida) described by Heron-Allen & Earland (1932) and Earland (1933; 1934; 1936).* **8.** British Museum (Natural Hisory), London., pp. 152.

Brönnimann, P. and Whittaker, J.E., 1988b. The trochamminaceous test and the taxonomic criteria used in the classification of the superfamily Trochamminacea. in *Second workshop on Agglutinated Foraminifera,* **41,** F. Roegl and F. M. Gradstein (eds). Geologische Bundesanstalt, 23-39.

Brönnimann, P. and Whittaker, J.E., 1990. Revision of the Trochamminacea and Remaneicacea of the Plymouth District, S.W. England, described by Heron-Allen and Earland (1930). in *Paleoecology, biostratigraphy, paleoceanography and taxonomy of agglutinated foraminifera,* **327,** C. Hemleben, M. A. Kaminski, W. Kuhnt and D. B. Scott (eds). D. Reidel Publishing Company, 105-137.

Buzas, M.A., 1990. Another look at confidence limits for species proportions. *Journal of Paleontology,* **64** (5): 842-843.

Buzas, M.A., Culver, S.J. and Jorissen, F.J., 1993. A Statistical Evaluation of the Microhabitats of Living (Stained) Infaunal Benthic Foraminifera. *Marine Micropaleontology,* **20** (3-4): 311-320.

Cain, W.F. and Suess, H.E., 1976. Carbon-14 in tree rings. *Journal of Geophysical Research,* **81** 3688-3694.

Campbell, I.D., Campbell, C., Apps, M.J., Rutter, N.W. and Bush, A.B.G., 1998. Late Holocene ~1500 yr periodicities and their implications. *Geology,* **26** 471-473.

Campbell-Scientific, 1999. PC200W - Datalogger Support Starter Software. 2.0.

Campin, J.-M., Fichefet, T. and Duplessy, J.-C., 1999. Problems with using radiocarbon to infer ocean ventilation rates for past and present climates. *Earth and Planetary Science Letters,* **165** (1): 17-24.

Cayan, D.R., 1992. Latent and Sensible Heat-Flux Anomalies over the Northern Oceans - Driving the Sea-Surface Temperature. *Journal of Physical Oceanography,* **22** (8): 859-881.

Chambers, F.M. and Blackford, J.J., 2001. Mid- and late-Holocene climatic changes: a test of periodicity and solar forcing in proxy-climate data from blanket peat bogs. *Journal of Quaternary Science,* **16** (4): 329-338.

Chambers, F.M. and Brain, S.A., 2002. Paradigm shifts in late-Holocene climatology? *The Holocene,* **12** (2): 239-249.

Chambers, F.M., Ogle, M.I. and Blackford, J.J., 1999. Palaeoenvironmental evidence for solar forcing of Holocene climate: links to solar science. *Progress in Physical Geography,* **23** (2): 181-204.

Chandler, R.E. and Wheater, H.S., 2002. Analysis of rainfall variability using generalized linear models: A case study from the west of Ireland. *Water Resources Research,* **38** (10): art. no.-1192.

Chapman, M.R. and Shackleton, N.J., 2000. Evidence of 550-year and 1000-year cyclicities in North Atlantic circulation patterns during the Holocene. *The Holocene,* **10** (3): 287-291.

Chen, F. and Ghil, M., 1995. Interdecadal Variability of the Thermohaline Circulation and High-Latitude Surface Fluxes. *Journal of Physical Oceanography,* **25** (11): 2547-2568.

Chester, r., 1990. *Marine Geochemistry.* Unwin Hyman Ltd, London. pp. 698.

Christiansen, C., Conradsen, K., Emelyanov, E., Trimonis, E., Heinemeier, J. and Rud, N., 1993. Hydrographic Changes in the Southern Kattegat (Scandinavia) During the Early Holocene Transgression. *Boreas,* **22** (4): 349-356.

Christiansen, C., Kunzendorf, H., Laima, M.J.C., Lund-Hansen, L.C. and Pedersen, A.M., 1996. Recent changes in environmental conditions in the southwestern Kattegat, Scandinavia. in *5th MARSKAT meeting,* **430,** R. Boe and T. Thorsnes (eds). Universitetsforlaget, 137-144.

Clark, P.U., Pisias, N.G., Stocker, T.F. and Weaver, A.J., 2002. The role of the thermohaline circulation in abrupt climate change. *Nature,* **415** (6874): 863-869.

Clemens, S.C., 2005. Millennial-band climate spectrum resolved and linked to centennial-scale solar cycles. *Quaternary Science Reviews,* **24** (5-6): 521-531.

Conradsen, K., 1993. Recent Benthic Foraminifera in the Southern Kattegat, Scandinavia - Distributional Pattern and Controlling Parameters. *Boreas,* **22** (4): 367-382.

Conradsen, K., Bergsten, H., Knudsen, K.L., Nordberg, K. and Seidenkrantz, M.S., 1994. Recent benthic foraminiferal distribution in the Kattegat and the Skagerrak, Scandinavia. in *Cushman Foundation for Foraminiferal Research. Special Publication,* **32,** H. P. Sejrup and K. L. Knudsen (eds). 53-68.

Conradsen, K. and Heier-Nielsen, S., 1995. Holocene Paleoceanography and Paleoenvironments of the Skagerrak-Kattegat, Scandinavia. *Paleoceanography,* **10** (4): 801-813.

Cook, E.R., D'Arrigo, R.D. and Mann, M.E., 2002. A well-verified, multiproxy reconstruction of the winter North Atlantic Oscillation index since AD 1400. *Journal of Climate,* **15** (13): 1754-1764.

Cooper, M.C., O'Sullivan, P.E. and Shine, A.J., 2000. Climate and solar variability recorded in Holocene laminated sediments - a preliminary assessment. *Quaternary International,* **68** 363-371.

Corliss, B.H., 1985. Microhabitats of Benthic Foraminifera within Deep-Sea Sediments. *Nature,* **314** (6010): 435-438.

Corliss, B.H., McCorkle, D.C. and Higdon, D.M., 2002. A time series study of the carbon isotopic composition of deep- sea benthic foraminifera. *Paleoceanography,* **17** (3): art. no.-1036.

Corliss, B.H. and Vanweering, T.C.E., 1993. Living (Stained) Benthic Foraminifera within Surficial Sediments of the Skagerrak. *Marine Geology,* **111** (3-4): 323-335.

Cortijo, E., Labeyrie, L., Elliot, M., Balbon, E. and Tisnerat, N., 2000. Rapid climatic variability of the North Atlantic Ocean and global climate: a focus of the IMAGES program. *Quaternary Science Reviews,* **19** (1-5): 227-241.

Craig, H., 1953. The geochemistry of the stable carbon isotopes. *Geochemica et Cosmochimica Acta,* **3** 53-92.

Craig, H., 1954. Carbon 13 in plants and the relationships between carbon 13 and carbon 14 variations in nature. *The Journal of Geology,* **62** (2): 115-149.

Craig, H., 1965. Measurement of oxygen isotope paleotemperatures. in *Stable Isotopes in Oceanographic Studies and Paleotemperatures,* E. Tongiorgi (eds). Laboratory of Nuclear Geology, National Research Council, Pisa. 161-182.

Craig, R.E., 1958. *Hydrography of Scottish Coastal Waters.*

Crowley, T.J., 2000. Causes of Climate Change Over the Past 1000 Years. *Science,* **289** (5477): 270-277.

Crutzen, P., 2002. Geology of mankind. *Nature,* **415** 23.

Cullen, H., D'Arrigo, R.D., Cook, E.R. and Mann, M.E., 2001. Multiproxy reconstructions of the North Atlantic Oscillation. *Paleoceanography,* **16** (1): 27-39.

Curry, R., Dickson, B. and Yashayaev, I., 2003. A change in the freshwater balance of the Atlantic Ocean over the past four decades. *Nature,* **426** (6968): 826-829.

Curry, W.B., Marchitto, T.M., McManus, J., Oppo, D.W. and Laarkamp, K.L., 1999. Millennial-scale Changes in Ventilation of the Thermocline, Intermediate and Deep Water of the Glacial North Atlantic. in *Mechanisms of Global Change at Millennial Time Scales,* Geophysical Monograph, **112,** P. U. Clark, R. S. Webb and L. D. Keigwin (eds). American Geophysical Union,

Czaja, A., Robertson, A.W. and Huck, T., 2003. The Role of Atlantic Ocean-Atmosphere Coupling in Affecting North Atlantic Oscillation Variability. in *The North Atlantic Oscillation: Climatic Significance and Environmental Impact,* Geophysical Monograph, **134,** J. W. Hurrell, Y. Kushnir, G. Ottersen and M. Visbeck (eds). American Geophysical Union, Washington DC. 147-172.

Dahl-Jensen, D., Mosegaard, K., Gundestrup, N., Clow, G.D., Johnsen, S.J., Hansen, A.W. and Balling, N., 1998. Past temperatures directly from the Greenland Ice Sheet. *Science,* **282** (5387): 268-271.

Dansgaard, W., Johnsen, S.J., Clausen, H.B., Dahl-Jensen, D., Gundestrup, N.S., Hammer, C.U., Hvidberg, C.S., Steffensen, J.P., Sveinbjornsdottir, A.E., Jouzel, J. and Bond, G., 1993. Evidence for general instability of past climate from a 250-kyr ice-core record. *Nature,* **364** (6434): 218-220.

Davis, J.C., 2002. *Statistics and Data Analysis in Geology.* John Wiley and Sons, pp. 638.

Dawson, A., Elliott, L., Noone, S., Hickey, K., Holt, T., Wadhams, P. and Foster, I., 2004. Historical storminess and climate 'see-saws' in the North Atlantic region. *Marine Geology,* **210** (1-4): 247-259.

Dawson, A.G., Elliott, L., Mayewski, P., Lockett, P., Noone, S., Hickey, K., Holt, T., Wadhams, P. and Foster, I., 2003. Late-Holocene North Atlantic climate "seesaws", storminess changes and Greenland ice sheet (GISP2) palaeoclimates. *The Holocene,* **13** (3): 381-392.

Dawson, A.G., Hickey, K., Holt, T., Elliott, L., Dawson, S., Foster, I.D.L., Wadhams, P., Jonsdottir, I., Wilkinson, J., McKenna, J., Davis, N.R. and Smith, D.E., 2002. Complex North Atlantic Oscillation (NAO) Index signal of historic North Atlantic storm-track changes. *Holocene,* **12** (3): 363-369.

de Vernal, A., Hillaire-Marcel, C., Peltier, W.R. and Weaver, A.J., 2002. Structure of the upper water column in the northwest North Atlantic: Modern versus Last Glacial Maximum conditions. *Paleoceanography,* **17** (4): 2-10.

Dearing, J., 1998. Magnetic Susceptibility. in *Environmental Magnetism: a practical guide,* **Technical Guide 6,** J. Walden, F. Oldfield and J. Smith (eds). Quaternary Research Association, London. 35-62.

Delaney, M.L., 1998. Phosphorus accumulation in marine sediments and the oceanic phosphorus cycle. *Global Biogeochemical Cycles,* **12** (4): 563–572.

Delworth, T.L. and Mann, M.E., 2000. Observed and simulated multidecadal variability in the Northern Hemisphere. *Climate Dynamics,* **16** 661-676.

Dennison, J.M. and Hay, W.W., 1967. Estimating the needed sampling area for subaquatic ecologic studies. *Journal of Paleontology,* **41** (3): 706-708.

Denton, G.H. and Karlen, W., 1973. Holocene climatic variations; their pattern and possible cause. *Quaternary Research,* **3** (2): 155-205.

Dickson, B., Yashayaev, I., Meincke, J., Turrell, B., Dye, S. and Holfort, J., 2002. Rapid freshening of the deep North Atlantic Ocean over the past four decades. *Nature,* **416** (6883): 832-837.

Dickson, R., Lazier, J., Meincke, J., Rhines, P. and Swift, J., 1996. Long-term coordinated changes in the convective activity of the North Atlantic. *Progress in Oceanography,* **38** 241-295.

Dickson, R.R. and Curry, R.Y.I., 2003. Recent changes in the North Atlantic. in *Royal Society discussion meeting,* **361,** J. H. Lawton, J. Marotzke, R. Marsh and I. N. McCave (eds). Royal Society of London, 1917-1934.

Dickson, R.R., Meincke, J., Malmberg, S.A. and Lee, A.J., 1988. The Great Salinity Anomaly in the Northern North-Atlantic 1968- 1982. *Progress in Oceanography,* **20** (2): 103-151.

Dix, J.K. and Duck, R.W., 2000. A high-resolution seismic stratigraphy from a Scottish sea loch and its implications for Loch Lomond Stadial deglaciation. *Journal of Quaternary Science,* **15** (6): 645-656.

Drinkwater, K.F., Belgrano, A., Borja, A., Conversi, A., Edwards, M., Greene, C.H., Ottersen, G., Pershing, A.J. and Walker, H., 2003. The Response of Marine Ecosystems to Climate Variability Associated with the North Atlantic Oscillation. in *The North Atlantic Oscillation: Climatic Significance and Environmental Impact,* Geophysical Monograph, **134,** J. W. Hurrell, Y. Kushnir, G. Ottersen and M. Visbeck (eds). American Geophysical Union, Washington DC. 211-234.

Druffel, E.R.M., 1997. Pulses of rapid ventilation in the North Atlantic surface ocean during the past century. *Science,* **275** (5305): 1454-1457.

Duplessy, J.C., Lalou, C. and Vinot, A.C., 1970. Differential isotopic fractionations in benthic foraminifera and paleotemperatures reassessed. *Science,* **168** 250-251.

Edwards, A. and Sharples, F., 1986. *Scottish sea lochs: a catalogue.* Scottish Marine Biological Association/ Nature Conservancy Council, Oban/Peterborough. pp.

Edwards, R.J., van de Plassche, O., Gehrels, W.R. and Wright, A.J., 2004. Assessing sea-level data from Connecticut, USA, using a foraminiferal transfer function for tide level. *Marine Micropaleontology,* **51** 239-255.

Eiríksson, J., Knudsen, K.L., Haflidason, H. and Heinemeier, J., 2000. Chronology of late Holocene climatic events in the northern North Atlantic based on AMS C-14 dates and tephra markers from the volcano Hekla, Iceland. *Journal of Quaternary Science,* **15** (6): 573-580.

Ellet, D.J. and Edwards, A., 1983. Oceanography and inshore hydrography of the Inner Hebrides. *Proceedings of the Royal Society of Edinburgh,* **83 B** (143-160):

Ellett, D.J., 1979. Some oceanographic features of Hebridean waters. *Proceedings of the Royal Society of Edinburgh,* **77 B** 61-74.

Ellett, D.J. and Edwards, A., 1983. Oceanography and inshore hydrography of the Inner Hebrides. *Proceedings of the Royal Society of Edinburgh,* **83 B** (143-160):

Elliot, M., Labeyrie, L. and Duplessy, J.-C., 2002. Changes in North Atlantic deep-water formation associated with the Dansgaard–Oeschger temperature oscillations (60–10 ka). *Quaternary Science Reviews,* **21** (10): 1153-1165.

Elliott, A.J., Gillibrand, P.A. and Turrell, W.R., 1992. Tidal mixing near the sill of a Scottish sea loch. in *Dynamics and Exchanges in Estuaries and the Coastal Zone, Coastal and Estuarine Studies,* **40,** D. Prandle (eds). American Geophysical Union, Washington DC. 35-56.

Emiliani, C., 1955. Pleistocene temperatures. *Journal of Geology,* **63** 538-578.

Emrich, K., Ehhalt, D.H. and Vogel, J.C., 1970. Carbon isotope fractionation during the precipitation of calcium carbonate. *Earth and Planetary Science Letters,* **8** 363-371.

Epstein, S., Buchsbaum, R., Lowenstam, H.A. and Urey, H.C., 1953. Revised carbonate-water isotopic temperature scale. *Geological Society American Bulletin,* **64** 1315-1326.

Epstein, S. and Mayeda, T., 1953. Variation of O^{18} content of waters from natural sources. *Geochimica et Cosmochimica Acta,* **4** 213-224.

Erez, J., 1978. Vital effect on stable-isotope composition seen in foraminifera and coral skeletons. *Nature,* **273** 199-202.

Erez, J. and Luz, B., 1983. Experimental paleotemperature equation for planktonic foraminifera. *Geochemica et Cosmochimica Acta,* **47** 1025-1031.

The Icelandic Forest Service Eysteinsson, T., 2005. *Forestry in a treeless land.* http://www.skogur.is/Apps/WebObjects/Skogur.woa/1/wa/dp?id=1000172&wosid=zd8rD1OQbTNOJmbBYt25a0. Last updated not known, accessed on 2005.

Facorellis, Y., Maniatis, Y. and Kromer, B., 1998. Apparent ^{14}C ages of marine mollusk shells from a Greek Island: Calculation of the marine reservoir effect in the Aegean Sea. *Radiocarbon,* **40** (2): 963-973.

Farmer, D.M. and Freeland, H.J., 1983. The Physical Oceanography of Fjords. *Progress in Oceanography,* **12** (2): 147-219.

Farmer, J.G., Mackenzie, A.B., Sugden, C.L., Edgar, P.J. and Eades, L.J., 1997. A comparison of the historical lead pollution records in peat and freshwater lake sediments from central Scotland. *Water Air and Soil Pollution,* **100** (3-4): 253-270.

Feely, R.A., Sabine, C.L., Lee, K., Berelson, W., Kleypas, J., Fabry, v.J. and Millero, F.J., 2004. Impact of Anthropogenic CO_2 on the $CaCO_3$ System in the Oceans. *Science,* **305** 362-366.

Feyling-Hanssen, R.W., 1964. *Foraminifera in late Quaternary deposits from the Oslofjord area.* pp. 225,383.

Feyling-Hanssen, R.W., 1976. The stratigraphy of the Quaternary Clyde Foreland Formation, Baffin Island, illustrated by the distribution of benthic foraminifera. *Boreas,* **5** (2): 77-94.

Feyling-Hanssen, R.W., Joergensen, J.A., Knudsen, K.L. and Andersen, A.-L.L., 1971. Late Quaternary foraminifera from Vendsyssel, Denmark and Sandnes, Norway. *Bulletin of the Geological Society of Denmark = Meddelelser fra Dansk Geologisk Forening,* **21** (2-3): 67-71.

Filipsson, H.L. and Nordberg, K., 2004a. A 200-year environmental record of a low-oxygen fjord, Sweden, elucidated by benthic foraminifera, sediment characteristics and hydrographic data. *Journal of Foraminiferal Research,* **34** (4): 277-293.

Filipsson, H.L. and Nordberg, K., 2004b. Climate variations, an overlooked factor influencing the recent marine environment. An example from Gullmar Fjord, Sweden, illustrated by benthic foraminifera and hydrographic data. *Estuaries,* **27** (5): 867-881.

Filipsson, H.L., Nordberg, K. and Gustafsson, M., 2004. Seasonal study of delta O-18 and delta C-13 in living (stained) benthic foraminifera from two Swedish fjords. *Marine Micropaleontology,* **53** (1-2): 159-172.

Fisher, R.A., Corbett, A.S. and Williams, C.B., 1943. The relationship between the number of species and the number of individuals in a random sample of an animal population. *Journal of Animal Ecology,* **12** 42-58.

Frank, N., Paterne, M., Ayliffe, L., van Weering, T., Henriet, J.P. and Blamart, D., 2004. Eastern North Atlantic deep-sea corals: tracing upper intermediate water Delta C-14 during the Holocene. *Earth and Planetary Science Letters,* **219** (3-4): 297-309.

Fromentin, J.M. and Planque, B., 1996. Calanus and environment in the eastern North Atlantic .2. Influence of the North Atlantic Oscillation on C-finmarchicus and C-helgolandicus. *Marine Ecology-Progress Series,* **134** (1-3): 111-118.

Furevik, T., 2001. Annual and interannual variability of Atlantic Water temperatures in the Norwegian and Barents Seas: 1980-1996. *Deep Sea Research Part I: Oceanographic Research Papers,* **48** (2): 383-404.

Gade, H.G. and Edwards, A., 1980. Deep-water renewal in fjords. in *Fjord oceanography,* H. J. Freeland, D. M. Farmer and C. D. Levings (eds). Plenum Press, New York. 435-489.

Ganachaud, A. and Wunsch, C., 2000. Improved estimates of global ocean circulation, heat transport and mixing from hydrographic data. *Nature,* **408** (6811): 453-457.

Gehrels, W.R., 2000. Using foraminiferal transfer functions to produce high-resolution sea-level records from salt-marsh deposits,Maine, USA. *Holocene,* **10** (3): 367-376.

Gehrels, W.R., Belknap, D.F., Black, S. and Newham, R.M., 2002. Rapid sea-level rise in the Gulf of Maine, USA, since AD 1800. *Holocene,* **4** (4): 383-389.

Geyh, M.A. and Schlüchter, C., 1998. Calibration of the ^{14}C time scale beyond 22,000 BP. *Radiocarbon,* **40** (1): 475-482.

Gillett, N.P., Graf, H.F. and Osborn, T.J., 2003. Climate Change and the North Atlantic Oscillation. in *The North Atlantic Oscillation: Climatic Significance and Environmental Impact,* Geophysical Monograph, **134,** J. W. Hurrell, Y. Kushnir, G. Ottersen and M. Visbeck (eds). American Geophysical Union, Washington DC. 193-209.

Gillibrand, P.A., 1993. *Circulation and mixing in a Scottish sea loch.* Ph.D. thesis. School of Ocean Sciences, University of Wales, Bangor, Bangor. pp. 133.

Gillibrand, P.A., 2001. Calculating Exchange Times in a Scottish Fjord Using a Two-dimensional, Laterally-integrated Numerical Model. *Estuarine, Coastal and Shelf Science,* **53** (4): 437-449.

Gillibrand, P.A., Cage, A.G. and Austin, W.E.N., 2005. A preliminary investigation of basin water response to climate forcing in a Scottish fjord: evaluating the influence of the NAO. *Continental Shelf Research,* **25** (5-6): 571-587.

Gillibrand, P.A. and Turrell, W.R., 1997. The use of simple models in the regulation of the impact of fish farms on water quality in Scottish sea lochs. *Aquaculture,* **159** (1-2): 33-46.

Gillibrand, P.A., Turrell, W.R. and Elliott, A.J., 1995. Deep-Water Renewal in the Upper Basin of Loch Sunart, a Scottish Fjord. *Journal of Physical Oceanography,* **25** (6): 1488-1503.

Gillibrand, P.A., Turrell, W.R., Moore, D.C. and Adams, R.D., 1996. Bottom water stagnation and oxygen depletion in a Scottish sea loch. *Estuarine Coastal and Shelf Science,* **43** (2): 217-235.

Giraudeau, J., Jennings, A.E. and Andrews, J.T., 2004. Timing and mechanisms of surface and intermediate water circulation changes in the Nordic Seas over the last 10,000 cal years: a view from the North Iceland shelf. *Quaternary Science Reviews,* **23** 2127–2139.

Glud, R.N., Gundersen, J.K., Roy, H. and Jorgensen, B.B., 2003. Seasonal dynamics of benthic O-2 uptake in a semienclosed bay: Importance of diffusion and faunal activity. *Limnology and Oceanography,* **48** (3): 1265-1276.

Godwin, H., 1962. Half-life of radiocarbon. *Nature,* **195** 984.

Gooday, A.J., 1988. A response by benthic Foraminifera to the deposition of phytodetritus in the deep sea. *Nature,* **332** 71-73.

Gooday, A.J., 2002. Organic-walled allogromiids: Aspects of their occurrence, diversity and ecology in marine habitats. *Journal of Foraminiferal Research,* **32** (4): 384-399.

Gooday, A.J. and Hughes, J.A., 2002. Foraminifera associated with phytodetritus deposits at a bathyal site in the northern Rockall Trough (NE Atlantic): seasonal contrasts and a comparison of stained and dead assemblages. *Marine Micropaleontology,* **46** (1-2): 83-110.

Gooday, A.J. and Rathburn, A.E., 1999. Temporal variability in living deep-sea benthic foraminifera: a review. *Earth-Science Reviews,* **46** (1-4): 187-212.

Goslar, T., Arnold, M., Bard, E., Kuc, T., Pazdur, M.F., Ralska-Jasiewiczowa, M., Rózanski, K., Tisnerat, N., Walanus, A., Wicik, B. and Wieckowski, K., 1995. High concentration of atmospheric ^{14}C during the Younger Dryas cold episode. *Nature,* **377** (414-417):

Gove, H.E., 2000. Some comments on accelerator mass spectrometry. *Radiocarbon,* **42** (1): 127-135.

Graham, D.W., Corliss, B.H., Bender, M.L. and Keigwin, L.D., 1981. Carbon and Oxygen Isotopic Disequilibria of Recent Deep-Sea Benthic Foraminifera. *Marine Micropaleontology,* **6** (5-6): 483-497.

Greene, C.H. and Pershing, A.J., 2003. The flip-side of the North Atlantic Oscillation and modal shifts in slope-water circulation patterns. *Limnology and Oceanography,* **48** (1): 319-322.

Grossman, E.L., 1984a. Carbon Isotopic Fractionation in Live Benthic Foraminifera - Comparison with Inorganic Precipitate Studies. *Geochimica Et Cosmochimica Acta,* **48** (7): 1505-1512.

Grossman, E.L., 1984b. Stable Isotope Fractionation in Live Benthic Foraminifera from the Southern-California Borderland. *Palaeogeography Palaeoclimatology Palaeoecology,* **47** (3-4): 301-327.

Grossman, E.L., 1987. Stable Isotopes on Modern Benthic Foraminifera: A Study of Vital Effect. *Journal of Foraminiferal Research,* **17** (1): 48-61.

Grove, J.M., 2001. The Initiation of the "Little Ice Age" in Regions Round the North Atlantic. *Climatic Change,* **48** (1): 53-82.

Gruber, N. and Keeling, C.D., 2001. An improved estimate of the isotopic air-sea disequilibrium of CO2: Implications for the oceanic uptake of anthropogenic CO2. *Geophysical Research Letters,* **28** (3): 555-558.

Gruber, N., Keeling, C.D., Bacastow, R.B., Guenther, P.R., Lueker, T.J., Wahlen, M., Meijer, H.A.J., Mook, W.G. and Stocker, T.F., 1999. Spatiotemporal patterns of carbon-13 in the global surface oceans and the oceanic Suess effect. *Global Biogeochemical Cycles,* **13** 307-335.

Gustafsson, M. and Nordberg, K., 2000. Living (Stained) benthic foraminifera and their response to the seasonal hydrographic cycle, periodic hypoxia and to primary production in Havstens Fjord on the Swedish west coast. *Estuarine Coastal and Shelf Science,* **51** (6): 743-761.

Gustafsson, M. and Nordberg, K., 2001. Living (stained) benthic foraminiferal response to primary production and hydrography in the deepest part of the Gullmar Fjord, Swedish West Coast, with comparisons to Hoglund's 1927 material. *Journal of Foraminiferal Research,* **31** (1): 2-11.

Gustafsson, M. and Nordberg, K., 2002. The impact of climate and shore-level displacement on the late-Holocene environmental development of Havstens Fjord and Koljö Fjord, Swedish west coast. *The Holocene,* **12** (3): 325-338.

Hald, M., Husum, K., Vorren, T.O., Grosfjeld, K., Jensen, H.B. and Sharapova, A., 2003. Holocene climate in the subarctic fjord Malangen, northern Norway: a multi-proxy study. *Boreas,* **32** (4): 543-559.

Hall, I.R., Bianchi, G.G. and Evans, J.R.J.R., 2004. Centennial to millennial scale Holocene climate-deep water linkage in the North Atlantic. *Quaternary Science Reviews,* **23** (14-15): 1529-1536.

Hammer, Ø., Harper, D.A.T. and Ryan, P.D., 2001. *PAST: Paleontological Statistics Software Package for Education and Data Analysis.* http://palaeo-electronica.org/2001_1/past/issue1_01.htm. Last updated accessed on 4.

Hannah, F. and Rogerson, A., 1997. The temporal and spatial distribution of foraminiferans in marine benthic sediments of the Clyde Sea area, Scotland. *Estuarine Coastal and Shelf Science,* **44** (3): 377-383.

Hansen, B., Osterhus, S., Hatun, H., Kristiansen, R. and Larsen, K.M.H., 2003. The Iceland-Faroe inflow of Atlantic water to the Nordic Seas. *Progress in Oceanography,* **59** (4): 443-474.

Hansen, B., Turrell, W.R. and Osterhus, S., 2001. Decreasing overflow from the Nordic seas into the Atlantic Ocean through the Faroe Bank channel since 1950. *Nature,* **411** (6840): 927-930.

Hansen, J., Nazarenko, L., Ruedy, R., Sato, m., Willis, J., Del Genio, A., Koch , D., Lacis, A., Lo, K., Menon, S., Novakov, T., Perlwitz , J., Russell, G., Schmidt, G.A. and Tausnev, N., 2004. Earth's Energy Imbalance: Confirmation and Implications. *Science,* **1110252**

Hanson, A.K., Jr. and Donaghay, P.L., 1998. Micro- to Fine-scale Chemical Gradients and Layers in Stratified Coastal Waters. *Oceanography,* **11** (1): 10-17.

Harkness, D.D., 1983. The extent of natural ^{14}C deficiency in the coastal environment of the United Kingdom. in *First international symposium; ^{14}C and archaeology,* **8,** W. G. Mook and H. T. Waterbolk (eds). Conseil de l'Europe, 351-364.

Haug, G.H., Guenther, D., Peterson, L.C., Sigman, D.M., Hughen, K. and Aeschlimann, B., 2003. Climate and the collapse of Maya civilization. *Science,* **299** (5613): 1731-1735.

Haynes, J.R., 1973. *Cardigan Bay Recent foraminifera (Cruises of the R. V. Antur, 1962-1964).* British Museum (Natural History), London. pp. 245.

Haynes, J.R., 1981. *Foraminifera.* MacMillan Publishers Ltd., London and Basingstoke. pp. 433.

Hayward, B.W., Holzmann, M., Grenfell, H.R., Pawlowski, J. and Triggs, C.M., 2004. Morphological distinction of molecular types in Ammonia - towards a taxonomic revision of the world's most commonly misidentified foraminifera. *Marine Micropaleontology,* **50** (3-4): 237-271.

Hedges, R.E.M., 1983. ^{14}C dating by the accelerator technique. in *First international symposium; ^{14}C and archaeology,* **8,** W. G. Mook and H. T. Waterbolk (eds). Conseil de l'Europe, 165-175.

Heier-Nielsen, S., Heinemeier, J., Nielsen, H.L. and Rud, N., 1995. Recent Reservoir Ages for Danish Fjords and Marine Waters. *Radiocarbon,* **37** (3): 875-882.

Heinz, P., Kitazato, H., Schmiedl, G. and Hemleben, C., 2001. Response of deep-sea benthic foraminifera from the Mediterranean Sea to simulated phytoplankton pulses under laboratory conditions. *Journal of Foraminiferal Research,* **31** (3): 210-227.

Heiri, O., Lotter, A.F. and Lemcke, G., 2001. Loss on ignition as a method for estimating organic and carbonate content in sediments; reproducibility and comparability of results. *Journal of Paleolimnology,* **25** (1): 101-110.

Hellings, L., Dehairs, F., Tackx, M., Keppens, E. and Baeyens, W., 1999. Origin and fate of organic carbon in the freshwater part of the Scheldt Estuary as traced by stable carbon isotope composition. *Biogeochemistry,* **47** (2): 167-186.

Heron-Allen, E. and Earland, A., 1916. The foraminifera of the West of Scotland. *Transactions of the Linnean Society of London, Series 2 (Zoology),* **11** 197-300.

Hill, A.E., Horsburgh, K.J., Garvine, R.W., Gillibrand, P.A., Slesser, G., Turrell, W.R. and Adams, R.D., 1997. Observations of a density-driven recirculation of the Scottish coastal current in the Minch. *Estuarine Coastal and Shelf Science,* **45** (4): 473-484.

Höglund, H., 1947. Foraminifera in the Gullmar fjord and the Skagerrak. *Zoologiska bidrag från Uppsala,* **26** 328.

Hohenegger, J., 2005. Estimation of environmental paleogradient values based on presence/absence data: a case study using benthic foraminifera for paleodepth estimation. *Palaeogeography Palaeoclimatology Palaeoecology,* **217** (1-2): 115-130.

Holliday, N.P., 2003. Air-sea interaction and circulation changes in the northeast Atlantic. *Journal of Geophysical Research,* **108** (C8): 3259, doi:10.1029/2002JC001344.

HOLSMEER, 2004. *Executive summart and detailed report: Late HOLocene Shallow Marine Environments of Europe.* http://www.bangor.ac.uk/os/holsmeer/FWV%20section%205-6.pdf

Holsten, J., Stott, L. and Berelson, W., 2004. Reconstructing benthic carbon oxidation rates using [delta]13C of benthic foraminifers. *Marine Micropaleontology,* **53** (1-2): 117-132.

Hormes, A., Muller, B.U. and Schluchter, C., 2001. The Alps with little ice: evidence for eight Holocene phases of reduced glacier extent in the Central Swiss Alps. *Holocene,* **11** (3): 255-265.

Horton, B. and Edwards, R.J., 2005. The application of local and regional transfer functions to the reconstruction of Holocene sea levels, north Norfolk, England. *The Holocene,* **15** (2): 216-228.

Howe, J.A., Shimmield, T., Austin, W.E.N. and Longva, O., 2002. Post-glacial depositional environments in a mid-high latitude glacially-overdeepened sea loch, inner Loch Etive, western Scotland. *Marine Geology,* **185** (3-4): 417-433.

Hughen, K., Lehman, S., Southon, J., Overpeck, J., Marchal, O., Herring, C. and Turnbull, J., 2004a. C-14 activity and global carbon cycle changes over the past 50,000 years. *Science,* **303** (5655): 202-207.

Hughen, K.A., Baillie, M.G.L., Bard, E., Beck, J.W., Bertrand, C.J., Blackwell, P.G., Buck, C.E., Burr, G.S., Cutler, K.B., Damon, P.E., Edwards, R.L., Fairbanks, R.G., Friedrich, M., Guilderson, T.P., Kromer, B., McCormac, F.G., Manning, S., Bronk Ramsey, C., Reimer, P.J., Reimer, R.W., Remmele, S., Southon, J., Stuiver, M., Talamo, S., Taylor, F.W., van der Plicht, J. and Weyhenmeyer, C.E., 2004b. Marine04 Marine Radiocarbon Age Calibration, 0–26 Cal Kyr BP. *Radiocarbon,* **46** (3): 1059-1086.

Hughes, J.A., Gooday, A.J. and Murray, J.W., 2000. Distribution of live benthic Foraminifera at three oceanographically dissimilar sites in the northeast Atlantic: preliminary results. *Hydrobiologia,* **440** (1-3): 227-238.

Hunt, B.G., 1998. Natural climatic variability as an explanation for historical climatic fluctuations. *Climatic Change,* **38** 133-157.

Hurrell, J.W., 1995. Decadal Trends in the North-Atlantic Oscillation - Regional Temperatures and Precipitation. *Science,* **269** (5224): 676-679.

Hurrell, J.W., 1996. Influence of variations in extratropical wintertime teleconnections on Northern Hemisphere temperature. *Geophysical Research Letters,* **23** (6): 665-668.

Hurrell, J.W., Kushnir, Y., Visbeck, M. and Ottersen, G., 2003. An Overview of the North Atlantic Oscillation. in *The North Atlantic Oscillation: Climate Significance and Environmental Impact,* **134,** J. W. Hurrell, Y. Kushnir, G. Ottersen and M. H. Visbeck (eds). Geophysical Monograph Series, 1-35.

Husum, K. and Hald, M., 2004a. A continuous marine record 8000-1600 cal. yr BP from the Malangenfjord, north Norway: foraminiferal and isotopic evidence. *The Holocene,* **14** (6): 877-887.

Husum, K. and Hald, M., 2004b. Modern foraminiferal distribution in the subarctic Malangenfjord and adjoining shelf, northern Norway. *Journal of Foraminiferal Research,* **34** 34-48.

Hut, G., 1987. *Consultants group meeting in stable isotope reference samples for geochemical and hydrological investigations.*

Imbrie, J. and Kipp, N.G., 1971. A new micropaleontologic method for quantitative application to a late Pleistocene Carribian core. in *Late Cenozoic Glacial Ages,* K. K. Turekian (eds). Yale University Press, New Haven. 71-191.

Inall, M. and Griffiths, C., 2003. The Tiree Passage Time Series: 1981 – 2003. *DEFRA,* **MECN: Tiree Passage**

Israelson, C. and Buchardt, B., 1991. The isotopic composition of oxygen and carbon in some fossil and recent bivalve shells from East Greenland. *LUNDQUA Rep,* **33** 117-123.

Jennings, A.E., Hagen, S., Harðardóttir, J., Stein, R., Ogilvie, A.E.J. and Jónsdóttir, I., 2001. Oceanographic Change and Terrestrial Human Impacts in a Post A.D. 1400 Sediment Record from the Southwest Iceland Shelf. *Climatic Change,* **48** (1): 83 - 100.

Jiang, H. and Eiriksson, J.S.M.K.K.-L.S.M.-S., 2005. Evidence for solar forcing of sea-surface temperature on the North Icelandic Shelf during the late Holocene. *Geology,* **33** (1): 73-76.

Jiang, H., Seidenkrantz, M.-S., Knudsen, K.L. and Eiriksson, J., 2002. Late-Holocene summer sea-surface temperatures based on a diatom record from the North Icelandic Shelf. *The Holocene,* **12** (2): 137-147.

Johnsen, S.J., Clausen, H.B., Dansgaard, W., Fuhrer, K., Gundestrup, N., Hammer, C.U., Iversen, P., Jouzel, J., Stauffer, B. and Steffensen, J.P., 1992. Irregular glacial interstadials recorded in a new Greeland ice core. *Nature,* **359** (6393): 311-313.

Johnsen, S.J., Dahl-Jensen, D., Gundestrup, N., Steffensen, J.P., Clausen, H.B., Miller, H., Masson-Delmotte, V., Sveinbjörnsdottir, A.E. and White, J., 2001. Oxygen isotope and palaeotemperature records from six Greenland ice-core stations: Camp Century, Dye-3, GRIP, GISP2, Renland and NorthGRIP. *Journal of Quaternary Science,* **16** (4): 299-307.

Jones, P.D., Jonsson, T. and Wheeler, D., 1997. Extension to the North Atlantic Oscillation using early instrumental pressure observations from Gibraltar and south- west Iceland. *International Journal of Climatology,* **17** (13): 1433-1450.

Jones, P.D. and Lister, D., 2004. The development of monthly temperature series for Scotland and Northern Ireland. *International Journal of Climatology,* **24** (5): 569-590.

Joos, F., Plattner, G.-K., Stocker, T.F., Marchal, O. and Schmittner, A., 1999. Global Warming and Marine Carbon Cycle Feedbacks on Future Atmospheric CO_2. *Science,* **284** 464-467.

Jorissen, F.J., 1999. Benthic foraminiferal microhabitats below the sediment-water interface. in *Modern Foraminifera.,* B. K. Sen Gupta (eds). Kluwer, 161-179.

Jorissen, F.J., de Stigter, H.C. and Widmark, J.G.V., 1995. A conceptual model explaining benthic foraminiferal microhabitats. *Marine Micropaleontology,* **26** (1-4): 3-15.

Juggins, S., 2003a. C^2 - Software for ecological and palaeoecological data analysis and visualisation. 1.4.

University of Newcastle Juggins, S., 2003b. *C^2 - Software for ecological and palaeoecological data analysis and visualisation. User guide version 1.3.* http://www.campus.ncl.ac.uk/staff/Stephen.Juggins/software/code/C2.pdf. Last updated 25/11/2003, accessed on 2003.

Keigwin, L.D. and Boyle, E.A., 2000. Detecting Holocene changes in thermohaline circulation. *Proceedings of the National Academy of Sciences of the United States of America,* **97** (4): 1343-1346.

Keir, R., Rehder, G., Suess, E. and Erlenkeuser, H., 1998. The delta C-13 anomaly in the northeastern Atlantic. *Global Biogeochemical Cycles,* **12** (3): 467-477.

Keith, M.L. and Anderson, G.M., 1963. Radiocarbon Dating: Fictitious Results with Mollusk Shells. *Science,* **141** (3581): 634-637.

Keith, M.L., Anderson, G.M. and Eichler, R., 1964. Carbon and oxygen isotopic composition of mollusks shells from marine and fresh-water environments. *Geochimica et Cosmochimica Acta,* **28** 1757-1786.

Kelly, M., Funder, S., Houmark-Nielsen, M., Knudsen, K.L., Kronborg, C., Landvik, J. and Sorby, L., 1999. Quaternary glacial and marine environmental history of northwest Greenland: a review and reappraisal. *Quaternary Science Reviews,* **18** (3): 373-392.

Kerr, R., 2000. A North Atlantic Climate Pacemaker for the Centuries. *Science,* **288** (5473): 1984-1985.

Kershaw, P.J., Heldal, H.E., Mork, K.A. and Rudjord, A.L., 2004. Variability in the supply, distribution and transport of the transient tracer ^{99}Tc in the NE Atlantic. *Journal of Marine Systems,* **44** (1-2): 55-81.

Kim, S.-T. and O'Neil, J.R., 1997. Equilibrium and nonequilibrium oxygen isotope effects in synthetic carbonates. *Geochimica et Cosmochimica Acta,* **61** (16): 3461-3475.

King, P., Kennedy, H., Newton, P.P., Jickells, T.D., Brand, T., Calvert, S., Cauwet, G., Etcheber, H., Head, B. and Khripounoff, A., 1998. Analysis of total and organic carbon and total nitrogen in settling oceanic particles and a marine sediment: an interlaboratory comparison. *Marine Chemistry,* **60** (3-4): 203-216.

Klinck, J.M., O'Brien, J.J. and Svendsen, H., 1981. A Simple Model of Fjord and Coastal Circulation Interaction. *Journal of Physical Oceanography,* **11** 1612-1626.

Klitgaard-Kristensen, D. and Buhl-Mortensen, L., 1999. Benthic foraminifera along an offshore-fjord gradient: a comparison with amphipods and molluscs. *Journal of Natural History,* **33** (3): 317-350.

Klitgaard-Kristensen, D., Sejrup, H.P. and Haflidason, H., 2002. Distribution of recent calcareous benthic foraminifera in the northern North Sea and relation to the environment. *Polar Research,* **21** (2): 275-282.

Körtzinger, A., Quay, P.D. and Sonnerup, R.E., 2003. Relationship between anthropogenic CO2 and the 13C Suess effect in the North Atlantic Ocean. *Global Biogeochemical Cycles,* **17** (1): doi:10.1029/2001GB001427.

Kovach, W.L., 1995. Multivariate Data Analysis. in *Statistical Modelling of Quaternary Science Data,* D. Maddy and J. S. Brew (eds). Quaternary Research Association, Cambridge. 1-38.

Kristensen, D.K., Sejrup, H.P., Haflidason, H., Berstad, I.M. and Mikalsen, G., 2004. Eight-hundred-year temperature variability from the Norwegian continental margin and the North Atlantic thermohaline circulation. *Paleoceanography,* **19** (2): art. no.-PA2007.

Kristensen, P., Heiernielsen, S. and Hylleberg, J., 1995. Late-Holocene Salinity Fluctuations in Bjornsholm Bay, Limfjorden, Denmark, as Deduced from Microfossil and Macrofossil Analysis. *Holocene,* **5** (3): 313-322.

Kroon, D., Shimmield, G., Austin, W.E.N., Derrick, S., Knutz, P. and Shimmield, T., 2000. Century- to millennial-scale sedimentological–geochemical records of glacial–Holocene sediment variations from the Barra Fan (NE Atlantic). *Journal of the Geological Society,* **157** (3): 643-653.

Kroopnick, P.M., 1985. The Distribution of C-13 of Sigma-Co2 in the World Oceans. *Deep-Sea Research Part a-Oceanographic Research Papers,* **32** (1): 57-84.

Kryc, K.A. and Murray, R.W.M.D.W., 2003. Al-to-oxide and Ti-to-organic linkages in biogenic sediment; relationships to paleo-export production and bulk Al/Ti. *Earth and Planetary Science Letters,* **211** (1-2): 125-141.

Kucera, M., Weinelt, M., Kiefer, T., Pflaumann, U., Hayes, A., Weinelt, M., Chen, M.T., Mix, A.C., Barrows, T.T., Cortijo, E., Duprat, J., Juggins, S. and Waelbroeck, C., 2005. Reconstruction of sea-surface temperatures from assemblages of planktonic foraminifera: multi-technique approach based on geographically constrained calibration data sets and its application to glacial Atlantic and Pacific Oceans. *Quaternary Science Reviews,* **24** (7-9): 951-998.

Kuzmina, S.I., Bengtsson, L., Johannessen, O.M., Drange, H., Bobylev, L.P. and Miles, M.W., 2005. The North Atlantic Oscillation and greenhouse-gas forcing. *Geophysical Research Letters,* **32** (L04703): doi: 10.1029/2004GL021064.

Labitzke, K. and Matthes, K., 2003. Eleven-year solar cycle variations in the atmosphere; observations, mechanisms and models. *The Holocene,* **13** (3): 311-317.

Laj, C., Mazaud, A. and Duplessy, J.C., 1996. Geomagnetic intensity and ^{14}C abundance in the atmosphere and ocean during the past 50kyr. *Geophysical Research Letters,* **23** (16): 2045-2048.

Larsen, E., Sejrup, H.P., Johnsen, S.J. and Knudsen, K.L., 1995. Do Greenland Ice Cores Reflect Nw European Interglacial Climate Variations. *Quaternary Research,* **43** (2): 125-132.

Lee, J.J. and Anderson, O.R., 1991. *Biology of Foraminifera.* Academic Press Limited, London. pp.

Lee, J.J., Faber, W.W., Anderson, O.R. and Pawlowski, J., 1991. Life cycles of foraminifera. in *Biology of Foraminifera,* J. J. Lee and O. R. Anderson (eds). Academic Press Limited, London. 285-335.

Lees, J., 1998. Evaluating magnetic parameters for use in source identifcation and modelling of natural and environmental materials. in *Environmental Magnetism: a practical guide,* **Technical Guide 6,** J. Walden, F. Oldfield and J. Smith (eds). Quaternary Research Association, London. 113-138.

Lepš, J. and Šmilauer, P., 2003. *Multivariate Analysis of Ecological data using CANOCO.* Cambridge University Press, Cambridge. pp. 269.

Levin, I. and Hesshaimer, V., 2000. Radiocarbon - A unique tracer of global carbon cycle dynamics. *Radiocarbon,* **42** (1): 69-80.

Libby, W.F., 1955. *Radiocarbon dating.* University of Chicago Press, pp.

Libby, W.F., Anderson, E.C. and Arnold, A.J., 1949. Age determination by radiocarbon content: world-wide assay of natural radiocarbon. *Science,* **109** 227-228.

Linick, T.W., Damon, P.E., Donahue, D.J. and Jull, A.J.T., 1989. Accelerator mass spectrometry: the new revolution in radiocarbon dating. *Quaternary International,* **1** 1-6.

Lloyd, R.M., 1964. Variations in the oxygen and carbon isotope ratios of Florida Bay mollusks and their environmental significance. *Journal of Geology,* **72** 84-111.

Loeblich, A.R. and Tappan, H., 1987. *Foraminiferal genera and their classification.* Von Nostrand Reinhold Co, New York. pp.

Loubere, P., Fariduddin, M. and Murray, R.W., 2003. Patterns of export production in the eastern equatorial Pacific over the past 130,000 years. *Paleoceanography,* **18** (2): art. no. 1028.

Lowe, J.J. and Walker, M.C., 1997. *Reconstructing Quaternary Environments.* Longman Limited, pp. 446.

Lozano, I., Devoy, R.J.N., May, W. and Andersen, U., 2004. Storminess and vulnerability along the Atlantic coastlines of Europe: analysis of storm records and of a greenhouse gases induced climate scenario. *Marine Geology,* **210** (1-4): 205-225.

Lubinski, D.J., Polyak, L. and Forman, S.L., 2001. Freshwater and Atlantic water inflows to the deep northern Barents and Kara seas since ca 13 14C ka: : foraminifera and stable isotopes. *Quaternary Science Reviews,* **20** (18): 1851-1879.

Luterbacher, J., Rickli, R., Xoplaki, E., Tinguely, C., Beck, C., Pfister, C. and Wanner, H., 2001. The Late Maunder Minimum (1675–1715) – A Key Period for Studying Decadal Scale Climatic Change in Europe. *Climatic Change,* **49** (4): 441-462.

Lynch-Stieglitz, J., Curry, W.B. and Slowey, N., 1999. A geostrophic transport estimate for the Florida Current from the oxygen isotope composition of benthic foraminifera. *Paleoceanography,* **14** (3): 360-373.

Lysa, A., Sejrup, H.P. and Aarseth, I., 2004. The late glacial-Holocene seismic stratigraphy and sedimentary environment in Ranafjorden, northern Norway. *Marine Geology,* **211** (1-2): 45-78.

Macdonald, A.M. and Wunsch, C., 1996. An estimate of global ocean circulation and heat fluxes. *Nature,* **382** (6590): 436-439.

Mackensen, A. and Bickert, T., 1999. Stable Carbon Isotopes in Benthic Foraminifera: Proxies for Deep and Bottom Water Circulation and New Production. in *Use of Proxies in Palaeoceanography: Examples from the South Atlantic,* G. Fischer and G. Wefer (eds). Springer-Verlag, Berlin Heidelberg. 229-254.

Mackensen, A., Hubberten, H.W., Bickert, T., Fischer, G. and Futterer, D.K., 1993. The Delta-C-13 in Benthic Foraminiferal Tests of Fontbotia- Wuellerstorfi (Schwager) Relative to the Delta-C-13 of Dissolved Inorganic Carbon in Southern-Ocean Deep-Water - Implications for Glacial Ocean Circulation Models. *Paleoceanography,* **8** (5): 587-610.

Mackensen, A., Schumacher, S., Radke, J. and Schmidt, D.N., 2000. Microhabitat preferences and stable carbon isotopes of endobenthic foraminifera: clue to quantitative reconstruction of oceanic new production? *Marine Micropaleontology,* **40** (3): 233-258.

MacKenzie, A.B., Farmer, J.G. and Sugden, C.L., 1997. Isotopic evidence of the relative retention and mobility of lead and radiocaesium in Scottish ombrotrophic peats. *Science of the Total Environment,* **203** (2): 115-127.

Macklin, M.G., Bonsall, C., Davies, F.M. and Robinson, M.R., 2000. Human-environment interactions during the Holocene: new data and interpretations from the Oban area, Argyll, Scotland. *Holocene,* **10** (1): 109-121.

Malmgreen, B.A., Kucera, M., Nyberg, J. and Waelbroeck, C., 2001. Comparison of statistical and arti¢cial neural network techniques for estimating past sea surface temperatures from planktonic foraminifer census data. *Paleoceanography,* **16** 520-530.

Mangerud, J., 1972. Radiocarbon dating of marine shells, including a discussion of apparent age of Recent shells from Norway. *Boreas,* **1** 149-172.

Mangerud, J. and Gulliksen, S., 1975. Apparent radiocarbon ages of Recent marine shells from Norway, Spitsbergen, and Arctic Canada. *Quaternary Research,* **5** (2): 263-273.

Manighetti, B. and McCave, I.N., 1995. Late-Glacial and Holocene Paleocurrents around Rockall Bank, Ne Atlantic-Ocean. *Paleoceanography,* **10** (3): 611-626.

Manley, G., 1974. Central England temperatures: monthly means 1659 to 1973. *Quarterly Journal of the Royal Meteorological Society,* **100** 389-405.

Mann, K.H. and Lazier, J.R.N., 1991. *Dynamics of Marine Ecosystems: Biological-Physical Interactions in the Oceans.* Blackwell Scientific Publications, pp. 466.

Mann, M.E., 2001. Climate during the past millennium. *Weather,* **56** 91-102.

Mann, M.E., Bradley, R.S. and Hughes, M.K., 1998. Global-scale temperature patterns and climate forcing over the past six centuries. *Nature,* **392** (6678): 779-787.

Mann, M.E. and Jones, P.D., 2003. Global surface temperatures over the past two millennia. *Geophysical Research Letters,* **30** (15): 1820, doi:10.1029/2003GL017814.

Mann, M.E. and Park, J., 1994. Global-scale mode of surface temperature variability on interannual to century timescales. *Journal of Geophysical Research,* **99** (D12): 25,819-25,833.

Marchetto, A., 1994. Rescaling species optima estimated by weighted averaging. *Journal of Paleolimnology,* **12** 155-162.

Marchitto, T.M., Curry, W.B. and Oppo, D.W., 1998. Millennial-scale changes in North Atlantic circulation since the last glaciation. *Nature,* **393** (6685): 557-561.

Marchitto, T.M. and deMenocal, P.B., 2003. Late Holocene variability of upper North Atlantic Deep Water temperature and salinity. *Geochemistry Geophysics Geosystems,* **4** art. no.-1100.

Marotzke, J., 2000. Abrupt climate change and thermohaline circulation: Mechanisms and predictability. *Proceedings of the National Academy of Sciences of the United States of America,* **97** (4): 1347-1350.

Marshall, J., Kushner, Y., Battisti, D., Chang, P., Czaja, A., Dickson, R., Hurrell, J., McCartney, M., Saravanan, R. and Visbeck, M., 2001. North Atlantic climate variability: Phenomena, impacts and mechanisms. *International Journal of Climatology,* **21** (15): 1863-1898.

Martin, W.R., McNichol, A.P. and McCorkle, D.C., 2000. The radiocarbon age of calcite dissolving at the sea floor: estimates from pore water data. *Geochimica et Cosmochimica Acta,* **64** (8): 1391-1404.

Maslin, M., Pike, J., Stickley, C. and Ettwein, V., 2003. Evidence of Holocene variability in marine sediments. in *Global Change in the Holocene,* A. Mackay, R. W. Battarbee, H. J. B. Birks and F. Oldfield (eds). Arnold, 185-209.

Mayewski, P.A., Meeker, L.D., Twickler, M.S., Whitlow, S., Yang, Q.Z., Lyons, W.B. and Prentice, M., 1997. Major features and forcing of high-latitude northern hemisphere atmospheric circulation using a 110,000-year-long glaciochemical series. *Journal of Geophysical Research-Oceans,* **102** (C12): 26345-26366.

Mayewski, P.A., Rohling, E.E., Stager, J.C., Karlen, W., Maasch, K.A., Meeker, L.D., Meyerson, E.A., Gasse, F., Van Kreveld, S., Holmgren, K., Lee-Thorp, J., Rosqvist, G., Rack, F., Staubwasser, M., Schneider, R.R. and Steig, E.J., 2004. Holocene Climate Variability. *Quaternary Research,* **62** (3): 243-255.

McCartney, M., 1997. Climate change: Is the ocean at the helm? *Nature,* **388** 521 - 522.

McCave, I.N., Manighetti, B. and Robinson, S.G., 1995. Sortable Silt and Fine Sediment Size Composition Slicing - Parameters for Paleocurrent Speed and Paleoceanography. *Paleoceanography,* **10** (3): 593-610.

McConnaughey, T., 1989a. C-13 and O-18 Isotopic Disequilibrium in Biological Carbonates .1. Patterns. *Geochimica Et Cosmochimica Acta,* **53** (1): 151-162.

McConnaughey, T., 1989b. C-13 and O-18 Isotopic Disequilibrium in Biological Carbonates .2. Invitro Simulation of Kinetic Isotope Effects. *Geochimica Et Cosmochimica Acta,* **53** (1): 163-171.

McConnaughey, T.A., Burdett, J., Whelan, J.F. and Paull, C.K., 1997. Carbon isotopes in biological carbonates: Respiration and photosynthesis. *Geochimica et Cosmochimica Acta,* **61** (3): 611-622.

McCorkle, D.C., Corliss, B.H. and Farnham, C.A., 1997. Vertical distributions and stable isotopic compositions of live (stained) benthic foraminifera from the North Carolina and California continental margins. *Deep Sea Research Part I: Oceanographic Research Papers,* **44** (6): 983-1024.

McCorkle, D.C. and Emerson, S.R., 1988. The Relationship between Pore Water Carbon Isotopic Composition and Bottom Water Oxygen Concentration. *Geochimica Et Cosmochimica Acta,* **52** (5): 1169-1178.

McCorkle, D.C., Emerson, S.R. and Quay, P.D., 1985. Stable Carbon Isotopes in Marine Porewaters. *Earth and Planetary Science Letters,* **74** (1): 13-26.

McCorkle, D.C., Keigwin, L.D., Corliss, B.H. and Emerson, S.R., 1990. The influence of microhabitats on the carbon isotopic composition of deep-sea benthic foraminifera. *Paleoceanography,* **5** 161-185.

McCrea, J.M., 1950. On the isotopic chemistry of carbonates and a paleotemperature scale. *Journal of Chemical Physics,* **18** 849-857.

McDermott, F., Mattey, D.P. and Hawkesworth, C., 2001. Centennial-Scale Holocene Climate Variability Revealed by a High-Resolution Speleothem ^{18}O Record from SW Ireland. *Science,* **294** (5545): 1328-1331.

McKay, W.A., Baxter, M.S., Ellet, D.J. and Meldrum, D.T., 1986. Radiocaesium and Circulation Patterns West of Scotland. *Journal of Environmental Radioactivity,* **4** 205-232.

Meeker, L.D. and Mayewski, P.A., 2002. A 1400-year high-resolution record of atmospheric circulation over the North Atlantic and Asia. *Holocene,* **12** (3): 257-266.

Met Office *http://www.met-office.gov.uk/education/training/ukclimate.html*. http://www.met-office.gov.uk/education/training/ukclimate.html. Last updated accessed on 16/04/2003.

Middleburg, J.J. and Nieuwenhuize, J., 1998. Carbon and nitrogen stable isotopes in suspended matter and sediments from the Schlede Estuary. *Marine Chemistry,* **60** 217-225.

Mikalsen, G., Flatebo, T. and Sejrup, H.P., 1999. *Distributions and ecology of benthic foraminiferal faunas in fjord basins of western Norway*. Papers thesis. Department of Geology, University of Bergen, Bergen. pp. 1-15.

Mikalsen, G. and Sejrup, H.P., 1999. *A high-resolution 2500 year temperature record from Sognesjoen, western Norway; possible correlations to atmosperhic delta ^{14}C cycles*. Papers thesis. Department of Geology, University of Bergen, Bergen. pp. 7.

Mikalsen, G. and Sejrup, H.P., 2000. Oxygen isotope composition of fjord and river water in the Sognefjorden drainage area, western Norway. Implications for paleoclimate studies. *Estuarine Coastal and Shelf Science,* **50** (4): 441-448.

Mikalsen, G., Sejrup, H.P. and Aarseth, I., 2001. Late-Holocene changes in ocean circulation and climate: foraminiferal and isotopic evidence from Sulafjord, western Norway. *Holocene,* **11** (4): 437-446.

Mix, A.C., Morey, A.E., Pisias, N.G. and Hostetler, S.W., 1999. Foraminiferal faunal estimates of paleotemperature: Circumventing the no-analog problem yields cool ice age tropics. *Paleoceanography,* **14** (3): 350-359.

Moberg, A., Sonechkin, D.M., Holmgren, K., Datsenko, N.M. and Karlen, W., 2005. Highly variable Northern Hemisphere temperatures reconstructed from low- and high-resolution proxy data. *Nature,* **433** (7026): 613-617.

Mook, W.G., 1971. Palaeotemperatures and chlorinities from stable carbon and oxygen isotopes in shell carbonate. *Palaeogeography Palaeoclimatology Palaeoecology,* **9** 245-263.

Mook, W.G. and Streurman, H.J., 1983. Physical and chemical aspects of radiocarbon dating. in *First international symposium; ^{14}C and archaeology,* **8,** W. G. Mook and H. T. Waterbolk (eds). Conseil de l'Europe, 31-55.

Mook, W.G. and Vogel, J.C., 1968. Isotopic equilibrium between shells and their environment. *Science,* **159** 874-875.

Morford, J.L. and Emerson, S., 1999. The geochemistry of redox sensitive trace metals in sediments. *Geochimica et Cosmochimica Acta,* **63** (11-12): 1735-1750.

Murray, J.W., 1971. *An Atlas of British Recent Foraminiferids.* pp. 244.

Murray, J.W., 1973. *Distribution and ecology of benthic foraminiferids.* Heinemann Educational Books, London. pp. 274.

Murray, J.W., 1979. British nearshore foraminiferids. *Synopses of the British Fauna, New Series,* **no. 16** (16): 1-68.

Murray, J.W., 1982. Benthic foraminifera: The validity of living, dead or total assemblages for the interpretation of palaeocology. *Journal of Micropalaeontology,* **1** 137-140.

Murray, J.W., 1983. Population-Dynamics of Benthic Foraminifera - Results from the Exe Estuary, England. *Journal of Foraminiferal Research,* **13** (1): 1-12.

Murray, J.W., 1991a. Ecology and distribution of benthic foraminifera. in *Biology of Foraminifera,* J. J. Lee and O. R. Anderson (eds). Academic Press Limited, London. 221-255.

Murray, J.W., 1991b. *Ecology and palaeoecology of benthic foraminifera.* Longman, Harlow. pp. 397.

Murray, J.W., 2000a. The enigma of the continued use of total assemblages in ecological studies of benthic foraminifera. *Journal of Foraminiferal Research,* **30** (3): 244-245.

Murray, J.W., 2000b. Revised taxonomy, An Atlas of British Recent Foraminiferids. *Journal of Micropalaeontology,* **19** 44-44.

Murray, J.W., 2003a. Foraminiferal assemblage formation in depositional sinks on the continental shelf west of Scotland. *Journal of Foraminiferal Research,* **33** (2): 101-121.

Murray, J.W., 2003b. An Illustrated Guide to the Benthic Foraminifera of the Hebridean Shelf, West of Scotland, With Notes on Their Mode of Life. *Palaeontologica Electronica,* **5** (2): 31 pp.

Murray, J.W. and Alve, E., 1999a. Natural dissolution of modern shallow water benthic foraminifera: taphonomic effects on the palaeoecological record. *Palaeogeography, Palaeoclimatology, Palaeoecology,* **146** (1-4): 195-209.

Murray, J.W. and Alve, E., 1999b. Taphonomic experiments on marginal marine foraminiferal assemblages: how much ecological information is preserved? *Palaeogeography Palaeoclimatology Palaeoecology,* **149** (1-4): 183-197.

Murray, J.W. and Alve, E., 2000. Do calcareous dominated shelf foraminiferal assemblages leave worthwhile ecological information after their dissolution? in *Proceedings of the Fifth International Workshop on Agglutinated Foraminifera.,* **7,** M. B. Hart, M. A. Kaminski and C. W. Smart (eds). Grzybowski Foundation Special Publication, 311-331.

Murray, J.W., Alve, E. and Cundy, A., 2003. The origin of modern agglutinated foraminiferal assemblages: evidence from a stratified fjord. *Estuarine, Coastal and Shelf Science,* **58** (3): 677-697.

Murray, J.W. and Bowser, S.S., 2000. Mortality, protoplasm decay rate, and reliability of staining techniques to recognize 'living' foraminifera: A review. *Journal of Foraminiferal Research,* **30** (1): 66-70.

Nagy, J. and Alve, E., 1987. Temporal changes in foraminiferal faunas and impact of pollution in Sandebukta, Oslo Fjord. *Marine Micropaleontology,* **12** (2): 109-128.

Noller, J.S., 2000. Lead-210 Geochronology. in *Quaternary Geochronology: methods and applications.,* **AGU Reference Shelf 4,** J. S. Noller, J. M. Sowers and W. R. Lettis (eds). American Geophysical Union, Washington, DC. 115-121.

Nordberg, K., Filipsson, H.L., Gustafsson, M., Harland, R. and Roos, P., 2001. Climate, hydrographic variations and marine benthic hypoxia in Koljo Fjord, Sweden. *Journal of Sea Research,* **46** (3-4): 187-200.

Nordberg, K., Gustafsson, M. and Krantz, A.L., 2000. Decreasing oxygen concentrations in the Gullmar Fjord, Sweden, as confirmed by benthic foraminifera, and the possible association with NAO. *Journal of Marine Systems,* **23** (4): 303-316.

Nydal, R., 2000. Radiocarbon in the ocean. *Radiocarbon,* **42** (1): 81-98.

O' Brien, S.R., Mayewski, P.A., Meeker, L.D., Meese, D.A., Twickler, M.S. and Whitlow, S.I., 1995. Complexity of Holocene Climate as Reconstructed from a Greenland Ice Core. *Science,* **270** (5244): 1962-1964.

Oldfield, F., Asioli, A., Accorsi, C.A., Mercuri, A.M., Juggins, S., Lagone, L., Rolph, T., Trincardi, F., Wolff, G., Gibbs, Z., Vigliotti, L., Frignani, M., van der Post, K. and Branch, N., 2004. A high resolution late Holocene palaeo environmental record from the central Adriatic Sea. *Quaternary Science Reviews,* **22** (2-4): 319-342.

Oliver, M.A., Webster, R., Edwards, K.J. and Whittington, G., 1997. Multivariate, autocorrelation and spectral analyses of a pollen profile from Scotland and evidence for periodicity. *Review of Palaeobotany and Palynology,* **96** (1-2): 121-144.

Olsson, I.U., 1968. Modern aspects of radiocarbon dating. *Earth-Science Reviews,* **4** 203-218.

Olsson, I.U., 1980. Content of ^{14}C in marine mammals from northern Europe. *Radiocarbon,* **22** (3): 662-675.

Olsson, I.U. and Osadebe, F.A.N., 1974. Carbon isotope variations and fractionation corrections in ^{14}C dating. *Boreas,* **3** 139-146.

O'Neil, J.R., Clayton, R.N. and Mayeda, T., 1969. Oxygen isotope fractionation in divalent metal carbonates. *Journal of Chemical Physics,* **51** 5547-5558.

Open-University, 1995. *Seawater: Its Composition Properties and Behaviour.* Butterworth Heineman, pp. 166.

Open-University, 1997. *Waves, tides and shallow-water processes.* Butterworth Heineman, pp. 187.

Oppo, D.W., McManus, J.F. and Cullen, J.L., 2003. Palaeo-oceanography: Deepwater variability in the Holocene epoch. *Nature,* **422** (6929): 277-278.

O'Sullivan, P.E., Moyeed, R., Cooper, M.C. and Nicholson, M.J., 2002. Comparison between instrumental, observational and high resolution proxy sedimentary records of Late Holocene climatic change - a discussion of possibilities. *Quaternary International,* **88** 27-44.

Owen, R., Kennedy, H. and Richardson, C., 2002. Isotopic partitioning between scallop shell calcite and seawater: Effect of shell growth rate. *Geochimica Et Cosmochimica Acta,* **66** (10): 1727-1737.

Parker, D.E., Legg, T.P. and Folland, C.K., 1992. A new daily Central England Temperature Series, 1772-1991. *International Journal of Climatology,* **12** 317-342.

Parker, W.C. and Arnold, A.J., 1999. Quantitative methods of data analysis in foraminiferal ecology. in *Modern Foraminifera,* B. K. Sen Gupta (eds). Kluwer Academic Publishers, Great Britain. 71-89.

Patterson, R.T., Gehrels, W.R., Belknap, D.F. and Dalby, A.P., 2004. The distribution of salt marsh foraminifera at Little Dipper Harbour New Brunswick, Canada: applicable transfer functions in sea-level research. *Quaternary International,* **120** 185-194.

Perez-Arlucea, M., Mendez, G., Clemente, F., Nombela, M., Rubio, B. and Filgueira, M., 2005. Hydrology, sediment yield, erosion and sedimentation rates in the estuarine environment of the Ria de Vigo, Galicia, Spain. *Journal of Marine Systems,* **54** (1-4): 209-226.

Petit, J.R., Jouzel, J., Raynaud, D., Barkov, N.I., Barnola, J.-M., Basile, I., Bender, M., Chappellaz, J., Davis, M., Delayque, G., Delmotte, M., Kotlyakov, V.M., Legrand, M., Lorius, C., Pépin, L., Ritz, C., Saltzman, E. and Stievenard, M., 1999. Climate and atmospheric history of the past 420,000 years from the Vostok ice core, Antarctica. *Nature,* **399** (429-436):

Pfister, C., Schwarz-Zanetti, G., Wegmann, M. and Luterbacher, J., 1998. Winter air temperature variations in western Europe during the Early and High Middle Ages (AD 750–1300). *The Holocene,* **8** (5): 535-552.

Pilcher, J.R., 1991. Radiocarbon Dating. in *Quaternary Dating Methods - A User's Guide.,* **4,** P. L. Smart and P. D. Frances (eds). Quaternary Research Association Technical Guide, 16-36.

Pingree, R.D. and Griffiths, D.K., 1978. Tidal Fronts on the Shelf Seas Around the British Isles. *Journal of Geophysical Research,* **89** 4615-4622.

Piotrowski, A.M., Goldstein, S.L., Hemming, S.R. and Fairbanks, R.G., 2004. Intensification and variability of ocean thermohaline circulation through the last deglaciation. *Earth and Planetary Science Letters,* **225** (1-2): 205-220.

Plassen, L. and Vorren, T.O., 2002. Late Weichselian and Holocene sediment flux and sedimentation rates in Andfjord and Vågsfjord, North Norway. *Journal of Quaternary Science,* **17** (2): 161-180.

Polyak, L., Stanovoy, V. and Lubinski, D.J., 2003. Stable isotopes in benthic foraminiferal calcite from a river- influenced Arctic marine environment, Kara and Pechora Seas. *Paleoceanography,* **18** (1): art. no.-1003.

Prentice, J.C., 1980. Multidimensional scaling as a research tool in Quaternary palynology: a review of theory and methods. *Review of Palaeobotany and Palynology,* **31** 71– 104.

Proctor, C.J., Baker, A. and Barnes, W.L., 2002. A three thousand year record of North Atlantic climate. *Climate Dynamics,* **19** (5-6): 449-454.

Proctor, C.J., Baker, A., Barnes, W.L. and Gilmour, R.A., 2000. A thousand year speleothem proxy record of North Atlantic climate from Scotland. *Climate Dynamics,* **16** (10-11): 815-820.

Quay, P., Sonnerup, R., Westby, T., Stutsman, J. and McNichol, A., 2003. Changes in the 13C/12C of dissolved inorganic carbon in the ocean as a tracer of anthropogenic CO2 uptake. *Global Biogeochemical Cycles,* **17** (1): doi:10.1029/2001GB001817.

Qvale, G., Markussen, B. and Thiede, J., 1984. Benthic foraminifers in fjords; response to water masses. *Norsk Geologisk Tidsskrift,* **64** (3): 235-249.

Rahmstorf, S., 1995. Bifurcations of the Atlantic thermohaline circulation in response to changes in the hydrological cycle. *Nature,* **378** 145-149.

Rahmstorf, S., 1996. On the freshwater forcing and transport of the Atlantic thermohaline circulation. *Climate Dynamics,* **12** 799-811.

Rahmstorf, S., 2000. The thermohaline ocean circulation - a system with dangerous thresholds? *Climatic Change,* **46** 247-256.

Rahmstorf, S., 2002. Ocean circulation and climate during the past 120,000 years. *Nature,* **419** 207-214.

Rahmstorf, S., 2003. Timing of abrupt climate change: A precise clock. *Geophysical Research Letters,* **30** (10): 1510 doi:10.1029/2003GL017115.

Rathburn, A.E., Corliss, B.H., Tappa, K.D. and Lohmann, K.C., 1996. Comparisons of the ecology and stable isotopic compositions of living (stained) benthic foraminifera from the Sulu and South China Seas. *Deep Sea Research Part I: Oceanographic Research Papers,* **43** (10): 1617-1646.

Reid, G.C., 1997. Solar Forcing of Global Climate Change Since The Mid-17th Century. *Climatic Change,* **37** (2): 391-405.

Reilly, J., Prinn, R., Harnisch, J., Fitzmaurice, J., Jacoby, H., Kicklighter, D., Melillo, J., Stone, P., Sokolov, A. and Wang, C., 1999. Multi-gas assessment of the Kyoto Protocol. *Nature,* **401** 549-555.

http://radiocarbon.pa.qub.ac.uk/marine Reimer, P.J., 2004. *Marine Reservoir Correction Database*. http://radiocarbon.pa.qub.ac.uk/marine. Last updated 14/02/2004, accessed on 2000.

Reimer, P.J., Baillie, M.G.L., Bard, E., Bayliss, A., Beck, J.W., Bertrand, C.J., Blackwell, P.G., Buck, C.E., Burr, G.S., Cutler, K.B., Damon, P.E., Edwards, R.L., Fairbanks, R.G., Friedrich, M., Guilderson, T.P., Hogg, A.G., Hughen, K.A., Kromer, B., McCormac, F.G., Manning, S., Bronk Ramsey, C., Reimer, R.W., Remmele, S., Southon, J., Stuiver, M., Talamo, S., Taylor, F.W., van der Plicht, J. and Weyhenmeyer, C.E., 2004a. IntCal04 Terrestrial radiocarbon age calibration, 0-26 cal kyr BP. *Radiocarbon,* **46** (3): 1029–1058.

Reimer, P.J., Brown, T.A. and Reimer, R.W., 2004b. Discussion: Reporting and Calibration of Post-Bomb^{14}C Data. *Radiocarbon,* **46** (3): 1299-1304.

Reimer, P.J., McCormac, F.G., Moore, J., McCormick, F. and Murray, E.V., 2002. Marine radiocarbon reservoir corrections for the mid- to late Holocene in the eastern subpolar North Atlantic. *Holocene,* **12** (2): 129-135.

Reverdin, G., Cayan, D. and Kushnir, Y., 1997. Decadal variability of hydrography in the upper northern North Atlantic in 1948-1990. *Journal of Geophysical Research-Oceans,* **102** (C4): 8505-8531.

Reverdin, G., Niiler, P.P. and Valdimarsson, H., 2003. North Atlantic Ocean surface currents. *Journal of Geophysical Research,* **108** (C1 3002): doi:10.1029/2001JC001020.

Rial, J.A., 2004. Abrupt climate change: chaos and order at orbital and millennial scales. *Global and Planetary Change,* **41** (2): 95-109.

Rind, D., 2002. The Sun's Role in Climate Variations. *Science,* **296** 673-677.

Risebrobakken, B., Jansen, E., Andersson, C., Mjelde, E. and Hevrøy, K., 2003. A high-resolution study of Holocene paleoclimatic and paleoceanographic changes in the Nordic Seas. *Paleoceanography,* **18** (1): 1017, doi:10.1029/2002PA000764.

Roberts, N., 1998. *The Holocene: An Environmental History*. Blackwell Publishers Ltd, Oxford. pp. 316.

Rodwell, M.J., Rowell, D.P. and Folland, C.K., 1999. Oceanic forcing of the wintertime North Atlantic Oscillation and European climate. *Nature,* **398** (6725): 320-323.

Rohling, E.J. and Cooke, S., 1999. Stable oxygen and carbon isotopes in foraminiferal carbonate shells. in *Modern Foraminifera.,* B. K. S. Gupta (eds). Kluwer Academic Publishers, 239-258.

Rohling, E.J., Mayewski, P.A., Abu-zied, R.H., Casford, J.S.L. and Hayes, A., 2002. Holocene atmosphere-ocean interactions: records from Greenland and the Aegean Sea. *Climate Dynamics,* **18** (7): 587-593.

Rohling, E.J. and Pälike, H., 2005. Centennial-scale climate cooling with a sudden cold event around 8,200 years ago. *Nature,* **434** 975-979.

Romanek, C.S., Grossman, E.L. and Morse, J.W., 1992. Carbon Isotopic Fractionation in Synthetic Aragonite and Calcite - Effects of Temperature and Precipitation Rate. *Geochimica Et Cosmochimica Acta,* **56** (1): 419-430.

Ropes, J.W., Jones, D.S., Murawski, S.A., Serchuk, F.M. and Jearld, A., 1984. Documentation of Annual Growth Lines in Ocean Quahogs, Arctica- Islandica Linne. *Fishery Bulletin,* **82** (1): 1-19.

Ruprecht, E., Schroder, S.S. and Ubl, S., 2002. On the relation between NAO and water vapour transport towards Europe. *Meteorologische Zeitschrift,* **11** (6): 395-401.

Sabine, C.L., Feely, R.A., Gruber, N., Key, R.M., Lee, K., Bullister, J.L., Wanninkhof, R., Wong, C.S., Wallace, D.W.R., Tilbrook, B., Millero, F.J., Peng, T.H., Kozyr, A., Ono, T. and Rios, A.F., 2004. The Oceanic Sink for Anthropogenic CO_2. *Science,* **305** (5682): 367-371.

Saunders, M.A. and Qian, B., 2002. Seasonal predictability of the winter NAO from north Atlantic sea surface temperatures. *Geophysical Research Letters,* **29** (22): 2049, doi:10.1029/2002GL014952.

Sauter, E.J., Schluter, M. and Suess, E., 2001. Organic carbon flux and remineralization in surface sediments from the northern North Atlantic derived from pore-water oxygen microprofiles. *Deep-Sea Research Part I-Oceanographic Research Papers,* **48** (2): 529-553.

Schmidt, M.W., Spero, H.J. and Lea, D.W., 2004. Links between salinity variation in the Caribbean and North Atlantic thermohaline circulation. *Nature,* **428** (6979): 160-163.

Schmiedl, G., Pfeilsticker, M., Hemleben, C. and Mackensen, A., 2004. Environmental and biological effects on the stable isotope composition of recent deep-sea benthic foraminifera, from the western Mediterranean Sea. *Marine Micropaleontology,* **51** (1-2): 129-152.

Schone, B.R., Oschmann, W., Rossler, J., Castro, A.D.F., Houk, S.D., Kroncke, I., Dreyer, W., Janssen, R., Rumohr, H. and Dunca, E., 2003. North Atlantic Oscillation dynamics recorded in shells of a long-lived bivalve mollusk. *Geology,* **31** (12): 1037-1040.

Schonfeld, J., Zahn, R. and de Abreu, L., 2003. Surface and deep water response to rapid climate changes at the Western Iberian Margin. *Global and Planetary Change,* **36** (4): 237-264.

Schulz, M., Paula, A. and Timmermann, A., 2004. Glacial–interglacial contrast in climate variability at centennial-to-millennial timescales: observations and conceptual model. *Quaternary Science Reviews,* **23** (20-22): 2219-2230.

Scott, G.A., Scourse, J.D. and Austin, W.E.N., 2003. The distribution of benthic foraminifera in the Celtic Sea: The significance of seasonal stratification. *Journal of Foraminiferal Research,* **33** (1): 32-61.

Scourse, J., Marret, F., Versteegh, G.J.M., Jansen, J.H.F., Schefu, E. and van der Plicht, J., *in press*. High-resolution last deglaciation record from the Congo fan reveals significance of mangrove pollen and biomarkers as indicators of shelf transgression. *Quaternary Research,*

Scourse, J.D. and Austin, W.E.N., 2002. Quaternary shelf sea palaeoceanography: recent developments in Europe. *Marine Geology,* **191** (3-4): 87-94.

Scourse, J.D., Austin, W.E.N., Long, B.T., Assinder, D.J. and Huws, D., 2002. Holocene evolution of seasonal stratification in the Celtic Sea: refined age model, mixing depths and foraminiferal stratigraphy. *Marine Geology,* **191** (3-4): 119-145.

Scourse, J.D., Kennedy, H., Scott, G.A. and Austin, W.E.N., 2004. Stable isotopic analyses of modern benthic foraminifera from seasonally stratified shelf seas: disequilibria and the 'seasonal effect'. *Holocene,* **14** (5): 747-758.

Seidenkrantz, M.S., Kristensen, P. and Knudsen, K.L., 1995. Marine Evidence for Climatic Instability During the Last Interglacial in Shelf Records from Northwest Europe. *Journal of Quaternary Science,* **10** (1): 77-82.

Seidov, D. and Maslin, M., 2001. Atlantic ocean heat piracy and the bipolar climate see-saw during Heinrich and Dansgaard-Oeschger events. *Journal of Quaternary Science,* **16** (4): 321-328.

Sejrup, H.P., Birks, H.J.B., Klitgaard Kristensen, D. and Madsen, H., 2004. Benthonic foraminiferal distributions and quantitative transfer functions for the northwest European continental margin. *Marine Micropaleontology,* **53** (1-2): 197-226.

Sejrup, H.P., Fjaeran, T., Hald, M., Beck, L., Hagen, J., Miljeteig, I., Morvik, I. and Norvik, O., 1981. Benthonic foraminifera in surface samples from the Norwegian Continental Margin between 62°N and 65°N. *Journal of Foraminiferal Research,* **11** (4): 277–295.

Sejrup, H.P., Haflidason, H., Flatebo, T., Kristensen, D.K., Grosfjeld, K. and Larsen, E., 2001. Late-glacial to Holocene environmental changes and climate variability: evidence from Voldafjorden, western Norway. *Journal of Quaternary Science,* **16** (2): 181-198.

Sen Gupta, B.K., 1999. Systematics of modern Foraminifera. in *Modern Foraminifera,* B. K. Sen Gupta (eds). Kluwer Academic Publishers, 7-36.

Shackleton, N.J., 1967. Oxygen isotope analyses and Pleistocene temperatures re-assessed. *Nature,* **215** 15-17.

Shackleton, N.J., 1974. Attainment of isotopic equilibrium between ocean water and the benthonic foraminifera genus Uvigerina: Isotopic changes in the ocean during the last glacial. *Centre National de la Recherche Scientifique Colleagues Internationeaux,* **219** 203-209.

Shackleton, N.J., 1977. The oxygen isotope record of the Late Pleistocene. *Philosophical Transactions of the Royal Society of London Series,* **B280** 169-182.

Shackleton, N.J., 1987. Oxygen isotopes, ice volume and sea-level. *Quaternary Science Reviews,* **6** 183-190.

Shannon, C.E. and Weaver, W., 1949. *The mathematical theory of communication.* University of Illnois Press, Urbana. pp. 117.

Shennan, I., Hamilton, S., Hillier, C. and Woodroffe, S., 2005. A 16 000-year record of near-field relative sea-level changes, northwest Scotland, United Kingdom. *Quaternary International,* **133-134** 95-106.

Shennan, I., Innes, J.B., Long, A.J. and Zong, Y.Q., 1995. Late Devensian and Holocene Relative Sea-Level Changes in Northwestern Scotland - New Data to Test Existing Models. *Quaternary International,* **26** 97-123.

Shi, G.R., 1993. Multivariate Data-Analysis in Paleoecology and Paleobiogeography - a Review. *Palaeogeography Palaeoclimatology Palaeoecology,* **105** (3-4): 199-234.

Shindell, D.T., Schimdt, G.A., Miller, R.L. and Mann, M.E., 2003. Volcanic and Solar Forcing of Climate Change during the Preindustrial Era. *Journal of Climate,* **16** 4094-4102.

Shindell, D.T., Schmidt, G.A., Mann, M.E., Rind, D. and Waple, A., 2001. Solar Forcing of Regional Climate Change During the Maunder Minimum. *Science,* **294** (5549): 2149-2152.

Shultz, D.J. and Calder, J.A., 1976. Organic carbon $^{13}C/^{12}C$ variations in estuarine sediments. *Geochimica et Cosmochimica Acta,* **40** 381-385.

Siani, G., Paterne, M., Arnold, M., Bard, E., Metivier, B., Tisnerat, N. and Bassinot, F., 2000. Radiocarbon reservoir ages in the Mediterranean Sea and Black Sea. *Radiocarbon,* **42** (2): 271-280.

Simpson, J.H., Edelsten, D.J., Edwards, A., Morris, N.G.G. and Tett, P.B., 1979. The Islay front: physical structure and phytoplankton distribution. *Estuarine Coastal and Marine Science,* **9** 713-726.

Simpson, J.H. and Hunter, J.R., 1974. Fronts in the Irish Sea. *Nature,* **250** 404-406.

Simpson, J.H. and Rippeth, T.P., 1993. The Clyde Sea - a Model of the Seasonal Cycle of Stratification and Mixing. *Estuarine Coastal and Shelf Science,* **37** (2): 129-144.

Skinner, L.C. and McCave, I.N., 2003. Analysis and modelling of gravity- and piston coring based on soil mechanics. *Marine Geology,* **199** (1-2): 181-204.

Skrabal, S.A. and Terry, C.M., 2002. Distributions of dissolved titanium in porewaters of estuarine and coastal marine sediments. *Marine Chemistry,* **77** (2-3): 109-122.

Slonosky, V.C. and Yiou, P., 2001. The North Atlantic Oscillation and its relationship with near surface temperature. *Geophysical Research Letters,* **28** (5): 807-810.

Smith, J., 1998. An introduction to the magnetic properties of natural materials. in *Environmental magnetism; a practical guide,* **Technical Guide 6,** J. Walden, F. Oldfield and J. Smith (eds). Quaternary Research Association, Cambridge. 5-25.

Smittenberg, R.H., Baas, M., Green, M.J., Hopmans, E.C., Schouten, S. and Sinninghe Damste, J.S., 2005. Pre- and post-industrial environmental changes as revealed by the biogeochemical sedimentary record of Drammensfjord, Norway. *Marine Geology,* **214** (1-3): 177-200.

Sonnerup, R.E., Quay, P.D., McNichol, A.P., Bullister, J.L., Westby, T.A. and Anderson, H.L., 1999. Reconstructing the oceanic 13C Suess effect. *Global Biogeochemical Cycles,* **13** (4): 857–872.

Spero, H.J., Bijma, J., Lea, D.W. and Bemis, B.E., 1997. Effect of seawater carbonate concentration on foraminiferal carbon and oxygen isotopes. *Nature,* **390** (6659): 497-500.

Spero, H.J. and Lea, D.W., 1996. Experimental determination of stable isotope variability in *Globigerina bulliodes*: implications for paleoceanographic reconstructions. *Marine Micropaleontology,* **28** 231-246.

Spiker, E.C., 1980. The behaviour of ^{14}C and ^{13}C in estuarine water: Effects of in situ CO_2 production and atmospheric exchange. *Radiocarbon,* **22** (3): 647-654.

Stauffer, B., 1999. Climate change - Cornucopia of ice core results. *Nature,* **399** (6735): 412-413.

Stocker, T.F. and Marchal, O., 2000. Abrupt climate change in the computer: Is it real? *Proceedings of the National Academy of Sciences of the United States of America,* **97** (4): 1362-1365.

Stocker, T.F. and Schmittner, A., 1997. Influence of CO2 emission rates on the stability of the thermohaline circulation. *Nature,* **388** 862-865.

Stuiver, M. and Braziunas, T.F., 1989. Atmospheric C-14 and Century-Scale Solar Oscillations. *Nature,* **338** (6214): 405-408.

Stuiver, M. and Braziunas, T.F., 1993. Modeling Atmospheric ^{14}C Influences and ^{14}C Ages of Marine Samples to 10,000 BC. *Radiocarbon,* **35** (1): 137-189.

Stuiver, M., Braziunas, T.F., Becker, B. and Kromer, B., 1991. Climatic, Solar, Oceanic, and Geomagnetic Influences on Late- Glacial and Holocene Atmospheric C-14/C-12 Change. *Quaternary Research,* **35** (1): 1-24.

Stuiver, M. and Grootes, P., 2000. GISP2 Oxygen Isotope Ratios. *Quaternary Research,* **53** (3): 277-284.

Stuiver, M., Kromer, B., Becker, B. and Ferguson, C.W., 1986a. Radiocarbon age calibration back to 13,300 years BP and the ^{14}C ages matching of the German oak and US bristlecone pine chronologies. *Radiocarbon,* **28** 969-979.

Stuiver, M. and Pearson, G.W., 1993. High-Precision Bidecadal Calibration of the Radiocarbon Time Scale, Ad 1950-500 Bc and 2500-6000 Bc. *Radiocarbon,* **35** (1): 1-23.

Stuiver, M., Pearson, G.W. and Braziunas, T., 1986b. Radiocarbon Age Calibration of Marine Samples Back to 9000 cal yr BP. *Radiocarbon,* **28** (2B): 980-1021.

Stuiver, M. and Polach, H.A., 1977. Discussion reporting of ^{14}C data. *Radiocarbon,* **19** (3): 355-363.

Stuiver, M., Reimer, P.J., Bard, E., Beck, J.W., Burr, G.S., Hughen, K.A., Kromer, B., McCormac, G., Van der Plicht, J. and Spurk, M., 1998a. INTCAL98 radiocarbon age calibration, 24,000-0 cal BP. *Radiocarbon,* **40** (3): 1041-1083.

Stuiver, M., Reimer, P.J. and Braziunas, T.F., 1998b. High-precision radiocarbon age calibration for terrestrial and marine samples. *Radiocarbon,* **40** (3): 1127-1151.

Suess, H.E., 1955. Radiocarbon concentration in modern wood. *Science,* **122** 415-417.

Sutton, R.T. and Allen, M.R., 1997. Decadal predictability of North Atlantic sea surface temperature and climate. *Nature,* **388** (6642): 563-567.

Tachikawa, K. and Elderfield, H., 2002. Microhabitat effects on Cd/Ca and delta C-13 of benthic foraminifera. *Earth and Planetary Science Letters,* **202** (3-4): 607-624.

ter Braak, C.J.F., 1995. Non-linear methods for multivariate statistical calibration and their use in palaeoecology: a comparison of inverse (k-nearest neighbours, partial least squares and weighted averaging partial least squares) and classical approaches. *Chemometrics and Intelligent Laboratory Systems,* **28** (1): 165-180.

ter Braak, C.J.F., Juggins, S., Birks, H.J.B. and van der Voet, H., 1993. Weighted averaging partial least squares regression (WA-PLS): definition and comparison with other methods for species-environment calibration. in *Multivariate Environmental Statistics,* G. P. Patil and C. R. Rao (eds). Elsevier Science,

ter Braak, C.J.F. and Looman, C.W.N., 1986. Weighted averaging, logistic regression and the Gaussian response model. *Vegetatio,* **65** 3-11.

Thiede, J., Qvale, G., Skarbø, O. and Strand, J.E., 1981. Benthonic foraminiferal distributions in a southern Norwegian fjord system: a re-evaluation of Oslo Fjord data. *Special Publications of the International Association of Sedimentologists,* **5** 469-495.

Thomason, J.C., Hills, J.M. and Bennett, A.M., 1997. Dynamics of a massive freshwater influx in the Clyde Estuary. *Estuarine Coastal and Shelf Science,* **44** (4): 385-393.

Thornton, S.F. and McManus, J., 1994. Application of Organic Carbon and Nitrogen Stable isotopes and C/N ratios as Source indicators of Organic Matter Provenance in Estuarine Systems: Evidence from the Tay Estuary, Scotland. *Estuarine, Coastal and Shelf Science,* **38** 219-233.

Treasurer, J.W., 2001. A parasitic marine isopod Aega tridens leach on mackerel Scomber scomber L. in British Waters. *Bulletin of the European Association of Fish Pathologists,* **21** (1): 37-39.

Turrell, W.R., Slesser, G., Payne, R., Adams, R.D. and Gillibrand, P.A., 1996. Hydrography of the East Shetland Basin in relation to decadal North Sea variability. *ICES Journal of Marine Science,* **53** 899-916.

Urey, H.C., 1947. The thermodynamic properties of isotopic substances. *Journal of the Chemical Society,* 562-581.

van der Plicht, J., Beck, J.W., Bard, E., Baillie, M.G.L., Blackwell, P.G., Buck, C.E., Friedrich, M., Guilderson, T.P., Hughen, K.A., Kromer, B., McCormac, F.G., Bronk Ramsey, C., Reimer, P.J., Reimer, R.W., Remmele, S., Richards, D.A., Southon, J., Stuiver, M. and Weyhenmeyer, C.E., 2004. NotCal04—Comparison/Calibration 14C Records 26–50 Cal Kyr BP. *Radiocarbon,* **46** (3): 1225-1238.

van Geel, B., van der Plicht, J. and Renssen, H., 2003. Major Delta C-14 excursions during the late glacial and early Holocene: changes in ocean ventilation or solar forcing of climate change? *Quaternary International,* **105** 71-76.

van Kreveld, S., Sarnthein, M., Erlenkeuser, H., Grootes, P., Jung, S., Nadeau, M.J., Pflaumann, U. and Voelker, A., 2000. Potential links between surging ice sheets, circulation changes, and the Dansgaard-Oeschger cycles in the Irminger Sea, 60 - 18 kyr. *Paleoceanography,* **15** (4): 425-442.

Velinsky, D.J. and Fogel, M.L., 1999. Cycling of dissolved and particulate nitrogen and carbon in the Framvaren Fjord, Norway: stable isotopic variations. *Marine Chemistry,* **67** (3-4): 161-180.

Verardo, D.J., Froelich, P.N. and McIntyre, A., 1990. Determination of Organic-Carbon and Nitrogen in Marine- Sediments Using the Carlo-Erba-Na-1500 Analyzer. *Deep-Sea Research Part a-Oceanographic Research Papers,* **37** (1): 157-165.

Vilks, G. and Deonarine, B., 1988. Labrador Shelf benthic foraminifera and stable oxygen isotopes of Cibicides lobatulus related to the Labrador Current. *Canadian Journal of Earth Sciences = Journal Canadien des Sciences de la Terre,* **25** (8): 1240-1255.

Vincent, E., Killingley, J.S. and Berger, W.H., 1981. Stable Isotope Composition of Benthic Foraminifera from the Equatorial Pacific. *Nature,* **289** (5799): 639-643.

Vinot-Bertouille, A. and Duplessy, J.C., 1973. Individual isotopic fractionation of carbon and oxygen in benthic foraminifera. *Earth and Planetary Science Letters,* **18** 247-252.

Visbeck, M., Chassignet, E.P., Curry, R.G., Delworth, T.L., Dickson, R.R. and Krahmann, G., 2003. The Ocean's Response to North Atlantic Oscillation Variability. in *The North Atlantic Oscillation: Climatic Significance and Environmental Impact,* Geophysical Monograph, **134,** J. W. Hurrell, Y. Kushnir, G. Ottersen and M. Visbeck (eds). American Geophysical Union, Washington DC. 113-145.

Vlag, P.A., Kruiver, P.P. and Dekkers, M.J., 2004. Evaluating climate change by multivariate statistical techniques on magnetic and chemical properties of marine sediments (Azores region). *Palaeogeography Palaeoclimatology Palaeoecology,* **212** (1-2): 23-44.

Voelker, A.H.L., 2002. Global distribution of centennial-scale records for Marine Isotope Stage (MIS) 3: a database. *Quaternary Science Reviews,* **21** (10): 1185-1212.

Walden, J., Oldfield, F. and Smith, J., 1998. *Environmental magnetism; a practical guide.* Quaternary Research Association, Cambridge. pp. 243.

Walden, J. and Smith, J.P., 1995. Factor Analysis: A Practical Application. in *Statistical Modelling of Quaternary Science Data,* **Technical Guide No. 5,** D. Maddy and J. S. Brew (eds). Quaternary Research Association, 39-64.

Walker, M.J.C., Bjorck, S., Lowe, J.J., Cwynar, L.C., Johnsen, S., Knudsen, K.L. and Wohlfarth, B., 1999. Isotopic 'events' in the GRIP ice core: a stratotype for the Late Pleistocene. *Quaternary Science Reviews,* **18** (10-11): 1143-1150.

Walsh, J.J., Rowe, G.T., Iverson, R.L. and McRoy, C.P., 1981. Biological export of shelf carbon is a sink of the global CO_2 cycle. *Nature,* **219** 196-201.

Walton, W.R., 1952. Techniques for recognition of living foraminifera. *Contributions from the Cushman Foundation for Foraminiferal Research,* **3** 56-60.

Wanner, H., Bronnimann, S., Casty, C., Gyalistras, D., Luterbacher, J., Schmutz, C., Stephenson, D.B. and Xoplaki, E., 2001. North Atlantic Oscillation - Concepts and studies. *Surveys in Geophysics,* **22** (4): 321-382.

Weaver, A.J. and Hughes, T.M.C., 1994. Rapid Interglacial Climate Fluctuations Driven by North- Atlantic Ocean Circulation. *Nature,* **367** (6462): 447-450.

Wefer, G., 1976. Environmental effects on growth rates of benthic foraminifera (shallow water, Baltic Sea). in *First international Symposium on Benthonic Foraminifera of Continental Margins,* C. T. Schafer and B. R. Pelletier (eds). Atlantic Geoscience Society, 39-50.

Wefer, G. and Berger, W.H., 1991. Isotope Paleontology - Growth and Composition of Extant Calcareous Species. *Marine Geology,* **100** (1-4): 207-248.

Weidman, C.R. and Jones, G.A., 1993. A Shell-Derived Time History of Bomb ^{14}C on Georges Bank and Its Labrador Sea Implications. *Journal of Geophysical Research-Oceans,* **98** (C8): 14577-14588.

Weidman, C.R., Jones, G.A. and Lohmann, K.C., 1994. The long-lived mollusc *Arctica Islandica*: A new paleoceanographic tool for the reconstruction of bottom temperatures for the continental shelves of the northern North Atlantic Ocean. *Journal of Geophysical Research-Oceans,* **99** (C11): 18,305 - 18,314.

White, J.W.C., Gorodetzky, D., Cook, E.R. and Barlow, L.K., 1996. Frequency analysis of an annually resolved, 700 year paleoclimate record from the GISP-2 ice core. in *Climatic variations and forcing mechanisms of the last 2000 years,* NATO ASI Series, 1, **41,** P. D. Jones, R. S. Bradley and J. Jouzel (eds). Springer Berlin, 193-212.

White, W.B., Lean, J., Cayan, D.R. and Dettinger, M.D., 1997. Response of global upper ocean temperature to changing solar irradiance. *Journal of Geophysical Research,* **102** (C2): 3255–3266.

Wilbur, K.M., 1960. Shell structure and mineralization in mollusks. in *Calcification in Biological Systems,* **64,** R. F. Sogonnaes (eds). American Association in Advanced Science, 15.

Wilson-Finelli, A., Chandler, G.T. and Spero, H.J., 1998. Stable isotope behavior in paleoceanographically important benthic foraminifera: Results from microcosm culture experiments. *Journal of Foraminiferal Research,* **28** (4): 312-320.

Wohletz, K.H., 2000. Were the Dark Ages triggered by volcano-related climate changes in the 6th century? *EOS Transactions of the American Geophysical Union,* **48** (81): F1305.

Wollenburg, J.E. and Kuhnt, W., 2000. The response of benthic foraminifers to carbon flux and primary production in the Arctic Ocean. *Marine Micropaleontology,* **40** (3): 189-231.

Woodruff, F., Savin, S.M. and Douglas, R.G., 1980. Biological fractionation of oxygen and carbon isotopes by Recent benthic foraminifera. *Marine Micropaleontology,* **5** 3-11.
Wu, L.X. and Liu, Z.Y., 2005. North Atlantic decadal variability: Air-sea coupling, oceanic memory, and potential northern hemisphere resonance. *Journal of Climate,* **18** (2): 331-349.

Wunsch, C., 2000. On sharp spectral lines in the climate record and the millennial peak. *Paleoceanography,* **15** (4): 417-424.

Xing, J.X. and Davies, A.M., 2001. The influence of shelf edge flows and wind upon the circulation on the Malin Shelf and in the Irish Sea. *Continental Shelf Research,* **21** (1): 21-45.

Yarincik, K.M., Murray, R.W., Lyons, T.W., Peterson, L.C. and Haug, G.H., 2000. Oxygenation history of bottom waters in the Cariaco Basin, Venezuela, over the past 578,000 years: Results from redox-sensitive metals (Mo, V, Mn, and Fe). *Paleoceanography,* **15** (6): 593-604.

Yoneda, M., Kitagawa, H., van der Plicht, J., Uchida, M., Tanaka, A., Uehiro, T., Shibata, Y., Morita, M. and Ohno, T., 2000. Pre-bomb marine reservoir ages in the western north Pacific: Preliminary result on Kyoto University collection. *Nuclear Instruments & Methods in Physics Research Section B- Beam Interactions with Materials and Atoms,* **172** 377-381.

Zahn, R., Winn, K. and Sarnthein, M., 1986. Benthic foraminiferal d13C and accumulation rates of organic carbon: Uvigerina peregrina group and Cibicidoides wuellerstorfi. *Paleoceanography,* **1** (1): 27-42.

Zeebe, R.E., 1999. An explanation of the effect of seawater carbonate concentration on foraminiferal oxygen isotopes. *Geochimica et Cosmochimica Acta,* **63** (13-14): 2001-2007.

Zielinski, G.A., 2000. Use of paleo-records in determining variability within the volcanism–climate system. *Quaternary Science Reviews,* **19** (1-5): 417-438.

Appendix 8 - Information for Loch Sunart sample sites selected for foraminiferal analyses. In addition to benthic foraminiferal abundance data, species % abundance data, and species diversity data; environmental data such as bottom water temperature (BWT) and salinity (BWS), sediment grain size composition and organic matter content are also provided.

Station	Latitude	Longitude	Depth (m)	Collection date	Summer BWT	Winter BWT	Summer BWS	Winter BWS	% Organic matter	% CaCO3	% Clay	% Silt	% Sand	% > 125 microns	Mean grain size	Median grain size	Modal grain size	Skewness:	Kurtosis:	d10:	d50:	d90:
LS-53	56.6851	-5.5466	5	Jun-01	12.0		31.0		1.4	3.0	0.0	2.9	97.1	92.5	732.8	605.3	663.9	0.7	-0.5	165.1	605.3	1542.7
LS-68	56.6865	-5.5691	11	Jun-01	12.8	7.3	30.7	32.4	3.8		0.7	23.9	75.5	56.9	290.9	164.7	168.8	2.4	6.0	21.7	164.7	693.9
LS-147	56.6872	-5.5818	16	Jun-02	12.6	7.3	31.1	32.5	7.0	3.2	2.4	56.4	41.2	22.0	93.7	44.4	96.5	4.1	23.2	6.2	44.4	217.4
LS-72	56.6866	-5.5839	30	Jun-01	12.4	7.3	32.5	32.5	3.4	2.4	0.5	18.1	81.5	72.9	648.2	528.3	1162.3	0.6	-0.8	24.5	528.3	1517.3
LS-149	56.6842	-5.6216	59	Jun-02	12.1	7.3	33.0	32.7	18.0	9.7	3.5	78.2	18.3	7.3	42.6	21.1	18.0	3.6	16.6	4.5	21.1	99.8
LS-211	56.6825	-5.6338	93	Jun-02	11.9	7.3	33.1	32.9	6.7	2.2	1.8	26.9	71.3	50.3	285.1	151.8	168.8	2.6	6.0	20.2	151.8	659.8
LS-110	56.6796	-5.6469	53	Jul-01	12.3	7.3	33.1	32.8	2.5	9.5	1.0	17.3	81.7	79.5	625.6	489.2	1026.0	0.7	-0.5	14.2	489.2	1447.7
LS-112	56.6807	-5.6499	45	Jul-01	12.3	7.3	33.1	32.8	2.5	9.5	1.9	31.7	66.3	58.0	261.6	159.5	185.3	2.7	7.9	7.4	159.5	574.5
LS-76	56.6930	-5.6857	12	Jun-01	12.3	7.4	31.4	32.9	4.0	1.8	2.1	40.0	57.9	31.5	136.3	81.8	105.9	2.4	7.1	6.6	81.8	328.9
LS-2	56.6925	-5.7064	64	Jun-00	11.8		33.6		11.8	17.5	2.6	48.4	49.1	34.3	135.0	69.0	254.7	1.6	2.5	6.0	69.0	364.8
LS-80	56.6965	-5.7080	44	Jun-01	11.8	7.3	33.6	33.5	12.1	9.3	2.6	50.0	47.4	30.2	133.2	59.9	234.6	2.0	4.5	5.9	59.9	371.1
LS-173	56.7020	-5.7261	31	Jun-02	11.9	7.4	33.6	33.5	4.5	4.5	5.8	54.9	39.3	23.4	75.3	28.1	116.3	2.1	5.2	3.1	28.1	205.9
LS-176	56.7050	-5.7372	46	Jun-02	11.8	7.4	33.6	33.5	8.3	5.9	7.2	67.3	25.6	14.3	57.5	15.7	9.4	3.4	14.3	2.7	15.7	156.8
LS-45	56.6993	-5.7731	72	Apr-01	11.6	7.3	33.8	33.6	13.8	7.6	2.5	46.7	50.8	38.4	136.7	78.2	274.9	1.1	0.5	6.1	78.2	358.6
LS-210	56.6988	-5.7753	70	Jun-02	11.6	7.3	33.8	33.6	10.1	7.1	6.1	86.2	7.8	3.2	24.2	12.9	13.6	3.9	18.9	3.1	12.9	52.7
LS-101	56.6874	-5.8059	23	Jul-01	12.2	7.4	33.7	33.5	5.3	8.3	3.6	41.5	54.9	42.0	346.1	82.2	1800.7	1.7	1.5	4.9	82.2	1288.7
LS-201	56.6829	-5.8096	68	Jun-02	11.7		33.6		10.9	9.5	7.1	72.3	20.5	8.2	71.2	31.9	45.8	2.6	7.6	3.4	31.9	195.2
LS-202	56.6795	-5.8099	97	Jun-02	11.6	7.4	33.8	33.7	12.0	8.2	7.4	85.4	7.1	2.4	22.1	11.6	11.3	3.8	17.9	2.6	11.6	49.8
LS-200	56.6833	-5.8128	55	Jun-02	11.8	7.5	33.8	33.6	11.3	8.4	6.6	74.6	18.8	6.3	57.9	31.1	41.7	2.9	10.9	3.6	31.1	143.7
LS-90	56.6740	-5.8130	36	Jul-01	12.0	7.5	33.8	33.5	5.3	8.3	7.1	67.1	25.8	14.2	57.4	17.6	9.4	3.2	12.9	2.7	17.6	156.8
LS-199	56.6840	-5.8135	17	Jun-02	12.4	7.4	33.2	33.3	1.5	10.8	3.6	41.5	54.9	42.0	346.1	82.2	1800.7	1.7	1.5	4.9	82.2	1288.7
LS-198	56.6660	-5.8434	121	Jun-02	11.6	7.4	33.8	33.7	6.8	4.3	5.3	66.7	28.1	17.6	61.7	18.7	12.0	2.6	7.9	3.5	18.7	185.1
LS-41	56.6701	-5.8649	65	Apr-01	11.9	7.4	33.9	33.6	6.1	15.8	2.8	46.1	51.2	37.2	81.4	0.7	171.2	3.5	6.2	81.4	372.4	
LS-197	56.6736	-5.8658	111	Jun-02	11.7	7.4	33.9	33.6	6.1	15.8	3.1	32.8	64.1	59.0	646.1	471.0	1909.0	0.6	-1.0	9.0	471.0	1631.0
LS-192	56.6727	-5.9185	90	Jun-02	11.9	7.5	34.0	33.9	4.5	14.5	3.1	32.8	64.1	59.0	646.1	471.0	1909.0	0.6	-1.0	9.0	471.0	1631.0
LS-193	56.6669	-5.9198	51	Jun-02	12.3	7.5	34.1	33.7	3.9	9.5	3.0	29.8	67.3	64.1	307.0	244.2	324.3	1.2	1.3	6.0	244.2	758.6
LS-189	56.6706	-5.9467	75	Jun-02	12.3	7.5	34.2	33.9	3.6	7.4	4.0	35.0	61.0	57.9	323.0	197.5	245.2	1.9	3.2	4.4	197.5	1017.3
LS-184	56.6498	-5.9806	17	Jun-02	12.4	7.5	33.8	33.8	4.3	25.7	1.0	9.9	89.1	83.7	834.5	787.6	1584.0	0.3	-1.2	94.3	787.6	1692.0
LS-27	56.6622	-5.9920	113	Apr-01	12.4	7.5	34.1	33.9	11.1	11.9	3.0	51.0	46.0	30.1	114.3	57.8	208.8	2.2	7.5	5.7	57.8	293.5
LS-181	56.6804	-6.0117	36	Jun-02	12.5	7.5	34.1	33.8	5.5	8.6	7.2	64.0	28.8	20.4	80.5	17.2	9.4	3.0	9.9	2.7	17.2	242.1
LS-22	56.6722	-6.0135	45	Apr-01	12.5	7.5	34.2	34.0	9.4	11.3	3.4	59.1	37.5	19.3	76.9	39.2	74.5	2.0	4.5	5.0	39.2	205.5

Station	% Broken specimens	% Stained specimens	No. benthic foraminifera	No planktonic	Specimens/g	Calcareous specimens/g	Specimens/cm3	Calcareous specimens/cm3	Shannon H	Simpson 1-D	Fisher alpha	% Agglutinated	% Porcelaneous	% Hyaline	Adercotryma glomeratum	Agglutinated Ind	Agglutinated sp. Large fora	Alveolophragmium crassim	Ammoscalaria runiana	Ammoscalaria pseudospiral	Cribrostomoides cf. nitida	Cribrostomoides jefferysi
53	3	83	163	0	652	652	10	10	0.1	0.0	0.7	0.0	0.0	100.0	0.0	0.0	0.0	0.0	0.0	0.0	0.0	0.0
68	7	1	321	0	14675	1463	117	12	1.2	0.4	6.7	90.0	0.3	9.7	0.3	5.0	0.0	0.0	0.0	0.3	0.0	0.3
147	11	4	317	0	31950	907	197	6	1.0	0.4	6.4	97.2	0.0	2.8	0.0	1.0	2.5	0.0	8.8	0.0	0.0	0.6
72	7	2	324	0	6246	1137	49	9	1.9	0.6	10.0	81.6	0.3	18.1	0.6	0.6	0.0	0.0	5.9	0.0	0.0	1.3
149	35	30	311	2	2686	409	9	1	1.2	0.4	6.1	84.9	0.3	14.8	0.6	1.6	0.3	0.0	3.2	0.0	0.0	0.0
211	25	5	363	0	9014	1713	78	15	2.0	0.8	9.2	81.0	0.3	18.7	0.3	0.3	2.5	0.0	30.3	0.0	0.0	0.6
110	57	2	343	1	8831	6456	152	111	2.0	0.7	9.0	27.1	3.5	69.4	0.0	0.6	0.9	0.0	2.6	0.0	0.0	0.0
112	37	4	352	0	6931	3623	116	61	2.5	0.9	9.0	46.4	2.0	51.6	0.0	1.7	0.0	0.0	9.9	2.3	0.0	0.0
76	1	11	285	0	19390	5579	211	61	2.2	0.7	10.6	70.6	0.7	28.7	4.3	0.4	0.4	0.4	2.5	0.4	0.0	0.0
2			353	0	24416	18537			3.3	0.9	19.7	24.1	2.8	73.1	1.7	0.0	0.0	0.0	0.8	0.0	0.0	0.0
80	34	3	328	0	24764	17063	89	61	2.7	0.9	12.0	30.9	1.2	67.9	2.4	1.5	0.0	0.0	2.4	0.0	0.0	0.0
173	47	1	566	0	168139	119717	1064	758	2.6	0.9	9.5	28.8	0.4	70.8	0.4	0.2	0.5	0.0	4.6	0.0	0.0	0.0
176	46	1	508	0	260060	184294	1343	951	2.3	0.8	11.6	29.1	0.0	70.9	0.2	0.2	0.6	0.0	1.6	0.0	0.0	0.0
45	29	25	454	4	8100	6246	170	131	3.1	0.9	17.2	23.4	2.0	74.6	5.5	0.2	0.2	0.0	5.7	0.0	0.0	0.0
210	72	2	419	0	29434	25149	239	204	2.2	0.8	6.1	14.6	0.0	85.4	0.0	1.0	0.0	0.0	0.2	0.0	0.0	0.0
101	37	4	394	0	20225	13347	285	188	2.7	0.9	13.1	34.0	3.6	62.4	0.0	0.3	0.0	0.0	1.8	0.0	0.0	0.0
201	26	5	459	0	12344	9439	45	35	2.3	0.8	11.6	23.5	0.2	76.3	2.6	0.2	0.0	0.0	2.4	0.0	0.0	0.0
202	30	32	348	2	6436	5208	25	20	2.8	0.9	11.7	19.5	2.9	77.6	4.3	0.6	0.3	0.0	1.7	0.0	0.0	0.0
200	40	2	409	0	72192	48187	355	237	2.8	0.9	15.1	31.2	0.0	68.8	5.3	1.3	0.8	0.0	1.3	0.0	0.0	0.0
90	24	3	340	0	1485	1083	15	11	2.6	0.9	14.3	27.1	0.6	72.4	2.4	0.0	0.0	0.0	0.0	0.0	0.3	0.3
199	66	2	351	0	85052	78751	945	875	2.0	0.7	10.1	7.4	0.6	92.0	0.0	0.3	0.0	0.0	0.0	0.0	0.0	0.0
198	41	3	402	0	109424	77305	1043	737	2.3	0.9	8.2	29.4	0.0	70.6	0.5	0.0	0.0	0.0	3.2	0.0	0.0	0.0
41	46	4	468	0	20464	13512	527	348	2.8	0.9	12.6	34.0	1.1	65.0	1.5	0.0	0.0	0.0	4.1	0.0	0.0	0.0
197	29	19	338	0	2779	1710	105	65	2.7	0.9	13.9	38.5	7.1	54.4	0.9	0.0	0.0	0.0	5.9	0.0	0.0	0.0
192	41	4	451	0	8569	6213	146	106	2.6	0.9	12.1	27.5	3.8	68.7	0.4	0.2	0.0	0.0	1.8	0.0	0.0	0.0
193	60	1	393	0	77552	59200	809	617	2.1	0.8	9.3	23.7	1.8	74.6	0.3	0.0	0.0	0.0	0.8	0.0	0.0	0.0
189	53	1	439	0	65128	50886	824	643	2.1	0.8	8.3	21.9	5.0	73.1	0.5	0.2	0.0	0.0	0.0	0.0	0.0	0.0
184	55	1	486	1	32762	30195	734	676	2.2	0.7	13.2	8.0	5.1	86.8	0.0	0.6	0.0	0.0	0.0	0.0	0.0	0.0
27	16	12	526	40	18556	17258	259	241	3.6	1.0	22.6	14.3	2.7	83.1	0.0	1.7	0.0	0.0	1.0	0.0	0.0	0.0
181	27	2	406	0	148055	117058	1328	1050	2.8	0.9	13.3	20.9	2.2	76.8	0.5	0.5	0.0	0.0	2.5	0.0	0.0	0.0
22	30	1	378	0	5030	4032	23	19	2.3	0.8	7.3	19.8	0.0	80.2	2.6	0.0	0.0	0.0	3.2	0.0	0.0	0.0

Station	Cribrostomoides kosterensi	Cribrostomoides spp.	Cornuspira involvens	Difflugia oblonga	Eggerella artica	Eggerelloides scaber	Haplophragmoides bradyi	Haplophragmoides fragile	Haplophragmoides glomera	Haplophragmoides membra	Haplophragmoides sp. A (H	Haplophragmoides sp.	Hippocrepinna spp.	Jadammina macrasens	Marsipella sp. A (Haynes)	Millaminna fusca	Paratrochammina haynesi	Psammosphaera bowmanni	Quinqueloculina agglutinat	Recurvoides trochamminfor	Rhabdammina sp.	Rheophax arctica
53	0.0	0.0	0.0	0.0	0.0	0.0	0.0	0.0	0.0	0.0	0.0	0.0	0.0	0.0	0.0	0.0	0.0	0.0	0.0	0.0	0.0	0.0
68	0.0	0.0	0.0	0.0	0.0	75.1	0.0	0.0	0.0	0.0	0.0	0.3	0.0	0.0	0.0	0.9	0.0	0.0	0.0	0.0	0.0	0.0
147	0.6	0.0	0.3	0.0	0.0	78.5	0.0	0.0	0.0	0.0	0.0	0.0	0.0	0.0	0.0	0.3	0.3	0.3	0.0	0.9	0.0	0.0
72	0.3	0.3	3.4	0.0	0.0	59.1	0.0	0.0	0.0	0.3	0.0	0.0	0.0	0.0	0.0	0.0	0.0	0.0	0.3	1.3	0.6	0.0
149	0.0	0.6	0.0	0.0	0.0	74.9	0.0	0.0	0.0	0.0	1.0	0.0	0.0	0.0	0.0	0.0	0.0	0.0	0.0	0.6	0.0	0.0
211	0.0	0.0	0.0	0.0	0.0	38.3	0.0	0.0	0.0	0.0	0.0	0.0	0.0	0.0	0.0	0.3	0.0	0.3	0.0	1.1	0.8	0.0
110	0.9	0.0	0.0	0.0	0.0	6.1	0.0	0.0	0.0	0.0	0.0	0.0	0.0	0.0	0.0	0.0	0.0	0.0	0.0	0.3	0.3	0.0
112	3.2	0.0	0.0	0.0	0.0	21.9	0.0	0.0	0.0	0.0	0.0	0.0	0.0	0.0	0.0	0.0	0.0	0.0	0.0	0.3	0.3	0.0
76	0.4	0.0	0.0	0.0	0.0	51.6	0.0	0.0	0.0	0.0	0.0	0.0	0.0	0.0	0.0	0.0	0.0	0.0	0.4	3.6	1.4	0.4
2	0.0	0.0	0.3	0.0	0.0	3.1	0.0	0.3	0.3	0.0	0.0	0.0	0.0	0.3	0.0	0.0	0.0	0.0	0.0	0.3	0.0	0.0
80	0.0	0.0	0.3	0.0	0.0	8.9	2.4	0.0	0.0	0.0	1.8	0.0	0.0	0.0	0.0	0.0	0.0	0.0	0.0	0.0	0.3	0.0
173	0.0	0.0	0.0	0.0	0.0	1.4	0.0	0.0	0.0	0.0	0.0	0.0	0.0	0.0	0.0	0.0	0.0	0.0	0.0	0.0	0.0	0.0
176	0.0	0.0	0.0	0.0	0.0	2.2	0.2	0.0	0.0	0.0	0.0	0.0	0.0	0.2	0.0	0.2	0.0	0.0	0.0	0.2	0.2	0.0
45	0.0	0.2	0.0	0.0	0.0	4.2	0.4	0.0	0.0	0.0	0.0	0.0	0.0	0.0	0.0	0.0	0.0	0.2	0.0	1.5	0.2	0.0
210	0.5	0.0	0.0	0.0	0.0	11.2	0.0	0.0	0.0	0.0	0.0	0.0	0.0	0.0	0.0	0.0	0.0	0.0	0.2	0.0	0.0	0.0
101	0.0	0.0	0.3	0.0	0.0	4.8	0.0	0.0	0.0	0.0	1.0	0.0	0.5	0.0	0.3	0.0	0.0	0.0	0.0	0.0	0.5	0.0
201	0.0	0.0	0.0	0.0	0.2	5.9	0.4	0.0	0.0	0.0	0.0	0.0	0.0	0.0	0.0	0.0	0.0	0.0	0.0	1.3	0.0	0.0
202	0.0	0.0	0.0	0.0	0.0	3.7	2.6	0.0	0.0	0.0	0.0	0.0	0.0	0.0	0.0	0.0	0.0	0.0	0.0	3.2	0.0	0.0
200	0.0	0.0	0.0	0.0	0.0	7.1	0.0	0.0	0.0	0.0	0.0	0.0	0.0	0.0	0.0	0.3	0.0	0.0	0.0	1.0	1.5	0.0
90	0.0	0.0	0.0	0.0	0.0	11.8	0.0	0.0	0.0	0.0	0.0	0.0	0.0	0.0	0.0	0.6	0.3	0.0	0.0	0.3	0.6	0.0
199	0.0	0.0	0.3	0.0	0.0	0.9	0.0	0.0	0.0	0.0	0.0	0.0	0.0	0.0	0.0	0.0	0.0	0.0	0.0	0.0	0.3	0.0
198	0.0	0.0	0.0	0.0	0.0	4.2	0.0	0.0	0.0	0.0	0.0	0.0	0.0	0.0	0.0	0.0	0.0	0.2	0.2	0.0	0.0	0.0
41	0.0	0.0	0.0	0.0	0.0	8.3	0.0	0.0	0.0	0.0	0.0	0.0	0.0	0.0	0.0	0.2	0.0	0.0	0.0	0.4	0.9	0.0
197	0.6	0.0	0.0	0.0	0.0	1.5	0.0	0.0	0.0	0.0	0.0	0.0	0.0	0.0	0.0	0.0	0.0	0.0	0.3	2.1	0.3	0.0
192	0.0	0.0	0.0	0.0	0.0	4.4	0.0	0.0	0.0	0.0	0.0	0.0	0.0	0.0	0.0	0.0	0.0	0.2	0.2	0.0	0.0	0.0
193	0.0	0.0	0.0	0.0	0.0	1.0	0.0	0.0	0.0	0.0	0.0	0.0	0.0	0.0	0.0	0.0	0.0	0.0	0.0	0.3	0.0	0.0
189	0.0	0.0	0.0	0.0	0.0	1.1	0.0	0.0	0.0	0.0	0.0	0.0	0.0	0.0	0.0	0.0	0.0	0.0	0.0	0.0	0.0	0.0
184	0.0	0.0	0.0	0.0	0.0	0.8	0.0	0.0	0.0	0.0	0.0	0.0	0.0	0.0	0.0	0.0	0.0	0.0	0.0	0.2	0.0	0.0
27	0.4	0.0	0.0	0.0	0.0	4.9	0.0	0.0	0.0	0.0	0.0	0.0	0.0	0.0	0.0	0.0	0.2	0.2	0.0	1.1	0.4	0.0
181	0.0	0.0	0.0	0.0	0.0	5.4	0.0	0.0	0.0	0.0	0.0	0.0	0.0	0.0	0.0	0.0	0.0	0.0	0.0	0.0	0.2	0.0
22	0.0	0.0	0.0	0.3	0.0	8.5	0.0	0.0	0.0	0.0	0.0	0.0	0.0	0.0	0.0	0.0	0.0	0.0	0.0	0.0	0.3	0.0

Station	Rheophax scotti	Rheophax spp.	Rheophax subfusiformis	Spiroplectammina earlandi	Spiroplectammina wrightii	Textularia sp.	Textularia earlandi	Trochammina adaptera	Trochammina astrifica	Trochammina cf. stellata	Trochammina cf. parvus	Trochammina cf. rotalis	Trochammina intermediate	Trochammina cf inflata	Trochammina ochrea	Trochammina ind	Vernueilla advena	Cornuloculina balkwilli	Masslina secans	Milionella subrotunda	Miliolina ind	Prygo depressa
53	0.0	0.0	0.0	0.0	0.0	0.0	0.0	0.0	0.0	0.0	0.0	0.0	0.0	0.0	0.0	0.0	0.0	0.0	0.0	0.0	0.0	0.0
68	1.2	0.0	5.3	0.0	0.3	0.0	0.0	0.0	0.0	0.0	0.0	0.0	0.0	0.3	0.0	0.6	0.0	0.0	0.0	0.0	0.0	0.0
147	0.0	0.6	1.6	0.0	0.0	0.0	0.0	0.3	0.0	0.0	0.0	0.0	0.0	0.0	0.0	0.3	0.0	0.0	0.0	0.0	0.0	0.0
72	0.0	0.0	5.0	1.3	0.6	0.0	0.0	0.3	0.0	0.0	0.0	0.3	0.0	0.0	0.0	0.0	0.0	0.0	0.0	0.0	0.0	0.0
149	0.0	0.0	0.0	1.0	0.0	0.0	0.0	0.0	0.0	0.0	0.0	0.0	0.0	0.0	0.3	0.3	0.3	0.0	0.0	0.0	0.0	0.0
211	1.7	0.0	1.1	2.5	0.6	0.3	0.0	0.0	0.0	0.0	0.0	0.0	0.0	0.0	0.0	0.3	0.0	0.0	0.0	0.0	0.0	0.0
110	0.0	0.0	1.2	0.0	14.3	0.0	0.0	0.0	0.0	0.0	0.0	0.0	0.0	0.0	0.0	0.0	0.0	0.0	0.0	0.0	0.3	0.0
112	0.0	0.0	1.7	0.9	4.1	0.0	0.0	0.0	0.0	0.0	0.0	0.0	0.0	0.0	0.0	0.0	0.0	0.0	0.0	0.0	2.0	0.0
76	0.0	0.0	2.9	0.0	0.7	0.0	0.7	0.4	0.0	0.0	0.0	0.0	0.0	0.0	0.0	0.0	0.0	0.0	0.0	0.4	0.0	0.0
2	0.3	0.3	0.0	0.0	14.7	0.0	0.6	0.0	0.6	0.0	0.0	0.0	0.0	0.0	0.0	0.0	0.6	0.0	0.0	0.0	0.3	0.0
80	0.0	0.0	2.1	0.6	7.0	0.0	0.0	0.3	0.0	0.3	0.0	0.0	0.0	0.0	0.0	0.3	0.0	0.0	0.0	0.0	0.0	0.0
173	0.0	0.0	0.0	0.0	21.7	0.0	0.0	0.0	0.0	0.0	0.0	0.0	0.0	0.0	0.0	0.0	0.0	0.0	0.0	0.0	0.0	0.0
176	0.0	0.0	0.0	0.0	23.4	0.0	0.0	0.0	0.0	0.0	0.0	0.0	0.0	0.0	0.0	0.0	0.0	0.0	0.0	0.0	0.0	0.0
45	0.0	0.0	0.7	0.2	4.0	0.0	0.0	0.0	0.0	0.0	0.0	0.0	0.0	0.0	0.0	0.0	0.0	0.0	0.0	0.0	0.2	0.2
210	0.0	0.0	0.0	0.2	1.2	0.0	0.0	0.0	0.0	0.0	0.0	0.0	0.0	0.0	0.0	0.0	0.0	0.0	0.0	0.0	0.0	0.0
101	0.0	0.0	0.0	0.0	24.6	0.0	0.0	0.0	0.0	0.0	0.0	0.0	0.0	0.0	0.0	0.0	0.0	0.0	0.0	0.0	0.0	0.0
201	0.0	0.0	0.4	0.0	9.6	0.0	0.0	0.2	0.0	0.0	0.0	0.0	0.2	0.0	0.0	0.0	0.0	0.0	0.0	0.2	0.0	0.0
202	0.3	0.0	0.0	0.0	1.4	0.0	0.0	0.9	0.3	0.0	0.0	0.0	0.0	0.0	0.3	0.0	0.0	0.0	0.0	0.0	0.0	0.0
200	0.0	0.0	1.3	0.3	10.6	0.0	0.0	0.3	0.0	0.0	0.0	0.0	0.0	0.3	0.0	0.0	0.3	0.0	0.0	0.0	0.0	0.0
90	0.0	0.0	0.6	0.6	9.1	0.0	0.0	0.0	0.0	0.0	0.0	0.0	0.0	0.0	0.0	0.0	0.3	0.0	0.0	0.6	0.0	0.0
199	0.0	0.0	0.0	0.3	5.4	0.0	0.0	0.0	0.0	0.0	0.0	0.0	0.0	0.0	0.0	0.0	0.0	0.0	0.0	0.0	0.0	0.0
198	0.0	0.0	0.5	0.0	20.1	0.0	0.0	0.2	0.0	0.0	0.0	0.0	0.0	0.0	0.0	0.0	0.0	0.0	0.0	0.0	0.0	0.0
41	0.0	0.2	0.4	1.5	15.8	0.0	0.0	0.6	0.0	0.0	0.0	0.0	0.0	0.0	0.0	0.0	0.0	0.0	0.0	0.0	0.2	0.0
197	0.0	0.0	0.6	0.0	26.0	0.0	0.0	0.3	0.0	0.0	0.0	0.0	0.0	0.0	0.0	0.0	0.0	0.0	0.0	0.0	1.5	0.0
192	0.0	0.2	0.4	0.2	19.1	0.0	0.0	0.0	0.0	0.0	0.2	0.0	0.0	0.0	0.0	0.0	0.0	0.0	0.0	0.7	0.2	0.0
193	0.0	0.0	0.0	0.0	21.1	0.0	0.0	0.0	0.0	0.0	0.0	0.0	0.0	0.0	0.0	0.0	0.3	0.0	0.3	0.0	0.0	0.0
189	0.0	0.2	0.0	0.0	19.8	0.0	0.0	0.0	0.0	0.0	0.0	0.0	0.0	0.0	0.0	0.0	0.0	0.0	0.0	0.0	2.5	0.0
184	0.0	0.0	0.0	0.2	5.1	0.0	0.0	0.2	0.2	0.0	0.0	0.0	0.0	0.4	0.0	0.2	0.0	0.0	0.6	0.0	0.4	0.0
27	0.0	0.0	0.4	0.4	0.8	0.0	0.0	0.4	0.0	0.0	0.0	0.0	0.0	0.4	0.4	1.5	0.0	0.2	0.0	0.0	0.6	0.0
181	0.0	0.0	0.7	0.2	10.8	0.0	0.0	0.0	0.0	0.0	0.0	0.0	0.0	0.0	0.0	0.0	0.0	0.0	0.0	0.5	0.5	0.2
22	0.0	0.0	1.3	0.3	3.2	0.0	0.0	0.0	0.3	0.0	0.0	0.0	0.0	0.0	0.0	0.0	0.0	0.0	0.0	0.0	0.0	0.0

Station	Prygo willamsoni	Prygo sp.	Quinqueloculina aspera	Quinqueloculina bicornis	Quinqueloculina cf. cliarens	Quinqueloculina seminlum	Quinqueloculina stalkeri	Quinqueloculina spp.	Spiroloculina rotunda	Triloculina trihedra	Acervulina inhaerens	Ammonia becarrii	Amphicoryna scalaris	Anomalina globulosa	Asterigerinata mamilla	Astrononion gallowayi	Bolivina albatrossi	Bolivina cf. variablis	Bolivina cf. skagerrakensis	Bolivina cf. striatula	Bolivina pseudoplicata	Bolivina pseudopunctata
53	0.0	0.0	0.0	0.0	0.0	0.0	0.0	0.0	0.0	0.0	0.0	0.0	0.0	0.0	0.0	0.0	0.0	0.0	0.0	0.0	0.0	0.0
68	0.0	0.0	0.0	0.0	0.0	0.3	0.0	0.0	0.0	0.0	0.0	2.8	0.0	0.0	0.0	0.0	0.0	0.0	0.0	0.0	0.0	0.3
147	0.0	0.0	0.0	0.0	0.0	0.0	0.0	0.0	0.0	0.0	0.0	0.0	0.0	0.0	0.3	0.0	0.0	0.0	0.0	0.0	0.0	0.0
72	0.0	0.0	0.0	0.0	0.0	0.0	0.0	0.3	0.0	0.0	0.0	5.0	0.0	0.0	2.5	0.0	0.0	0.0	0.0	0.0	0.0	0.0
149	0.0	0.0	0.0	0.0	0.0	0.3	0.0	0.0	0.0	0.0	0.0	5.8	0.0	0.0	0.0	0.0	0.0	0.0	0.0	0.0	0.0	0.0
211	0.0	0.0	0.0	0.0	0.0	0.3	0.0	0.0	0.0	0.0	0.0	8.8	0.3	0.0	0.3	0.0	0.0	0.0	0.0	0.0	0.0	0.8
110	0.0	0.0	0.0	0.0	0.0	3.2	0.0	0.0	0.0	0.0	0.3	5.5	0.0	0.0	6.1	0.0	0.0	0.0	0.0	0.0	0.3	0.3
112	0.0	0.0	0.0	0.0	0.0	0.0	0.0	0.0	0.0	0.0	0.6	24.2	0.0	0.0	6.4	0.0	0.0	0.0	0.0	0.0	0.0	0.0
76	0.0	0.0	0.0	0.0	0.0	0.0	0.0	0.4	0.0	0.0	0.0	7.2	0.0	0.0	0.0	0.0	0.0	0.0	0.0	0.0	0.0	0.4
2	0.0	0.0	0.0	0.0	0.0	0.8	1.4	0.0	0.0	0.3	0.0	4.5	0.0	0.0	1.1	0.6	0.0	0.0	0.0	0.3	2.8	1.7
80	0.0	0.0	0.0	0.0	0.3	0.0	0.0	0.9	0.0	0.0	0.0	5.5	0.3	0.0	1.8	0.0	0.0	0.0	0.0	0.0	0.9	0.9
173	0.2	0.0	0.0	0.0	0.0	0.2	0.0	0.0	0.0	0.0	0.2	12.9	0.0	0.0	3.2	0.0	0.0	0.0	0.2	0.0	4.2	0.7
176	0.0	0.0	0.0	0.0	0.0	0.0	0.0	0.0	0.0	0.0	0.0	7.1	0.0	0.0	0.2	0.0	0.0	0.2	0.0	0.0	0.8	0.6
45	0.2	0.0	0.0	0.0	0.0	1.3	0.0	0.0	0.0	0.0	0.0	3.3	0.0	0.0	0.0	0.0	0.0	0.0	0.0	0.0	2.2	2.9
210	0.0	0.0	0.0	0.0	0.0	0.0	0.0	0.0	0.0	0.0	0.0	17.4	0.0	0.0	15.0	0.0	0.0	0.0	0.0	0.0	0.0	0.0
101	0.0	0.0	0.0	0.0	0.3	1.8	0.3	1.3	0.0	0.0	2.0	3.0	0.0	0.0	14.0	0.0	0.3	0.0	0.0	0.0	0.5	0.5
201	0.0	0.0	0.0	0.0	0.0	0.0	0.0	0.0	0.0	0.0	0.0	2.8	0.7	0.0	0.4	0.0	0.0	0.0	0.0	0.0	0.0	0.2
202	0.0	0.0	0.0	0.0	0.0	2.6	0.0	0.0	0.0	0.3	0.0	3.2	0.0	0.0	0.0	0.0	0.0	0.0	0.0	0.0	1.7	4.3
200	0.0	0.0	0.0	0.0	0.0	0.0	0.0	0.0	0.0	0.0	0.0	3.0	0.0	0.0	0.8	0.0	0.0	0.0	0.0	0.0	1.0	1.5
90	0.0	0.0	0.0	0.0	0.0	0.0	0.0	0.0	0.0	0.0	0.0	4.1	0.3	0.0	0.6	0.3	0.9	0.0	0.0	0.0	0.9	0.3
199	0.0	0.0	0.0	0.0	0.0	0.0	0.0	0.6	0.0	0.0	0.0	4.0	0.0	0.0	49.6	0.0	0.0	0.0	0.0	0.0	0.9	0.0
198	0.0	0.0	0.0	0.0	0.0	0.0	0.0	0.0	0.0	0.0	0.0	20.6	0.0	0.0	0.7	0.0	0.0	0.0	0.0	0.0	0.0	0.0
41	0.0	0.0	0.0	0.0	0.0	0.0	0.0	0.6	0.2	0.0	0.2	12.2	0.4	0.0	2.1	0.0	0.0	0.0	0.0	0.0	0.2	0.4
197	0.3	0.0	0.0	0.9	0.0	3.3	0.0	0.3	0.6	0.3	0.0	8.3	0.0	0.0	0.9	0.0	0.0	0.0	0.0	0.6	0.0	0.3
192	0.0	0.0	0.0	0.4	0.0	2.2	0.0	0.0	0.2	0.0	1.1	14.0	0.0	0.0	3.1	0.4	0.0	0.0	0.0	0.0	0.0	0.0
193	0.0	0.0	0.0	0.3	0.0	1.3	0.0	0.0	0.0	0.0	0.0	19.3	0.0	0.0	4.3	0.0	0.0	0.0	0.0	0.0	0.0	0.3
189	0.0	0.2	0.0	0.0	0.0	2.1	0.0	0.2	0.0	0.0	0.0	31.4	0.0	0.0	0.9	0.0	0.0	0.0	0.0	0.0	0.2	0.0
184	0.0	0.0	0.0	0.4	0.0	3.1	0.2	0.0	0.4	0.0	8.8	1.4	0.0	0.0	7.8	0.0	0.0	0.0	0.0	0.0	0.2	0.8
27	0.0	0.0	0.0	0.0	0.0	1.1	0.0	0.6	0.0	0.4	0.0	4.6	0.4	0.0	0.8	0.2	0.0	0.0	0.0	0.0	3.0	3.2
181	0.0	0.0	0.7	0.0	0.0	0.2	0.0	0.0	0.0	0.0	0.0	18.5	0.2	0.0	5.9	0.0	0.0	0.0	0.0	0.0	0.5	0.0
22	0.0	0.0	0.0	0.0	0.0	0.0	0.0	0.0	0.0	0.0	0.0	25.4	0.0	0.3	0.8	0.0	0.0	0.0	0.0	0.0	0.0	0.0

Station	Bolivina pygmae	Bolivina spathula	Bolivina spp.	Bolivina variablis	Bucella frigida	Bulimina elongata	Bulimina gibba	Bulimina marginata	Buliminella elegantissima	Bulimina spp.	Bulimina sp. trigonal	Cassidulina carinata	Cassidulina cf. bradyi	Cassudilina laegivata	Cassudilina obtusa	Cassidulina reniforme	Cassidulina spp.	Cibicides lobatulus	Dentalina spp.	Discorbis chasteri	Elphidium albiumbilicatum	Elphidium arctica & asklunc
53	0.0	0.0	0.0	0.0	0.0	0.0	0.0	0.0	0.0	0.0	0.0	0.0	0.0	0.0	0.0	0.0	0.0	0.0	0.0	0.0	0.0	0.0
68	0.0	0.0	0.0	0.0	0.0	0.0	0.0	0.6	0.3	0.0	0.0	0.0	0.0	0.0	0.0	0.0	0.0	0.3	0.0	0.0	0.0	0.0
147	0.0	0.0	0.0	0.0	0.0	0.0	0.3	0.0	0.3	0.0	0.0	0.0	0.0	0.0	0.0	0.0	0.0	0.0	0.0	0.0	0.0	0.0
72	0.0	0.0	0.0	0.0	0.0	0.3	0.3	1.3	0.6	0.0	0.0	0.0	0.0	0.0	0.0	0.0	0.0	2.2	0.0	0.0	0.0	0.0
149	0.0	0.0	0.0	0.0	0.0	0.3	0.3	5.1	0.0	0.3	0.0	0.0	0.0	0.0	0.0	0.0	0.0	0.6	0.0	0.0	0.0	0.0
211	0.0	0.0	0.0	0.0	0.0	0.6	0.0	2.8	0.3	0.0	0.0	0.0	0.0	0.0	0.0	0.0	0.0	1.7	0.0	0.0	0.0	0.0
110	0.0	0.0	0.0	0.3	0.0	0.0	0.0	0.3	0.0	0.0	0.0	0.0	0.0	0.0	0.0	0.3	0.0	48.7	0.0	0.0	0.0	0.0
112	0.0	0.3	0.0	0.0	0.0	0.0	0.3	2.3	0.0	0.0	0.0	0.0	0.0	0.0	0.0	0.0	0.0	7.6	0.0	0.0	0.0	0.0
76	0.0	0.4	0.0	0.0	0.0	0.0	1.1	1.1	0.0	0.0	0.0	0.0	0.0	0.0	0.0	0.0	0.0	0.4	0.0	0.0	0.0	0.0
2	0.3	0.6	0.0	4.8	0.8	1.7	0.3	13.9	0.3	0.0	0.0	0.3	0.0	0.0	2.0	0.0	0.0	7.6	0.0	0.0	1.1	0.0
80	0.0	0.9	0.0	0.0	0.0	0.0	0.0	34.6	0.0	0.0	0.0	0.0	0.0	0.0	0.0	0.3	0.0	1.5	0.0	0.0	0.3	0.0
173	0.0	1.1	0.0	0.0	0.0	0.0	0.2	17.0	0.0	0.0	0.9	0.0	0.0	0.0	0.4	0.0	0.0	10.8	0.0	0.0	0.0	0.0
176	0.0	1.4	0.2	0.0	0.0	2.2	0.4	34.4	0.2	0.0	0.0	0.0	0.0	0.0	0.0	0.0	0.2	3.5	0.0	0.0	0.0	0.0
45	0.0	2.0	0.0	0.2	0.2	4.4	2.0	19.6	0.2	1.1	0.0	0.0	0.0	0.0	0.0	1.3	0.2	2.2	0.0	0.0	0.0	0.0
210	0.0	0.0	0.0	0.0	0.0	0.7	0.0	0.7	0.0	0.0	0.0	0.0	0.7	0.0	0.0	0.0	0.0	24.3	0.0	0.0	0.0	0.0
101	0.0	0.0	0.0	0.0	0.5	0.5	0.0	7.4	0.0	0.0	0.0	0.0	0.0	0.0	0.0	0.5	0.0	16.2	0.0	0.0	0.0	0.0
201	0.0	1.1	0.0	0.7	0.0	0.7	0.0	43.4	0.0	0.0	0.0	0.0	0.2	0.0	0.0	0.4	0.0	0.4	0.0	0.0	0.0	0.0
202	0.0	0.6	0.3	0.0	0.0	4.0	2.3	27.9	0.0	0.0	0.6	0.0	0.0	0.0	1.1	0.0	0.0	1.4	0.0	0.0	0.0	0.0
200	0.0	0.5	1.0	0.0	0.0	3.0	1.5	30.2	0.5	1.0	0.0	0.0	0.0	0.0	0.8	0.8	0.5	2.3	0.3	0.0	0.5	0.0
90	0.3	0.9	0.0	0.0	0.3	0.0	0.0	31.5	0.3	0.0	0.0	0.0	0.0	0.0	0.0	1.5	0.0	1.8	0.0	0.0	0.3	0.0
199	0.0	0.3	0.0	1.1	0.0	0.0	0.0	1.7	0.0	0.0	0.0	0.0	0.0	0.0	0.3	0.0	0.0	17.9	0.0	0.0	0.0	0.0
198	0.0	1.0	0.0	0.2	0.0	0.0	0.0	15.9	0.0	0.0	0.0	0.0	0.0	0.0	0.0	0.0	0.2	14.9	0.0	0.0	0.2	0.0
41	0.0	0.4	0.0	0.0	0.0	2.6	1.3	9.8	0.0	0.0	0.4	0.0	0.0	0.0	0.0	0.0	0.2	17.1	0.0	0.0	0.0	0.0
197	0.0	0.3	0.0	0.6	0.0	0.0	0.6	5.3	0.0	0.0	0.0	0.0	0.0	0.0	0.0	0.0	0.0	15.4	0.0	0.0	0.0	0.0
192	0.0	0.0	0.0	0.7	0.0	0.9	0.0	6.2	0.0	0.0	0.0	0.4	0.0	0.0	0.0	0.0	0.2	26.4	0.0	0.0	0.0	0.0
193	0.0	0.5	0.0	0.0	0.0	0.5	0.5	1.3	0.0	0.3	0.0	0.0	0.0	0.0	0.0	0.0	0.0	32.6	0.0	0.0	0.0	0.0
189	0.0	0.0	0.0	0.0	0.0	1.8	0.5	1.6	0.0	0.0	0.0	0.0	0.0	0.9	0.0	0.0	0.0	24.6	0.0	0.0	0.0	0.9
184	0.0	0.2	0.0	0.4	0.0	0.4	0.4	0.0	0.0	0.0	0.0	0.0	0.0	0.0	0.0	0.0	0.0	49.0	0.0	0.0	0.0	0.0
27	0.4	3.0	0.0	1.7	0.2	1.3	0.0	6.7	0.0	0.4	0.0	0.0	0.0	0.2	1.9	0.4	0.2	4.8	0.0	0.4	0.0	0.0
181	0.0	1.2	0.2	0.2	0.0	0.7	0.7	4.7	0.0	0.0	0.0	0.0	0.0	0.7	0.0	0.0	0.0	13.3	0.0	0.0	0.0	0.0
22	0.3	0.3	0.3	0.3	0.0	0.0	0.0	18.3	0.0	0.0	0.0	0.0	0.0	0.3	0.0	0.3	0.0	6.1	0.0	0.0	0.0	0.0

Station	Elphidium barletti	Elphidium crispum	Elphidium cf excavatum	Elphidium excavatum	Elphidium excavatum cf se	Elphidium gerthi	Elphidium incertum	Elphidium macellum	Elphidium magellanicum	Elphidium magrataceum	Elphidium ind	Elphidium willamsoni	Epistominella exigua	Epistominella narensis	Epistominella vitrea	Fissurina ellipitica	Fissurina laegivata	Fissurina lagenoides	Fissurina lucida	Fissurina marginata	Fissurina quadrata	Fissurina spp
53	0.0	0.0	0.0	0.6	0.0	0.6	0.0	0.0	0.0	0.0	0.0	98.2	0.0	0.0	0.0	0.0	0.0	0.0	0.0	0.0	0.0	0.0
68	0.0	0.0	0.0	1.2	0.0	0.3	0.0	0.0	0.3	0.0	0.0	1.2	0.0	0.0	0.0	0.0	0.0	0.0	0.0	0.0	0.0	0.0
147	0.0	0.0	0.0	0.0	0.0	0.0	0.0	0.0	0.3	0.0	0.3	0.0	0.0	0.0	0.3	0.0	0.0	0.0	0.3	0.0	0.0	0.0
72	0.0	0.0	0.0	1.9	0.0	0.0	0.0	0.0	0.6	0.3	0.0	0.0	0.0	0.0	0.0	0.0	0.0	0.0	0.0	0.0	0.0	0.0
149	0.0	0.0	0.0	0.0	0.0	0.0	0.0	0.0	0.0	0.0	0.0	0.0	0.0	0.0	0.0	0.0	0.0	0.0	0.0	0.0	0.0	0.0
211	0.0	0.0	0.0	0.0	0.0	0.0	0.3	0.0	0.3	0.0	0.0	0.0	0.0	0.0	0.0	0.0	0.0	0.0	0.0	0.0	0.0	0.0
110	0.0	0.3	0.0	0.0	0.0	0.0	0.0	0.0	0.0	0.0	0.0	0.0	0.0	0.0	0.0	0.9	0.0	0.0	0.0	0.0	0.0	0.0
112	0.0	0.0	0.0	0.0	0.0	0.6	0.0	0.6	0.0	0.6	0.0	0.9	0.0	0.0	0.0	0.6	0.0	0.0	0.3	0.0	0.0	0.0
76	3.2	0.0	1.4	5.0	0.0	0.0	0.0	0.0	1.1	0.0	0.0	1.1	0.0	0.0	0.0	0.0	0.0	0.0	0.4	0.0	0.0	0.0
2	0.0	0.0	0.0	3.4	0.0	0.8	0.0	0.0	0.8	0.6	0.0	0.0	0.6	0.0	0.0	1.7	0.0	0.0	0.0	0.0	0.8	0.0
80	0.0	0.0	0.0	6.7	0.0	0.0	0.0	0.0	0.3	0.0	1.5	0.0	0.3	0.3	0.0	0.0	0.0	0.0	0.3	0.0	0.0	0.3
173	0.0	0.9	0.7	6.4	0.0	0.0	0.0	0.0	0.2	0.4	0.0	0.0	0.0	0.0	0.4	1.2	0.0	0.0	0.2	0.0	0.0	0.0
176	0.0	0.0	0.0	8.1	0.0	0.0	0.0	0.0	0.2	0.2	0.2	0.0	0.0	0.0	0.2	0.6	0.0	0.0	0.0	0.0	0.0	0.8
45	0.0	0.0	0.0	3.5	0.0	0.0	0.0	0.0	0.4	0.0	0.0	0.2	0.0	0.0	2.0	0.0	0.0	0.0	0.2	0.2	0.0	0.2
210	0.0	0.0	0.0	6.9	0.0	0.2	1.0	14.6	0.0	1.2	0.0	0.2	0.0	0.0	0.2	0.0	0.0	0.0	0.2	0.0	0.0	0.0
101	0.0	0.0	0.0	3.6	0.0	0.3	0.0	0.0	1.0	0.0	0.0	0.0	0.0	0.3	0.0	0.3	0.0	0.0	0.3	0.0	0.0	0.0
201	0.0	0.0	0.0	9.6	0.0	0.0	0.0	0.0	0.0	0.0	0.0	0.0	0.0	0.0	2.2	0.0	0.0	0.0	0.4	0.0	0.0	0.0
202	0.0	0.0	0.0	2.6	0.0	0.3	0.9	0.0	1.1	0.0	0.3	0.0	0.0	0.0	1.1	0.0	0.0	0.0	0.0	0.0	0.0	0.0
200	0.0	0.0	0.0	7.1	0.3	0.3	0.0	0.0	0.3	0.0	0.3	0.0	0.0	0.0	2.0	0.0	0.0	0.0	0.0	0.0	0.0	0.3
90	0.0	0.0	0.0	8.8	0.0	0.0	0.0	0.0	0.0	0.0	0.0	0.0	0.0	0.0	0.0	0.0	0.9	0.0	0.0	0.0	0.0	0.0
199	0.6	0.9	0.0	2.3	0.0	1.1	0.0	0.9	0.0	0.3	1.4	0.3	0.0	0.0	0.3	0.0	0.0	0.0	0.0	0.0	0.0	0.3
198	0.0	0.0	0.0	5.0	0.2	0.0	0.0	0.5	0.0	0.2	0.2	0.0	0.0	0.0	0.0	0.0	0.0	0.0	0.2	0.0	0.0	0.0
41	0.0	0.0	0.0	5.8	0.0	0.2	0.0	0.4	0.0	0.0	0.0	0.0	0.0	0.0	0.4	0.4	0.0	0.0	0.0	0.0	0.0	0.0
197	0.0	0.0	0.0	2.4	0.0	0.0	0.0	0.0	0.3	0.0	0.0	0.3	0.0	0.0	0.9	0.3	0.0	0.0	0.0	0.3	0.0	0.0
192	0.0	0.0	0.0	4.4	0.0	0.0	0.0	1.1	0.0	0.2	0.0	0.0	0.0	0.0	0.2	0.9	0.0	0.0	0.0	0.0	0.0	0.0
193	0.0	1.3	0.0	2.0	0.0	0.3	0.0	0.0	0.0	0.0	0.0	0.0	0.0	0.3	0.0	0.3	0.0	0.0	0.0	0.0	0.0	0.0
189	0.0	0.7	0.0	1.1	0.0	0.0	0.0	0.5	0.0	0.0	0.0	0.0	0.0	0.2	0.0	0.2	0.0	0.0	0.2	0.0	0.0	0.0
184	0.0	0.0	0.8	0.0	0.0	0.8	0.2	2.9	0.0	0.0	0.2	0.0	0.0	0.0	0.2	0.0	0.0	0.0	0.4	0.0	0.0	0.0
27	0.0	0.0	0.0	8.2	0.0	0.2	0.0	0.0	0.4	0.2	0.0	0.4	0.0	0.0	4.6	0.0	0.0	0.0	0.4	1.5	0.2	0.4
181	0.0	0.0	0.0	14.0	0.0	0.2	0.0	5.7	0.2	0.0	0.2	0.0	0.0	0.0	0.0	0.2	0.0	0.0	0.0	0.0	0.0	0.0
22	0.0	0.0	0.0	20.4	0.0	0.0	0.0	0.0	0.0	0.0	0.3	0.0	0.0	0.0	0.0	0.0	0.0	0.0	0.0	0.0	0.0	0.3

Station	Globocassidulina subglobos	Guttulina lactea	Guttulina spp.	Gyroidina spp.	Haynesina germanica	Hyalinea balthica	Islandiella narcossi	Islandiella spp.	Lagena gracillima	Lagena hirtshalsensis	Lagena semilineata	Lagena semistriata	Lagena spp.	Lagena substriata	Lagena striata	Lenticula spp.	Larmackina halitodae	Melonis barleeanum	Melonis spp.	Nonionella turgida	Nonion auricula	Nonion depressulus
53	0.0	0.0	0.0	0.0	0.6	0.0	0.0	0.0	0.0	0.0	0.0	0.0	0.0	0.0	0.0	0.0	0.0	0.0	0.0	0.0	0.0	0.0
68	0.0	0.0	0.0	0.0	0.9	0.0	0.0	0.0	0.0	0.0	0.0	0.0	0.0	0.0	0.0	0.0	0.0	0.0	0.0	0.0	0.0	0.6
147	0.0	0.0	0.0	0.0	0.0	0.0	0.0	0.0	0.0	0.0	0.0	0.3	0.0	0.0	0.0	0.0	0.0	0.0	0.0	0.0	0.0	0.0
72	0.0	0.0	0.0	0.0	0.0	0.0	0.0	0.0	0.0	0.0	0.0	0.0	0.0	0.3	0.0	0.0	0.0	0.0	0.0	0.9	0.0	0.0
149	0.0	0.0	0.0	0.0	0.0	0.0	0.0	0.0	0.0	0.0	0.0	0.0	0.0	0.0	0.0	0.0	0.0	0.0	0.0	0.3	0.0	0.0
211	0.0	0.0	0.0	0.0	0.0	0.0	0.0	0.0	0.0	0.0	0.0	0.0	0.3	0.0	0.0	0.0	0.0	0.0	0.0	0.8	0.0	0.0
110	0.0	0.0	1.5	0.0	0.0	0.0	0.0	0.0	0.0	0.0	0.0	0.0	0.0	0.0	0.0	0.0	0.0	0.0	0.0	0.6	0.0	0.0
112	0.0	0.3	0.0	0.0	0.0	0.0	0.0	0.0	0.0	0.0	0.0	0.0	0.6	0.0	0.0	0.0	0.0	0.0	0.0	0.3	0.0	0.0
76	0.0	0.0	0.0	0.0	0.0	0.0	0.0	0.0	0.0	0.0	0.0	0.0	0.0	0.4	0.0	0.0	0.0	0.0	0.0	1.8	0.0	0.0
2	0.0	0.0	1.1	0.0	0.0	0.0	0.0	0.0	0.3	0.0	0.0	0.0	0.0	0.0	0.3	0.0	0.0	0.0	0.0	1.7	2.0	2.9
80	0.0	0.0	0.0	0.0	0.0	0.9	0.0	0.0	0.0	0.0	0.0	0.0	0.0	0.0	0.0	0.0	0.0	0.0	0.0	5.8	0.0	0.3
173	0.0	0.0	0.0	0.0	0.0	0.5	0.4	0.0	0.0	0.0	0.0	0.0	0.0	0.0	0.2	0.0	0.0	0.9	0.0	1.1	0.0	0.0
176	0.0	0.0	0.0	0.0	0.0	1.4	0.2	0.0	0.0	0.0	0.0	0.0	0.0	0.0	0.0	0.2	0.0	1.2	0.0	2.8	0.0	0.0
45	0.4	0.0	0.0	0.4	0.0	0.2	0.0	0.0	0.0	0.0	0.0	0.0	0.0	0.0	0.0	0.0	0.0	0.4	0.0	11.9	0.0	0.4
210	0.0	0.0	0.0	0.0	1.7	0.0	0.0	0.0	0.0	0.0	0.0	0.2	0.0	0.2	0.0	0.0	0.0	0.0	0.0	0.2	0.0	0.0
101	0.0	0.0	0.3	0.0	0.0	0.0	0.0	0.0	0.0	0.0	0.0	0.0	0.3	0.0	0.0	0.0	0.0	0.0	0.0	1.3	1.0	0.0
201	0.4	0.0	0.0	0.0	0.2	0.9	0.0	0.7	0.0	0.0	0.0	0.0	0.0	0.2	0.0	0.0	0.0	0.4	0.0	6.8	0.0	0.0
202	0.0	0.0	0.0	0.0	0.0	0.0	0.3	0.0	0.0	0.0	0.0	0.0	0.0	0.3	0.0	0.0	0.0	0.0	0.0	11.2	0.9	0.0
200	0.3	0.0	0.0	0.0	0.0	1.3	0.3	0.0	0.3	0.0	0.0	0.0	0.0	0.0	0.0	0.3	0.0	0.3	0.0	5.0	0.0	0.0
90	0.0	0.0	0.0	0.0	0.0	0.3	0.0	0.0	0.3	0.0	0.3	0.0	0.3	0.0	0.0	0.0	0.0	0.0	0.0	10.0	0.0	0.0
199	0.0	0.0	0.0	0.0	0.0	0.0	0.0	0.0	0.0	0.0	0.0	0.0	0.0	0.0	0.0	0.0	0.0	0.0	0.0	0.3	0.0	0.6
198	0.0	0.0	0.2	0.0	0.0	1.5	0.0	0.0	0.0	0.0	0.0	0.0	0.0	0.0	0.0	0.0	0.0	1.2	0.0	3.2	0.0	0.0
41	0.0	0.0	0.0	0.0	0.0	0.6	0.0	0.0	0.0	0.0	0.0	0.0	0.0	0.0	0.0	0.0	0.0	0.4	0.0	3.8	0.0	0.2
197	0.0	0.0	0.0	0.0	0.0	0.0	0.0	0.0	0.0	0.0	0.3	0.0	0.0	0.0	0.0	0.0	0.0	0.0	0.0	8.6	0.6	0.0
192	0.0	0.0	0.0	0.0	0.0	0.4	0.0	0.0	0.0	0.0	0.0	0.0	0.0	0.0	0.0	0.0	0.0	0.2	0.0	2.0	0.0	0.0
193	0.0	0.0	0.3	0.0	0.0	0.3	0.5	0.0	0.0	0.0	0.0	0.0	0.0	0.0	0.0	0.0	0.0	5.9	0.0	0.3	0.0	0.0
189	0.0	0.0	0.0	0.0	0.0	0.2	0.0	0.0	0.0	0.0	0.0	0.0	0.0	0.0	0.0	0.0	0.0	3.9	0.0	0.0	0.0	0.0
184	0.0	0.0	0.0	0.0	0.0	0.0	0.0	0.0	0.0	0.0	0.0	0.0	0.0	0.0	0.0	0.0	0.0	0.0	0.0	0.4	0.2	0.0
27	0.2	0.0	0.2	0.0	0.4	0.4	0.4	0.0	0.0	0.2	0.0	0.0	0.0	0.0	0.0	0.0	0.2	0.2	0.0	6.1	1.1	0.0
181	0.0	0.0	0.0	0.0	0.0	0.7	0.0	0.0	0.0	0.0	0.0	0.0	0.0	0.0	0.0	0.0	0.0	1.2	0.0	1.5	0.0	0.0
22	0.0	0.0	0.0	0.0	0.0	2.6	0.0	0.0	0.0	0.0	0.0	0.0	0.0	0.0	0.0	0.3	0.0	1.3	0.0	0.0	0.0	0.0

Station	Nonion iridae	Nonion orbiculare	Nonion pauperatum	Nonion spp.	Oolina borealis	Oolina cf caudigera	Oolina cf lineata	Oolina hexagona	Oolina melo	Oolina spp.	Oolina squamosa	Oolina williamsoni	Parafissurina himatiostoma	Patellina corrugata	Planorbi distoma	Rosalina anomala	Rosalina cf. bradyi	Rosalina bradyi	Rosalina irregularis	Rosalina millettii	Rosalina praegeri	Rosalina spp.
53	0.0	0.0	0.0	0.0	0.0	0.0	0.0	0.0	0.0	0.0	0.0	0.0	0.0	0.0	0.0	0.0	0.0	0.0	0.0	0.0	0.0	0.0
68	0.0	0.0	0.0	0.0	0.0	0.0	0.0	0.0	0.0	0.0	0.0	0.0	0.0	0.0	0.0	0.0	0.0	0.0	0.0	0.0	0.0	0.0
147	0.0	0.0	0.0	0.0	0.0	0.0	0.0	0.0	0.0	0.0	0.0	0.0	0.0	0.0	0.0	0.0	0.0	0.0	0.0	0.0	0.3	0.0
72	0.0	0.0	0.0	0.0	0.0	0.0	0.0	0.0	0.0	0.0	0.0	0.3	0.0	0.0	0.0	0.0	0.0	0.0	0.0	0.0	0.9	0.0
149	0.0	0.0	0.0	0.0	0.0	0.0	0.0	0.0	0.0	0.0	0.0	0.0	0.0	0.0	0.0	0.0	0.0	0.0	0.0	0.0	0.0	0.0
211	0.0	0.0	0.0	0.0	0.0	0.0	0.0	0.0	0.3	0.0	0.0	0.3	0.0	0.0	0.0	0.0	0.0	0.0	0.0	0.0	0.0	0.0
110	0.0	0.0	0.3	0.3	0.0	0.0	0.0	0.0	0.3	0.0	0.3	0.3	0.0	0.0	0.0	0.3	0.0	0.0	0.0	0.0	1.7	0.3
112	0.0	0.0	0.0	0.0	0.0	0.0	0.3	0.3	0.0	0.0	0.0	0.3	0.0	0.0	0.0	0.0	0.0	0.0	0.0	0.0	3.2	0.0
76	0.0	0.0	0.0	0.0	0.0	0.0	0.0	0.0	0.0	0.0	0.0	0.0	0.0	0.0	0.0	0.0	0.0	0.0	0.0	0.0	0.7	0.0
2	0.0	0.0	2.5	0.0	0.0	0.0	0.3	0.3	0.0	0.0	0.0	0.0	0.0	0.8	0.0	0.3	0.0	0.0	0.0	0.0	4.8	0.0
80	0.0	0.0	0.0	0.0	0.0	0.0	0.0	0.0	0.0	0.0	0.0	0.0	0.0	0.0	0.3	0.3	0.0	0.0	0.0	0.0	0.0	0.0
173	0.0	0.0	0.0	0.2	0.0	0.0	0.0	0.0	0.0	0.0	0.0	0.0	0.0	0.0	0.0	0.0	0.0	0.0	0.0	0.0	3.2	0.0
176	0.0	0.0	0.0	0.0	0.0	0.0	0.0	0.2	0.0	0.0	0.0	0.0	0.0	0.0	0.0	0.8	0.0	0.0	0.0	0.0	1.2	0.2
45	0.0	0.0	0.2	0.2	0.0	0.0	0.0	0.0	0.0	0.0	0.0	0.0	0.2	0.2	0.0	0.2	0.0	0.0	0.0	0.0	0.0	0.0
210	0.0	0.0	0.0	0.0	0.0	0.0	0.0	0.0	0.0	0.0	0.0	0.2	0.0	0.0	0.0	0.0	0.0	0.0	0.0	0.0	0.0	0.0
101	0.0	0.0	0.0	0.0	0.0	0.0	0.3	0.5	0.0	0.0	0.0	0.0	0.0	0.0	0.0	0.0	0.0	0.3	0.0	0.0	4.3	0.0
201	0.0	0.0	0.2	0.0	0.0	0.0	0.0	0.0	0.4	0.0	0.0	0.0	0.0	0.2	0.0	0.2	0.0	0.2	0.0	0.0	0.2	0.0
202	0.0	0.0	0.0	0.0	0.0	0.0	0.0	0.0	0.0	0.0	0.0	0.0	0.0	0.0	0.0	0.0	0.0	0.0	0.0	0.0	0.0	0.3
200	0.0	0.0	0.0	0.0	0.3	0.0	0.0	0.0	0.0	0.0	0.0	0.0	0.0	0.0	0.0	0.0	0.0	0.0	0.0	0.0	0.0	0.0
90	0.0	0.0	0.0	0.0	0.0	0.0	0.0	0.0	0.0	0.3	0.0	0.0	0.0	0.3	0.0	0.0	0.3	0.0	0.0	0.3	2.4	0.0
199	0.0	0.0	0.3	0.0	0.0	0.0	0.0	0.0	0.0	0.0	0.0	0.3	0.0	0.0	0.0	0.3	0.0	0.0	0.0	0.0	4.6	0.0
198	0.0	0.0	0.0	0.0	0.0	0.0	0.0	0.0	0.0	0.0	0.0	0.0	0.0	0.0	0.0	0.0	0.0	0.0	0.0	0.0	2.7	0.2
41	0.0	0.0	0.0	0.2	0.0	0.2	0.0	0.0	0.0	0.0	0.0	0.2	0.0	0.4	0.2	0.0	0.0	0.0	0.0	0.0	2.8	0.0
197	0.0	0.0	0.3	0.3	0.0	0.0	0.0	0.3	0.0	0.0	0.0	0.0	0.0	0.0	0.0	0.0	0.0	0.0	0.0	0.0	3.8	0.0
192	0.0	0.0	0.0	0.0	0.0	0.0	0.0	0.0	0.4	0.0	0.0	0.0	0.0	0.0	0.2	0.2	0.2	0.0	0.0	0.0	2.4	0.2
193	0.0	0.0	0.0	0.3	0.0	0.0	0.0	0.0	0.3	0.0	0.0	0.0	0.0	0.0	0.0	0.0	0.0	0.0	0.0	0.0	2.3	0.3
189	0.0	0.7	0.0	0.0	0.0	0.0	0.0	0.0	0.0	0.0	0.0	0.2	0.0	0.0	0.0	0.0	0.0	0.0	0.0	0.0	0.9	0.0
184	0.0	0.0	0.0	0.0	0.4	0.0	0.0	0.0	0.0	0.0	0.0	0.0	0.0	0.0	1.4	0.2	6.0	0.0	0.0	0.0	1.6	0.2
27	0.8	0.0	0.4	0.0	0.0	0.0	0.0	0.0	0.0	0.0	0.0	0.0	0.0	0.4	0.0	0.2	0.8	1.1	0.0	0.0	1.7	0.8
181	0.0	0.0	0.0	0.0	0.0	0.0	0.0	0.0	0.0	0.0	0.0	0.0	0.0	0.2	0.2	0.7	0.0	0.2	0.0	0.0	1.7	0.0
22	0.0	0.0	0.0	0.0	0.0	0.0	0.0	0.0	0.0	0.0	0.0	0.0	0.0	0.0	0.0	0.3	0.0	0.0	0.3	0.0	2.1	0.0

Station	Rosalina willamsoni	Stainforthia fusiformis	Stainforthia loeblichi	Stainforthia schreibersiana	Stainforthia sp.	Trifarina angulosa	Trifarina fluens	Indeterminate spp.	Planktonic spp.
53	0.0	0.0	0.0	0.0	0.0	0.0	0.0	0.0	0.0
68	0.0	0.3	0.0	0.0	0.0	0.0	0.0	0.0	0.0
147	0.0	0.0	0.0	0.0	0.0	0.0	0.0	0.3	0.0
72	0.0	0.0	0.0	0.0	0.0	0.0	0.0	0.3	0.0
149	0.0	0.0	0.3	0.0	0.3	0.0	0.0	1.3	0.6
211	0.0	0.0	0.0	0.0	0.3	0.0	0.0	1.1	0.0
110	0.0	0.0	0.0	0.0	0.0	0.0	0.0	0.3	0.3
112	0.0	0.9	0.0	0.0	0.0	0.0	0.3	0.0	0.0
76	0.0	0.4	0.0	0.0	0.0	0.0	0.0	0.0	0.0
2	0.3	2.5	0.0	0.0	0.0	1.7	0.0	0.6	0.0
80	0.0	2.4	0.0	0.0	0.0	0.9	0.0	0.0	0.0
173	0.0	0.2	0.4	0.0	0.0	1.9	0.0	0.2	0.0
176	0.0	0.6	0.0	0.0	0.0	0.4	0.0	0.2	0.0
45	0.0	7.5	0.7	0.2	0.0	0.2	0.0	1.8	0.9
210	0.0	0.0	0.0	0.0	0.0	0.0	0.0	0.0	0.0
101	0.0	0.0	0.0	0.0	0.0	0.8	0.0	3.0	0.0
201	0.0	0.9	0.0	0.2	0.0	0.7	0.2	0.0	0.0
202	0.0	8.6	1.4	0.0	0.0	0.0	0.0	0.9	0.6
200	0.0	0.8	0.0	0.0	0.0	0.3	0.0	0.8	0.0
90	0.0	1.8	0.9	0.0	0.0	0.3	0.3	0.9	0.0
199	0.0	0.6	0.0	0.0	0.0	0.3	0.0	1.4	0.0
198	0.0	0.2	0.2	0.0	0.0	0.0	0.2	0.2	0.0
41	0.0	0.4	0.2	0.0	0.0	0.0	0.0	0.6	0.0
197	0.0	2.4	0.3	0.0	0.0	0.0	0.0	1.5	0.0
192	0.0	0.2	0.0	0.0	0.0	0.2	0.0	2.0	0.0
193	0.0	0.0	0.0	0.0	0.0	0.0	0.3	0.8	0.0
189	0.0	0.0	0.0	0.0	0.0	0.0	0.0	2.5	0.0
184	0.0	0.0	0.0	0.0	0.0	0.2	0.0	1.2	0.2
27	0.0	8.0	1.1	0.0	0.0	0.6	0.0	0.0	7.6
181	0.0	0.2	0.2	0.0	0.0	0.7	0.2	1.5	0.0
22	0.0	0.0	0.0	0.0	0.0	0.0	0.0	0.0	0.0